10/4-11-90 J5(1)

SANDIA REPORT

SAND89—2612/B • UC—132
Unlimited Release
Printed January 1990

Multiwell Experiment Final Report: IV. The Fluvial Interval of the Mesaverde Formation

Multiwell Experiment Project Groups
at Sandia National Laboratories
and
CER Corporation

Prepared by
Sandia National Laboratories
Albuquerque, New Mexico 87185 and Livermore, California 94550
for the United States Department of Energy
under Contract DE-AC04-76DP00789

SF2900Q(8-81)

Issued by Sandia National Laboratories, operated for the United States Department of Energy by Sandia Corporation.

Printed in the United States of America. This report has been reproduced directly from the best available copy.

Available to DOE and DOE contractors from
Office of Scientific and Technical Information
PO Box 62
Oak Ridge, TN 37831

Prices available from (615) 576-8401, FTS 626-8401

Available to the public from
National Technical Information Service
US Department of Commerce
5285 Port Royal Rd
Springfield, VA 22161

NTIS price codes
Printed copy: A99
Microfiche copy: A01

SAND--89-2612/Pt.B

DE90 007938

SAND89-2612/Part B
Unlimited Release
UC Category 132

MULTIWELL EXPERIMENT FINAL REPORT: IV. THE FLUVIAL INTERVAL OF THE MESAVERDE FORMATION

Compiled by the
Multiwell Experiment Project Groups
Sandia National Laboratories
Albuquerque, NM 87185
and
CER Corporation
Las Vegas, NV 89109
for the
U.S. Department of Energy

Printed January, 1990

Abstract

The Department of Energy's Multiwell Experiment (MWX) is a field laboratory in the Piceance Basin of Colorado which has two overall objectives: to characterize the low permeability gas reservoirs in the Mesaverde Formation and to develop technology for their production. Different depositional environments have created distinctly different reservoirs in the Mesaverde, and MWX has addressed each of these in turn. This report presents a comprehensive summary of results from the fluvial interval which lies between 4400 ft and 6000 ft at the MWX site. The reservoirs consist of heterogeneous, amalgamated point-bar sequences which form broad meanderbelts which create irregular, but roughly tabular, reservoirs with widths of 1000-2500 ft. Separate sections of this report are background and summary; site descriptions and operations; geology; log analysis; core analysis; in situ stress; well testing, stimulation, fracture diagnostics, and reservoir evaluation in two separate sandstones; stress, fracture diagnostic, and stimulation experiments in an additional sandstone; supporting laboratory studies; and a bibliography. Additional detailed data, results, analyses, and data file references are presented as appendices which are included on microfiche. The results show that stimulation of fluvial reservoirs can be successful if proper care is taken to minimize damage to the natural fracture system. Both an accelerated leakoff phenomenon and the ability to alter the in situ stress were quantified. Overall, the fluvial interval offers the highest production potential of the three nonmarine intervals studied.

CONTENTS
PART A--CHAPTERS 1 THROUGH 6
(See Part B for Sections 7 through 12)

CONTENTS, PART A

CONTENTS
PART B--CHAPTERS 7 THROUGH 11 (MICROFICHE APPENDICES INSIDE BACK COVERO
(See Part A for Chapters 1 through 6)

CONTENTS, PART B

CONTENTS, PART B

CONTENTS, PART B

CONTENTS, PART B

CONTENTS, PART B

7.0 FLUVIAL B SANDSTONE STIMULATION EXPERIMENT

7.1 PRE-STIMULATION RESERVOIR TESTING AND ANALYSIS

P. T. Branagan
CER Corporation

7.1.1 INTRODUCTION

On June 8, 1986, testing of the fluvial B sandstone commenced with the gas perforation breakdown or microfracturing of all 3 MWX wells. Immediately following, a pre-stimulation interference well test was initiated utilizing MWX-1 as the production well and MWX-2 and MWX-3 as observation wells. The following were the primary objectives of the fluvial B sand pre-stimulation testing:

- Derive average reservoir flow capacity and assess the contribution from natural fractures.
- Quantify real and apparent reservoir boundaries.
- Determine the degree of reservoir/natural fracture anisotropy.
- Separate interference diffusive pressure response from poroelastic effects.
- Provide additional in situ stress data and leakoff values for gaseous fracturing fluid components.
- Assess the variations in well production and interference pressure transients for liquid-filled and dry wellbores.

To minimize liquids in the wellbore, nitrogen (N_2) gas was used as the fracturing fluid. Workover operations were performed without liquids in

the wellbore to provide an essentially dry wellbore and natural fractures for the first fluvial B interference test. Also, minimizing wellbore liquids ensured dry natural fractures in the near well vicinity of the observation wells. This reduced uncertainty in assessing the results of the interference pressure transient data of both the microfracturing and well tests.

The objectives of both the microfracturing and pre-stimulation interference test was to establish base case conditions for reservoir model development, stimulation design, and post-stimulation enhancement determinations.

7.1.2 GASEOUS PERFORATION BREAKDOWN/MICROFRACTURING

The primary objective of the gas perforation breakdown was to induce short, dry, unpropped, fractures in each of the three MWX wells to provide clear and relatively conductive flow paths from the in situ fracture system to each wellbore. In addition, bottomhole pressure measurements gathered during each of the microfracturing tests yielded values of instantaneous shut-in pressure (ISIP) and closure pressure from which the minimum in situ stress was derived. During the breakdowns, transient pressures at the observation wells provided clear evidence of pressure interference. Previous reservoir test behavior indicated that conventional KCl-water breakdowns caused water blocks within the natural fractures which substantially reduced their flow capacity and the ability of the reservoir to produce gas. The reduction in flow capacity caused by liquids within the natural fractures makes the comparative assessment of future stimulations an ambiguous task. The comparison may have uncertainties that are extremely large and potentially undefinable due to variations in capillary pressures and flow capacity within the natural fracture system when liquids are present. Extremely low gas production in the marine Cozzette sandstone was followed by substantially increased production after a small volume of liquids were recovered. This was a clear example of

reservoir behavior where liquids in the fractures block or impede gas production.

7.1.3 SITE PREPARATIONS

Preparation of the MWX wells began with workover operations on MWX-2. The B sandstone was perforated with jet charges, after which, the tubulars and packer assemblies were set. Table 7.1.1 is a summary of pertinent well data for all three MWX wells during the fluvial B pre-frac tests.

Bottomhole pressure gauges were placed and isolated from the tubing with the bottomhole shut-in tools in the observation wells, MWX-2 and MWX-3, for about 60 days during the pre-frac interference test. Since the testing period was lengthy and the anticipated pressure transients at the observation wells were estimated to be very small (1 to 3 psi/day), it was necessary to pressure test each of the bottomhole assemblies for leaks. Following successful pressure testing for downhole leaks, reservoir and interference tests were initiated.

7.1.4 RESERVOIR CHARACTERISTICS

The fluvial lenticular sandstones at MWX can be characterized as very tight, low porosity, lenticular reservoirs that have small length to width ratios indicative of point bar deposits. Although the sandstone matrices are extremely tight, they are probably coupled to a relatively large set of natural fractures that ultimately makes these reservoirs potentially some of the more favorable lenticular producers at the MWX site. However, the complexity of the depositional environment and the subsequent impact of operations to connect the natural fracture system with the wellbore may cause initial well testing to indicate smaller than actual reservoir capacity.

The natural fractures may also extend beyond the reservoir body and into the adjacent siltstones and thus complicate well testing and

interpretation, and the design and execution of hydraulic fracturing operations. The largest natural fractures observed in the MWX cored intervals were, in fact, found in the fluvial siltstones that adjoin the sandstones. Figure 7.1.1 shows the fracture distribution and widths for the MWX fluvial and coastal intervals.

Figure 7.1.2 is a correlation of the lower fluvial interval for the three MWX wells. The fluvial B and adjoining intervals were cored and subsequently analyzed by various labs. Figure 7.1.3 and Table 7.1.2 provide good correlated core and log data from which to select reservoir net pay, total porosity, water saturation and dry Klinkenberg matrix permeability. Special core analysis, including restored state Klinkenberg matrix permeability measurements at various water saturations is shown in Figure 7.1.4. This data, when combined with the effective overburden pressure lab data, yields reliable in situ matrix permeability information for the fluvial B sandstone. Table 7.1.3 presents core, log, laboratory information and outcrop data from which a reservoir description for the fluvial B sandstone was developed. This information is used to develop the base case model of the fluvial B naturally fractured sandstone reservoir.

7.1.5 FLUVIAL B INTERFERENCE TESTS

Interference testing in the fluvial B sandstone began Monday, June 15, 1986, utilizing MWX-2 and MWX-3 as observation wells and MWX-1 as the production well. Figure 7.1.5 is a composite plot of MWX flow rate and bottomhole pressure data taken between June 16 and August 27. (Selected digitized well test data are given in Appendix F.) The zero reference time for the plot is 12 noon, June 14. A one day shut-in was performed between the second and third day, Wednesday, June 18 and Thursday, June 19. This shut-in was designed to provide a pressure pulse within the reservoir that might be observed in the interference wells. No clear pressure disturbances were observed. Both observation wells had slowly decreasing pressures and remained above the measured initial reservoir pressure of 3410 psi, probably due to the microfracturing injection process.

7.1.5.1 Drawdown Test

The initial flow rate in the production well, MWX-1, was held between 50 and 60 MSCFD, at a bottomhole pressure of about 700 psi. During the week of June 28 through July 3, the flow rate began slowly dropping from about 50 to 55 MSCFD to about 38 to 43 MSCFD. The flow test was allowed to become a constant pressure test in order to maintain the largest possible pressure drop in the production well and thus induce the greatest pressure transient into the reservoir.

Figures 7.1.6 and 7.1.7 are bottomhole pressure plots of the observation wells, MWX-2 and MWX-3, respectively, for the first 15 to 20 days of the interference test. The perturbations in MWX-3 during days 9 and 12 are the result of a leaky bottomhole seal. The large excursion during day 15 is the result of unseating the pressure tool downhole. Careful examination of these data do not reveal any clear evidence of pressure communication between the observation wells and MWX-1.

A 550 psi difference between surface and bottomhole pressure in MWX-1 indicated a liquid column standing in the wellbore. A short wellbore pressure survey was completed to determine the pressure gradient in the lower portion of the well. Figure 7.1.8 is a plot of the pressure survey data along with an insert of the calculated pressure gradient. The gradient between 4500 ft and 5800 ft is seen to be roughly constant at 0.10 psi/ft, much higher than a gradient of 0.0097 psi/ft for a dry gas with a specific gravity of 0.62 at an average wellbore pressure of 500 psi. Thus, the difference between the measured and calculated gradient was attributed to the inclusion of entrained liquids in the wellbore, probably on the order of 4 to 6 bbls.

The well was blown to the flare pit to unload as much of the wellbore liquids as possible. Several barrels of liquid were visually estimated to have been recovered. The liquid was extremely flammable and determined

from sample analysis to be condensate. Note in Figure 7.1.5 that the bottomhole pressure dropped from about 730 psi to about 350 psi following the removal of the wellbore liquids (day 21).

Figures 7.1.9 and 7.1.10 present the bottomhole pressure data for MWX-2 and MWX-3 during the liquid blow down in MWX-1. Note the sensitivity of this data and the fact that 0.05 psi can readily be resolved for MWX-2. Even on this very sensitive scale, there does not appear to be any indications that the fast pressure drop occurring in MWX-1 during the blow down was observable in either of the observation wells. Note that MWX-2 pressure is still falling, while MWX-3 is rising. These overall pressure transients are remnants of the perturbations that were introduced earlier during the breakdown and subsequent seating of the bottomhole pressure tools.

7.1.5.2 Preliminary Modeling

In an attempt to quantify the nature and productive mechanisms of the fluvial B sandstone, a series of computer model runs were used to supplement the analytic effort. Production data from MWX-1 indicated the reservoir to be capable of producing 25 to 30 MSCFD. An isotropic, homogeneous reservoir model was developed to determine the minimum average flow capacity required to produce 25 MSCFD. The resulting model suggested that for a 17-ft thick reservoir, the average permeability required to radially produce 25 MSCFD was 10 μd. This is about 100 times more permeable than the maximum core derived matrix restored state permeability (reference Figures 7.1.3 and 7.1.4). The model further indicated that after several days of production, the pressure transient at MWX-2 should be about 10 psi, and thus be resolvable with the present observation well system.

The next modeling scenario was designed to determine whether the inclusion of the gas breakdown fractures could be the sole enhancement

mechanism that would permit a 0.1 μd homogeneous matrix reservoir to produce 25 MSCFD. A revised model was developed to include a homogeneous matrix 17 ft thick with a permeability of 0.1 μd and the following breakdown fracture parameters:

$$w_f = 0.001 \text{ in.}$$
$$k_f = 2 \text{ darcy}$$
$$x_f = 100 \text{ ft}$$
$$h_f = 17 \text{ ft}$$

This model indicated the well would not be capable of producing 20 MSCFD for more than several days, and that the production would be principally wellbore and fracture dominated. Consequently, no pressure transients would be observed at either observation well. Thus, unless the breakdown fracture in MWX-1 was in excess of 100 ft, it can be concluded that the enhanced production mechanism in and around MWX-1 is not the result of a single fracture such as the breakdown fracture. Therefore it appears that the fluvial B sandstone is a naturally fractured reservoir containing numerous closely spaced fractures.

The next set of computer runs assumed the natural fracture system flow capacity was severely anisotropic, with the maximum value directed along the direction of maximum principle stress. This makes the smaller value of natural fracture flow capacity point toward the observation wells and would thus minimize the pressure transients in that direction. This is similar to the final descriptions for the other reservoirs tested at MWX which showed flow capacity ratios of 50:1 and 100:1. In order to replicate the MWX well test data, an injection was simulated (similar to the breakdown) in the observation location for MWX-2, followed by a falloff, before producing MWX-1. The largest value of anisotropy appears to make the observation of the transient from MWX-1 very difficult to distinguish from the falloff occurring in MWX-2 and thus may be a fair representation of the fluvial B sand. The 100:1 ratio equates to one set of fractures having a

permeability of about 15 darcies while the orthogonal set would be 0.15 darcies.

The drawdown testing provided the following information:

- An average total reservoir flow capacity of 8 to 12 μd.
- A 100 fold increase in flow capacity over the matrix value.
- Pressure interference data indicating the natural fracture flow capacity exhibits severe anisotropy, probably as much as 100:1.

7.1.5.3 Initial Buildup Test

On July 11 (day 27), MWX-1 was shut-in for a short period to induce a pressure transient that might be observable at observation wells, MWX-2 and MWX-3. The pressure buildup continued through July 13 (day 29). Figure 7.1.11 is a log-log plot of the pressure buildup data from MWX-1. Note the long period during which the buildup rate is on a slope of 1 and thus indicates the extended time that wellbore storage controls bottomhole pressure. The small pressure drop that can be seen to occur at 674 hrs is the result of a surface wellhead leak that was subsequently repaired.

Figure 7.1.12 is a Horner plot of the MWX-1 pressure buildup. Note that extrapolating this data to an infinite buildup, (i.e., a Horner time = 1), will yield an average reservoir pressure well in excess of initial pressure (3430 psi). This is the result of both the wellbore storage effects and the fact that the reservoir is not acting in a radial or pseudo-radial fashion. It would be expected that the pressure rate of rise would be severely curtailed, thus producing a relatively flat slope on this type plot in order to extrapolate to a P* of about 3430 psi. Note that these data do not indicate the presence of boundaries.

No attempt was made to calculate flow capacity from the Horner plot since the final slope of this short shut-in is clearly not the appropriate slope to make such a derivation. The well was returned to production at a flow rate about 18 to 20 MSCFD with a bottomhole pressure of 600 psi (Figure 7.1.5, day 29).

Figures 7.1.13 and 7.1.14 are expanded views of the bottomhole pressure data from the observation wells, MWX-2 and MWX-3, respectively, during the buildup and drawdown of MWX-1 on days 24 through 33. There appear to be no pressure changes that are related to either the buildup or production pressure transients initiated in MWX-1.

A second pressure survey was performed in MWX-1 on July 25 (day 41). The flow rate from MWX-1 was held at about 18 MSCFD during the last 3 weeks (days 31 to 52) of the drawdown. The bottomhole pressure rises during this constant production period from about 500 psi to slightly above 1000 psi, while the surface pressure continued to decrease. Thus, it was assumed that liquids, although not produced at the surface, were nevertheless entering the wellbore and increasing the bottomhole fluid density. A new pressure survey indicated the density of the wellbore fluid ranged from 0.16 psi/ft at the perforations to about 0.12 psi/ft at about 1200 ft. Thus, the wellbore fluid was probably composed of natural gas (80 percent) with a distributed quantity of entrained liquids (20 percent) in vapor phase. No solid column of liquids was observed.

The use of MWX-3 as an observation well for interference testing was terminated July 24 (day 40) when the seated bottomhole pressure tool was released and the well was produced to the flare pit. During nearly 6 weeks of pressure interference testing, it was not possible to observe any pressure transients that could be attributed to production in MWX-1. MWX-2 remained shut-in for about another week, but it also provided no evidence of pressure transients from MWX-1. The lack of pressure interference at either observation well suggests that: (1) there is no communication between MWX-1 and the other two wells; or (2) the production is dominated

by anisotropic flow such that the transient remains below the resolution of the data acquisition system, e.g., 0.05 to 0.10 psi.

7.1.5.4 Argon Injection Test Into MWX-2

The elimination of liquids during completion and workover operations essentially eliminates water blockage near the observation wells as a disruptive source masking the pressure transients. Although the total production from MWX-1, 1400 MSCF, was not of the magnitude from previous tested intervals, it should have been sufficient to cause an observable pressure transient at either MWX-2 or MWX-3. This lack of observable interference pressure was frustrating, and contradictory with the production data, even when a very anisotropic fracture system is assumed. To better quantify the fracture communication between wells and determine the anisotropic permeability, a tracer interference test using argon gas was conducted in the fluvial B sandstone.

An argon tracer test of the fluvial B sand was conducted July 31 (day 47) with the injection of approximately 235,000 SCF of argon gas into MWX-2. Since MWX-1 had been producing for a total of 45 days, the large pressure gradient existing between MWX-1 and MWX-2 should provide a positive flow from MWX-2 to MWX-1. Several days before the argon injection, MWX-3 was put on production in an attempt to provide another low pressure sink for gases originating from MWX-2. The reservoir pressure profile would probably be very elliptic because of MWX-1 production. The streamlines from MWX-2 may therefore all turn toward MWX-1 with few, if any, low potential streamlines terminating at MWX-3.

Real time gas chromatographic data from MWX-1 and MWX-3 were provided using three separate gas chromatograph systems. The gas produced from each well could be switched to any of the gas chromatographs to provide maximum coverage during critical periods. Calibration gas analyses and background argon/oxygen, concentrations of about 0.1 percent, indicated that measurement of argon/oxygen changes of down to 0.2 percent were possible.

Figure 7.1.15 is a summary plot of the argon injection data showing the bottomhole pressure and surface flow rate for MWX-2. MWX-1 and MWX-3 were both flowing at about 20 MSCFD and 28 MSCFD, respectively. It was determined that high bottomhole pressures resulted during the argon injection and thus the injection was more of an argon frac than an injection. The low viscosity of argon gas, however, would preclude the creation of an extended fracture. Further, following 3 to 4 days of gas sampling, the presence of argon was not detectable in the produced gas from either of the production wells.

7.1.5.5 Final Buildup Test

MWX-3 was taken off production August 3 (day 50) and the bottomhole pressure instrument was seated in the downhole shut-in tool with nitrogen. MWX-2 was shut-in downhole immediately following the argon injection on July 31 (day 47) to gather falloff data. Both MWX-2 and MWX-3 were now prepared as observation wells for the final MWX-1 pressure buildup test.

An extended pressure buildup of MWX-1 using the downhole shut-in tool was initiated August 5 (day 52). Some operational problems occurred during the seating procedure that caused the early shut-in and buildup pressures to be more dependent on surface pumping conditions than reservoir buildup pressure. Once the tool was properly seated, the pressure buildup appeared to be proceeding in a normal fashion.

On August 7 (day 54), the bottomhole pressure appeared to level out and fall (Figure 7.1.5). During the next several days bottomhole pressure dropped from a peak of 3260 psi to about 2780 psi. This apparent loss of bottomhole pressure does not appear to be the result of liquid imbibition and the two previous buildups (90 hrs and 630 hrs) did not show signs of reservoir depletion. The data would seem to indicate the mechanism causing this irregular pressure behavior is pressure dependent.

To ensure the problems did not result from either the bottomhole pressure tool or a leak around the downhole shut-in tool, the test was

concluded August 12 and MWX-1 was returned to production at 90 MSCFD. After about 6 hours the flow rate was reduced to about 20 MSCFD at a bottomhole pressure of about 1000 psi.

The MWX-1 flow test was conducted for about 4 days and the well was again shut-in bottomhole for a final pressure buildup test (day 63). As with the previous buildup test, the anomalous pressure behavior was evident, with pressures reaching about 3100 psi and then decreasing to about 2750 psi in a 3-day period.

The anomalous behavior during the two pre-frac pressure buildups is attributed to a pressure dependent leak in the bridge plug located below the fluvial E sand. This bridge plug subsequently failed during fracture operations, again leading credence to the above conclusion.

7.1.6 MWX-3 WELL TESTING

Concurrent with the interference testing, a short drawdown/ buildup test was conducted in MWX-3. The test was conducted from July 24 (day 40) to August 30 (day 77). The MWX-3 well test was performed during the final buildup of MWX-1, after the pressure anomaly occurred in MWX-1, in an attempt to provide reliable data for subsequent reservoir modeling.

Figure 7.1.16 presents the flow rate and bottomhole pressure for MWX-3 during the testing period. The test consisted of a 9-day drawdown period in which MWX-3 was produced at an initial rate of 50 MCFD that quickly fell to 25-30 MCFD. MWX-3 was then shut-in bottomhole for a 27-day pressure buildup test beginning on day 49.

Figure 7.1.17 is a Horner plot of the pressure buildup data. The shape of the Horner plot appears to be characteristic of a stimulated/fractured reservoir, possibly the result of the breakdown procedures using nitrogen fracturing. Figure 7.1.18 is a log-log pressure and pressure derivative plot of the MWX-3 well test data. Again, the unit

slope region is very short in duration (less than 0.2 hr) due to the bottomhole shut-in. Also, the derivative curve is characteristic of a stimulated reservoir, exhibiting a continual increase throughout the test.

7.1.7 PRE-STIMULATION RESERVOIR MODELING

The preliminary reservoir modeling conducted during the fluvial B sandstone interference testing was used as a baseline for the final pre-stimulation reservoir modeling. Due to the anomalous pressure buildup behavior of MWX-1, additional reservoir modeling was not conducted. Figure 7.1.19 is a log-log plot of final MWX-1 pressure buildup test illustrating the pressure anomaly at 28 hours after shut-in.

As a result, all subsequent reservoir modeling will be directed toward evaluating the short well test conducted in MWX-3. The pre-stimulation reservoir modeling of the fluvial B sandstone from MWX-3 well test data proceeded in two phases to provide a broad-based study of reasonable reservoir configurations.

7.1.7.1 Naturally Fractured Reservoir Modeling

The naturally fractured reservoir modeling utilized a fully transient naturally fractured reservoir simulator capable of modeling the combined effects of transient matrix flow, anisotropic natural fracture properties, hydraulic fractures and reservoir layering.[1,2] Figure 7.1.20 is a conceptual drawing of the fluvial B reservoir model, illustrating the net reservoir thickness (17 ft), natural fracture spacing (10 ft), natural fracture width (0.001 in.), drainage radius (5500 ft), and maximum and minimum natural fracture permeability (2000 and 20 md, respectively) for a 100:1 anisotropic system. The naturally fractured fluvial B reservoir model is an extension of the preliminary simulation studies conducted during the well test operations and utilizes much of the baseline reservoir data presented in the previous section (Tables 7.1.2 and 7.1.3). The exact input data are shown in Table 7.1.4.

A series of simulations were conducted to evaluate various combinations of natural fracture properties. Figure 7.1.21 illustrates the simulated bottomhole pressure and surface flow rate for an isotropic naturally fractured reservoir having a natural fracture permeability of 2 darcies, natural fracture spacing of 10 ft, and a matrix permeability of 0.001 md. The figure clearly shows that the predicted production of 75-100 MCFD is much higher than the actual production of 25 to 30 MCFD (Figure 7.1.16). Figure 7.1.22 is a log-log comparison of the actual pressure buildup data and the simulation results indicating that the data do not compare favorably.

The next set of simulations utilized an anisotropic natural fracture permeability of 1.25 and 0.125 darcies. Figure 7.1.23 presents the simulation data, showing that the predicted production rates are very similar to the actual rates seen in Figure 7.1.16. Figure 7.1.24 compares the actual log-log pressure buildup data to the model predicted data, showing that the shape of the actual and model curves are similar, but the magnitude of the pressures are different.

The natural fracture anisotropy was then increased to 100 to 1, using natural fracture permeabilities of 2 and 0.02 darcies, with all other data remaining unchanged. Figure 7.1.25 shows the model predicted data and shows slightly lower production rates compared to the previous case. However, the simulated rates are still very close to the actual MWX-3 production rates. Figure 7.1.26 compares the simulated pressure buildup behavior to the actual data, showing a much better match than previously obtained. The simulated buildup pressures are seen to be somewhat higher than the actual pressures.

Figure 7.1.27 shows the model predicted pressures and rates for an isotropic case with a 1000 to 1 ratio in natural fracture permeability (2 darcies and 2 md). The simulated production rates are slightly less than the 100 to 1 case previously shown, but are still comparable with the actual data. Figure 7.1.28 compares the simulated pressure buildup data to

the actual data, indicating a very good match of both the pressure and pressure derivative data. There is a departure between the model data and the actual well behavior at 100 to 200 hours.

The Horner plots for the above simulation cases are compared to the actual data in Figure 7.1.29. Again, the 100 to 1 and 1000 to 1 anisotropy appear to provide the best match. As with the log-log comparisons, there is a departure between the model predicted pressures and the actual data at later shut-in times (Horner time of 2). The reason for this departure could not be quantified with the limited duration of the MWX-3 well test.

To illustrate the pressure profile around the MWX producing well, several pressure maps were produced using both 2- and 3-dimensional plotting techniques. The pressure maps were constructed from simulation data at the end of the MWX-1 drawdown, after approximately 50 days of production. Figures 7.1.30 and 7.1.31 illustrate the pressure profile for an isotropic natural fractured reservoir; the former is a 3D plot, while the latter is an areal view with the locations of MWX-1, MWX-2 and MWX-3 shown for reference. Figure 7.1.31 illustrates that pressure interference should been detectable in MWX-2 and possibly MWX-3 if the reservoir was isotropic. Figures 7.1.32 and 7.1.33 illustrate, as 3D and areal plots, respectively, the pressure distribution in a naturally fractured reservoir with a 100 to 1 anisotropy. The areal pressure profile shown in Figure 7.1.33 indicates that pressure interference will not be detected in MWX-2 or MWX-3 at the end of the drawdown period if the reservoir anisotropy is 100 to 1.

7.1.7.2 Homogeneous Reservoir Modeling

As was discussed previously (Section 7.1.5.2), the MWX-3 well test data has the characteristic shape of a stimulated reservoir. The previous section (7.1.7.1) illustrated that the inclusion of a highly anisotropic set of natural fractures could produce the same pressure buildup behavior as seen in the actual MWX-3 data. To provide a complete analysis, a set of

reservoir simulations was conducted using a single phase, homogeneous reservoir model that was capable of simulating production from a well containing a single fracture. Figure 7.1.34 is an illustration of the reservoir model used for the homogeneous simulations. The location of MWX-1, MWX-2 and MWX-3 are shown on Figure 7.1.34 along with a breakdown fracture in MWX-3. The objective of the homogeneous modeling was to provide a comparison of the pressure buildup behavior of a homogeneous reservoir to that of a naturally fractured reservoir.

A series of simulation runs were performed to provide a general understanding of the effects of various hydraulic fracture conductivities and matrix permeabilities on the simulated pressure buildup behavior. The input data for the homogeneous modeling is identical to that used in the naturally fractured modeling, with the exception of hydraulic fracture and matrix properties. The homogeneous simulation assumed an isotropic reservoir with a 100-ft hydraulically induced fracture that results from the initial completion operations. Figure 7.1.35 compares the log-log pressure behavior for a simulation case having a matrix permeability of 0.001 md and a hydraulic fracture conductivity of 5 d-ft. The figure shows that the model predicted data is much lower than the actual data and the model predicted derivative curve is shifted to the right. The simulated production rate was 12.8 MCFD, about half the actual rate.

The hydraulic fracture conductivity was reduced to 0.083 d-ft for the next simulated case. Figure 7.1.36 compares the model and actual data. The model predicted pressures are now above the actual data, while the derivative curves compare more favorably. However, the reduction in fracture conductivity resulted in a simulated flow rate of only 6.6 MCFD, much lower than the actual MWX-3 production rate (reference Figure 7.1.16). The final simulation compared the simulated pressure buildup behavior of a reservoir containing a 100-ft, 0.42 d-ft fracture and having a matrix permeability of 0.004 md, to the actual MWX-3 data. In this case, the matrix permeability has been increased by a factor of 4 from all previous cases (0.001 to 0.004 md). Figure 7.1.37 compares the model and actual

data. The simulated pressure data are still somewhat high, but the simulated pressure derivative data are very similar to the actual data.

Figure 7.1.38 compares the Horner plots of the previous two homogeneous simulation cases. The figure shows that both cases have similar curve shapes when compared to the actual data. The final simulation (0.42 d-ft fracture conductivity) is approximately 200 psi above the actual data for most of the buildup period. The homogeneous simulation illustrates that similar pressure buildup behavior can be expected for both anisotropic naturally fractured reservoirs and homogeneous reservoirs that contain a breakdown fracture of moderate length and conductivity.

7.1.8 SUMMARY

- MWX-1 well test data appears to have a superimposed pressure perturbation, most probably caused by a leaking bridge plug which subsequently failed during stimulation.

- Interference pressure data during the nitrogen perforation breakdowns suggest that some communication between wells must exist.

- Interference pressure data during well tests indicates that the permeability between wells is low, possibly due to low conductivity cross natural fractures.

- Argon tracer tests confirm the hypothesis of very low conductivity cross fractures between wells.

- Acceptable models for the fluvial B sand include:

  - a highly anisotropic (100:1), naturally fractured, tight (0.1 μd) matrix reservoir; and

  - a homogeneous, tight (0.4 μd) reservoir.

7.1.9 REFERENCES

1. Branagan, P. T., et al., "Designing and Evaluating Hydraulic Fracture Treatments in Naturally Fractured Reservoirs," SPE/DOE 16434, Proceedings of the 1987 SPE/DOE Low Permeability Reservoir Symposium, Denver, CO, May 18-19, 1987.

2. Branagan, P. T., et al., "Preface Interference Testing of a Naturally Fractured, Tight Fluvial Reservoir," SPE 17724, Proceedings of the 1988 SPE Gas Technology Symposium, Dallas, TX, June 13-15, 1988.

TABLE 7.1.1 MWX WELL CONFIGURATIONS FOR THE FLUVIAL B SAND TESTS

Well	Perforated Interval	Bridge Plug	Packer	Bottomhole Seat
MWX-1	5822-45 ft	5950 ft	5791 ft	5786 ft
MWX-2	5822-42 ft	5846 ft	5797 ft	5795 ft
MWX-3	5828-48 ft	5896 ft	5811 ft	5809 ft

TABLE 7.1.2 SELECTED CORE- AND LOG-DERIVED DATA FOR THE LOWER FLUVIAL INTERVAL

Zone	Zone Depth, ft	Pay Sand (h),* ft	Porosity (ϕ), fraction	Porosity-feet (ϕ x h), ft	Water Saturation (S_w), fraction	Hydrocarbon-feet, (ϕ x (1-S_w) x h), ft	S_{xo} - Sw (ΔS_w), fraction	Permeability-feet (kh), md-ft	Volume Clay (V_{cl}), fraction	Volume Carbonate (VCO_3), fraction	Core Porosity, fraction	Stressed Core Permeability, md	Core Water Saturation, fraction	Core Grain Density, gm/cc	Cation Exchange Capacity, meq/100 gm
F	5,478.5-5,491.5	13.5	.060	.81	.649	.29	.136	.0388	.092	.080	.062	.0050	.512	2.64	1.72
E_2	5,525.0-5,531.5	7.0	.045	.32	.646	.11	.045	.0085	.126	.151	.043	--	.725	2.66	--
E_1	5,544.0-5,565.0	21.5	.060	1.30	.640	.47	.109	.0723	.056	.100	.064	.0041	.519	2.64	2.00
D_1	5,624.5-5,635.5	11.5	.064	.73	.602	.30	.104	.0534	.083	.148	.056	--	.516	2.66	--
C_2	5,714.5-5,737.5	23.5	.078	1.83	.630	.69	.034	.1701	.078	.071	.081	.0073	.436	2.66	3.02
B	5,827.0-5,843.0	16.5	.071	1.18	.538	.56	.170	.1555	.055	.188	.061	.0071	.505	2.65	2.07
A_2	5,957.0-5,971.0	14.5	.048	.70	.479	.37	.153	.0439	.103	.122	.050	.0017	.527	2.66	--
A_1	5,977.0-5,983.5	7.0	.062	.44	.629	.17	-.023	.0489	.106	.116	.056	.0020	.477	2.66	--

TABLE 7.1.3 RESERVOIR BASE CASE DATA FOR THE FLUVIAL B SANDSTONE

Gross Pay, H	22 ft
Net Pay, h	16.5 ft
Total Porosity, ϕ_t	6.8 percent
Water Saturation, S_w	49.5 percent
Gas Porosity, ϕ_g	3.5 percent
Minimum Matrix Perm., k_m	0.03 μd (MWX-2 core at 49.5 percent, Fig. 7.1.4)
Maximum Matrix Perm., k_m	0.30μd (Extrapolated to the best dry core values at 5827.5 ft)
Martrix Block Spacing, S	10 ft
Natural Fracture Width, w	0.001 in.
Natural Fracture Perm., k_f	5000 md or 1500 md

TABLE 7.1.4 FLUVIAL B BASE CASE RESERVOIR PROPERTIES

Depth	d = 5,850 ft
Net Pay Height	h = 17 ft
Reservoir Temperature	T = 174° F
Initial Pressure	p_i = 3,450 psia
Gas Gravity	SG = 0.626 (air = 1)
Reservoir Boundaries	r_e = 5,500 ft x 5,500 ft
Wellbore Radius	r_w = 7 in.
Matrix Gas Porosity	ϕ_{gm} = 4%
Matrix Block Size	S = 10 ft
Matrix Permeability	k_m = 0.1 μd
Natural Frac Width	w_f = 0.001 in.
Natural Frac Permeability (max)	k_{fmax} = 2,000 md
Natural Frac Permeability (min)	k_{fmin} = 20 md

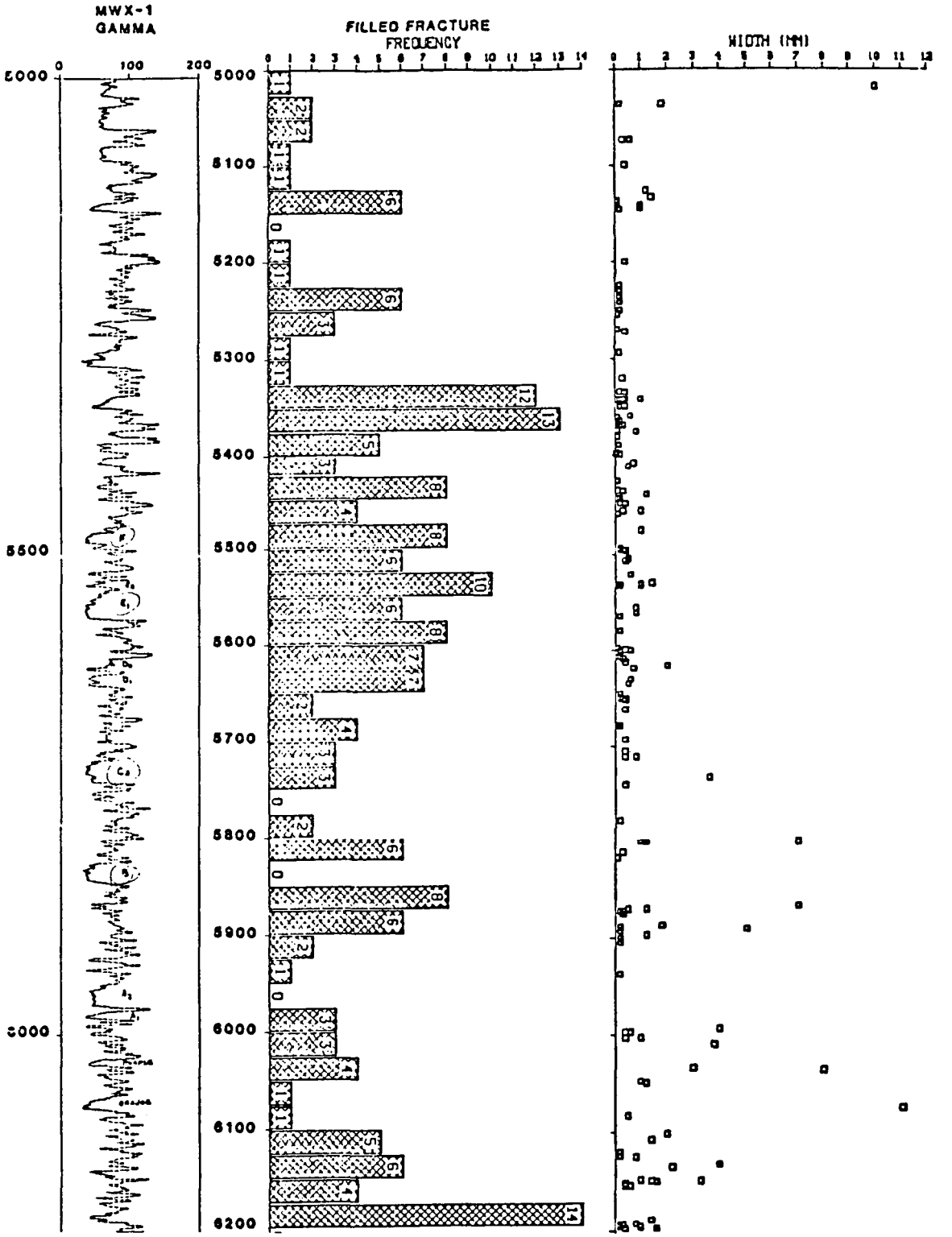

Figure 7.1.1 Core Fracture Frequency and Width Distribution

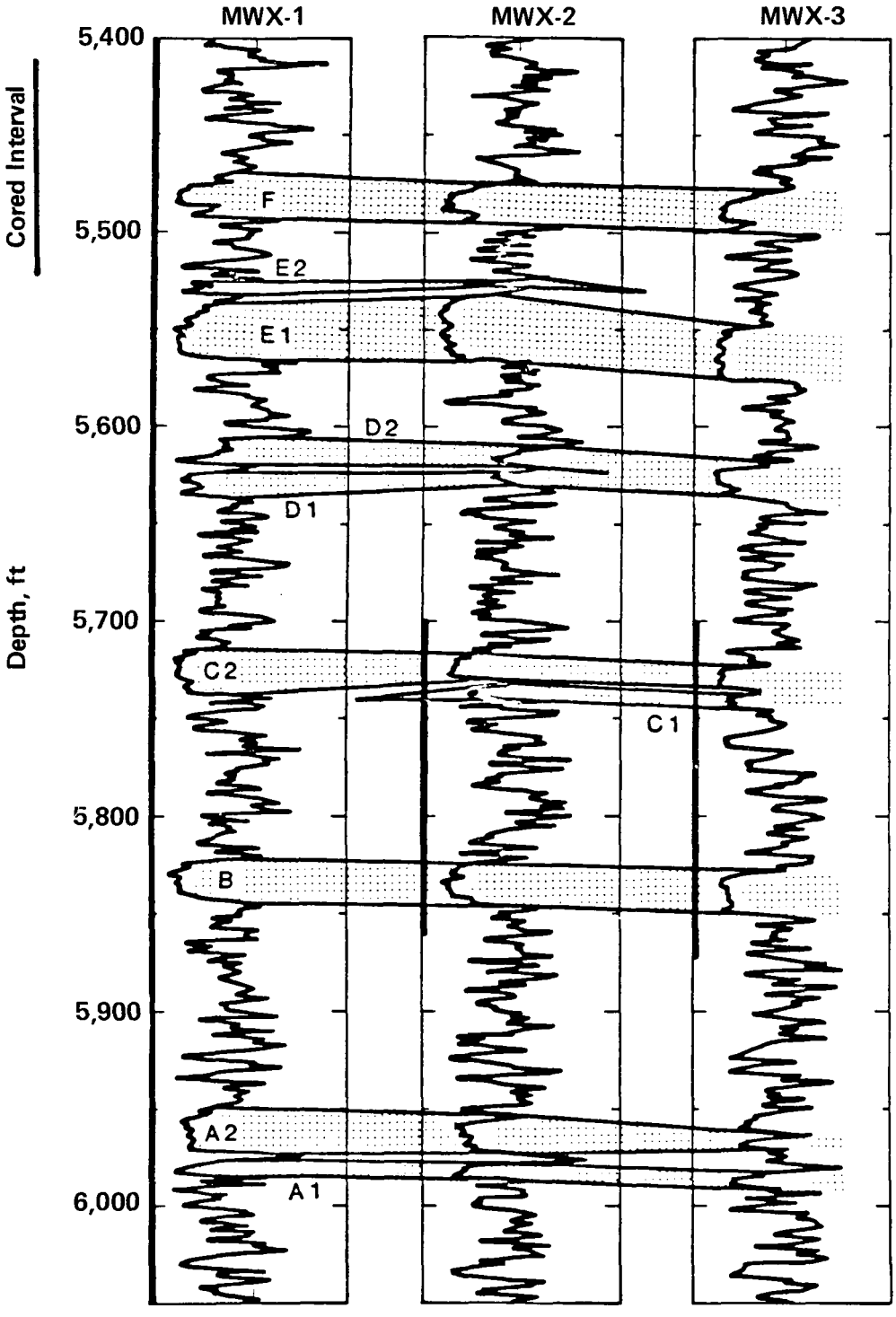

Figure 7.1.2 Lower Fluvial Interval

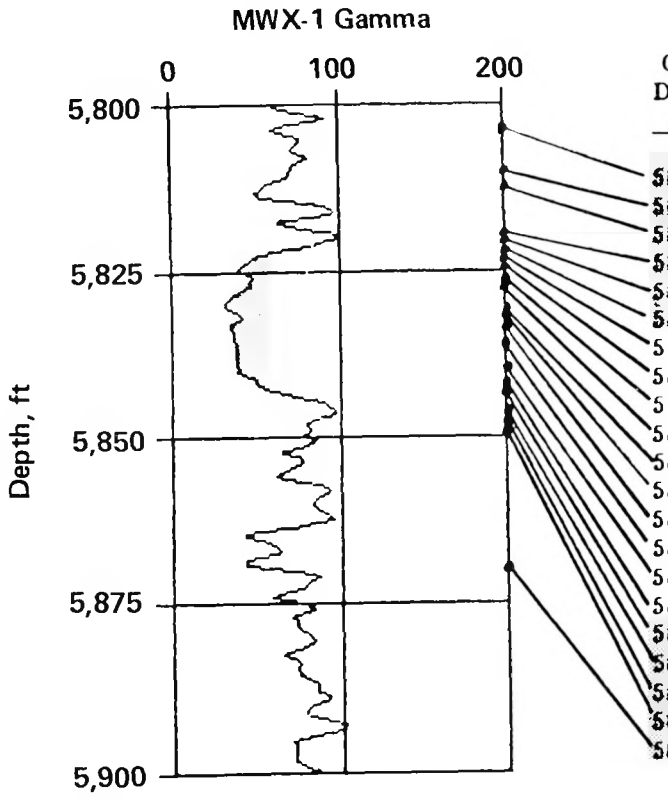

Core Depth, (ft)	(~Log Depth)	Water Saturation Percent		Porosity Percent	Effective Overburden Pressure, psi: 1000 Klinkenberg Permeability millidarcys	2000 Klinkenberg Permeability millidarcys	4000 Klinkenberg Permeability millidarcys
5806.5	(5804.5)	70.7		4.1	0.0036	0.0018	
5812.4	(5810.5)	77.4		2.9	0.0003	0.0001	<0.0001
5814.5	(5812.5)	92.6		2.1	0.0006	0.0003	0.0001
5821.6	(5819.5)	91.7		1.6	<0.0001	<0.0001	<0.0001
5822.5	(5820.5)	90.5		1.4	0.0001	0.0001	<0.0001
5824.4	(5822.5)	77.8		0.7	0.0001	0.0001	<0.0001
5825.5	(5823.5)	57.7		1.9	0.0003	0.0002	0.0001
5826.5	(5824.5)	63.4		4.3	0.0016	0.0008	0.0003
5827.8	(5826.0)	46.4		6.0	0.0089	0.0042	0.0027
5829.6	(5827.5)	44.1		9.9	0.0798	0.0379	0.0199
5832.3	(5830.5)	43.1	net	7.8	0.0151	0.0068	0.0045
5833.3	(5831.5)	51.7	pay	6.1	0.0095	0.0043	0.0021
5835.6	(5833.5)	45.5		6.9	0.0158	0.0071	0.0044
5837.6	(5835.5)	49.3		7.4	0.0080	0.0057	0.0022
5840.4	(5838.5)	58.0		5.6	0.0087	0.0044	0.0027
5842.8	(5841.0)	64.4		4.9	0.0080	0.0040	0.0016
5844.4	(5842.5)	78.9		1.0	0.0002	0.0001	<0.0001
5847.8	(5846.0)	89.5		0.8	0.0001	0.0001	<0.0001
5849.6	(5847.5)	71.4		0.3	0.0001	0.0001	<0.0001
5850.6	(5848.5)	60.0		0.4	0.0001	0.0001	<0.0001
5870.4	(5868.5)	81.8		4.2	0.0036	0.0019	

Figure 7.1.3 Fluvial B Core Data

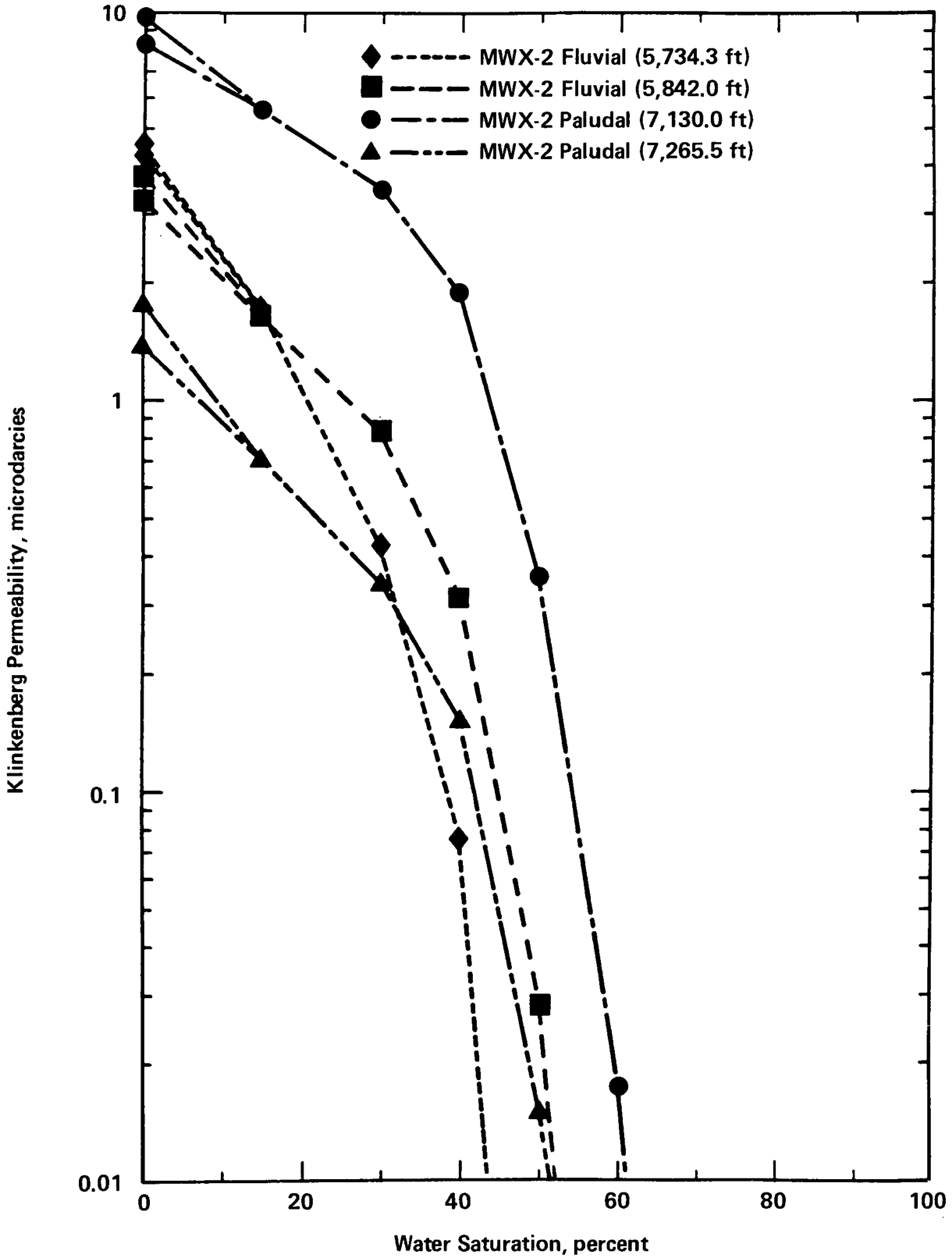

Figure 7.1.4 Effect of Water Saturation on Permeability

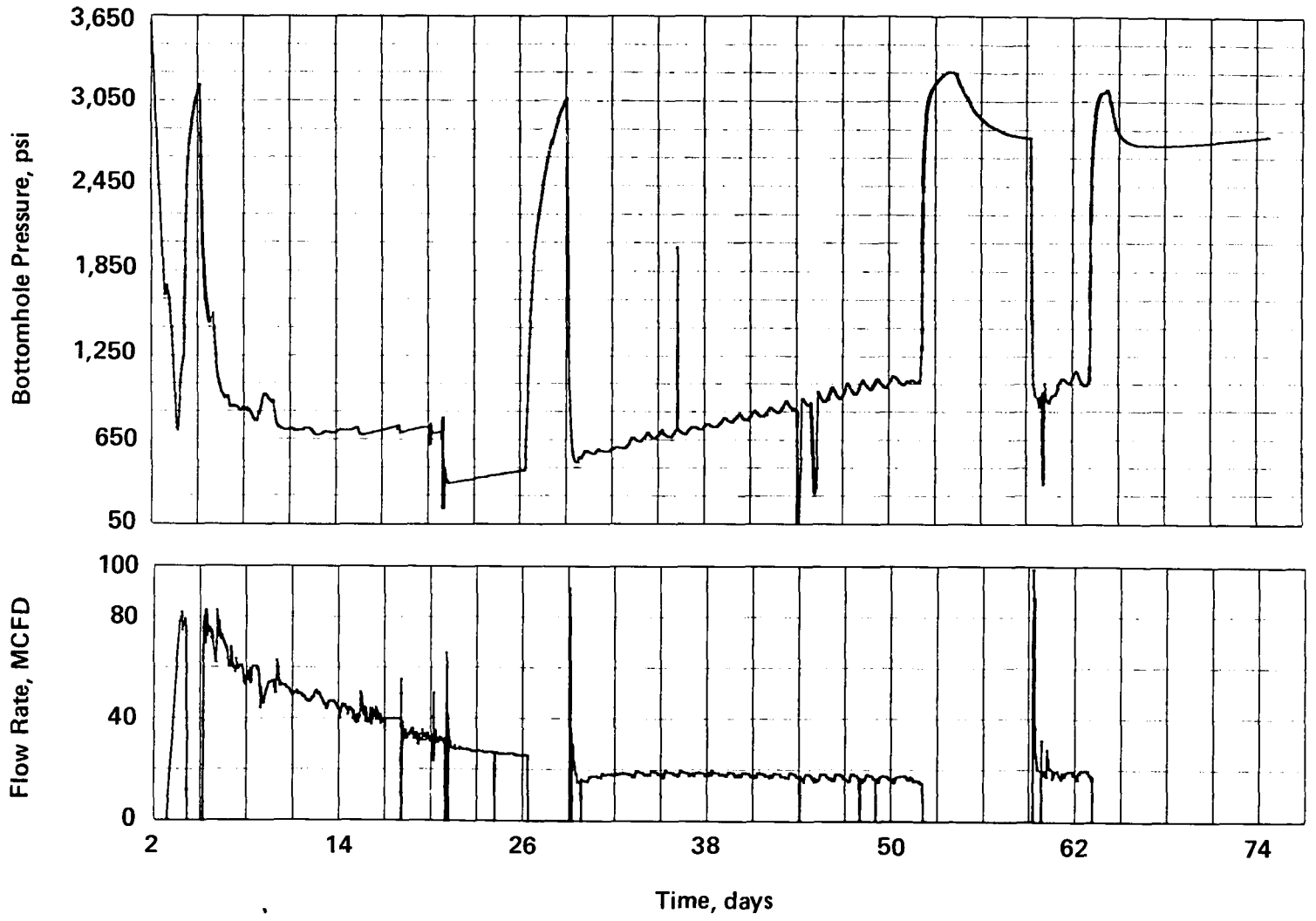

Figure 7.1.5 MWX-1 Flow Rate and Pressure Data, June 26-August 27, 1986

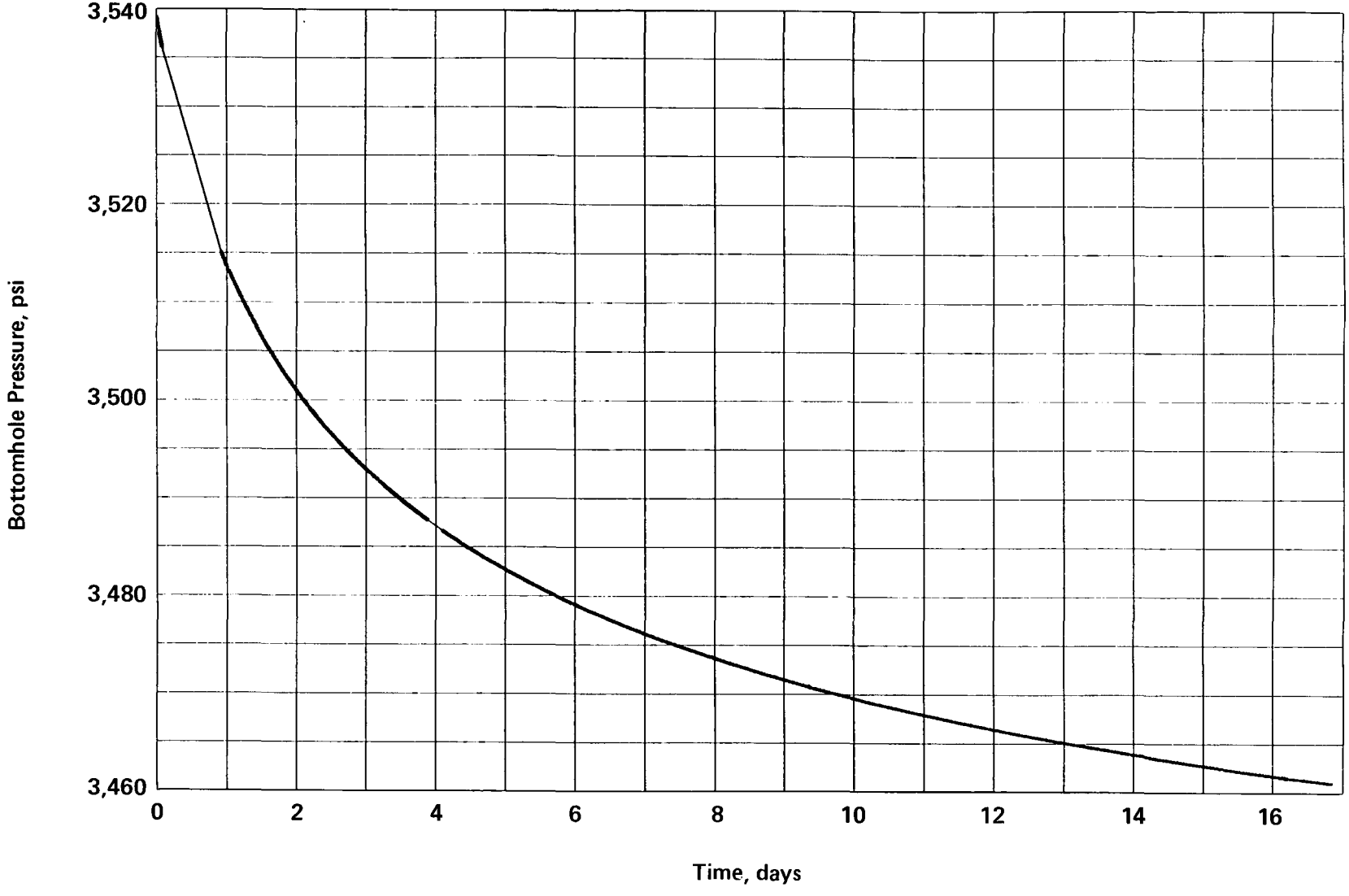

Figure 7.1.6 Interference Pressure, MWX-2

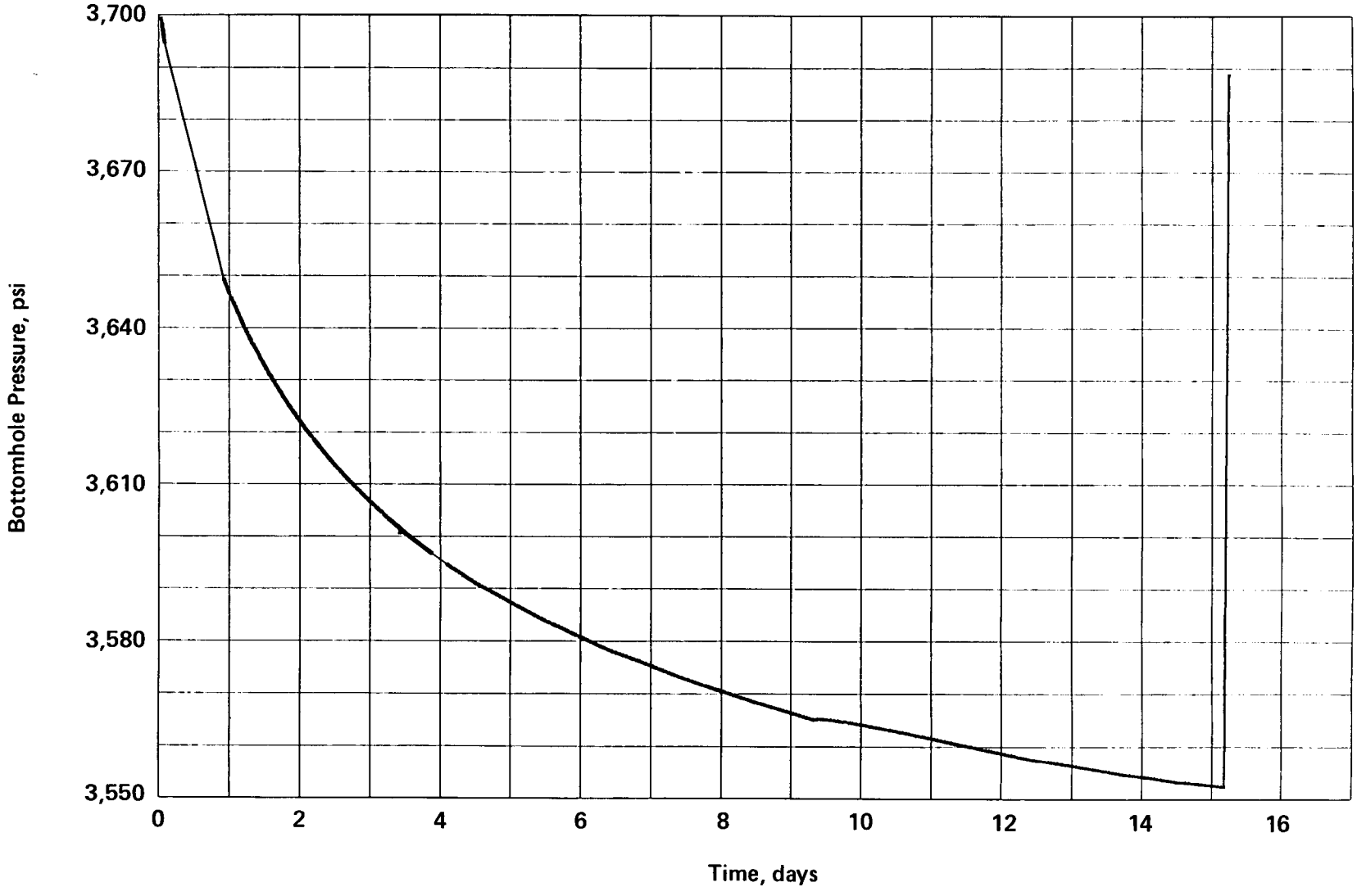

Figure 7.1.7 Interface Pressure, MWX-3

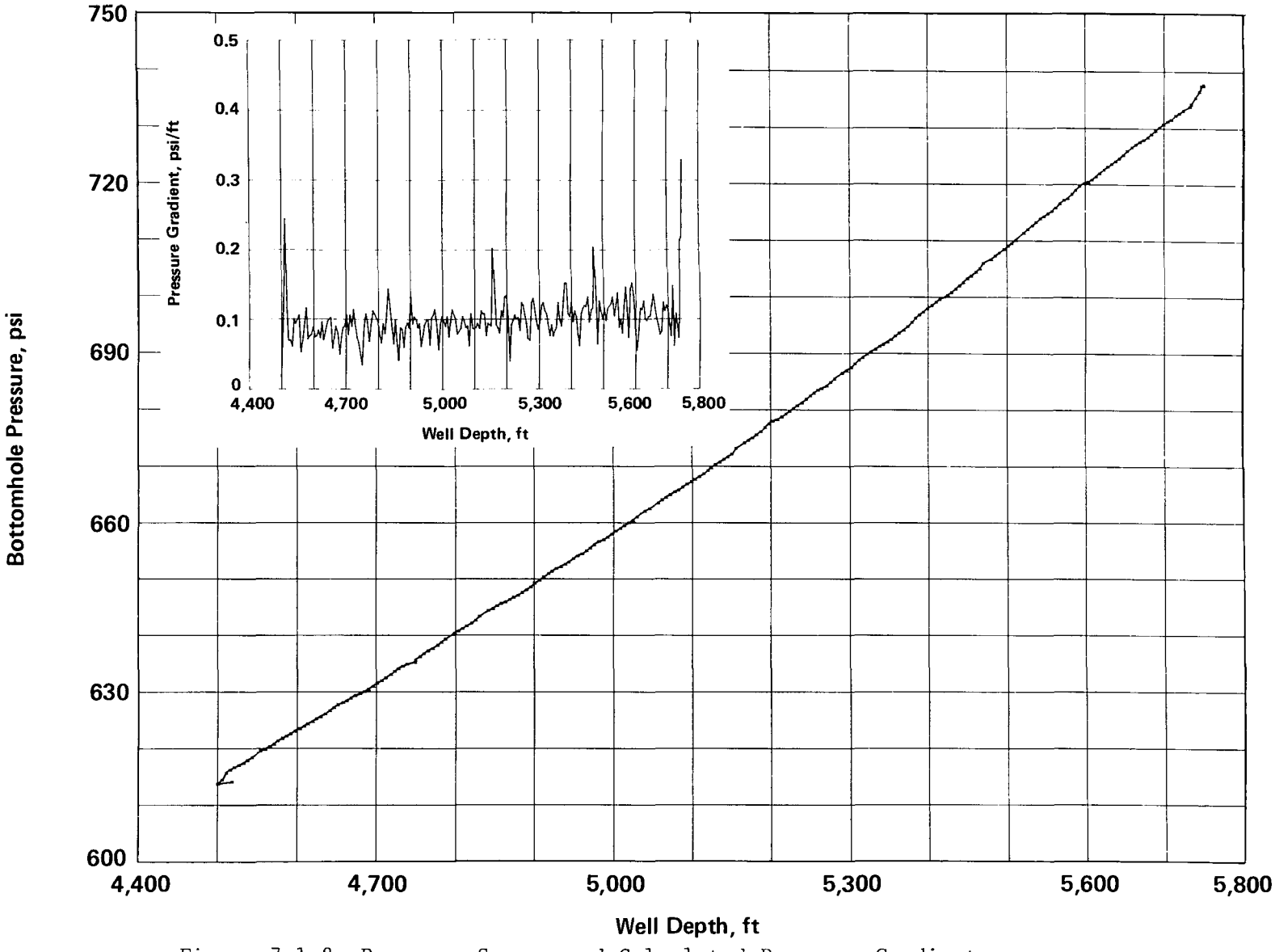

Figure 7.1.8 Pressure Survey and Calculated Pressure Gradient

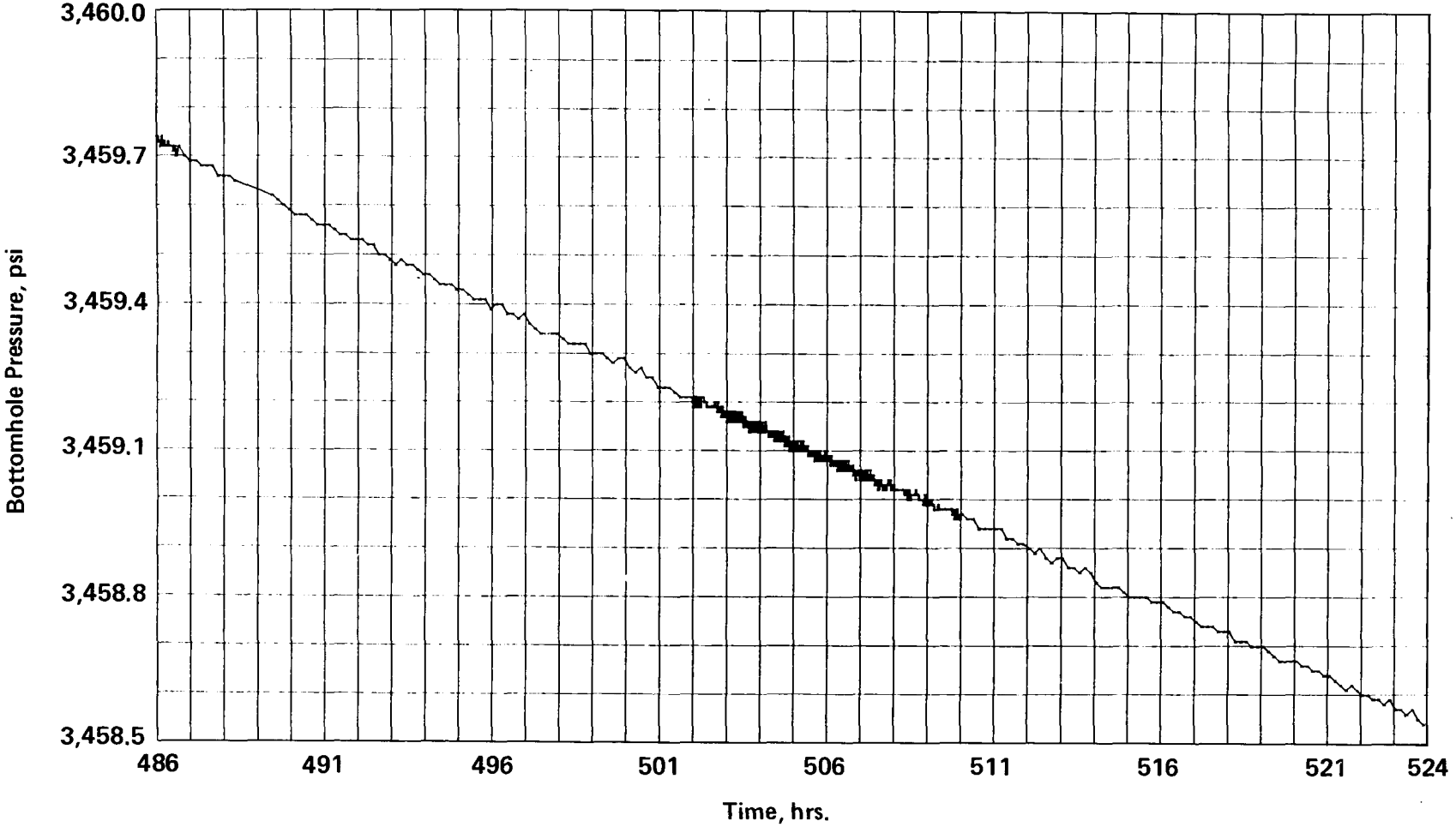

Figure 7.1.9 Bottomhole Pressure, MWX-2

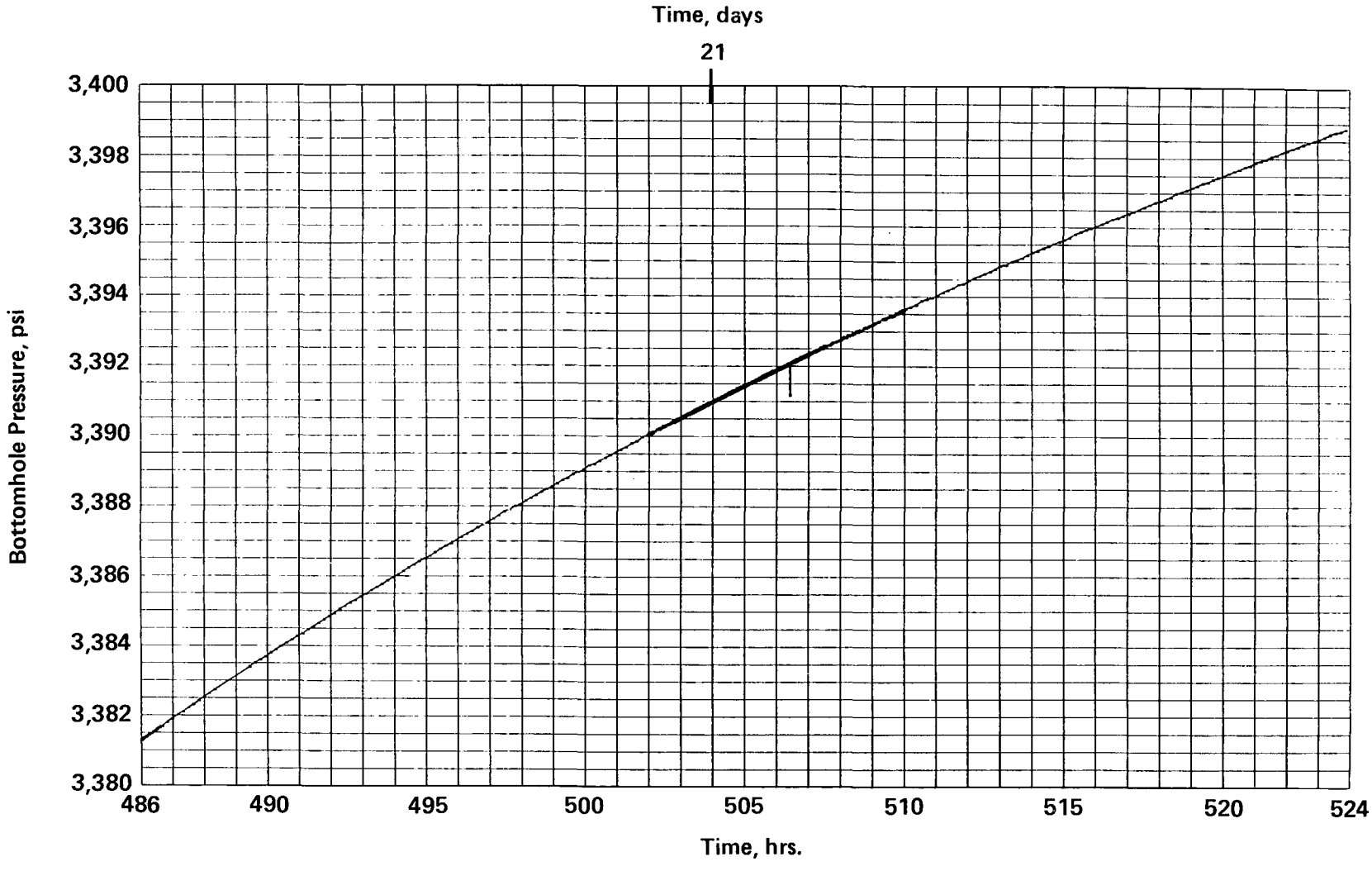

Figure 7.1.10 Bottomhole Pressure, MWX-3

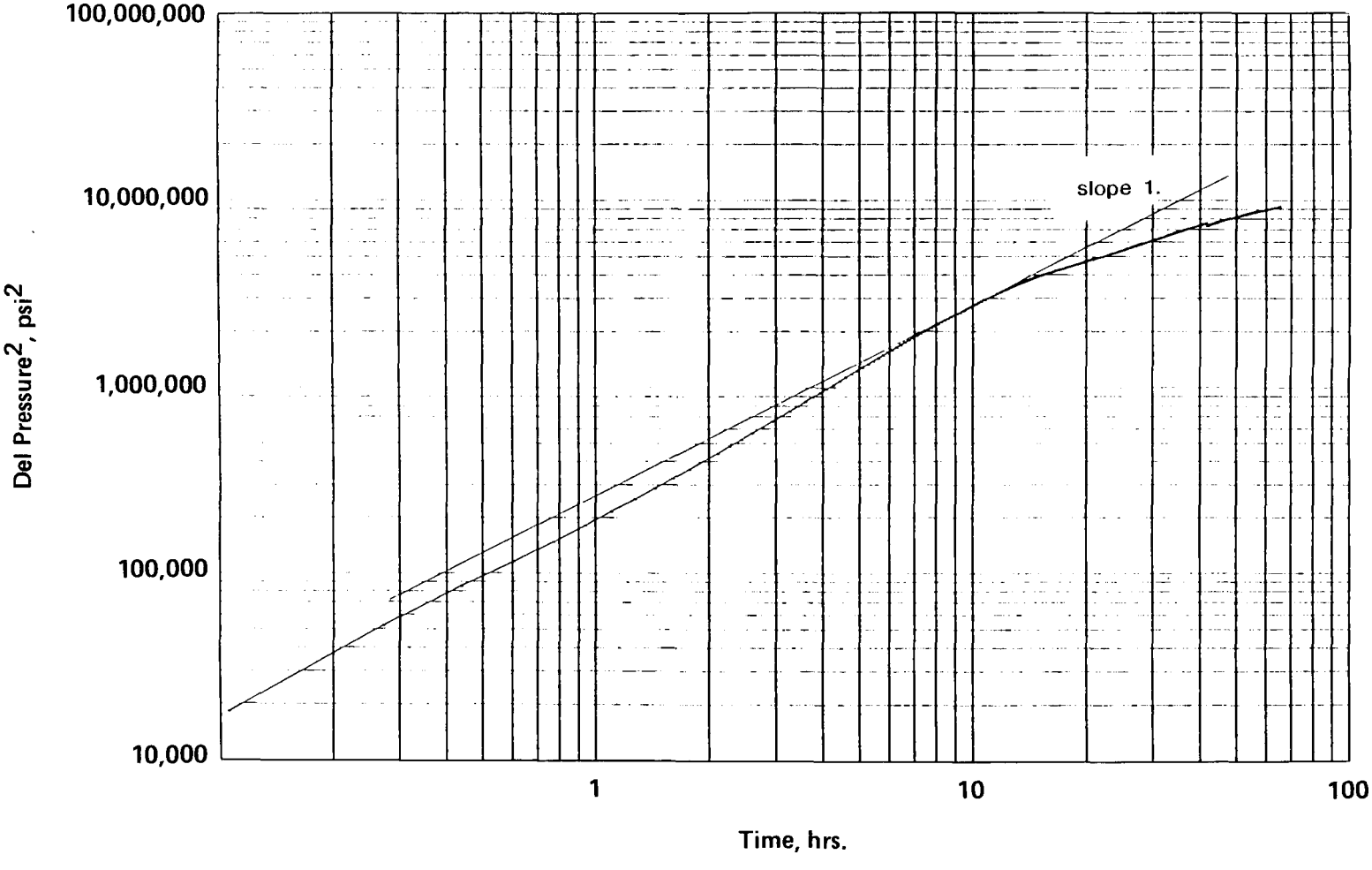

Figure 7.1.11 Pressure Buildup, MWX-1, Log-Log Plot

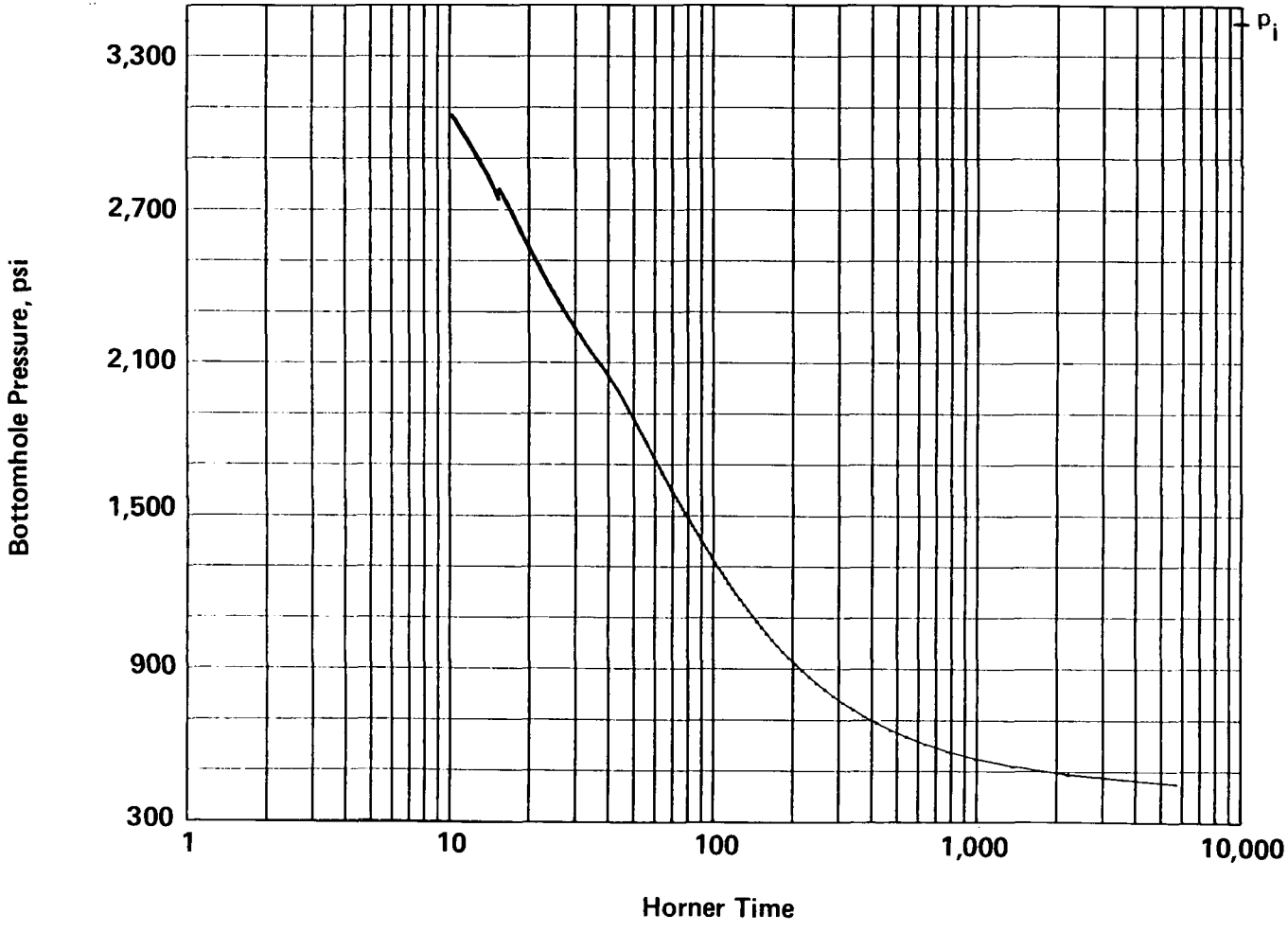

Figure 7.1.12 Pressure Buildup, MWX-1, Horner Plot

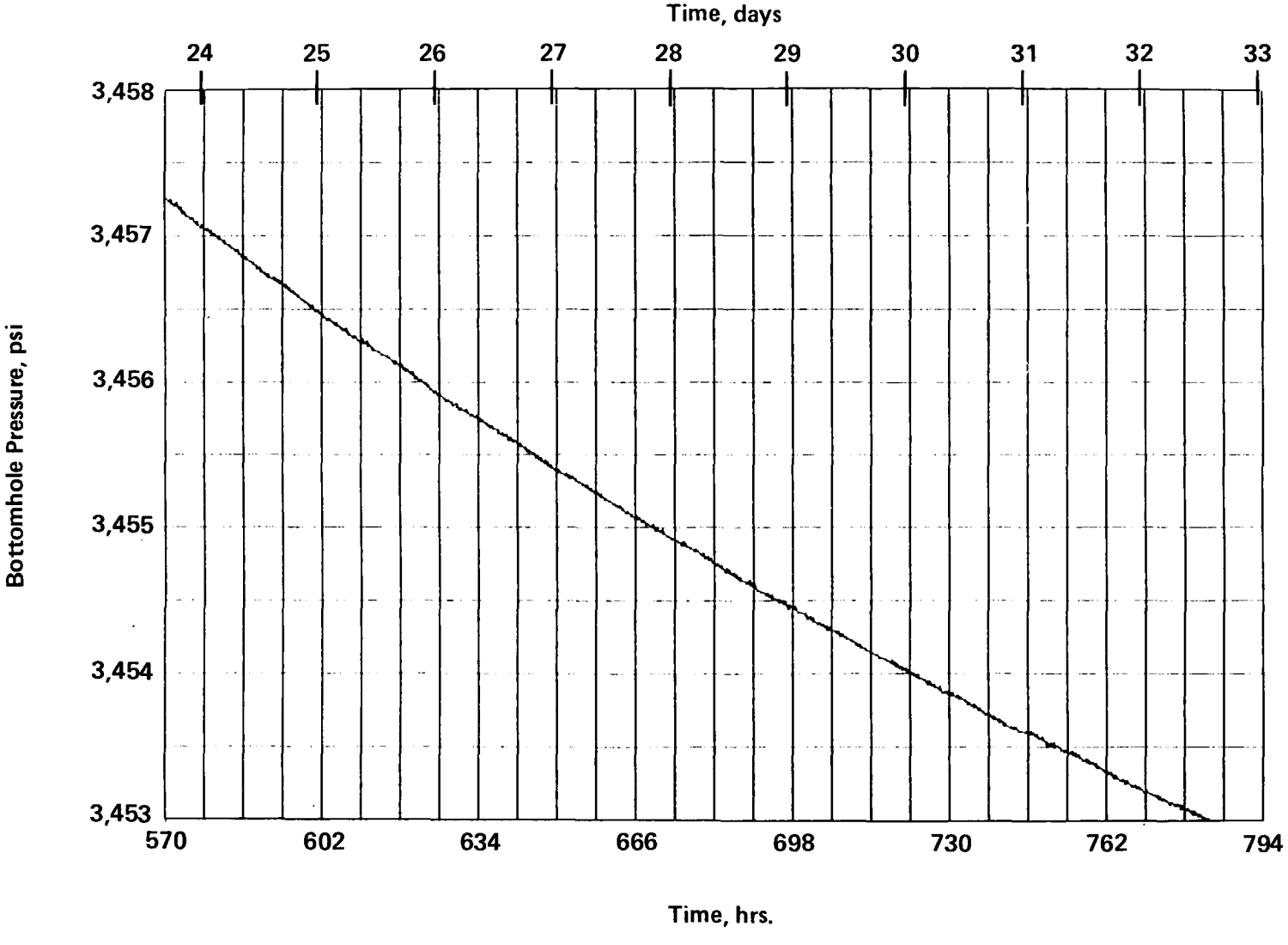

Figure 7.1.13 Bottomhole Pressure, MWX-2

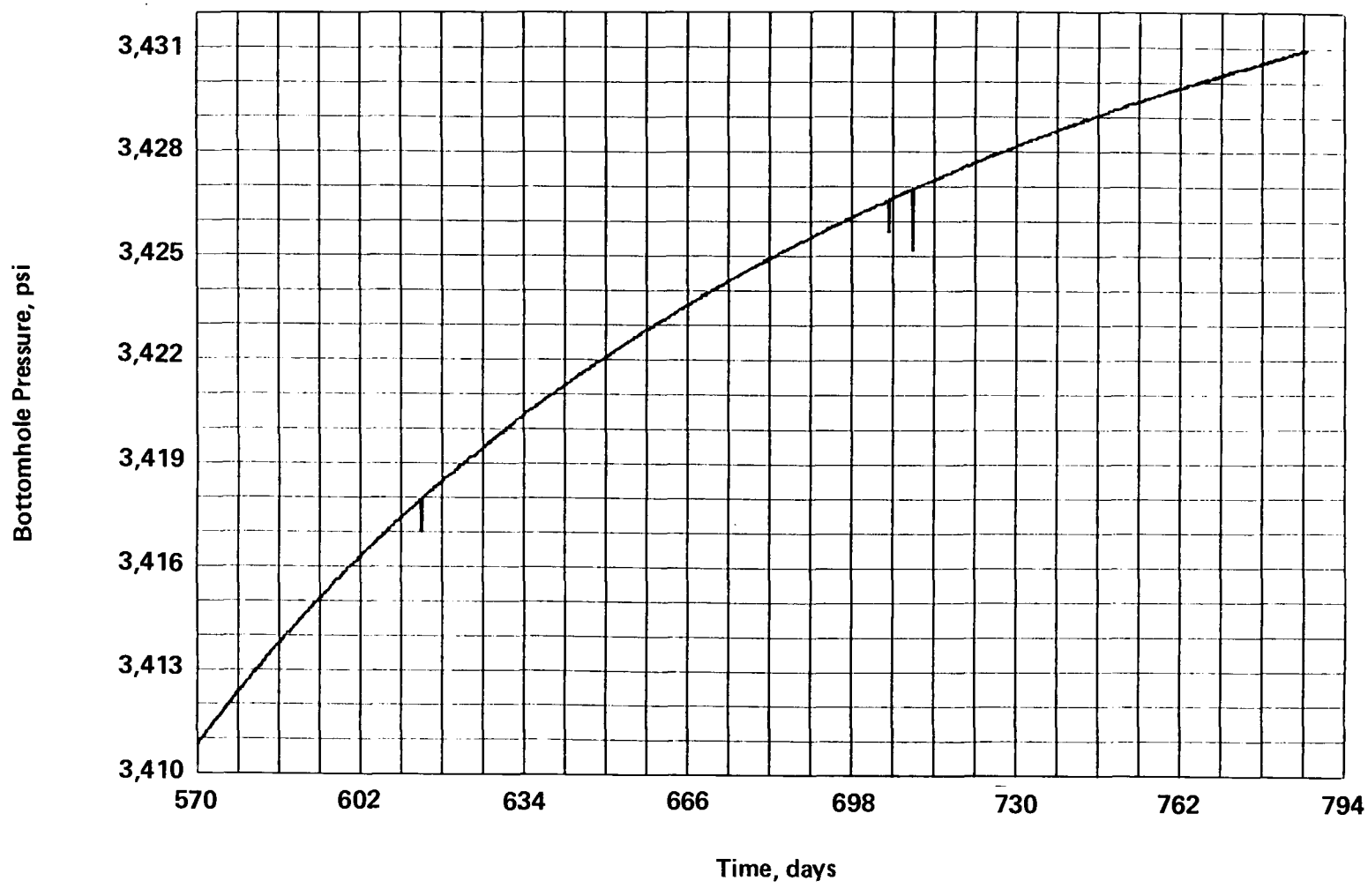

Figure 7.1.14 Bottomhole Pressure, MWX-3

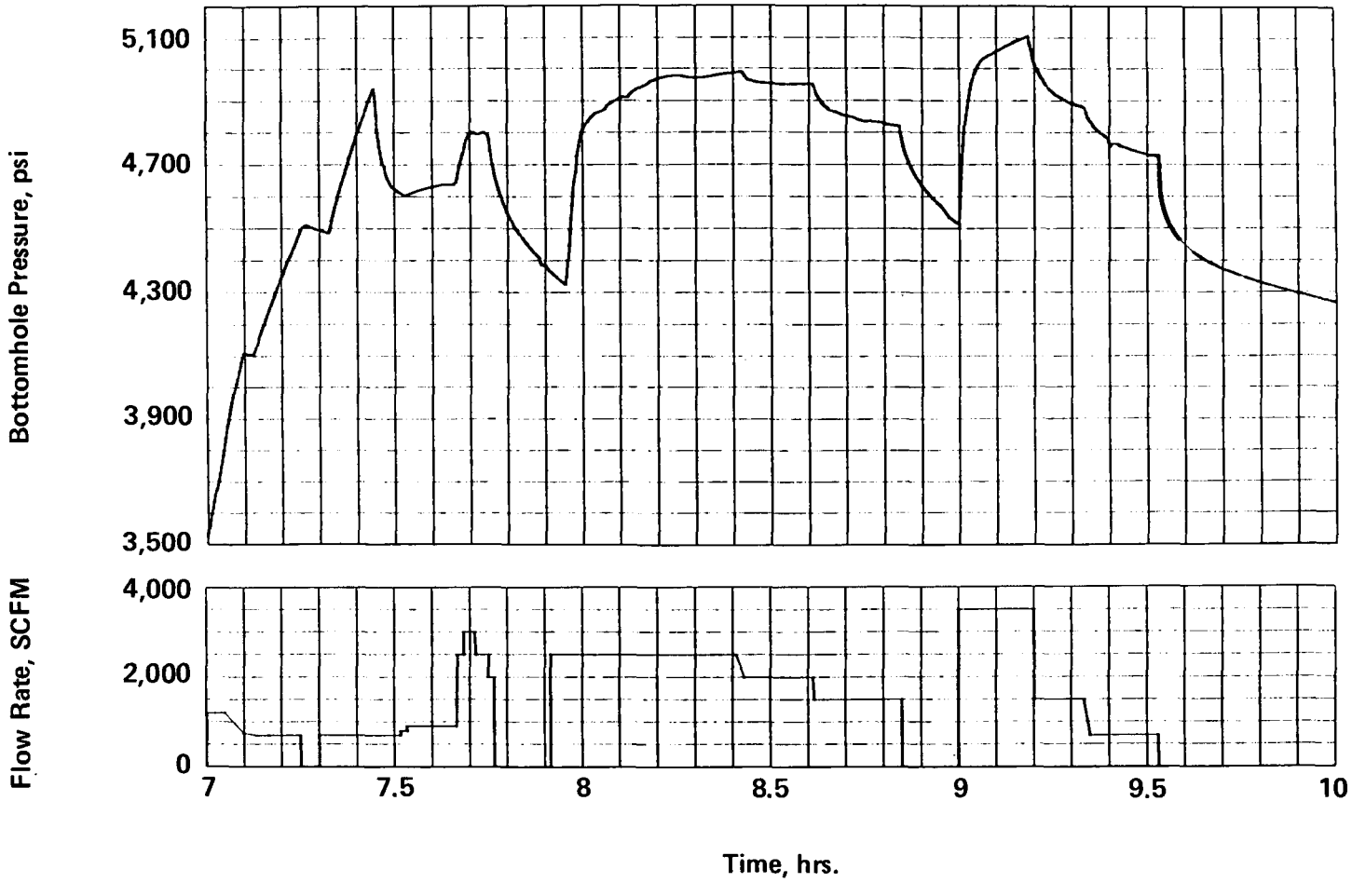

Figure 7.1.15 Argon Injection Data, MWX-2

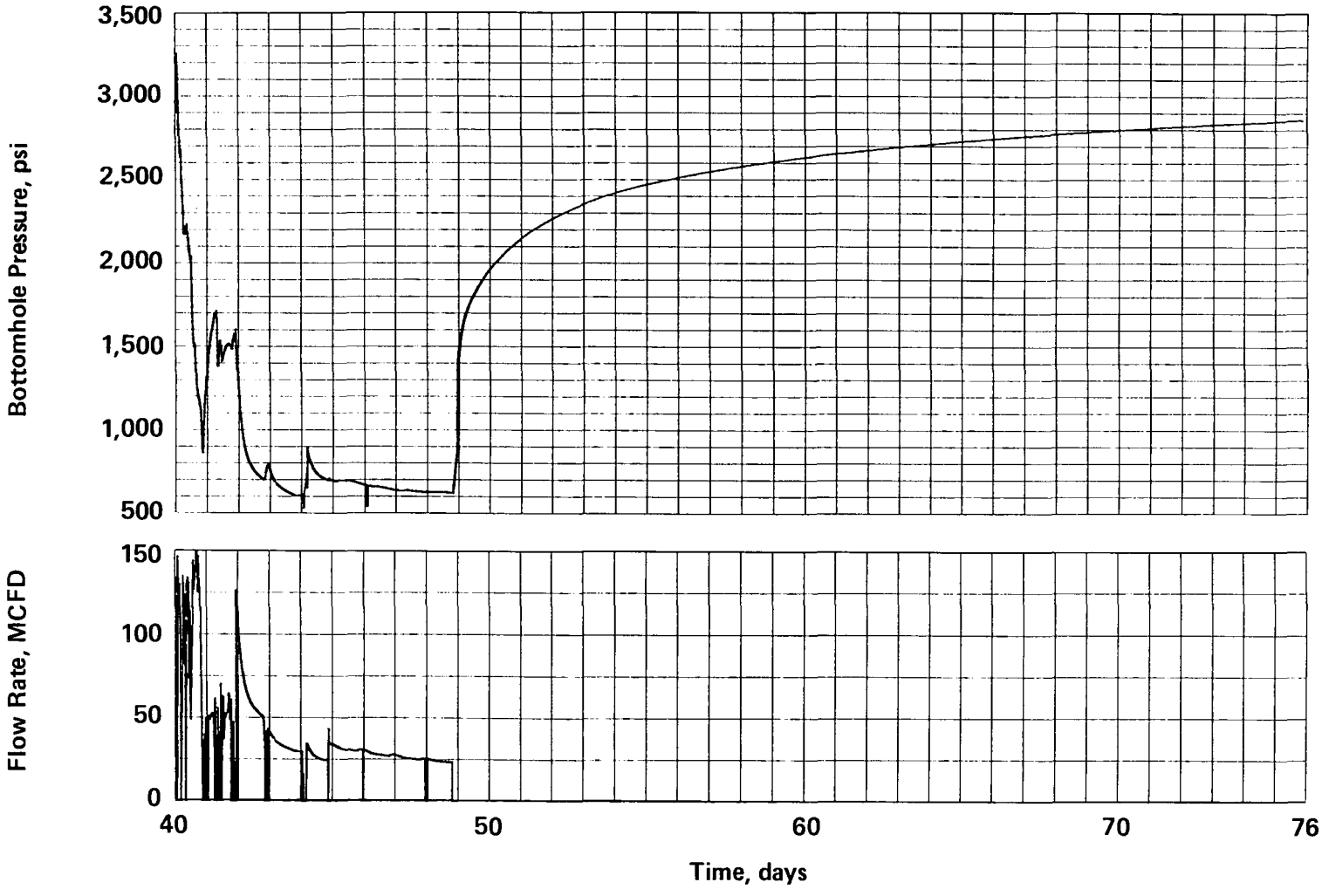

Figure 7.1.16 MWX-3 Flow Rate and Pressure Data, July 24-August 30, 1986

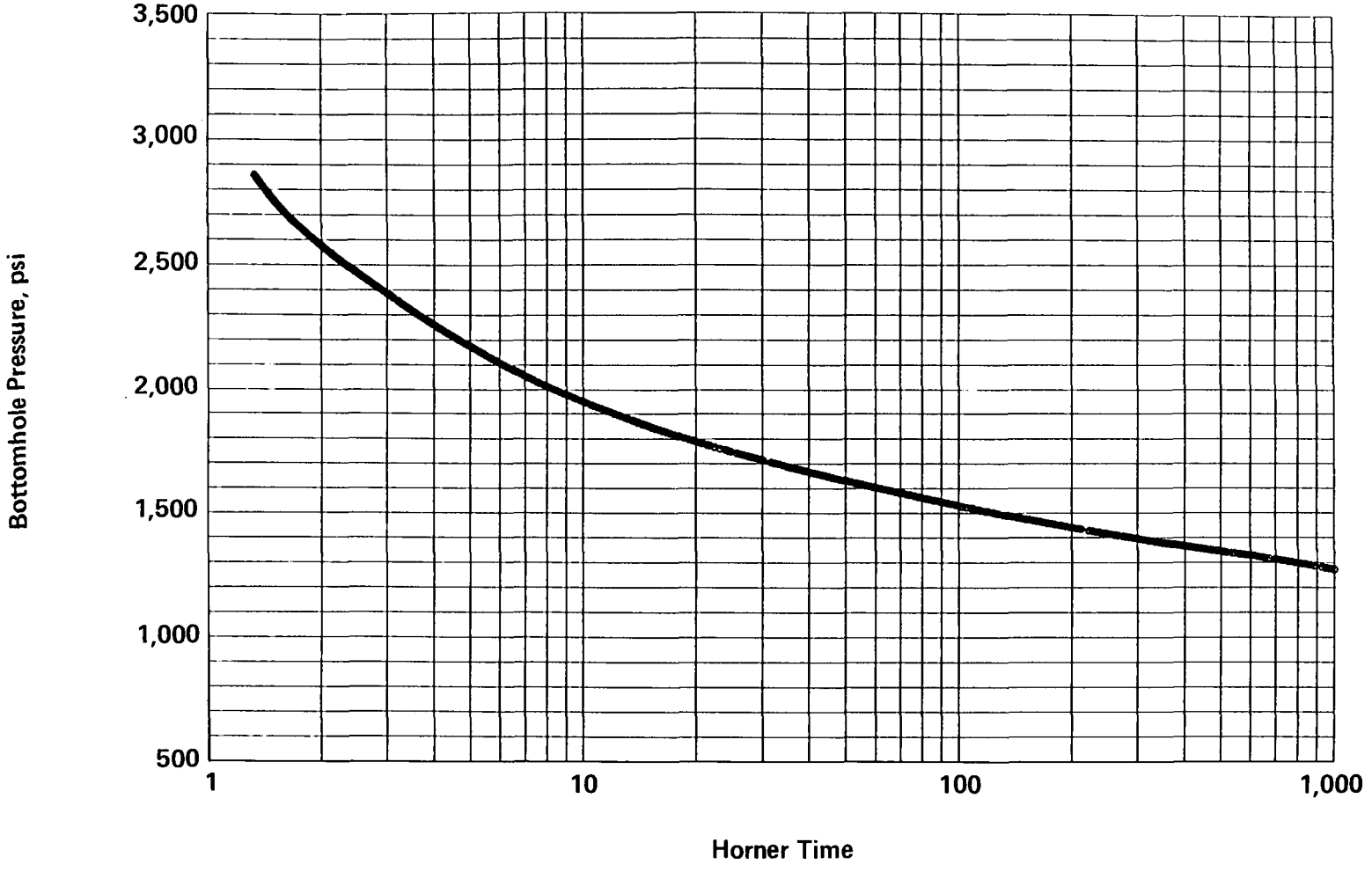

Figure 7.1.17 Pressure Buildup, MWX-3, Horner Plot

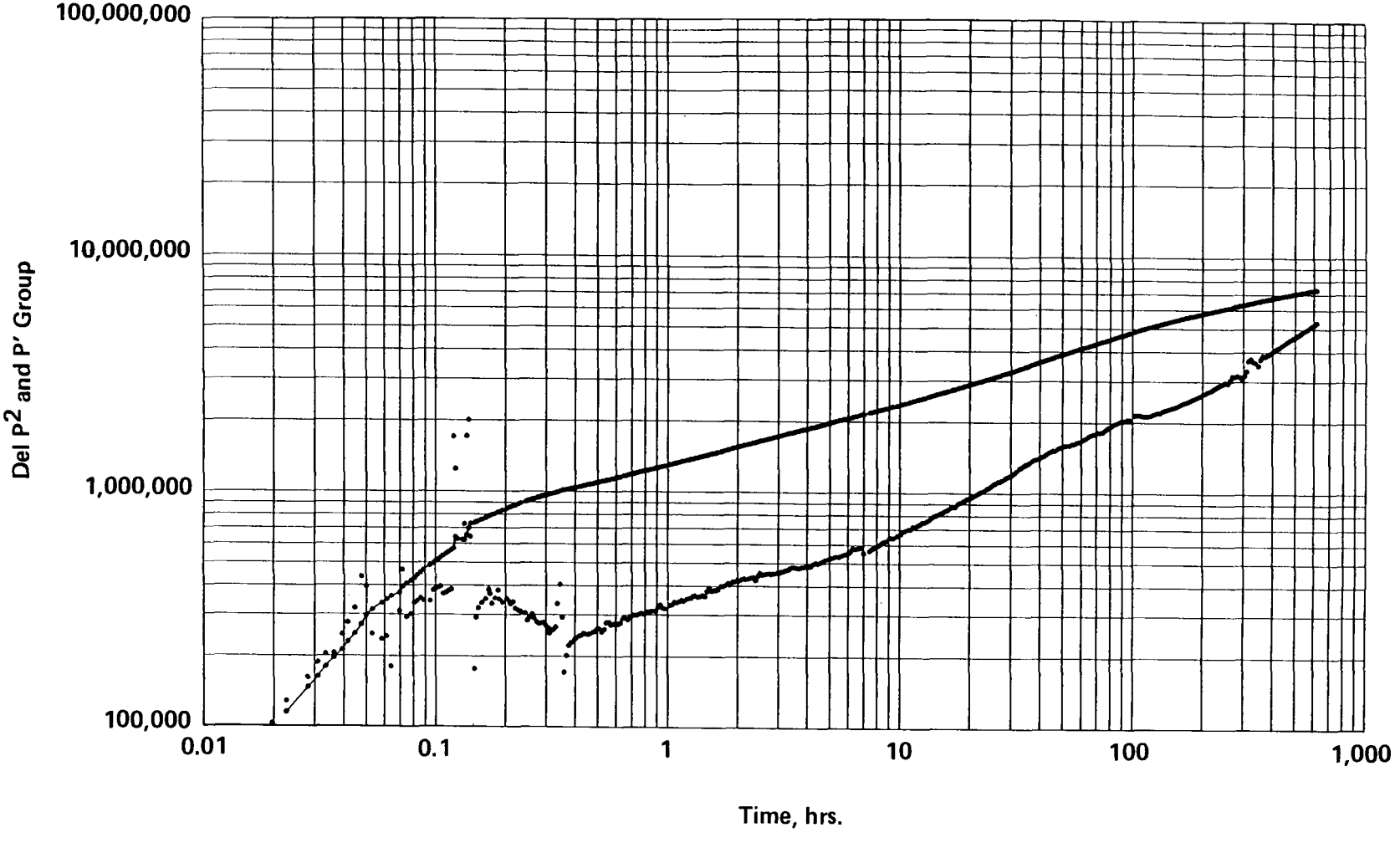

Figure 7.1.18 Pressure Buildup, MWX-3, Log-Log and Derivative Plots

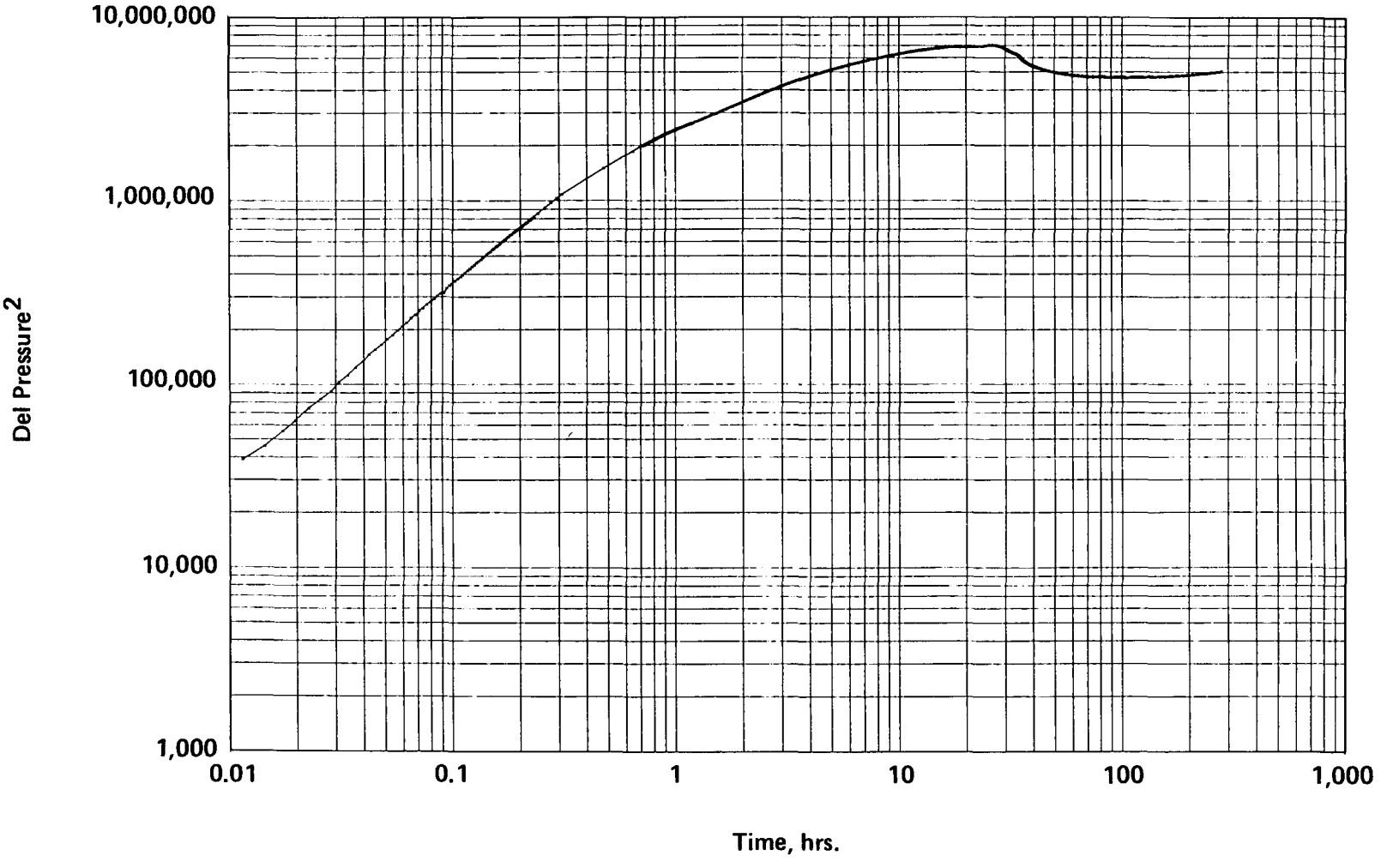

Figure 7.1.19 Pressure Buildup, MWX-1, Log-Log Plot

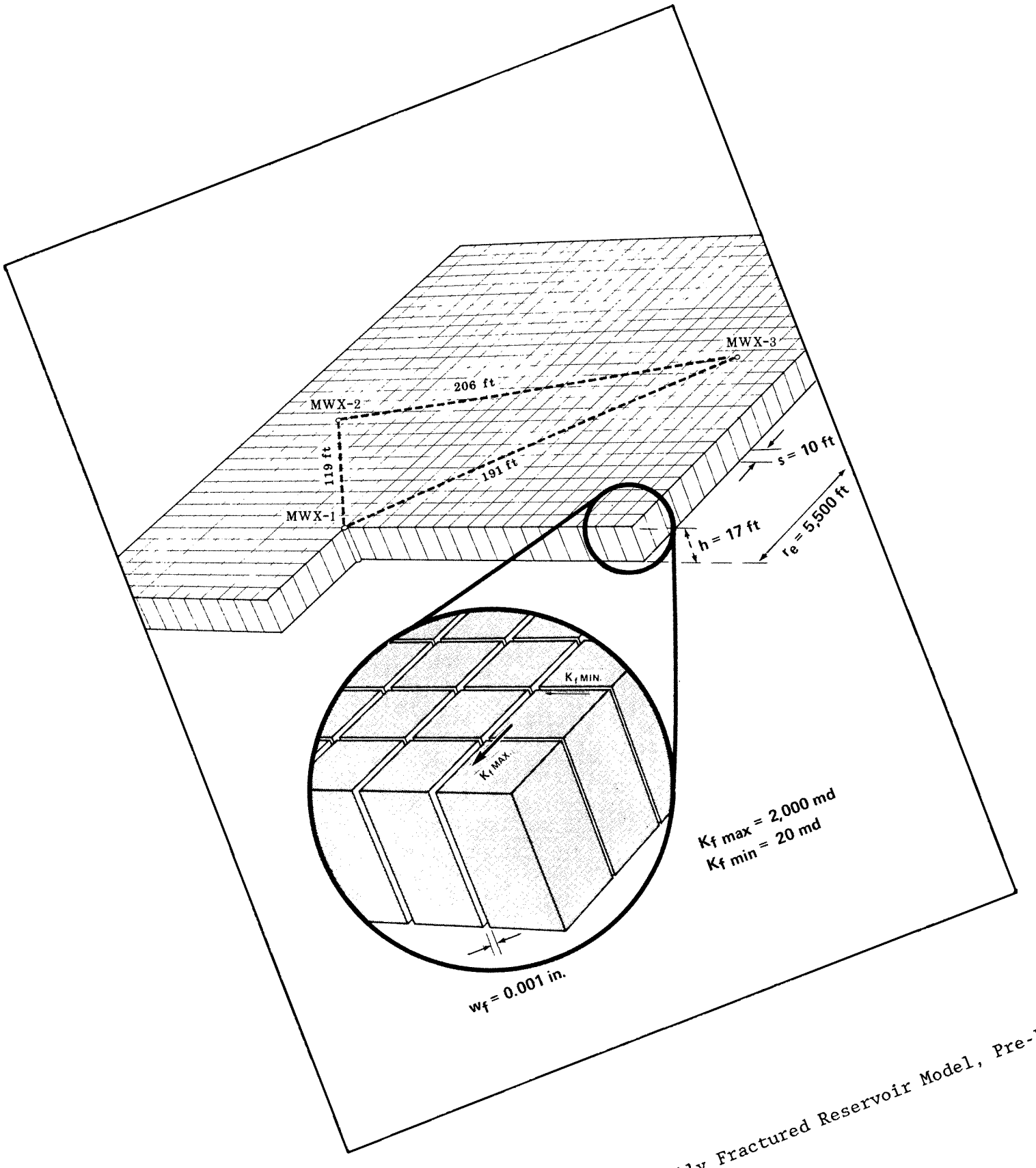

Figure 7.1.20 Fluvial B Naturally Fractured Reservoir Model, Pre-Frac

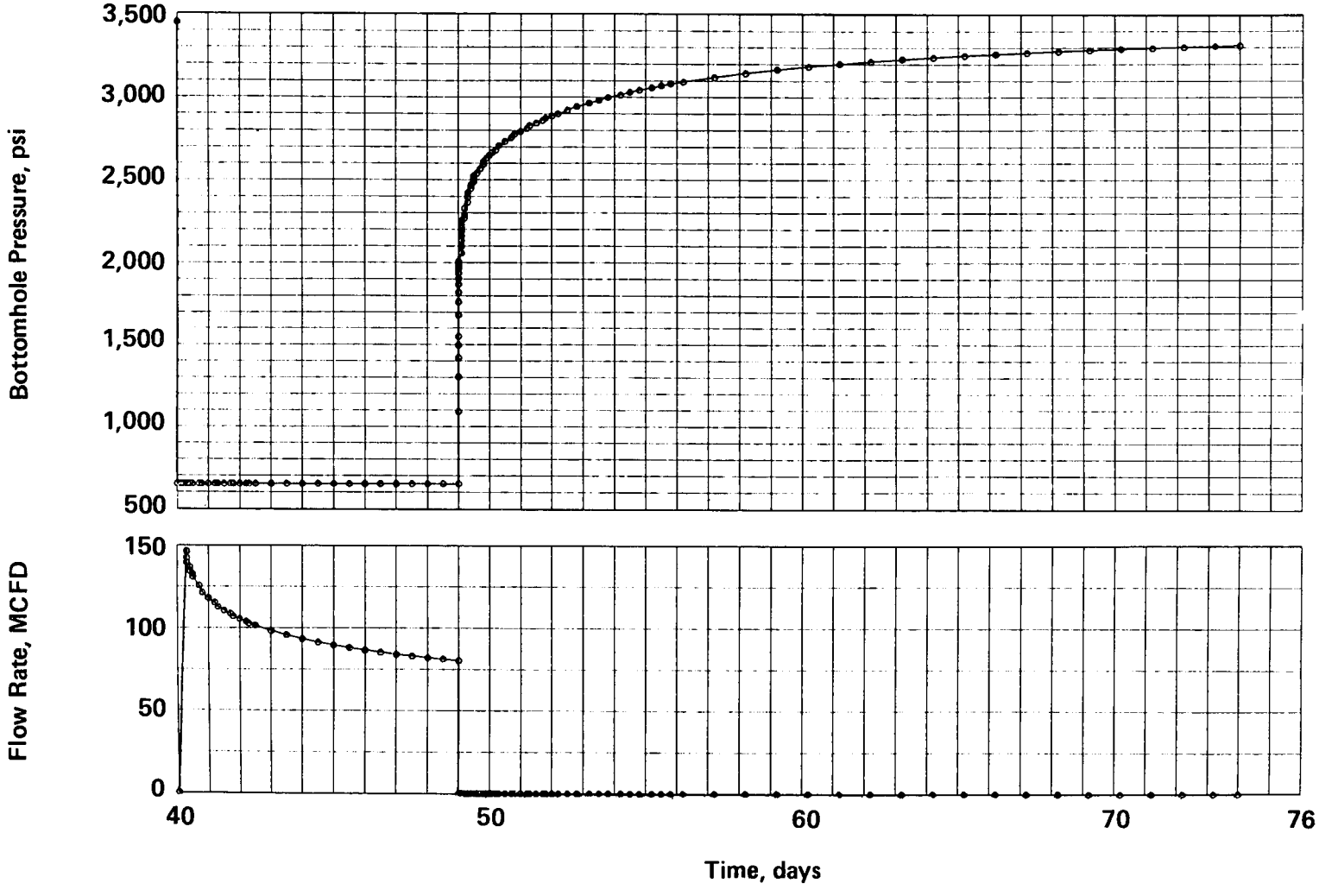

Figure 7.1.21 Simulated Flow Rate and Pressure Data, Isotropic

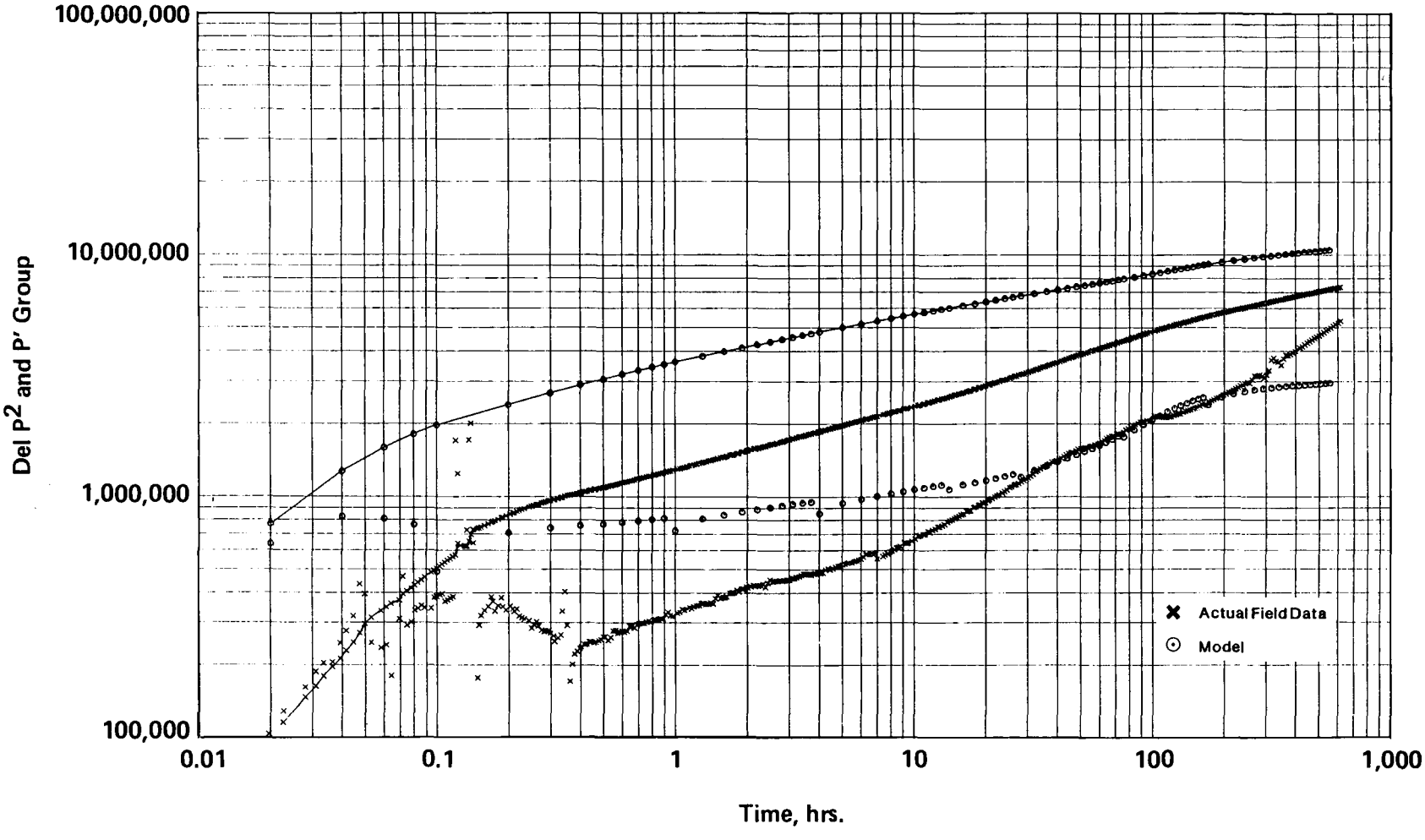

Figure 7.1.22 Comparison of Simulated and Field Pressures, Isotropic

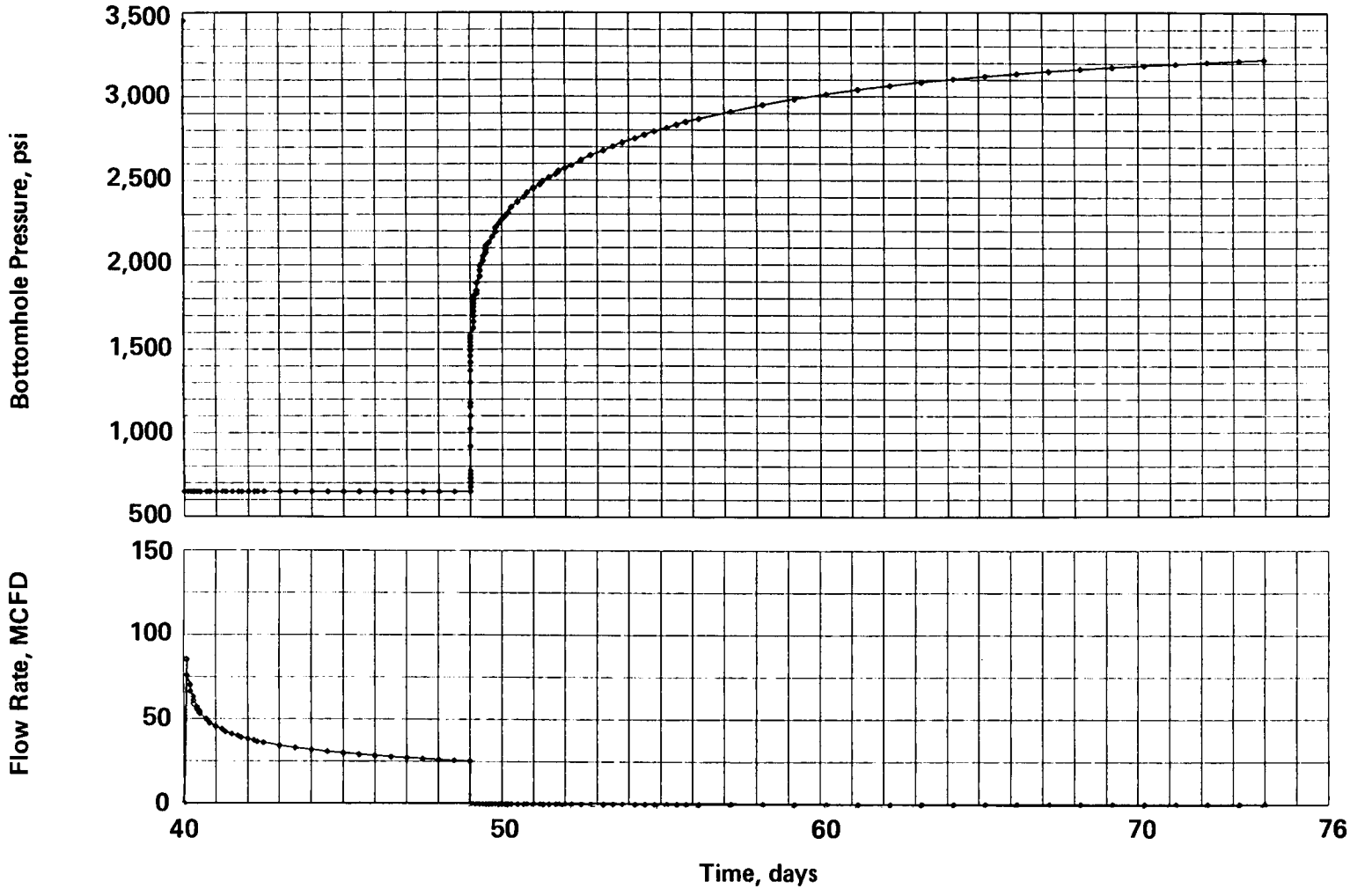

Figure 7.1.23 Simulated Flow Rate and Pressure Data, Anisotropic, 10:1

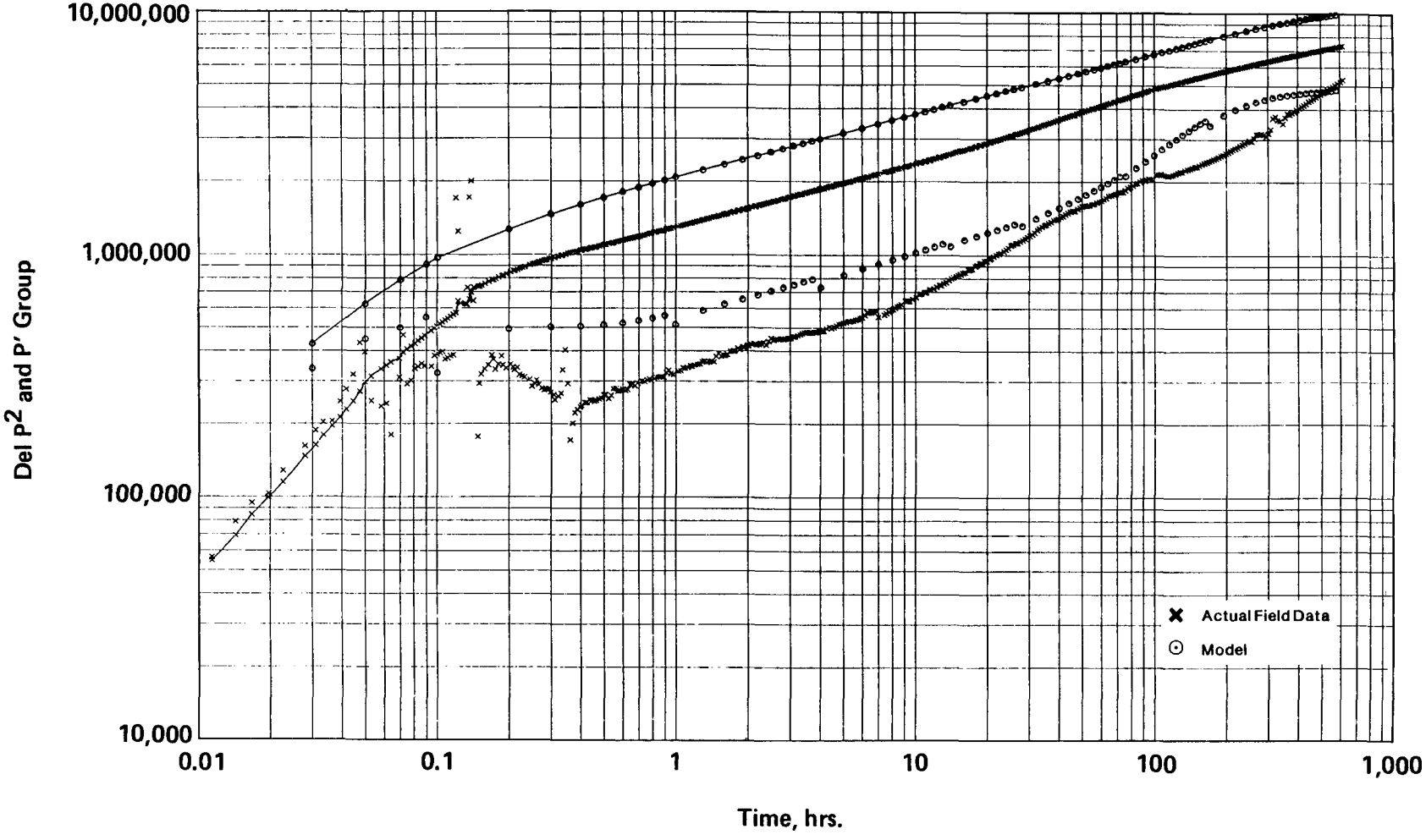

Figure 7.1.24 Comparison of Simulated and Field Pressures, Anisotropic, 10:1

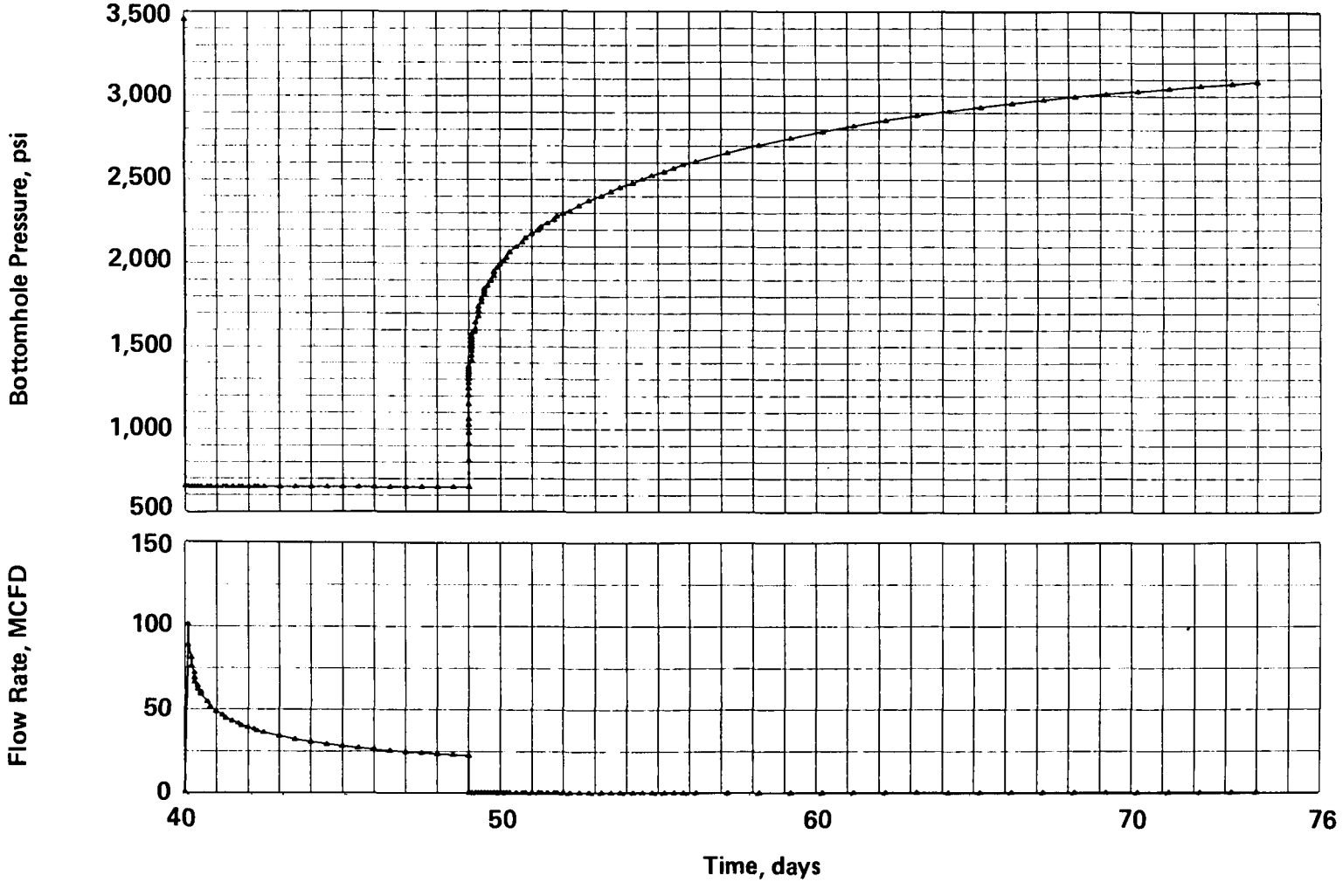

Figure 7.1.25 Simulated Flow Rate and Pressure Data, Anisotropic, 100:1

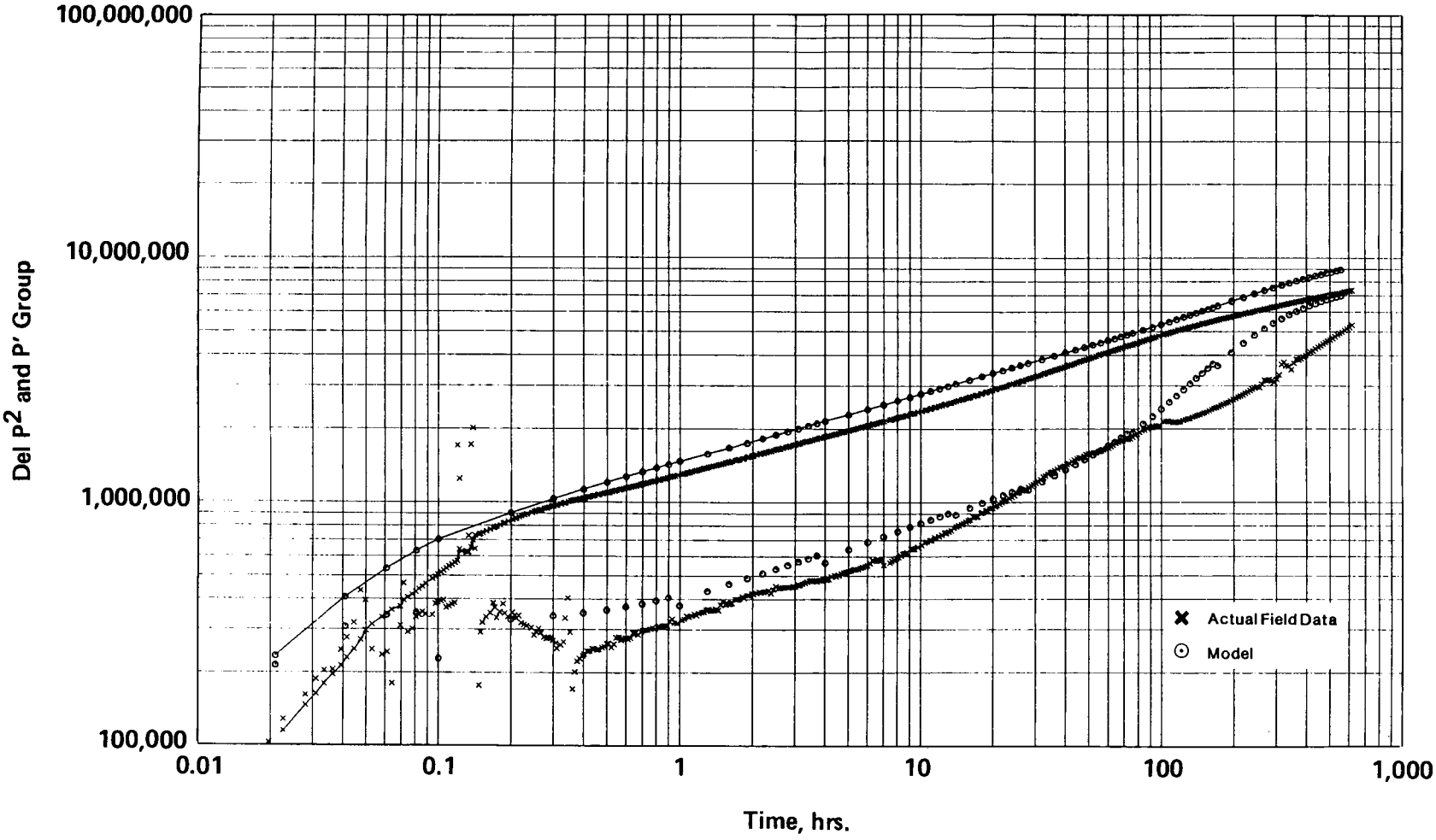

Figure 7.1.26 Comparison of Simulated and Field Pressures, Anisotropic, 100:1

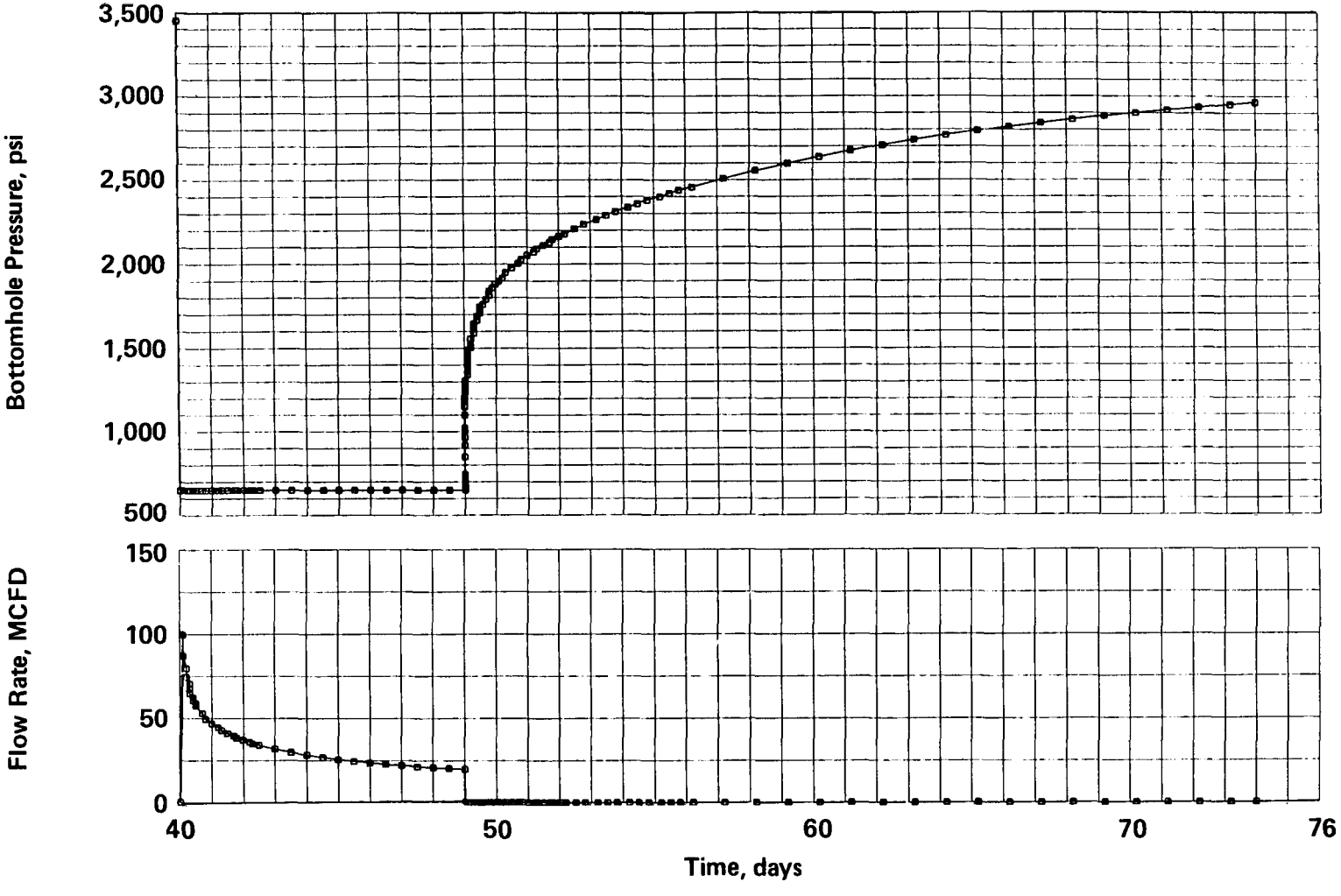

Figure 7.1.27 Simulated Flow Rate and Pressure Data, Anisotropic, 1000:1

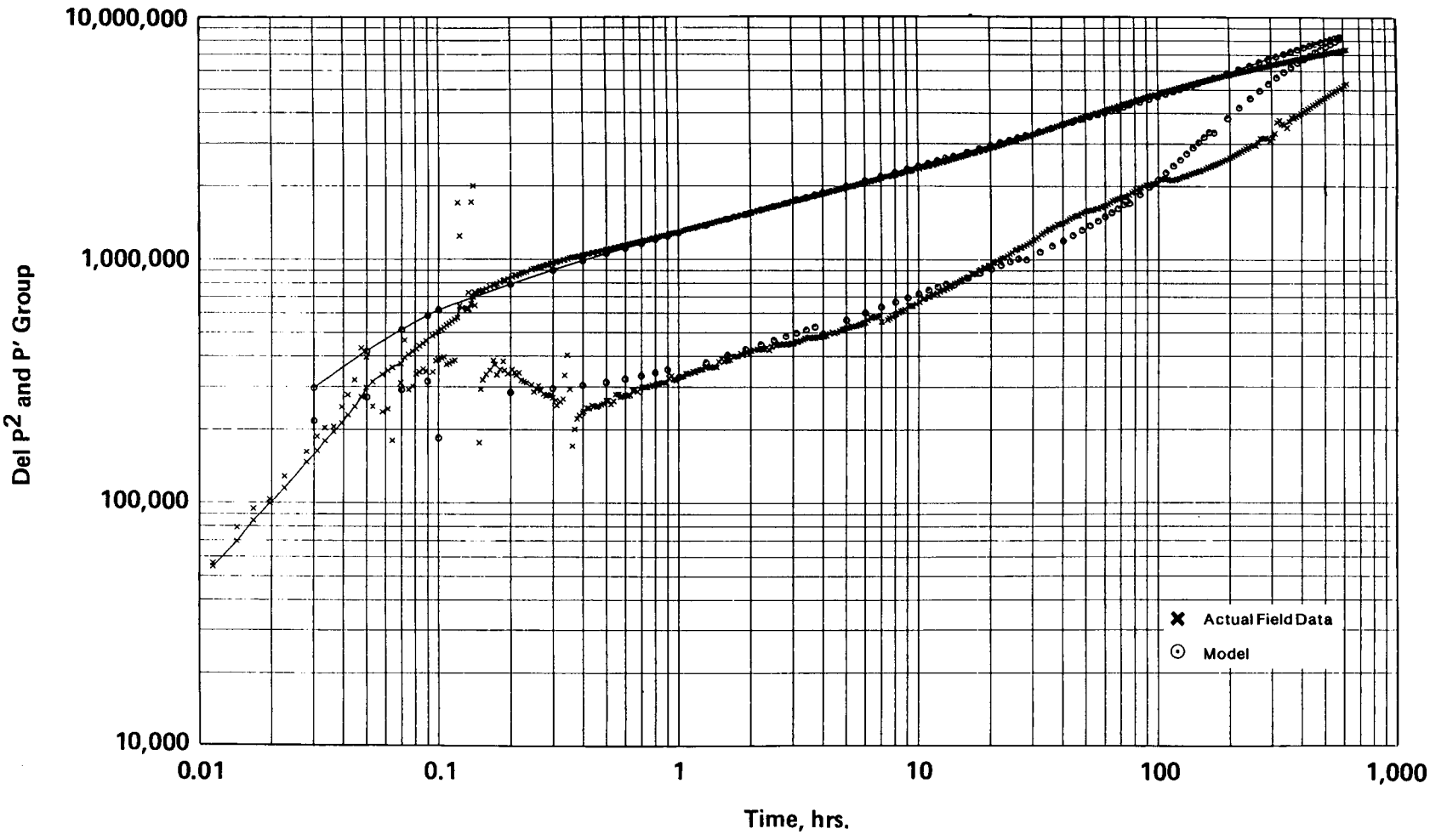

Figure 7.1.28 Comparison of Simulated and Field Pressures, Anisotropic, 1000:1

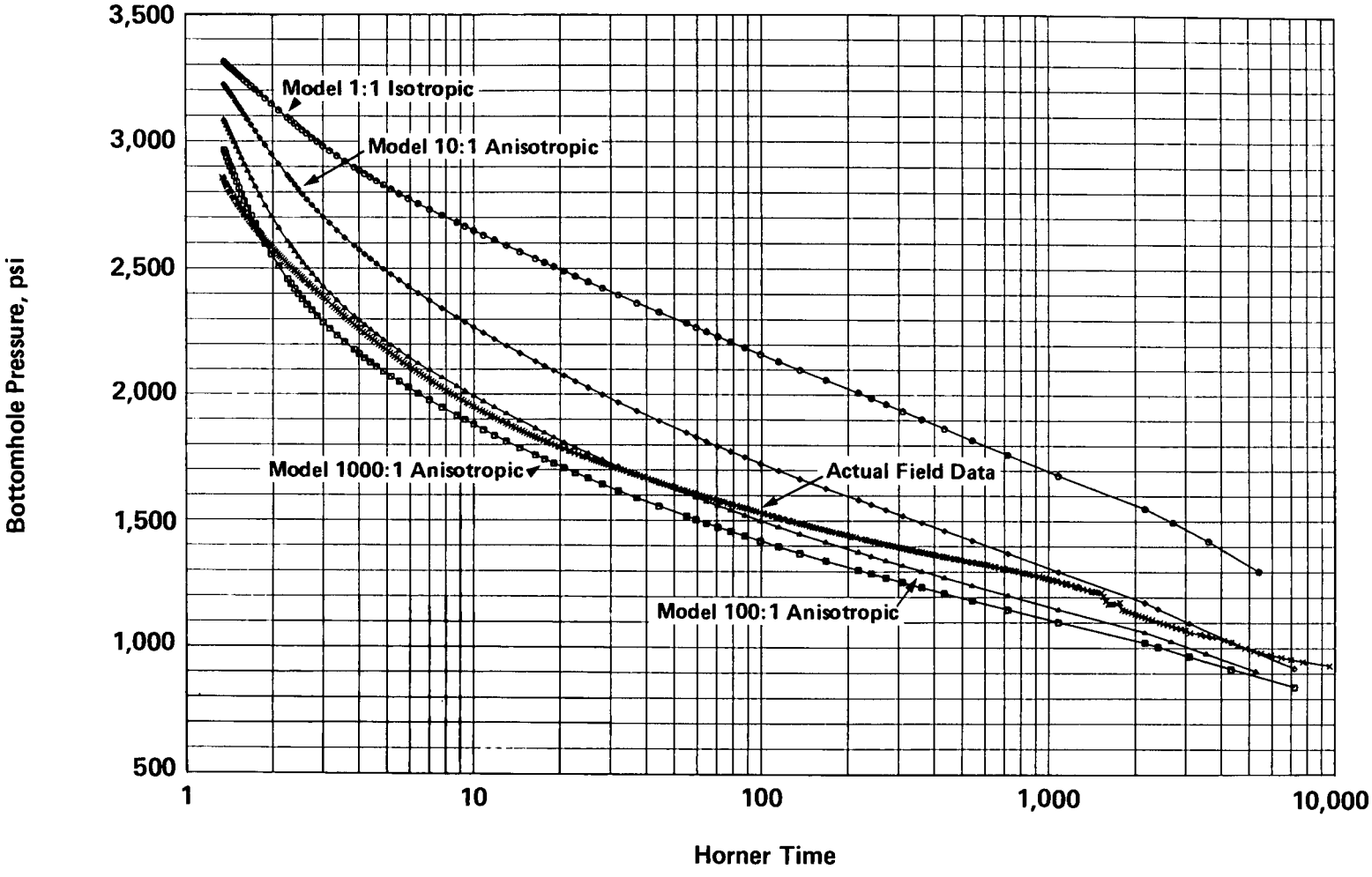

Figure 7.1.29 Comparison of Simulated and Field Pressures, Horner Plots

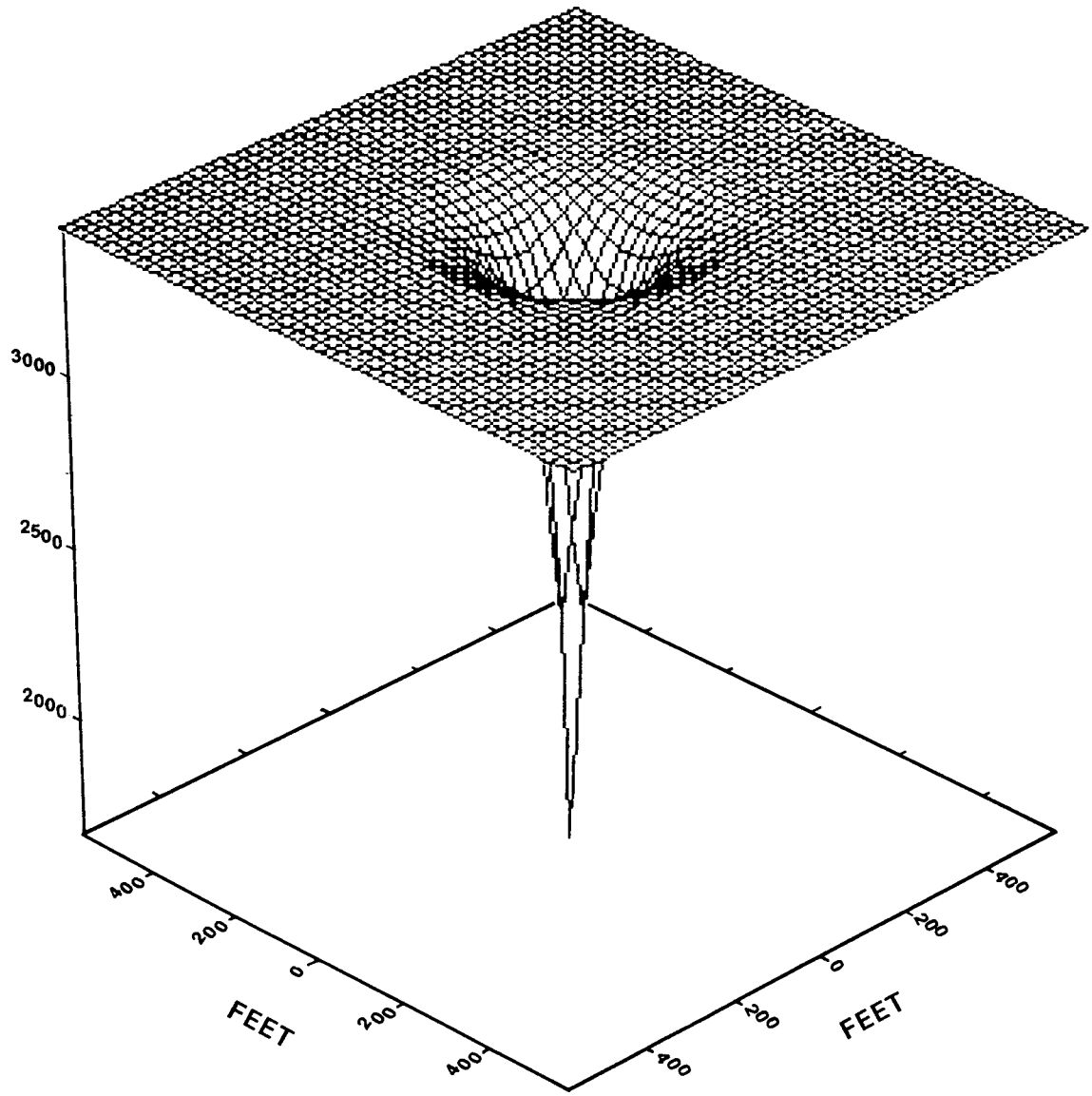

Figure 7.1.30 Pressure Profiles, Isotropic

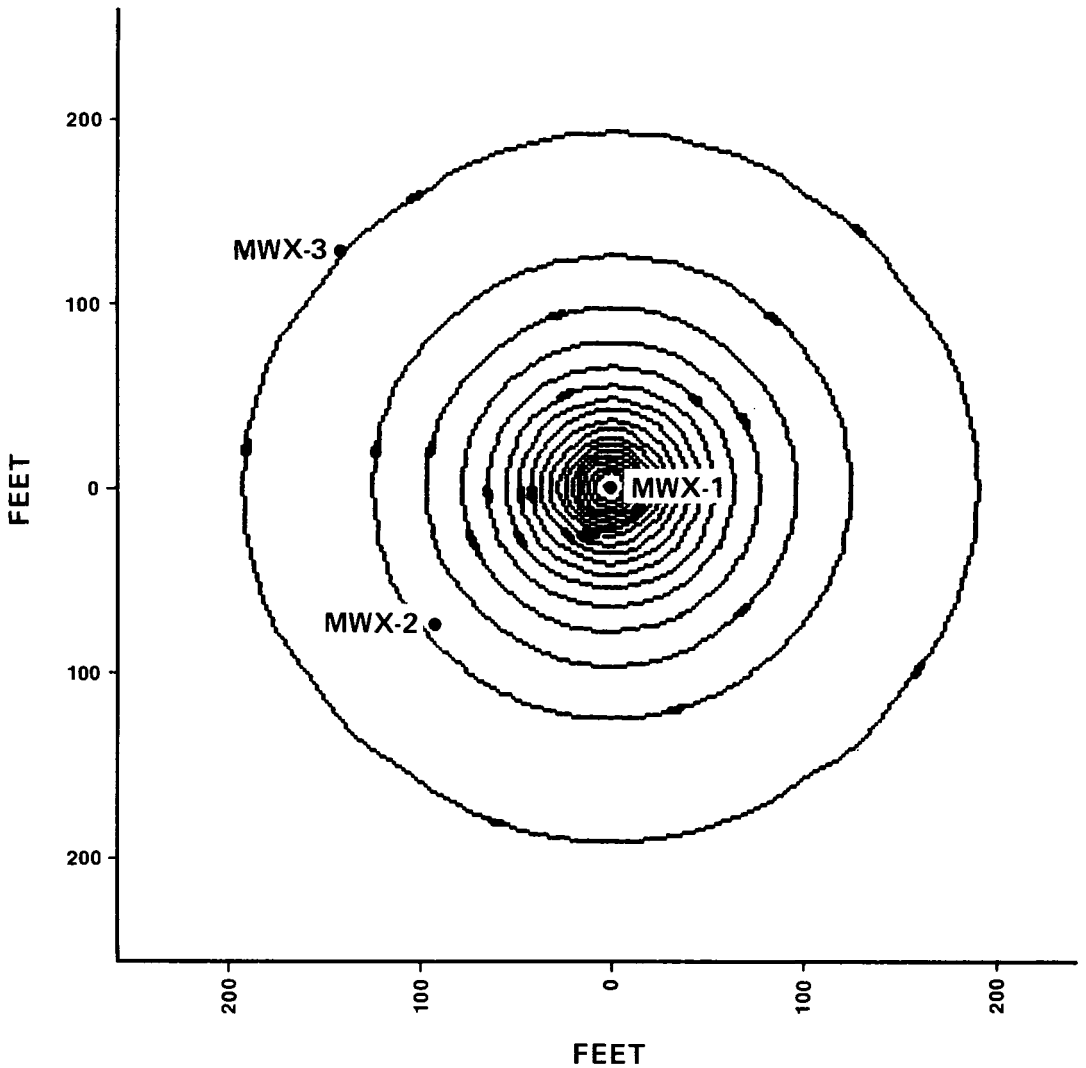

Figure 7.1.31 Pressure Profiles, Isotropic

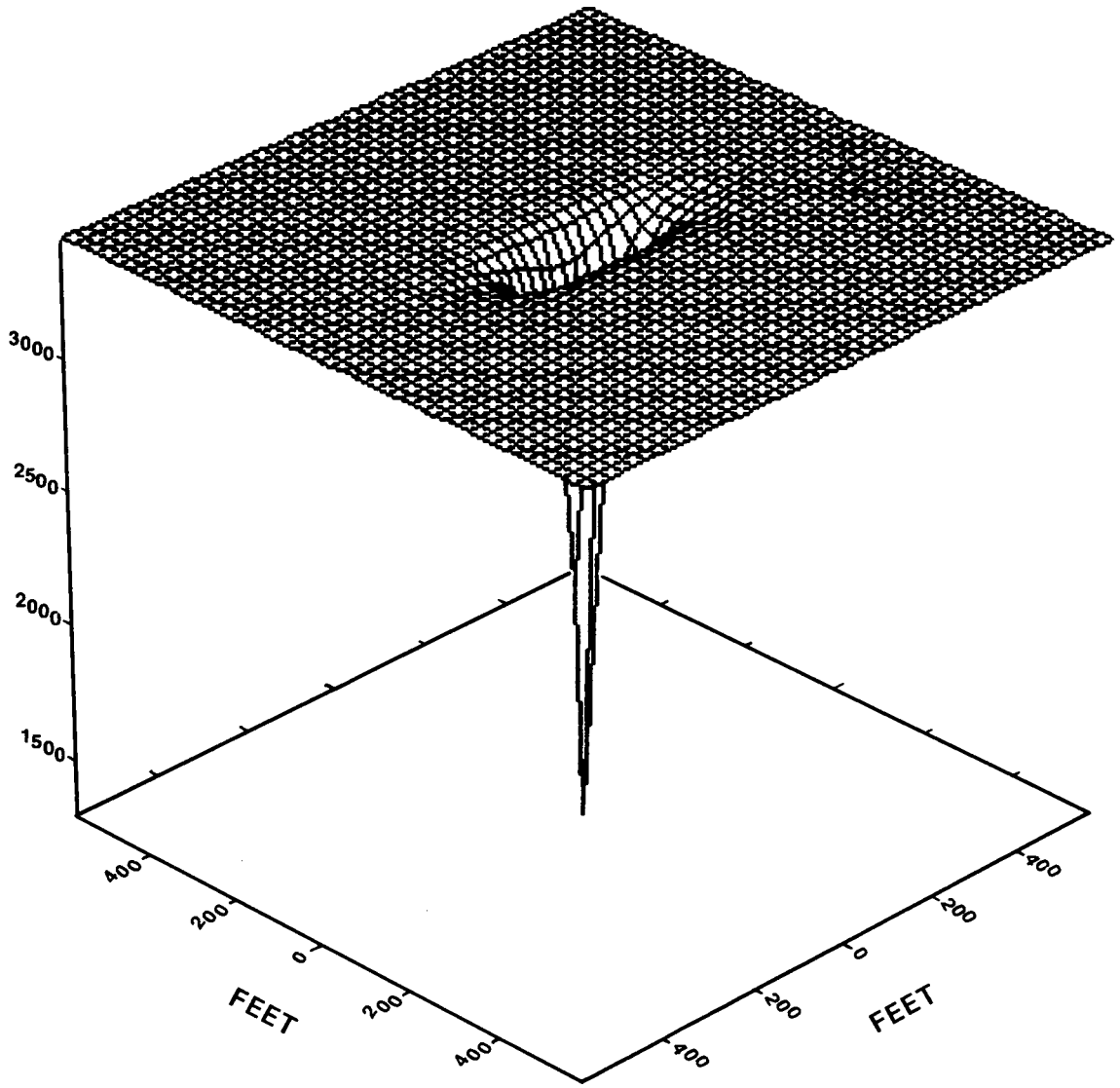

Figure 7.1.32 Pressure Profiles, Anisotropic, 100:1

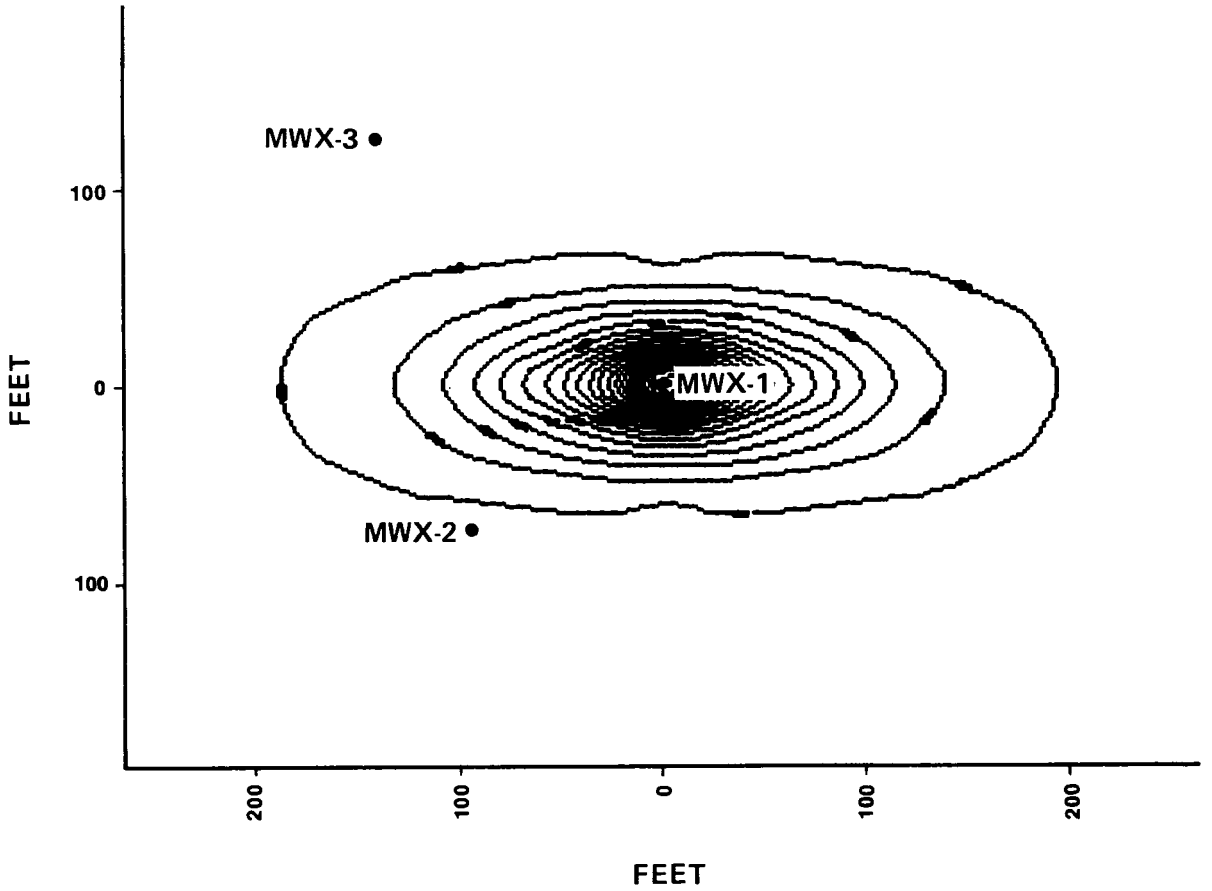

Figure 7.1.33 Pressure Profiles, Anisotropic, 100:1

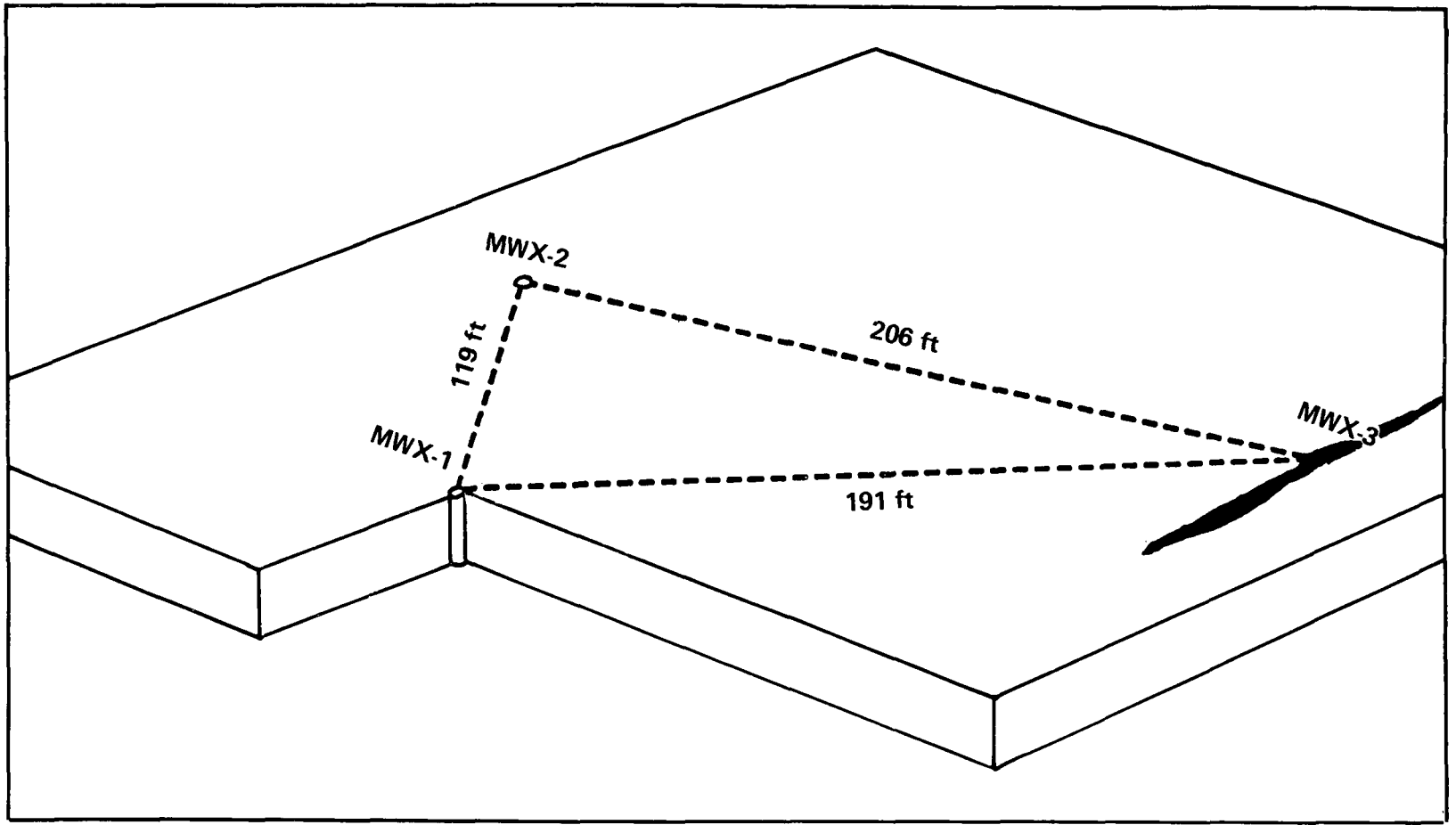

Figure 7.1.34 Fluvial B Homogeneous Reservoir Model with Hydraulic Fracture

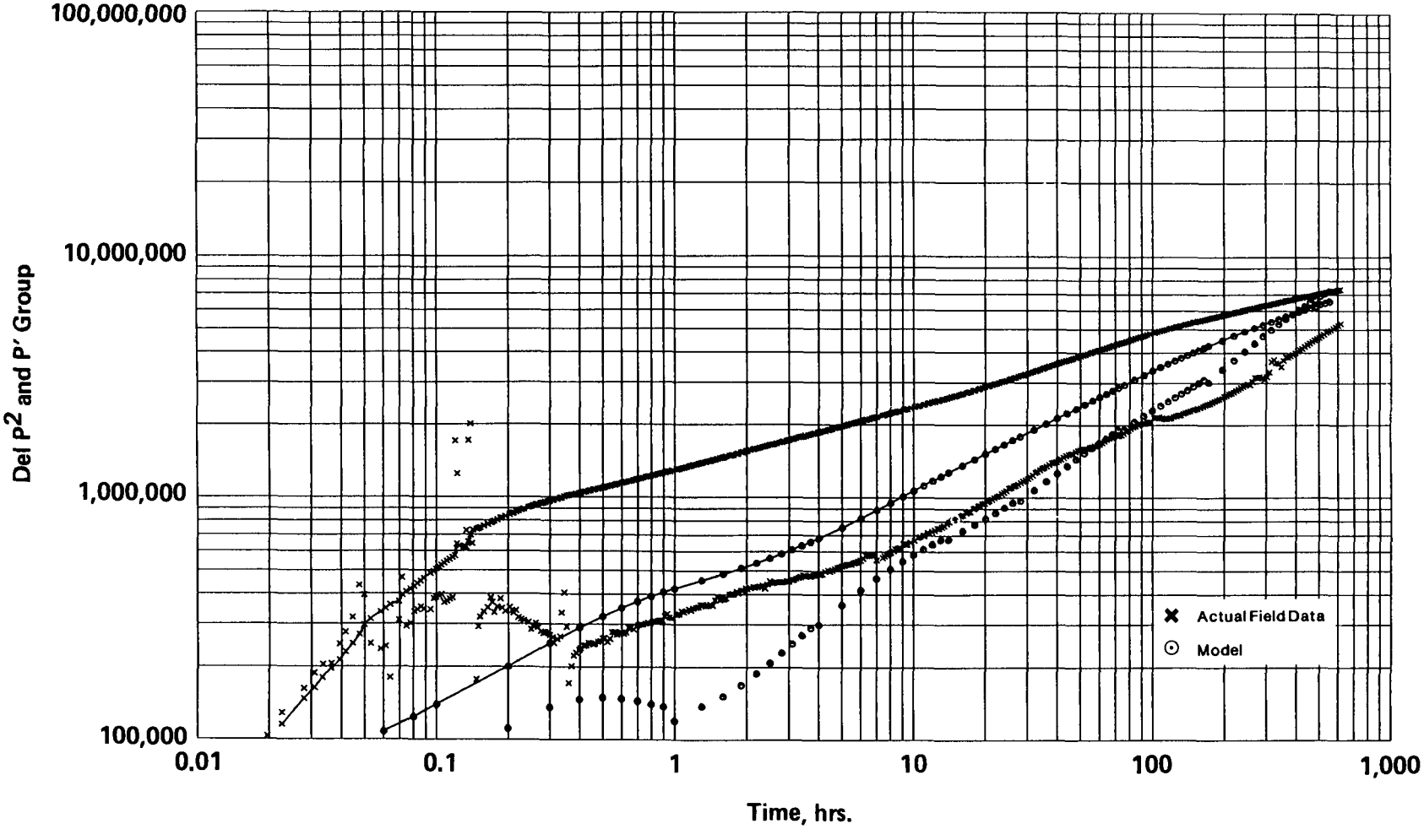

Figure 7.1.35 Comparison of Simulated and Field Pressures

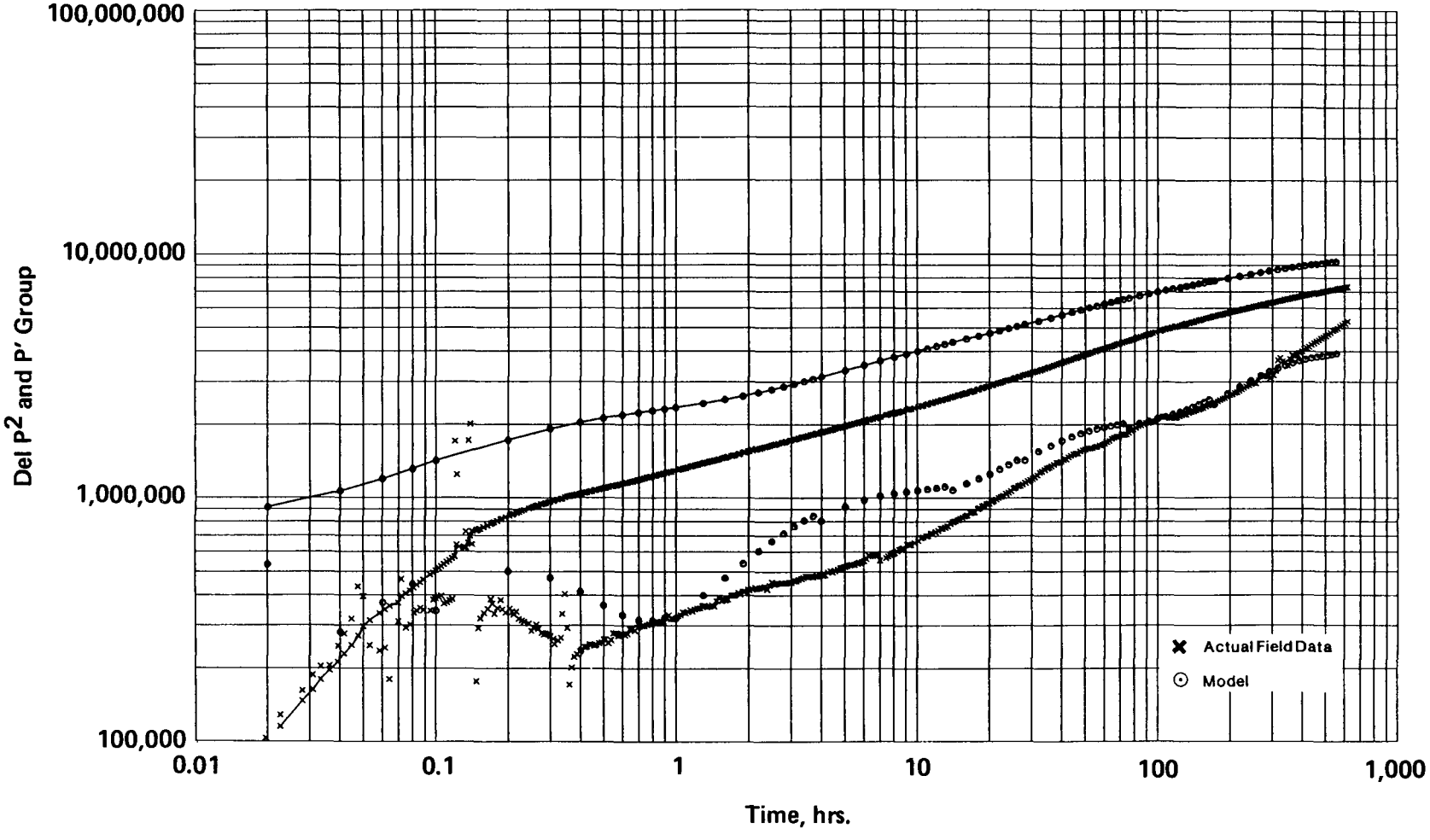

Figure 7.1.36 Comparison of Simulated and Field Pressures

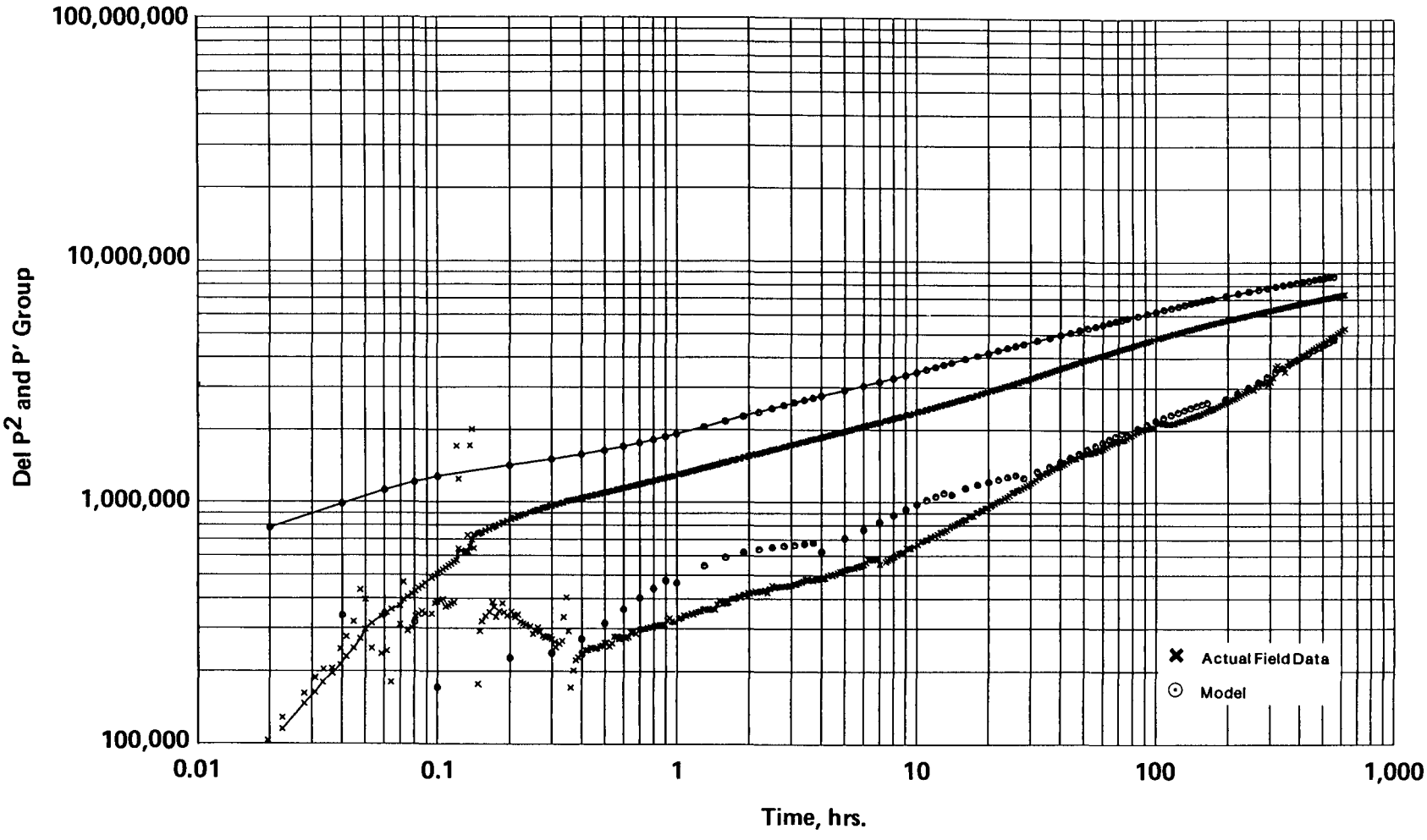

Figure 7.1.37 Comparison of Simulated and Field Pressures

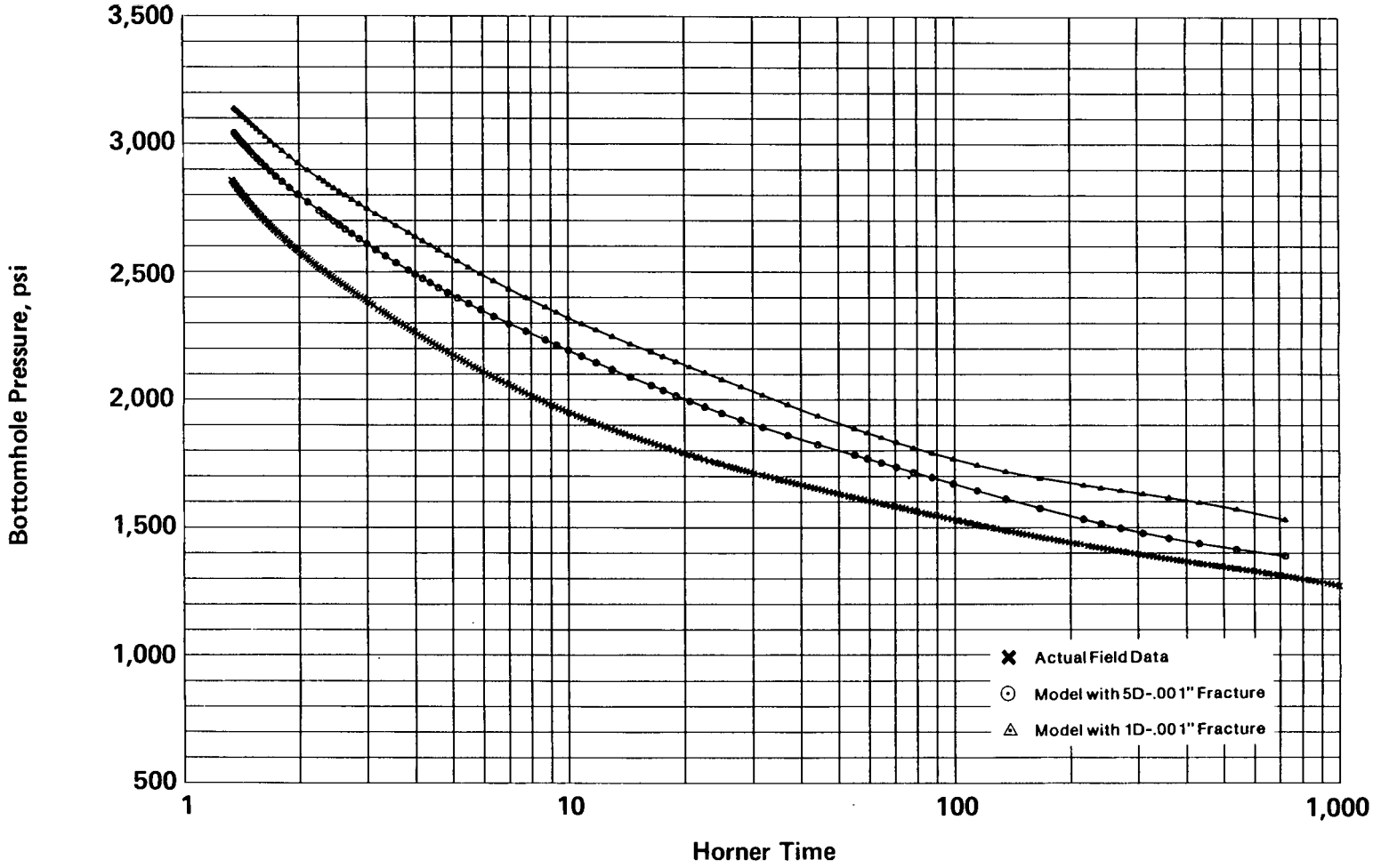

Figure 7.1.38 Comparison of Simulated and Field Pressures, Horner Plot

FLUVIAL B SANDSTONE STIMULATION EXPERIMENT

7.2 STIMULATION AND ANALYSIS

N. R. Warpinski
Sandia National Laboratories

7.2.1 OBJECTIVE

Hydraulic fracturing experiments in the fluvial B sandstone were conducted September-November of 1986. These experiments included step-rate/flow-back tests to estimate the closure stress, a foam minifrac to define leakoff characteristics and the nitrogen-foam stimulation treatment. The objective was to stimulate essentially the entire width of this meander belt sandstone reservoir, to determine production potential, and to investigate the possibility of damaging the natural fractures with treatment fluids.

7.2.2 BACKGROUND

The fluvial interval of the Mesaverde is the nonmarine section that is characterized by accumulated point bar deposits that form wide meander belt lenses. The widths of these lenses are considerably greater than the distributary channels found in the coastal and paludal intervals, providing considerably more gas-in-place for each individual lens. Thus, the fluvial interval is the primary lenticular target at MWX. On the other hand, such an agglomeration of point bar deposits, with the associated scour surfaces, shale breaks, etc., will undoubtedly result in a very unhomogeneous reservoir. This is complicated further by natural fractures, which are the primary production mechanism. Inspection of core in this zone has shown that most natural fractures terminate at shale/mudstone breaks, so interconnectivity between adjacent point bars may not be aided much by these fractures. Figure 7.2.1 shows an estimate of the lens size with respect to the wellbore spacing (see Section 3.3).

The fluvial B sandstone is the second major fluvial sandstone lens (from the bottom of the section) at MWX. The depth is 5822-5845 ft in MWX-1, the

production well. Core was obtained in all three wells, so good reservoir data are available. Several natural fractures were found in the B sandstone and all were less than 0.5 mm wide and 1 ft long (see Section 3.4). One of these was in the production well at the very base of the sand; it was vertical and completely calcite filled. Many fractures were observed in the siltstones above and below the B sandstone and some of these are several millimeters wide and fairly porous.

Porosities of the B sandstone range from 6-10% with matrix permeabilities from 5-25 md at 3000 psi confining stress and no water saturation. At in situ water saturation conditions (~55%), the matrix permeability is reduced about an order of magnitude. Well test permeabilities are considerably higher, about 10 μd for the system as whole (see Section 7.1).

Young's modulus for the B sandstone is about 4.5×10^6 psi and Poisson's ratio is about 0.18. The mudstones above and below the B sandstone are quite variable, and have Young's moduli that may be considerably greater or less than the sandstone. This is shown in Figure 7.2.2. Fracture toughness measurements of the B sandstone are typically 2000 psi$\sqrt{\text{in.}}$ while the surrounding mudstones are closer to 1500 psi$\sqrt{\text{in.}}$

Stress tests in and around the B sandstone showed that relatively large stress contrasts between the sands and mudstones were common (see Section 6.0). Figure 7.2.3 shows the stress test data obtained from the lower fluvial zone. Good stress contrasts are found below, and possibly just above, the B sandstone, but the stress contrasts are considerably smaller higher up.

7.2.3 STEP-RATE/PUMP-IN/FLOW-BACK TESTS

Before testing the B sandstone, the perforations in all three wells were broken down with small N_2 fracs. Nitrogen was used in order to avoid any liquid damage to the natural fractures. We tried to measure the ISIP at the end of each N_2 pump, but no clear ISIP was discernible and the stress could

have been anywhere in the range of about 4300-4700 psi. In addition, these tests were performed prior to several weeks of drawdown, during which the reservoir pressure dropped from about 3450 psi to about 3000 psi in the near-wellbore area at the time of the experiments.

September 4-5, 1986, we performed step-rate and flow-back tests to try to characterize the closure stress in the production well. Nitrogen was again used in order to minimize liquids. During these two days, a nitrogen step-rate/flow-back test, three nitrogen pump-in/flow-back tests, and one KCl-water pump-in/flow-back test were conducted.

The purpose of these tests was to measure the closure stress in the interval at the time of fracturing, to estimate the treatment pressures for hydraulic fracture design, and to get some initial data on leakoff for the following foam-frac operations. Nitrogen was used for these tests in an attempt to minimize fluids injected into the reservoir. The last pump-in/flow-back test, using 3% KCl water, was originally scheduled to be a 75 quality, nitrogen-foam, pump-in/flow-back test, but we did not feel that we could adequately measure or control the foam flow-back rates and this test was switched to KCl.

7.2.3.1 Wellbore Configuration and Instrumentation for Flow-Back Tests

The bottom-hole configuration for MWX-1 during these tests is shown in Figure 7.2.4. There are 46 perforations from 5822-5845 ft and 100 ft of rat hole below the perfs. A packer was set at 5753 ft with a tubing tail at 5792 ft. The bottom-hole pressure/temperature tool was located in a $4\text{-}^1/_2$-in. casing joint just above the packer. The difference in hydrostatic head between the gauge location and the perforations is only about 10-20 psi for N_2 at pressure, and has therefore been ignored.

7.2.3.2 Nitrogen Step-Rate Test

The nitrogen step-rate test was conducted with eight five-minute steps between about 500 and 10,000 SCFM. The actual steps and the pressure data are given in Table 7.2.1 and Figure 7.2.5.

The standard step-rate results plot is shown in Figure 7.2.6. For the fracture extension pressure, the first break from radial flow behavior is used. This is the same number that would be obtained from a semilog plot. The extension pressure here is about 4650 psi and this value is usually a couple of hundred psi above the closure stress in KCl-water flow-back tests, so a closure stress value is expected to be around 4450 psi.

7.2.3.3 Flow-Back Tests

Flow-back tests are generally considered to be fairly accurate techniques for determining the closure stress, at least in conventional reservoirs. These tests are usually conducted with KCl water and we knew of no previous experience with nitrogen as the test fluid. However, it was considered to be sufficiently important to minimize water on the formation that we decided to try using N_2 in this zone.

The first flow-back was conducted immediately after the step-rate injection. While the pressure during the flow-back can be seen in Figure 7.2.5, an expanded plot of the pressure in the region of interest is shown in Figure 7.2.7. The flow-back rate during this period is also shown. The surface rate is decreasing continuously, but the downhole pressure is also decreasing, so that the actual bottom-hole rate is decreasing at a relatively slow rate.

In Figure 7.2.7, there is no obvious reversal in curvature (from positive to negative), but rather a change from positive curvature to no curvature. This can be seen more clearly by fitting the data in a least-squares procedure to a polynomial. Derivatives can then be easily calculated to determine if any curvature change is occurring and where it occurs. In this test, the first derivative shows that the curvature became flat at about 60.5 minutes, which corresponds to a pressure of 4260 psi. This is borne out by the second derivative, which curiously reaches a minimum near zero, but never totally reverses. The possible meaning of this minimum will be discussed later.

The data for the second flow-back test are shown in Figures 7.2.8 and 7.2.9. Figure 7.2.8 shows data for the whole test (injection and flow-back), while Figure 7.2.9 shows the data particular to the flow-back. Note that the injection pressure for N_2 at 10,000 SCFM (about seven bpm bottom-hole-equivalent rate) is 5200 psi. This is on the order of 700 psi above the expected closure stress and is typical of the relatively high treatment pressures that have been observed in all zones at the MWX site.

This second flow-back was conducted at an initial value of 1200 MSCFD, a higher rate than the previous test. The flow-back portion looks similar to the post-step-rate flow-back, but the point where the minimum in the second derivative occurs is probably an artifact of the fitting procedure. Just before this minimum point, we switched from one-second to one-minute data and there are too few data points after 28 minutes to constrain the fit adequately. It is easy to change the character of the curve fit (after 28 minutes) by changing the order of the polynomial.

Results for flow-back number 3 are shown in Figures 7.2.10 and 7.2.11 and the flow-back data in Figure 7.2.11 are very similar to the previous two tests. Again, the curve fits after 22.5 minutes should be dismissed because of lack of sufficient data and constraint on the fit. Nevertheless, the minimum in curvature is before this at 21.3 minutes and 4270 psi. No total reversal in curvature is seen here. The flow-back rate at the start of this test was 1600 MSCFD.

Figures 7.2.12 and 7.2.13 show the results for nitrogen flow-back number 4. At a flow-back rate starting at about 2800 MSCFD, there is finally some slight reversal in curvature. This occurs at about 12.5 minutes at 4410 psi. There is also the same general character in this test as was observed in the previous flow-backs. A minimum in the second derivative occurs at about 13.5 minutes at 4270 psi.

The data for the KCl-water flow-back are shown in Figure 7.2.14. We had difficulties keeping a constant rate and no reversal in curvature was seen. A second KCl-water test was attempted, but the bottom-hole pressure/temperature gauge was lost downhole and testing was stopped.

7.2.3.4 Discussion of Flow-Back Tests

It is clear from these data that determination of the closure stress is not straightforward in these nitrogen flow-backs. Table 7.2.2 summarizes the information obtained. The inflection point from flow-back number 4 is a tempting choice for closure, but examination of the pressure data shows that the change in curvature is slight and transitory. The minimum in the second derivative in all tests is intriguing because of the invariance in the value, but it is not clear that any special physical significance should be associated with that point.

It might be helpful to review what probably occurs during a flow-back. When a liquid is used for a flow-back, the results are fairly well understood. The initial pressure decline at the start of flow-back is not usually analyzed because it is a combination of flow-back, the leakoff into the formation, continued extension of the fracture and rearrangement of the fluid in the fracture. However, after a short time, the crack will probably stop extending, a relatively steady flow-back rate will have been established throughout the fracture/wellbore system, and some relatively steady leakoff rate will have been achieved. As the pressure decreases and closure begins, the fracture first closes near the wellbore because the pressure is lowest there (negative pressure gradient in the fracture because of reverse flow). This causes the pressure in the wellbore to drop even faster because there is no longer an open conduit for fluid support from the fracture. This is generally seen as a reversal in curvature, but the ability to achieve this reversal depends strongly on the flow-back rate (probably because of the delicate, competing balance between flow-back, leakoff, and fracture fluid dynamics).

With gas, the situation is not quite so clear. Because of the low viscosity of the nitrogen, leakoff into the formation may be as large or larger than the flow-back rate and pressures may actually decrease at a slower rate at closure. Even when the fracture closes, there is still a residual fracture width that is highly conductive to nitrogen. A significant amount of gas could still be injected into the fracture (from

the wellbore) and the amount injected should decrease as the pressure decreases. Thus, if the volume lost from leakoff is greater than from flowback, the rate of pressure decrease should be steadily decreasing throughout the flow-back, although the rate of decrease may change for the closed fracture configuration compared to the open fracture. This might be the significance of the minimum in the second derivative.

Another possible scenario, which may better explain these results, is one where the leakoff rate is less than the flow-back rate (as in the liquid case), but the highly conductive fracture keeps supporting the wellbore after closure. In this case, the rate of pressure decline should decrease as the fracture narrows, but once the fracture closes, the residual width will not change much with pressure changes and support from the fracture may become much less sensitive to pressure in the wellbore. The pressure in the wellbore will now only affect the pressure gradient down the fracture and not the width of the fracture as well. The balance between the gas that can be produced through the closed fracture and the flow-back rate determines whether the rate of decrease will merely slow down or totally reverse at closure. The point where behavior changes from decreasing positive curvature to increasing positive curvature (minimum in the second derivative) probably indicates the transition from flow through an open fracture to flow through the residual fracture. This point is probably slightly below the closure stress because enough fracture length must close near the wellbore to make this noticeable and this will take additional pressure drop below closure. The major difference between this second scenario and the first one is the capability of developing a curvature reversal in the second one; such a reversal was seen in flow-back number 4, at the high flow-back rates.

We can speculate that the reason that the curvature minimum is so consistent is because it depends most strongly on the conductivity of the closed fracture, the length of the created fracture, the pressure in the fracture at closure, and the way the crack closes. None of these factors should change much from flow-back to flow-back, since the maximum length is probably attained in the step-rate test (the largest volume test).

The previous discussion suggests that the closure stress is no less than 4270 psi and, if the slight reversal in curvature in flow-back number 4 is due to closure, then it is about 4400 psi. This is consistent with stress-test data and the step-rate test and 4400 psi will be used for all following analyses. The accuracy of this number, however, is only ±150 psi.

7.2.4 MINIFRAC AND STIMULATION

A minifrac was conducted in the B sandstone on October 31 and, on the following day, the stimulation of the same interval was performed. Both of these tests were carried out with the same wellbore configuration, fluid system, and instrumentation. Quality control and operational data for both the minifrac and stimulation are found in Reference 1, which is given as Appendix G. Similarly, the digitized stimulation data are presented in Appendix H.

7.2.4.1 Wellbore Configuration and Instrumentation

The wellbore configuration for the B sandstone stimulations is shown in Figure 7.2.15. Bridge plugs were set below the zone at 6000 ft and 5950 ft (the lower one leaked). The tubing was landed open-ended at 5703 ft and a bottom-hole pressure/temperature gage was situated at 5650 ft. The surface instrumentation, as developed by Cipolla and CER, are shown schematically in Figure 7.2.16.[1] The treatment fluid was a 75-quality nitrogen foam and all fluid and sand components were measured in order to cross check rates. All flowmeters (low pressure magnetic, high pressure magnetic and nitrogen) and densitometers were provided by Dowell-Schlumberger.

Borehole-seismic geophone tools were located in each of the offset wells in an attempt to determine fracture geometry. Locations of the tools, calibrations, and results[2] are given in Section 7.4.

7.2.4.2 Fluid System

In order to minimize liquids, a 75-quality nitrogen foam was chosen to be the frac fluid. The gelling agent in the liquid phase is a Xanthan

polymer, because of its low residue and high foam stability. Dowell Schlumberger performed additional laboratory work to develop a breaker system for the Xanthan gel. The gel/breaker system appeared to function adequately during the treatment.

7.2.4.3 Minifrac Operations

The purpose of the minifrac was to confirm the design parameters for the full-scale stimulation, to test instrumentation and diagnostics, and to map the fracture. The design is shown in Table 7.2.3. We start the treatments by pressuring up the wellbore with nitrogen so that foam quality is not too high when foam is started and to achieve a steady nitrogen flow rate. The nitrogen also acts as a spearhead to clear out any liquids at the bottom of the wellbore.

Dowell-Schlumberger pumped the minifrac as planned on October 31, 1986. (Specific data are found in Appendices G and H.) All instrumentation functioned adequately. Figure 7.2.17 shows the bottom-hole pressure and surface foam rate during the treatment. The initial rate is decreasing as the nitrogen, which is being pumped at a constant surface rate, is being compressed. Foam hit the perfs at about 17 minutes, where the bottom-hole pressure suddenly increased. The long pressure decline was used for a Nolte pressure decline analysis.[3]

The Nolte-Smith plot[4] is shown in Figure 7.2.18. Throughout most of the minifrac the pressure is relatively flat. The type curve for the Nolte pressure decline analysis is shown in Figure 7.2.19. The fit is relatively good and a P^* value of about 160 psi was determined. This results in a calculated leakoff value of 0.00026 $ft/\sqrt{min}$, much lower than any previous zones that we have tested. This suggested that the design value of 0.001 $ft/\sqrt{min}$ was conservative and tip screenout was not likely.

Flowback of the zone began after the pressure decline and a temperature survey. Approximately half of the pumped liquids were recovered at this time.

7.2.4.4 Stimulation Operations

The objective of the stimulation was to create a relatively long propped fracture that would take advantage of the larger reservoir size of these fluvial lenses (compared to the coastal and paludal zones) and would minimize damage to the natural fractures.

The stimulation design is shown in Table 7.2.4. The proppant used was 20/40-mesh Proflow intermediate strength prop and the design foam flow rate at the perfs was 10 bpm. On November 1, 1986, the treatment was conducted.

The actual treatment was considerably more complex than designed because of some operational problems (Reference 1 and Appendices G and H). Figure 7.2.20 shows the bottom-hole pressure and surface foam flow rate during the job. The initial nitrogen pump-up, the pad and the first two stages were pumped as planned, but the pumper sanded out when we started the third stage. This occurred at about 138 minutes (Figure 7.2.20) and required a 12 minute shutdown to correct. At this point, the first stage of sand was just about to the perforations. When pumping resumed, there were two minor sand outs that required a decrease in sand concentration to correct. Within 10 minutes of the estimated time that sand first entered the perfs (about 150 minutes) the job screened out. Pressure began to rise dramatically compared to the pad stage, so we went directly to flush. During the flush, there were two sharp drops in pressure that are now attributed to movement of the lower bridge plugs. Pressure continued to rise to a final value that was about 2200 psi above closure stress at shut-in. The Nolte-Smith plot for the treatment is shown in Figure 7.2.21; the screenout is clear in this plot.

After the test, we discovered that the densitometer on the pod blender was not correctly calibrated and we had attempted to pump significantly higher concentrations than design. The one-ppg stage was actually about a 1.7-ppg bottom-hole equivalent concentration (seven ppg through the pump), the two-ppg stage was about 3.8 ppg (about 20 ppg through the pump). Sand-out occurred at the four-ppg stage, which was actually much greater (>25 ppg

through the pump). After clearing the sand out, the four-ppg stage was finished by actually pumping the designed concentration.

The downward movement of the bridge plug resulted in the loss of a significant volume of fluid and sand. After cleanup, the bridge plug was found at 6530 ft, a drop of about 600 ft, equivalent to about 21 bbl of casing volume. Most of this probably occurred during the large drop in pressure at about 165 minutes into the job (Figure 7.2.20).

However, even with the delays and operational problems, the job should not have screened out. The foam was sufficiently stable that the 10-minute shutdown should have had only negligible effect. The main focus of the post-frac stimulation analysis was to determine why screenout occurred so early.

7.2.4.5 Diagnostics

Temperature and gamma-ray surveys were performed after the treatment, but no useful information on fracture height was obtained from temperature logs during either the minifrac or the stimulation. The temperature log after the stimulation was blocked by sand at about 5775 ft.

The post-stimulation gamma ray survey run after the well was cleared is shown in Figure 7.2.22. The top of the tagged proppant is between 5805 ft and 5815 ft while the bottom is about 5860 ft.

7.2.4.6 Analysis of the Minifrac

Because of all the operational difficulties during the stimulation, and the similarity between the minifrac and the start of the stimulation (pumping of the pad), the key to understanding the main stimulation is probably to understand the minifrac. No operational problems occurred during the minifrac and all instrumentation worked adequately. As seen in Figure 7.2.18, the Nolte-Smith plot is anomalous only in the small slope. The Nolte pressure decline analysis looks good, but the leakoff coefficient

is considerably lower than previous zones that we have tested. Lengths obtained from the pressure decline analysis were also excessive.

Several pressure-history-match calculations were performed using a pseudo 3-D fracture simulator to evaluate fracture behavior. We used a Perkins and Kern geometry because of the large L/H aspect ratio and the compatibility with stress-induced height containment. The containment situation is shown in Figure 7.2.23; only stresses are considered for height growth because the large stress contrasts are expected to dwarf any other contributions from strength, modulus, etc. Note that Figure 7.2.23 has larger stress contrasts above the B sandstone than were actually measured. We could not obtain the necessary containment to produce the observed level of the treatment pressure without good containment. Since the first stress measurement point above the B sandstone was about 40 ft above the top of the B sandstone, we speculate that there may have been a layer with higher stress (overlying the sandstone) that we did not measure. As will be seen later, even this additional stress contrast is not sufficient to provide the total containment necessary. However, additional restraint on height growth is probably available from the reduced width in the high stress layers and also to inefficiencies in propagating across bedding.

Figure 7.2.24 shows two example calculations of the pressure response for estimated parameters compared to actual field data. There is no trouble matching the initial nitrogen stage, but the foam stage cannot be matched for normal conditions. The case using a 0.0005 $ft/\sqrt{min}$ leakoff coefficient matches the initial pressure rise and the long-term pressure decay, but it results in a pressure that continues to increase to a level that is much too high. While the maximum pressure level for the higher leakoff coefficient is better, the initial pressure rise and the shut-in response cannot be matched.

Examining the field pressure data, the interesting feature is the sudden flattening in the pressure at a level 1050 psi above the closure stress during pumping and the rapid drop to this same level at shut-in, after which the pressure decreases much more slowly. We first tried to match this

behavior using enhanced height growth. While height growth can flatten the pressure during pumping, it also causes a very slow pressure decline at shut-in. Additional leakoff height was added as height grew, but this could not flatten the pressure as much as needed. Finally, we tried an accelerated leakoff condition above 1050 psi. This was done by increasing the leakoff coefficient by a constant factor above some threshold value. To keep the results smooth and code convergent, the increased leakoff was actually linearly phased in between 1000 and 1100 psi. The final result of these calculations is shown in Figure 7.2.25; a factor of 50 increase in the leakoff coefficient was required to match the data for pressures above 1050 psi.

There are two possible mechanisms for this accelerated leakoff that seem reasonable here. The first is the possibility that the natural fractures begin to open at pressure levels above the threshold value. ASR data suggests that the difference in horizontal stresses in this zone is 600-800 psi, about the value of the pressure threshold. The second possibility is that at this pressure threshold value, there is just enough height growth (10-15 ft up and down) to break into some of the thin siltstones above and below the sand. Many of these siltstones have wide-open natural fractures and these may be taking excessive fluid.

In either case, the accelerated leakoff due to natural fractures is the only mechanism that seems to give a close pressure-history match with the field data. The length at the end of pumping was about 800 ft and the length after 10 minutes of shut-in was 910 ft (and growing very little). The maximum height was 52 ft, compared to an initial zone height of 22 ft, so containment was relatively good (this is with the additional stress contrast).

7.2.4.6 Analysis of the Stimulation

The accelerated leakoff hypothesis explains the early screenout seen in the stimulation and a history-match of the main treatment was performed to show how this would occur. Figure 7.2.26 shows the best history match for the entire treatment that we could obtain, including all of the operational

problems. The initial nitrogen pressure-up/fracture stage and the pad used the same parameters as were determined by the minifrac. The behavior is similar to the minifrac and the accelerated leakoff occurs at the same threshold pressure. When sand out occurred at the surface and the well was shut in for 12 minutes to clear the lines, only pad was in the formation and the pressure decline was also matched by the minifrac parameters.

Soon after pumping resumed, the sand hit the perfs and the pressure continued to rise well above the level found during the pad. This was accounted for by increasing the viscosity of the slurry caused by dehydration of the slurry due to the high fluid loss above the threshold pressure. This apparent increase in viscosity continues into the 3 ppg stage until the pressure begins to rise on a unit slope in the Nolte-Smith plot and a screenout occurs. When this happens there is still a large pad volume in the fracture, but it is out towards the fracture tip where the pressure is less than the threshold value. The screenout is not due to pad depletion, but rather to dehydration of the sand slurry until it is no longer movable.

The first small pressure drop after the start of the screenout (at 58 minutes in Figure 7.2.26) is due to the rate change that occurred at the start of flush (no longer pumping sand). The next two pressure drops (at 60 and 70 minutes) are probably caused by movement of the bridge plugs set below the interval. The extra volume of the casing that was available after the bridge plugs moved is known and we appropriately subtracted that volume from the volume injected into the fracture to achieve the match. During all these complications the screenout continued, reaching a final bottom-hole pressure of 6600 psi, about 2200 psi above closure.

This is by no means a unique solution to this stimulation, but it does show consistency between the minifrac and the stimulation, and also shows a plausible mechanism for the very early screenout. Additionally, the pressure drops observed during the screenout are consistent with the volume of wellbore exposed when the bridge plugs moved. Using this history match, total frac-wing length is 1060 ft but the propped length is only 318 ft. This happens because the pad, which is at low pressure, is very efficient.

Closer to the wellbore, where the sand is present, the pressure is above the threshold value and fluid is lost rapidly, thus dehydrating the prop.

At the time of screenout, the heights are large (>150 ft) in the near wellbore region, because of the high pressure, but they rapidly decrease to less than 50 ft within 100 ft of the wellbore. After screenout, the model was restricted so as not to allow additional height growth, because the screenout condition occurs throughout the sand-laden volume, rather than from a pad-depletion mechanism. Needless to say, conductivities within the fracture are likely to be quite high, because of a wide fracture produced by the screenout. Unfortunately, these high pressures at the end of the screenout make it quite likely that the formation, and particularly the natural fractures, have been significantly damaged by injection of liquid and gels. Even without a screenout, the accelerated leakoff probably causes damage to the natural fractures because fluid is injected when the natural fractures are dilated, but clean-up occurs when they are closed.

7.2.5 CONCLUSIONS

The nitrogen step-rate test gave a fracture extension pressure of about 4650 psi, which suggests that the closure stress is around 4450 psi. The nitrogen flow-back tests were not totally conclusive, but they suggest that the minimum possible closure stress is 4270 psi. One test showed a slight reversal in curvature at about 4400 psi. This value (4400 psi) was used for all subsequent analyses, although it is recognized that the possible error is $\pm$150 psi.

The reason for the early screenout in this job is probably an accelerated leakoff phenomenon that occurred above the threshold pressure of 1050 psi. This is likely due to either opening of natural fractures in zone or to height growth into open natural fractures that are prevalent in thin siltstones in this interval. While there were several operational difficulties (sand outs, bridge plug failures), they do not appear to have affected the results. However, they certainly complicated the analysis.

Well test results have shown that some of the stimulations at MWX have damaged the natural fractures. The accelerated lockoff mechanism appears to be a plausible mechanism for the damage. If the natural fractures in the zone open up during the treatment, then gel from the foam is readily injected into those natural fractures when they are dilated; on the other hand, frac-fluid recovery is attempted when the fractures are closed during drawdown. Thus, it is not unrealistic to expect damage. Even if the accelerated leakoff is due to height growth into fractured siltstones, the high pressure during the screenout could still have injected gel into the fractures.

This stimulation experiment again shows the value of a minifrac for evaluating treatment results. In this case, sufficient time was not allowed between the minifrac and the stimulation for a complete analysis, or we might have discovered the accelerated leakoff phenomena and tried some leakoff additive such as 100-mesh sand to minimize the deleterious results. This also shows that a pressure-history match should be used in tandem with the Nolte pressure decline in the minifrac analysis if a complete analysis is desired.

7.2.6 REFERENCES

1. Cipolla, C., Branagan, P., Wilmer, R. and Ferguson, D., "Fluvial B Fracturing QC and Operational Data," CER Corp Memorandum, February 2, 1987.

2. Thorne, B. J. and Morris, H. E., "Advances in Borehole Seismic Fracture Diagnostics," SPE 16405, proceedings 1987 SPE/DOE Joint Symposium on Low Permeability Reservoirs, Denver, CO, pp 165-172, May 1987.

3. Nolte, K. G., "A General Analysis of Fracturing Pressure Decline with Application to Three Models," SPE Formation Evaluation, Vol. 1, pp 571-583, December 1986.

4. Nolte, K. G. and Smith, M. B., "Interpretation of Fracturing Pressures," J. Pet. Tech., Vol. 33, pp 1767-1775, September 1981.

Table 7.2.1

Step-Rate Test Data

Surface Rate (SCFM)	Bottom-Hole Rate (bpm)	Bottom-Hole Pressure (psi)
600	0.5	4370
825	0.7	4655
1220	1.0	4770
1850	1.4	4840
3900	3.0	5000
5840	4.4	5100
7670	5.6	5185
9050	6.5	5215

Table 7.2.2

Summary of Flow-Back Results

Test	Curvature Reversal (psi)	Curvature Minimum (psi)
Step-Rate	-	4260
2	-	-
3	-	4270
4	4410	4270

Table 7.2.3

Minifrac Design

Stage	Fluid	N_2 Rate (SCFM)	Foam Rate (bpm)	Foam Volume (gal)
Pressure Up	N_2	12,000	-	-
Minifrac	Foam	12,000	10	8000
Flush	Foam	12,000	10	7770

Table 7.2.4

Stimulation Design

			Rates	
Stage	Volume (gal)	Sand (ppg)	N_2 (SCFM)	Slurry (bpm)
Pressure Up	-	-	12,000	0
Pad	8000	-	12,000	2.5
1	2500	1	12,000	2.9
2	2500	2	12,000	3.8
3	9000	4	12,000	4.3
Flush	7770	-	12,000	2.5

Total Injected--22,000 gal Foam, 46,000 lb Proflow

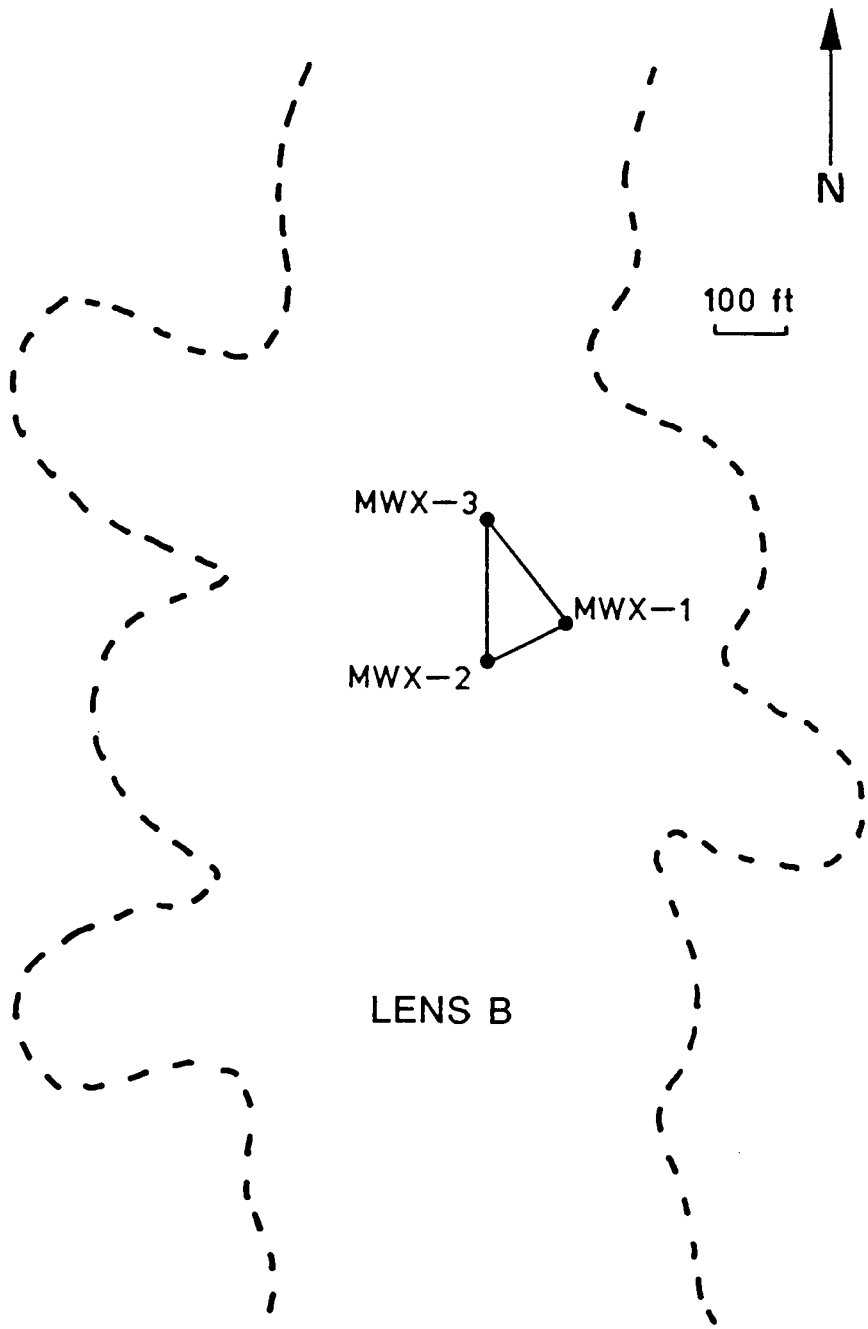

Figure 7.2.1. Possible Lens Sizes/Orientations for the Fluvial B Zone

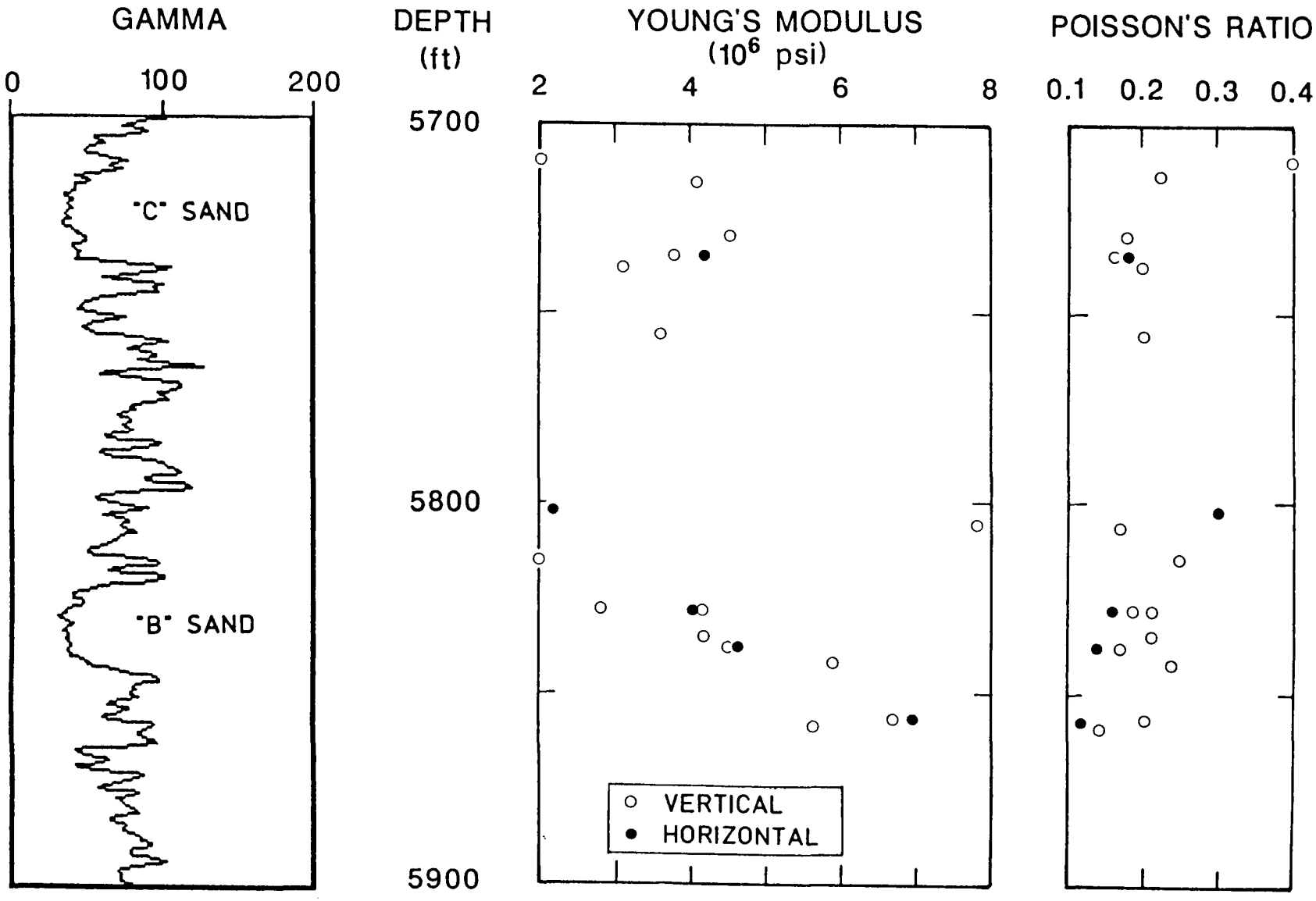

Figure 7.2.2. Rock Properties

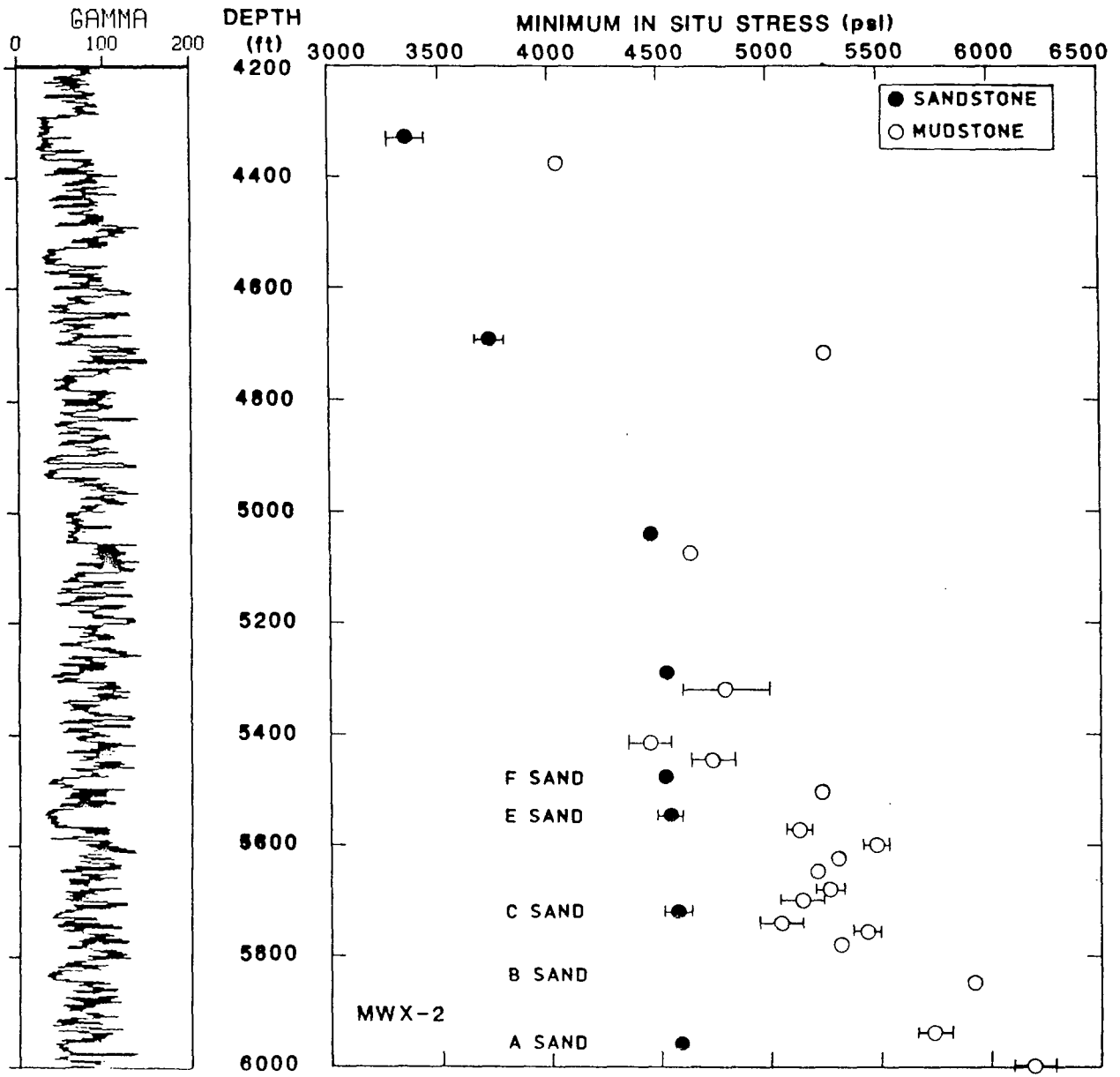

Figure 7.2.3. In Situ Stress Data

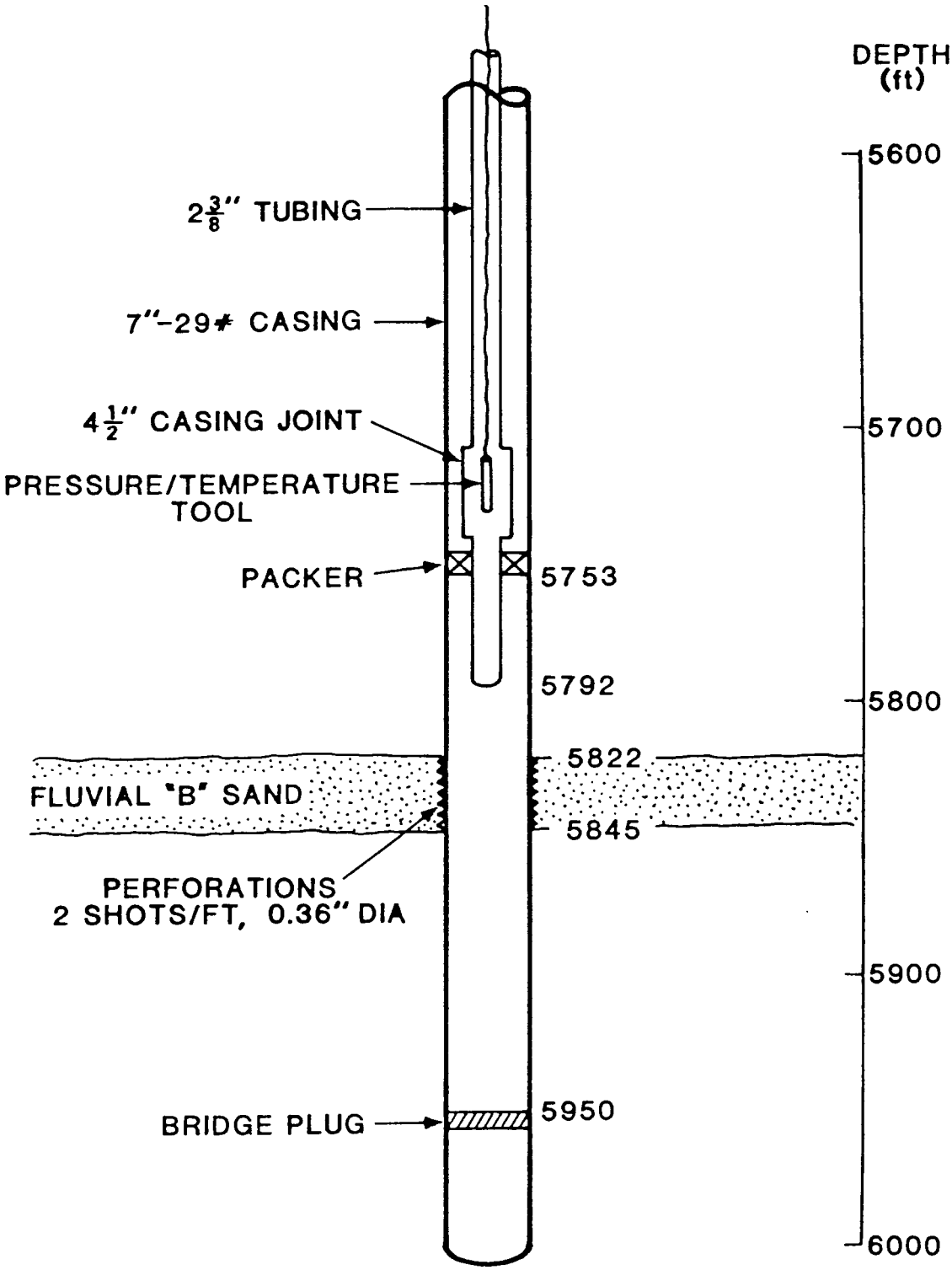

Figure 7.2.4. MWX-1 Configuration

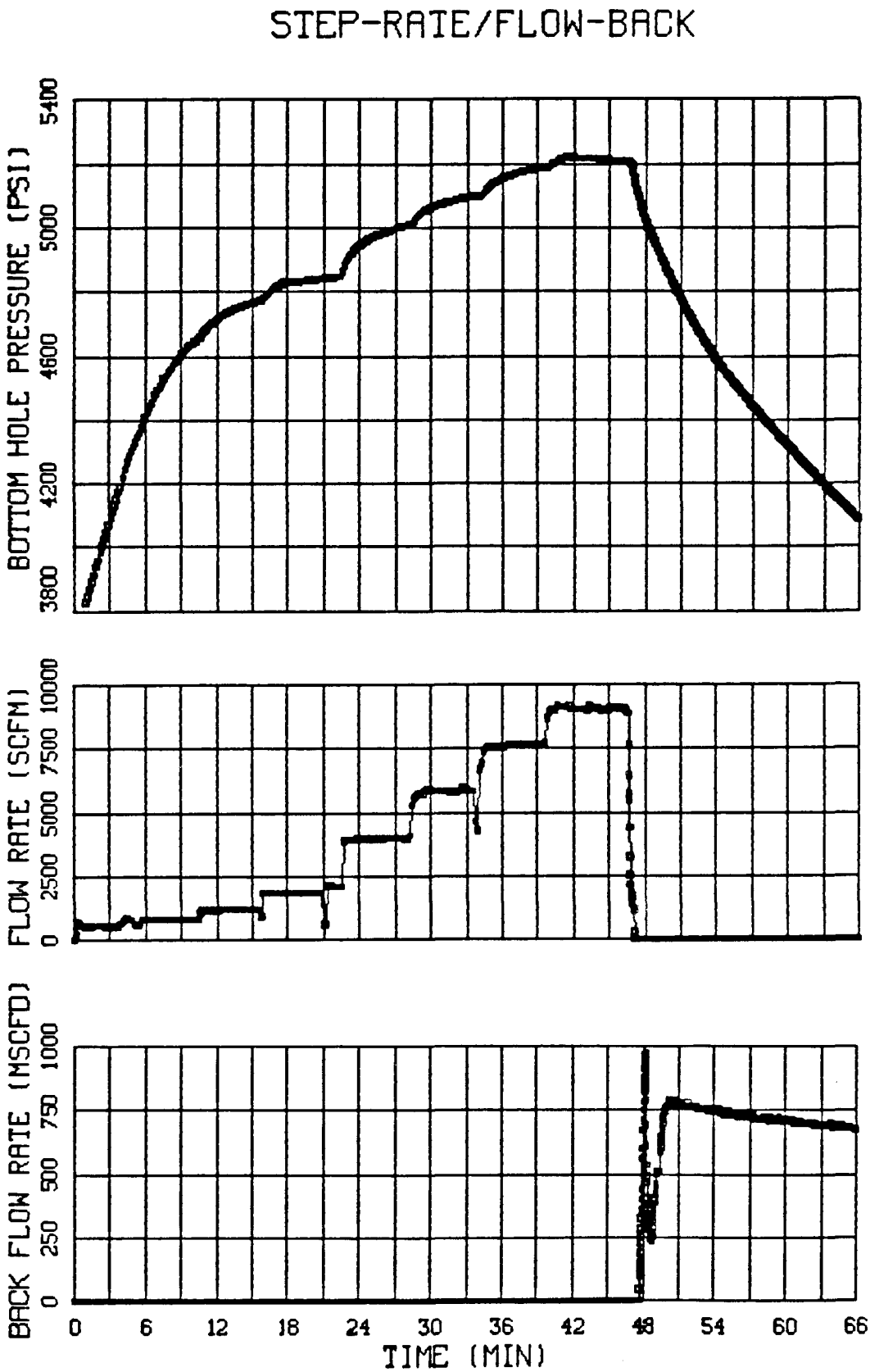

Figure 7.2.5. Step-Rate/Flow-Back Data

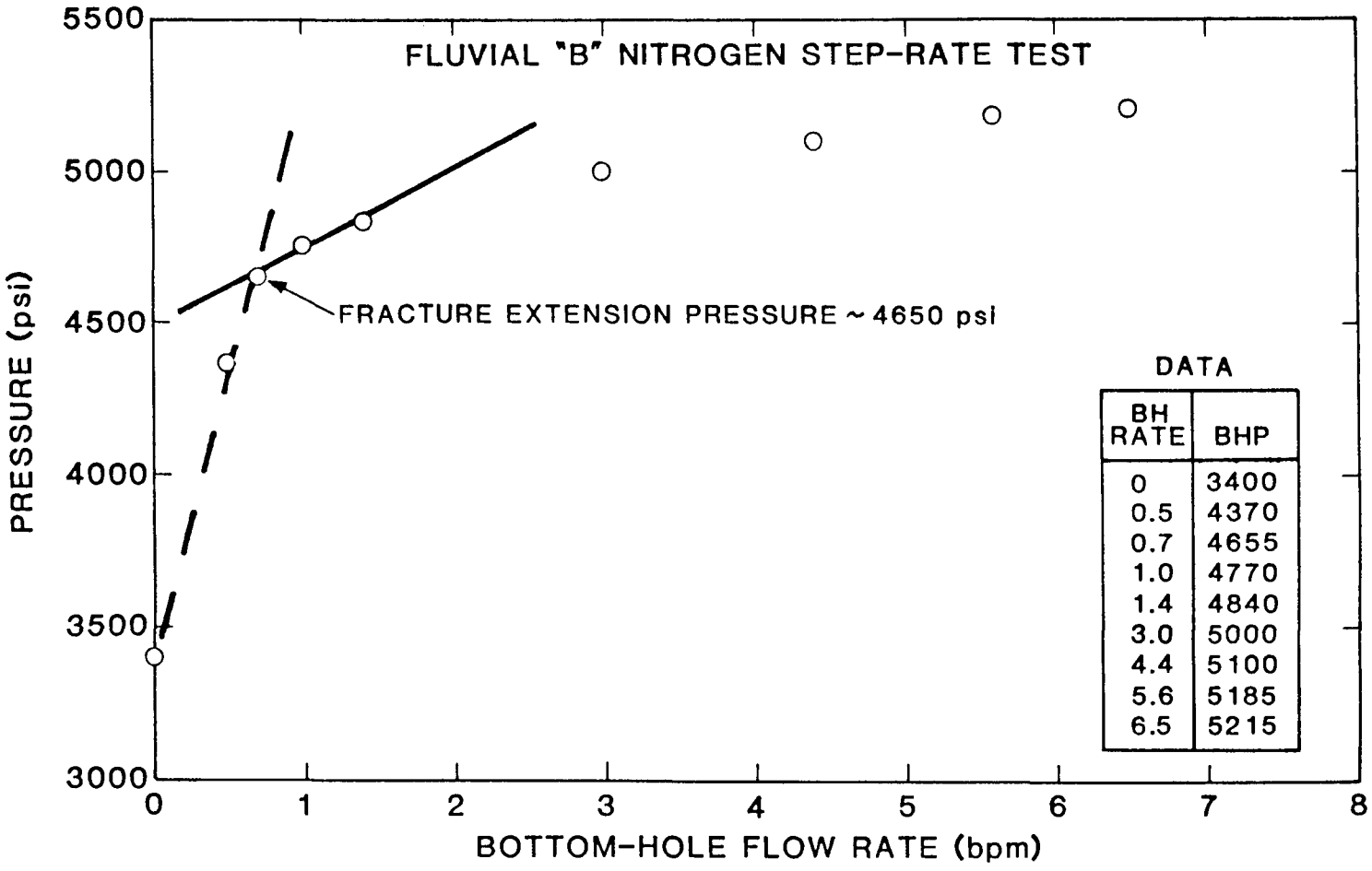

Figure 7.2.6. Step-Rate Test Results

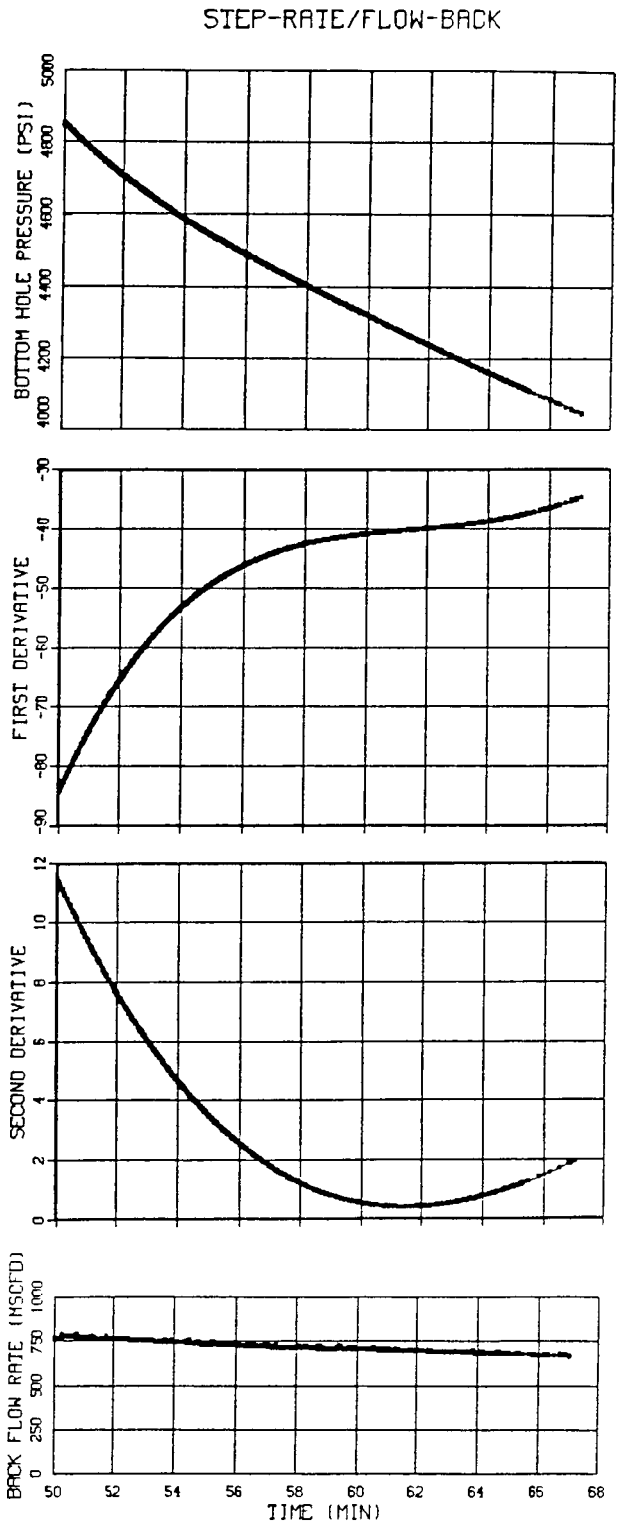

Figure 7.2.7. Flow-Back Results After Step-Rate Test

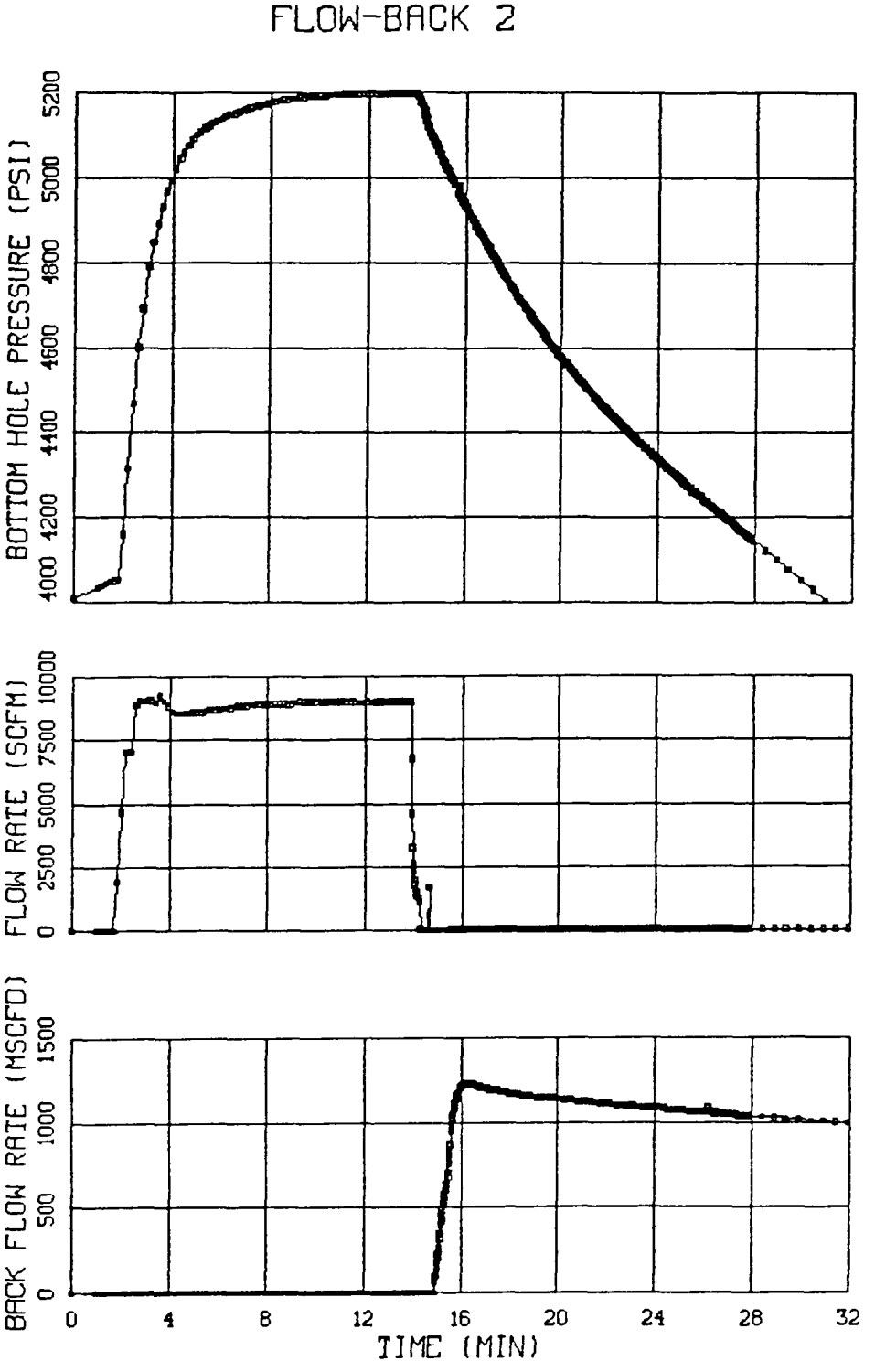

Figure 7.2.8. Pump-In/Flow-Back Test #2

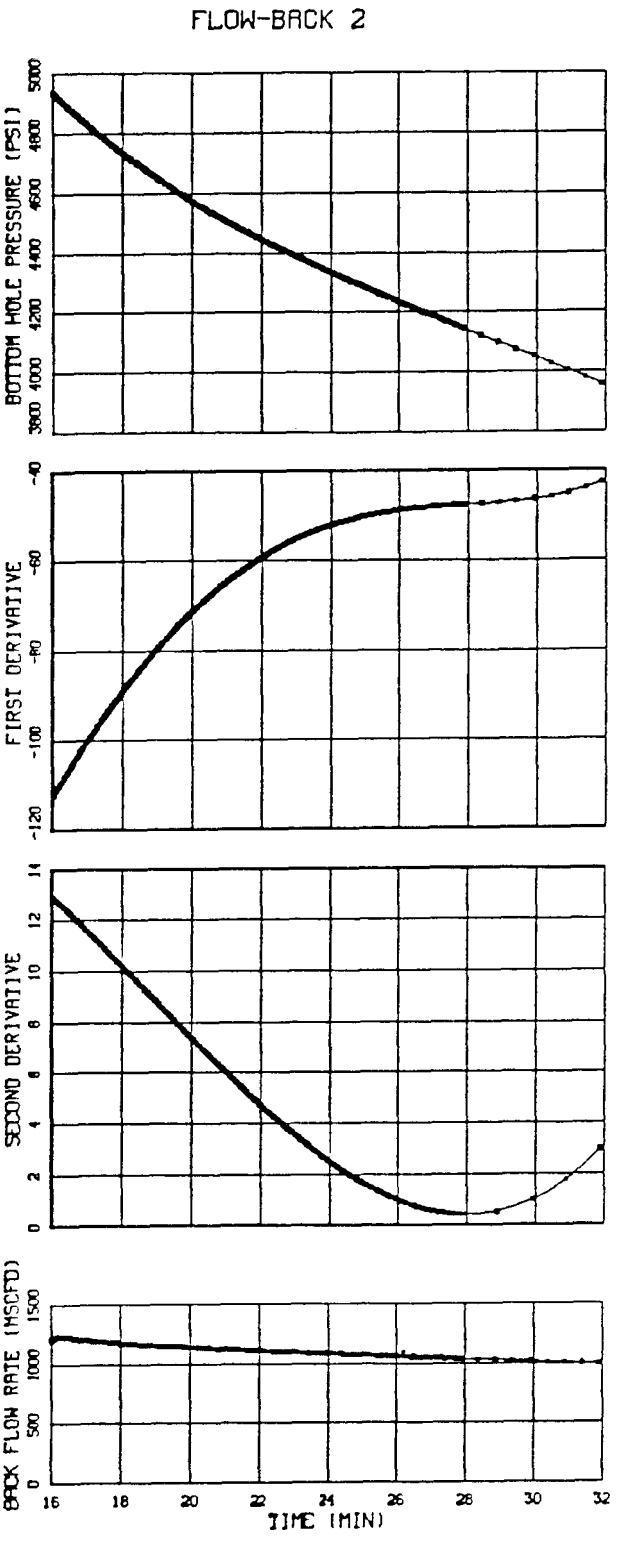

Figure 7.2.9. Flow-Back #2 Results

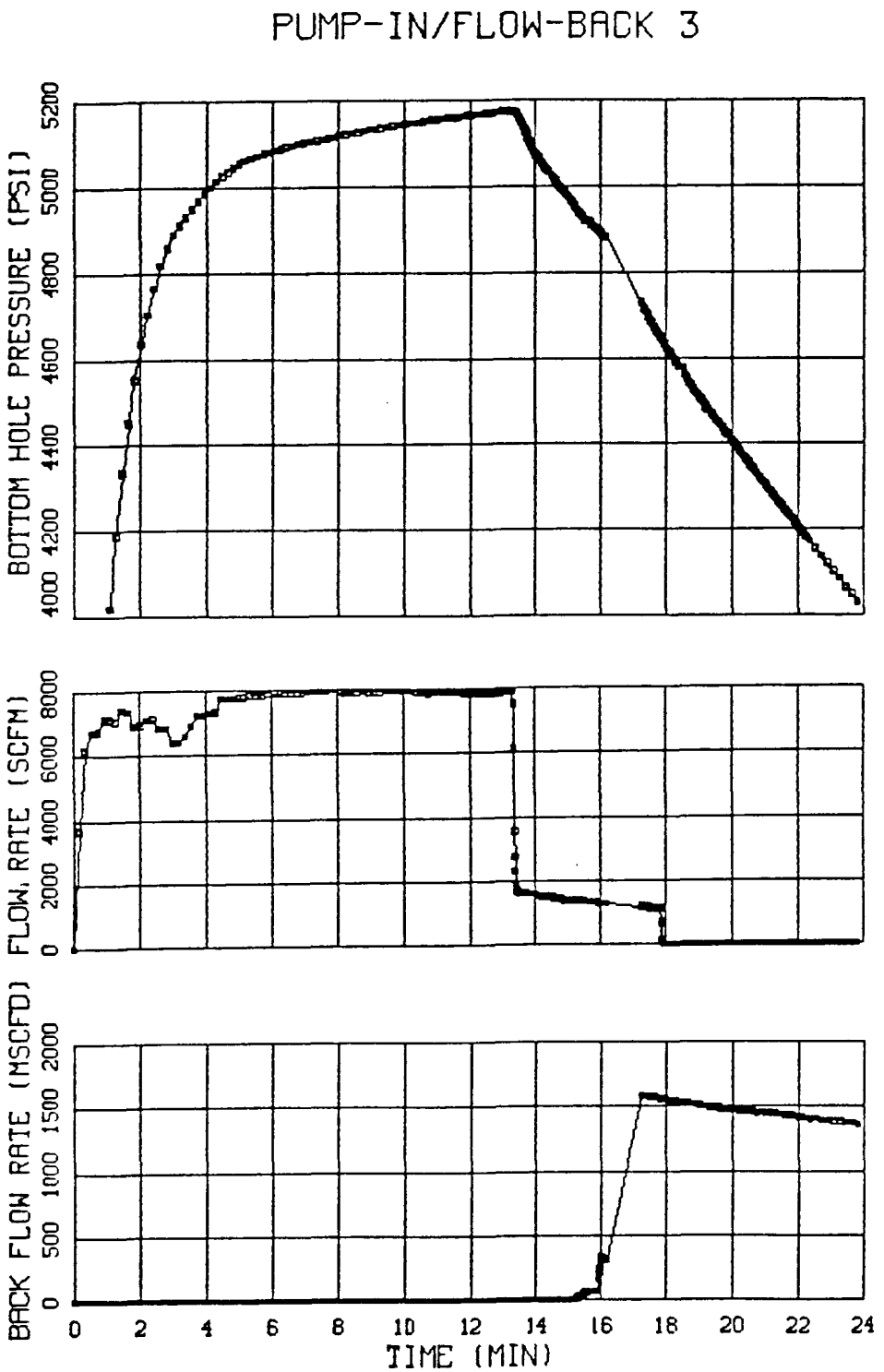

Figure 7.2.10. Pump-In/Flow-Back Test #3

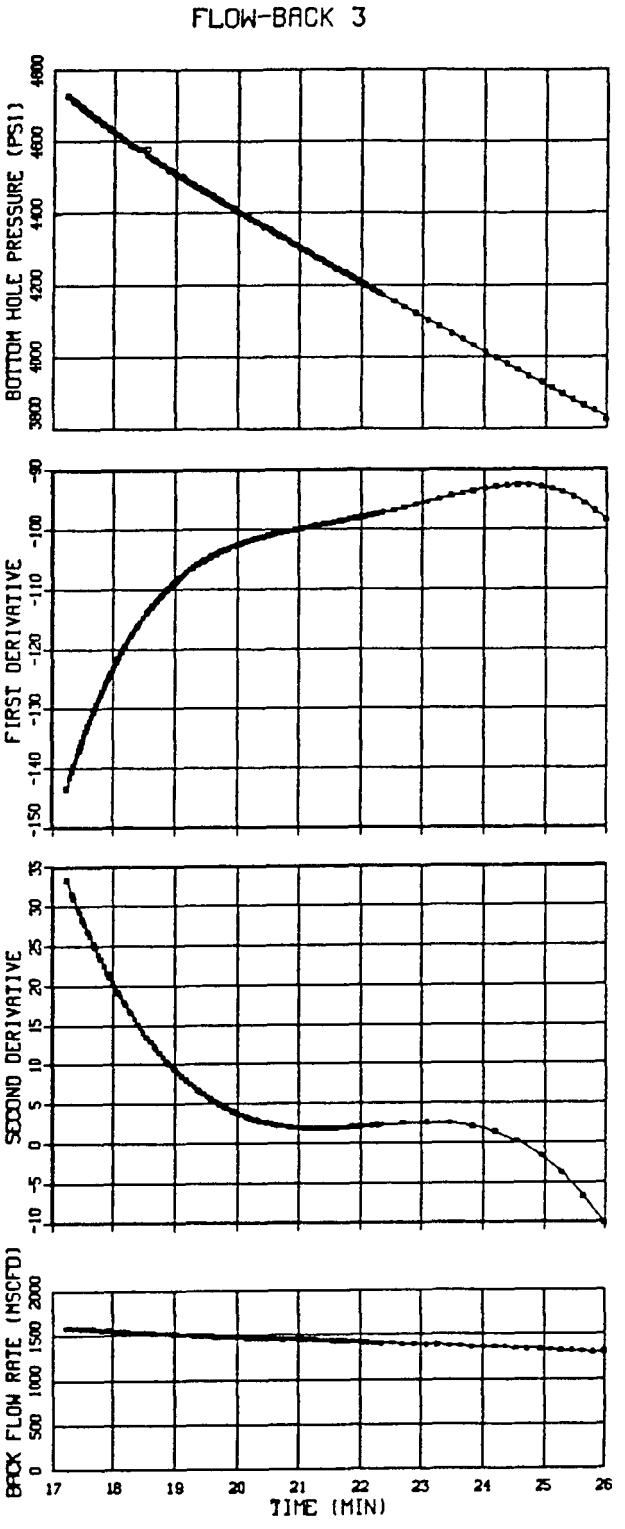

Figure 7.2.11. Flow-Back #3 Results

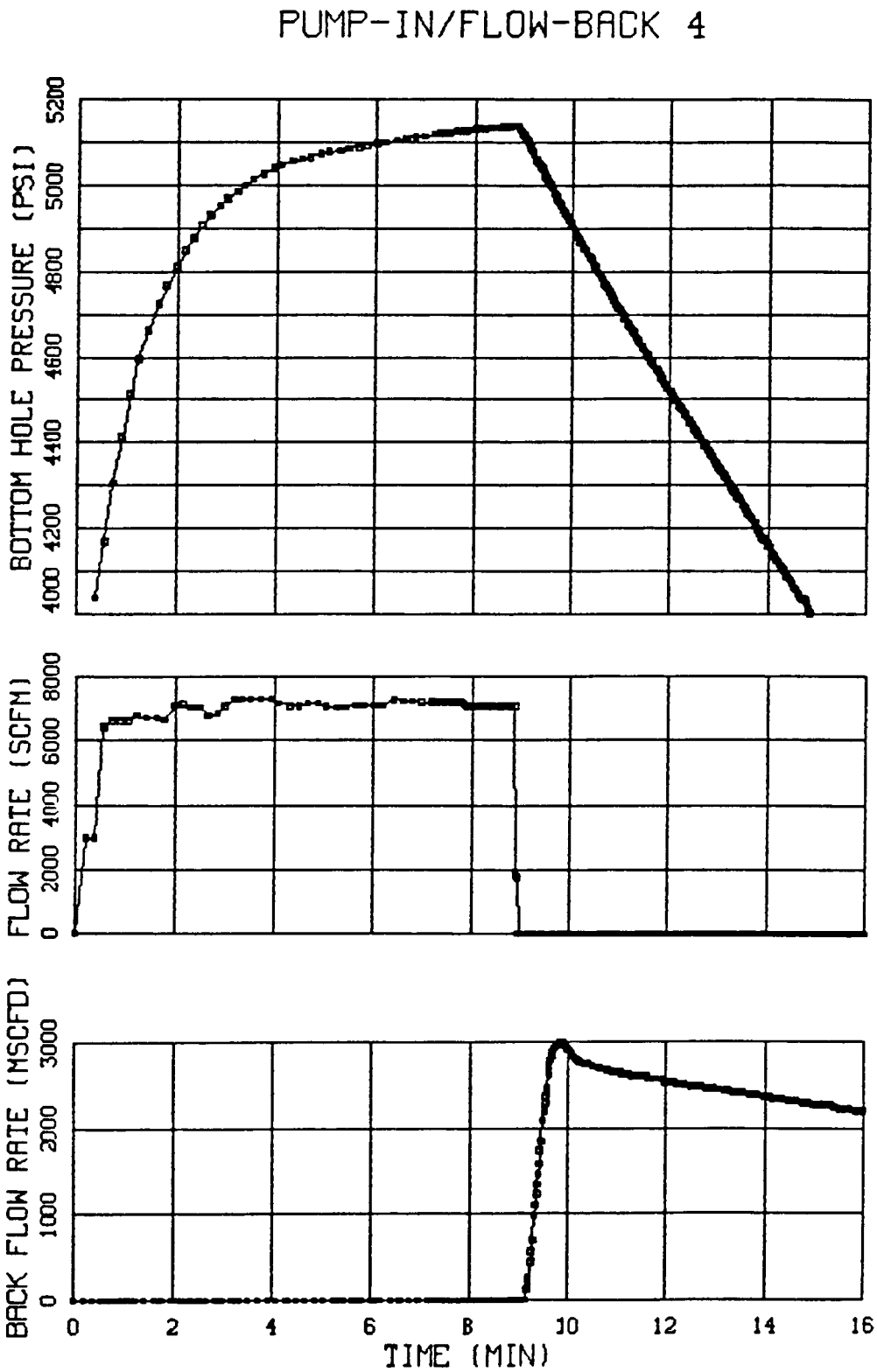

Figure 7.2.12. Pump-In/Flow-Back Test #4

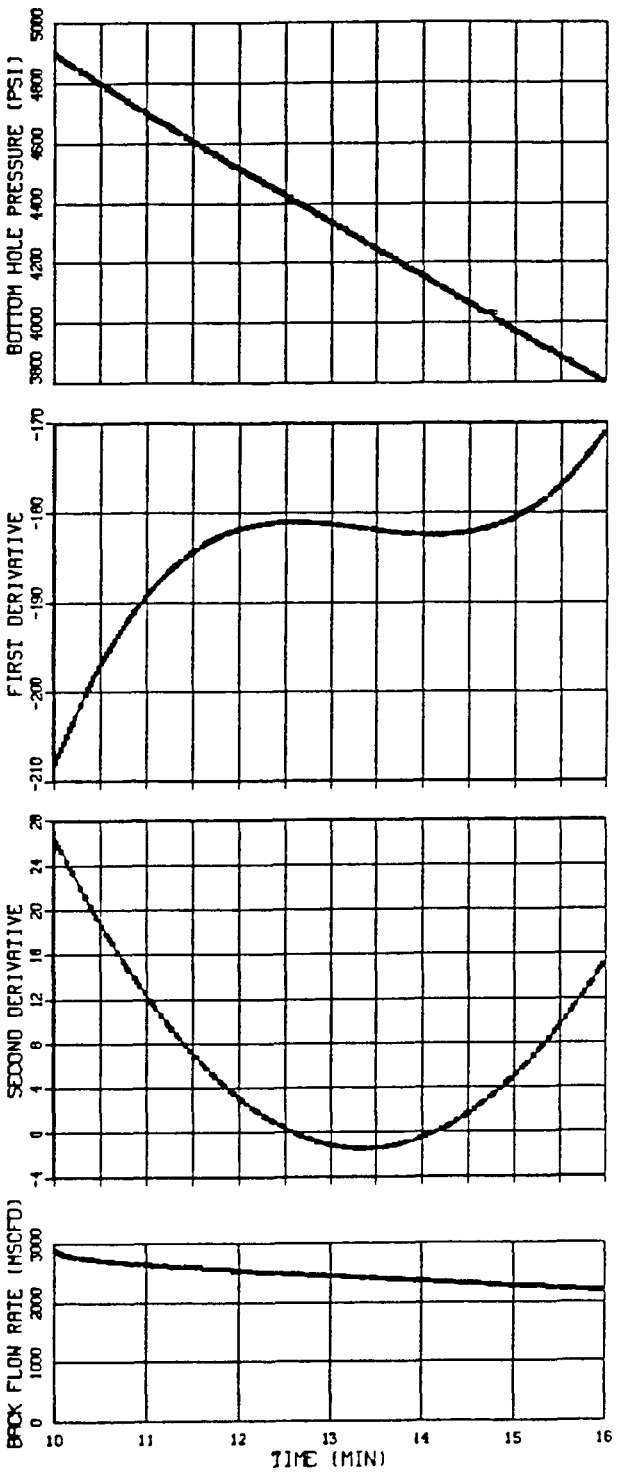

Figure 7.2.13. Flow-Back #4 Results

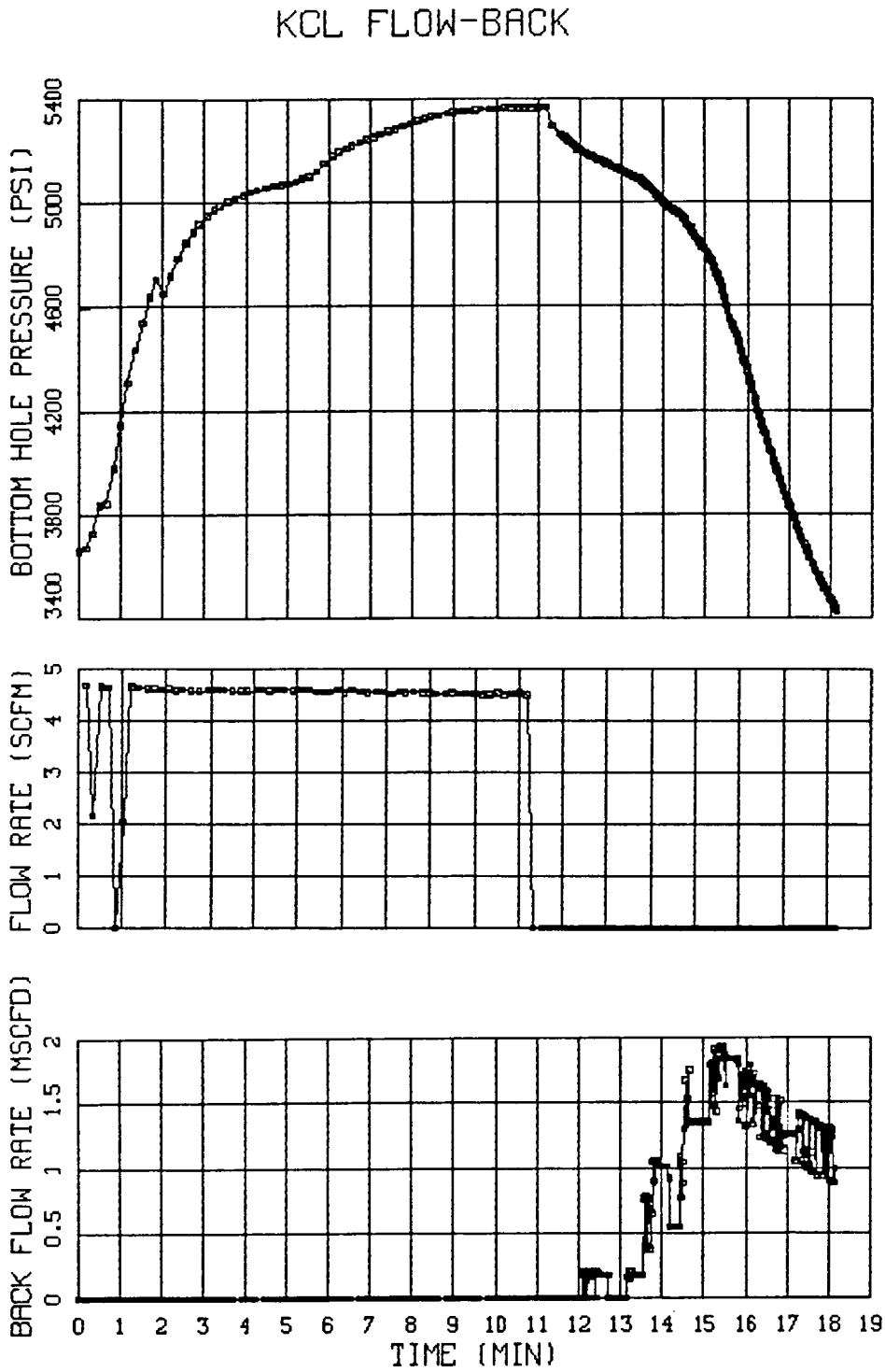

Figure 7.2.14. KC1 Flow-Back Data

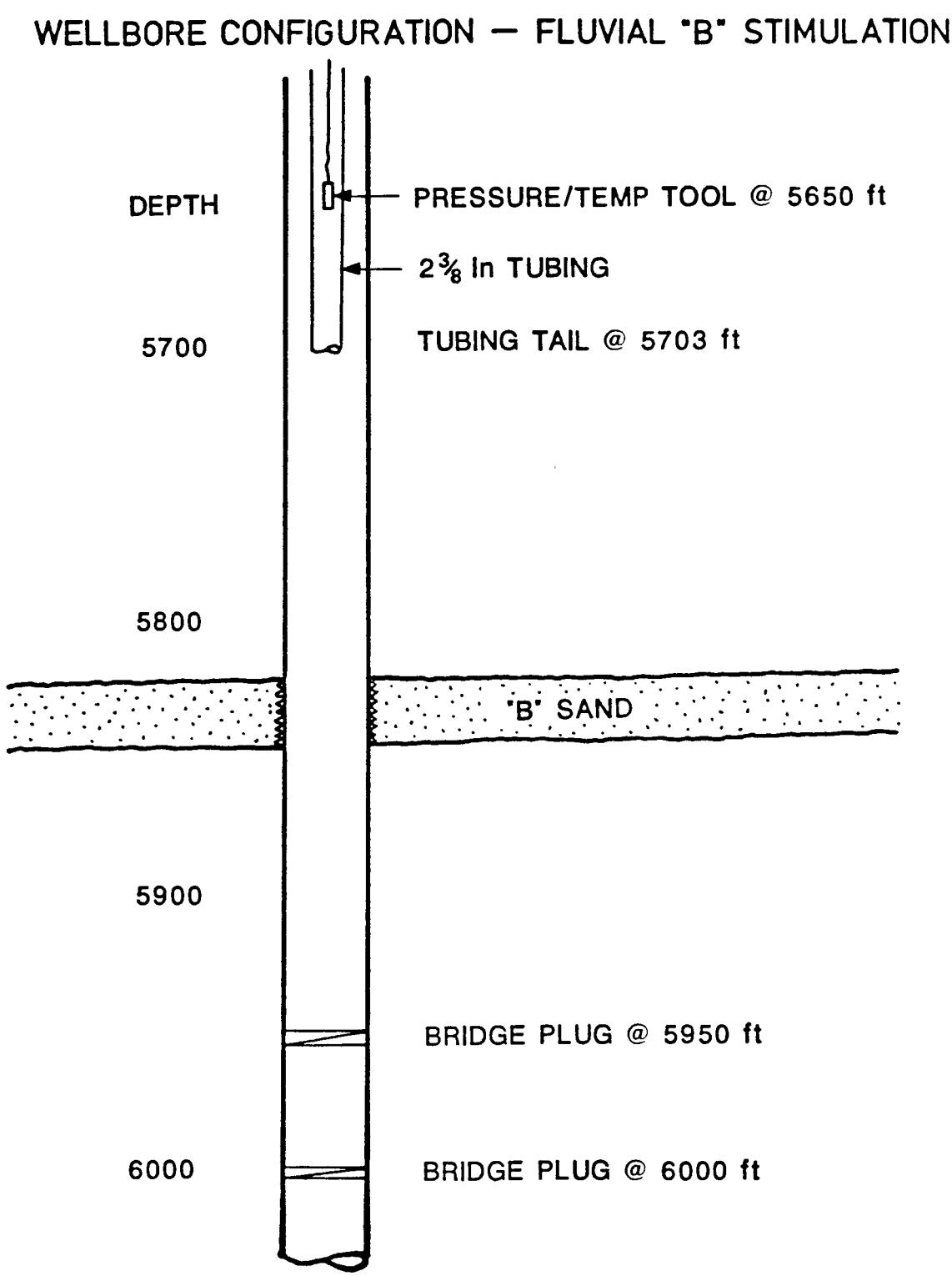

Figure 7.2.15. Wellbore Configuration

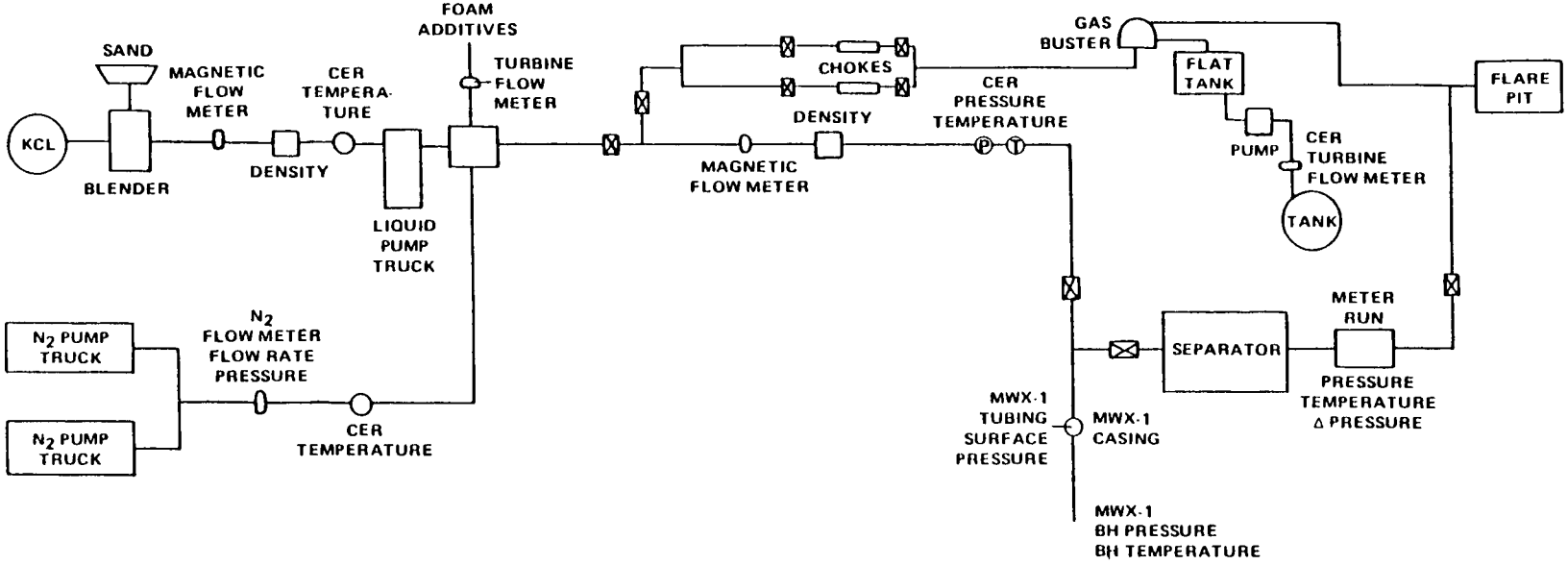

Figure 7.2.16. MWX Fluvial "B" Foam Fracture Treatment Instrumentation Diagram

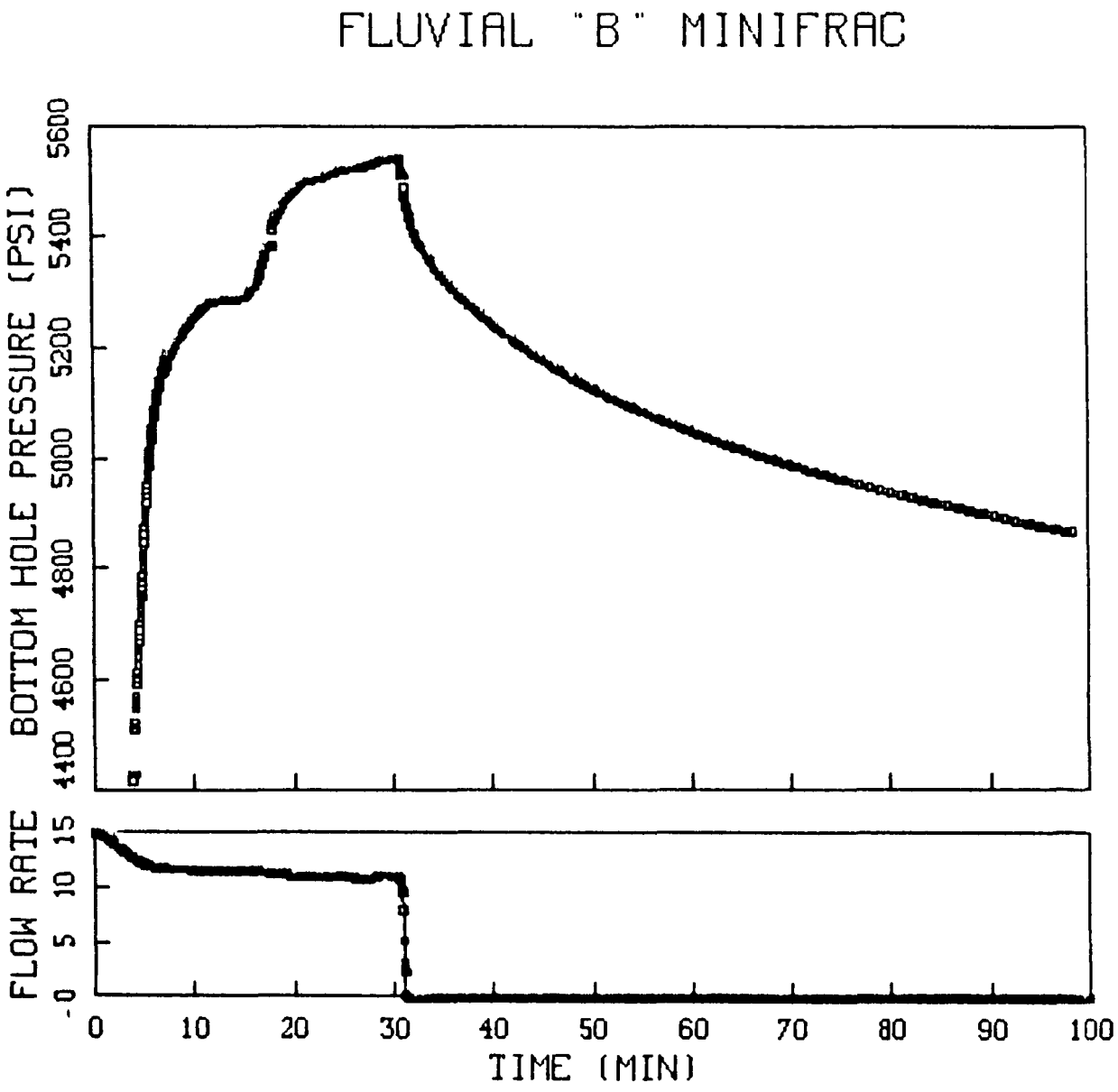

Figure 7.2.17. Minifrac Data

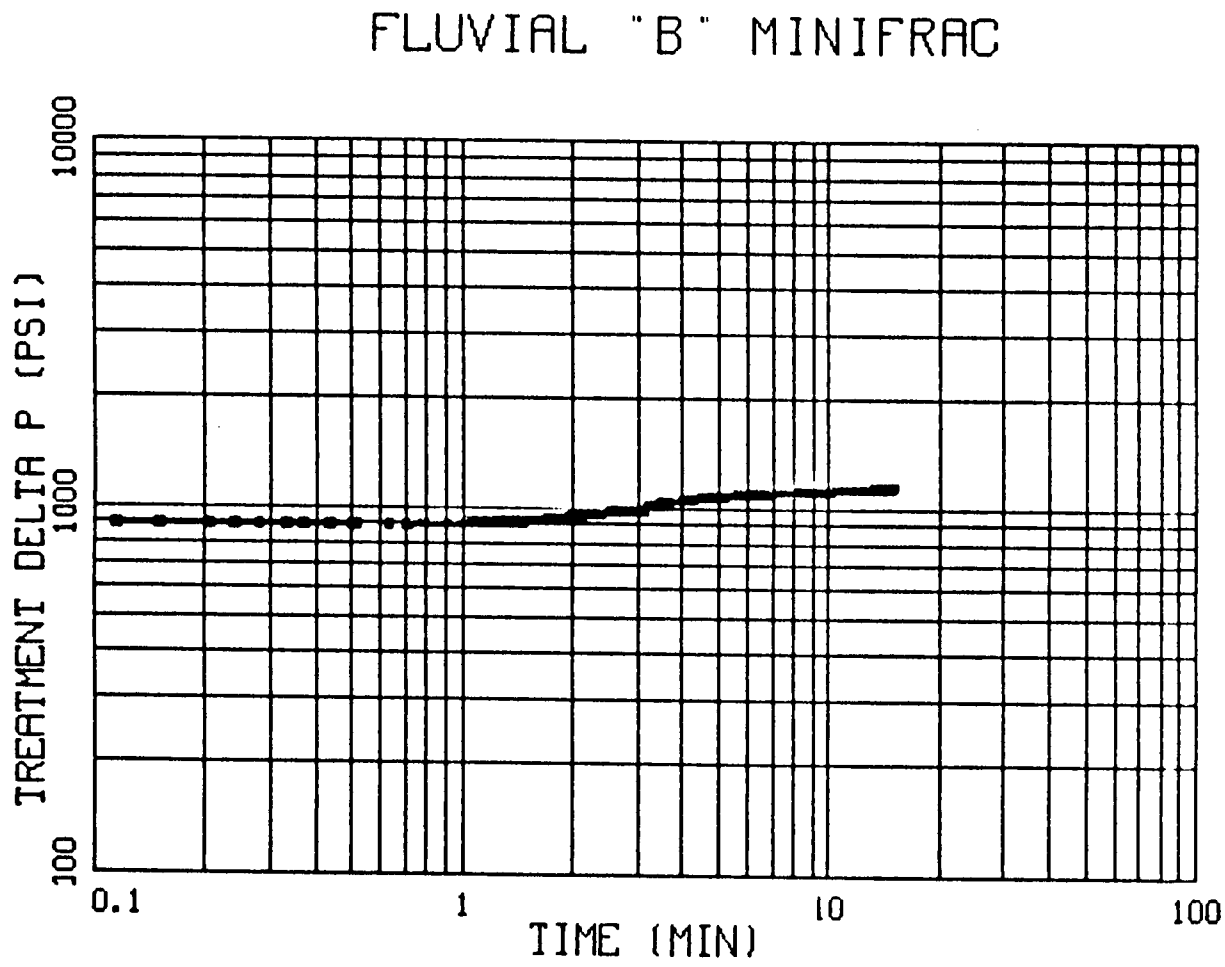

Figure 7.2.18. Minifrac Nolte-Smith Plot

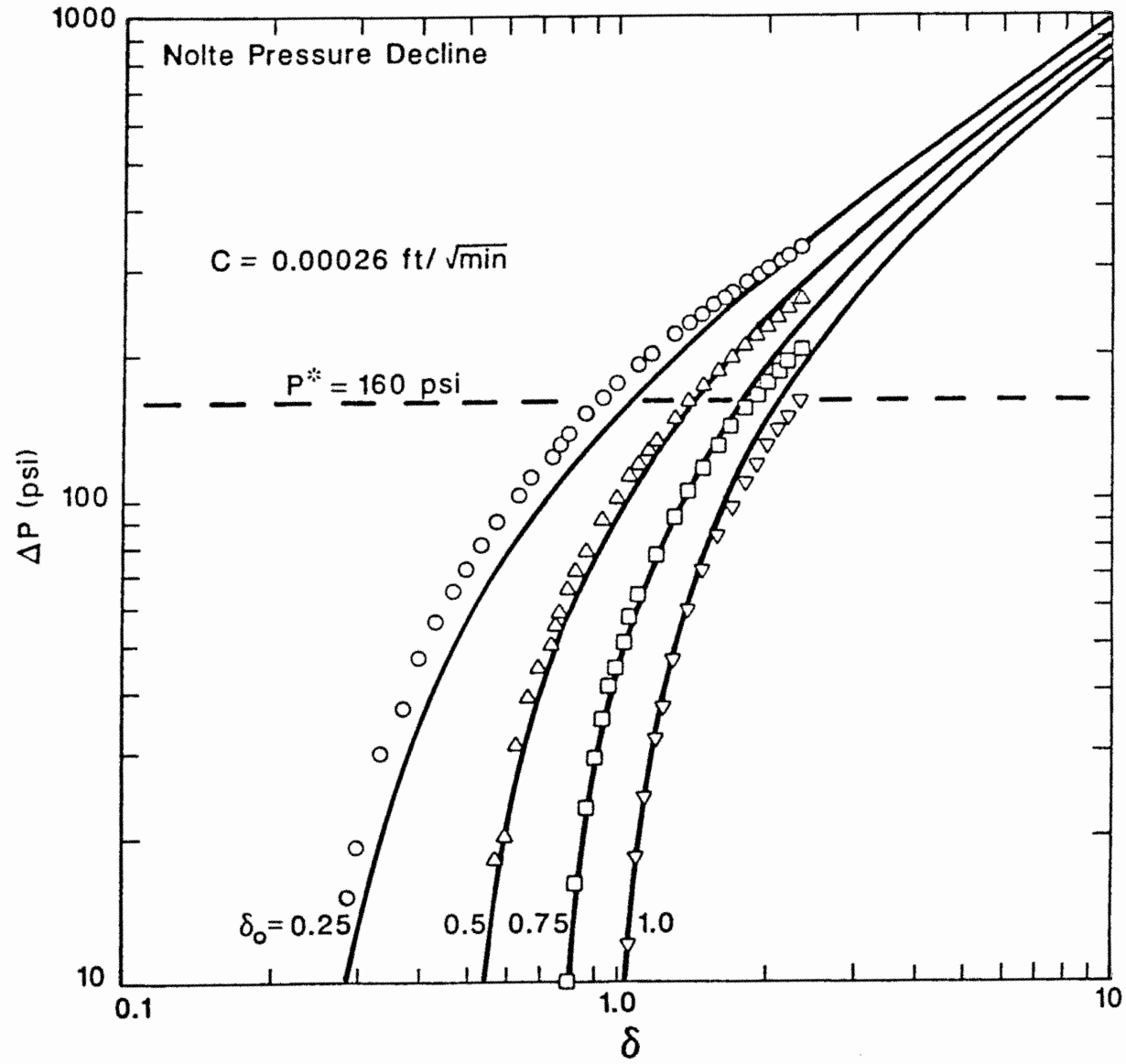

Figure 7.2.19. Minifrac Nolte Pressure-Decline Type Curve

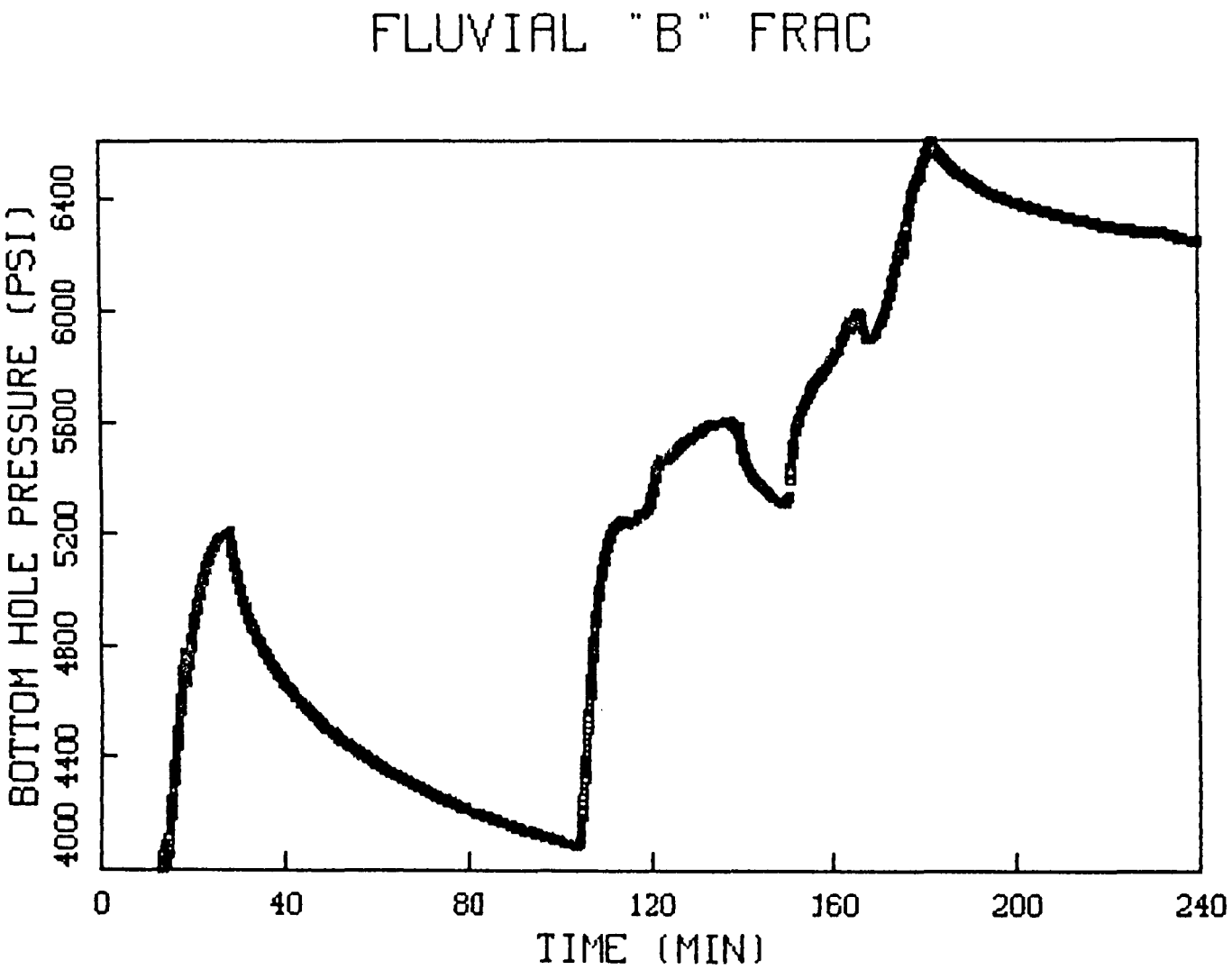

Figure 7.2.20. Stimulation Data

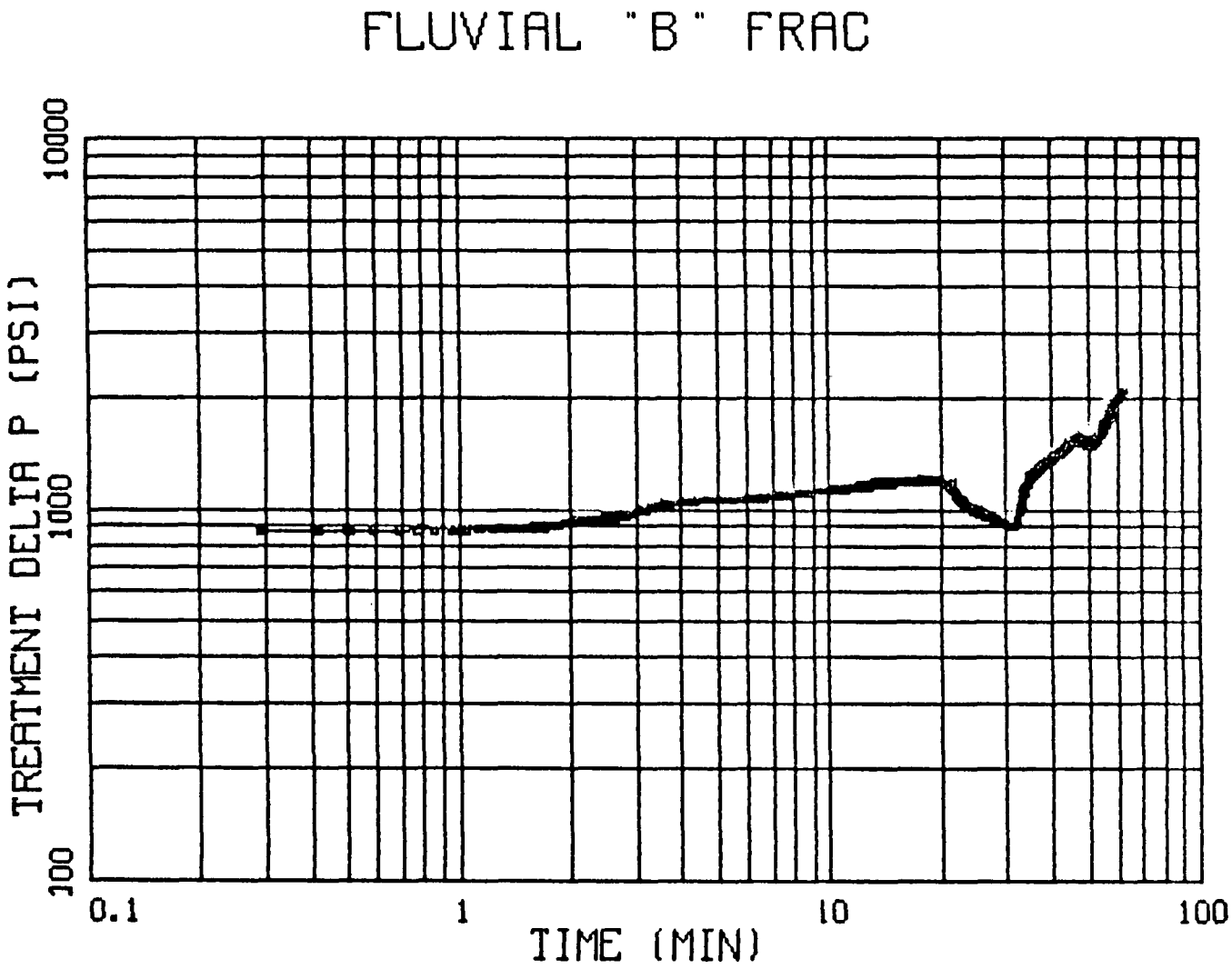

Figure 7.2.21. Stimulation Nolte-Smith Plot

PRE & POST-FRAC GAMMA SURVEYS
FLUVIAL "B" STIMULATION

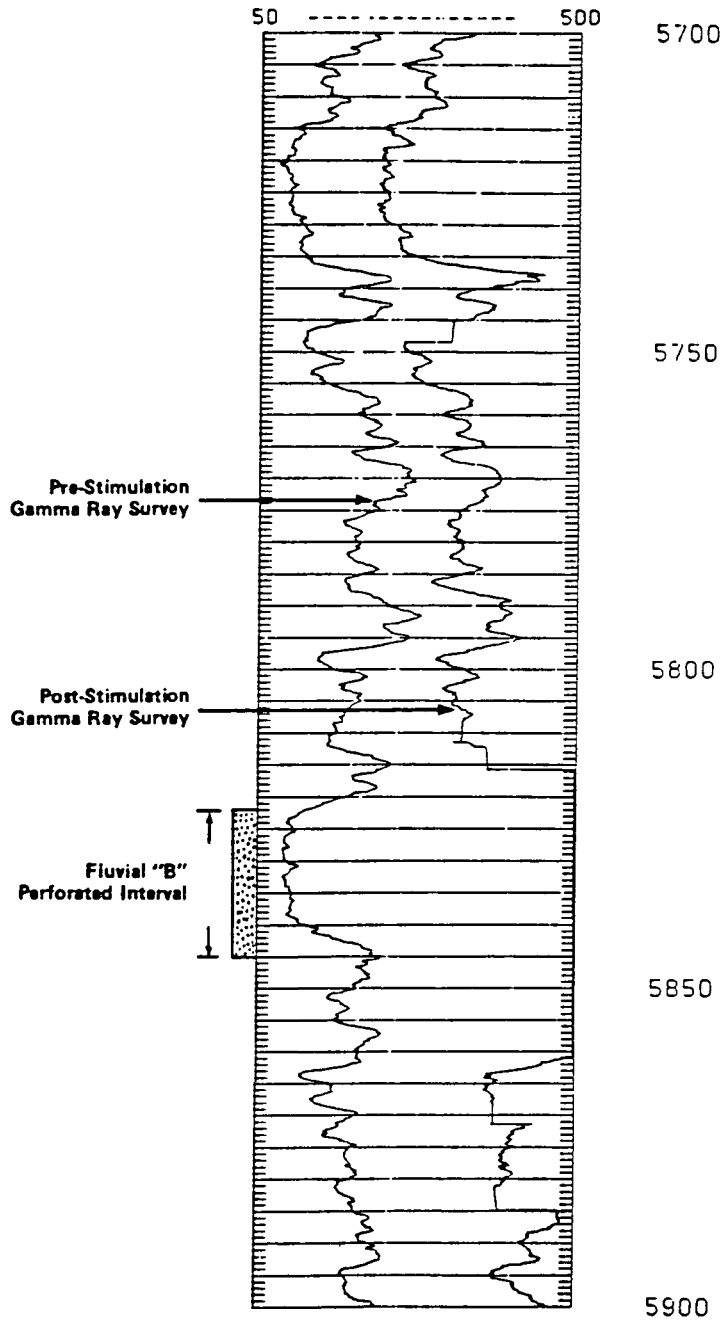

Figure 7.2.22. Gamma Survey

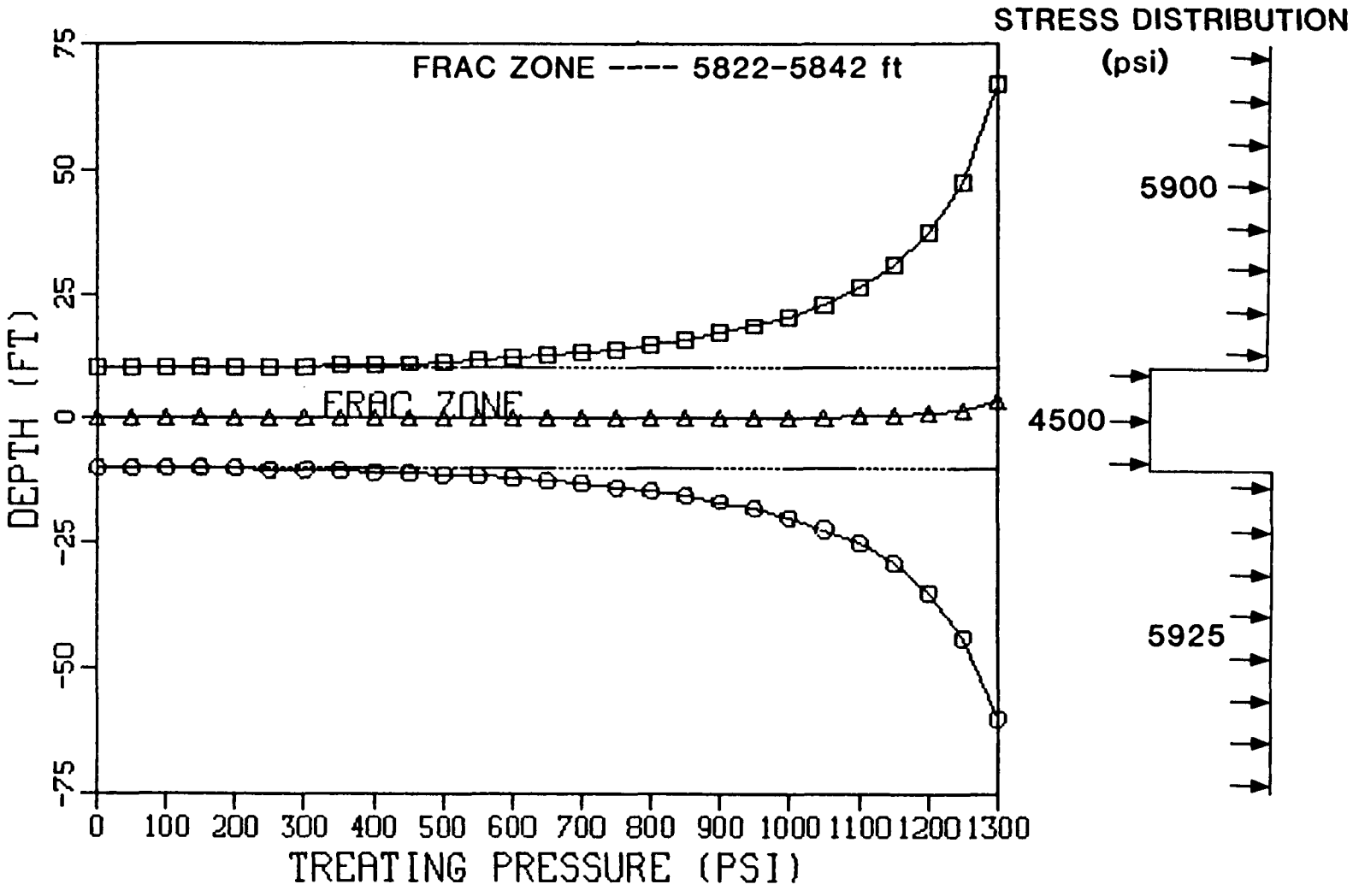

Figure 7.2.23. Containment for "B" Sand

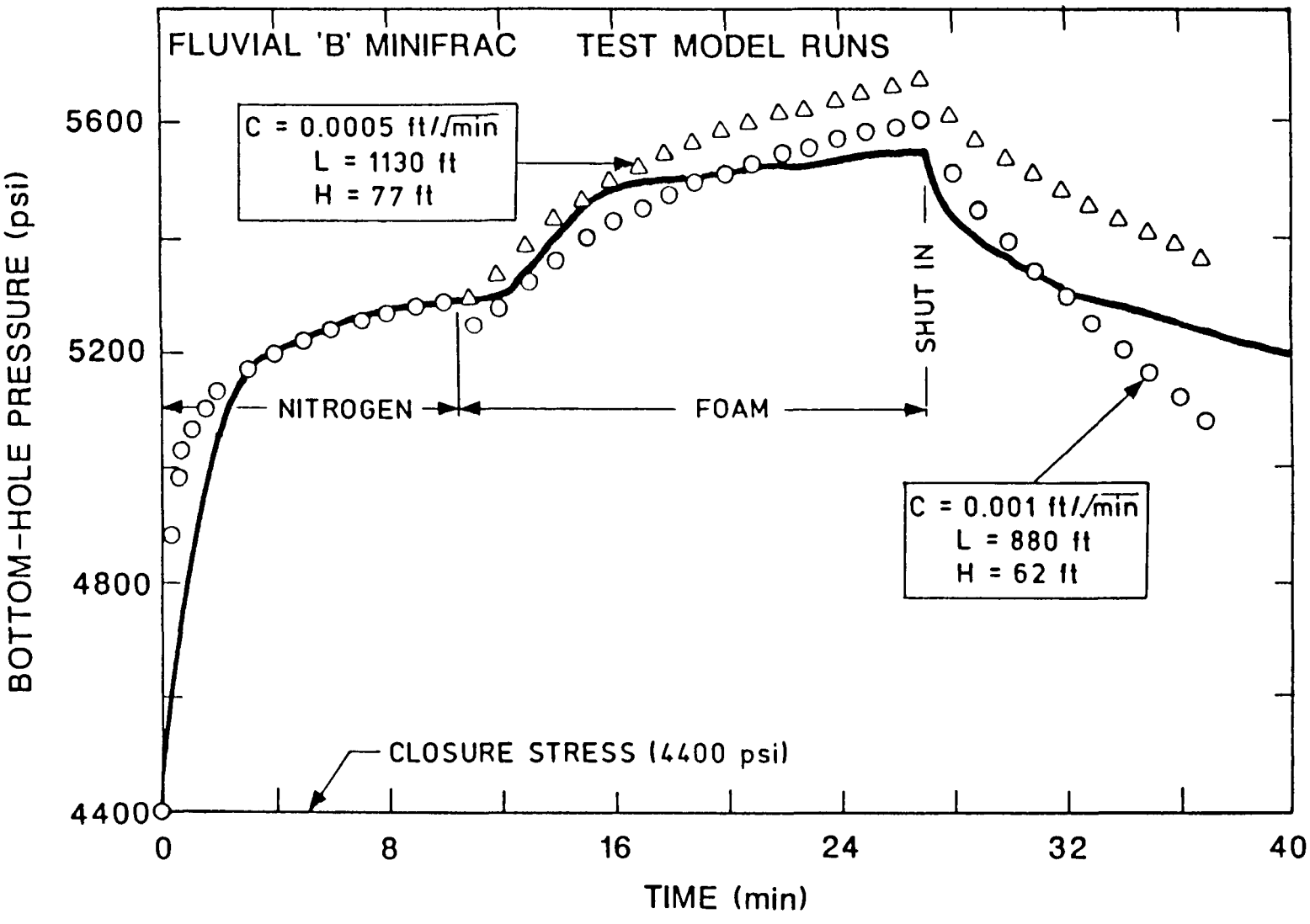

Figure 7.2.24. Initial History-Match Calculations for the Minifrac

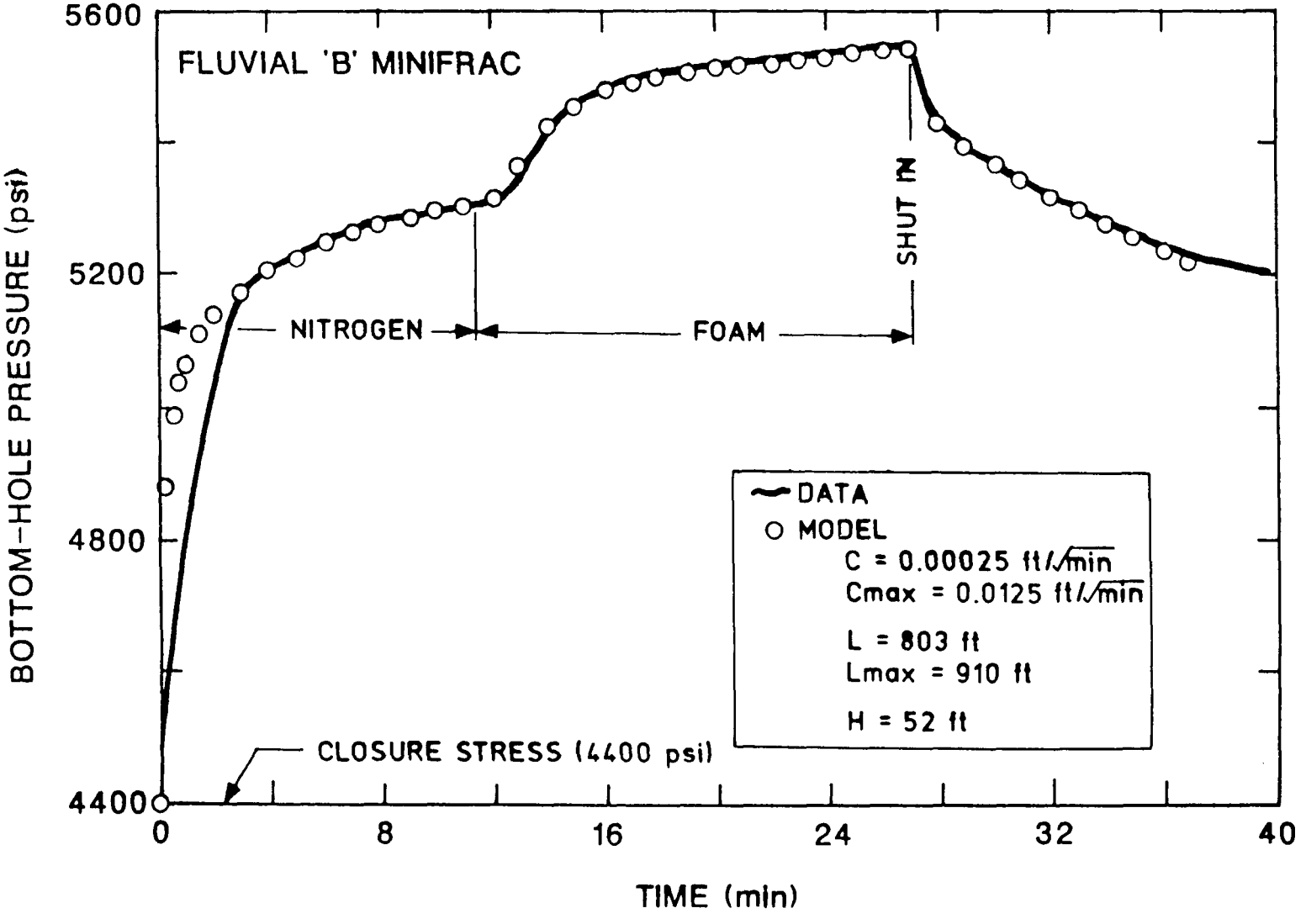

Figure 7.2.25. Final Pressure-History-Match for the Minifrac

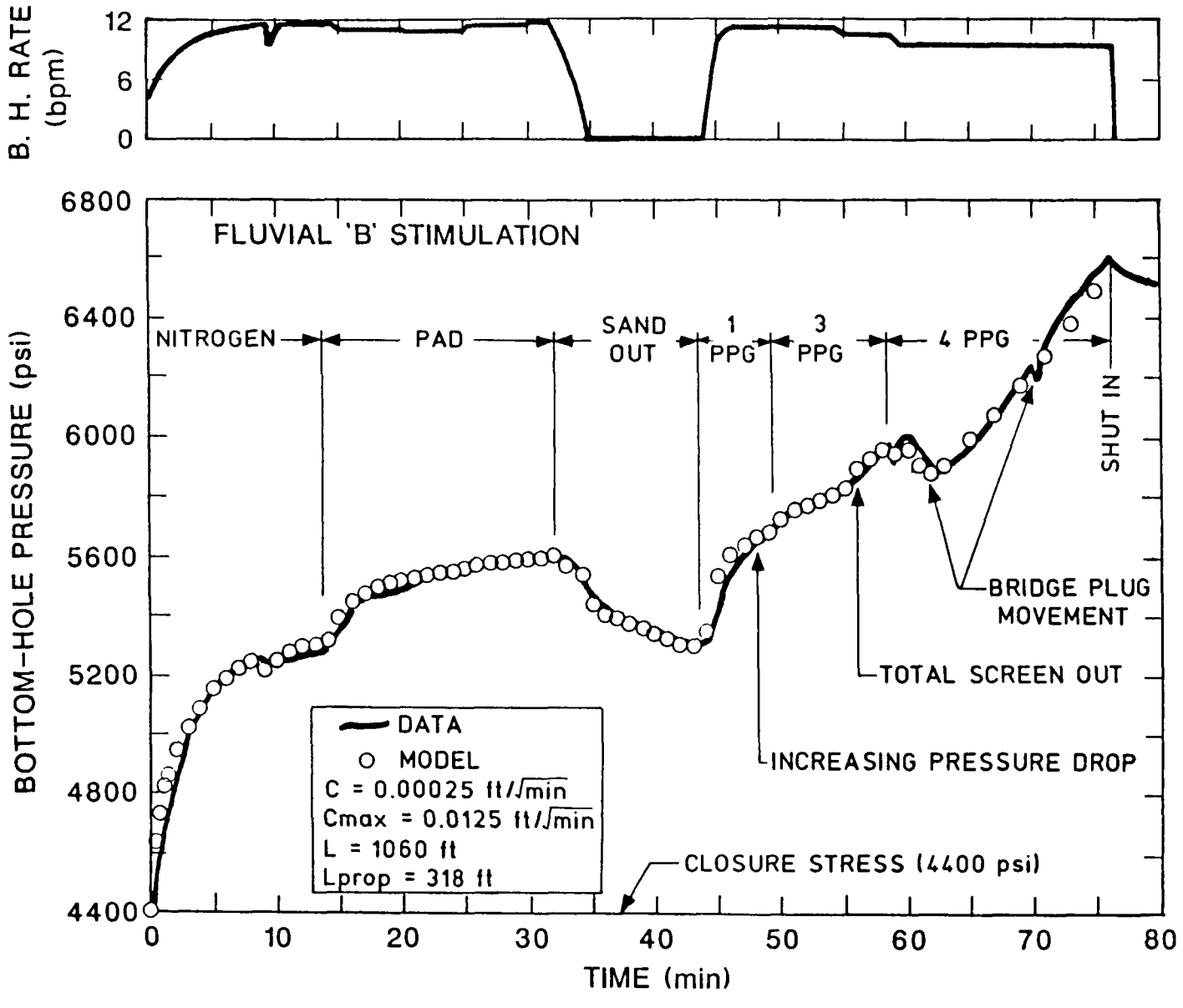

Figure 7.2.26. Final Pressure-History-Match Calculations for the Stimulation

FLUVIAL B SANDSTONE STIMULATION EXPERIMENT

7.3 POST-STIMULATION RESERVOIR TESTING AND ANALYSIS

P. T. Branagan
CER Corporation

7.3.1 POST-STIMULATION PRODUCTION AND TESTING

The fluvial B sandstone post-fracture well testing was conducted in two phases. Phase I was conducted in December, 1986, immediately following the stimulation and well cleanup operations. The MWX site was closed during the months of January and February, 1987, and all wells were shut-in. Phase II commenced on March 6 to evaluate the effects of the two-month shut-in. This two phase approach was developed based on previous MWX test results in the paludal interval, where a prolonged shut-in period enhanced well productivity.[1]

7.3.1.1 Phase I

Figure 7.3.1 presents the Phase I post-fracture production and bottomhole pressure data for MWX-1 during the 48-day testing period. (Digitized data for this test are given in Appendix I.) The flow rates were very sporadic due to irregular water production.

The post-fracture production rate fluctuated from an initial high of 50 MCFD to a stabilized rate of 20 to 30 MCFD during the last 9 days of the drawdown (Figure 7.3.1, days 21 through 30). The flowing bottomhole pressure varied considerably during the test, ranging from 400 to 1000 psi. The bottomhole pressure fluctuation appeared to be linked to periodic water removal from the wellbore. MWX-1 was shut-in periodically to allow the bottomhole pressure to buildup sufficiently to allow water removal. These buildup periods occurred in days 3, 7, 13 and 18. Since the bottomhole

quartz pressure gauge required servicing during days 19 and 21, MWX-1 had to be shut-in for tool removal, repair and emplacement.

Comparing the pre-fracture production rates (Figure 7.1.5) to the post-fracture rates (Figure 7.3.1) shows very little improvement after stimulation. The pre-fracture rate of 20 MCFD at 1000 psi flowing bottomhole pressure is very similar to the stabilized post-fracture rate of 25 MCFD at a varying bottomhole pressure of 400 to 1100 psi. The operational difficulties during the stimulation treatment (bridge plug movement and subsequent screen-out) preclude a quantitative assessment of stimulation effectiveness.

The Horner and log-log plots of the final fluvial B sand post-fracture buildup test are presented in Figures 7.3.2 and 7.3.3, respectively. Due to the complexities associated with both the MWX-1 pre-fracture well testing and the stimulation treatment, a quantitative analysis of the post-fracture well testing was not attempted. However, a qualitative assessment of the buildup characteristics can be made. Figure 7.3.2 does not exhibit the characteristic Horner shape of a hydraulically fractured well. The extrapolated P* appears to be approximately 3200 psi, about 200 psi lower than the initial reservoir pressure. The log-log plot, Figure 7.3.3, shows an extended wellbore storage period which does not indicate the existence of a hydraulically propped fracture. The pressure buildup behavior of MWX-1 appears to be influenced by the complications associated with the completion and stimulation operations.

7.3.1.2 Phase II

The Phase II well testing commenced on March 6, 1987, with initial flow rates of approximately 110 to 120 MCFD at 900 psi flowing bottomhole pressure. The test was designed to maintain a flowing bottomhole pressure in excess of 800 psi to avoid a pressure dependant productivity. Figure 7.3.4 presents the bottomhole pressure and surface flow rate for the Phase II test. The test consisted of a 14-day drawdown, followed by a 12-day

buildup. The flow test began with an initial bottomhole pressure of 3100 psi, and quickly dropped below 1000 psi after 2 days. The production rate during the final 5 days ranged from 35 to 30 MCFD. MWX-1 was shut-in for a 12-day buildup test on day 16.

A qualitative assessment of the MWX-1 productivity appears to indicate that well productivity is essentially the same compared to the initial Phase I productivity. Comparing Figures 7.3.1 and 7.3.4 indicates that the initial post-fracture flow rates were approximately 20 to 30 MCFD during the last 20 days of the Phase I drawdown and are similar to the Phase II rates of 30 to 35 MCFD. Therefore, the short, two-month shut-in does not appear to have allowed sufficient time for reservoir improvement, assuming it would occur.

Figure 7.3.5 is a log-log plot of the Phase II buildup, while Figure 7.3.6 is a Horner plot of the same data. The Phase I data are included in both plots for comparison. The log-log pressure and pressure derivative data for both the phase I and the Phase II buildup tests appears very similar, indicating no significant change or improvement in reservoir behavior. The Phase I and II Horner plots are also very similar and show no indication of any change in reservoir behavior as a result of the two-month winter shut-in. There appears to be no significant production enhancement from the stimulation treatment.

7.3.2 MODELING AND ANALYSIS

The expected production from MWX-1 for various fracture lengths was predicted using the reservoir models developed from the pre-fracture simulation study of the MWX-3 well test data. The expected post-fracture production was simulated using both the anisotropic naturally fractured and the homogeneous model.

7.3.2.1 Naturally Fractured Reservoir Model

Figure 7.3.7 compares the expected post-fracture flow rates for high conductivity, propped hydraulic fractures having lengths of 100, 250 and 750 ft during the first year of production. The orientation of the propped fracture is parallel to the high permeability natural fractures, intersecting the lower permeability natural fractures. Figure 7.3.8 illustrates the fracture orientation with respect to MWX-2 and MWX-3. The fracture orientation was estimated based on available in situ stress orientation data from strain relaxation, differential strain curve analysis, geological and outcrop studies and previous seismic monitoring of stimulation experiments in neighboring zones. The natural fracture anisotropy was assumed to be a function of the current in situ stress field, thus the high permeability natural fractures are oriented parallel to the minimum in situ stress.

The cumulative production for the first year is shown for comparison on Figure 7.3.7. It can be seen that a 750-ft hydraulic fracture would increase first year recovery by a factor of 4.3 compared to the unstimulated reservoir. A 250-ft hydraulic fracture would provide about twice the production compared to the unstimulated case. However, little production increase is realized for a 100-ft hydraulic fracture. It has been evident from previous MWX stimulation experiments that permeability impairment to the natural fractures can occur due to stimulation liquids and polymers[2,3]. Therefore, an additional set of prediction cases were evaluated with the inclusion of damage to natural fracture permeability.

The simulated post-fracture flow rates for the above cases with a 10-ft damage zone around the hydraulic fracture are shown in Figure 7.3.9. The damage zone in the model consists of reducing the permeability of the intersected natural fractures to the matrix value of 0.001 md for a distance of 10 ft around the hydraulic fracture. This figure shows that the production from a reservoir containing a 100-ft hydraulic fracture that has damaged the intersected natural fractures will actually reduce first year production from 4.2 MMCF to 2.0 MMCF. The simulated production from a 250-ft hydraulic fracture is almost identical to the unstimulated case when

the natural fracture system is damaged. However, the longer 750-ft hydraulic fracture does provide significant production enhancement, a 2.7-fold increase in gas production the first year. Comparing Figures 7.3.7 and 7.3.9 shows there is a large decrease in expected gas production when the natural fracture system is damaged for all fracture lengths evaluated. The 750-ft hydraulic fracture case would be expected to produce 18.1 MMCF without damage and 11.4 MMCF with damage, a 37 percent decrease in first year recovery.

7.3.2.2 Homogeneous Reservoir Model

The simulated production for the above three hydraulic fracture lengths (100, 250 and 750 ft) in a homogeneous reservoir are shown in Figure 7.3.10. Figure 7.3.11 is an illustration of the homogeneous reservoir model, showing the hydraulic fracture orientation and the location of MWX-1, MWX-2 and MWX-3. It should be noted that the base case homogeneous simulation does not include the breakdown fracture that was required to reproduce the MWX-3 pre-fracture well test behavior. Therefore, the flow rates on the order of 1 MCFD are much lower than the MWX field data.

The cumulative first year production for the 250-ft and 750-ft cases in a homogeneous reservoir are 6.9 MMCF and 19.7 MMCF, respectively. Comparing the same hydraulic fracture length in Figure 7.3.7 (naturally fractured reservoir with no damage) shows slightly less production for the 750-ft case, 18.1 MMCF, while the 250-ft case shows about 17 percent more production. The comparison serves to illustrate that longer hydraulic fractures are more effective in the homogeneous reservoir scenario compared to the naturally fractured case. Again, the homogeneous model assumes that MWX-3 production and pressure buildup behavior can be attributed to the existence of a 100-ft hydraulic fracture as a result of the initial nitrogen breakdown. It should be noted that the conductivity of a hydraulic fracture can be very small and yet still enhance production due to the small matrix permeability (0.001 to 0.004 md).

The above simulations were used to qualitatively evaluate the post-fracture production from MWX-1. Due to the lack of reliable pre-fracture well test data from MWX-1 and difficulties during the stimulation operation (Section 7.2), no quantitative post-stimulation reservoir modeling of the fluvial B sandstone was performed.

7.3.3 CONCLUSIONS

There are several possible explanations for the observed absence of enhanced productivity after the fluvial B sandstone stimulation. These complicating factors could have acted individually or in concert, thus rendering a quantitative analysis of the well testing data ambiguous.

- The hydraulic fracture did not extend into nor prop a significant portion of the fluvial B sandstone. This could be a result of the screen-out and/or the bridge plug movement which occurred during the stimulation treatment. Both of these events could have led to a very short propped fracture that would not contribute significantly to well productivity.

- The propped fracture and intersected natural fractures could be damaged as a result of liquids and stimulation polymers. This would negate much of the expected productivity increase and mask the appearance of the hydraulic fracture during buildup testing.

- The complicating effects of the anomalous pressure buildup behavior during the pre-fracture testing could be an indication that the completion in the MWX-1 fluvial B sandstone did not completely isolate the zone and communication within the wellbore exists. Again, the anomalous pressure behavior was pressure sensitive during the pre-fracture testing. The subsequent propped fracture treatment could have increased communication to neighboring zones, thus eliminating the pressure dependant behavior.

- The highly anisotropic natural fractures in the fluvial B sandstone could result in reduced stimulation effectiveness if the hydraulic fracture is oriented parallel to the high permeability natural fractures (as may be expected).

7.3.4 REFERENCES

1. Warpinski, N. R., et al., "Fracturing and Testing Case Study of Paludal, Tight, Lenticular Gas Sands," SPE Formation Evaluation, pp. 535-545, December 1987.

2. Branagan, P. T., et al., "Case History of Hydraulic Fracture Performance in the Naturally Fractured Paludal Zone: The Transitory Effects of Damage," SPE/DOE 16397, Proceedings of the 1987 SPE/DOE Low Permeability Reservoirs Symposium, Denver, CO, May 18-19, 1987.

3. Branagan P. T., et al., "Designing and Evaluating Hydraulic Fracture Treatments in Naturally Fractured Reservoirs," SPE/DOE 16434, Proceedings of the 1987 SPE/DOE Low Permeability Reservoirs Symposium, Denver, CO, May 18-19, 1987.

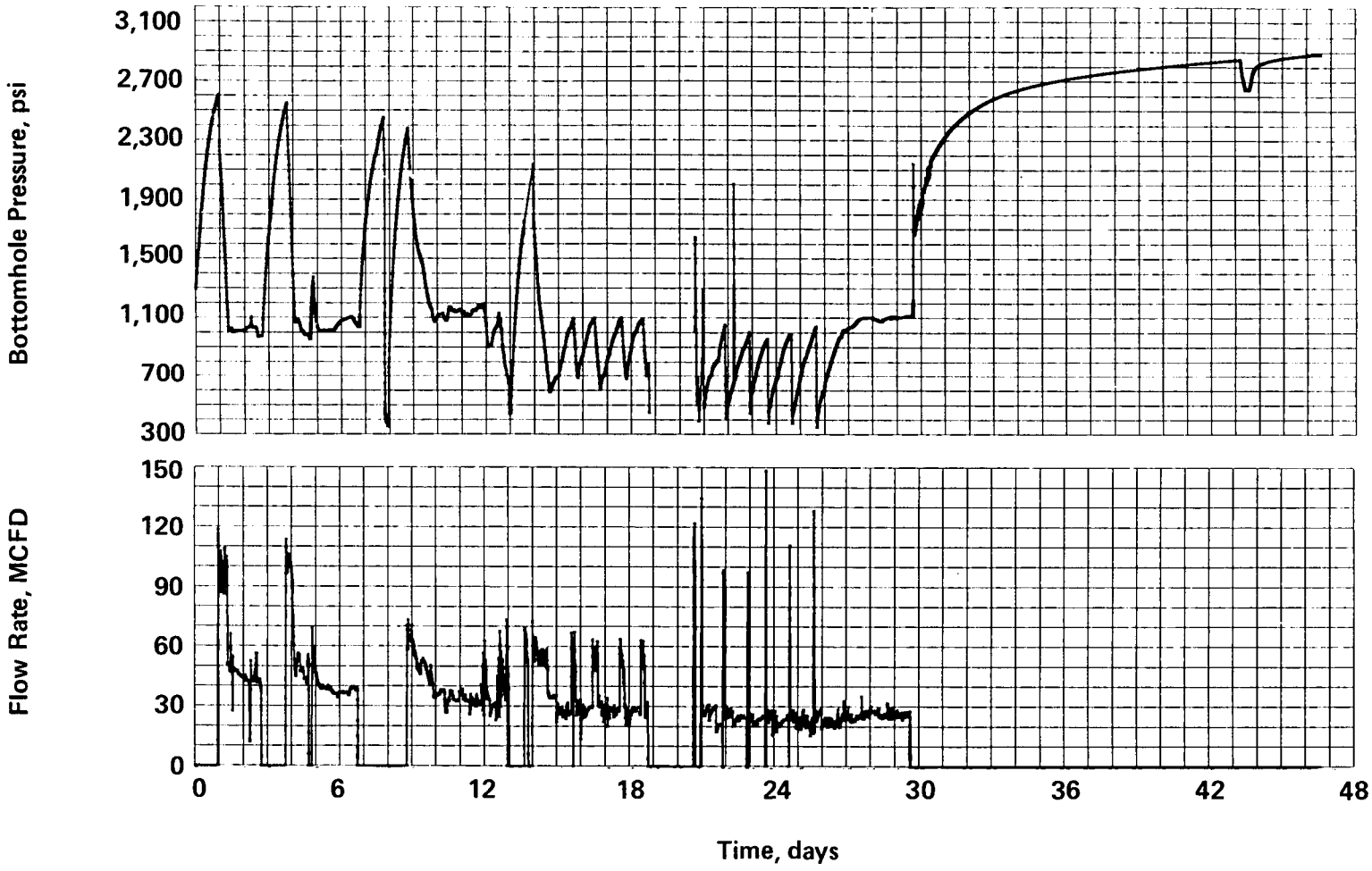

Figure 7.3.1 Post-Frac Flow and Pressure Data, Phase I, December Test

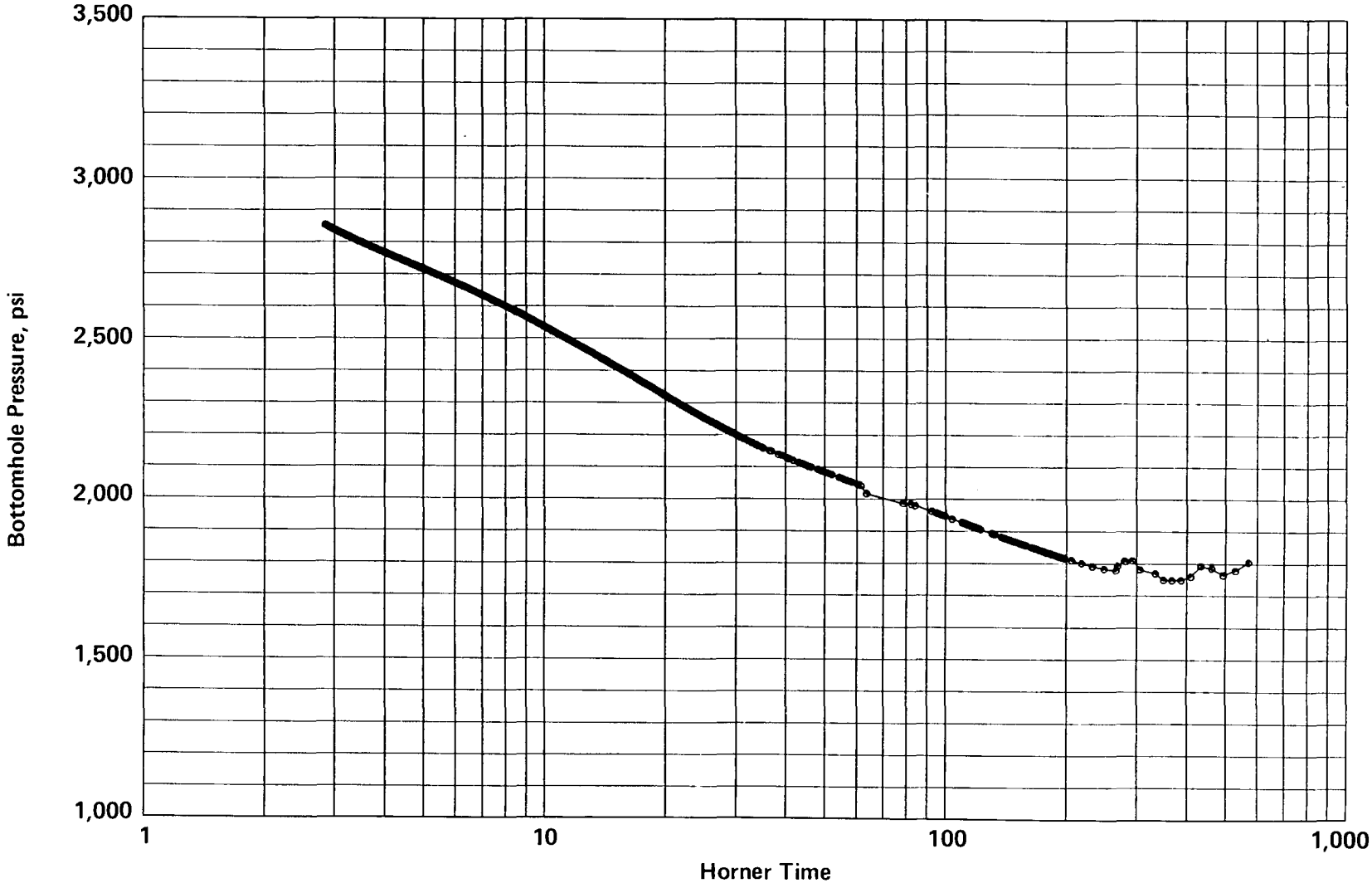

Figure 7.3.2 Post-Frac Buildup, Horner Plot

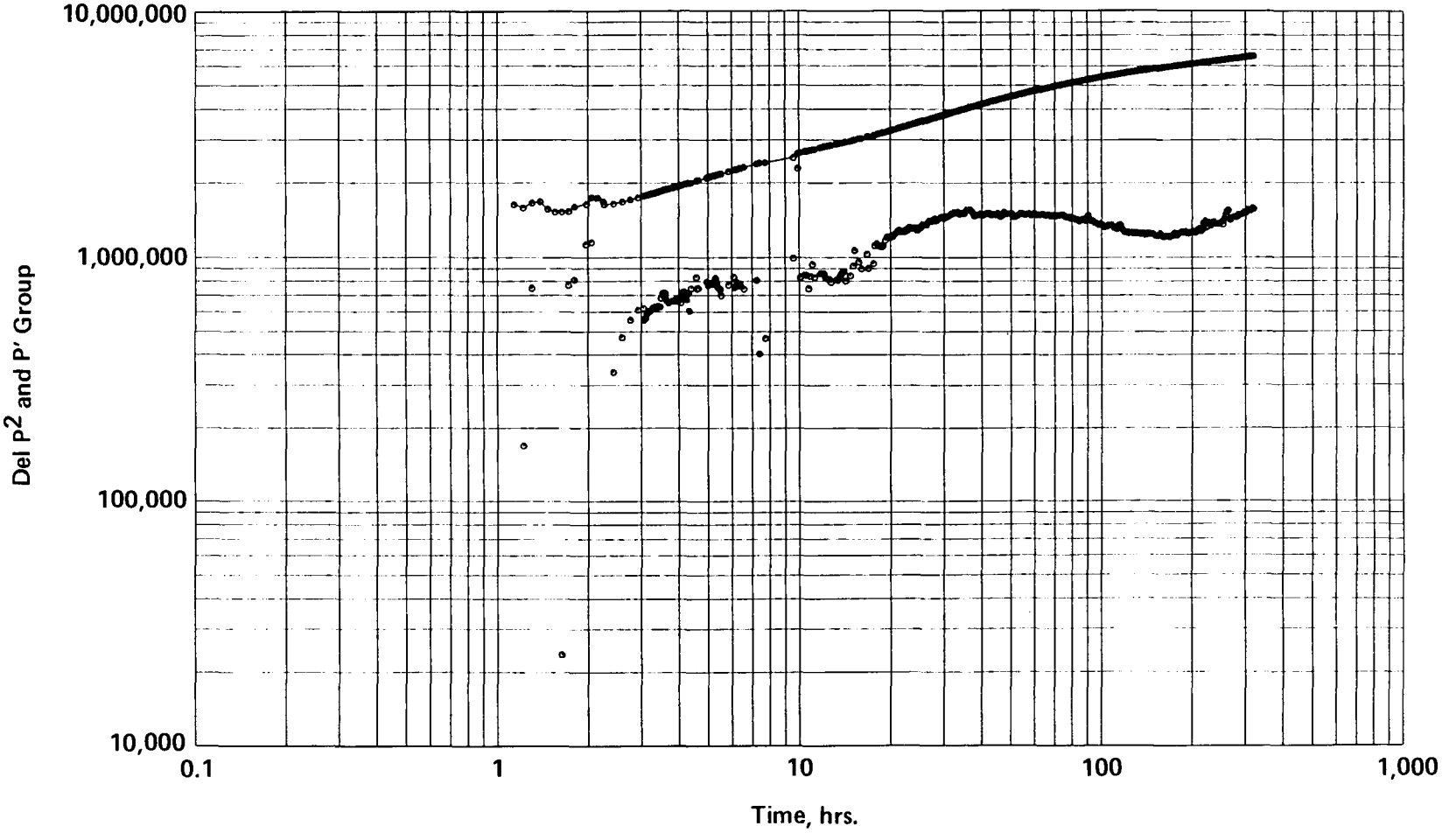

Figure 7.3.3 Post-Frac Buildup, Log-Log and Derivative Plots

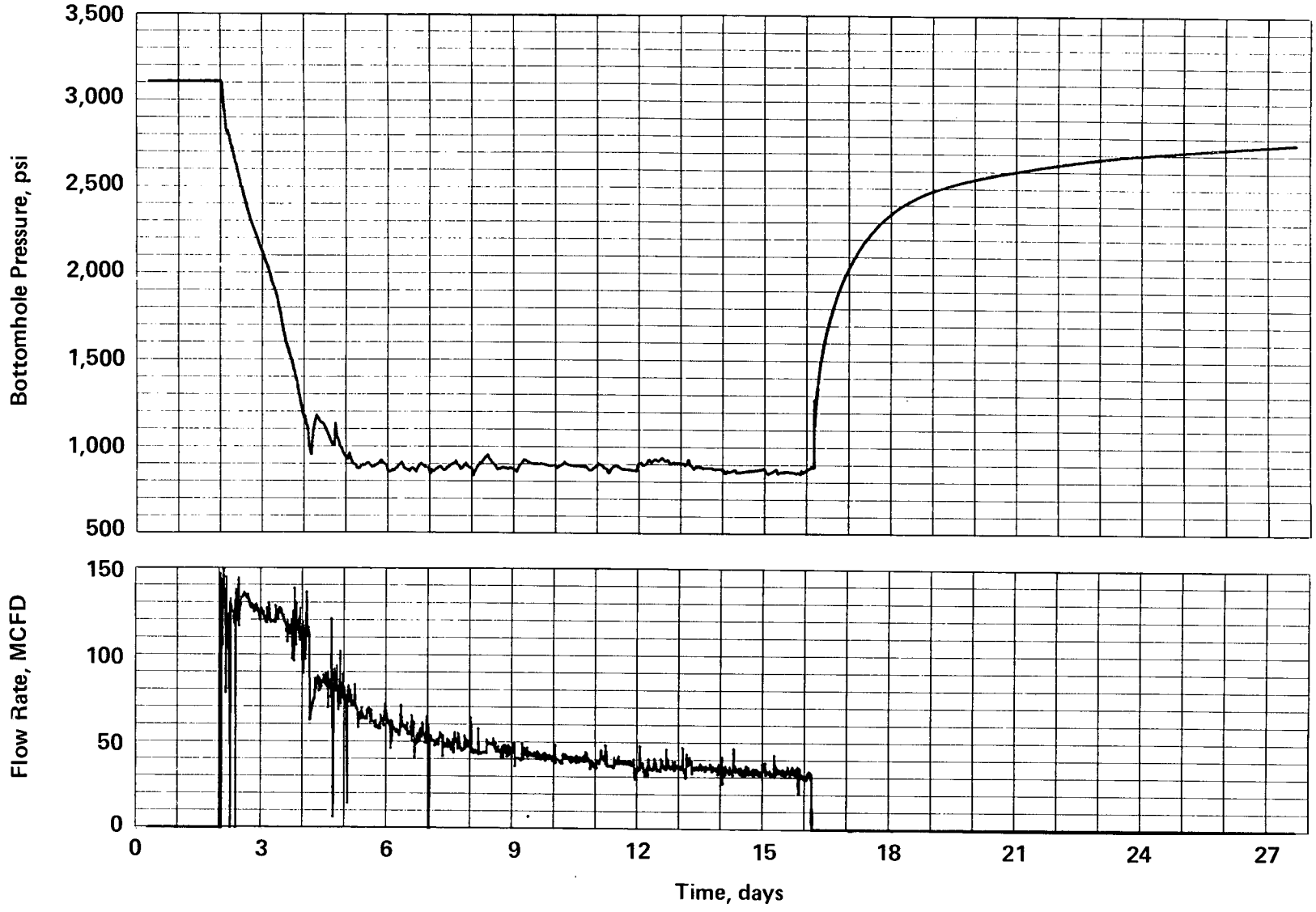

Figure 7.3.4 Post-Frac Flow and Pressure Data, Phase II, March Test

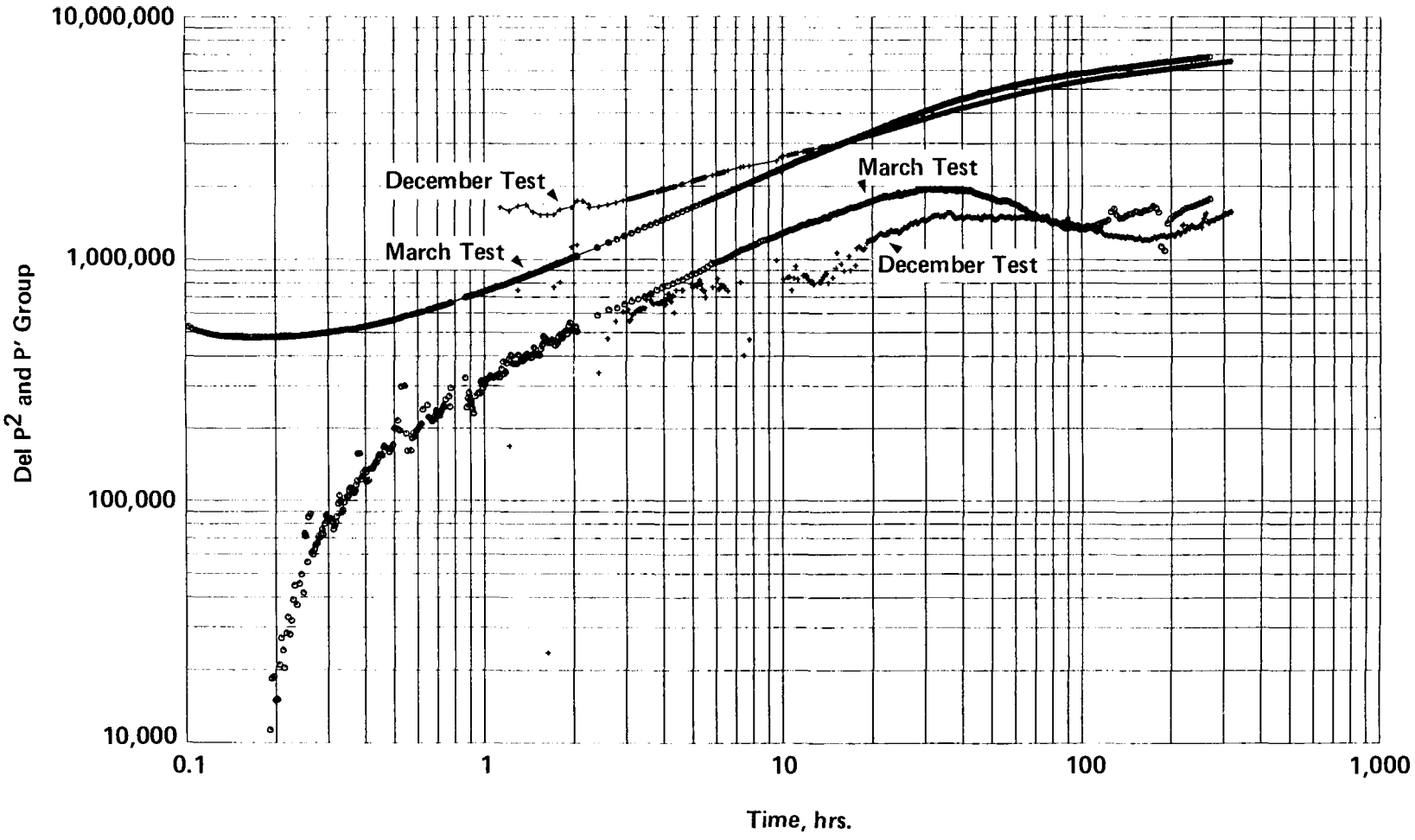

Figure 7.3.5 Post-Frac Buildup, Log-Log and Derivative Plots, Phase I, II

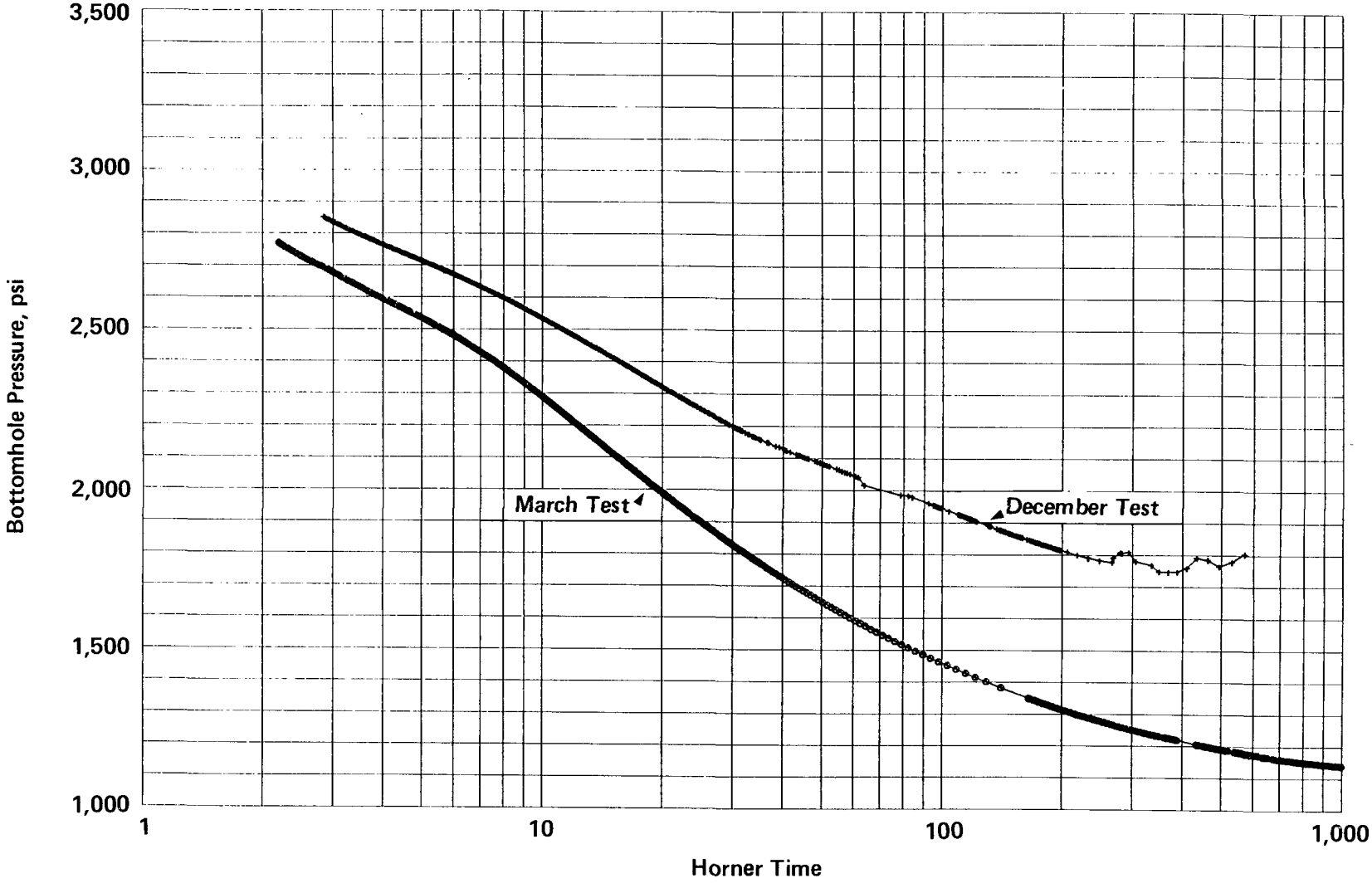

Figure 7.3.6 Post-Frac Buildup, Horner Plot, Phase I, II

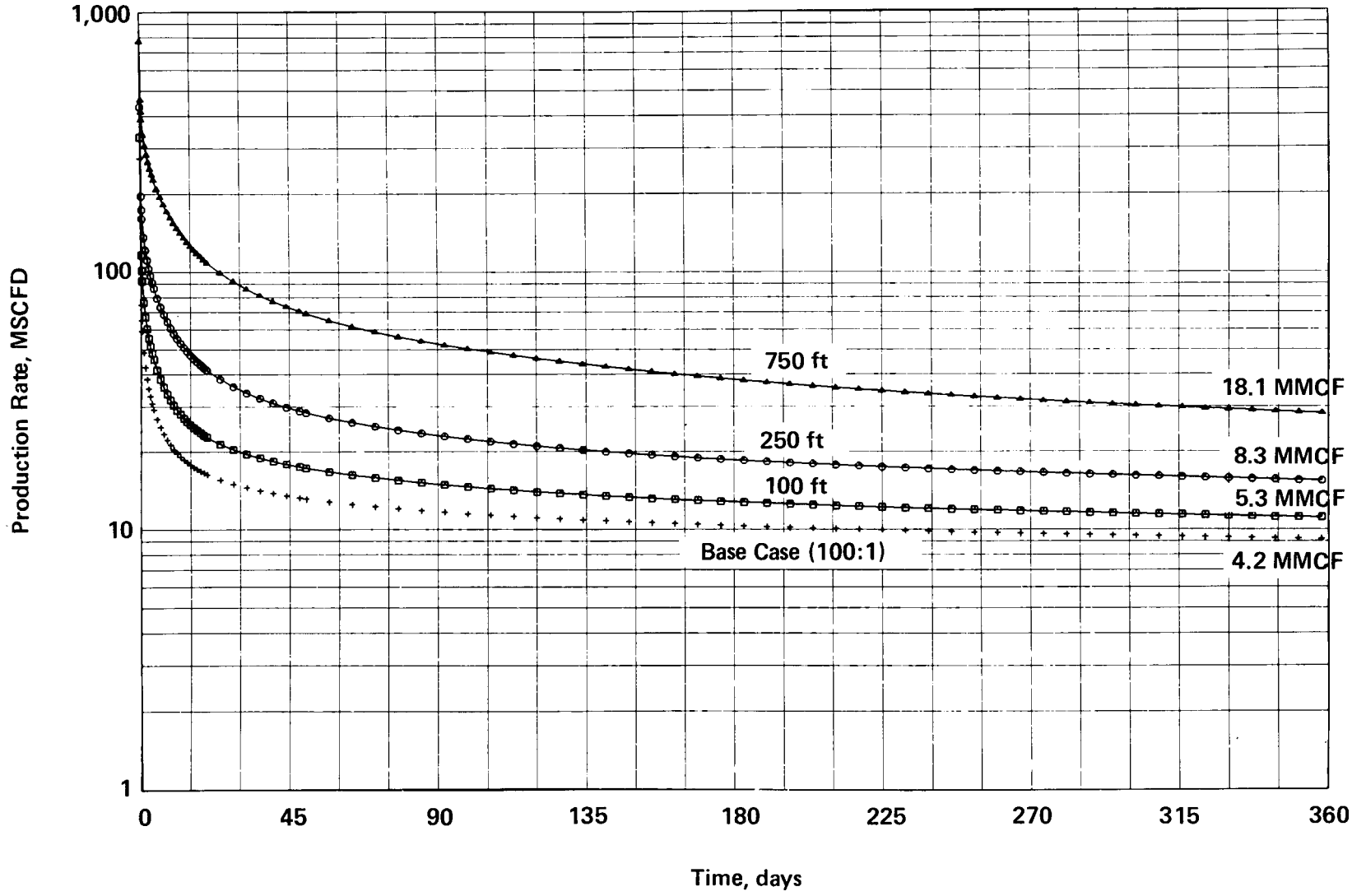

Figure 7.3.7 Calculated Post-Frac Flows, Fractured Reservoir, No Damage

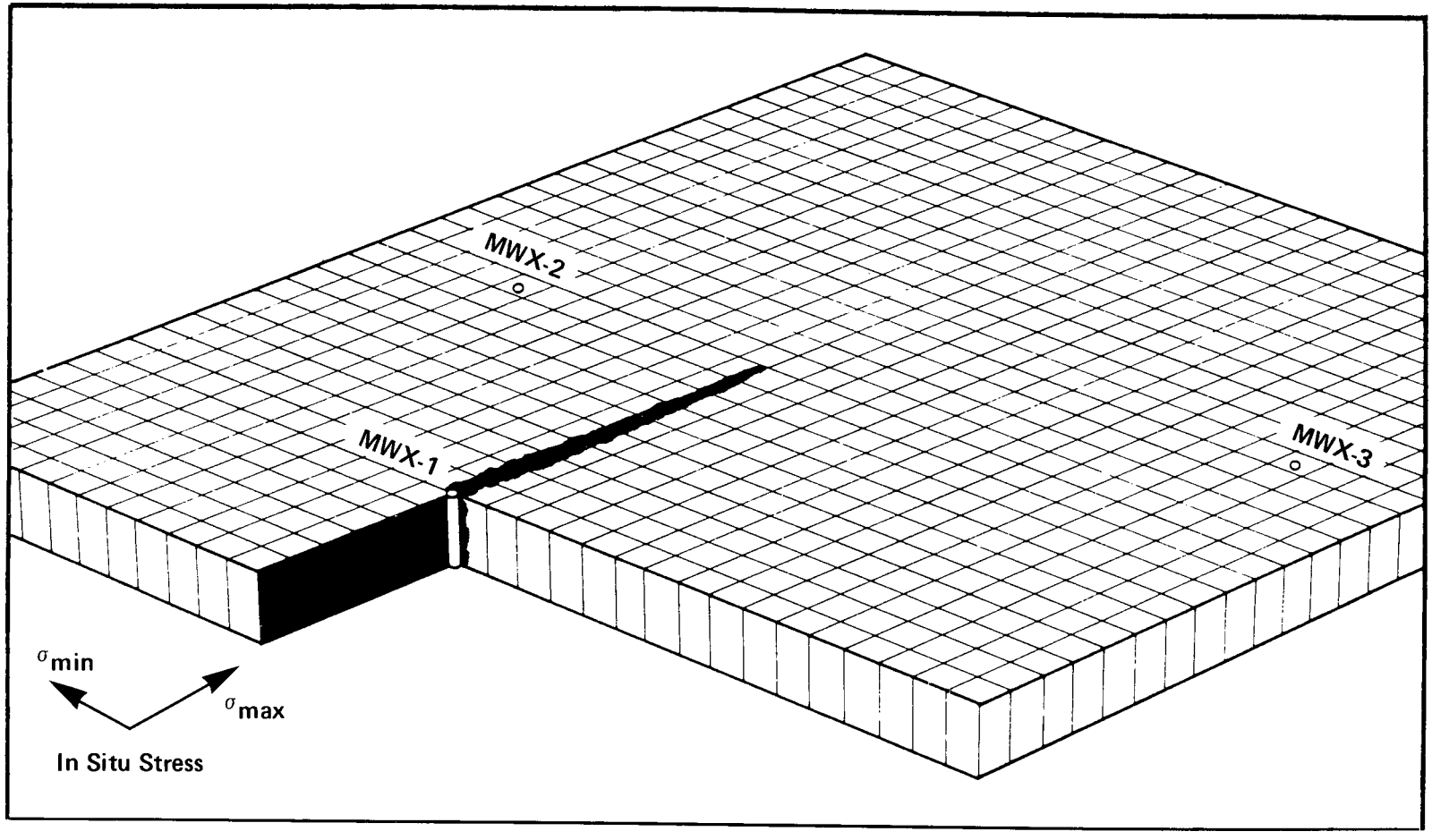

Figure 7.3.8 Hydraulic Fracture Orientation, Fractured Reservoir

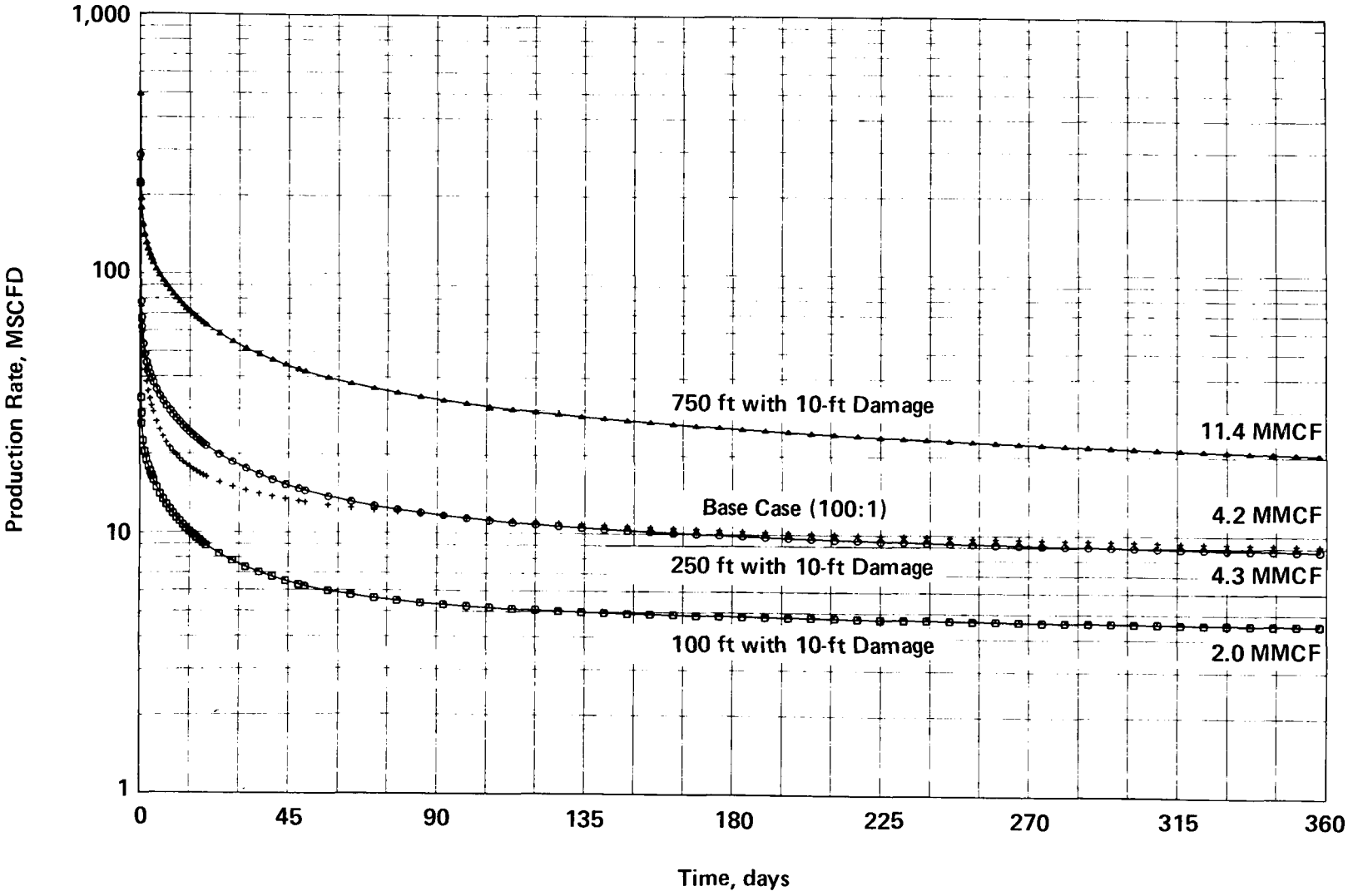

Figure 7.3.9 Calculated Post-Frac Flows, Fractured Reservoir, 10-ft Damage

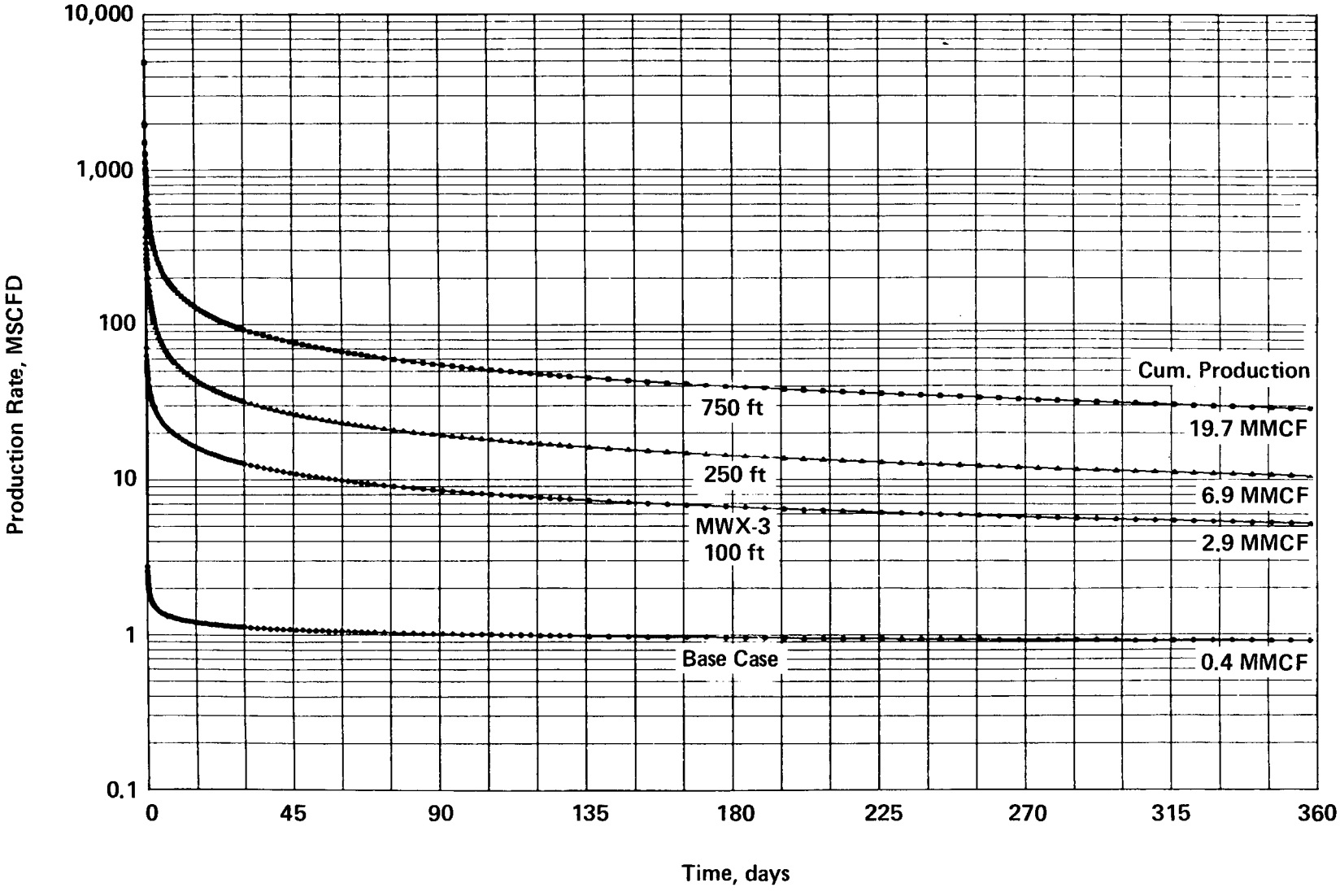

Figure 7.3.10 Calculated Post-Frac Flows, Homogeneous Reservoir, No Damage

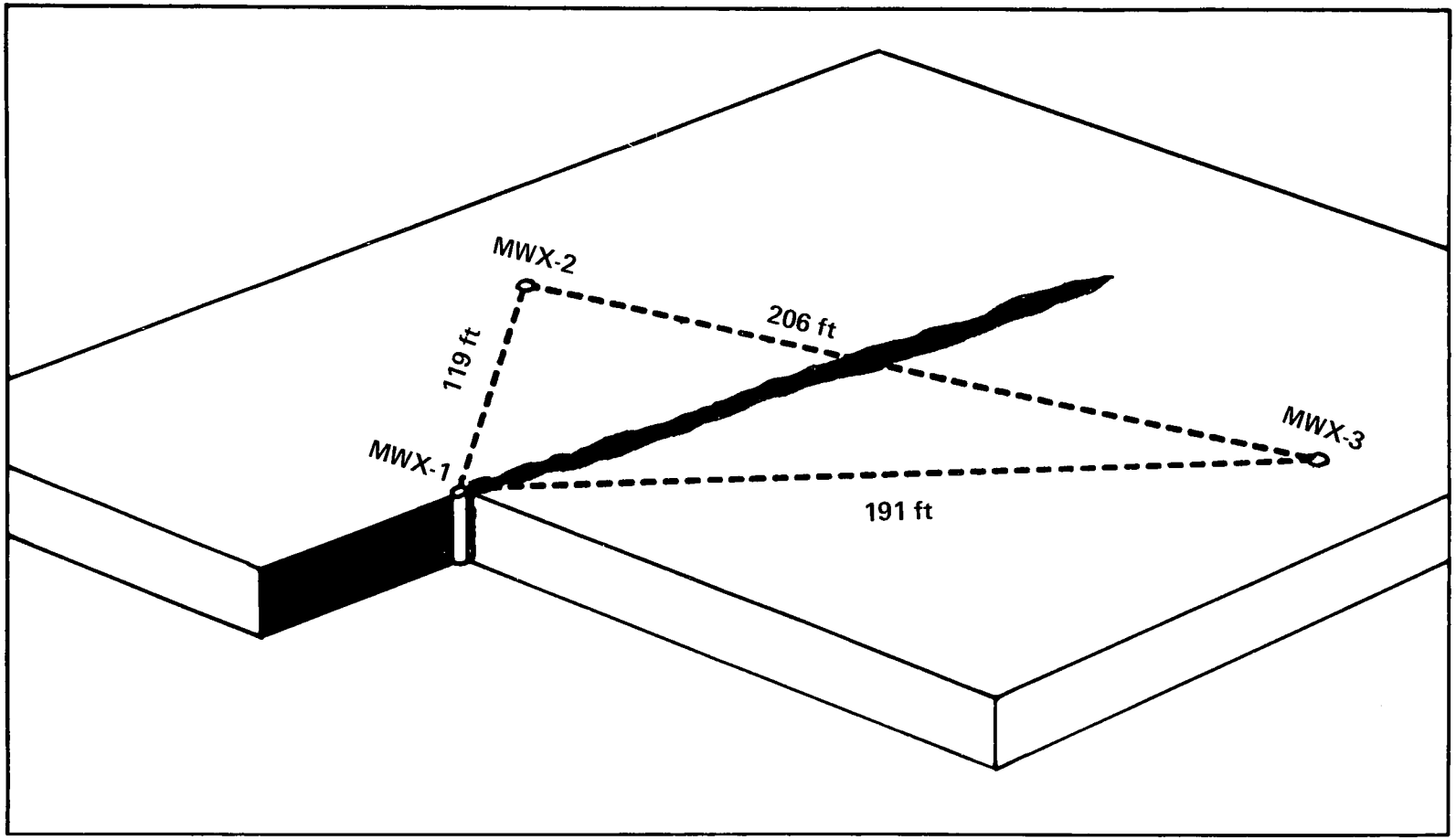

Figure 7.3.11 Hydraulic Fracture Orientation, Homogeneous Reservoir

7.0 FLUVIAL B SANDSTONE STIMULATION EXPERIMENT

7.4 BOREHOLE SEISMIC FRACTURE DIAGNOSTICS

B. J. Thorne
Sandia National Laboratories

7.4.1 INTRODUCTION

Recent redesign of the hardware, software, and data-reduction techniques associated with the Sandia Borehole Seismic System (BSS) have made possible better estimates of hydraulic fracture geometry. The BSS was upgraded to include several new diagnostic capabilities. Calibration and balancing of the data channels can now be achieved through the wireline using surface instrumentation. An increased digitization rate made possible the acquisition and processing of data that were previously inaccessible. A maximum likelihood microseismic event location scheme, based on the use of directional statistics, was used to compute the location of microseismic events and error estimates for these locations. The accuracy of the redesigned system, based on the ability to locate perforation shots, indicates a 25 ft uncertainty in the location of individual microseisms. These changes result in a fairly high level of confidence in the determination of the azimuth of the November 1, 1986, hydraulic fracture in the fluvial B sandstone.

7.4.2 INSTRUMENTATION UPGRADE

The principal thrust of the BSS upgrade was derived from certain aspects of the data set produced during the August 1, 1985, stimulation experiment in the coastal interval.[1] The new electronics make use of a null system and an improved calibration system which includes a synthetic event generator to produce sinusoidal signals of specified amplitude, frequency and phase. These make readjustments to maintain system balance possible while BSS tools are in place downhole. The new geophone array contains vertical and horizontal exciters which can be activated from the surface to confirm operation of the entire system. In addition, the

position of the clamp arm and the force which it exerts on the wellbore wall are continuously displayed on surface instrumentation while the BSS tool is in place.

The new analog to digital (A/D) conversion method is based on a Phoenix Data IDAS eight channel A/D converter with vector sample and hold. The IDAS is coupled to an IBM-PC Computer and an event detector which triggers the IBM-PC to store data when any of the six channels exceed a preset voltage. The new system is capable of simultaneously digitizing all six channels at a rate of 13.3 kHz per channel as compared to a maximum digitization rate of 2.3 kHz per channel for the old PDP-11/34 based system. Figure 7.4.1 shows time histories of the three data traces for the first 25 ms of a typical event recorded in well MWX-2, together with horizontal and vertical hodograms of the first 1.5 ms of the primary wave. Note the good signal to noise ratio of the time histories and the clear direction of breakout of the hodograms.

7.4.3 SINGLE-TOOL LOCATION OF A MICROSEISMIC EVENT

If the primary and secondary wave arrival times, T_P and T_S can be determined, then the distance D to a seismic source can be calculated by

$$D = V_F \, (T_S - T_P). \tag{7.4.1}$$

The "velocity factor",

$$V_F = V_S \, V_P/(V_P - V_S), \tag{7.4.2}$$

can be determined empirically from seismic sources at known distances, without knowledge of the primary wave velocity V_P or the secondary wave velocity V_S.

The primary wave travels faster than all other waves and, in a homogeneous isotropic medium, is polarized parallel to the direction of

travel. It is, therefore, possible to determine the direction from which it arrives at a triaxial geophone of known orientation, and thus the direction to the seismic source, by analysis of the three components of the first arrival of the signal. However, analysis of the triaxial geophone data can only determine this direction with a 180° ambiguity, i.e., it cannot distinguish between a compressional first arrival from a given direction and a dilatational first arrival from the opposite direction.

For data from the BSS, determination of the direction of primary wave polarization is done in two steps. First, the east and north components are analyzed by using spherical statistics to determine the azimuth of the polarization,[2] with resolution of the 180° ambiguity handled by the analyst based on knowledge of the probable location of the source or, preferably, by comparison of data from two BSS tools. Then a three-dimensional spherical statistical analysis of the data[2] is used to determine the elevation to the source. This approach yields a more accurate determination of the azimuth than use of three-dimensional spherical statistics for determination of both the azimuth and elevation, because the vertical component of the BSS data seems to have a different dominant frequency than the two horizontal components (See Figure 7.4.1). In addition to the azimuth and elevation of the direction of polarization, spherical statistics yields an estimate of the probable error in the form of standard deviations for both the azimuth and elevation.[2]

7.4.4 TWO-TOOL LOCATION OF A MICROSEISMIC EVENT

Given the azimuth, elevation, and distance to a microseismic event determined by two BSS tools, it is desirable to refer the two single-tool locations and their error measures to a common coordinate system and determine a most probable single location and an error measure for that location. This can be done by assuming a triangular probability distribution about each location based on the mean, mode, and standard deviation for the azimuth, elevation, and distance, and solving for the position which minimizes the error measure.[2] For a rectangular coordinate

system, the error measure is expressed as a standard deviation for each of the coordinate axes and can be thought of as an ellipsoid with axes parallel to the coordinate axes. The minimum error position is the position which minimizes the volume of this error ellipsoid.

Figure 7.4.2 illustrates the method as applied to a single microseism. In Figure 7.4.2(a) the 5800 ft depth horizontal position of the three wells is plotted in a rectangular coordinates system with origin at the stimulation well, MWX-1. The horizontal locations determined from BSS data taken in wells MWX-2 and MWX-3 are given by the triangle symbols nearest to the respective observation wells. The ellipse drawn about each of these two locations represents the horizontal projection of the error ellipsoid for that location. The third triangle symbol and the ellipse drawn about it represent the two-well minimum error horizontal location and the horizontal projection of the minimum error ellipsoid. Note that the ellipse about the minimum error position is smaller than the ellipse about either single-well location. The line through well MWX-1 is given by the spherical average of the three angles determined by these three locations and is at an azimuth of 70° west of north. Figure 7.4.2(b) gives the projection of these same three points into the vertical plane determined by this line. In Figure 7.4.2(b) the positions of the bottoms of the BSS tools in wells MWX-2 and MWX-3 are indicated by the square symbols on the projection of the well bore onto this plane. The square symbol on MWX-1 indicates the center of the perforation gun.

Depth is measured from the surface at well MWX-1 and the top and bottom of the fluvial B sandstone is indicated by horizontal lines. The lower triangle symbol corresponds to the location determined from well MWX-2 and the ellipse about it to the projection of the error ellipsoid for that location onto the vertical plane. The upper triangle symbol and ellipse correspond to the location determined from well MWX-3, with the third triangle symbol and ellipse corresponding to the minimum error location and ellipsoid.

7.4.5 DETERMINATION OF THE VELOCITY FACTOR

Before the distance to the source can be determined, the velocity factor, V_F, must be established. This is accomplished by analysis of data from seismic sources at known locations. Specifically, 20 ten-gram perforation shots were fired at an average depth of 5831 ft in well MWX-3 with a BSS tool in place at a depth of 5744 ft in well MWX-2. The velocity factor, V_F, was calculated for each shot from the known distance and the primary and secondary wave arrival times, using Equation 7.4.1. Without moving the BSS tool in well MWX-2, a second BSS tool was placed in well MWX-3 at a depth of 5731 ft, and 13 ten-gram perforation shots were fired at an average depth of 5835 ft in well MWX-1. Velocity factors proved to be different for all three paths as seen in Table 7.4.1.

Since it is well established that the MWX site is inhomogeneous and anisotropic, it is reasonable to assume that the different values of V_F for the three paths are a result of a variation in V_S, and perhaps V_P, with direction. In order to be able to use Equation 7.4.1 to compute the distance to a microseismic event, it is reasonable to compute V_F as a function of azimuth in a manner which agrees with the measured values. Since we have measured values for three azimuths, a three parameter model is required. A model which gives a minimum value for V_F at a critical azimuth α and a maximum value perpendicular to that azimuth was chosen in the form:

$$V_F(\theta) = V_1[1 - V_2\cos(2\theta - 2\alpha)] \qquad (7.4.3)$$

The values of V_F for the three azimuths measured dictate the following values for the three parameters in Equation 7.4.3:

α = 35.6° north of east
V_1 = 16.9 ft/ms (5150 m/s)
V_2 = 0.088

It is assumed that Θ is also measured in degrees north of east. This gives values of V_F in the range of 15.4 ft/ms to 18.4 ft/ms. The critical angle α does not seem to have physical significance at this time.

7.4.6 ORIENTATION OF BSS TOOLS

If it is assumed that the direction of polarization of the primary wave is the direction towards the source, as it would be in a homogeneous isotropic medium, then the orientation of the geophone axes can be determined from the same perforation shots used to determine the velocity factor function. Since the wells at the MWX site are very nearly vertical, the orientation of the vertical axis is known. This allows the elevation calculated from the BSS data to be compared to the known elevation to the center of the perforation gun, as a check on the assumption that the direction of polarization is the same as the direction to the source. It is unreasonable to assume that a correct orientation has been obtained if large errors in the elevation result. Table 7.4.2 gives the vertical errors for the three paths. Average vertical errors vary from -4.2° to 4.2°, indicating a scatter about zero consistent with the 2.9° to 3.7° standard deviations of the three data sets. Before the final observation depths were chosen, several tool positions were rejected in both wells because of large errors in elevation on previous perforation shot series. The reasons for unsatisfactory results at rejected positions is not clear. It is possible that the quality of the casing cement bond is the dominate factor. However, it could be the result of inhomogeneities in the formation causing the first arrival to be along a path different from the straight line path to the source.

The orientations obtained from both sets of perforation shots are given in Table 7.4.2. Orientations are measured from the y-geophone axis to north as shown in Figure 7.4.2(a). Thirteen perforation shots in well MWX-1 confirm the orientation of the BSS tool in well MWX-2 obtained from the 20 perforation shots in well MWX-3 to within a fraction of the 3.0° and

3.6° standard deviations of the two data sets. Thus, the assumption that the direction of primary wave polarization is the same as the direction towards the seismic source should be accurate to within 4° in both azimuth and elevation, even though the formation is neither homogeneous nor isotropic. Before the final observation depth in well MWX-2 was chosen, several tool positions were rejected because of large differences in orientation obtained from perforation shots in wells MWX-1 and MWX-3. Previous perforation shot series in wells MWX-1 and MWX-2 were used to pick the final observation depth in well MWX-3 based on confirmation of orientation. However, it was impossible to have a two-well final orientation of the BSS tool in well MWX-3 as perforations could not be shot in MWX-2 due to the presence of the BSS tool in that well.

7.4.7 TWO-TOOL LOCATION OF PERFORATION SHOTS

In order to estimate the accuracy which can be expected from the analyses method, data from the 13 perforation shots in well MWX-1 were analyzed as if they were microseismic events of unknown location. The resulting locations have horizontal components which fall within a circle of radius 25 ft about well MWX-1, as indicated by the triangle symbols in Figure 7.4.3(a). Figure 7.4.3(b) indicates that these locations are biased to lie above the center of the perforation gun and lie inside an ellipsoid with a vertical major axis extending 30 ft above and below the center of the perforation interval.

7.4.8 TWO-TOOL LOCATION OF THE FRACTURE

Over 100 microseismic events were recorded and digitized during pump in, shut in and flow back of the hydraulic fracture experiment conducted on November 1, 1986. The location of most of the microseismic events occurring during pump in could not be determined due to a high background noise, probably resulting either from flow of the frac fluid through the formation or from the pumping equipment. Most microseismic events detected during shut in and flow back had very good signal-to-noise ratios and could

be located from both wells. However, some of these events resulted in two single-well locations that were so far apart that it seemed unreasonable to believe the resulting two-well location. Still others resulted in two-well locations that were inconsistent with the differences in times of primary wave arrival at the two BSS tools and reasonable primary wave speeds.

A total of 29 microseismic events were detected which were located by both BSS tools and resulted in locations that were close enough together in both time and space to reasonably represent microseismic activity resulting from the stimulation. These locations indicate a fracture azimuth of 68° west of north, Figure 7.4.4(a). It is interesting to note that all of these locations lie between parallel vertical planes located 25 ft on either side of the vertical plane through well MWX-1 in this direction, consistent with the scatter of the locations determined for the perforation shots. This indicates that a fairly high level of confidence can be associated with the 68° west of north fracture azimuth determined from the two-well locations, in spite of the fact that spherical statistics on the set of angles measured from well MWX-1 to microseismic event locations yields a 21.3° standard deviation. This azimuth is in excellent agreement with fracture azimuth predictions based on previous measurements at this site.[3]

The projection of these locations onto the vertical plane through well MWX-1 at 68° west of north is shown in Figure 7.4.4(b). Most of these locations lie above the B sandstone. It is clear from Figure 7.4.4(b) that the scatter in the vertical direction has a more serious detrimental effect on determination of the fracture height than the scatter in the horizontal direction has on determination of the fracture azimuth. It is known from radioactive tracers in the proppant that the fracture broke out of the top of the formation by at least 10 ft at well MWX-1. This, added to the 30 ft uncertainty in the determination of the vertical location of the perforation shots, would lead to expected microseismic event locations associated with the top of the fracture at depths up to 5780 ft. All but two events lie below this level. However, it is obvious that the bottom of the fracture cannot be determined from these locations.

7.4.9 DIFFERENCES BETWEEN DATA FROM THE TWO OBSERVATION WELLS

Certain systematic differences between the data from the two observation wells become obvious after a thorough analysis of the data from perforation shots and microseismic events. At this time, causes for these differences have not been established, but it is tempting to speculate.

There seems to be an unexplained difference in signal strength between data from the BSS tools in wells MWX-2 and MWX-3. For microseismic events located equal distances from both observation wells, the signal strength from the BSS tool in well MWX-2 was approximately three times that from the BSS tool in well MWX-3. It has been suggested that the difference in signal strength between the two wells is a result of differences in the geological formations in which the two BSS tools were placed or differences in the strengths of the well casing cement bonds at the BSS tool locations.

Figure 7.4.5 shows 73 single-well locations given microseismic events based on data from well MWX-2. Some of these events occurred during pumping and have very large error ellipsoids. Less than 40 percent of these 73 events resulted in acceptable two-well locations for reasons mentioned above. In spite of the problems with this data set, Figure 7.4.5 can be used to illustrate several points.

Figure 7.4.5 shows several microseismic events located on the east wing of the fracture at distances of up to 130 ft from the stimulation well. This confirms existence of an east wing of the fracture. For all but one of these events, the signal strength from the BSS tool in well MWX-3 was too weak to give a consistent two-well locations. This is undoubtedly related to the above mentioned difference in signal strength between wells MWX-2 and MWX-3. The farthest event location on the east wing of the fracture in Figure 7.4.4 is more than 300 ft from the BSS tool in well MWX-3. Beyond this range, data from well MWX-3 produced no analyzable events that were in close enough agreement with the positions determined from well MWX-2 to result in acceptable two-well locations.

Figure 7.4.5(a) indicates a fracture azimuth of 80° west of north, 12° different from Figure 7.4.4(a). The cause of this difference is illustrated by the single microseismic event shown in Figure 7.4.2. In Figure 7.4.2, both single-well locations are closer to the corresponding observation well than the two-well location. This places them 10° above and below the 70° west of north azimuth of the two-well location, causing both of the single well azimuths to differ from the two-well azimuth by 10°. This is typical of most of the 29 locations in Figure 7.4.4. Microseismic events for which a two-well location was established, yielded two-well locations further from both observation wells than the single-well locations were from the well from which they were determined. It seems reasonable to assume that this pattern is caused by the anisotropic nature of the MWX site. Whether it is caused by violation of the assumption that the direction of polarization is the direction to the source or problems with the velocity model remains to be determined. It is clear, however, that errors in azimuth could result from dependence on data from only one observation well; thus, events locatable in two wells provide a significantly improved measure of the azimuth.

7.4.10 SUMMARY AND CONCLUSIONS

The upgrade of the BSS has allowed the collection of data from microseismic activity with a significant increase in resolution. In spite of the inhomogeneous anisotropic conditions existing at the MWX site, it was possible to orient the BSS tools in both observation wells by assuming the direction of primary wave polarization is the direction to the seismic source, with only small errors in elevation and an even smaller scatter in azimuth. This resulted in the ability to locate perforation shots at a known depth in well MWX-1 to within 25 ft in the horizontal and 30 ft in the vertical by using data from both observation wells. Data from the fluvial B stimulation on November 1, 1986, indicate a fracture azimuth of 68° west of north with a fairly high level of confidence. However, fracture height could not be established due to the almost total absence of microseismic events located near the bottom of the fracture. Systematic

differences between the data from the two observation wells indicate that dependence on data from a single observation well could result in errors in fracture azimuth for inhomogeneous anisotropic geologies such as the MWX site.

7.4.11 REFERENCES

1. Hart, C. M., R. A. Newell and H. E. Morris, "Borehole Seismic System Analyses for A Complex Data Set", Rough Draft Report, Sandia National Laboratories, April 1986.

2. Engi D., "A Numerical Signal Processing Technique for Borehole Seismic Fracture Diagnostics", Sandia National Laboratories Report, SAND86-1865, 1/87.

3. Teufel, L. W., C. M. Hart, A. R. Sattler and J. A. Clark, "Determination of Hydraulic Fracture Azimuth by Geophysical, Geological and Orientated Core Methods at the Multi-Well Site, Rifle, Colorado", SPE 13226, 59th Annual SPE Meeting, Houston, TX, 9/84.

Table 7.4.1 Velocity Factors

Observation Well	Perforation Well	Velocity Factor (ft/ms)	Standard Deviation (ft/ms)	Path Length (ft)	Path Azimuth (North of East)
MWX-2	MWX-3	17.5	0.8	224	-87.8°
MWX-2	MWX-1	15.5	1.2	150	26.8°
MWX-3	MWX-1	18.4	1.2	217	-53.2°

Table 7.4.2 Tool Orientation

Observation Well	Perforation Well	Tool Orientation	Standard Deviation	Vertical Error	Standard Deviation
MWX-2	MWX-3	29.9°	3.6°	4.2°	2.9°
MWX-2	MWX-1	30.8°	3.0°	-3.6°	3.2°
MWX-3	MWX-1	-73.3°	2.4°	-4.2°	3.7°

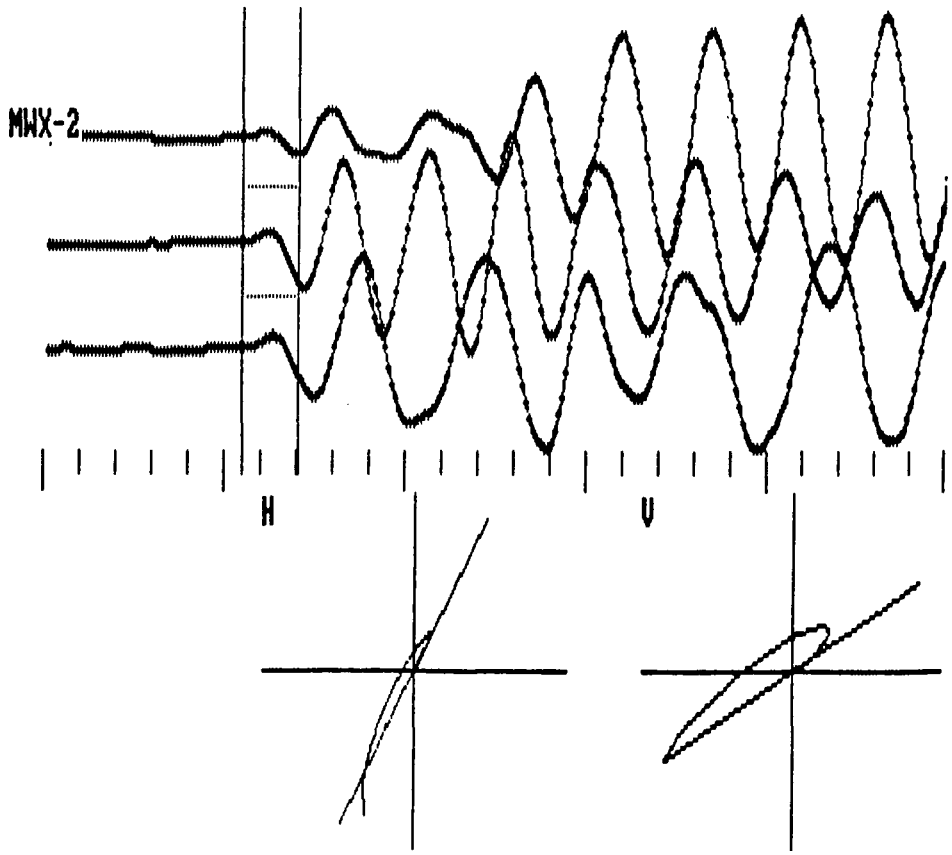

Figure 7.4.1. Microseismic event detected during the 1986 stimulation of the Fluvial Zone at the MWX site.

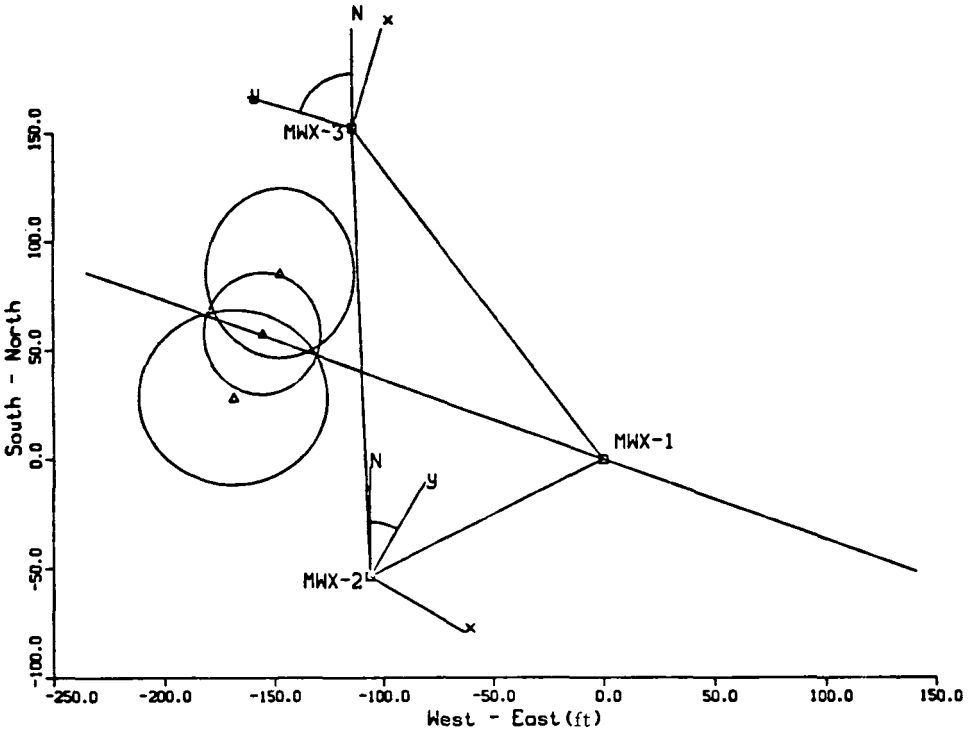

Figure 7.4.2(a). Horizontal projection of microseismic event location.

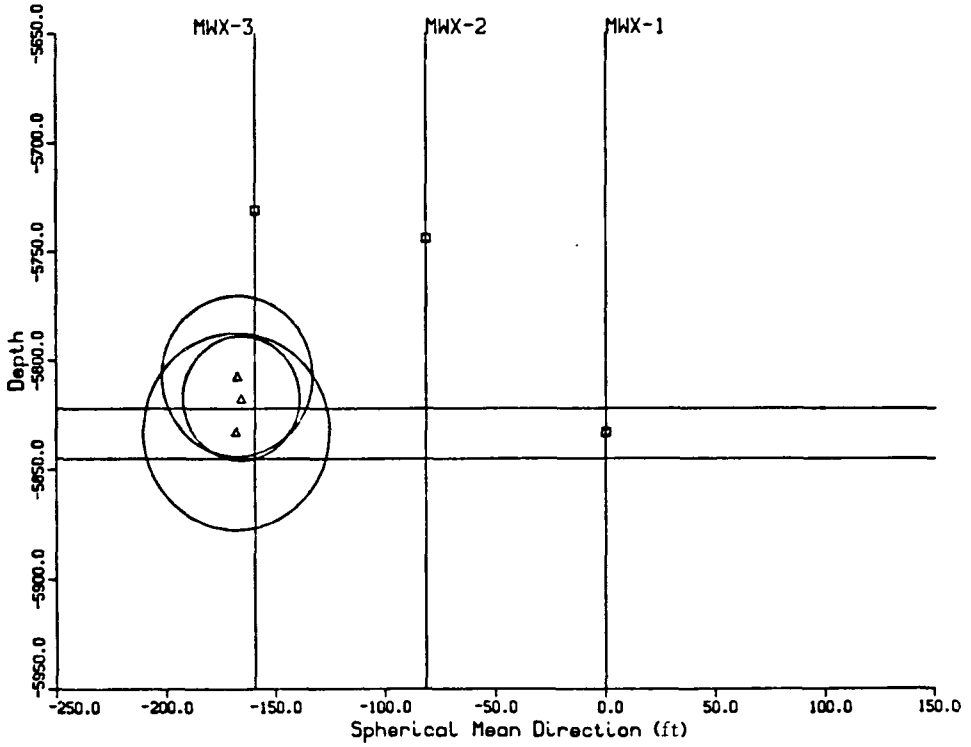

Figure 7.4.2(b). Vertical projection of microseismic event location.

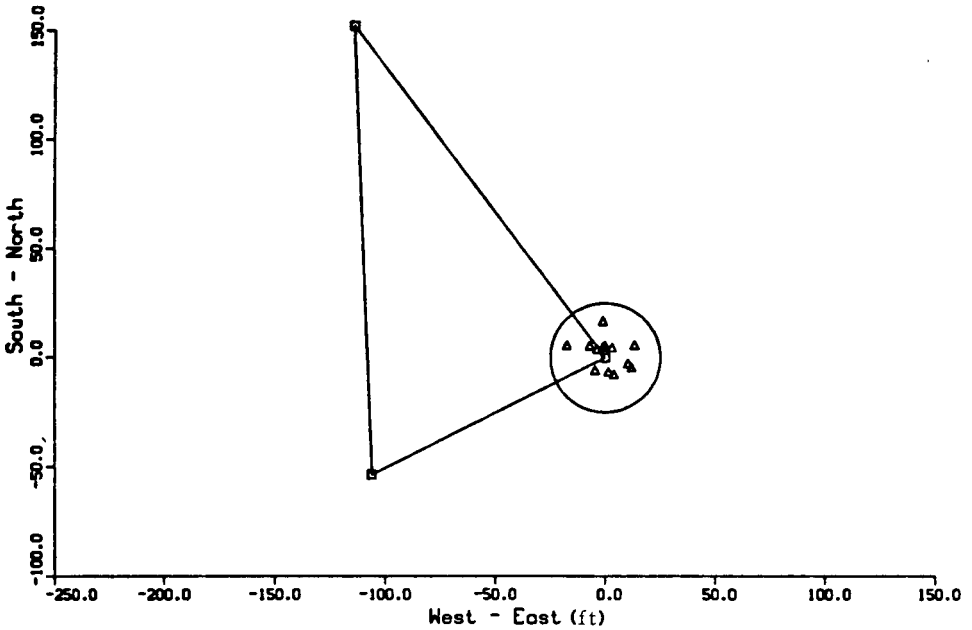

Figure 7.4.3(a). Horizontal projection of perforation shot locations.

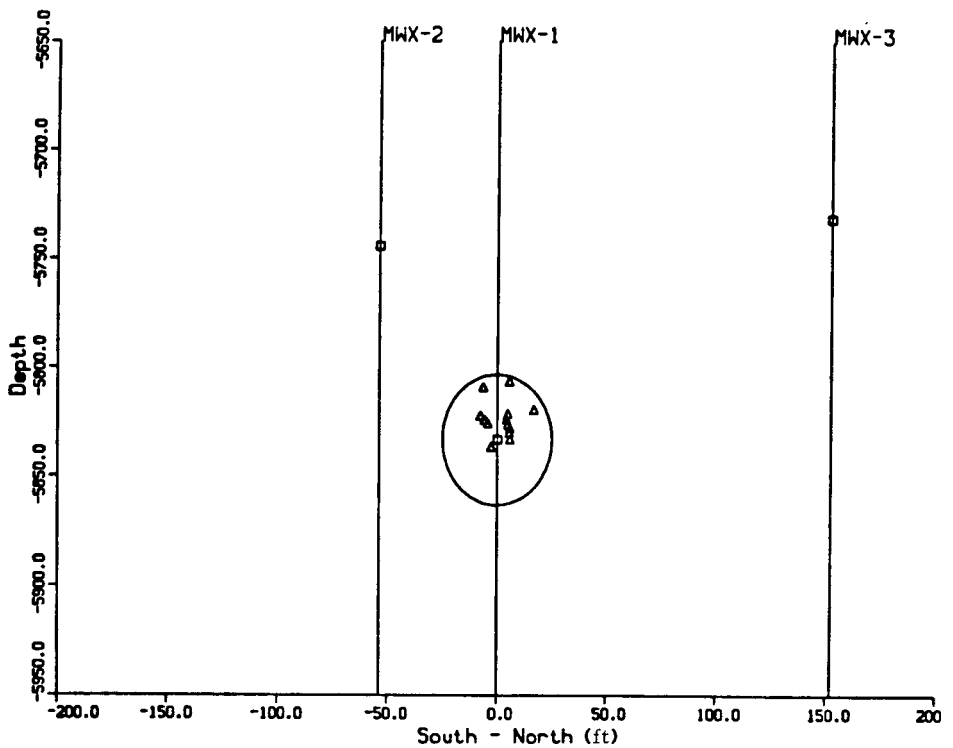

Figure 7.4.3(b). Vertical projection of perforation shot locations.

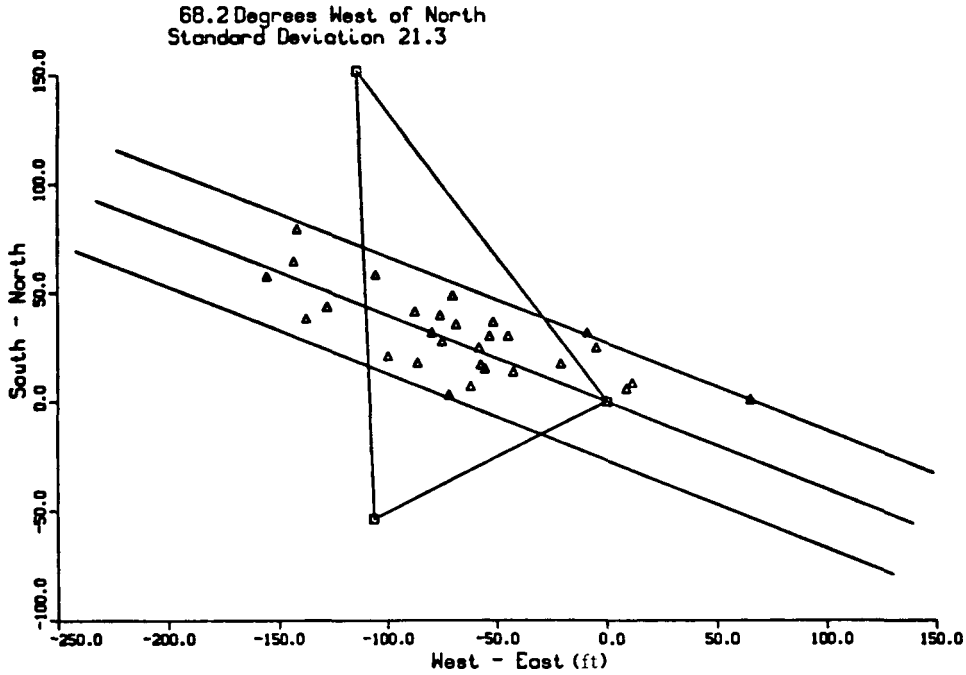

Figure 7.4.4(a). Horizontal projection of microseismic events for the 1986 stimulation of the Fluvial Zone at the MWX site.

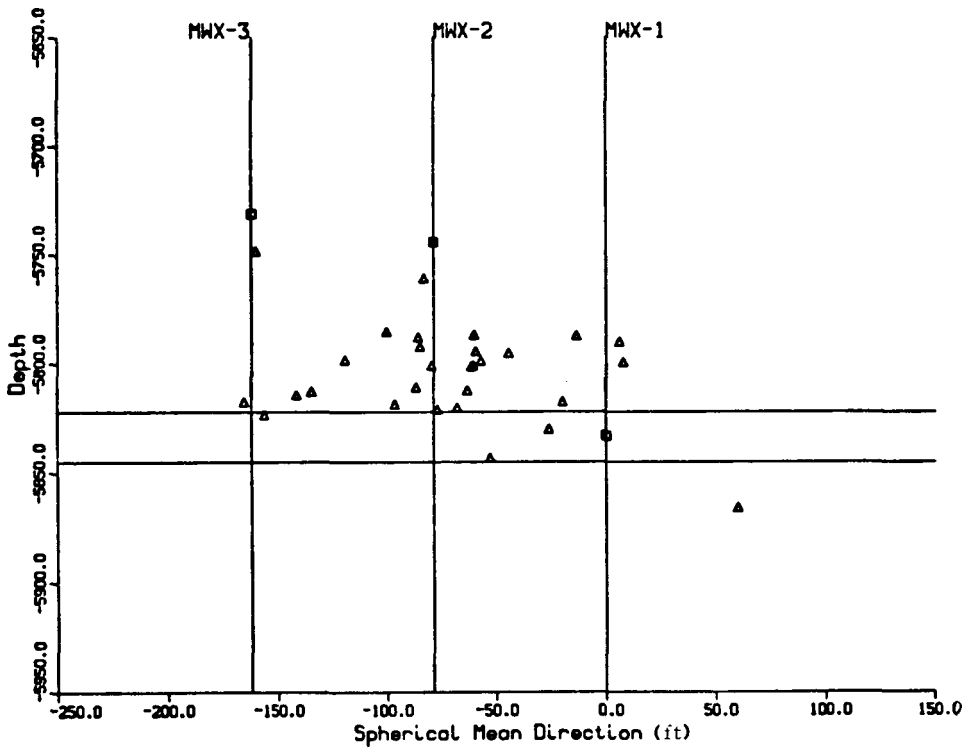

Figure 7.4.4(b). Vertical projection of microseismic events for the 1986 stimulation of the Fluvial Zone at the MWX site.

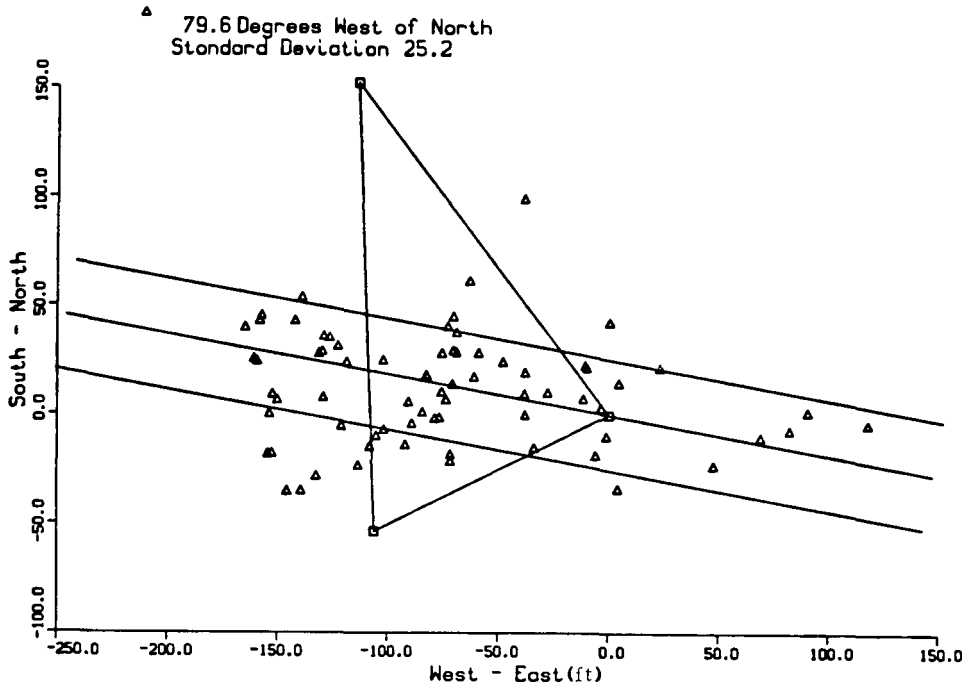

Figure 7.4.5(a). Horizontal projection of microseismic events located from Well MWX-2.

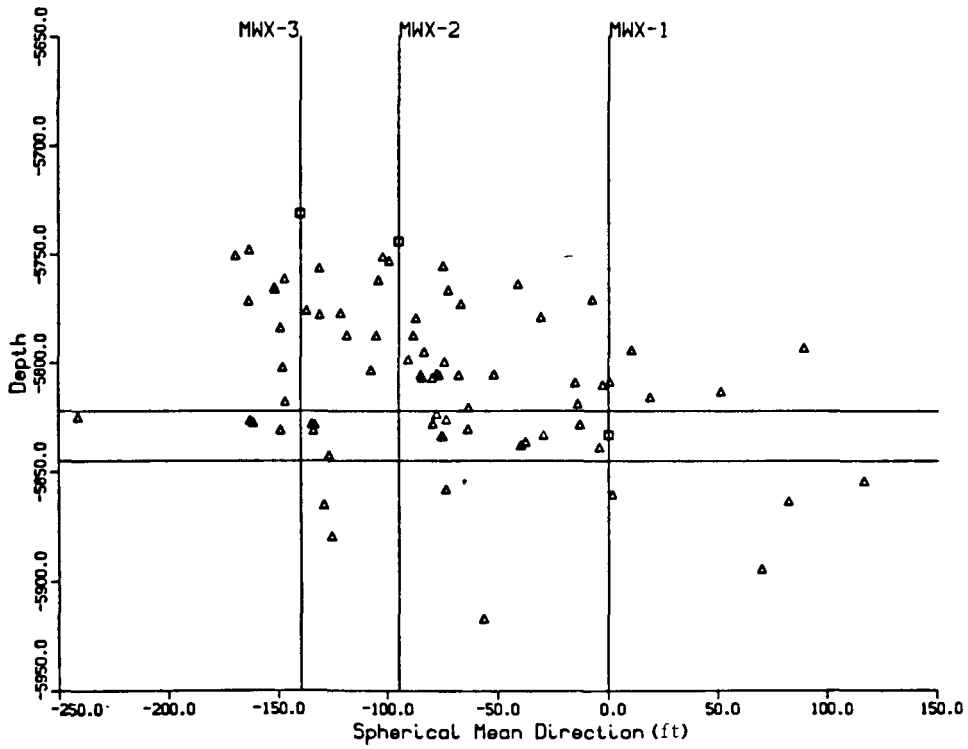

Figure 7.4.5(b). Vertical projection of microseismic events located from Well MWX-2.

8.0 FLUVIAL C SANDSTONE STIMULATION EXPERIMENT

8.1 LEAKOFF EXPERIMENTS AND ANALYSIS

N. R. Warpinski
Sandia National Laboratories

8.1.1 OBJECTIVE

A suite of fracturing experiments was conducted in the fluvial C sandstone at MWX. These experiments were performed in April and May 1987 and included pump-in/shut-in, step-rate/flow-back, pump-in/flow-back and datafrac tests. The objective of these tests was to characterize fracturing behavior in this interval and determine if accelerated leakoff conditions were present.

8.1.2 BACKGROUND

The previous results in the B sandstone of the fluvial interval (see Section 7.2) indicated that a dual leakoff phenomenon may have caused the early screenout that was observed in that zone. Below a threshold pressure (1050 psi above the closure stress), leakoff was relatively low (0.00025 ft/$\sqrt{}$min) and fracturing proceeded normally. Above this threshold pressure, leakoff was 50 times greater (0.0125 ft/$\sqrt{}$min) and screenout occurred only minutes after the start of sand injection. Tests in a lower zone, the coastal Yellow sand, may have shown the same behavior, although no quantitative analysis was possible.

We believe that this accelerated (or intensified) leakoff condition is caused by either (1) natural fractures within the pay zone opening when the injection pressure exceeds the threshold pressure or (2) sufficient fracture height growth at this pressure that the hydraulic fracture intersects many of the thin siltstones that contain wide, open natural fractures. These wide, open natural fractures are seen in thin beds (typically siltstones or sandstones) which are abundant in the fluvial interval, but they are not usually observed in the major reservoir units.

The purpose of this set of experiments was to determine if this pressure-sensitive leakoff is common in all sands in the fluvial interval, if the threshold pressure is relatively constant, and if some additive, such as 100-mesh sand, to the treatments would minimize the problem. The C sandstone was not a major target sand, so no pre-frac well tests were conducted. However, stress tests were performed throughout the interval.

8.1.3 FORMATION DATA

As seen in Figure 8.1.1 and in more detail in Figure 8.1.2, the C sandstone is 22 ft thick and lies at a depth of 5714-5736 ft. Table 8.1.1 gives known or estimated rock/reservoir data.

The matrix permeability, 6 μd dry at 3000 psi net stress, is reduced by about an order of magnitude at 55% water saturation for an in situ matrix permeability of about 0.5 μd. However, natural fractures give an effective permeability of about 12 μd based well testing in the B sand. The irreducible water saturations of 45-50% are determined from centrifuge capillary pressure tests up to 1000 psi displacement pressure.

Natural fractures in the C sandstone are thought to be very narrow and nearly unidirectional. Their orientation will approximately parallel the hydraulic fracture orientation. Many wider, and often highly porous, fractures are found in thin siltstones and sandstones above and below the C sandstone. The pressure sensitive leakoff may be due to either opening of the natural fractures within the reservoir sand or height growth into the abutting siltstones where fluid is lost to the open fractures.

Figure 8.1.3 shows a plot of Young's modulus and Poisson's ratio data in the region of the B and C sandstones. Young's modulus for the sand is about 4×10^6 psi and Poisson's ratio is about 0.18. Elastic parameters for the mudstones are quite variable.

In situ stress data for this region are shown in Figure 8.1.4. These stress tests were all conducted in MWX-2. There is an interesting feature

in the stresses in this fluvial region. Below about 5800 ft, the minimum stresses in the mudstones are all around 0.98-1.05 psi/ft gradients. Above 5800, the minimum stresses drop to 0.9-0.94 psi/ft gradients. Below 5800, stress contrasts between sands and shales are 1200-1500 psi. Above 5800, stress contrasts are 500-900 psi, suggesting that height growth may be more of a problem here in the C sandstone than it was in the B sandstone. The closure stress for the C sandstone is about 4575 psi.

8.1.4 WELL DATA

The well configuration is shown in Figure 8.1.5. The casing in the treatment well is 29-lb, seven-in., N80 pipe. There was a string of 2-3/8-in. tubing in the well, landed open-ended at 5650 ft. Inside the tubing, about 25-30 ft above the open end, a bottom-hole pressure/ temperature package was situated, thus placing it about 100 ft above the center of the C sandstone. The treatments were all conducted down the annulus, with a flush volume to the top of the perforations of about 181 bbl. Perforations were shot from 5720-5738 ft, avoiding the top of the zone where cement bonding was marginal. The perforation schedule had one shot/ft of 23-gm, 0.43-in.-diameter perfs and one shot/ft of 10-gm, 0.31-in.-diameter perfs. The smaller charges were shot singly to provide signals for orienting a geophone package in MWX-3.

8.1.5 FRACTURE EXPERIMENTS

8.1.5.1 Schedule of Tests

On April 28, 1987 the C sandstone interval was broken down using ball sealers for diverting. The following series of tests was then conducted in this interval:

KCl pump-in/shut-in test	4/28/87
KCl step-rate/flow-back test	4/29/87
Two KCl pump-in/flow-back tests	4/29/87

Foam minifrac	4/30/87
One-week flow and cleanup test	5/04/87
Foam + 100-mesh minifrac	5/12/87
One-week flow and cleanup test	5/19/87

Cipolla et al.[1] give a detailed description of these tests and plots of the data. This reference appears as Appendix J, while digitized stimulation data for the two minifracs are found in Appendix K.

8.1.5.2 Pump-In/Shut-In Test

The purpose of the pump-in/shut-in test was to determine fracture parameters for a case where the pressure in the fracture did not exceed the threshold pressure for intensified leakoff. KCl water was injected at seven bpm for 10 minutes and shut in for 45 minutes. This was sufficient shut-in time for the pressure decline analysis and for the pressure to drop below the closure stress. Figure 8.1.6 shows the bottom-hole pressure and flow-rate data for this test. We do not know what caused the nearly one hundred psi drop in pressure at six minutes. Otherwise the test appears normal. The Nolte-Smith plot[2] is shown in Figure 8.1.7; the slope appears to be on the order of 0.2, which is the expected value for a Newtonian fluid.

Figure 8.1.8 shows the standard Nolte[3] type curve for the shut-in data. The estimated P* is 220 psi. This yields a leakoff coefficient of 0.0003 ft/$\sqrt{}$min for a fracture height and leakoff height of 22 ft. Figure 8.1.9 shows the square-root-of-time plot and the derivative; it suggests that closure occurs at about 18 minutes after shut-in. This is at a pressure of about 4600 psi, in good agreement with the stress test in MWX-2. The G-function and dP/dG plots, as described by Castillo[4] are shown in Figure 8.1.10. They also indicate that closure occurred at about 18 minutes. The stabilized shut-in period, between the end of extension and the start of closure, only lasts for about 15 minutes, from 3-18 minutes. During this period, dP/dG (or P*) varies from 265 to 200 with an average value of 224, in good agreement with the type curve value.

Figure 8.1.11 shows the pressure-dependent leakoff results for an exponent of 1/2. The slope of the function is about -2.5 between three and 18 minutes, yielding an M value (see Castillo[4]) of $9x10^{-6}$. This gives a leakoff coefficient of 0.00032 ft/$\sqrt{}$min during the shut-in (4750 psi) and 0.00036 ft/$\sqrt{}$min during the pump (5200 psi). For all practical purposes, the leakoff is pressure insensitive.

Since water is the frac fluid, the compressibility-controlled leakoff (exponent = 1) is the same order of magnitude as the leakoff due to the viscosity of the frac fluid, so this case has been calculated also. Figure 8.1.12 shows these results and gives a slope of about -0.14. This yields an M value of $2.4x10^{-7}$ and a leakoff coefficient of 0.00033 ft/$\sqrt{}$min at shut-in and 0.0043 during pump, a slight pressure sensitivity. A comparison of Figures 8.1.11 and 8.1.12 would seem to indicate that the compressibility-controlled-leakoff case does a better job of adjusting the pressure behavior (constant slope during stabilized shut-in period). At these relatively low pump and shut-in pressures, there is no evidence of the factor of 50 increase in leakoff that we believe occurred in the B sandstone experiment.

8.1.5.3 Step-Rate/Flow-Back Test

A step-rate/flow-back test was conducted to estimate the minimum fracture extension pressure (step-rate) and closure stress (flow-back). KCl water was injected at rates from 1-7 bpm with a total volume of 71 bbl. Figure 8.1.13 shows the pressure and flow rate data and Figure 8.1.14 shows the step-rate data on linear and semilog plots. The semilog plot is usually a good technique for linearizing the two regimes. This suggests that the minimum fracturing pressure is about 4950 psi.

The flow-back portion of the test is shown in Figure 8.1.15. The initial flow-back rate was about 1.1 bpm, but this had dropped to about 0.9 bpm at closure. While there is clearly an inflection in the pressure data, the actual inflection point is difficult to determine. Figure 8.1.16 shows derivatives of the pressure data. Figure 8.1.16a is determined from a

five-point regression of the actual pressure vs time data. The point of maximum slope is difficult to discern and may occur anywhere between 24 and 28 minutes for a closure stress between 4800 and 5000 psi. When the point of curvature reversal cannot be determined from a regression, it often helps to determine the inflection point with a fourth or fifth order polynomial fit. A solid line showing the fit has been plotted in Figure 8.1.15 and the derivative results are shown in Figure 8.1.16b and c. The fitted inflection point is at 27 minutes for a closure stress of 4850 psi. This is considerably higher than the stress test and pump-in/shut-in results.

8.1.5.4 Pump-In/Flow-Back Tests

Two pump-in/flow-back tests were conducted to investigate the discrepancy in closure stress values seen in previous data. Both tests used KCl water injected at seven bpm for 10 minutes. The pressure, injection rate, and Nolte-Smith plot for the first pump-in/flow-back test are shown in Figure 8.1.17. The flow-back data are shown in Figure 8.1.18. The flow-back rate in this test was held at a fairly constant 1.5 bpm through closure. The solid line through the pressure data is a least-square, fourth-order, polynomial fit. The inflection point in the flowback is again determined from the derivatives shown in Figure 8.1.19. Again, it is difficult to determine a maximum in the actual data, as shown in the five-point, regression-derived derivative in Figure 8.1.19a. The fourth-order, polynomial fit yields an inflection point at 14 minutes for a closure stress of 4930 psi. This value is higher than the previous flowback result.

The injection data for the second pump-in/flow-back test are shown in Figure 8.1.20. The flow-back data are shown in Figure 8.1.21. The flow-back rate dropped from about 0.8 bpm at the start of flow-back to about 0.7 bpm at closure. In this flow-back, a third order polynomial fit the data to the required accuracy. The derivatives are shown in Figure 8.1.22. The five-point regression derivative suggests that closure may be as early as 25 minutes at a pressure of 4620 psi while the polynomial fit yields closure at 29.5 minutes at a pressure of 4475 psi. These values are much more in line with the stress-test and pump-in/shut-in stress values than the previous two

flow-backs. Figure 8.1.23 shows the estimated closure stress vs the flow-back rate. These data suggest that the apparent-closure-stress measurement may be rate dependent, but this may just be due to the difficulty in determining the inflection point in these tight, naturally fractured sands. For all analyses, 4575 psi will be used as the closure stress, based on stress tests, the pump-in/shut-in result and the final pump-in/flow-back test.

8.1.5.5 Minifrac #1

The purpose of the first minifrac was to determine if the intensified leakoff would occur during a fracture treatment of the C sandstone. The design schedule is shown in Table 8.1.2. The digitized stimulation record is given in Appendix K.

We always start the minifracs by pumping up the wellbore to 2500 psi bottomhole with nitrogen. This is done so that the initial foam injected into the wellbore does not have such a high quality (at low pressures) that it becomes unstable, to establish the nitrogen rate, and to clean out any residual bottom-hole liquids. 150 bbl (6300 gal) of 75-quality, 20 lb/1000 gal gel, nitrogen foam were injected in this minifrac. No breaker was used for this test. The flush was foam also and required an additional 181 bbl. The bottom-hole rate was 10 bpm at 5600 psi at 140°F. The nitrogen volume factor under these conditions is 1496 SCF/BBL. Estimated values of n′ and k′ are 0.5 and 0.007 lb-sec$^{n'}$/ft^2.

Figure 8.1.24 shows the important data for this minifrac, including surface foam rate, bottom-hole pressure and bottom-hole temperature. The injection pressure data and the Nolte-Smith plot are shown in Figure 8.1.25. There is some initial fracturing with nitrogen until the foam hits the perfs at about 17 minutes. During the foam injection, there appears to be three distinct fracturing phases. Initially the pressure rises rapidly as the foam begins fracturing. At about 20 minutes (5450 psi), the pressure flattens considerably and may be caused by the advent of intensified

leakoff. Finally at about 33 minutes (5590 psi) the pressure begins to slowly drop, perhaps due to height growth.

The pressure-decline data are shown in Figure 8.1.26 along with the resultant Nolte-type curve. The estimated match pressure is 93 psi which yields a leakoff coefficient of 0.000056 ft/$\sqrt{}$min. (The degradation coefficient is assumed to be unity for the 29-minute foam injection.) The plots of pressure versus G function and the derivative are shown in Figure 8.1.27. The P* value drops from 100 psi at 20 minutes to 80 psi at the end of the test. A pressure-sensitive leakoff analysis for frac-fluid, viscosity-controlled leakoff results in the plots shown in Figure 8.1.28. The pressure function stabilizes at a value of about -0.85. This yields an M value of 2×10^{-6} for a leakoff coefficient of 0.00076 ft/$\sqrt{}$min at 5300 psi and 0.000081 ft/$\sqrt{}$min at 5600 psi. No indications of any significant pressure-sensitive leakoff are seen in the pressure decline analysis.

8.1.5.6 Pressure History Match of Minifrac #1

Based on the results of the pressure decline analysis, one would conclude that leakoff is very low and a fracture treatment is not likely to screenout. However, this does not necessarily imply that leakoff during pumping conditions will also be low. Additionally, the low slope of the Nolte-Smith plot is a warning of some undesirable fracture growth, possibly height growth, high leakoff or a compliance change. As with the B sandstone minifrac (Section 7.2.4), the only means to recognize the fracture parameters during pumping is to perform a pressure history match in combination with the pressure decline analysis.

For the match calculations, a pseudo-3-D, Perkins and Kern geometry, finite-difference simulator was used. The height growth for this case is based primarily on in situ stresses, but a comparison of the stress data in Figure 8.1.4 with the magnitude of the treatment pressures shows that either the stress profile is missing some high stress regions or fracture height is also being controlled by other features. Given the stress data in Figure 8.1.4, it would be impossible to get treatment pressures above 5500 psi.

There is a possibility that some high stress regions were missed because of some poor cement bonding in this region. During stress testing, there was some difficulty breaking down most of the mudstone stress-test zones and high injection pressures were observed in many of zones.

The stress profile that was used is more in line with all of the stress results in lower zones and is shown in Figure 8.1.29. This profile is only three layers and assumes about a 1.0 psi/ft gradient for the mudstones. As will be seen later, this is still not sufficient to contain the fracture adequately (based primarily on borehole seismic data, Section 8.4). Also a maximum height restriction of 70 ft was put on the fracture, up to the point of declining pressure. This restriction is totally arbitrary, but is based on an inability to match the high pressure level with anything else and it agrees with the diagnostic information.

Figure 8.1.30 shows two initial calculations that illustrate some of the features of the fracture behavior. The initial nitrogen fracturing stage is easily matched, but it has only a minor effect on the rest of the treatment. A low leakoff coefficient, as determined from the pressure decline analysis, can model the initial pressure rise, but then pressures also continue to rise. A high leakoff coefficient can fit the maximum pressure better, but it cannot match the initial fracture behavior. Similarly, neither of these can match the shut-in behavior. The low leakoff yields a very slow pressure decline, much like that observed after about 47-48 minutes, but is nowhere close to matching the initial pressure decline. The high leakoff case has a rapid initial drop at shut-in, but then also continues to drop off too rapidly to match the data.

The key feature is the pressure flattening that occurs at about 18 minutes. This flattening can be matched with excessive height growth, but then the pressure would drop very slowly at shut-in because of the large amount of fluid storage in the extra height. Furthermore, there is no indication of excessive height from the geophone data.

As in the B sandstone, the only good match of this behavior is with an accelerated leakoff above some threshold pressure. A final match is shown in Figure 8.1.31. The threshold pressure is about 875 psi above closure and the factor of increased leakoff is 70, from 0.0001 ft/$\sqrt{}$min to 0.007 ft/$\sqrt{}$min. This gives a good pressure match up to about 30 minutes.

After 30 minutes, the decrease in pressure is most likely due to fracture height growth into a lower stress zone. This could also be obtained with an even higher leakoff, so much so that the length would start decreasing, but this seems unlikely because of the extremely high leakoff required. It also seems likely that it would shut itself off when the pressure drops a little, but this does not happen. Since there is insufficient data to estimate the locations of the high and low stress regions that might be controlling the height growth, an arbitrary artificial pressure-drop growth has been included in the fracture simulator. This is done by increasing the height a small percentage at each time step for a given pressure. Only fracture heights of 70 ft or more are allowed to increase. This artificial feature yields an estimate of the total additional height needed to give the observed pressure drop. In this case, it only takes an additional 7-14 ft of height growth, depending on how the width area factor is adjusted, to get the required pressure behavior. Unfortunately, the addition of the artificial pressure-drop growth does not allow a reasonable match of the shut-in behavior. If the fracture breaks into a lower stress zone, at shut-in the shale will close first, thus trapping the fluid in the low stress interval. The simulator cannot easily dispose of the trapped fluid (since conservation of mass is invoked) and the result gives too much storage and a smaller drop-off at shut-in than actually measured. This is unfortunate, because the shut-in behavior is a valuable part of the history data.

Obviously, parts of this modeling exercise are arbitrary and nonunique, but it is a fairly convincing case that shows that the intensified leakoff hypothesis is the best explanation for the pressure behavior. Because of uncertainties in the stresses and the resultant height growth, the factor of

70 increase is only an estimate of the change in leakoff. With a maximum height of 50 ft, 100 ft or some other value, the factor of 70 will change accordingly, as low as 50 or as high as 80. It appears that this intensified leakoff is a common feature in all the fluvial sandstones and possibly in the coastal and paludal intervals as well.

8.1.5.7 Minifrac #1 Clean-Up and Flow Test

After the first minifrac, the well was flowed back, cleaned up and tested for about a week. Cleanup was rapid and gas flow rates were 50-60 MCFD. Some of this rate was probably due to nitrogen returned from the minifrac. The well was then shut in to prepare for the second minifrac.

8.1.5.8 Minifrac #2

The purpose of the second minifrac was to determine if 100-mesh sand could control the excessive leakoff that was thought to be occurring in these fluvial sands. The design schedule is shown in Table 8.1.3. The digitized stimulation record is given in Appendix K.

Again, the foam frac was initiated by establishing the N_2 rate and pumping up to sufficient pressure that the initial foam quality is not too high as to be unstable. Four different 100-mesh sand concentrations were used to determine if there was any apparent optimum concentration. The purpose of the preflush was to determine if the effect of the 100-mesh sand was transitory, i.e., if leakoff control would decrease after 100-mesh was stopped. The design flow rate was 10 bpm bottom-hole. This test used the same foam system as the first minifrac, but the base gel viscosity of the second minifrac was somewhat lower than the first.

Figure 8.1.32 shows the important data for the second minifrac, including surface foam rate, bottom-hole pressure and bottom-hole temperature. From the available data, the bottom-hole rate is estimated to be 9.2 bpm. Figure 8.1.33 shows the bottom-hole pressure during the pumping

and the Nolte-Smith plot for the foam injection. The nitrogen fracturing behavior is considerably different than that of the first minifrac. This is probably due to a spearhead of a few barrels of KCl water present in the first minifrac because of incomplete removal of the KCl water from the well after the pump-in/flow-back tests. No water was found in the well prior to the second minifrac. In this test, foam hits the perfs at about 21 minutes and the 100-mesh sand stages hit in successive five-minute intervals. The preflush hits the perfs at about 46 minutes, which is coincidently the time at which the pressure levels off. It is not clear whether this is the advent of height growth or the return of higher leakoff conditions with the end of the sand. In any event, it is clear that the 100-mesh sand has a positive effect on leakoff, since the pressure continues to increase (after 26 minutes) instead of becoming flat as it does in the first minifrac (compare with Figure 8.1.25). The Nolte-Smith plot also has a larger slope in the second, as compared to the first minifrac.

Figure 8.1.34 shows the pressure decline data and the formal Nolte type curve. P^* is about 200 psi, which yields a leakoff coefficient of around 0.0001 ft/$\sqrt{}$min, about twice that obtained from the type curve analysis of minifrac #1. With such a low leakoff coefficient and small zone thickness, the derived length of several thousand feet is unbelieveably long.

A plot of the pressure versus the G function is shown in Figure 8.1.35, along with a five-point regression of the derivative. While there is a lot of scatter in the data, the average P^* from 25-100 minutes is also about 200 psi. It drops to around 150 psi later in the falloff. The pressure dependent leakoff analysis is shown in Figure 8.1.36. The linearization of G is marginally improved, yielding a slope of about -1.4; the derivative is a least-square polynomial fit as the regression data were too noisy. This results in an M value of 1.8×10^{-6} for a leakoff coefficient of 0.00011 ft/$\sqrt{}$min during shut-in and 0.00012 ft/$\sqrt{}$min during pumping. These values are nearly the same as the first minifrac.

It is not clear whether the linearization provides a better estimate of leakoff in either of the minifracs. The resultant leakoff coefficients

(linearized vs nonlinearized) are different by about a factor of two in the first minifrac, but are much closer in the second minifrac. In any event, the leakoff coefficient after the second minifrac is about twice the value after the first minifrac. This may be due to the 100-mesh sand, either propping open natural fractures within the zone or holding open the shales sufficiently that other leakoff zones are available.

8.1.5.9 Pressure History Match of Minifrac #2

The primary purpose of the second minifrac was to determine what effect the 100-mesh sand had on leakoff. To do this, the second minifrac was modeled using the same parameters as the first test. The only differences were (1) a slightly different nitrogen pump up, (2) a bottom-hole flow rate of 9.2 bpm compared to 10 bpm in the first minifrac, and (3) a lower foam viscosity for the second minifrac (estimated at $k' = 0.005$ lb-sec$^{n'}$/ft^2). The effect of the sand concentration was modeled with Steinour's relationship[5] for viscosity increase with sand concentration to account for the effect of the 100-mesh sand.

Figure 8.1.37 shows an example calculation through the first two sand stages for an intensified leakoff with a factor of 70 increase in leakoff above 875 psi (above closure). The 100-mesh sand has clearly resulted in different fracture behavior than the first minifrac. Figure 8.1.38 shows the final best match of the minifrac. It was obtained by reducing the factor of leakoff from 70 to 20 after the first two minutes of the 0.25 ppg sand stage. After 42 minutes, artificial pressure-drop height growth was applied again to get the pressure stabilization. Only 4-8 ft of additional growth was required at this point. Again, no shut-in analysis is available because of the excess storage that cannot be disposed of.

Since the height growth seems to occur just about the time the preflush hits the perfs, the final pressure stabilization was also modeled as a return to the factor of 70 leakoff. This is shown in Figure 8.1.39 and it cannot account for the pressure behavior. This is fairly convincing evidence that the pressure stabilization is due to height growth.

The important point is that the 100-mesh sand appears to have reduced leakoff from 0.007 ft/√min to 0.002 ft/√min, a 3.5 decrease. The 100-mesh sand also might delay height growth. It may also result in a higher leakoff coefficient after shut-in, which of course also means higher permeability feeding the hydraulic fracture once production is started. All of these are positive effects.

8.1.5.10 Post Minifrac #2 Clean-Up and Flow Test

After the second minifrac, the well was flowed back, cleaned up and produced for about a week. Gas flow rates were about the same as after the first minifrac and were probably supported somewhat by the injected nitrogen. We did not expect enhanced production, even with the 100-mesh sand, because of the large preflush which cleared out the near-wellbore area.

8.1.5.11 Diagnostics

Temperature logs were run after each of the minifracs, but no indication of fracturing, outside of the perforated interval and a few feet above and below, was evident. Temperature logs have not been particularly useful in the foam fractures conducted at MWX. A borehole seismic package was placed in MWX-3 during these operations and these results are given in Section 8.4.

8.1.6 DISCUSSION AND CONCLUSIONS

The C sandstone fracturing experiments were very successful and we accomplished our two primary objectives: (a) the treatments again showed evidence of the intensified leakoff that probably caused the screenout in the B sandstone, and (b) we found that 100-mesh sand was a relatively effective leakoff-control agent. Looking back at previous coastal and paludal tests,[6,7] it is possible that there was some intensified leakoff in those tests as well, but probably not such a high factor. The effect of the 100-mesh sand was positive. The positive effects include control of leakoff, possible delay of height growth, and increased permeability along

the sides of the hydraulic fracture as evidenced by increased leakoff after shut-in. The only possible deleterious effect of the fine-mesh sand is reduction of hydraulic-fracture conductivity, but with effective reservoir permeabilities of 10-15 md, a little loss of hydraulic-fracture conductivity will not be noticed.

The results again show that the optimum way to obtain stimulation design parameters is to combine a pressure decline analysis with a pressure history match. This yields the best possible insight into reservoir and fracture behavior.

The major problem with the pressure history match in these tests was fracture height. The stress tests did not show enough contrast to limit height as much as the geophone data and altered stress data showed (see Sections 8.2 and 8.4). Temperature logs were inconclusive. An arbitrary stress profile with a limiting height was used to get a reasonable fracture height calculation. These findings are not unexpected, however, as it has been shown that many factors control fracture height. In this case, the complicated bedding or the narrow widths in the higher stress mudstones may have made fracture height growth relatively inefficient. Height growth based on stress is a conservative calculation, as it probably gives the maximum possible height, and a time constant approach would not do any better here. A constant height model could have been used for these calculations, except that it would not have been easy to match the nitrogen fracturing stage, where heights are relatively small, and it would have been difficult to get the steep pressure increase when the foam hit the perfs without altering several other parameters. Even though it is somewhat arbitrary, this height growth model helps give the best picture of overall fracture behavior. These problems with modeling fracture height illustrate the importance of having some kind of reliable height diagnostic.

We have had some difficulty getting consistent closure stress measurements in these intervals using flowback tests. It is not clear whether there is some rate effect or the characteristics of flowback from a

tight, naturally fractured sandstone are such that the inflection point does not appear clearly. On the other hand, an initial pump-in/shut-in test with KCl water was very clear and consistent with the previous stress tests.

8.1.7 REFERENCES

1. Cipolla, C., R. Wilmer, D. Cowley, and D. Ferguson, "Multiwell Experiment Fluvial C Fracturing Quality Control and Monitoring Results," CER Corporation Report, June 12, 1987.

2. Nolte, K. G. and M. B. Smith, "Interpretation of Fracturing Pressures," JPT, Vol. 33, No. 9, pp 1767-1775, September 1981.

3. Nolte, K. G., "A General Analysis of Fracturing Pressure Decline with Application to Three Models," SPE Formation Evaluation, Vol. 1, No. 6, pp 571-583, December 1986.

4. Castillo, J. L., "Modified Fracture Pressure Decline Analysis Including Pressure-Dependent Leakoff," SPE 16417, presented at SPE/DOE Low Permeability Reservoirs Symposium, Denver, CO, pp 273-281, May 18-19, 1987.

5. Steinour, H. H., "Rate of Sedimentation," Industrial and Engineering Chemistry, Vol. 36, No. 9, pp 618-624, July 1944.

6. Northrop, D. A., ed., "Multiwell Experiment Final Report: 2. The Paludal Interval of the Mesaverde Formation," Sandia National Laboratories Report, SAND88-1008, May 1988.

7. Northrop, D. A., ed., "Multiwell Experiment Final Report: 3. The Coastal Interval of the Mesaverde Formation," Sandia National Laboratories Report, SAND88-3284, March 1989.

Table 8.1.1

C Sandstone Data

Gross Height	22 ft
Net Height	22 ft
Porosity	8%
Permeability, Matrix	6.0 μd dry at 3000 psi net stress 0.5 μd at 55% Sw and 3000 psi net stress
Water Saturation	55%-60%
Irreducible Water Saturation	45%-50%
Permeability, Effective	12 μd (from B Sandstone well tests)
Initial Reservoir Pressure	3400 psi
Initial Reservoir Temperature	160°F
Young's Modulus	4×10^6 psi
Poisson's Ratio	0.18

Table 8.1.2

Minifrac #1 Design Data

	Volume (bbl)	Volume N_2 (SCFM)	Volume Liquid (bbl)	Rate N_2 (SCFM)	Rate Liquid (bpm)
Pump up	-	150,000	-	11,220	-
Minifrac	150	170,000	37.5	11,220	2.5
Flush	181	205,000	45.3	11,220	2.5
		525,000	82.8		

Table 8.1.3

Minifrac #2 Design Data

	Volume (gal)	Volume N_2 (SCF)	Volume Liquid (bbl)	Rate N_2 (SCFM)	Rate Liquid (bpm)	100-Mesh Sand (ppg)
Pump up	-	150,000	-	11,200	-	-
Pad	2,000	53,510	12	11,200	2.5	-
Stage 1	2,000	53,500	12	11,200	2.5	0.25
Stage 2	2,000	53,500	12	11,200	2.5	0.5
Stage 3	2,000	53,500	12	11,200	2.5	0.75
Stage 4	2,000	53,500	12	11,200	2.5	1.0
Preflush	5,000	134,000	30	11,200	2.5	-
Flush	7,600	203,000	45	11,200	2.5	-
Totals	22,600	754,500	125			5000 lb

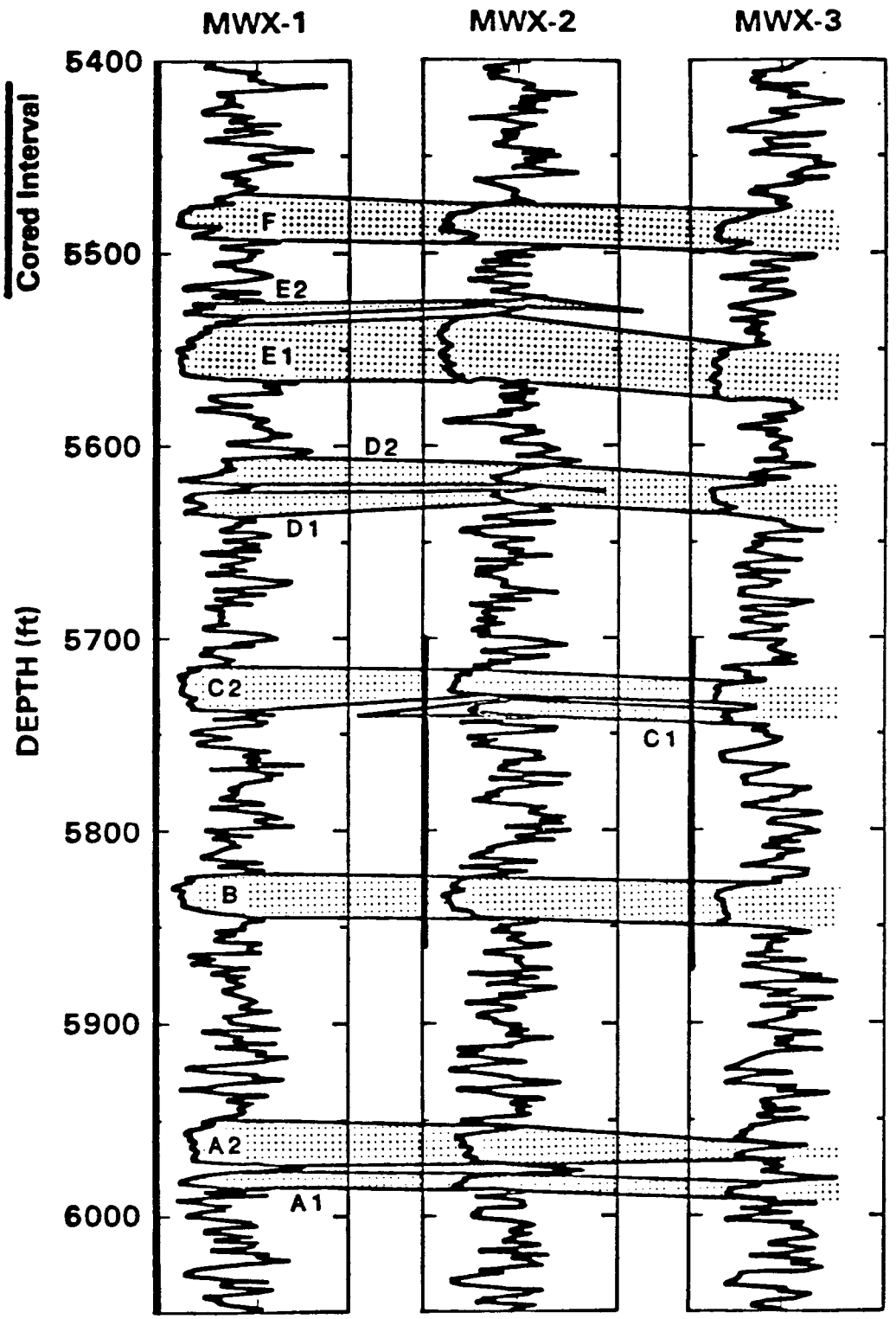

Figure 8.1.1. Lower Fluvial Lithology

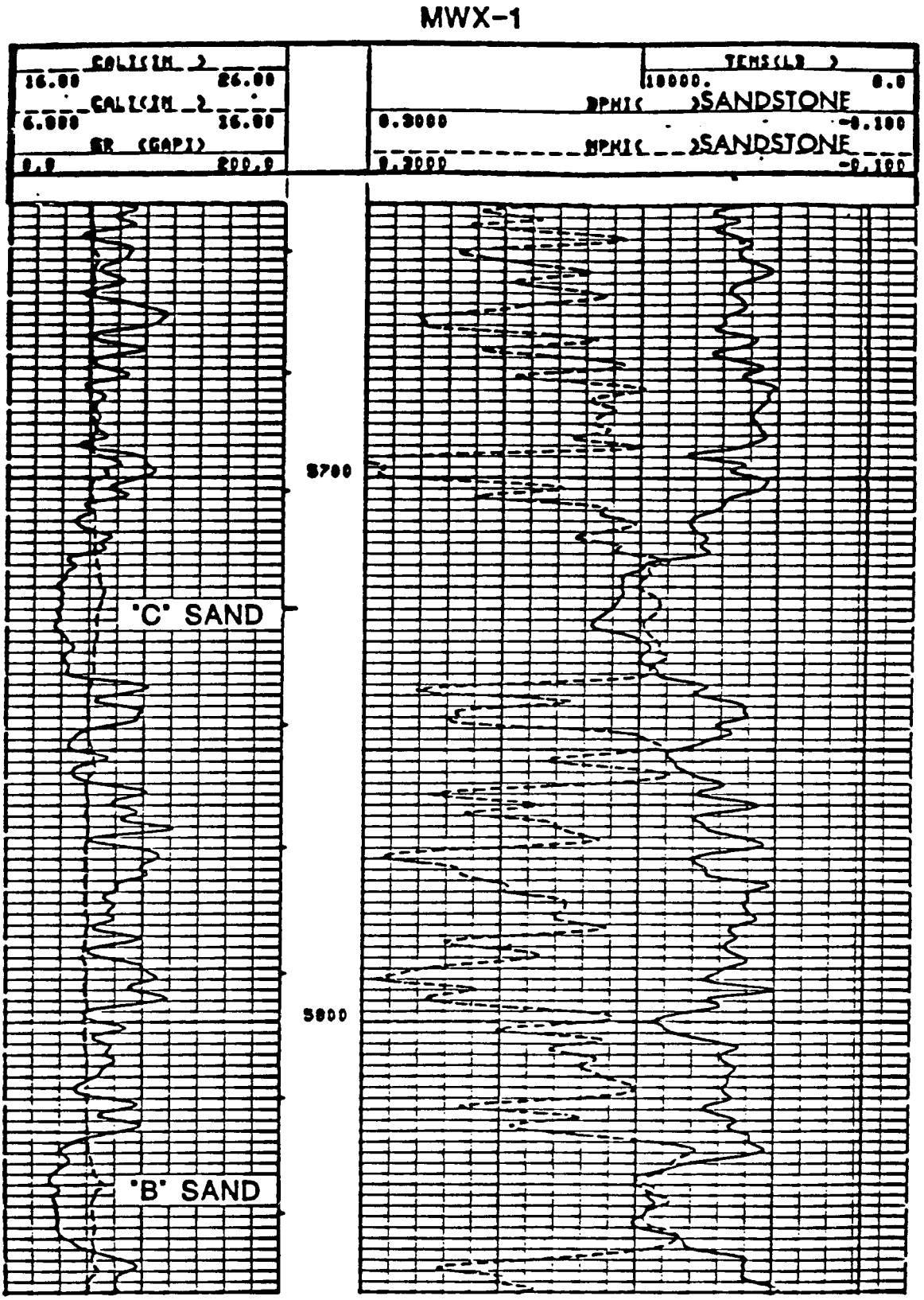

Figure 8.1.2. Logs in the Vicinity of the C Sandstone

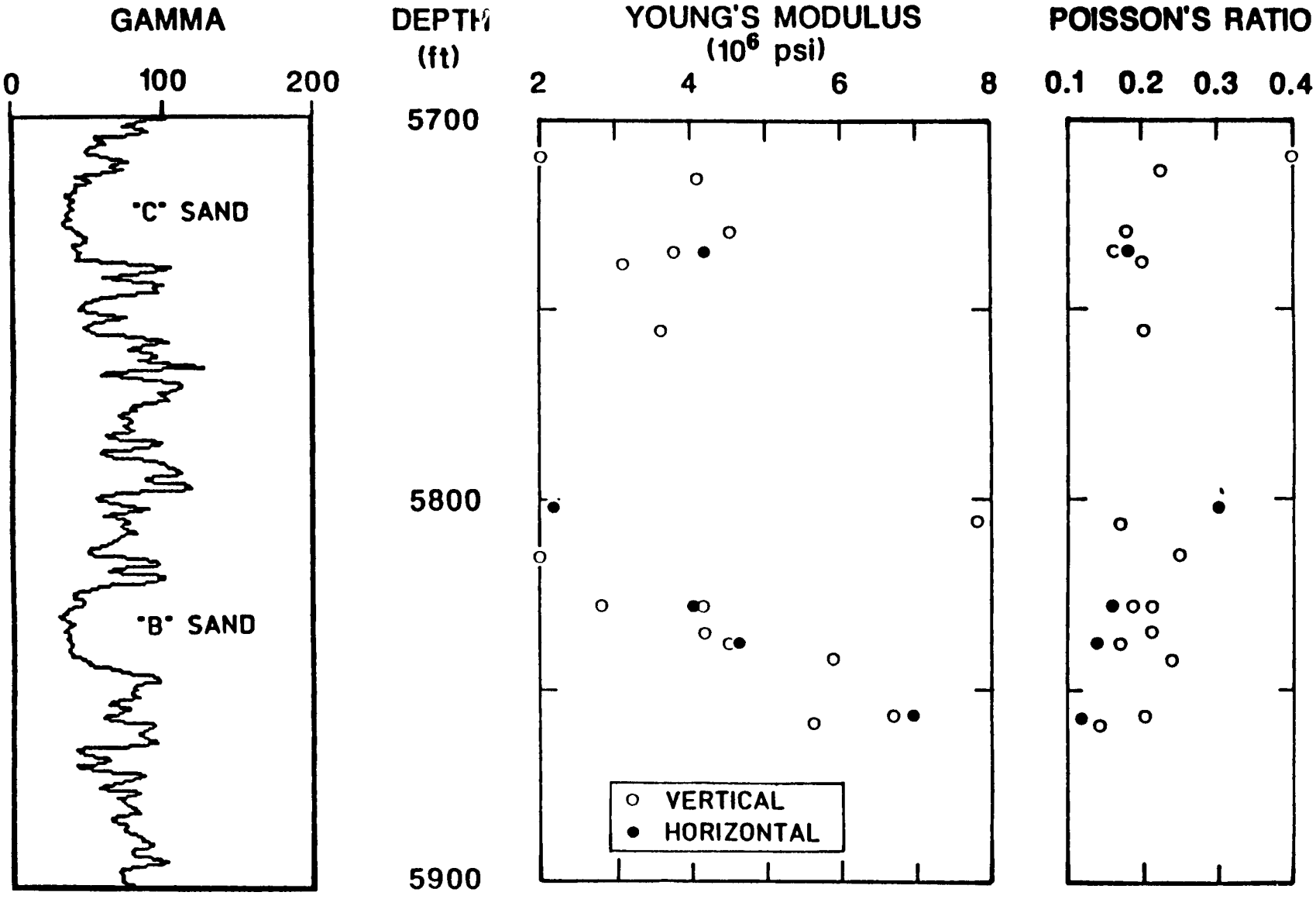

Figure 8.1.3. Rock Properties

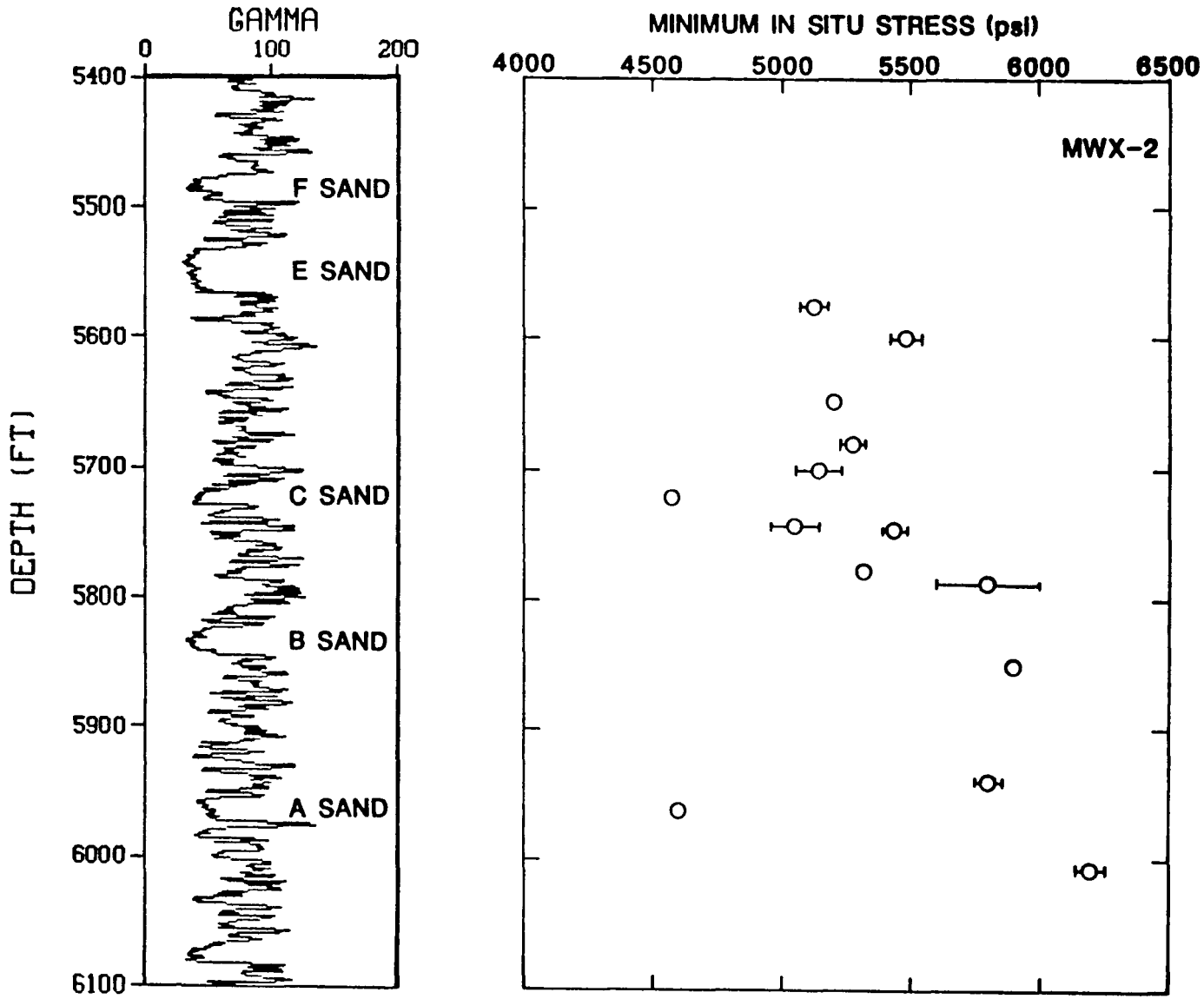

Figure 8.1.4. Stress Distribution

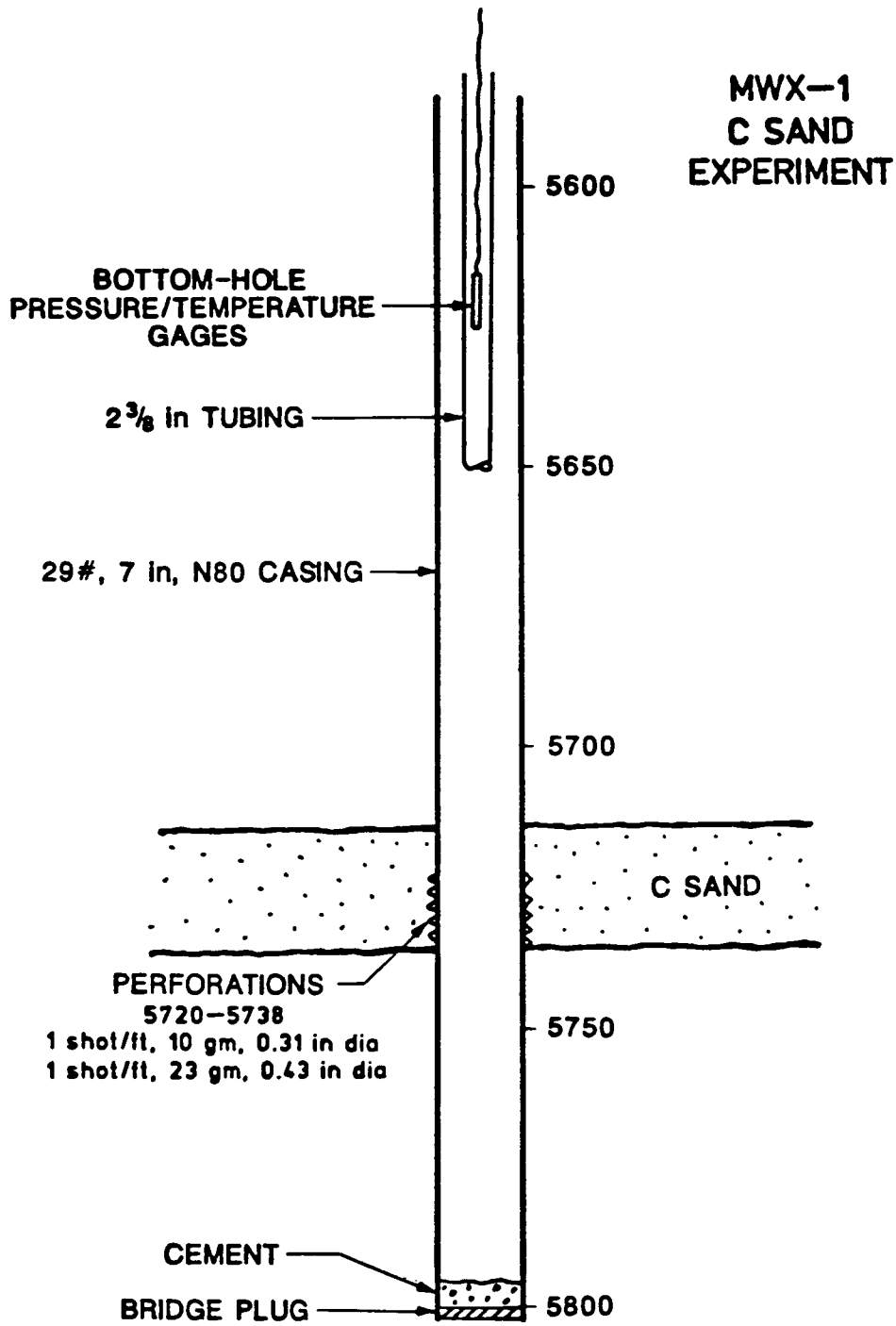

Figure 8.1.5. Well Configuration

Figure 8.1.6. Pump-In/Shut-In Flow Data

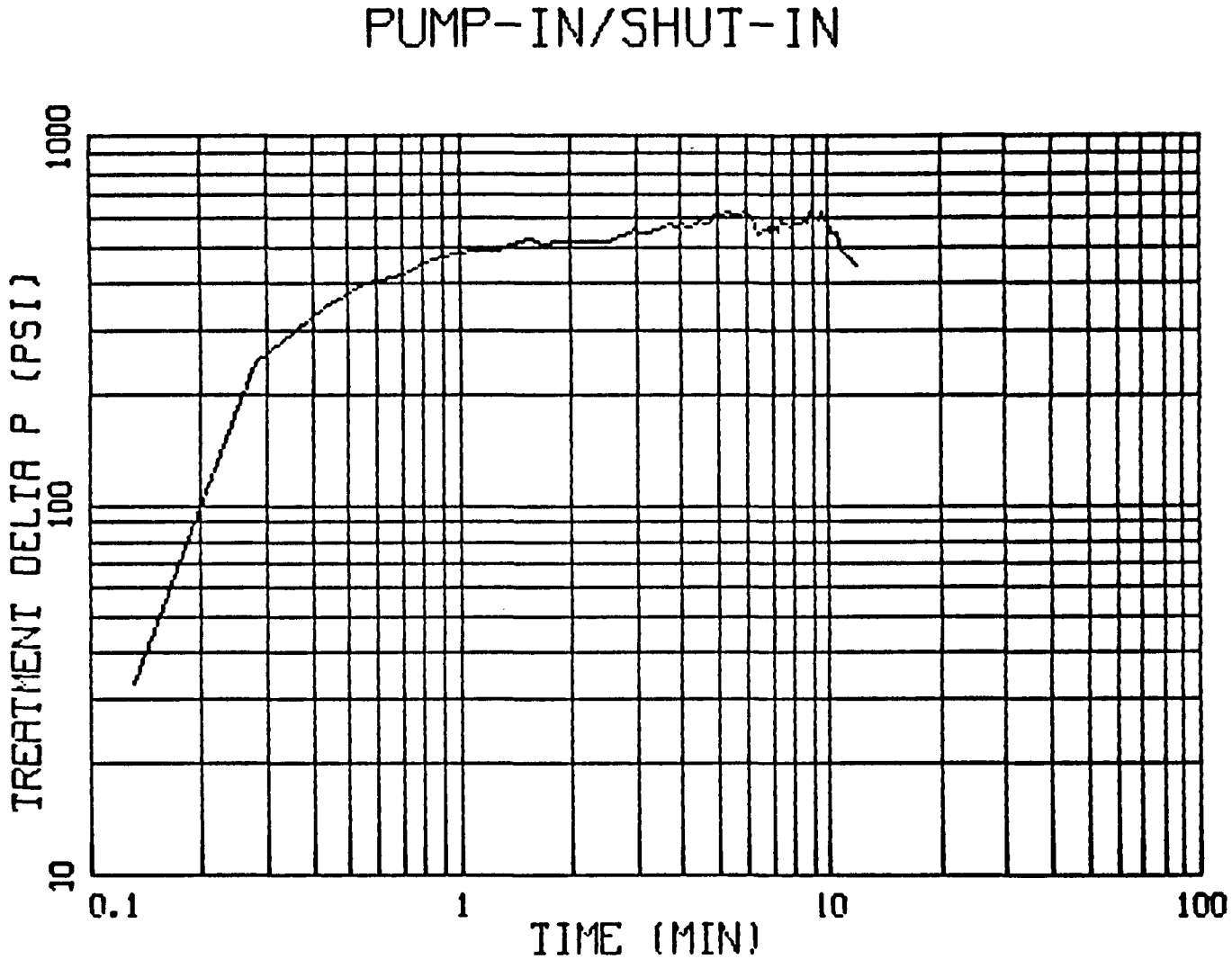

Figure 8.1.7. Pump-In/Shut-In Nolte-Smith Plot

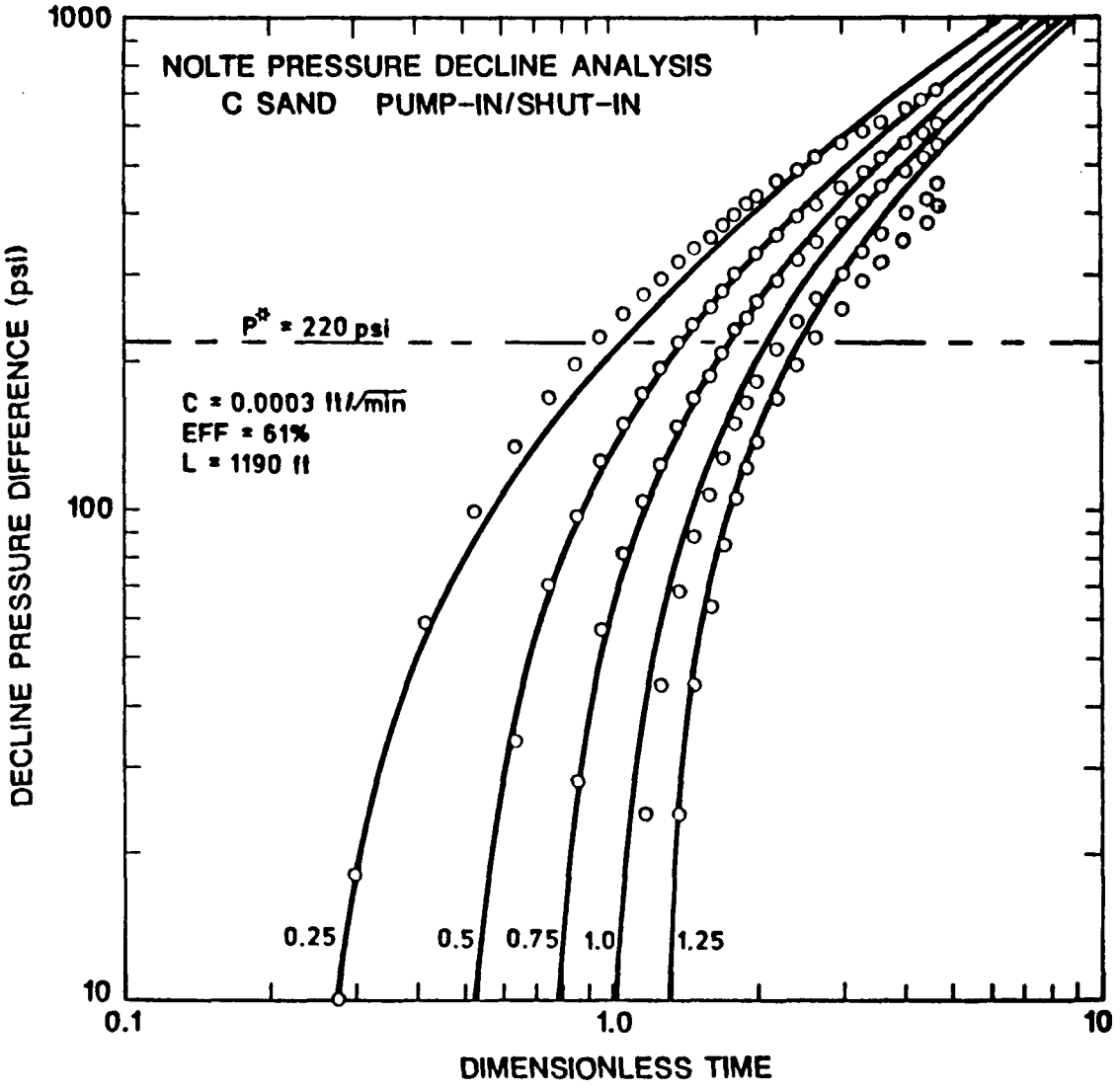

Figure 8.1.8. Pump-In/Shut-In Nolte Plot

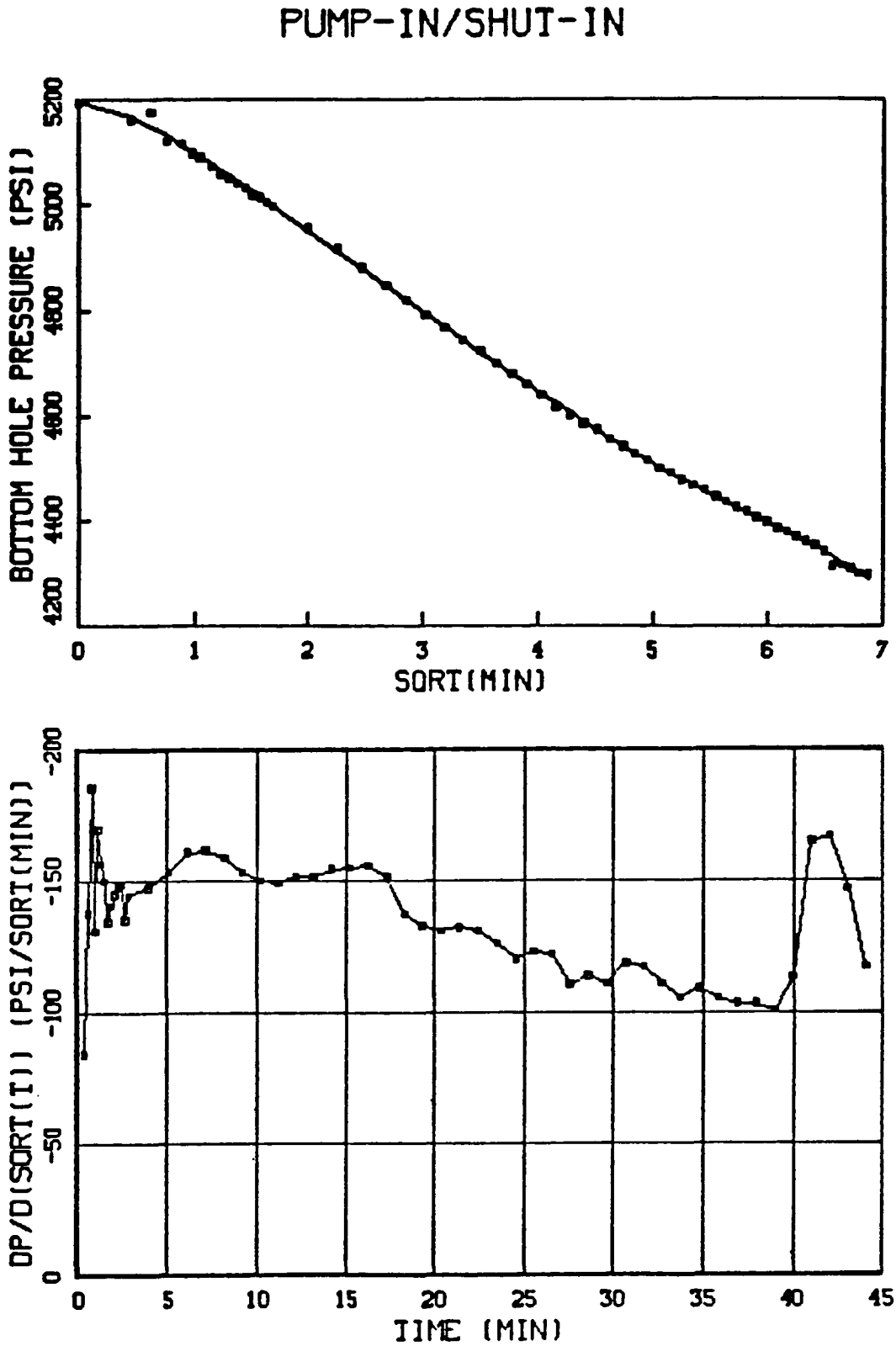

Figure 8.1.9. Pump-In/Shut-In Square Root of Time Plot

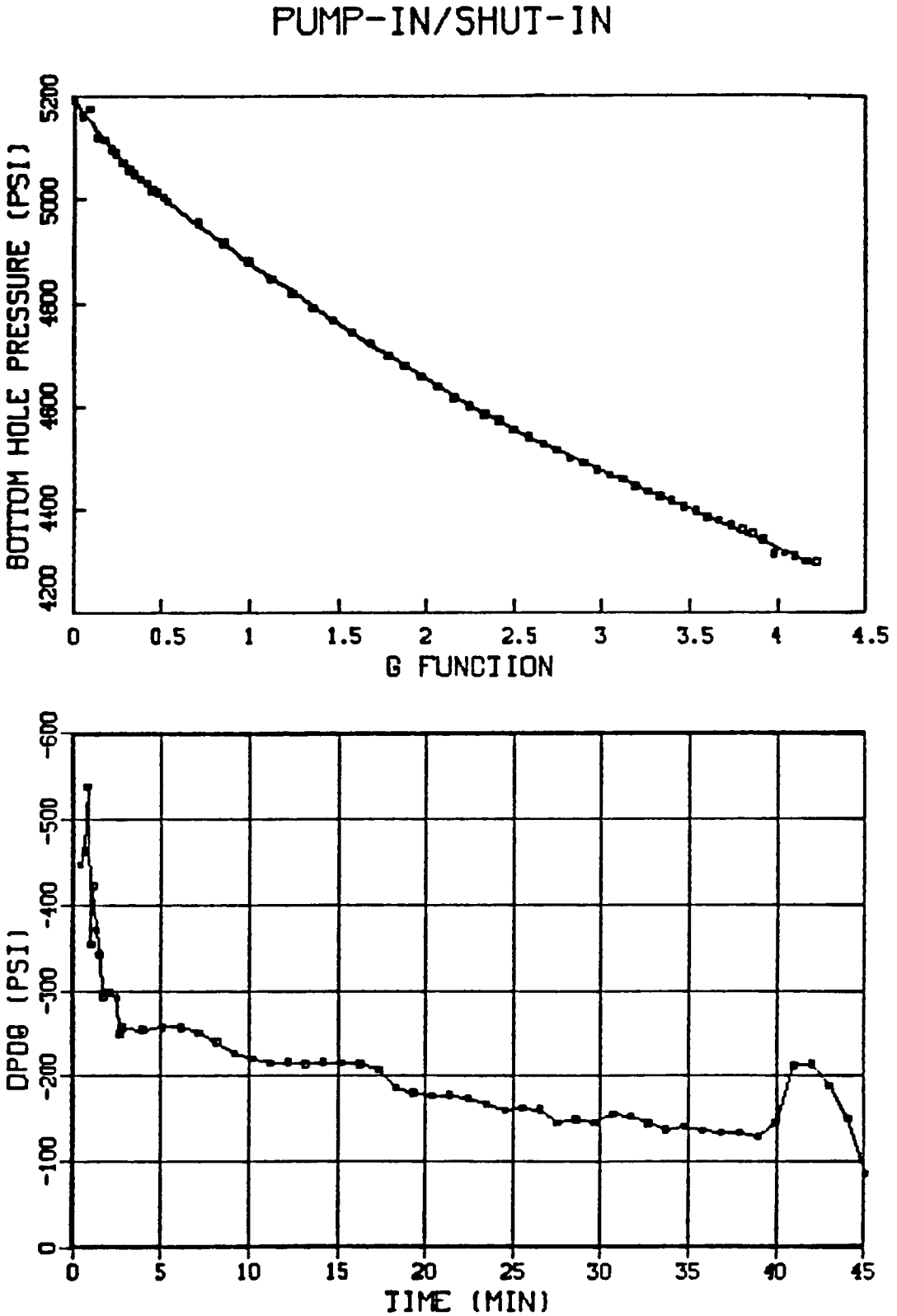

Figure 8.1.10. Pump-In/Shut-In Pressure vs G Function

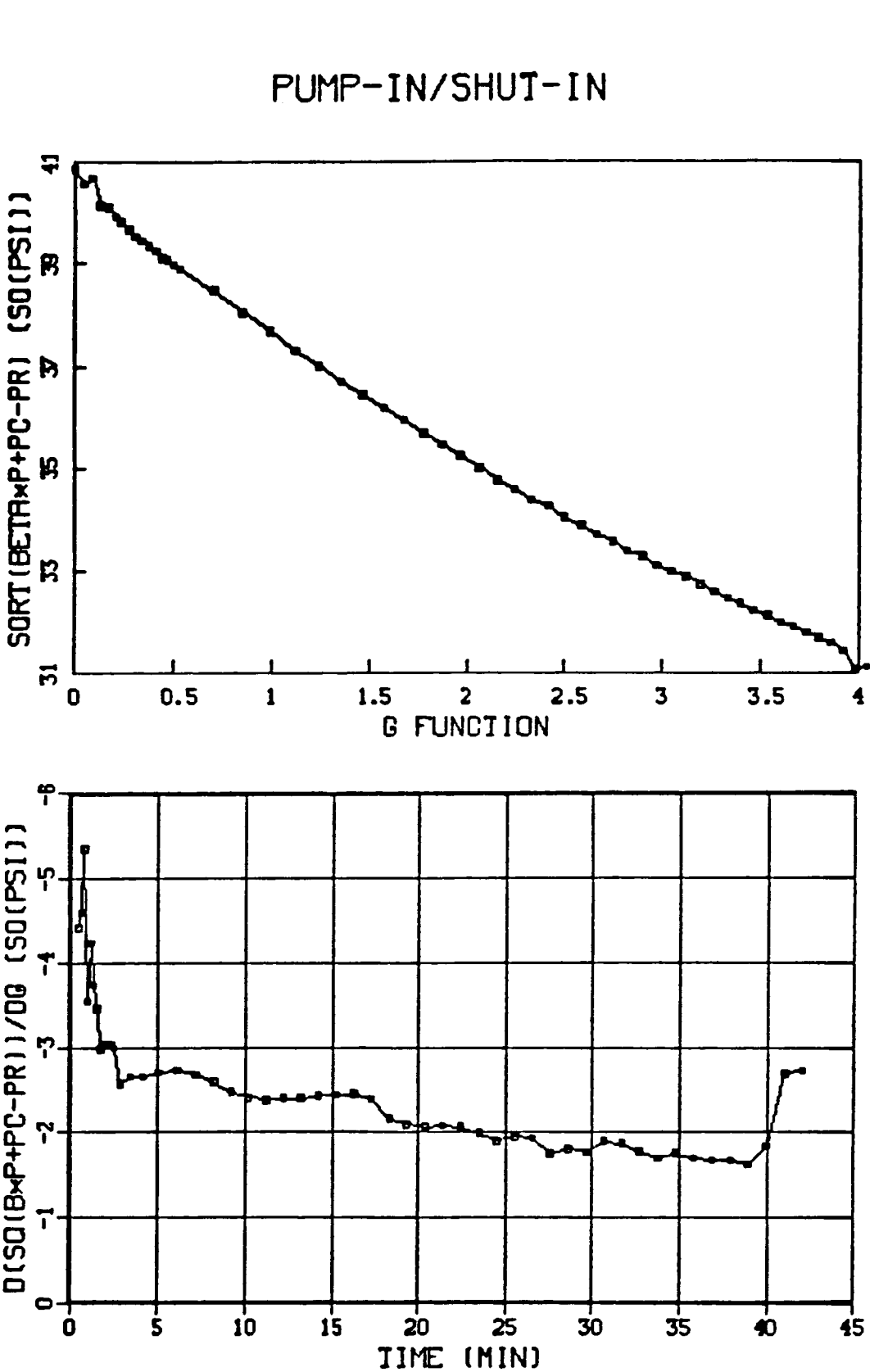

Figure 8.1.11. Pump-In/Shut-In Linearized G Function (exponent = 1/2)

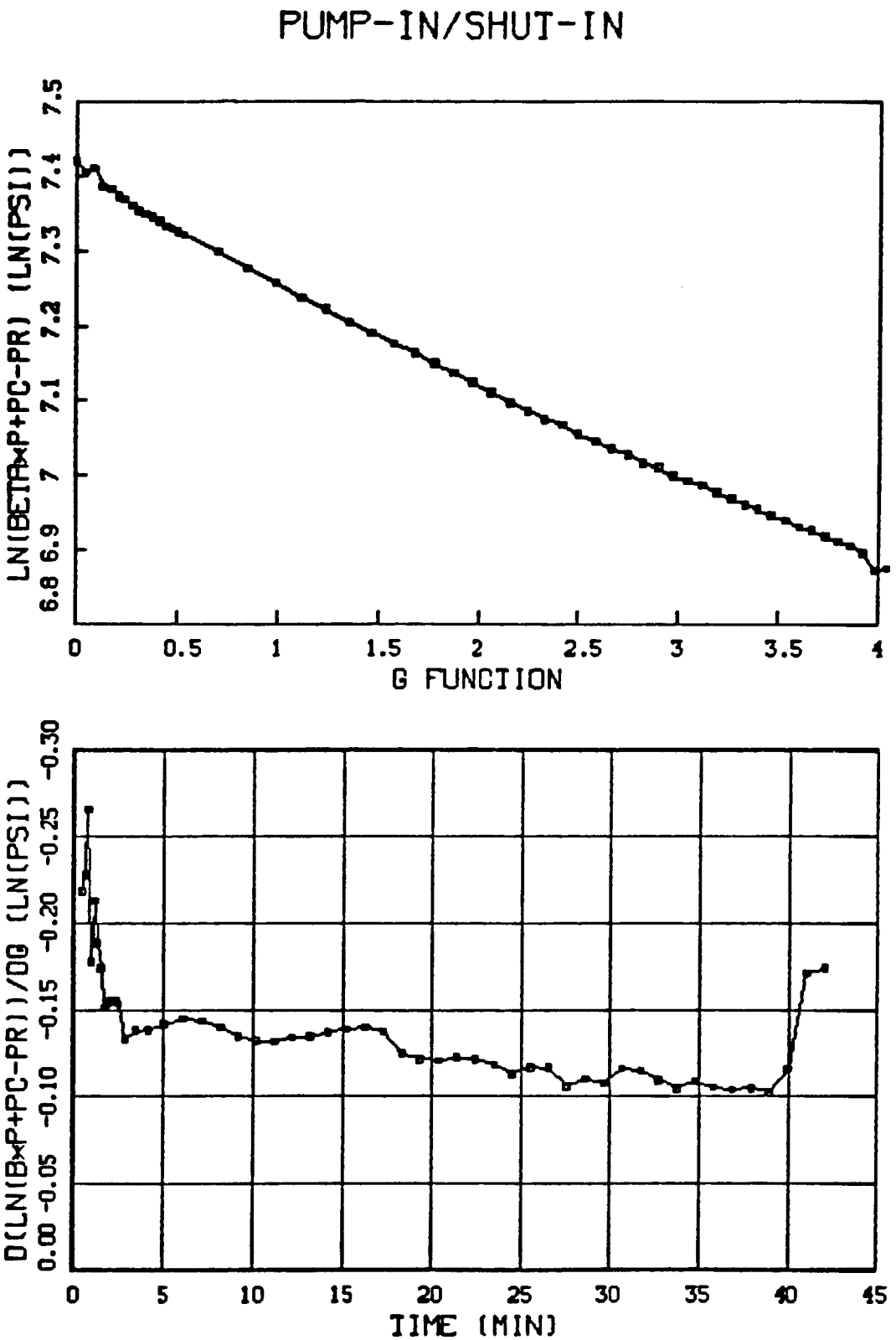

Figure 8.1.12. Pump-In/Shut-In Linearized G Function (exponent = 1)

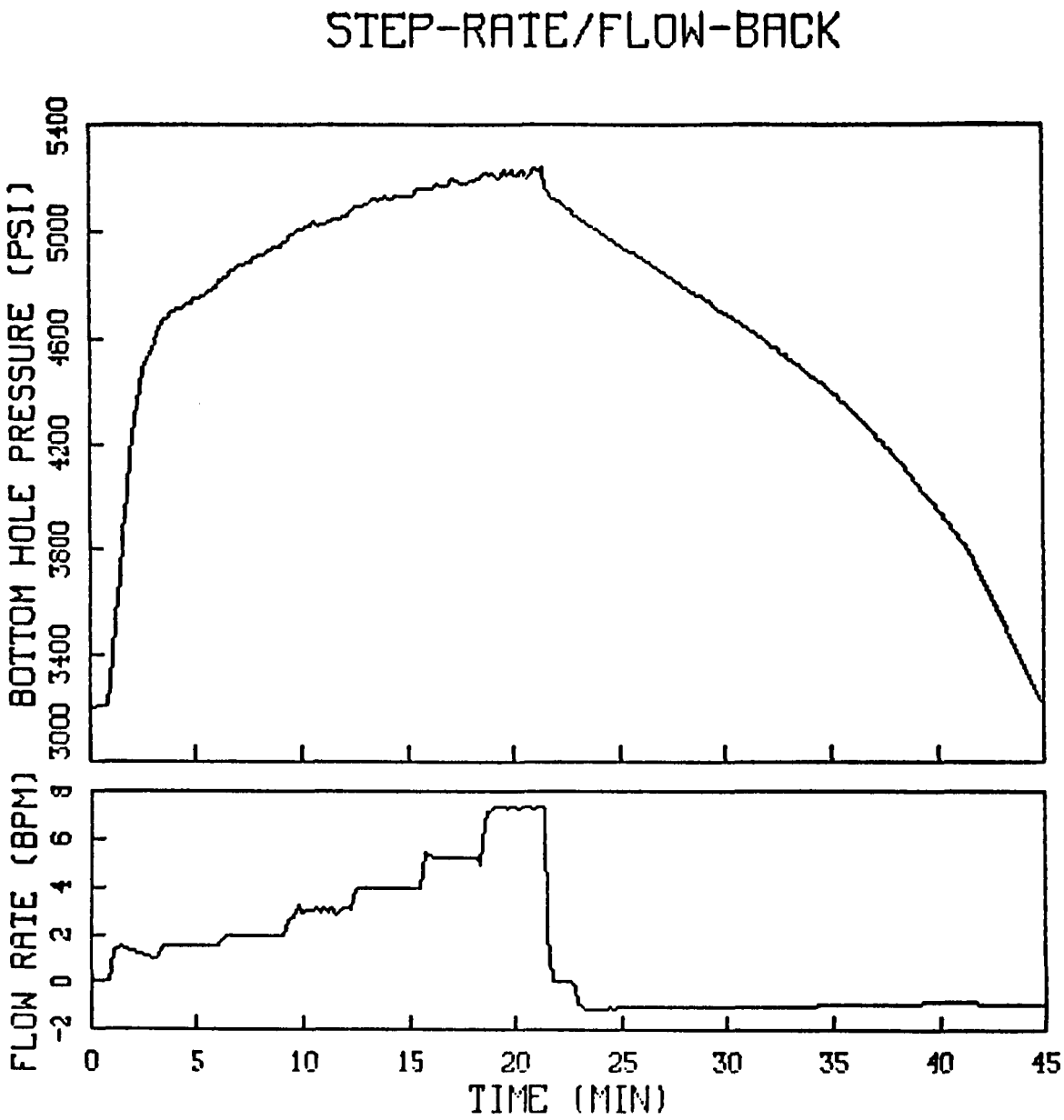

Figure 8.1.13. Step-Rate/Flow-Back Injection Data

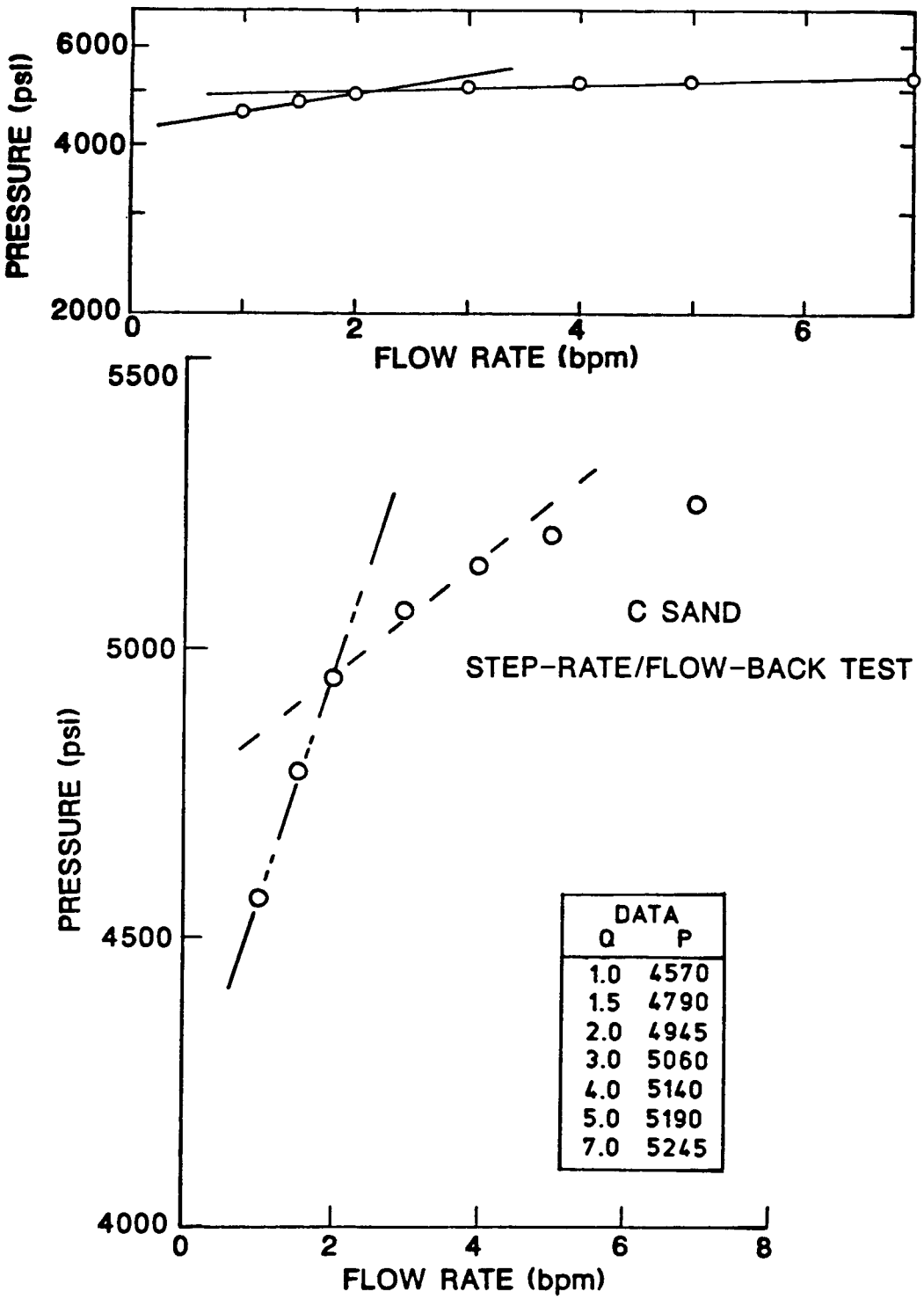

Figure 8.1.14. Step-Rate Data

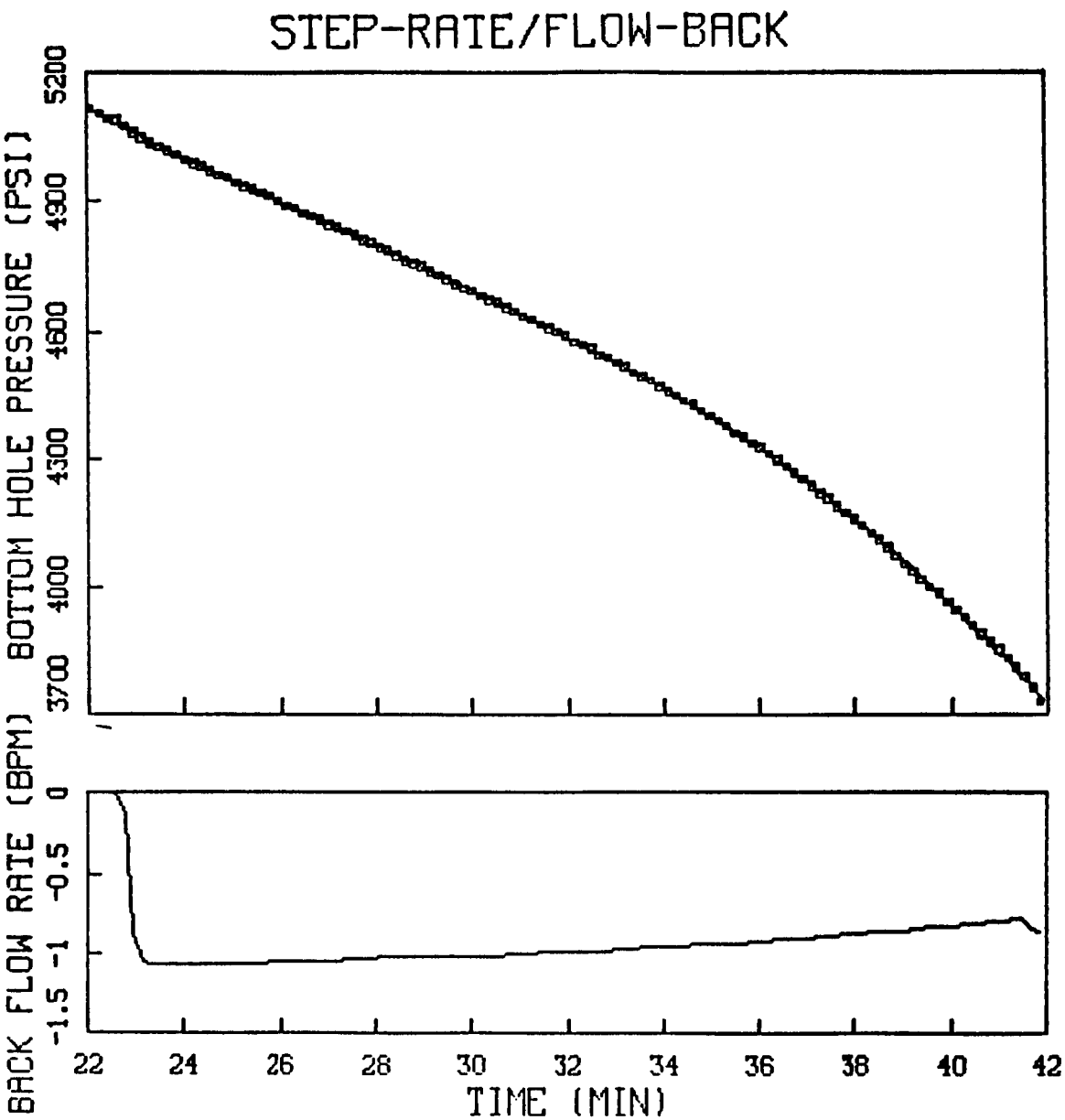

Figure 8.1.15. Flow-Back Data After Step-Rate Test

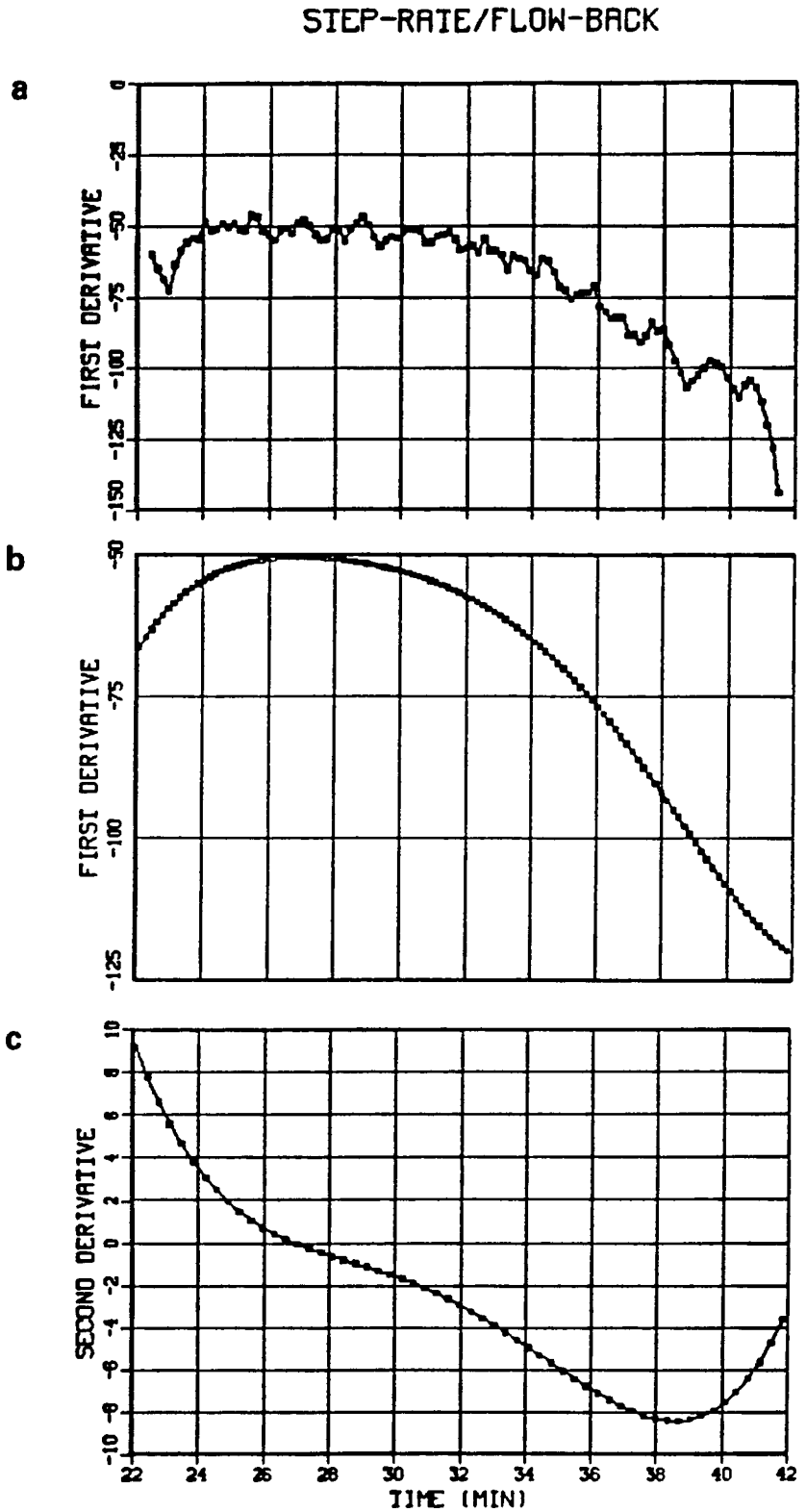

Figure 8.1.16. Flow-Back Derivative Results After Step-Rate Test

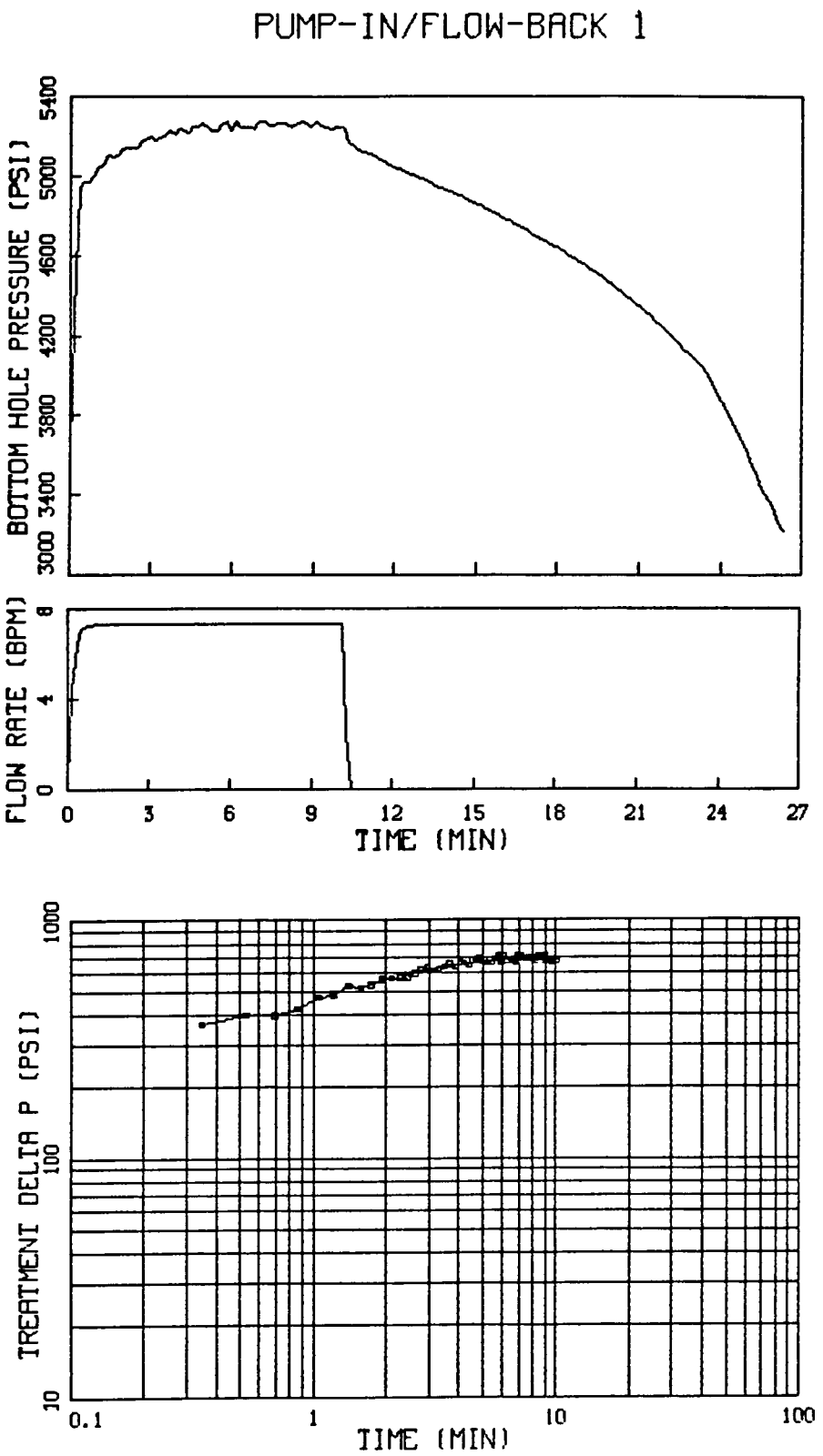

Figure 8.1.17. Pump-In/Flow-Back #1 Injection Data

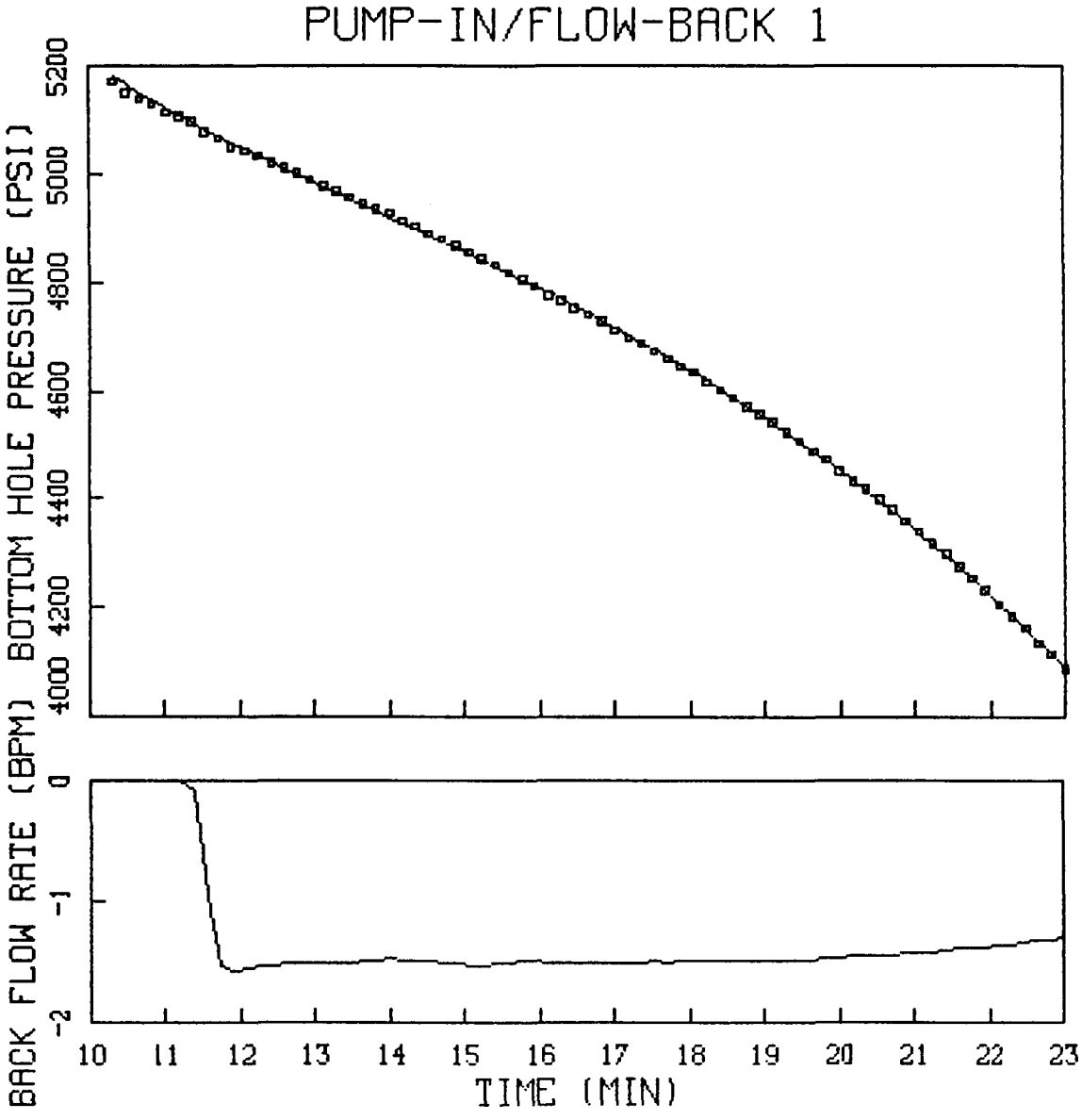

Figure 8.1.18. Flow-Back Data After Pump-In/Flow-Back #1

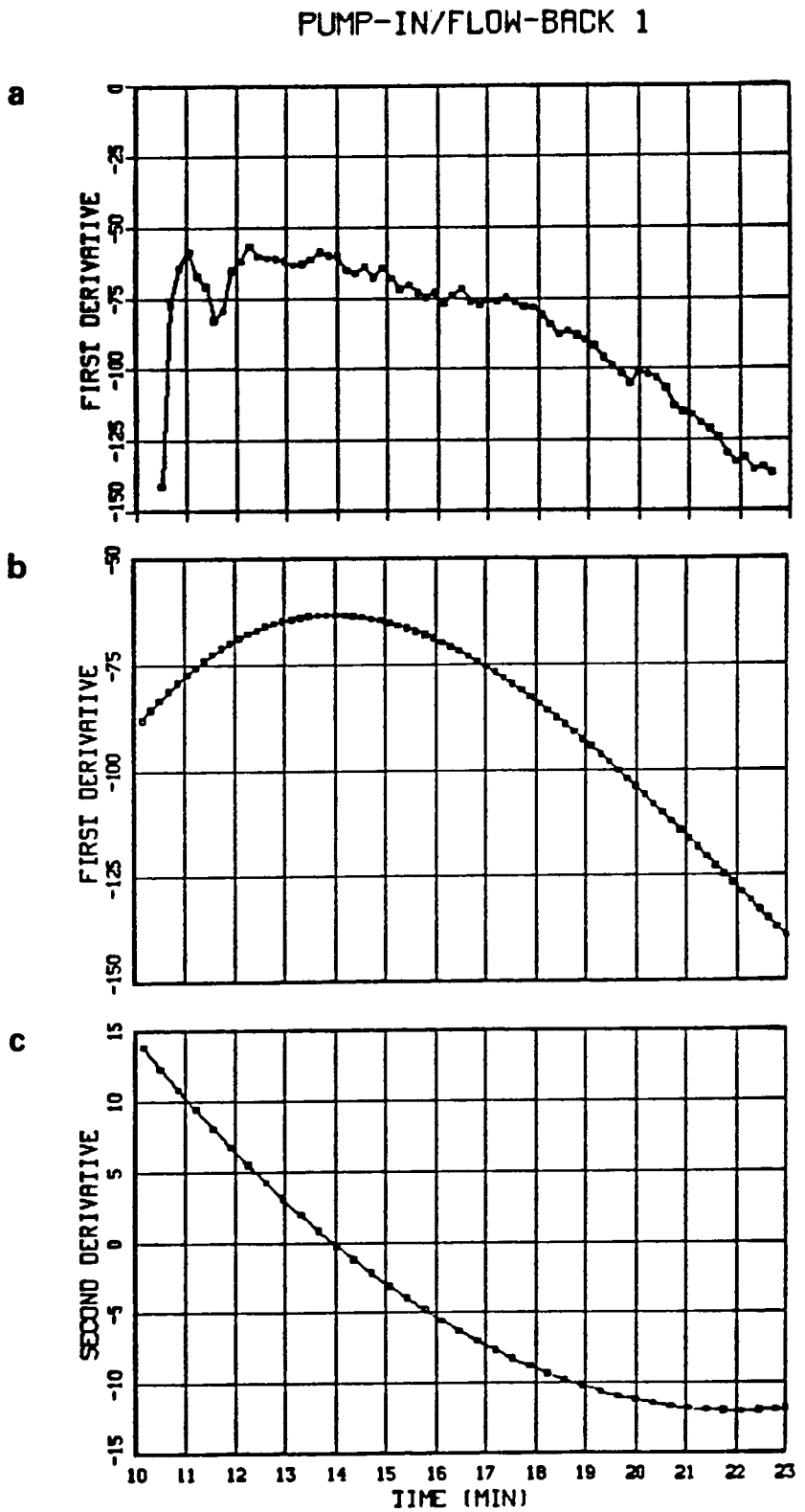

Figure 8.1.19. Flow-Back Derivative Results After Pump-In/Flow-Back #1

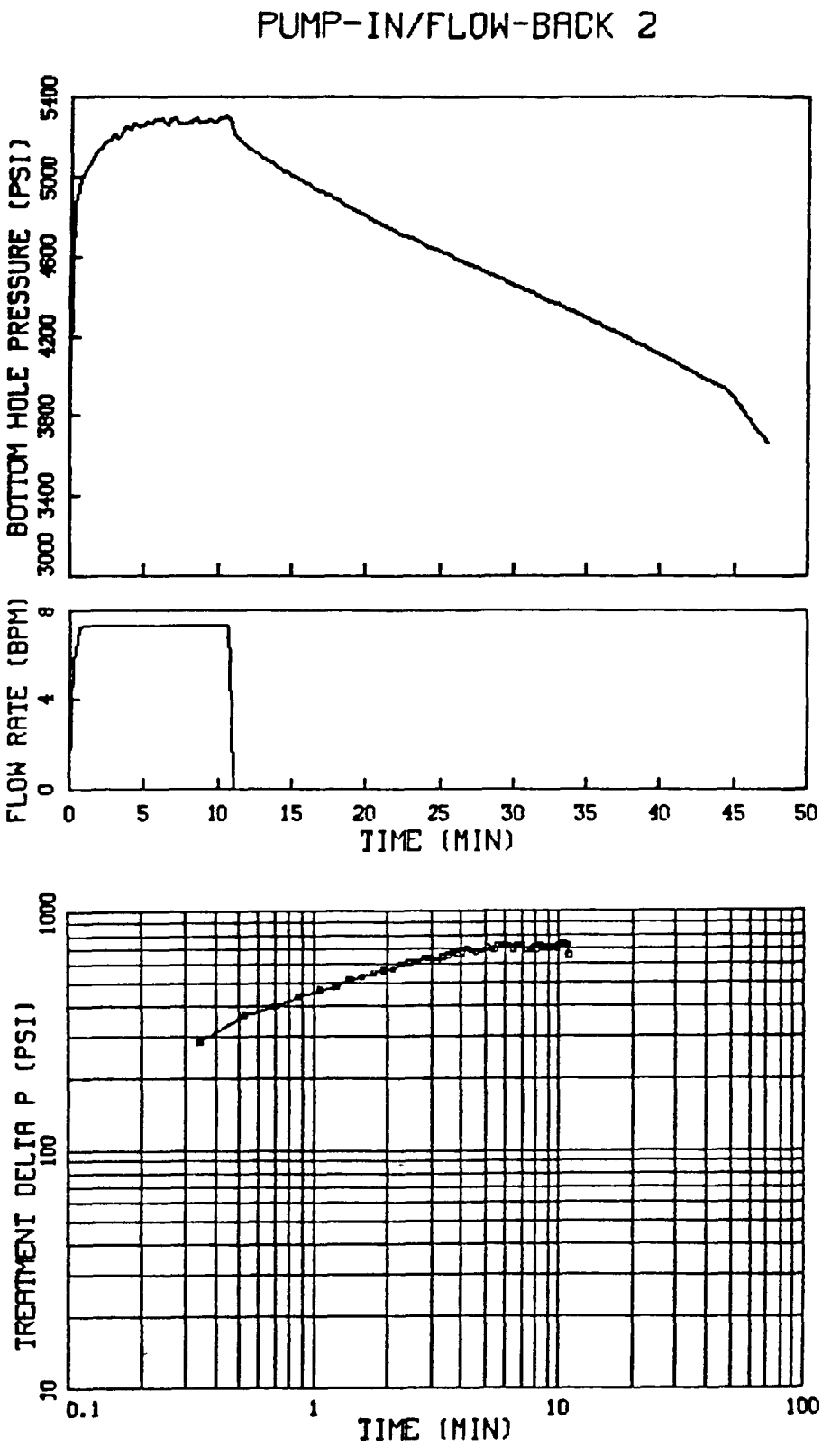

Figure 8.1.20. Pump-In/Flow-Back #2 Injection Data

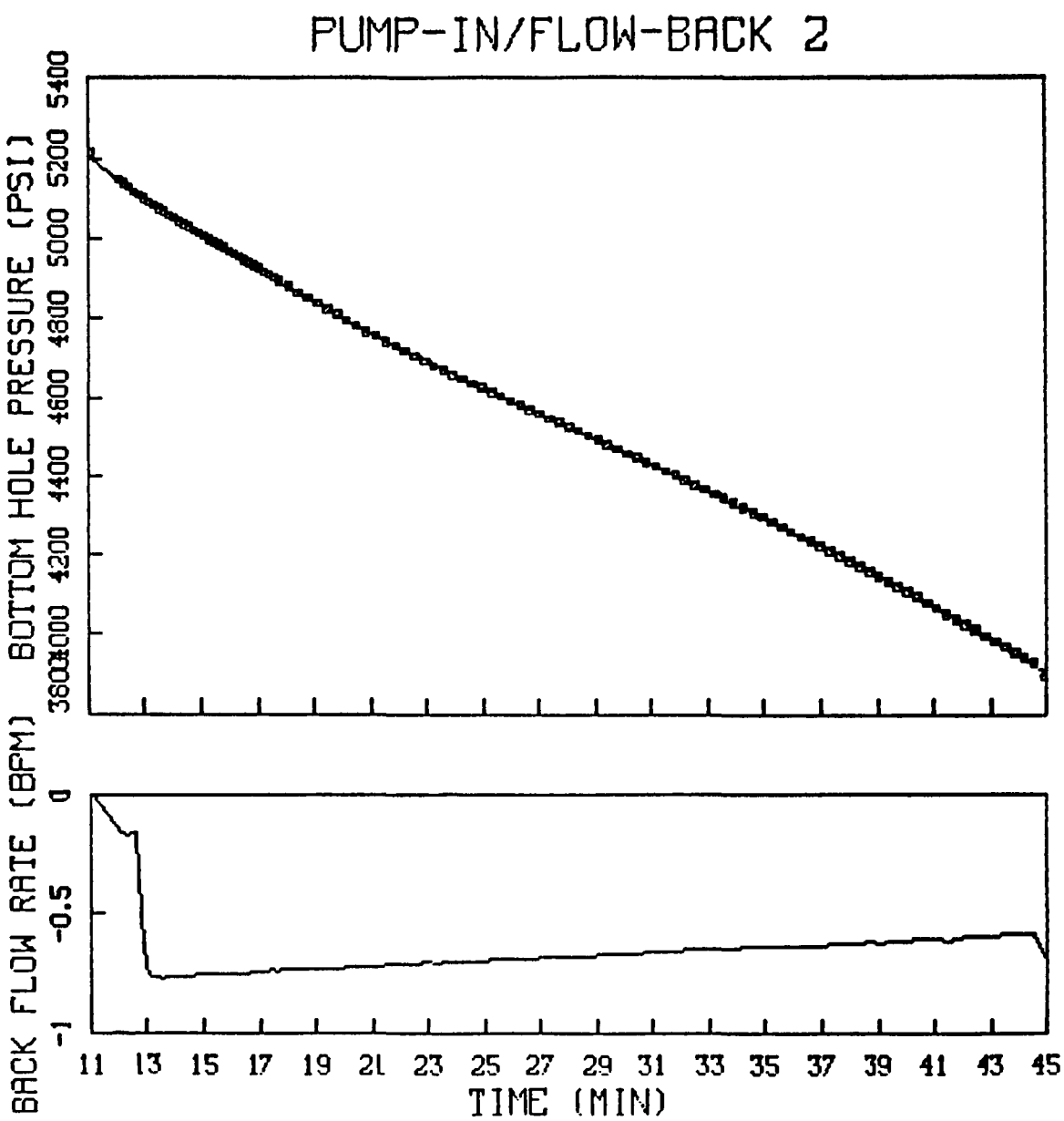

Figure 8.1.21. Flow-Back Data After Pump-In/Flow-Back #2

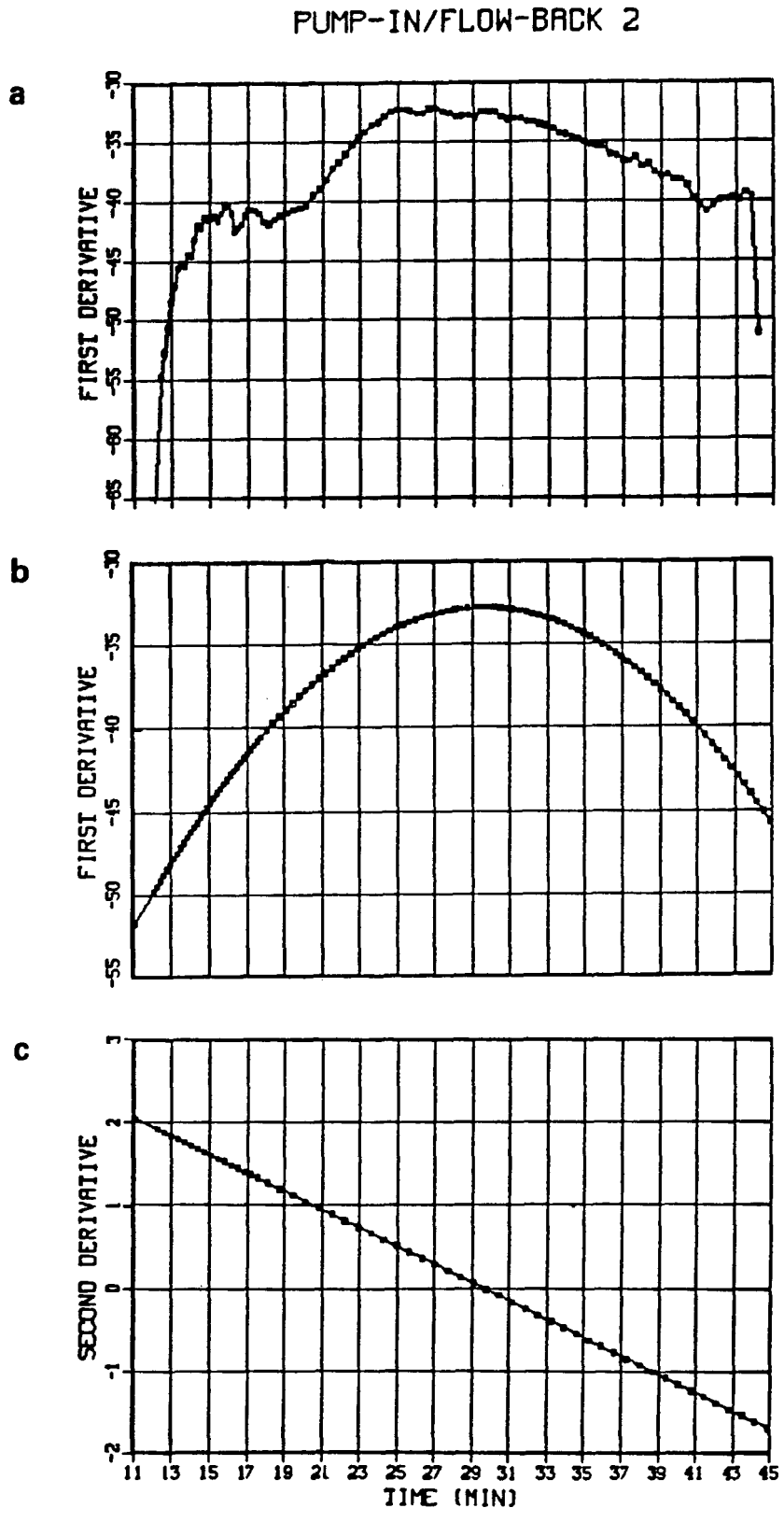

Figure 8.1.22. Flow-Back Derivative Results After Pump-In/Flow-Back #2

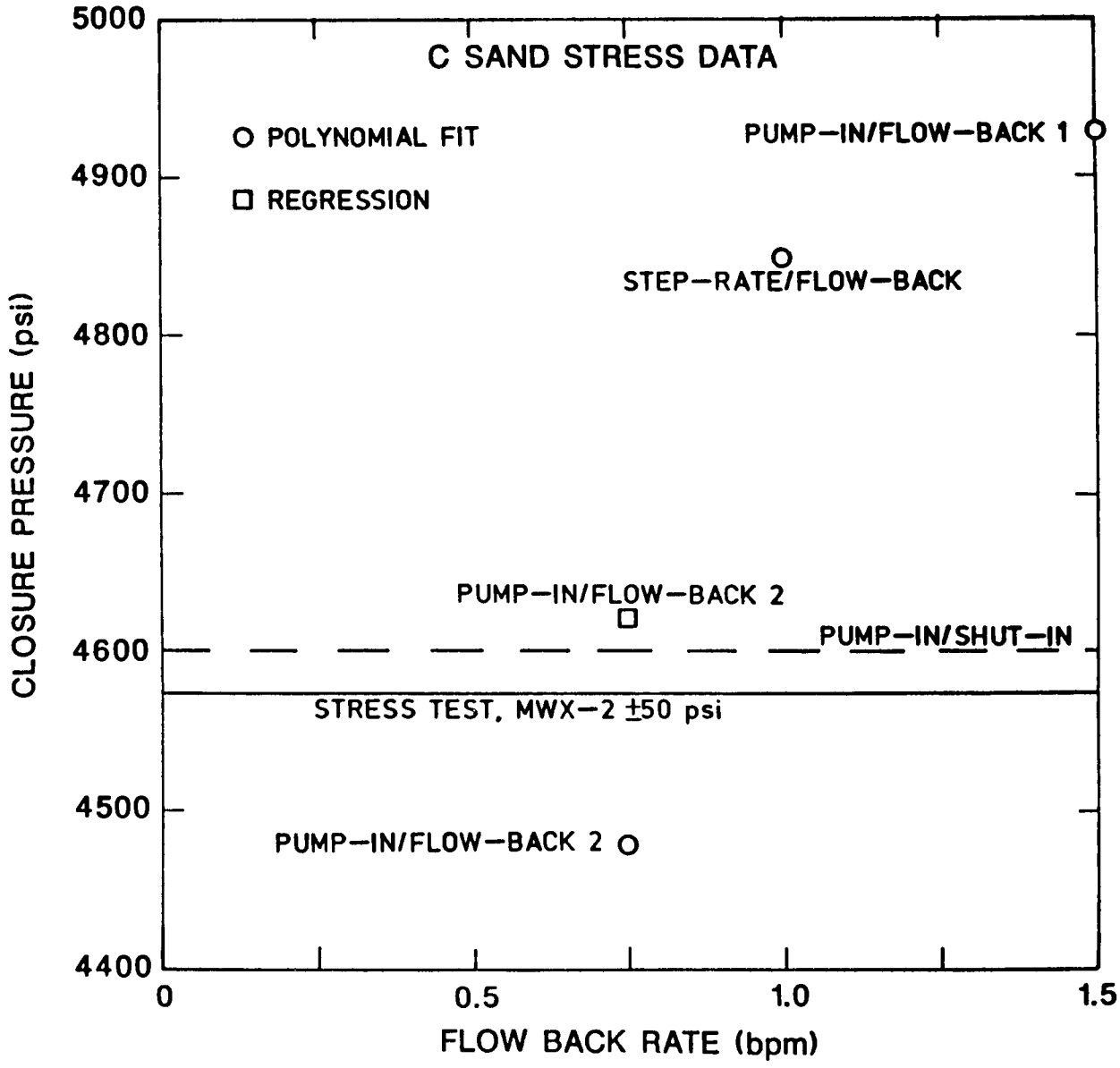

Figure 8.1.23. Flow-Back Closure Stress vs Flow-Back Rate

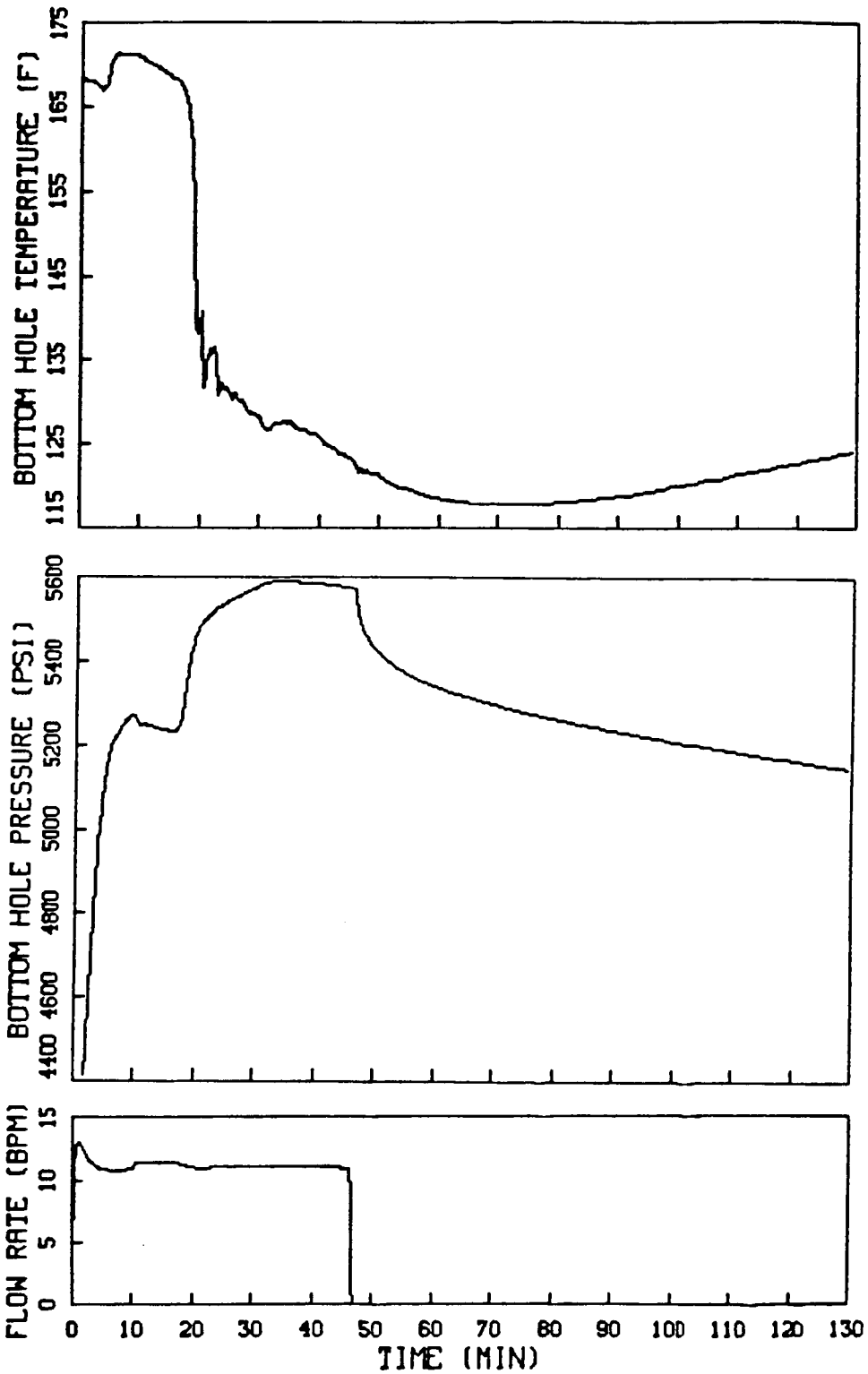

Figure 8.1.24. Minifrac #1 Injection Data

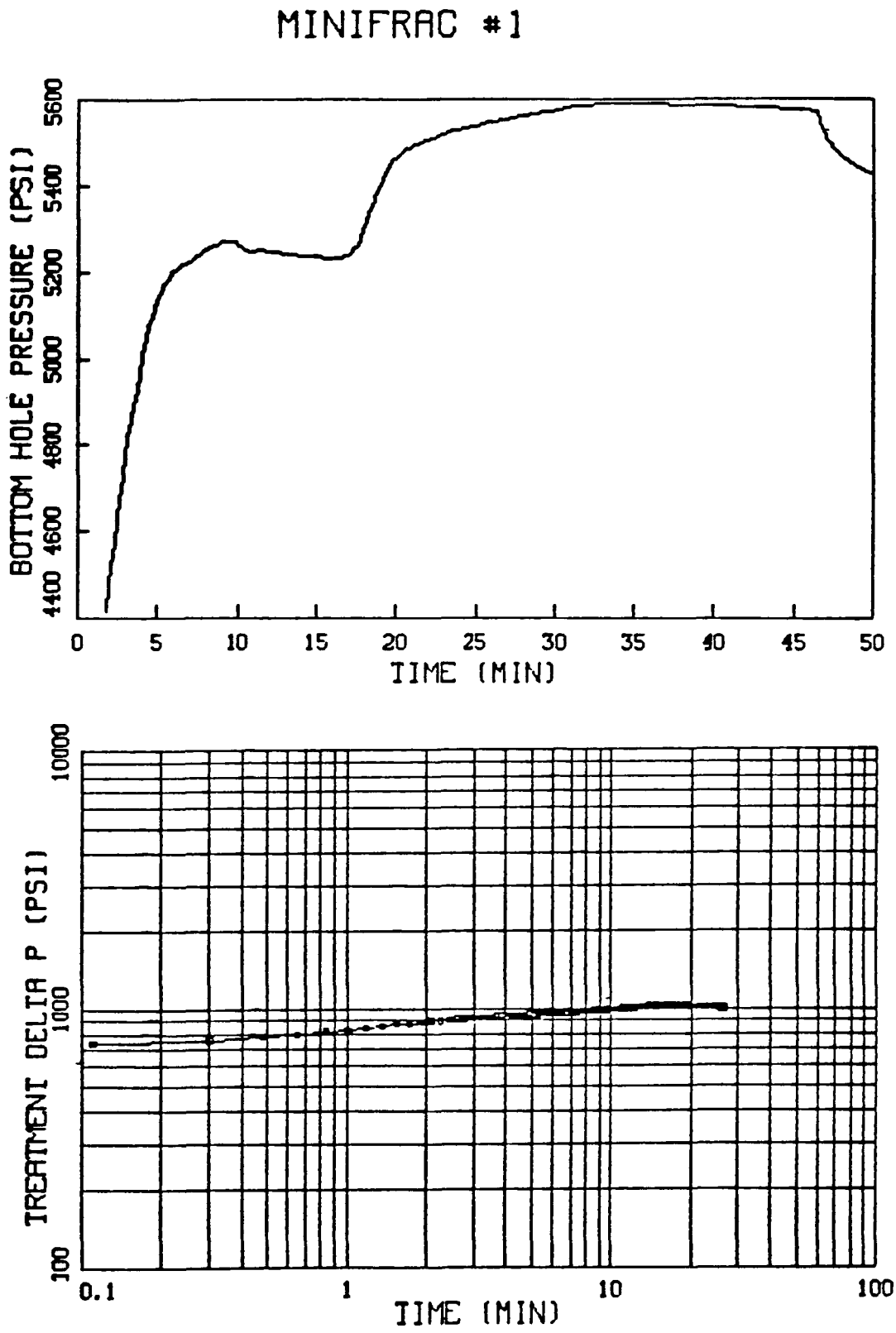

Figure 8.1.25. Minifrac #1 Treatment Pressure and Nolte-Smith Plot

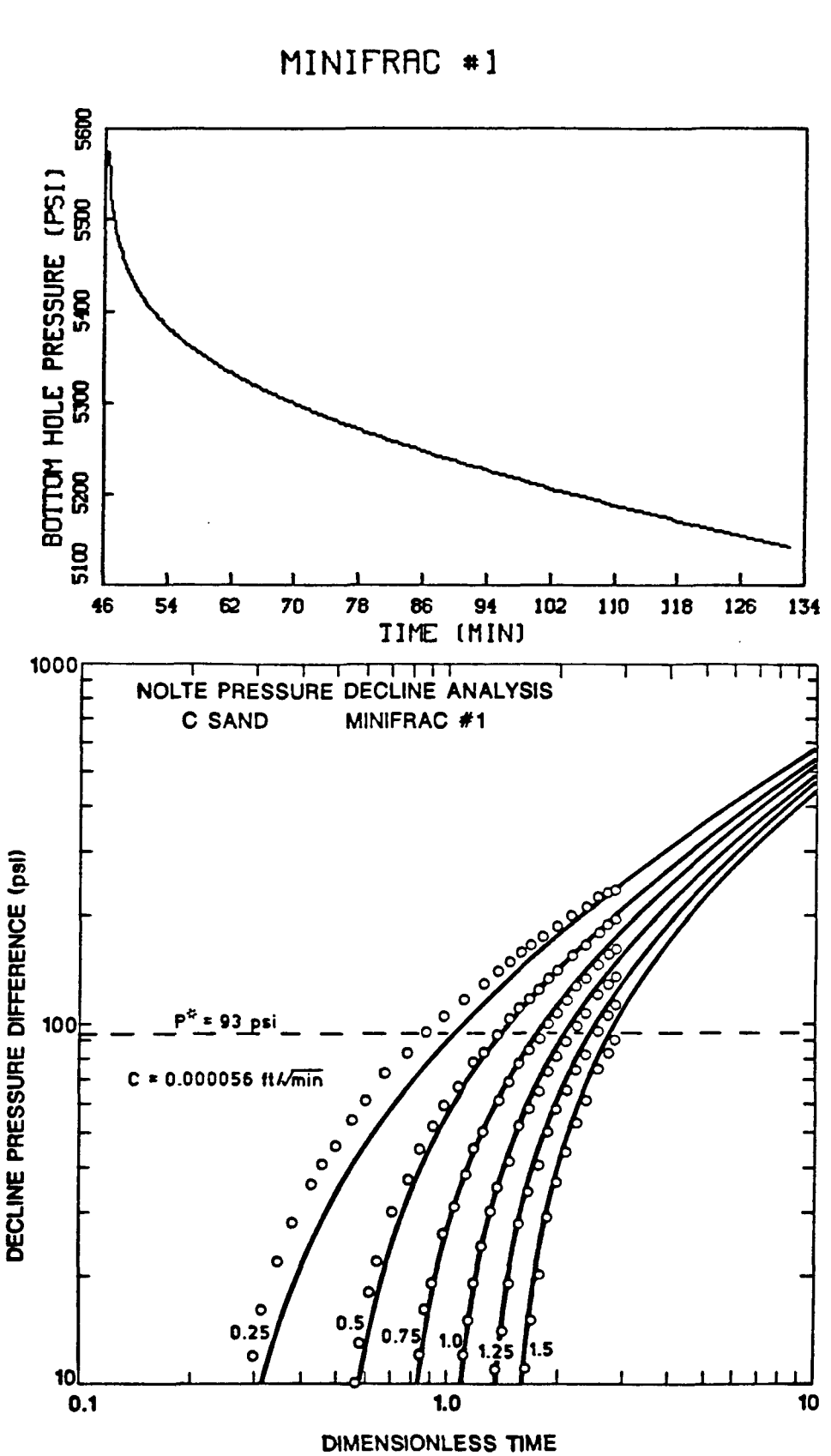

Figure 8.1.26. Minifrac #1 Pressure Decline Data and Nolte Plot

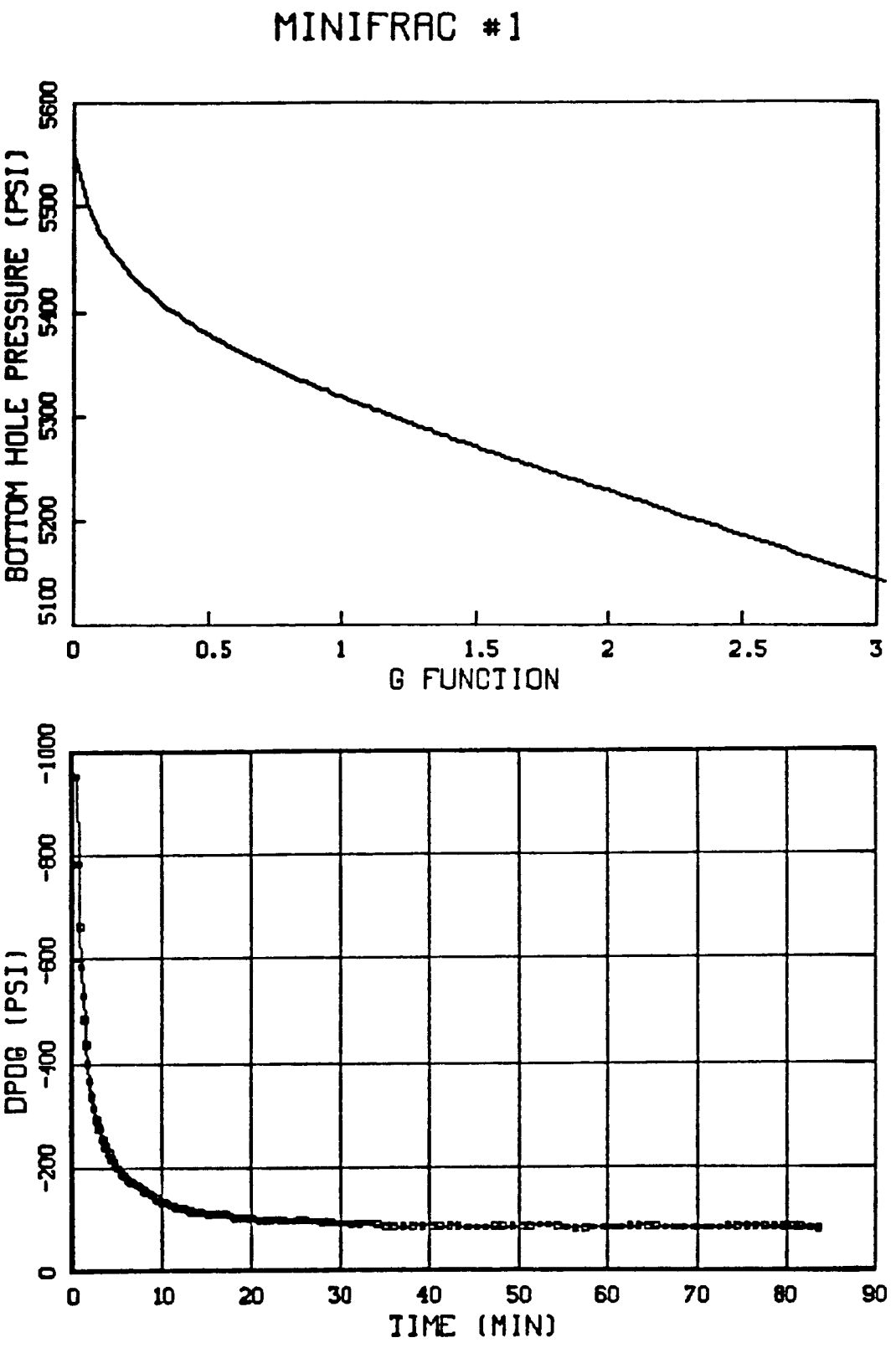

Figure 8.1.27. Minifrac #1 G Function Results

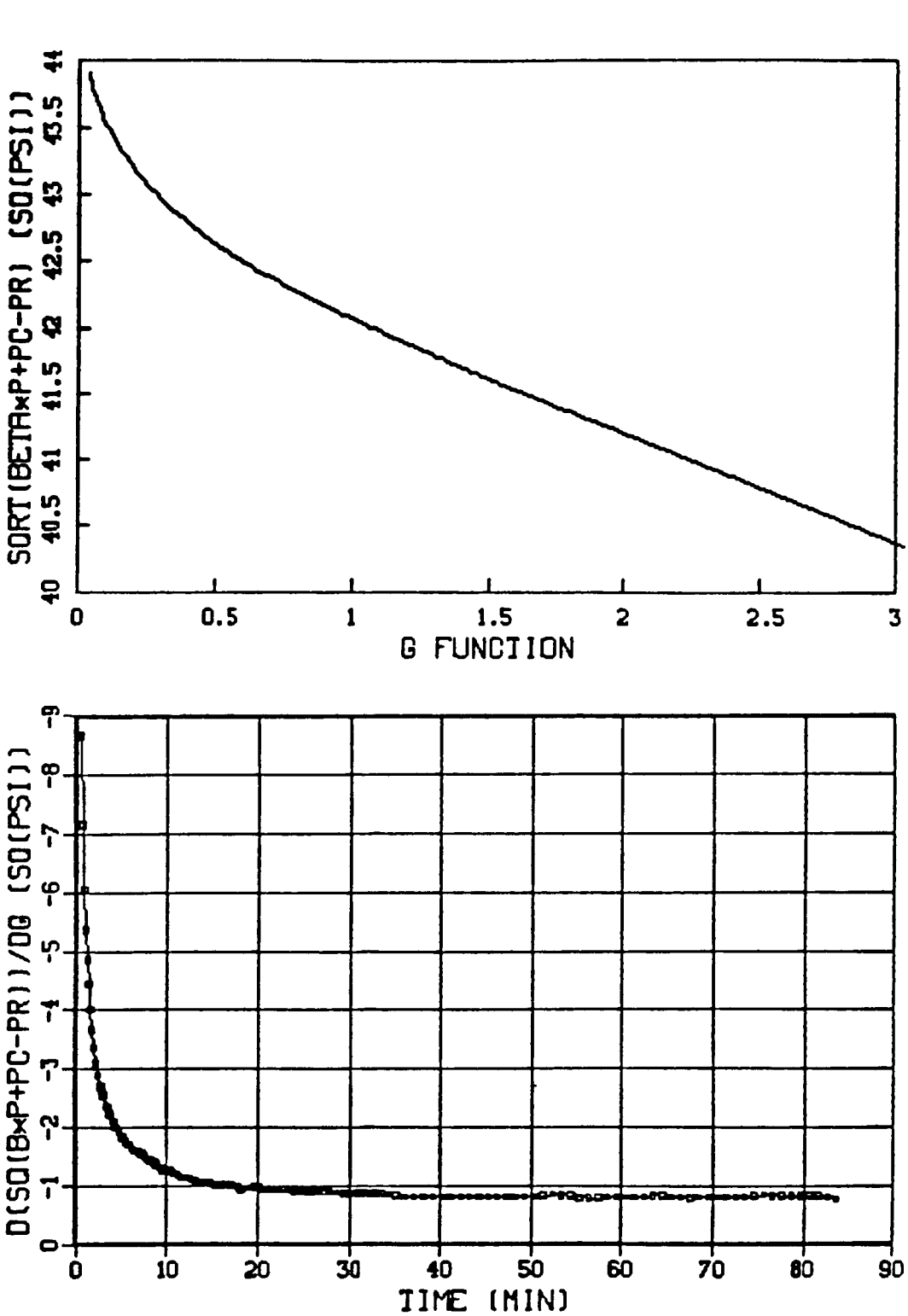

Figure 8.1.28. Minifrac # 1 Linearized G Function

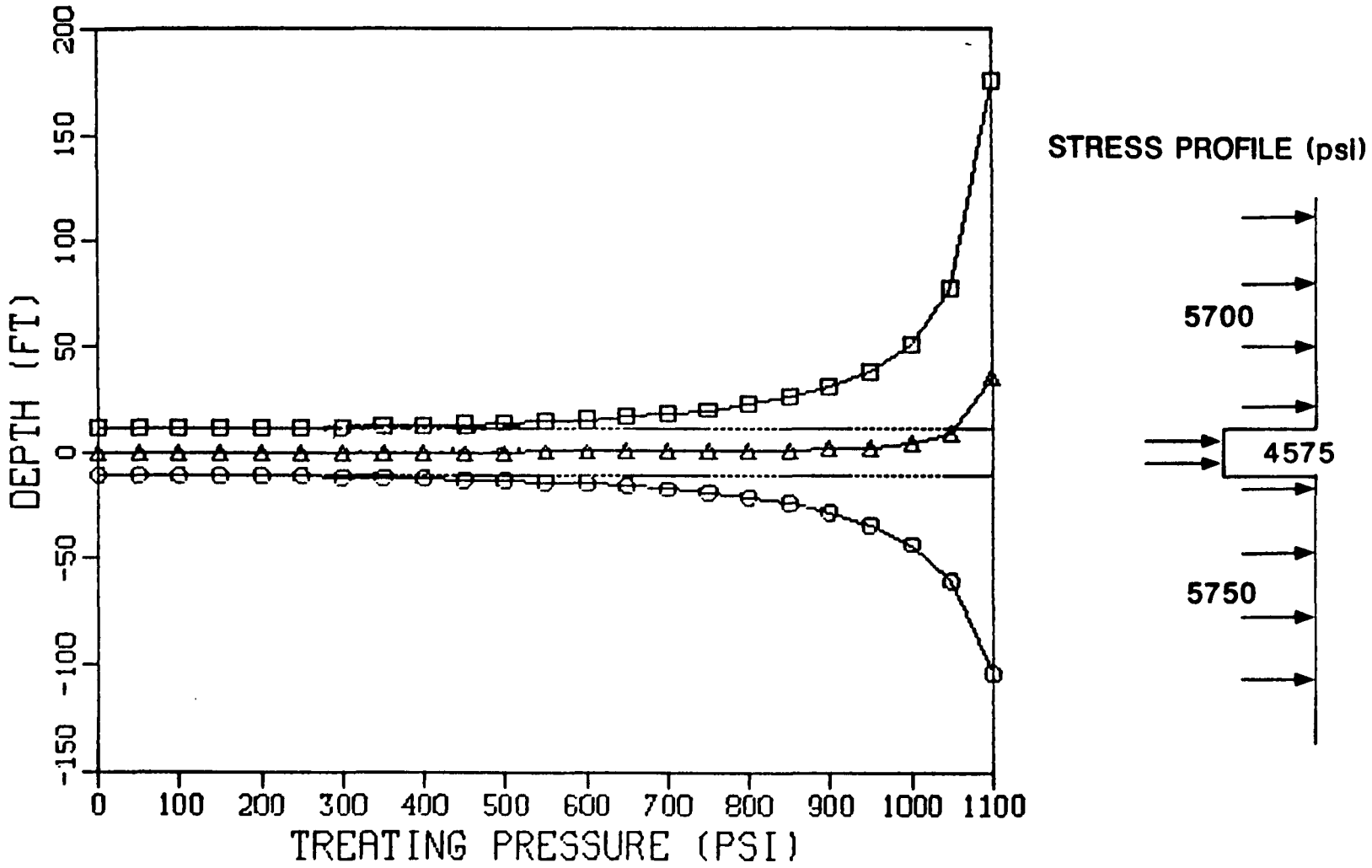

Figure 8.1.29. Stress Profile Used for Pressure History Match

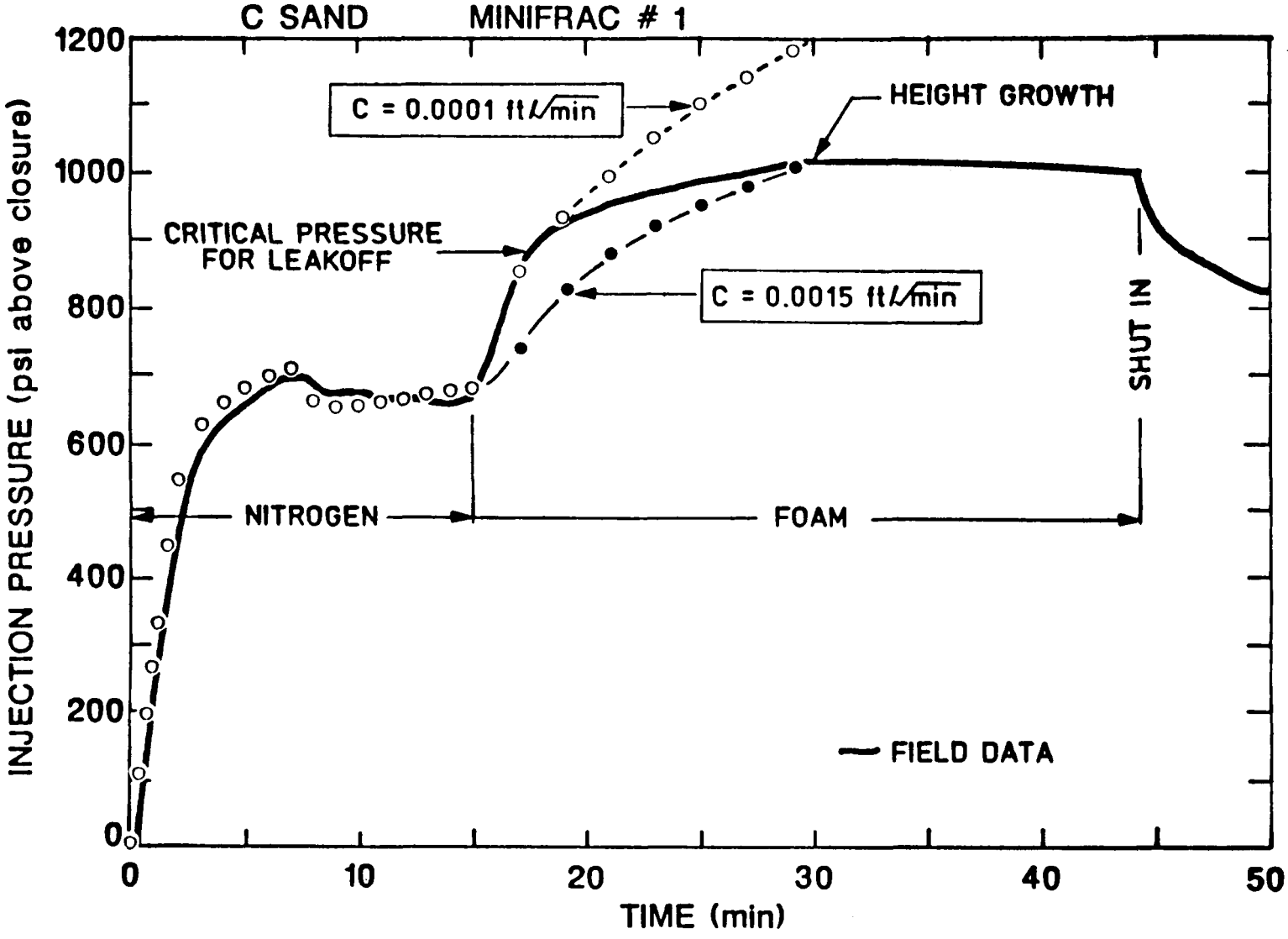

Figure 8.1.30. Pressure History Match Calculations for Normal Fracture Behavior

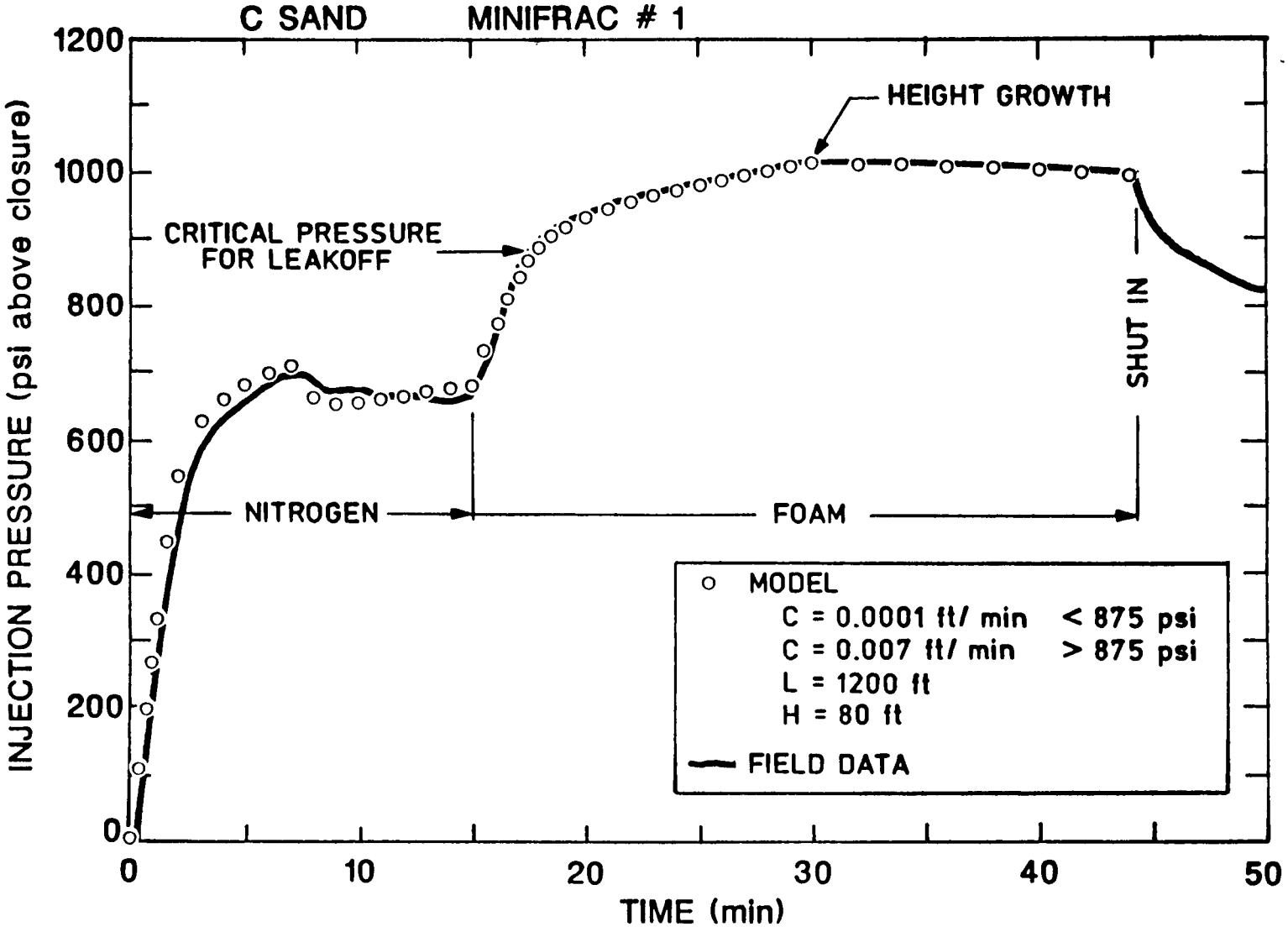

Figure 8.1.31. Pressure History Match for Intensified Leakoff

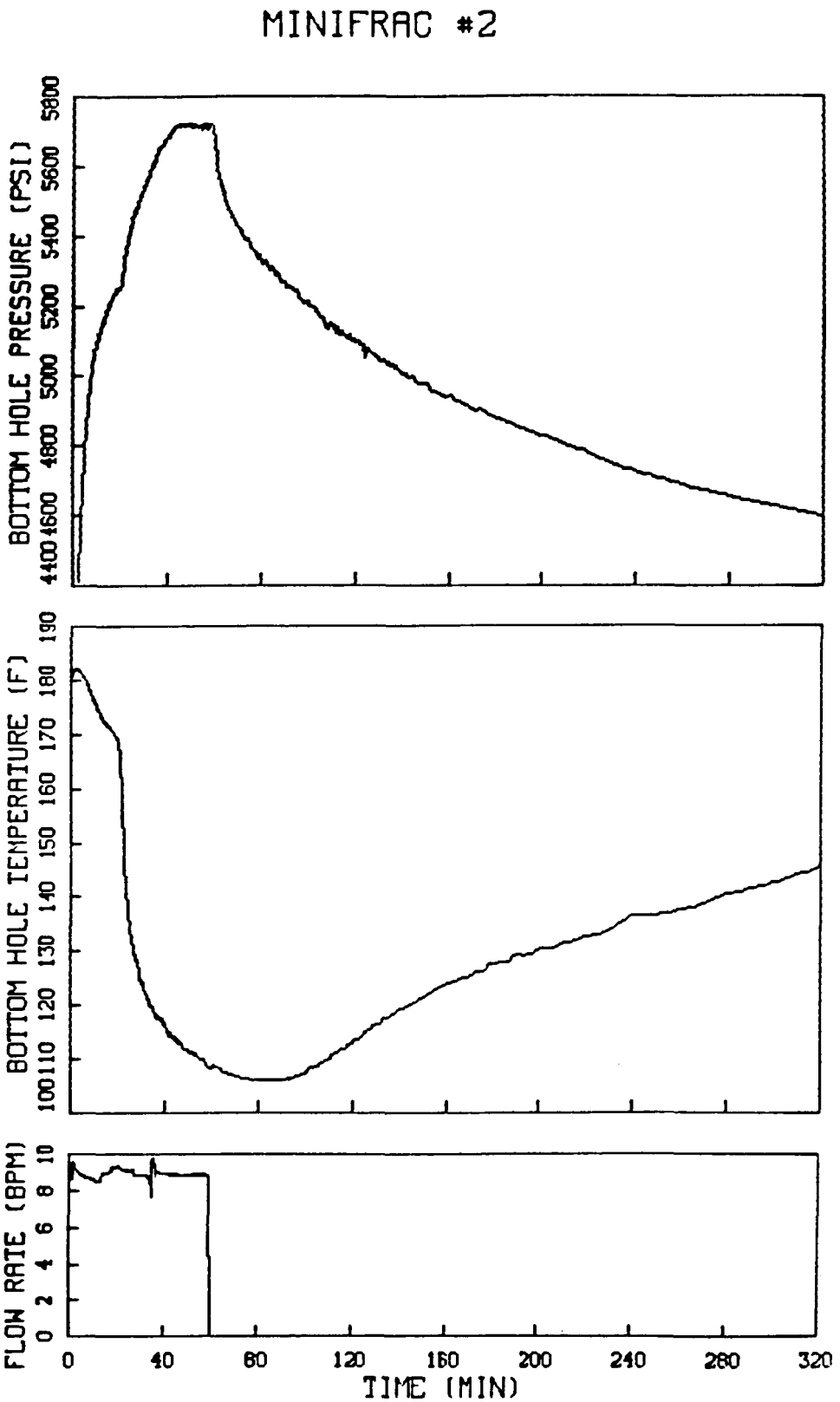

Figure 8.1.32. Minifrac #2 Injection Data

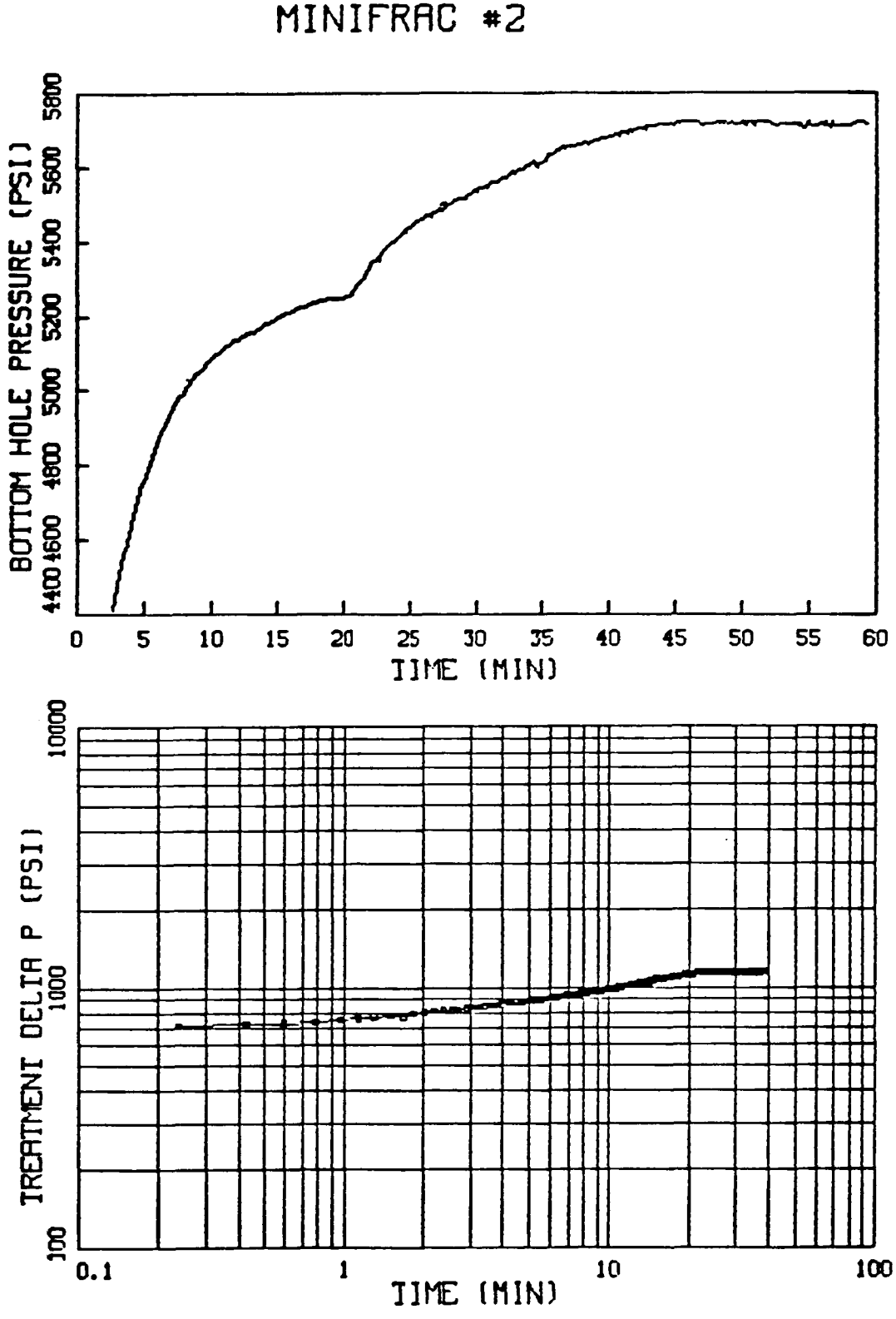

Figure 8.1.33. Minifrac #2 Treatment Pressure and Nolte-Smith Plot

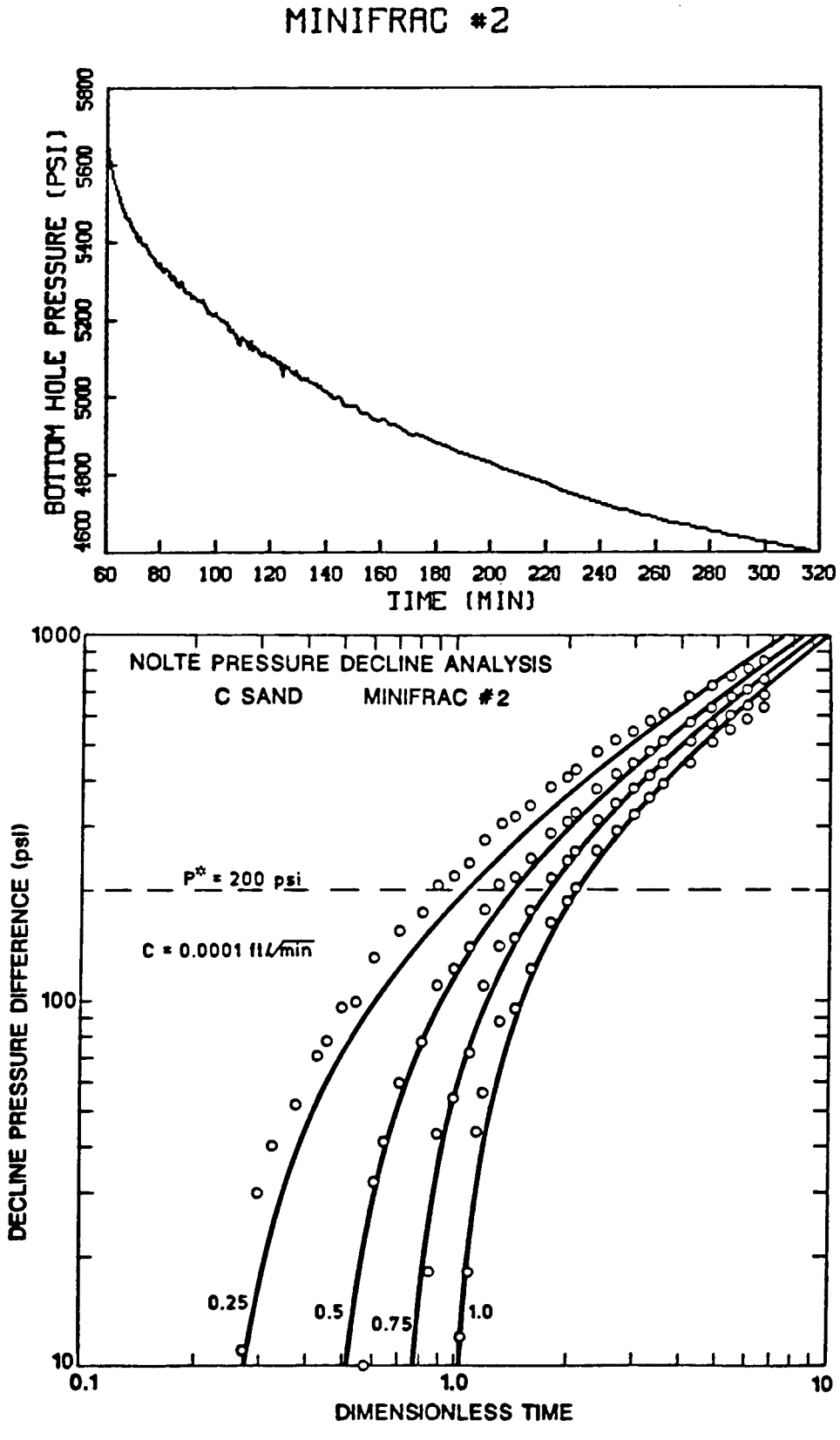

Figure 8.1.34. Minifrac #2 Pressure Decline Data and Nolte Plot

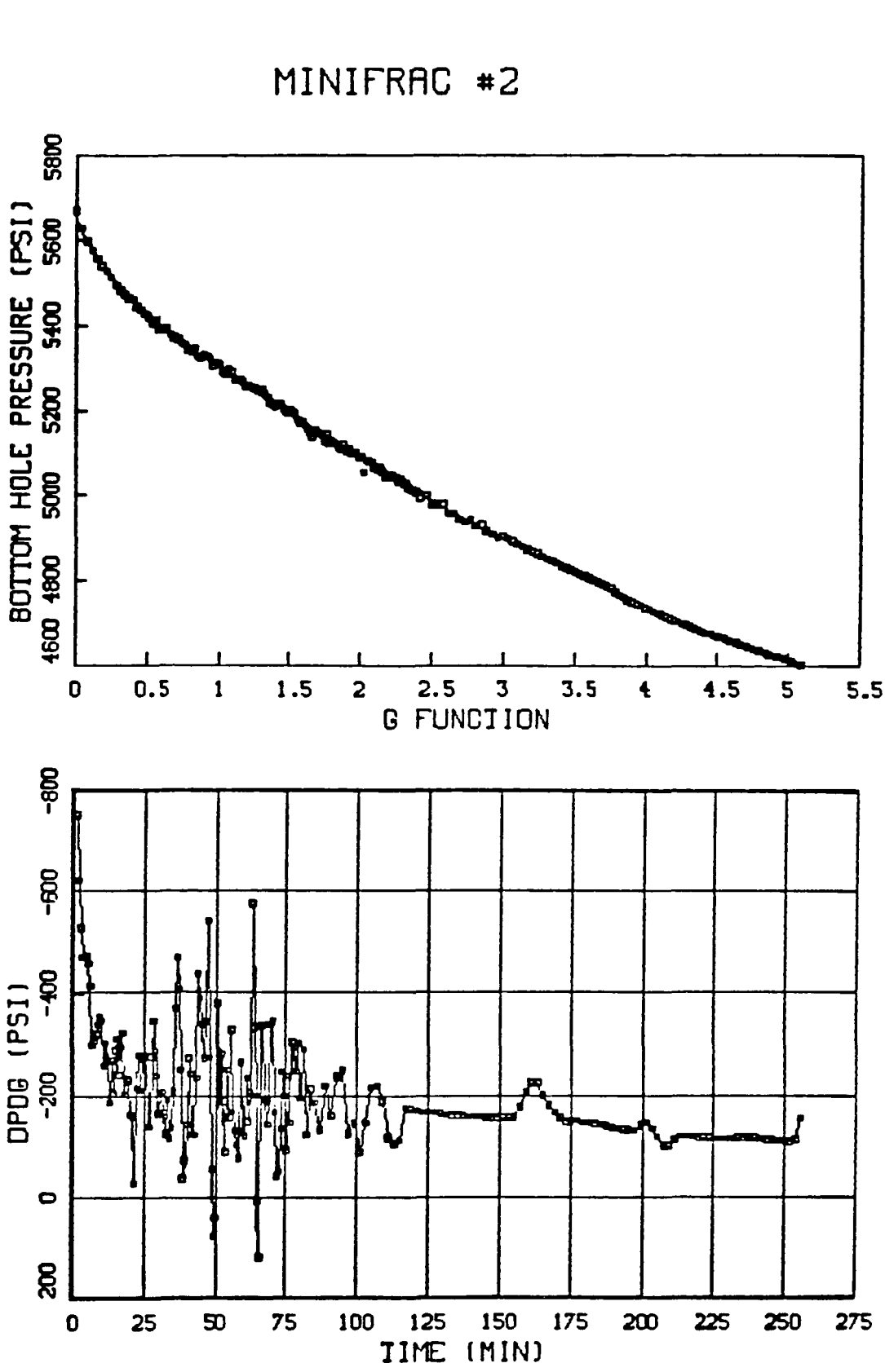

Figure 8.1.35. Minifrac #2 G Function Results

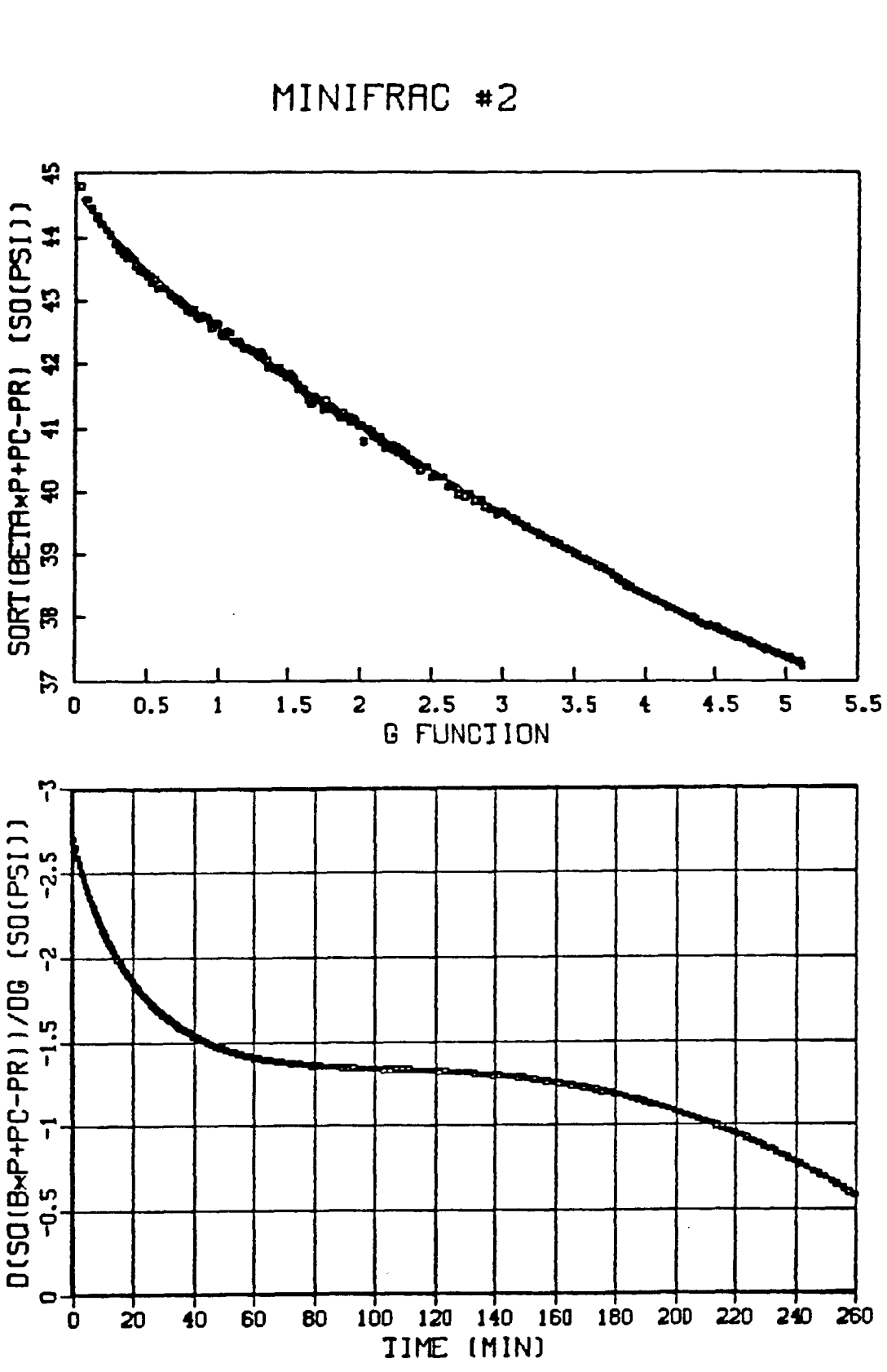

Figure 8.1.36. Minifrac #2 Linearized G Function

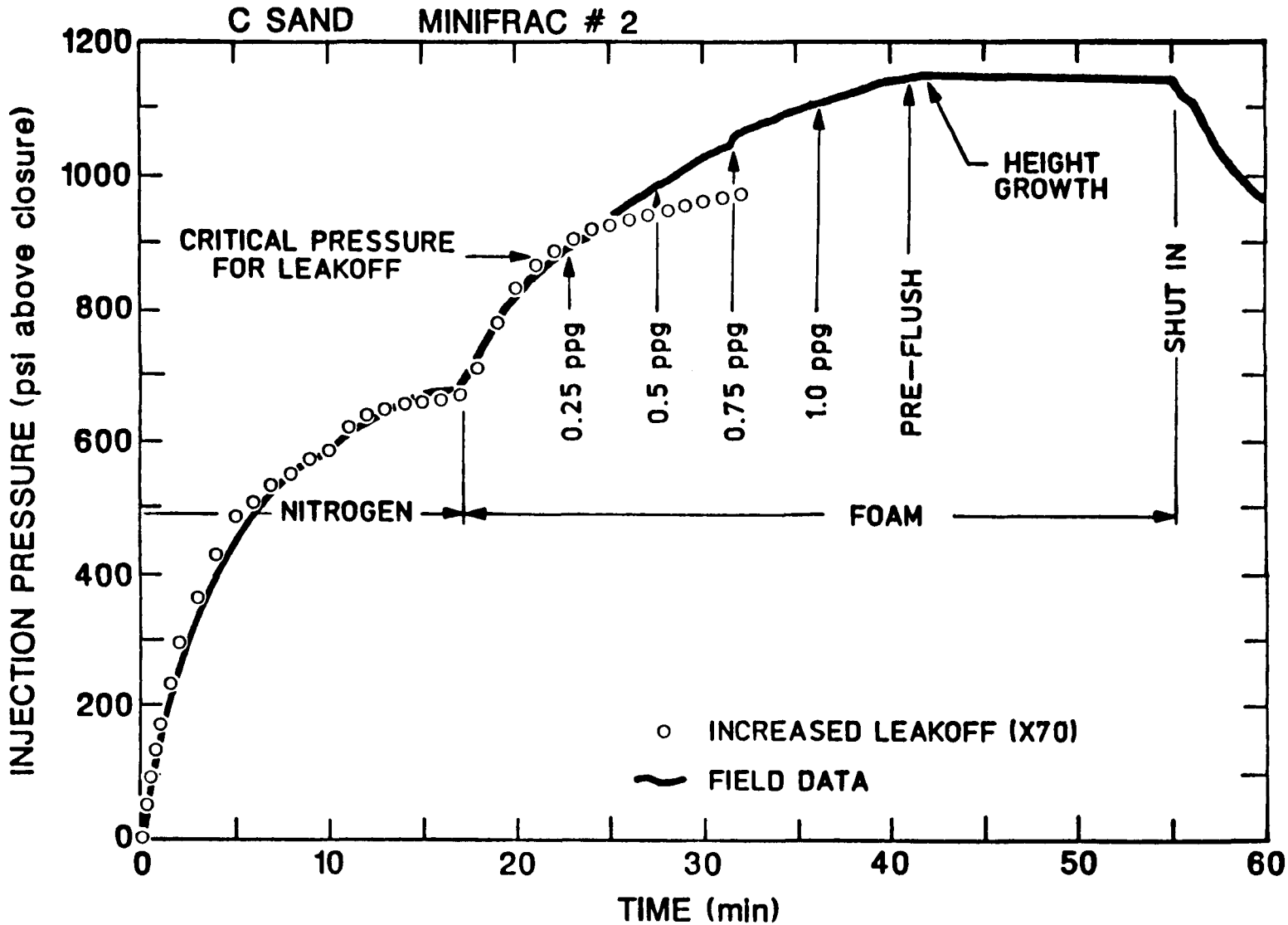

Figure 8.1.37. Pressure-History Match for Minifrac #2 Using Same Parameters as Minifrac #1

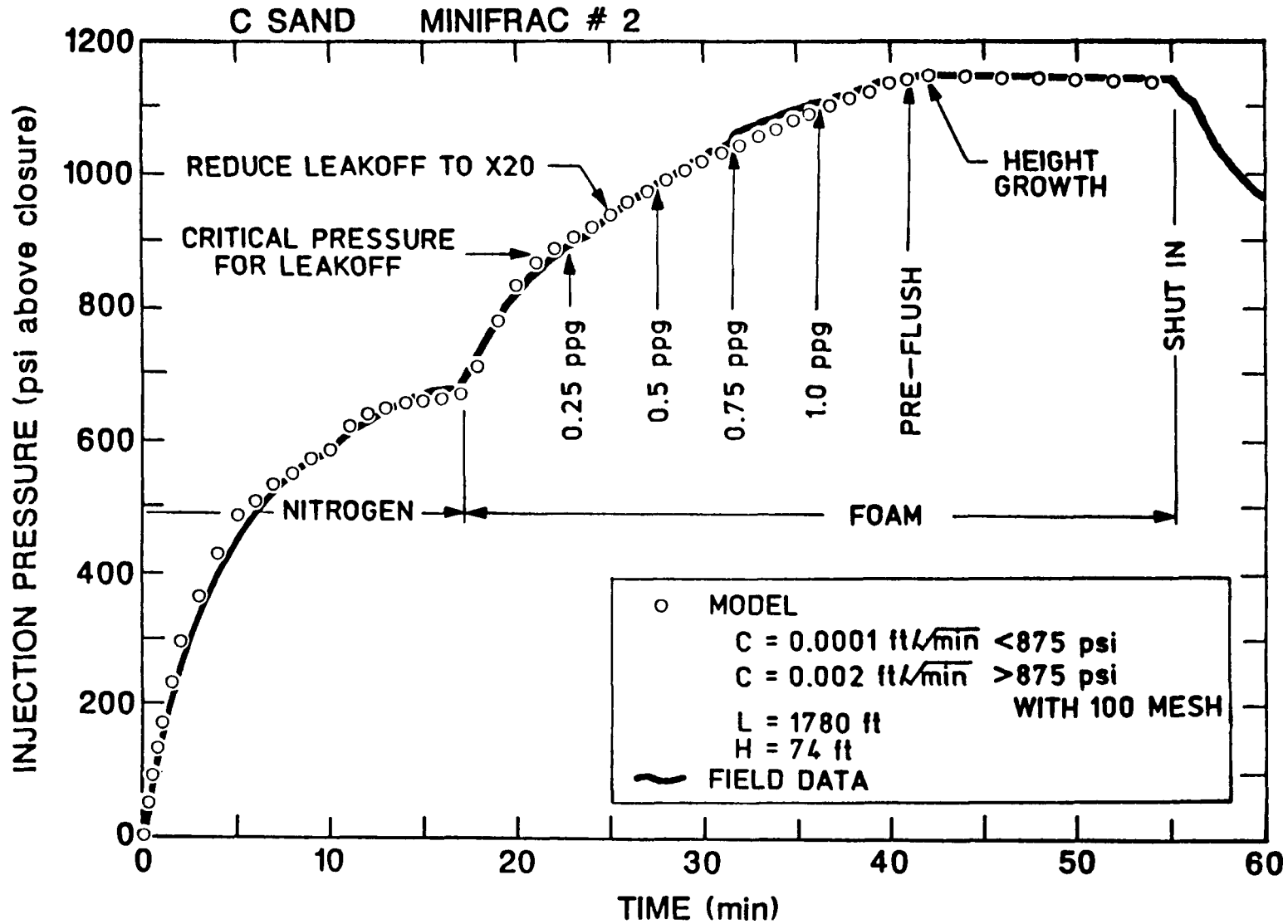

Figure 8.1.38. Final Pressure-History Match for Minifrac #2

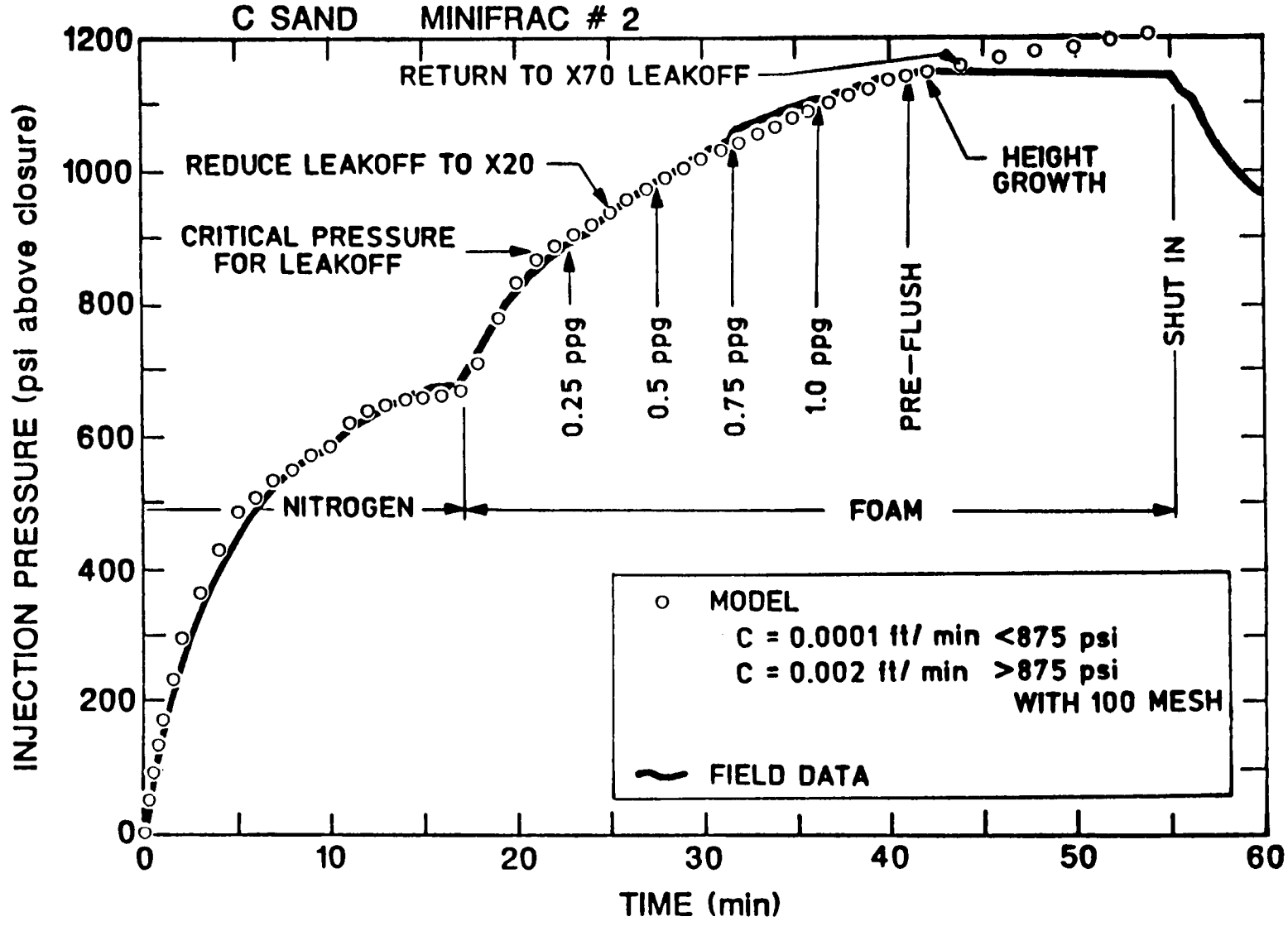

Figure 8.1.39. Pressure-History Match for a Return to Factor of 70 Leakoff

FLUVIAL C SANDSTONE STIMULATION EXPERIMENT

8.2 ALTERED STRESS EXPERIMENTS

N. R. Warpinski
Sandia National Laboratories

8.2.1 OBJECTIVE

The Altered Stress Experiments were conducted in April and May 1987 in conjunction with the C sandstone experiments. The purpose of these tests was to measure the stress alteration in one well as a result of hydraulic fracturing operations in a second well. In this case, stress tests were performed in MWX-2 to determine the stress changes induced by the minifracs conducted in MWX-1. Based on these field results, analytical and finite-element calculations were also performed to determine if the degree of stress change induced by a large treatment would be sufficient to reorient the stress field in order to obtain a better connection with the natural fracture system.

8.2.2 BACKGROUND

The in situ stress field that exists at depth in a rock mass is known to control many oil and gas stimulation parameters,[1-4] such as the orientation and height of a hydraulic fracture. In some reservoirs, the stress distribution is unfavorable for an effective stimulation and considerable research efforts have been directed towards mitigating undesirable effects. A particular example that is important at MWX is a hydraulic fracture that is not optimally oriented with respect to the permeability anisotropy, i.e., one that is parallel to the primary natural fracture direction.

Most efforts to control the fracture orientation have been modifications of the stimulation design or the drilling program. While modifications, such as altering the well layout, deviated drilling, or propellant fracturing , have been successful in some cases, they may not be practical in other situations. There is a second approach, however, that is usually overlooked. Instead of changing the stimulation design or drilling program,

it may be possible to alter the stress field to a more favorable orientation or magnitude. While at first it may seem somewhat pretentious to consider altering the stress field at 5000- to 10,000-ft depths, we should remember that significant stress perturbations are induced by any process that changes reservoir pressure or fractures the rock. A hydraulic fracture, because of the high pressure needed for fracture dilation and the large surface area created, is an effective mechanism for altering the stress field.

This section elaborates on the concept of stress alteration using hydraulic fractures and the ways it can be applied.[5] A description is given of the initial field test to measure the stress change in the vicinity of the minifracs in the C sandstone. This was achieved by conducting stress tests in MWX-2 while hydraulically fracturing MWX-1. Analytic calculations for homogeneous media and finite-element calculations for layered media are included for comparison with the field results. Reservoir simulations, showing the productivity enhancement expected from application of this concept, are described. Finally, practical capabilities of this altered-stress fracturing technique are discussed.

8.2.3 THE ALTERED STRESS SETTING

The nonmarine, lenticular sands of the fluvial interval have 0.1-2 μd matrix permeabilities, but limited natural fracture systems increase the effective reservoir system permeabilities to 10-50 μd.[6] Studies of outcrops and over 4100 ft of core--over 1100 ft of it oriented--have shown that the natural fractures are primarily unidirectional, resulting in an anisotropic permeability distribution. This has been substantiated with three-well interference test results[7] that show permeability anisotropy ratios of 10:1 to 100:1. In the few lenses where cross-fracture sets are observed, permeability anisotropies are still large. Thicknesses of the reservoirs range from a few ft to 40 ft, with estimated lens widths of 100-2500 ft depending on the depositional environment.[8] Since these reservoirs were deposited as sand channels or meander belts, lengths of the lenses are expected to be much greater than widths. Finally, the in situ stress field

is aligned with the natural fractures so that hydraulic fractures parallel the natural fractures.[9,10]

Stimulation and production of these reservoirs is not an easy task.[10] Hydraulic fractures will intersect only a few of the natural fractures and productivity enhancements of only about 2-4 times can be expected (Section 7.3). In addition, these natural fractures are extremely narrow and appear to be easily damaged by stimulation gels. Because of the limited lens size, long hydraulic fractures that can produce economically from the matrix alone are not feasible. Initial flow rates from many of these sands are only 10-70 MCFD, so the production resulting from a stimulation is often disappointing.

To overcome the coalignment of the natural fractures and the hydraulic fractures, techniques such as propellant fracturing[11] and directional drilling[12] have been suggested. Propellant fracturing can induce multiple, radially oriented fractures, but there is a limit to fracture lengths that can be achieved. Directional drilling in lenticular sands will intersect more natural fractures if the hole is oriented perpendicular to the natural fracture azimuth. However, if drilling damages the natural fractures or too few fractures are encountered in a lens, conventional stimulations in a directionally drilled hole will be no more effective than in vertical holes.

The altered-stress fracturing approach is an attempt to reorient the stress field in a region by conducting a hydraulic fracture nearby. Sneddon[13,14] calculated the stress distribution around 2-D and penny-shaped fractures and showed that the stress perturbation at a distance is proportional to the size and the pressure in the hydraulic fracture. Shuck[15] was granted a patent on the concept in 1977, the first suggestion of the technique of which we are aware. While the original concept of stress alteration using multiple wells is somewhat limited because of well spacing criteria, the technique is also applicable in deviated holes. Uhri[16] obtained a patent in 1987 on a method that could be used in deviated holes.

In addition, some stress modification applications may be useful in vertical wells.

Figure 8.2.1 shows the conceptual application of this approach at MWX. An offset well (in this figure MWX-2) would be used to create a hydraulic fracture that alters the stress field around the production well (MWX-1). To effect this, the offset well must be fractured first and continue to be treated while the production well is fractured. Obviously, timing, treating pressures, stresses, and distances between wells are important parameters. The high pressure in the first fracture would add additional stress to the virgin minimum in situ stress around the production well. If the difference in horizontal stresses is not too large, the wells are relatively close, and treatment pressures and fracture size in the offset wells are sufficiently large, enough stress can be added to the virgin minimum horizontal in situ stress to make it the maximum horizontal stress. Pumping must be maintained in the offset well fracture, because the stress perturbation will decay as the pressure declines. If a treatment in the production well is started under these conditions, the hydraulic fracture in the production well will propagate perpendicular to the usual direction. How far it will go before turning depends on many factors, but it can be roughly estimated.

For this idea to work in a given situation, there are a number of reservoir and well requirements that should be met.

- There must be a reason why altering the stress field will produce some advantage. At MWX, a hydraulic fracture parallels the highly anisotropic, natural fracture permeability system.

- The difference between the two principal horizontal stresses must not be too large, because the stress perturbation is proportional to the pressure in the offset hydraulic fracture which has a practical limit. At MWX, the stress difference is about 600 psi.[17]

- The wells should be as close together as possible since the stress perturbation decays rapidly with distance. At MWX, the effective distance is 90-100 ft. Application of this technique in deviated holes eliminates this requirement.

- There needs to be some mechanism to obtain high treatment pressures in the offset wells. This may be due to reservoir features such as good vertical stress contrasts, or induced features such as a screenout. At MWX, high treatment pressures are common, largely because of large stress contrasts that somewhat contain fracture height.[18]

- Some height growth must also be obtained to produce large perturbations at realistic distances from the offset well. The stress decay is also proportional to the height of the fracture. At MWX, fracture heights of 75-200 ft are common for relatively small treatments.

8.2.4 ANALYTIC CALCULATIONS

Some simple scoping calculations can help show the effects of the important parameters on the stress perturbation. Sneddon[13,14] gives the stress field around an infinitely long 2-D crack (plane strain) in a homogeneous, isotropic, elastic body, having Poisson's ratio of ν and the geometry shown in Figure 8.2.2, as

$$\frac{1}{2}\left(\sigma_x+\sigma_y\right) = -P\left\{\frac{r}{\sqrt{r_1 r_2}}\cos\left[\theta-\frac{1}{2}\left(\theta_1+\theta_2\right)\right] -1\right\} \quad , \tag{1}$$

$$\frac{1}{2}\left(\sigma_y-\sigma_x\right) = P\left\{\frac{r\,\sin\theta}{c}\left(\frac{c^2}{r_1 r_2}\right)^{3/2}\sin\left[\frac{3}{2}\left(\theta_1+\theta_2\right)\right]\right\} \quad , \tag{2}$$

$$\tau_{xy} = -P\left\{\frac{r\,\sin\theta}{c}\left(\frac{c^2}{r_1 r_2}\right)^{3/2}\cos\left[\frac{3}{2}\left(\theta_1+\theta_2\right)\right]\right\} \text{ and} \tag{3}$$

$$\sigma_z = \nu\left(\sigma_x+\sigma_y\right) \quad . \tag{4}$$

In Eqs. 1-4, P is the internal pressure, c is the crack half height (H/2), and the geometric relations are given by

$$r = \sqrt{x^2+y^2} \qquad \theta = \tan^{-1}(x/-y)$$

$$r_1 = \sqrt{x^2+(y+c)^2} \qquad \theta_1 = \tan^{-1}[x/(-y-c)]$$

$$r_2 = \sqrt{x^2+(y-c)^2} \qquad \theta_2 = \tan^{-1}[x/(c-y)] \quad . \qquad (5)$$

Negative values of θ, θ_1, and θ_2 should be replaced by $\pi+\theta$, $\pi+\theta_1$ and $\pi+\theta_2$, respectively. Examination of Eqs. 1-5 also suggests that all stresses can be normalized by the pressure, P, and all lengths can be normalized by the half height, c=H/2.

The results can be used to calculate the decay of the stress field with distance from the fracture. Figure 8.2.3 shows a plot of the induced stresses along the centerline, extending away from the crack. Both axes are normalized as discussed above. The induced σ_x at 2x/H=1.0 is about 65% of the treating pressure, but at 2x/H=2.0, it is already down to 28%. This suggests that wells need to be close, the pressure high, and height large. There is also a small contribution to the other principal horizontal stress, σ_z in this calculation, that will raise its value somewhat and make stress reversal slightly harder. At 2x/H=1.0, about 12% of the net treating pressure is added to the maximum horizontal stress, and at 2x/H=2.0, about 4% is added.

In order to get a reversal of the stresses, we require that $\sigma_{Hmin}+\sigma_x>\sigma_{Hmax}+\sigma_z$, where σ_{Hmin} and σ_{Hmax} are the virgin minimum and maximum horizontal principal stresses. For example, if the difference in stresses is initially 600 psi, then a treating pressure of 1130 psi is required to get stress reversal at a normalized distance of 1.0 and 2500 psi is required at 2.0. The requirements become excessive for normalized distances greater than 2.0.

This calculation assumes that the fracture length is large enough that it can be considered infinite, a good approximation in the practical application of this technique. However, an estimate of the effect of a short fracture can be made using equations that Sneddon[14] developed for a penny-shaped crack. The results are much more complicated than Eqs. 1-5 and are not given here. Figure 8.2.4 shows the normalized stress decay for the radial case. The radial and tangential stresses are the same along the centerline and they both depend upon Poisson's ratio. The perpendicular stress, σ_x, decays faster than the comparable stress in the 2-D case.

8.2.5 FIELD TEST

The MWX well spacings are ideal for testing the stress alteration capabilities of a hydraulic fracture at depth. In the spring of 1987, an opportunity arose to conduct what is essentially a pilot test by measuring the stress changes that were induced by a series of pump-in tests and two minifracs conducted in MWX-1. One of the offset wells, MWX-3, had a borehole geophone package located downhole in an attempt to map the minifracs from the created microseisms. The other offset well, MWX-2, was available for stress test measurements during these operations. (Note that this is the opposite configuration to the conceptual diagram shown in Figure 8.2.1. In this field test, stress is measured in the offset well (MWX-2) while the production well (MWX-1) is fractured.)

Prior to the minifracs, a series of stress tests[17,19] were conducted in MWX-2 to establish the baseline virgin stress condition (Section 6.0). The stress tests are small volume (10-50 gal) hydraulic fractures using low viscosity fluids (KCl water), pumped at low flow rates (2-15 gpm). The fracture is shut in with a bottom-hole closure tool and pressure is recorded with a surface recording, wireline run, bottom-hole quartz crystal oscillator gage. The quartz gage processor has been modified for faster pressure response, usually 5-10 measurements per second. Under most conditions, the instantaneous shut-in pressure (ISIP) determined from such a small fracture will closely approximate the minimum in situ stress.[17,19] Results of these tests gave a minimum in situ stress value of 4575 psi with

an uncertainty of ±50 psi. Young's modulus in this zone is about 4.5×10^6 psi, while Poisson's ratio is about 0.18.

Table 8.2.1 lists the series of pump-in tests and minifracs that were performed in MWX-1 and the associated stress tests for measuring the stress alteration in MWX-2. A few stress measurements were obtained during the KCl pump-in tests. During the first minifrac, three stress tests were conducted, with two more during the pressure decline and flow back. A second minifrac, which was conducted two weeks later, was considerably larger and used 100-mesh sand in an attempt to control fluid leakoff into natural fractures that seemed to occur during high pressure injections. Seven stress tests were conducted during this minifrac, seven during the pressure decline, and five during the flowback.

Figure 8.2.5 shows pressure records of the stress-test pumps that were performed during the pump-in tests and the first minifrac in MWX-1. The names next to each curve are consistent with the names given in Table 8.2.2. These data have been correlated so that the shut-in time is the same for all tests. It is clear from the increase in the injection pressure that the stresses around the offset well, MWX-2, are increasing considerably with the pressure in the treatment well.

One problem that occurred in these tests was an unclear ISIP, which made the determination of the stress relatively uncertain. To circumvent this difficulty, most of the stress-test pumps were conducted at the same rate (~15 gpm) and for the same length of time (~2 minutes) after reaching a pressure of 4500 psi. Since all of the stress-testing fracturing parameters (rate, viscosity, volume, height, etc.) are the same for each test, the change in the injection pressure should reflect the stress change induced by the hydraulic fracture in the treatment well. Care needs to be taken in determining the fracturing pressure for each pump, because the slight pressure increase that occurs just before shut-in in most tests is due to the movement of the wireline in order to lower the downhole seating mandrel

into the shut-in position. In Figure 8.2.5, the pressures at the 2.5-minute mark provides a good test-to-test comparison to estimate the stress change. Based on this approach, the induced stress change in MWX-2 due to the treatment in MWX-1 is as much as 240 psi.

One source of error in using the injection pressure is the slight increase in pressure with consecutive tests if fluid is allowed to remain in the stress test fracture. To minimize such cumulative effects, the pressure in the stress test well was bled down to the hydrostatic value after most stress tests. This allows the stresses and pore pressure to force out most residual water and yields a more complete closure of the fracture. Residual effects after this precaution are small.

Figure 8.2.6 shows the last stress test pressure record from the first minifrac, along with the two stress tests that were conducted after pumping stopped. The two post-minifrac stress tests were conducted back-to-back and confirm that the stress is dropping upon cessation of pumping.

Figure 8.2.7 shows a similar set of tests conducted during the second minifrac, which was conducted with 100-mesh sand. The second minifrac was a larger volume and achieved higher pressures by about 100 psi. The stress change in the offset well during these tests is as much as 300 psi. Of particular interest here is the large stress change that occurs during the last four tests with relatively small changes in treatment pressure (see Table 8.2.2). There is good evidence of height growth towards the end of treatment, with essentially flat to slightly declining injection pressures for the last 10-12 minutes. The increase in stress around the offset well at this time is due to height growth rather than pressure increase. Note also that the base stress level for the second minifrac is 25 psi higher than the first minifrac. This is based on stress tests conducted just prior to the second minifrac and is thought to be an effect of increased pore pressure in the reservoir after the first minifrac. However, this apparent stress increase may also be due to some residual width in the treatment hydraulic fracture because of incomplete closure at asperities.

Several of the stress tests conducted during the pressure decline (post-minimesh) and during the flow-back are shown in Figure 8.2.8, along with the last stress test from the 100-mesh minifrac. Again, the decrease in stress with reduction of pressure and time is apparent. This shows that the increase in stress measured in MWX-2 is not just an artifact of the stress-test procedure in MWX-2, or continued testing should result in a further increase in the pumping pressures. No such increase is observed here and the pressure behavior in MWX-2 follows the pumping behavior in MWX-1.

The final results of all these stress tests, compared to the bottom-hole pressure in the treatment, are shown in Table 8.2.2. Many of the initial stress tests conducted on 4/22/87 are not shown because they were conducted at different rates or with different volumes and cannot logically be compared. This is also true for two other tests. Selected data from Table 8.2.2 are plotted in Figure 8.2.9, with change in stress in the observation well as a function of net treatment pressure. This plot shows the loading behavior during pumping and the unloading behavior during pressure decline and flowback.

The loading behavior can be broken up into two regions. Below about 1000 psi in the treatment well, the stress change is relatively small with a slope of 0.11, as determined by a linear regression through the origin. Referring back to Figure 8.2.3, a normalized stress change of 0.11 would correspond to $2x/H=3.5$ for a homogeneous, elastic medium. Since x is fixed at 90 ft, this suggests that the height is about 50 ft. Above 1000 psi, the stress change increases rapidly, which will most likely occur if height is increasing significantly. This also assumes that length is already great enough that it can be considered infinite, a reasonable assumption considering the volume injected to achieve the higher pressures. The maximum value of normalized stress is 0.27, which corresponds to $2x/H=2.1$ for a height of 86 ft. Modest changes in height growth yield large changes in the induced stress. This occurs because reduced values of $2x/H$ provide rapidly increasing values of stress change, as can be seen in Figure 8.2.3. A second important point is that this technique is an excellent height

growth diagnostic. Since the stress change and pressure are both measured and x is fixed, the only variable that can account for the nonlinear behavior is the height.

The unloading behavior is also interesting because it indicates that there is considerable hysteresis, but the Y-axis offset essentially disappears during flowback. Some of this may be due to excess height that has not closed, possibly because it is propped with 100-mesh sand. Some of it may also be poroelastic, due to the charging of the reservoir with nitrogen from the foam.

8.2.6 FINITE-ELEMENT CALCULATIONS

The previous discussion is appropriate for a homogeneous, elastic body, but this test was actually conducted in a layered medium in which modulus and stress are considerably different in the reservoir rock compared to the surrounding mudstones. Modulus contrasts will affect these results because stiffer layers will take more of the stress. Stress contrasts are also important because the fracture width in high stress regions will be small so that less strain will be induced and the effect of extra height growth will be less than in a homogeneous formation. To evaluate these effects, a series of finite element calculations were performed using the JAC code.[20] This code allows several different materials and, most importantly, the application of a prestress to simulate the varied stresses in different layers. This is the optimum method to simulate layered stresses; the alternative of applying different stresses at the boundaries causes the stress layers to smear within the body, yielding misleading results. Several grid sizes were also used to assure that boundary distortions were not modifying the results.

Figure 8.2.10 shows the effect of modulus contrasts on the stress perturbations in the reservoir compared to the analytic solution. The data points on the analytic solution are a finite element solution for a uniform material that was run to assure that the code is set up correctly. Two

different size cracks have been considered for these tests, a small crack that is well contained and a larger crack with considerable height growth out of the zone. The modulus of the surrounding mudstones was reduced by a factor of 2, from 4.5×10^6 psi to 2.25×10^6 psi for the low modulus case and doubled to 9.0×10^6 psi for the high modulus case. Clearly, the more common situation of low-modulus bounding rocks increases the magnitude of the induced stress change for a given location, and the effect is quite large.

Figure 8.2.11 shows the effect of different in situ stresses in the abutting rocks with positive stress values indicating increasing compression. High stresses in the mudstones reduce the magnitude of stress change, and the effect increases with crack size. Low stress layers will, of course, enhance the induced stress change. Figure 8.2.12 shows several combined modulus and stress calculations. High stresses in the nonreservoir rocks are nearly compensated for by low modulus in the nonreservoir rocks, at least for small cracks.

Finally, Figure 8.2.13 shows our best estimate of the conditions around the C sandstone for three crack sizes. Stress contrasts are about 600 psi and Youngs modulus of the mudstones is 3.5×10^6 psi compared to 4.5×10^6 in the sandstone. The internal pressure used for all three calculations is 1000 psi. For a small crack, the effects of high stress and low modulus in the mudstones nearly cancel. For larger cracks, the effect of the high stress is more significant and the curves shift left.

Based on these new curves, a better estimate of the fracture height in the treatment can be obtained. For a normalized stress of 0.11 and using the middle crack height, a 2x/H value of 3.25 is estimated. This yields a crack height of 55 ft during the pump-in test and the initial growth of the minifracs. For a normalized stress of 0.27, 2x/H=1.67 on the large-height curve, which yields a height of 108 ft. This is in excellent agreement with borehole geophone results from the third well (MWX-3) which yielded a height on the order of 100 ft (see Section 8.4).

8.2.7 RESERVOIR SIMULATION CALCULATIONS

A series of reservoir simulations were performed to estimate the enhanced production that would occur for an altered stress fracture as opposed to a normal hydraulic fracture. In the model,[7] the high permeability fractures run parallel to the maximum principal stress direction (hydraulic fracture direction) and the minimum permeability is orthogonal to this. Transient phenomena within grid matrix blocks are incorporated by dividing each of the blocks into a graded set of seven concentric rectangular cells. This provides a realistic approximation of the pressure transients that occur in the matrix.

Table 8.2.3 shows the reservoir data that was used in the model. These data are from the B sandstone (Section 7.3) that is about 100 ft below the sand tested in the present experiments. However, extensive well tests were performed in the B sandstone and these model properties give a good match with the observed production. The anisotropy in this case is 100:1.

Figure 8.2.14 shows a comparison of one year of production for three cases. The base case has no stimulation and closely matches the production obtained in well tests. The 750-ft fracture case is for a conventional hydraulic fracture with essentially infinite conductivity and no damage to the reservoir. This fracture only intersects the low permeability natural fractures. After one year of production, flow rates are about 100 MSCFD with a cumulative produced volume of 52.4 MMSCF. The 100-ft fracture is orthogonal to the maximum stress direction, as if turned by an altered-stress fracture treatment, and therefore intersects the high permeability natural fractures. Flow rates after one year are about 120 MSCFD with a cumulative production of 62.5 MMSCF. The 100-ft altered-stress treatment is equivalent to about a 900-ft conventional treatment in this 100:1 anisotropic reservoir.

As one would expect, lower anistropy ratios will reduce the advantage while higher ratios will increase the advantage of the altered-stress

fracture. If damage occurs to the natural fractures during these treatments, the altered-stress fracture is more severely affected because there are fewer fractures of higher permeability to be damaged. However, cleanup of these fractures should be easier since they are higher permeability. Finally, the 100-ft length for the altered stress fracture was chosen as a conservative estimate for the length at this site. In principal, there is no reason why longer fractures could not be generated, giving an even greater advantage. On the other hand, the 750-ft conventional fracture is about the maximum useful length in this reservoir since the lens width is only about 1500-1800 ft.[6]

8.2.8 DISCUSSION

These field experiments show that the concept of altering the stress field is valid and can be applied in lenticular reservoirs. Stress changes of as much as 300 psi were observed during small minifracs, in which the treatment pressures reached 1120 psi above closure and estimated heights of 100 ft. Larger treatments with greater heights and treatment pressures could overcome the existing stress difference of about 600 psi. Assuming that a larger or more viscous treatment could easily achieve a height of 200 ft and treatment pressure of 2000 psi above closure, the change in the maximum stress would be 880 psi and the change in the minimum stress would be 140 psi. This would result in a net stress reversal of 140 psi if the initial stress difference is 600 psi. Many reservoirs will have smaller initial stress differences, and stress alteration could be more easily achieved.

However, this case also shows that there is a limit to the applicability of this technique using separate wells. A more likely application is in directionally drilled holes, as discussed by Uhri.[16] A first treatment could be conducted down the annulus while the second treatment is performed down tubing, at much closer distances than could be obtained in multiple wells. In addition, if the first treatment (to alter the stress) is initiated in a high stress shale or mudstone, high treating pressures and

large heights will be facilitated so that much greater stress changes will occur. This technique cannot be used to reverse the horizontal stresses in a vertical well when the overburden stress is also vertical. If dipping strata, topography or some other effect causes the stress field to be misaligned with the vertical, however, then this technique is feasible.

One problem with such a technique is the complexity of treatment operations, particularly if it is all being performed in one well. It may also not be possible to guarantee sufficient pressure in the offset fracture to reverse the stress field. This suggests that unusual fracture design techniques should be applied to the first fracture. One possibility is to design a tip screenout for the first fracture. This would ensure high pressures as well as making maintenance of those high pressures easy by allowing for relatively slow pumping of only liquids (after the tip screenout has formed). It may also be possible to induce a tip screenout and pack enough sand into the fracture so that no additional pumping is needed. The propped fracture width and the strain it produces is equivalent to the pressure required to create that width. If the first treatment is in a nonproductive rock or will not be produced, then cement could be used or tailed in after a tip screenout to squeeze the perforations, but this could be tricky. Very thick gels could also be tried.

The results of Figure 8.2.3 show that the stress perturbation at some distance from a fracture is independent of modulus. This is important because it suggests that the compliance of natural fractures will not attenuate the decay distance. In general, a more compliant formation will have a lower stress per unit strain than a stiffer material, but in this application, greater compliance also results in greater fracture widths and thus more strain. The two effects exactly cancel in a homogeneous formation. Layered formation will behave differently and the principal problem occurs if the reservoir rock is highly fractured and the surrounding layers are not. This may make the reservoir layer highly compliant which will result in significantly less stress change, as seen in Figure 8.2.10. At MWX, the nonreservoir layers have more and wider natural fractures than

the reservoir sandstones. Most fractures are found in thin siltstones that are embedded in the mudstone intervals and these fractures probably enhance the favorable modulus contrast that already exists.

Another possible application of the stress modification concept is for alteration of the vertical distribution of the minimum horizontal in situ stress. The basic idea here is that a hydraulic fracture creates a large compressive stress in the layer it resides, but it also induces large tensile stresses above and below. This could be used to advantage if hydraulic fractures are propagating into undesirable zones, such as aquifers. Figure 8.2.15 shows an example calculation for a reservoir rock that is 500 psi higher stress than a nearby aquifer. The initial stress condition and the new stress condition created by a 32-ft, 1000-psi hydraulic fracture are shown here. This rather crude calculation shows that a 500-psi unfavorable stress contrast can be altered into a favorable stress contrast of around 800 psi. Such an application is possible in a vertical hole, a deviated hole or even two adjacent wells.

If an altered stress concept is used to reorient the fracture, the initial breakdown technique in the production well should be carefully considered. A normal breakdown or ballout will initiate hydraulic fractures in the usual hydraulic fracture orientation. Afterward, attempts to start an altered-stress fracture may be difficult and the stress perturbations may be mitigated. It would be better to break down under reversed stress conditions so that the fracture is oriented correctly from the start. An alternate breakdown technique would be to use a propellant fracturing device[11] through perforations with at least 90° phasing. Fractures should initiate out of each set of perforations, giving reasonable initiation sites for the follow-on treatment.

Another important consideration for the altered-stress treatment is leakoff control. If the hydraulic fracture is altered to cross the most permeable natural fractures, then fluid leakoff may be much greater than normally found in the reservoir. Height containment conditions may also

suffer, particularly if the vertical distribution of the maximum stress is different from the vertical distribution of the minimum stress. This will occur if the shales are viscoelastic[17] and if tectonic or other strains are induced differently in the two principal directions.

An interesting result is the finding that this technique can be used as an accurate fracture height diagnostic. If stress measurements can be made in an offset well, it is relatively easy to determine when significant fracture height growth begins to occur. These results agreed well with height measurements using borehole geophones. No temperature log heights were discernible in these tests.

A note of caution should be added about extrapolating the finite-element calculations given in this paper to other zones. In uniform, homogeneous formations, the results of Figure 8.2.3 apply to any formation or zone with simply a change in the stress obtained for the out-of-plane direction (different Poisson's ratio). In layered materials, the thickness of the zone, the stress contrasts and the modulus contrasts also become important parameters. Attempts to extrapolate these results to larger or smaller zone thicknesses may cause significant errors.

In the field tests, it was disappointing to not see clear ISIP values that reflected the stress changes, but the fracture pressure approach is entirely valid and the results are in no way compromised. The problems with determining the ISIP could be due to the perforations, the cement, or the formation. Figure 8.2.16 shows the pressure record of the initial stress test in this zone, on 4/22/87. This test was obscured by a leak across the closure tool just seconds after the ISIP, but it provided the clearest ISIP of all of the tests conducted at any time. In this case, the ISIP is about 4575 psi, but possibly a little lower, as the initial shut-in does not continue long enough to make this certain. The second stress test, shown in Figure 8.2.17, shows the characteristics of all later tests, a continuing increase in the pressure and an unclear ISIP.

There are various possible techniques to extract the ISIP from unclear data, but none of them have good theoretical backing.[21] Figure 8.2.18 shows several of these techniques, including square-root-of-time, G-function, log-log and semilog plots. In all cases the ISIP is difficult to discern. The G-function shows no evidence of the ISIP and the square-root-of-time plot shows some change between 4500 and 4600 psi. The log-log plot is obtained by subtracting the pressure from the injection pressure at the end of pumping (4629 psi) and possibly shows something at 60 psi below the fracturing pressure, or 4570 psi. The semilog plot is obtained by subtracting the reservoir pressure (3300 psi) from the pressure during the decline and it indicates that there might be some changes between 1200 and 1300 psi above the reservoir pressure, or 4500-4600 psi.

Finally, Figure 8.2.19 shows another technique that we developed[21] to estimate the error in tests with unclear ISIP values. A radius of curvature of the pressure decline is calculated from the data, with results that are typical of Figure 8.2.19. In tests with a clear ISIP, there is a well-defined minimum in the radius of curvature with a very narrow width to that minimum. As the ISIP becomes less clear, the width of the minimum broadens, as shown here. It is highly likely that the ISIP is embedded somewhere in the minimum band, so this yields a reasonable estimate of the uncertainty. In this case the band occurs between 0.03 and 0.6 minutes after shut-in, which corresponds to pressures of 4590 and 4490 psi, a 100 psi range. The average value is 4540 psi, but there is no reason to believe that it is a best choice for an ISIP value. Combined with the stress test data of Figure 8.2.16, we believe that 4575 psi is the best estimate of the minimum stress in this zone. The uncertainty is +15 and -85 psi.

These results and calculations also show how important it is to know what the reservoir and the surrounding rocks look like. Natural fracture distributions, stress contrasts and modulus variations are all very important in this application. A method for in situ modulus measurements

would be valuable; current dynamic measurements using logs will not measure the effects of the natural fractures. Measurement of the stresses is critical.

Finally, the possibilities of this technique for enhancing gas production from tight, anisotropic reservoirs has been shown. A 100-ft fracture that intersects the natural fractures is equivalent to a 900-ft fracture that parallels the natural fractures for the case described in this paper. Since longer altered-stress fractures are possible, but longer hydraulic fractures are likely to extend outside the lens, the overall favorability of the altered-stress technique is even greater. The main problem is that closely spaced wells or deviated holes are required.

8.2.9 CONCLUSIONS

The altered-stress concept has been shown to be valid in both field tests and finite element calculations. Stress changes of as much as 300 psi were measured in an offset well during small minifrac treatments in the production well. Larger changes will occur with larger treatments.

Finite element calculations show the importance of the layering, with respect to both stress and modulus. High stresses in the nonreservoir rocks are somewhat compensated by lower modulus in the nonreservoir rocks.

This technique has been found to be an accurate fracture height diagnostic. Estimates of fracture height in these tests agree with borehole geophone measurements.

Reservoir modeling, using an anisotropic, naturally fractured, reservoir simulator, show that a relatively small altered stress fracture in an anisotropic reservoir will yield gas production equivalent to a conventional hydraulic fracture that is nine times longer.

8.2.10 NOMENCLATURE

c	- Fracture half height
E_1, E_2, E_3	- Young's modulus in reservoir layers
H	- Fracture height
P	- Fracture treatment pressure above closure
r	- Distance from center of fracture to point
r_1	- Distance from negative fracture tip to point
r_2	- Distance from positive fracture tip to point
x, y, z	- Cartesian coordinates
ν	- Poisson's ratio
θ	- Angle from center of fracture to point
θ_1	- Angle from negative fracture tip to point
θ_2	- Angle from positive fracture tip to point
$\sigma_x, \sigma_y, \sigma_z$	- Stresses induced by fracture in Cartesian coordinate directions
$\sigma_1, \sigma_2, \sigma_3$	- Stresses in reservoir layers

8.2.11 REFERENCES

1. Hubbert, M. K. and D. G. Willis, "Mechanics of Hydraulic Fracturing," Petroleum Transactions, AIME, Vol. 210, pp 153-166, 1957.

2. Perkins, T. K. and L. R. Kern, "Widths of Hydraulic Fractures," Journal of Petroleum Technology, September 1961, pp 937-949.

3. Simonson, E. R., A. S. Abou-Sayed, and R. J. Clifton, "Containment of Massive Hydraulic Fractures," Society of Petroleum Engineers Journal, Vol 18, February 1978, pp 27-32.

4. Warpinski, N. R., J. A. Schmidt, and D. A. Northrop, "In Situ Stresses: the Predominant Influence on Hydraulic Fracture Containment," Journal of Petroleum Technology, Vol 34, March 1982, pp 653-664.

5. Warpinski, N. R., and P. T. Branagan, "Altered Stress Fracturing," SPE 17533, Proceedings of the Rocky Mountain Regional Meeting of the Society of Petroleum Engineers, Casper, WY, May 11-13, 1988, pp. 465-476. Also Journal of Petroleum Technology, Vol. 41, pp 990-997, September 1989.

6. Lorenz, J. C. and S. J. Finley, "Differences in Fracture Characteristics and Related Production of Natural Gas in Different Zones of the Mesaverde Formation, Northwestern Colorado," SPE 16809, presented at 62nd Annual Technical Conference of SPE, Dallas, TX, September 27-30, 1987.

7. Branagan, P. T., C. L. Cipolla, S. J. Lee, and L. Yan, "Case History of Hydraulic Fracture Performance in the Naturally Fractured Paludal Zone: The Transitory Effects of Damage," SPE 16397, Proceedings 1987 SPE/DOE Joint Symposium on Low Permeability Reservoirs, Denver, CO, May 18-19, 1987.

8. Lorenz, J. C., "Reservoir Sedimentology in Mesaverde Rocks at the Multiwell Experiment Site and East Central Piceance Creek Basin," Sandia National Laboratories Report, SAND87-0040, January 1987.

9. Teufel, L. W., C. M. Hart, A, R. Sattler, and J. A. Clark, "Determination of Hydraulic Fracture Azimuth by Geophysical, Geological and Oriented-Core Methods at the Multiwell Experiment Site, Rifle, CO," SPE 13226, presented at 59th Annual Technical Conference of SPE, Houston, TX, September 16-19, 1984.

10. Lorenz, J. C., P. T. Branagan, N. R. Warpinski, and A. R. Sattler, "Fracture Characteristics and Reservoir Behavior of Stress-Sensitive Fracture Systems in Flat-Lying Lenticular Formations," SPE 15244, Proceedings, Unconventional Gas Technology Symposium of SPE, Louisville, KY, pp 423-430, May 18-21, 1986.

11. Cuderman, J. F. and D. A. Northrop, "A Propellant-Based Technology for Multiple Fracturing Wellbores to Enhance Gas Recovery: Application and Results in Devonian Shale," SPE 12838, Proceedings SPE Unconventional Gas Recovery Symposium, Pittsburgh, PA, pp 77-86, May 13-15, 1984.

12. Salamy, S. P., B. S. Saradji, C. O. Okaye, J. C. Mercer, and A. B. Yost, "Recovery Efficiency Aspects of Horizontal Well Drilling in Devonian Shale," SPE 61411, Proceedings 1987 SPE/DOE Joint Symposium on Low Permeability Reservoirs, Denver, CO, pp 217-226, May 18-19, 1987.

13. Sneddon, I. N. and H. A. Elliot, "The Opening of a Griffith Crack Under Internal Pressure," The Quarterly of Applied Mathematics, Vol. IV, No. 3, pp 262-267, 1946.

14. Sneddon, I. N., "The Distribution of Stress in the Neighbourhood of a Crack in an Elastic Solid," Proceedings, Royal Society, Series A, Vol 187, 1946, pp 229-260.

15. Shuck, L. Z., "Method for Selectively Orienting Induced Fractures in Subterranean Earth Formations," United States Patent 4,005,750, February 1, 1977.

16. Uhri, D. C., "Stimulation of Earth Formations Surrounding a Deviated Wellbore by Sequential Hydraulic Fracturing," United States Patent 4,687,061, August 18, 1987.

17. Warpinski, N. R. and L. W. Teufel, "In Situ Stresses in Low Permeability, Nonmarine Rocks," SPE 16402, Proceedings 1987 SPE/DOE Joint Symposium on Low Permeability Reservoirs, Denver, CO, pp 125-138, May 18-19, 1987.

18. Warpinski, N. R., P. T. Branagan, A. R. Sattler, J. C. Lorenz, D. A. Northrop, R. L. Mann, K-H. Frohne, "Fracturing and Testing Case Study of Paludal, Tight, Lenticular, Gas Sands," SPE Formation Evaluation, Vol. 2, No. 4, pp 535-545, December 1987.

19. Warpinski, N. R., P. T. Branagan, and R. Wilmer, "In Situ Stress Measurements at DOE's Multiwell Experiment Site, Mesaverde Group, Rifle, Colorado," Journal of Petroleum Technology, Vol. 37, pp 527-536, March 1985.

20. Biffle, J. H., "JAC--A Two-Dimensional Finite Element Computer Program for the Non-Linear Quasistatic Response of Solids with the Conjugate Gradient Method," Sandia National Laboratories Report, SAND81-0998, April 1984.

21. Warpinski, N. R., "Determining the Minimum In Situ Stress from Hydraulically Fracturing Through Perforations," International Journal of Rock Mechanics, October 1989.

Table 8.2.1

Activities in Altered-Stress Experiments

	MWX-1			MWX-2	
Date	Operation	Fluid	Volume	Stress Tests	Number
4/22/87	-			Initial Stress Tests	10
4/28/87	-			Pre-Pump-In Tests	3
4/28/87	Pump-In/Shut-In	KCl Water	70 bbl	Pump-In Test	1
4/28/87	-			Post-Pump-In Tests	2
4/29/87	Step-Rate/Flow-Back	KCl Water	71 bbl	-	
4/29/87	Pump-In/Flow-Back	KCl Water	70 bbl	Pump-In Test	1
4/29/87	-			Post-Pump-In Tests	1
4/30/87	Minifrac	N_2 Foam	150 bbl	Minifrac Tests	3
4/30/87	-			Post-Minifrac Tests	2
5/11/87	-			Pre-100-Mesh Minifrac Tests	3
5/12/87	100-Mesh Minifrac	N_2 Foam	400 bbl	100-Mesh Minifrac Tests	7
5/12/87	-			Post-100-Mesh Minifrac Tests	12

Table 8.2.2

Altered-Stress Field Results

		MWX-2		MWX-1	
Date	Stress Test	Pressure (psi)	Δ Stress (psi)	Pressure (psi)	ΔP (psi)
4/22/87	Initial Stress Test 2	4629	-	-	-
"	Initial Stress Test 3	4621	-	-	-
"	Initial Stress Test 9	4629	-	-	-
4/28/87	Pre-Pump-In Test 1	4611	-	-	-
"	Pre-Pump-In Test 3	4628	-	-	-
4/28/87	Pump-In/Shut-In	4681	57	5200	625
"	Post-Pump-In/Shut-In 1	4679	55	-	-
"	Post-Pump-In/Shut-In 2	4639	15	-	-
4/29/87	Pump-In/Flow-Back	4680	56	5210	635
"	Post-Pump-In/Flow-Back	4644	30	-	-
4/30/87	Minifrac 1	4718	94	5530	955
"	Minifrac 2	4811	187	5580	1005
"	Minifrac 3	4864	240	5580	1005
"	Post-Minifrac 1	4722	98	-	-
"	Post-Minifrac 2	4717	93	-	-
5/11/87	Pre-Minimesh 1*	4648	-	-	-
"	Pre-Minimesh 3	4655	-	-	-
5/12/87	Minimesh 1*	4688	38	5150	550
"	Minimesh 2	4751	101	5250	650
"	Minimesh 3	4781	131	5499	900
"	Minimesh 4	4849	199	5611	1011
"	Minimesh 5	4887	237	5700	1100
"	Minimesh 6	4914	264	5720	1120
"	Minimesh 7	4951	301	5720	1120
5/12/87	Post-Minimesh 1*	4828	178	5240	6405
"	Post-Minimesh 2	4872	222	5201	601
"	Post-Minimesh 3	4799	149	5056	456
"	Post-Minimesh 4	4804	154	4963	363
"	Post-Minimesh 5	4780	130	4850	250
"	Post-Minimesh 6	4763	123	4722	122
"	Post-Minimesh 7	4732	82	-	-
5/12/87	Minimesh Flow-Back 1*	4738	88	-	-
"	Minimesh Flow-Back 2	4711	61	-	-
"	Minimesh Flow-Back 3	4704	54	-	-
"	Minimesh Flow-Back 4	4675	25	-	-

* Minimesh is the name of the 100-mesh sand minifrac.

TABLE 8.2.3

Base Case Reservoir Properties for Simulations

Depth	5850 ft
Net Pay Height	17 ft
Reservoir Temperature	174°F
Initial Pressure	3450 psia
Gas Gravity	0.626 (air = 1.0)
Reservoir Boundaries	5500x5500 ft
Wellbore Radius	7.0 in.
Matrix Gas Porosity	4%
Matrix Block Size	10 ft
Matrix Permeability	0.1 μd
Natural Frac Width	0.001 in.
Natural Frac Perm (max)	15,000 md
Natural Frac Perm (min)	150 md

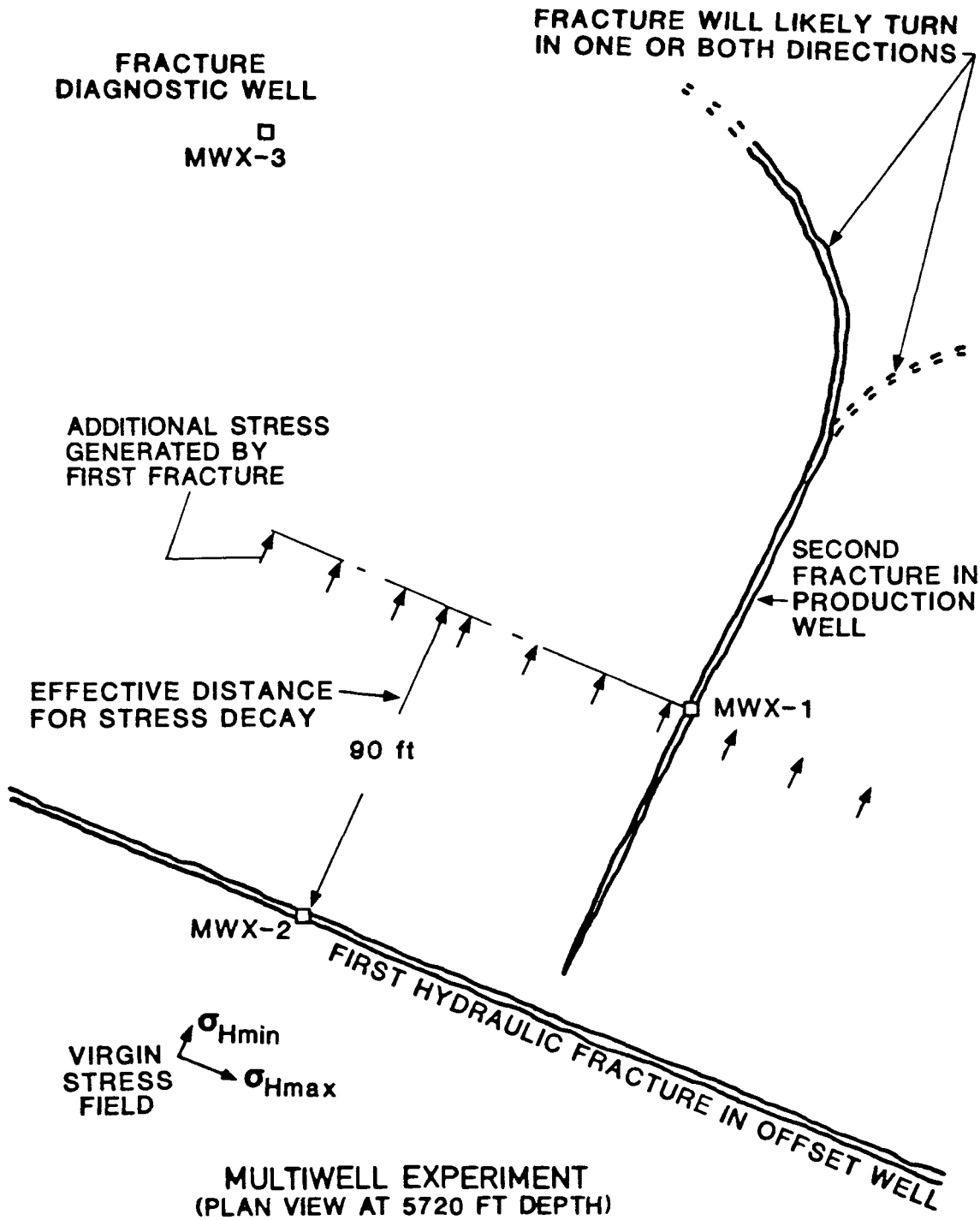

Figure 8.2.1. The Altered-Stress Concept at MWX

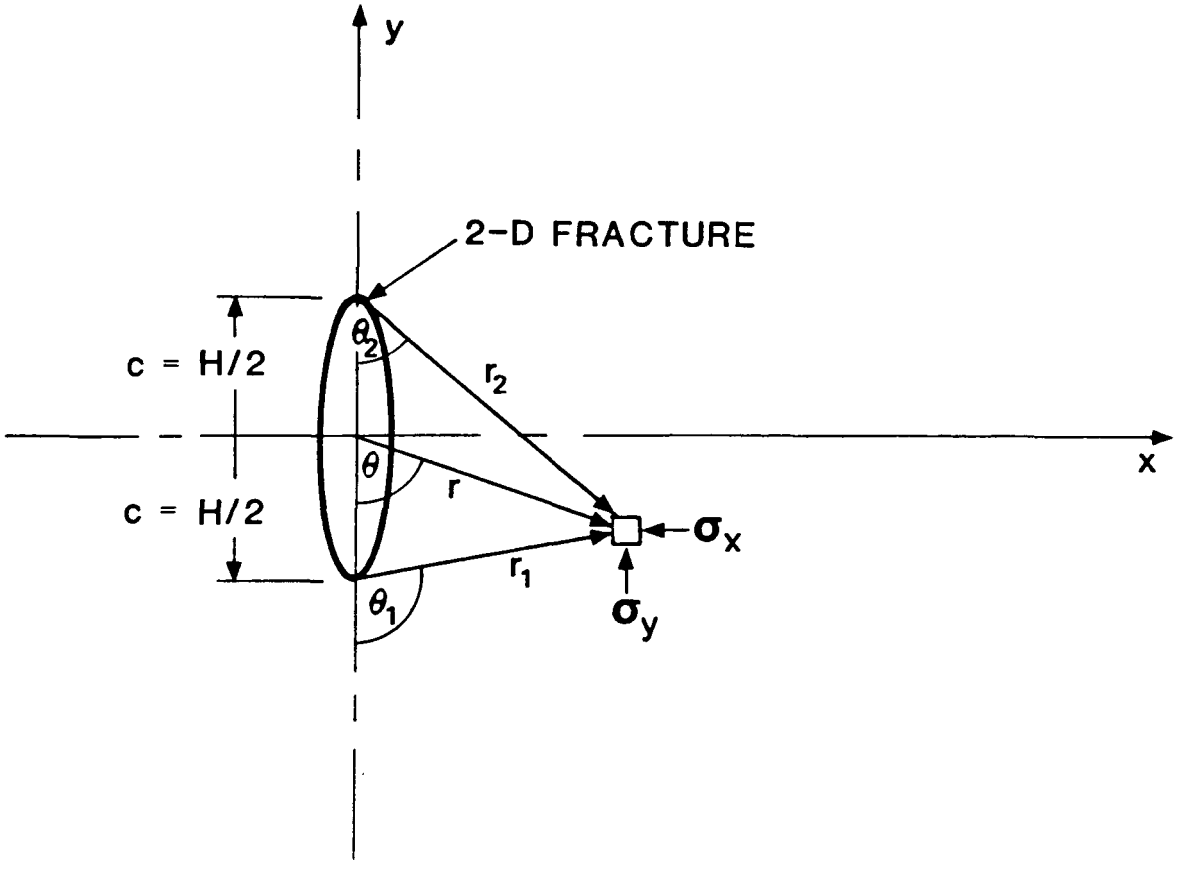

Figure 8.2.2. Geometry for 2-D Crack

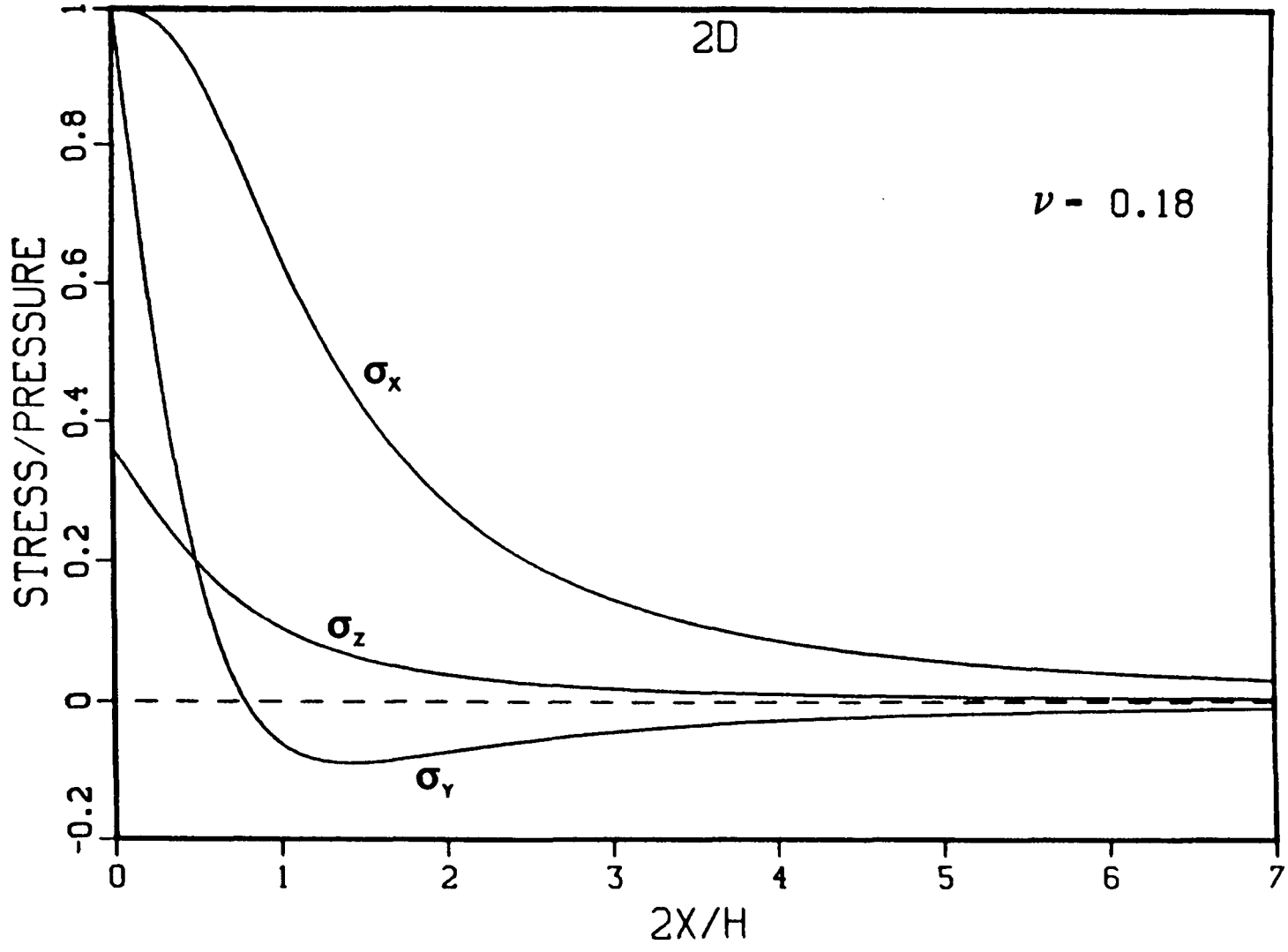

Figure 8.2.3. Analytic Results -- 2-D Crack

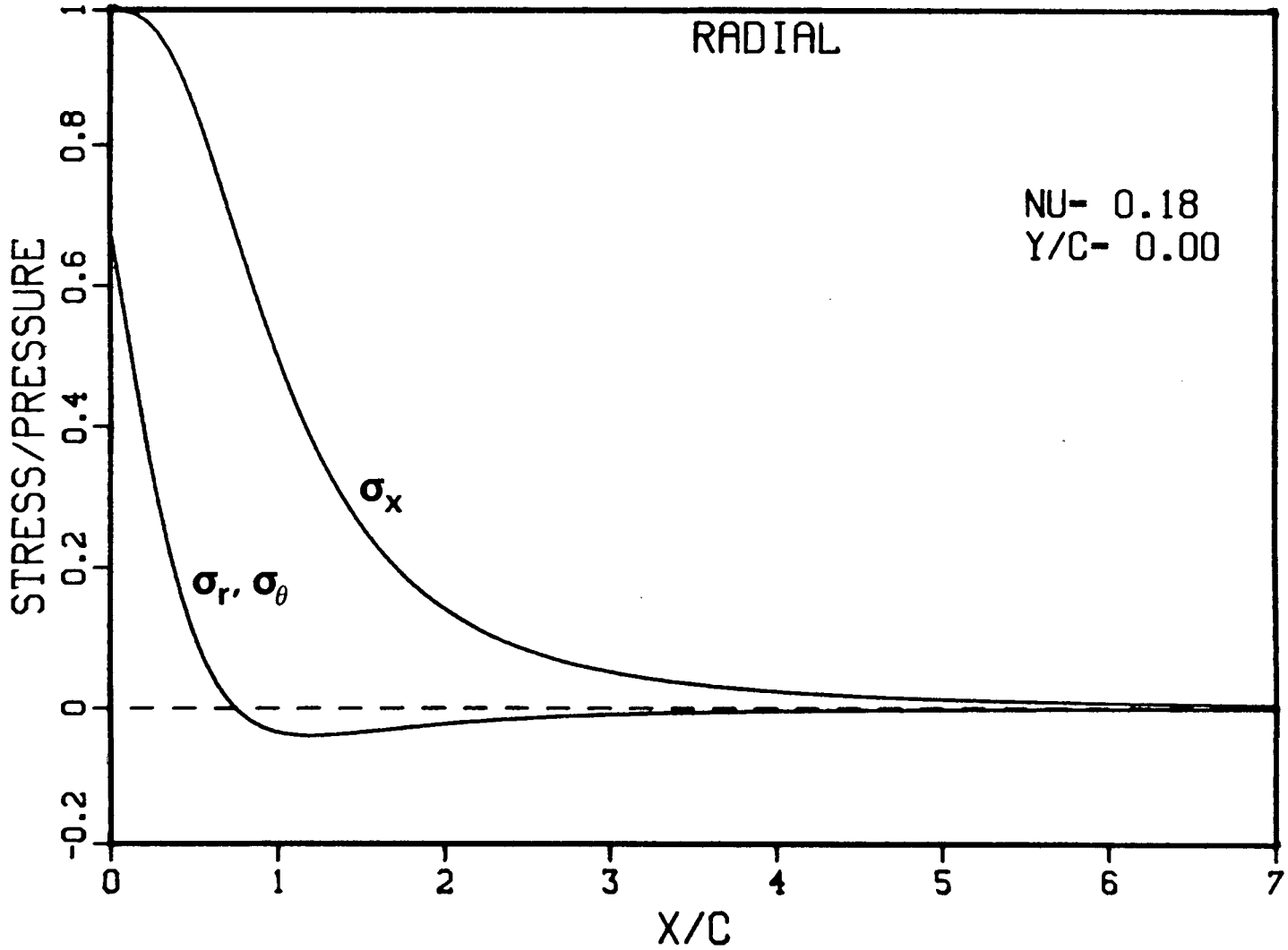

Figure 8.2.4. Analytic Results -- Radial (penny-shaped) Crack

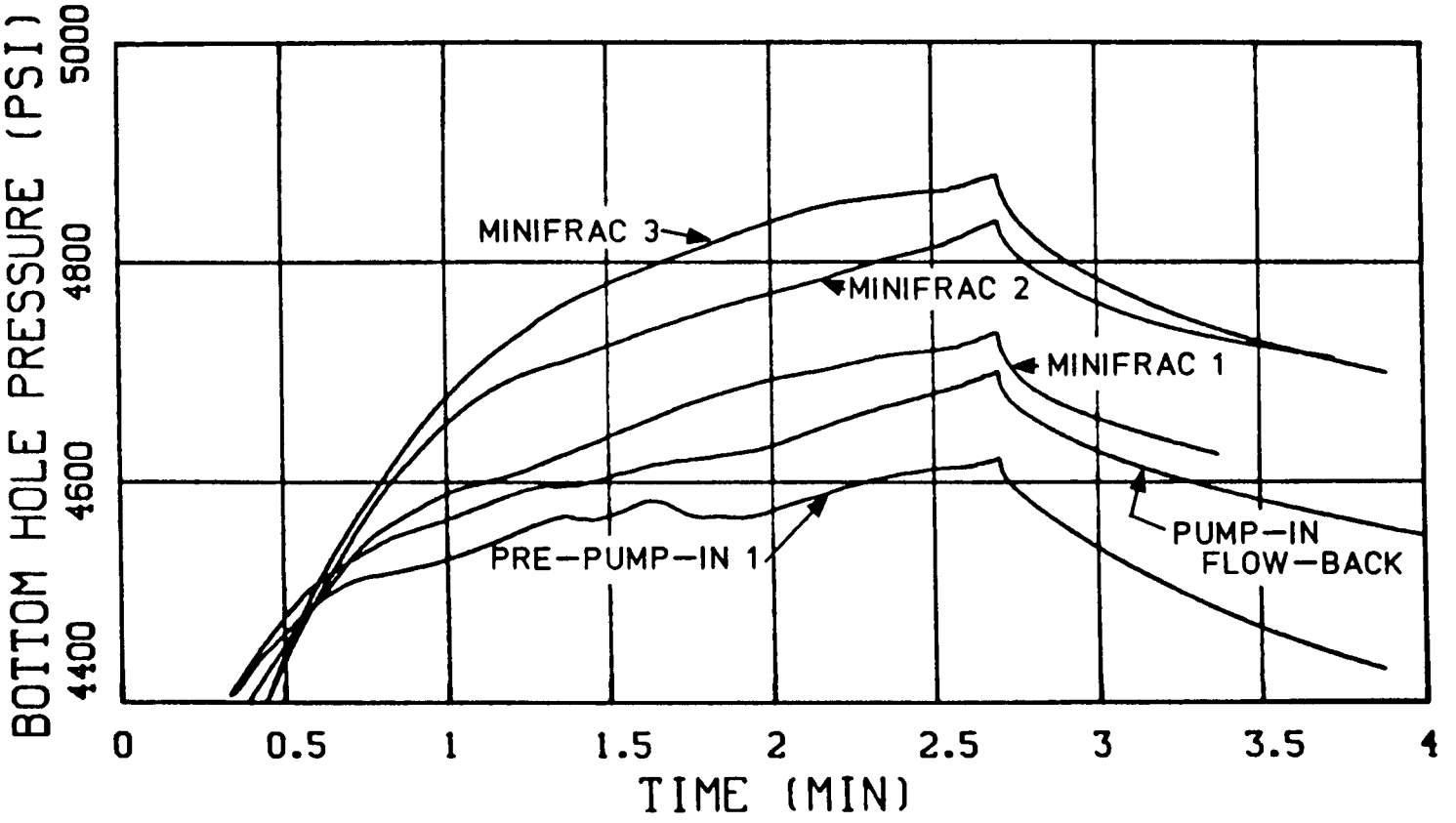

Figure 8.2.5. Pressure Data for Stress Tests During Minifrac and Pump-In

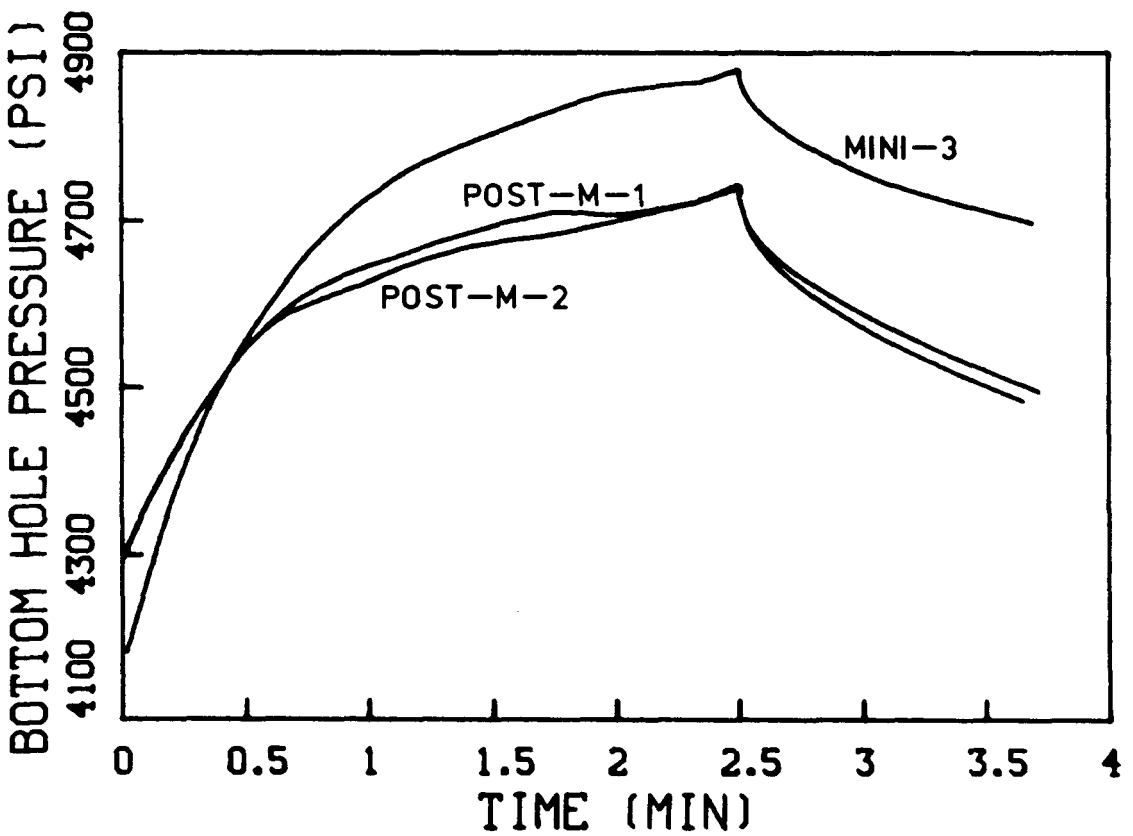

Figure 8.2.6. Pressure Data for Stress Tests After Minifrac #1

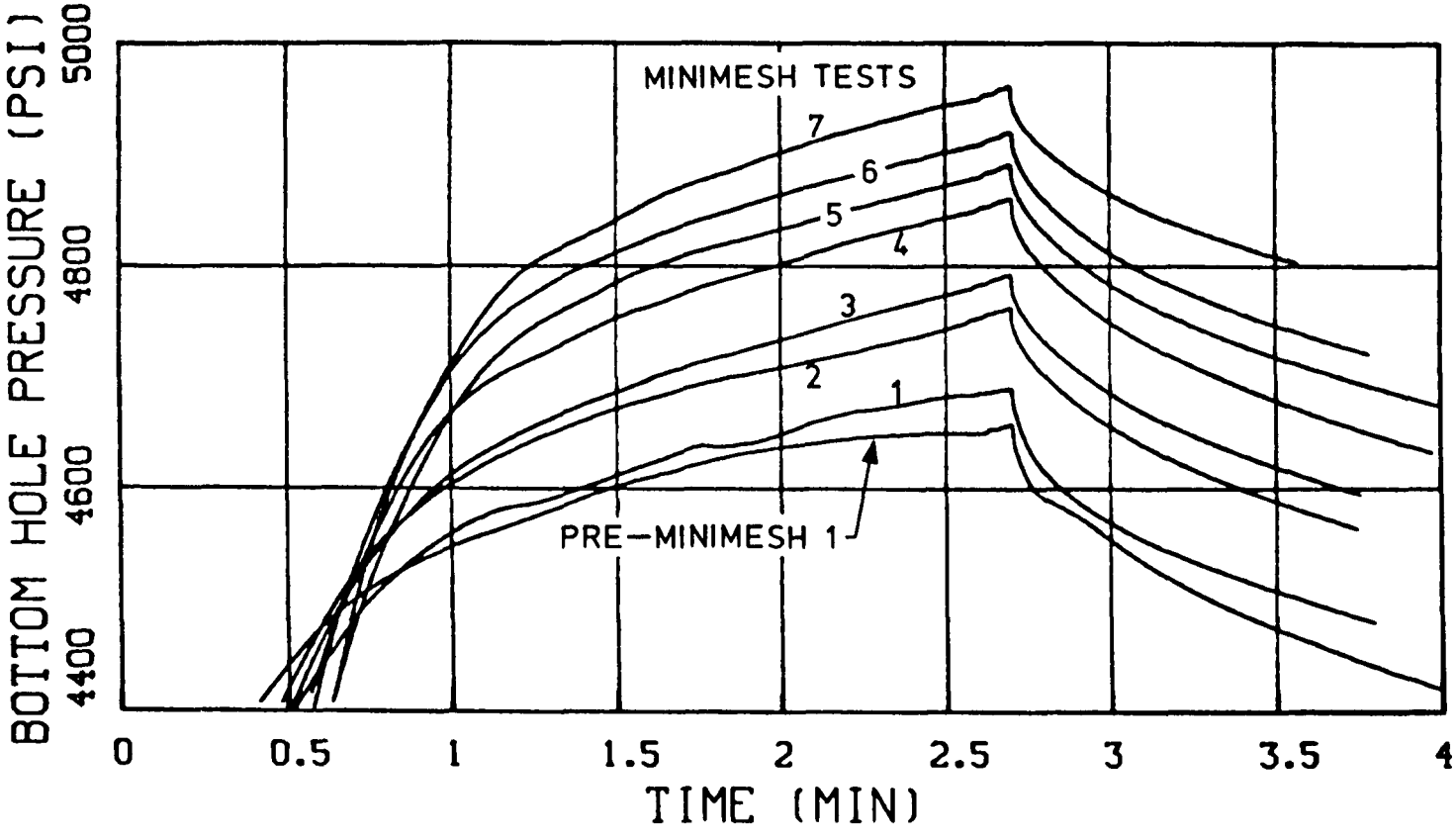

Figure 8.2.7. Pressure Data for Stress Tests During 100-Mesh Minifrac

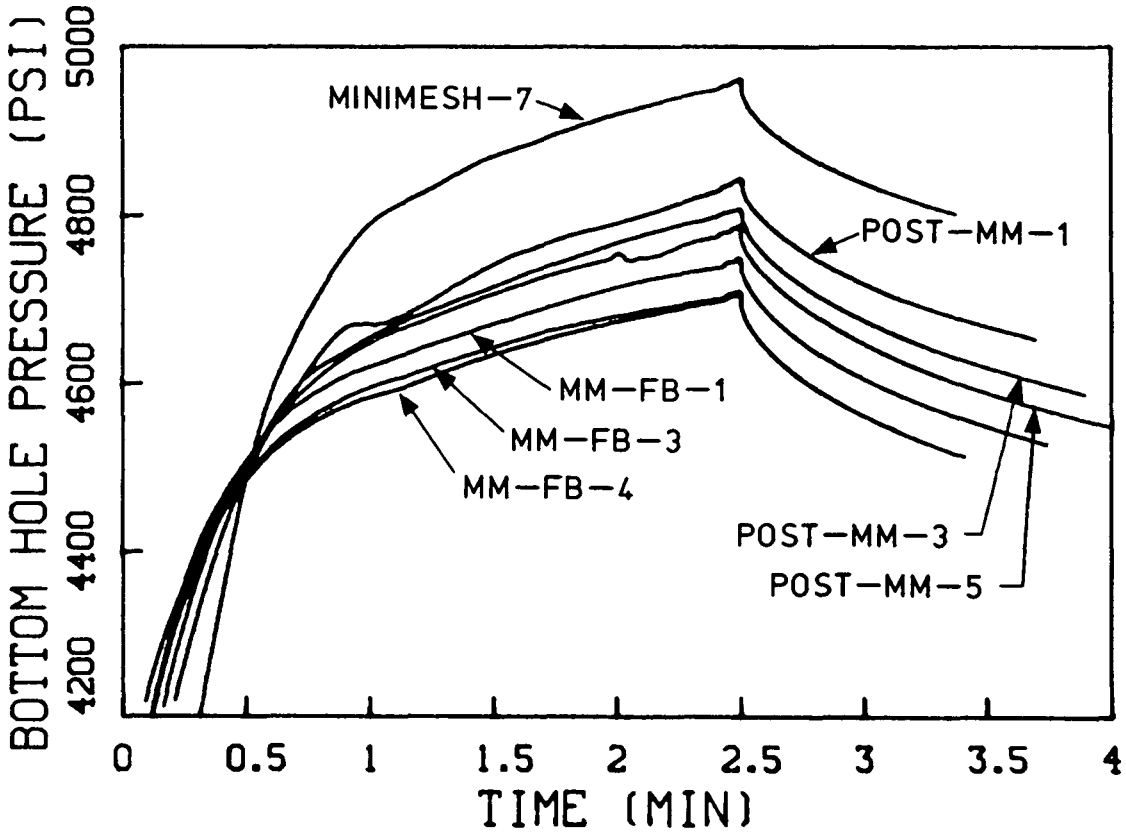

Figure 8.2.8. Pressure Data for Stress Tests After the 100-Mesh Minifrac

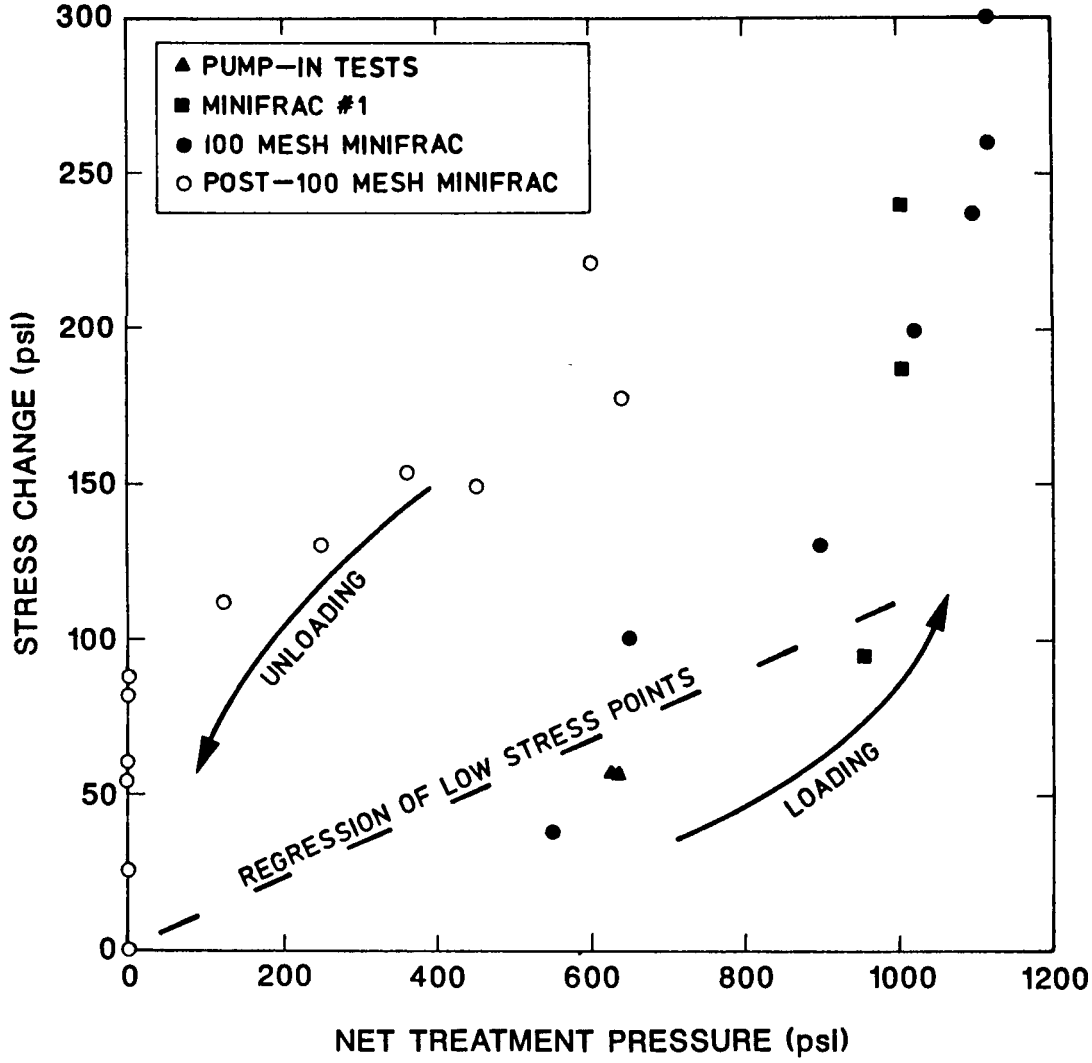

Figure 8.2.9. Stress Change in MWX-2 vs Treating Pressure in MWX-1

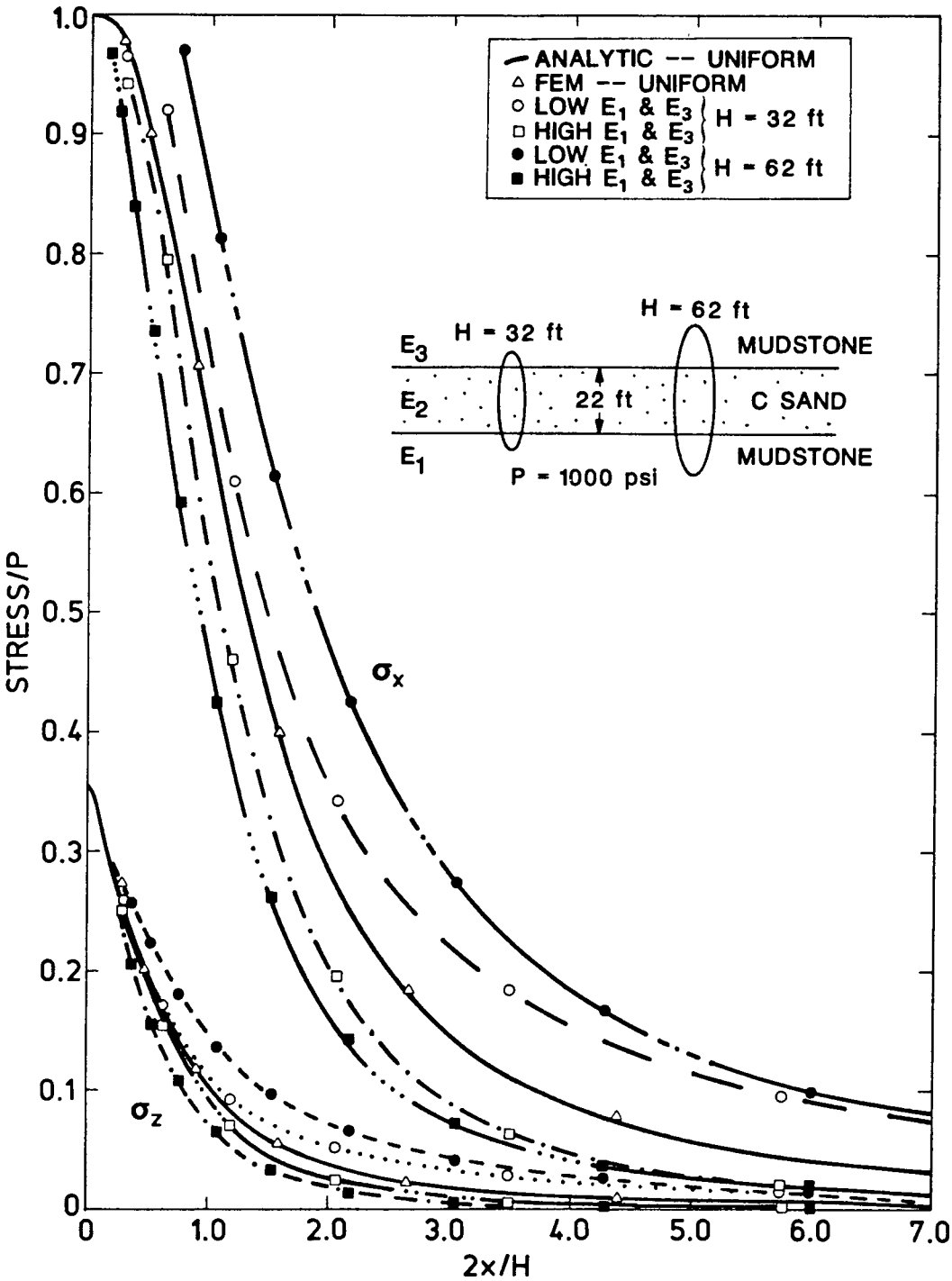

Figure 8.2.10. Finite-Element Calculations Showing Effect of Modulus

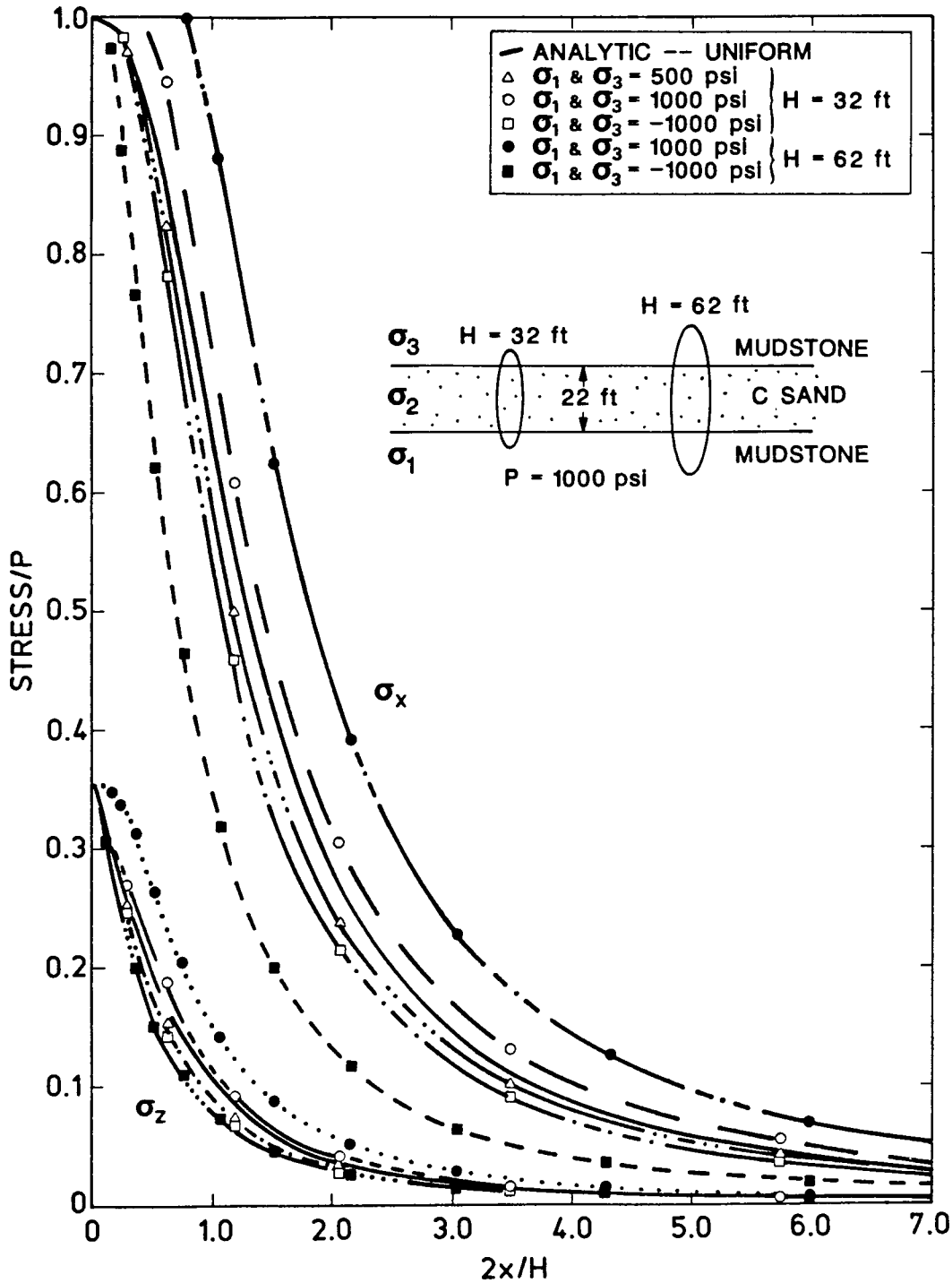

Figure 8.2.11. Finite-Element Calculations Showing Effect of Stress

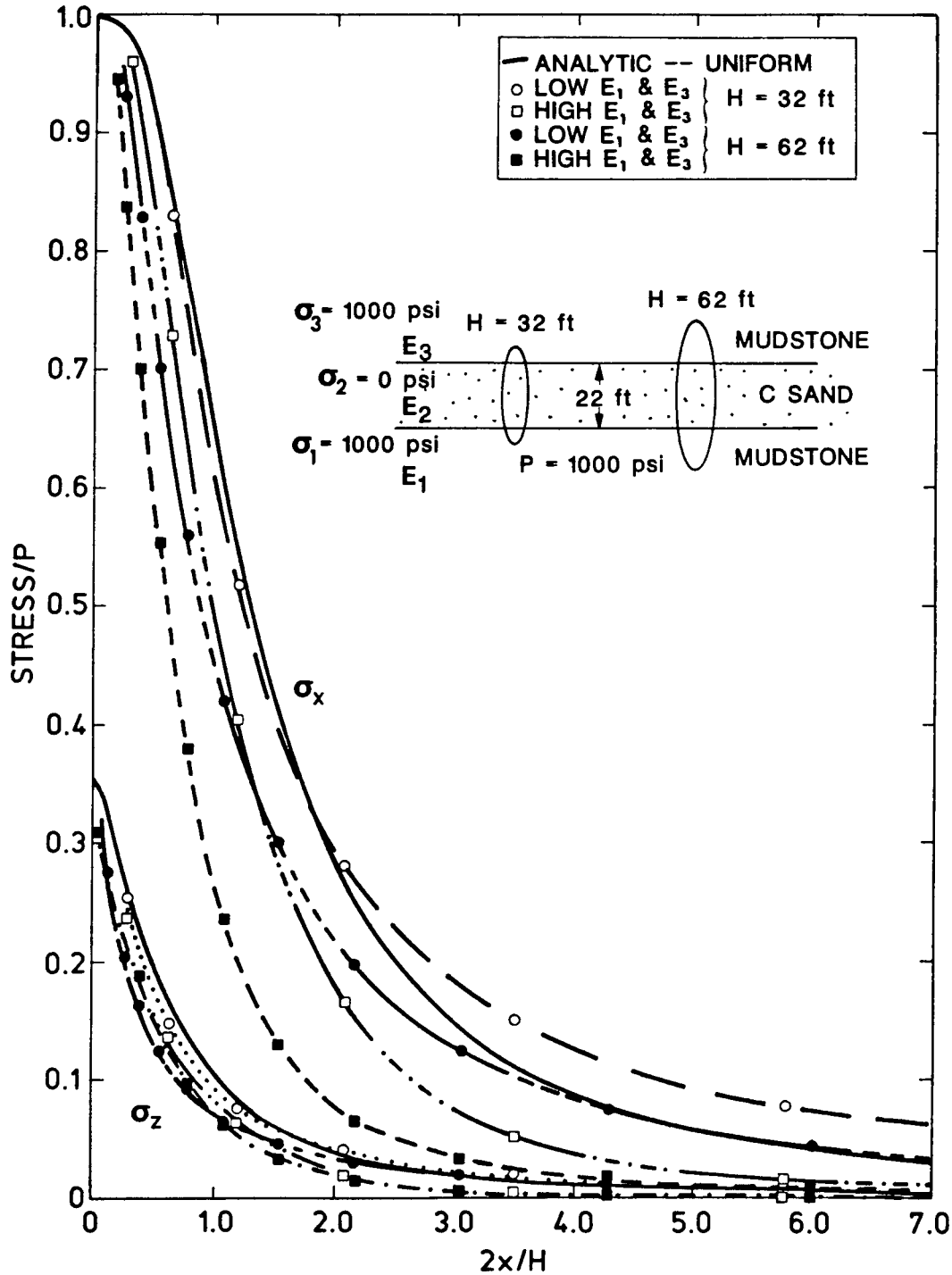

Figure 8.2.12. Finite-Element Calculations Showing Effect of Stress and Modulus

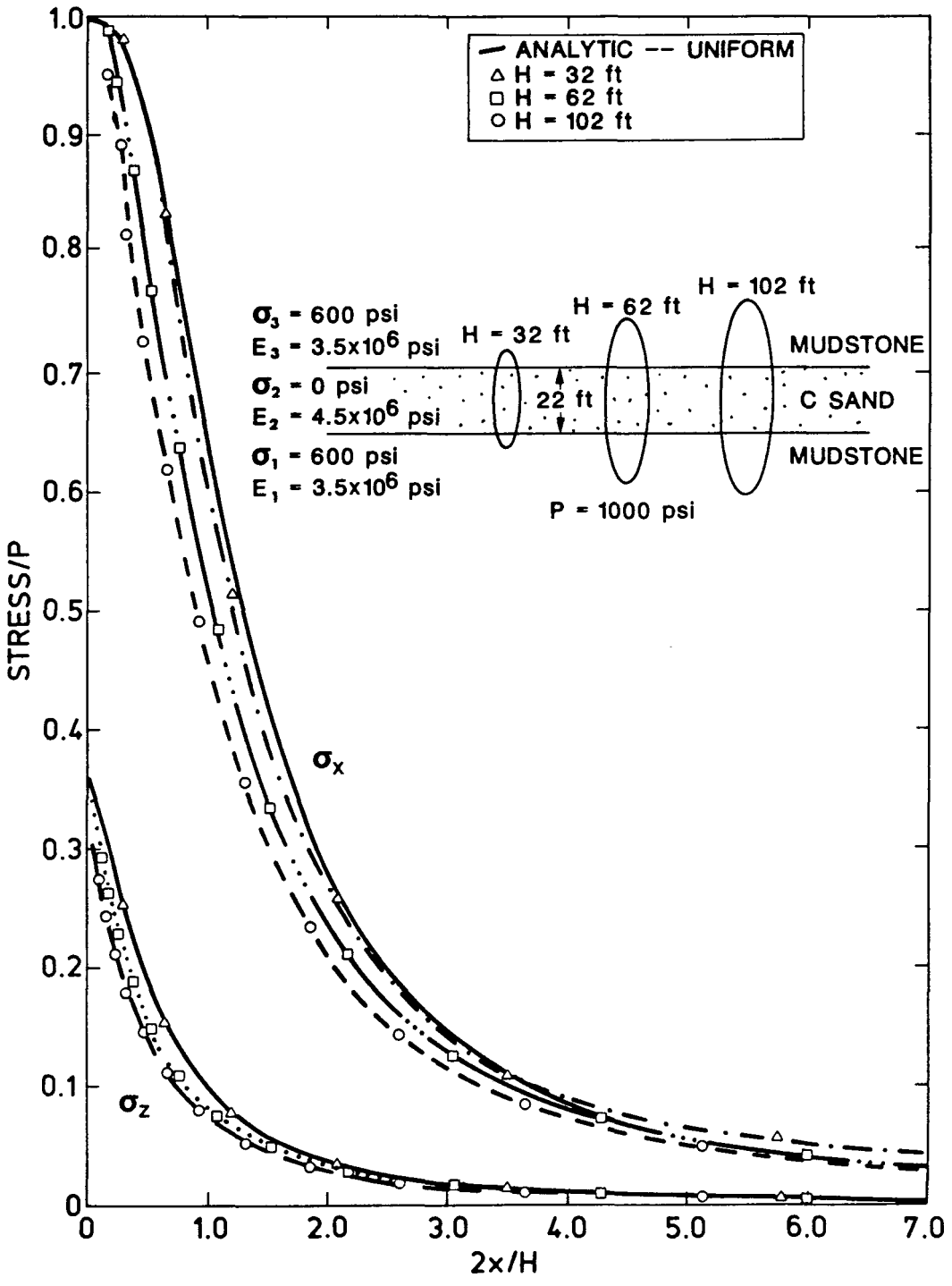

Figure 8.2.13. Finite-Element Calculations Approximating MWX Conditions

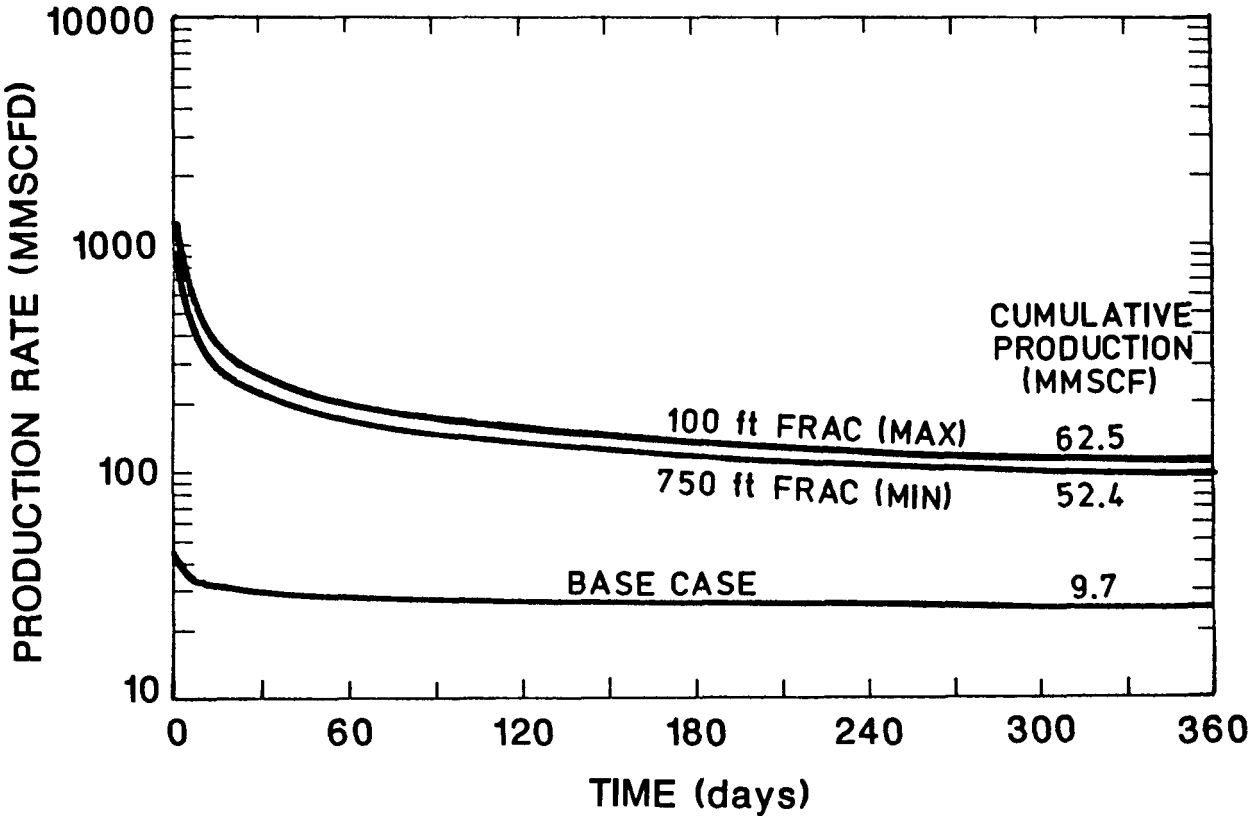

Figure 8.2.14. Gas Production Calculations

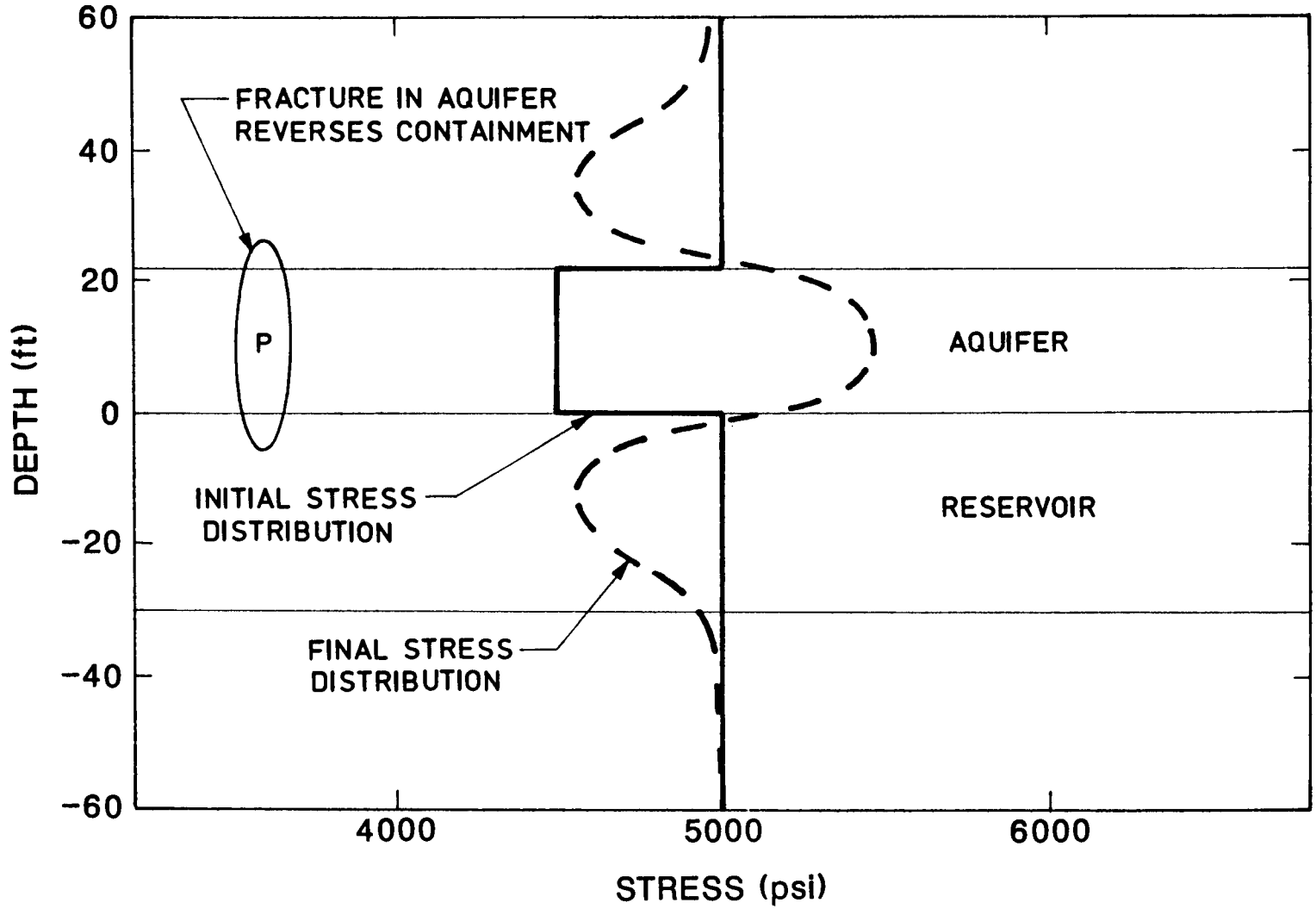

Figure 8.2.15. Example of Containment Modification Using Hydraulic Fractures

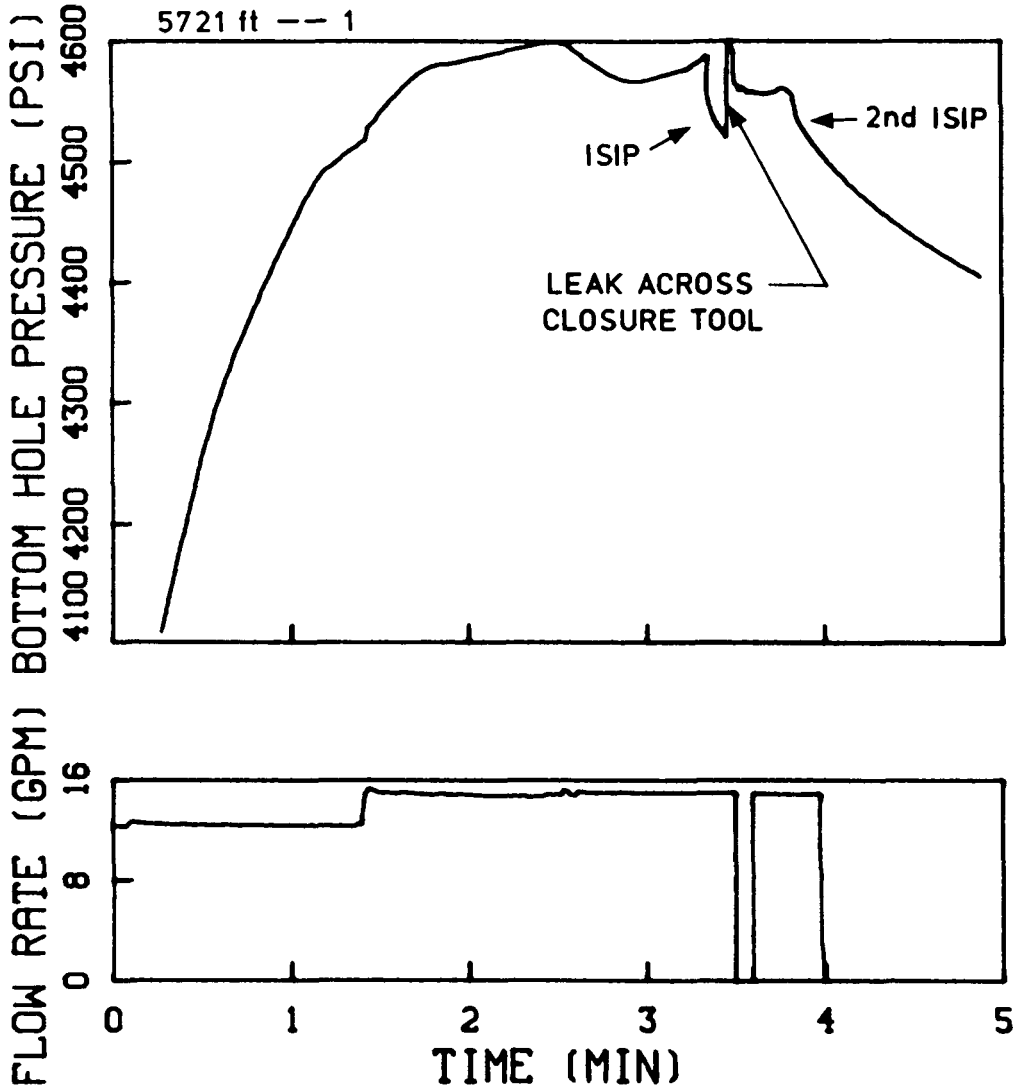

Figure 8.2.16. Initial Stress Test Data

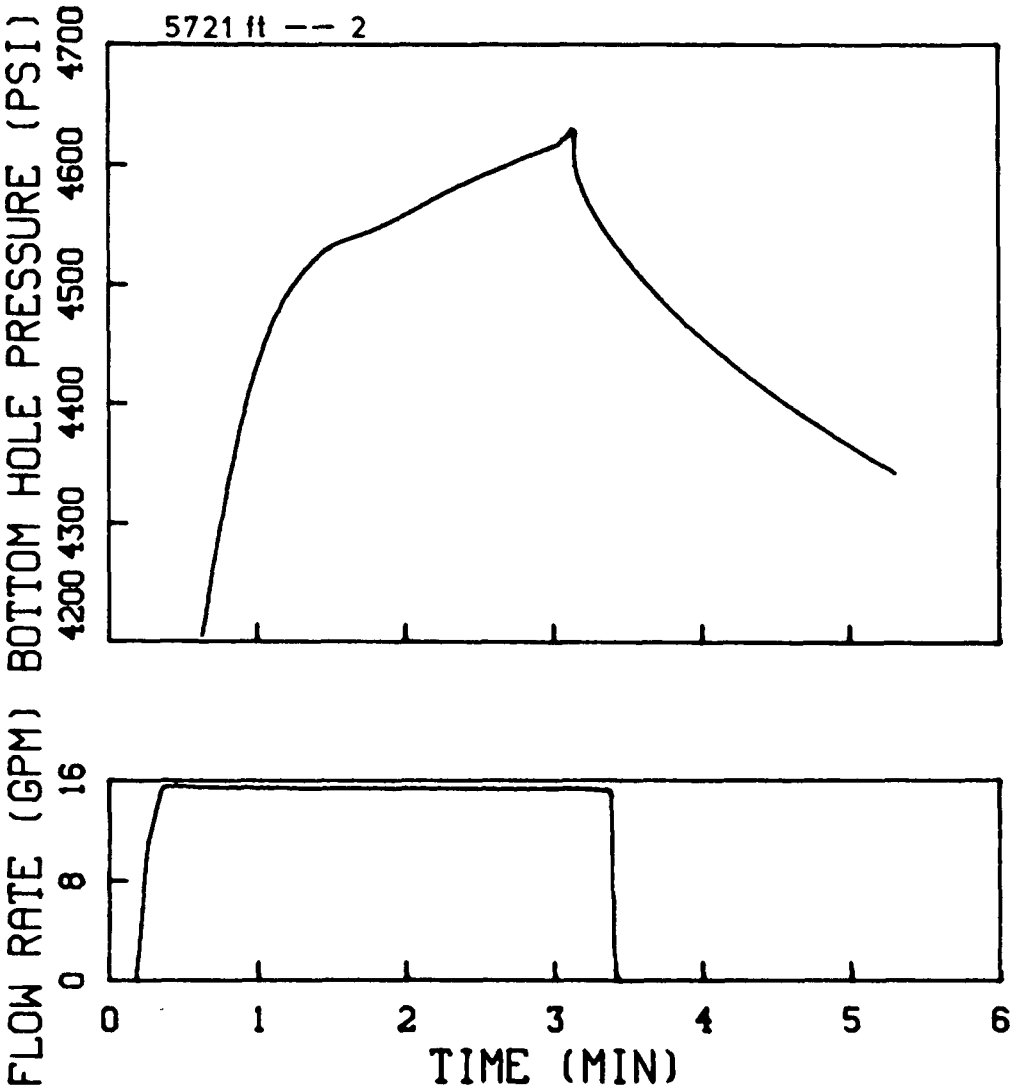

Figure 8.2.17. Second Stress Test Data

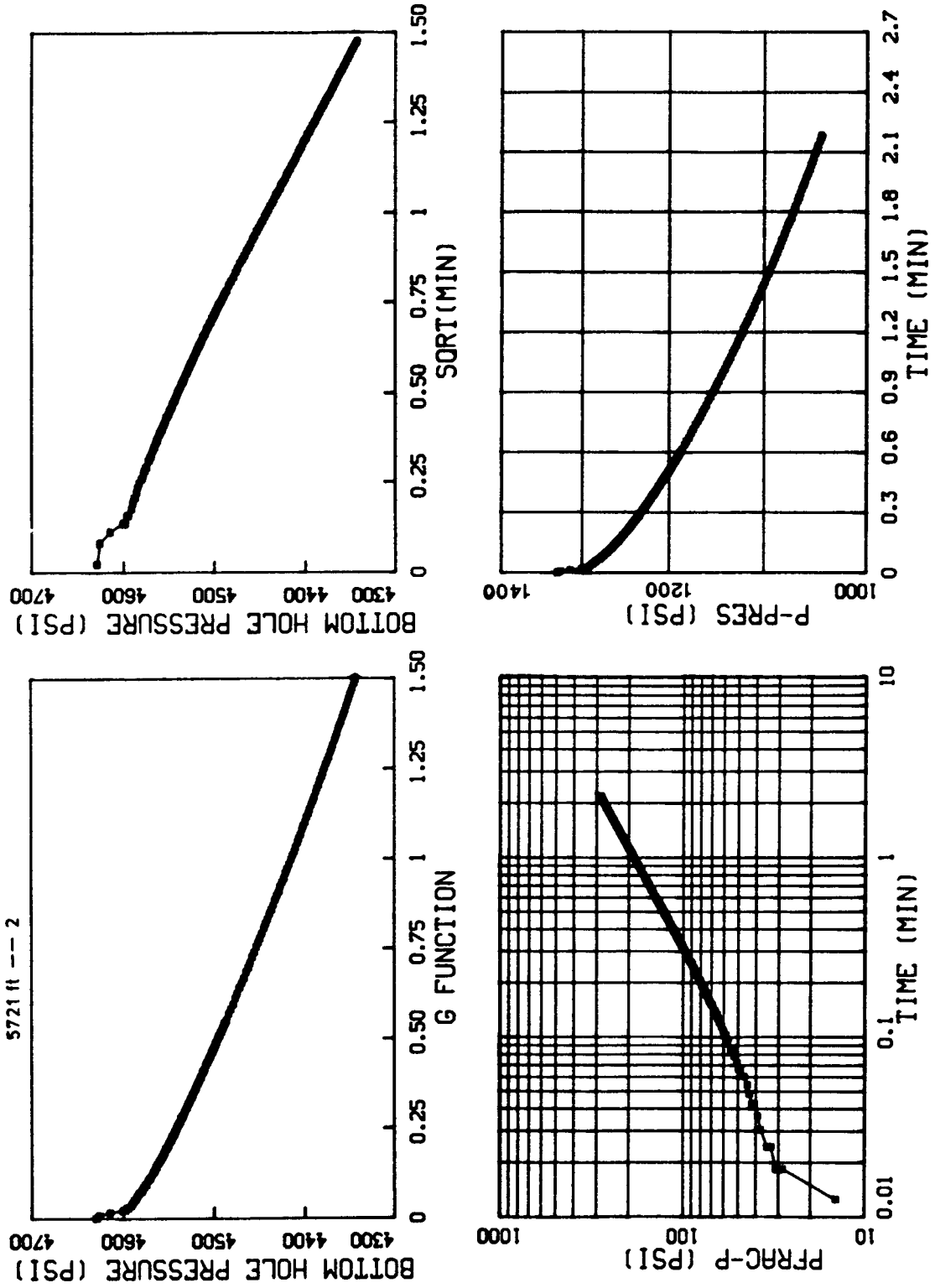

Figure 8.2.18. Plots for Extraction of the ISIP

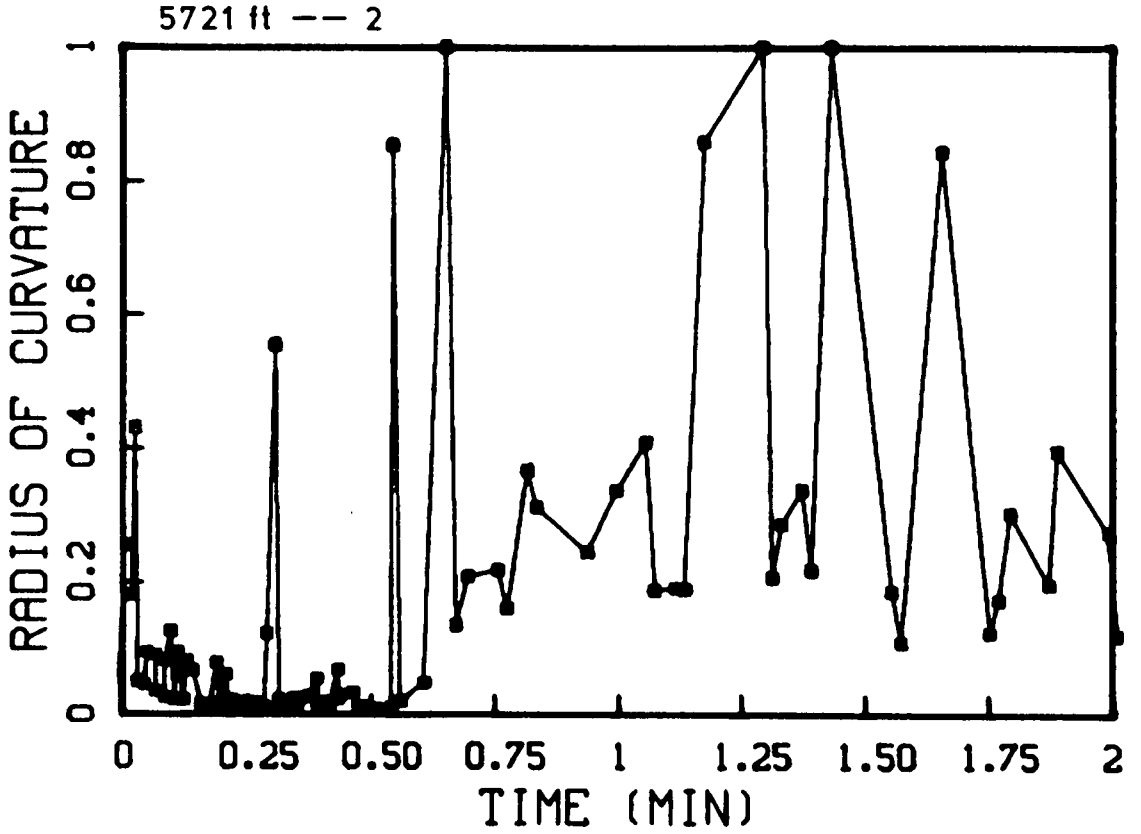

Figure 8.2.19. Normalized Radius of Curvature Data

FLUVIAL C SANDSTONE STIMULATION EXPERIMENT

8.3 RESERVOIR TESTING

P. T. Branagan
CER Corporation

8.3.1 INTRODUCTION

The fluvial C interval consists of two sandstones, designated C1 and C2. Figure 7.1.2 includes the fluvial C interval, showing the general thickness of the C1 and C2 sands in the three MWX wells. The C1 sandstone appears in MWX-2 and MWX-3, but is not present in MWX-1. However, the C2 sand is present in all three wells. The fluvial C well testing consisted of a 71-hour pressure drawdown test of the fluvial C2 sand in MWX-1.

8.3.2 RESERVOIR CHARACTERISTICS

The fluvial C2 sandstone is located at a depth of 5714 to 5737 ft in MWX-1. The well was perforated from 5720 to 5738 ft and a breakdown using 3 percent KCl water, containing 80 5/8-in. diameter ball sealers, was conducted at 3 BPM to insure the wellbore and reservoir were adequately connected.

Table 7.1.2 lists the MWX-1 reservoir characteristics from log and core analysis for the C2 sandstone. The net gas pay is approximately 23 ft, matrix porosity 7.8 percent, water saturation 63 percent, and dry stressed permeability is 0.0073 md from core tests. Comparison of B sandstone and C2 sandstone data in Table 7.1.2 shows that the two zones are very similar, although the net gas pay in the C2 sandstone is about 42 percent larger in contrast to the B sandstone.

8.3.3 WELL TEST RESULTS

The short (71 hour) pressure drawdown test in the C2 sandstone was intended only as a qualitative evaluation of the short term productivity of the zone. Figure 8.3.1 presents the bottomhole pressure and surface flow rate for the test period. The bottomhole pressure stabilized at 1000 to 1050 psi after 10 hours of flow, with a corresponding flow rate of approximately 60 MCFD. The bottomhole pressures and surface flow rates did not provide data applicable to quantitative analysis using either analytical or numerical methods.

However, this production and pressure behavior can be compared to the B sandstone to gain insight into the possible production mechanisms present. Referring to Figure 7.1.5, which presents the B sandstone pre-fracture well testing data, the flow rate and pressures can be compared for the two zones. The B sandstone production rates varied considerably during the initial testing, ranging from an initial high of 80 MCFD decreasing to 30 MCFD after 24 days. The B sandstone flow rates from days seven through 10, show an approximate flow rate of 60 MCFD at a bottomhole pressure of 850 psi. The C2 sandstone exhibited the same flow rate at a bottomhole pressure of 1025 psi. The B sandstone flow rates stabilized at later times at about 20 MCFD with a steadily increasing bottomhole pressure, 450 to 1050 psi, (days 29 through 50).

The anomalous production behavior in the B sandstones complicates direct comparisons. However, it does appear that the two sandstones have similar production characteristics. The initial C2 sandstone flow rate of 60 MCFD at 1025 psi indicates that it is slightly more productive than the B sandstone, which produced the same rate at about 850 psi bottomhole pressure. Also, the late time B sandstone rate of 20 MCFD at 1050 psi indicates that the fluvial C2 sandstone has a greater flow capacity. Based solely on net gas pay and core permeability (Table 7.1.2), the C2 sandstone should be about 40 percent more productive. The pre-frac B sandstone well test analysis and reservoir modeling presented in Section 7.1 indicated that the B sandstone was naturally fractured. The C2 sandstone also

appears to be naturally fractured based on its matrix permeability and the productivity.

8.3.4 CONCLUSIONS

The very short, qualitative flow test of the C2 sandstone indicates that it has similar production characteristics to the lower B sandstone. Thus, the C2 sandstone:

- appears to be naturally fractured,
- may be more productive than the B sandstone, and
- has a well developed natural fracture system, although the existence of reservoir anisotropy can not be inferred from the single well test.

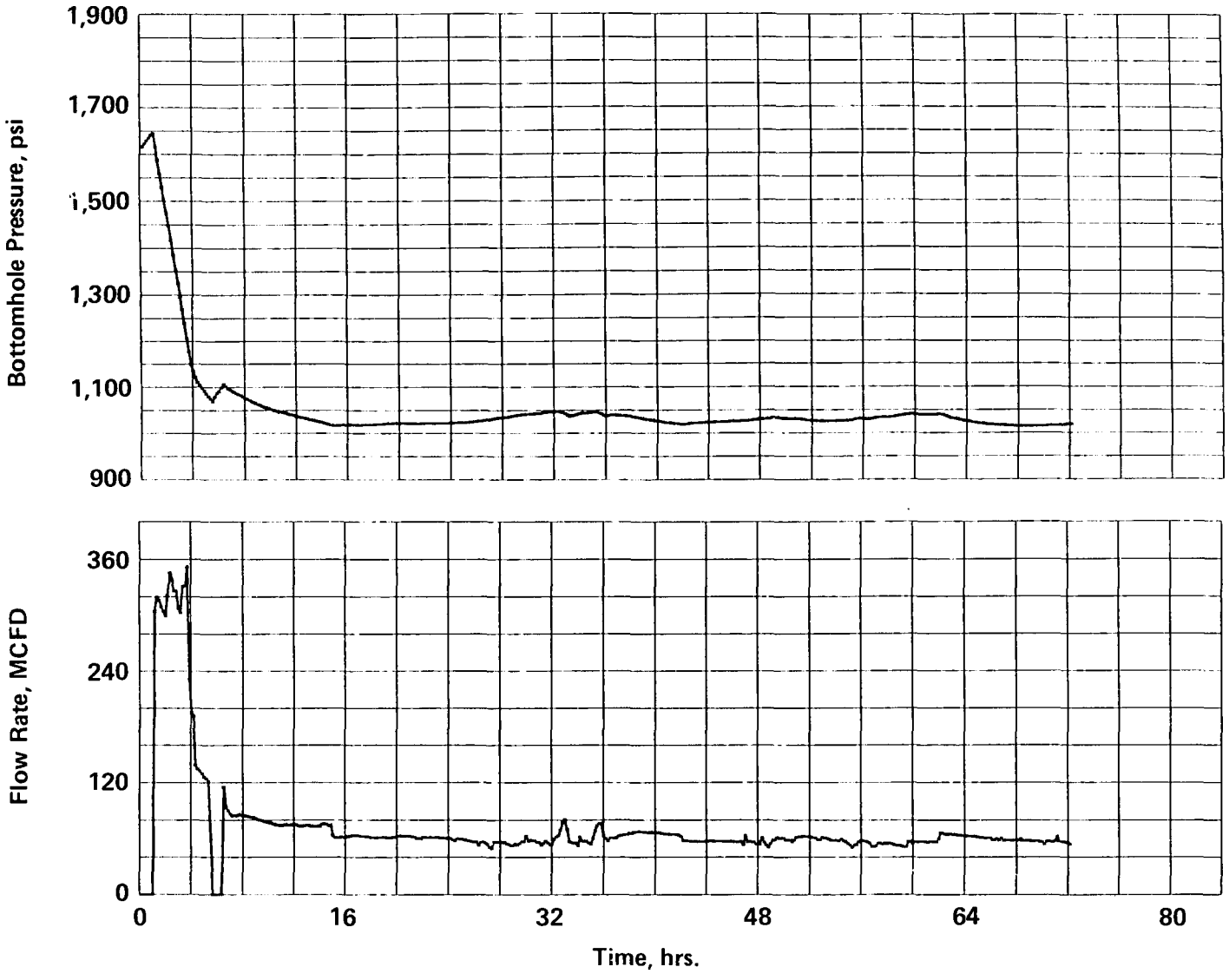

Figure 8.3.1 MWX-1 Flow Rate and Pressure Data

8.0 FLUVIAL C SANDSTONE STIMULATION EXPERIMENT

8.4 BOREHOLE SEISMIC FRACTURE DIAGNOSTICS

B. J. Thorne
Sandia National Laboratories

8.4.1 INTRODUCTION

During the spring 1986 stimulation experiment in the fluvial C sandstone it was not possible to place a Borehole Seismic System (BSS) tool in well MWX-2 because of stress tests being conducted in that well. However, it was possible to place the BSS tool in well MWX-3 in the center of the fluvial C sandstone. Since this allowed signals originating in the fluvial C to reach the BSS tool without having to pass through other layers, it was hoped that the data set would be simpler and easier to analyze, allowing for an accurate frac map with only one BSS tool.

Based on the ability to locate perforation shots, accuracy of this data set is substantially less than that in the fluvial B data set (7.4). The scatter in locations determined for microseismic events for the April 30 and May 12, 1987 hydraulic fractures in the fluvial C sandstone make a reasonable determination of the azimuth, wing length and height difficult.

The overall theory and procedures involved in microseismic event location were presented in Section 7.4. Similar procedures, although limited to one BSS, were employed in the fluvial C sandstone stimulation experiment.

8.4.2 INSTRUMENTATION UPGRADE

The only modification of the BSS since the 1986 experiment in the fluvial B sandstone, was a return to the concept of two gain levels. However, in the new BSS the low gain channel has a gain of 100 dB,

approximately the same as the high gain channel in 1985, while the high gain channel has a gain of 112 dB, four times the the level of the low gain channel. The idea behind using two channels is to increase the dynamic range of the BSS by using the low gain channel to avoid saturation on strong signals and the high gain channel to avoid electronic noise on weak signals.

Problems with the software for the Phoenix Data IDAS analog to digital (A/D) converter caused it to require over 30 seconds to write each event to disc. This resulted in not digitizing most of the signals recorded on the analog tape. These signals can be recovered by playing back the analog tape if we can get Phoenix Data to either fix the software or provide us with the source code so that we can fix it ourselves.

8.4.3 DETERMINATION OF THE VELOCITY FACTOR

Before the distance to the source can be determined, the velocity factor, V_F, must be established (Section 7.4.3). This is accomplished by analysis of data from seismic sources at known locations. For this test, a series of 18 ten-gram perforation shots was fired at an average depth of 5730 ft in well MWX-1 with a BSS tool in place at a depth of 5728 ft in well MWX-3. A second series of 10 ten-gram perforation shots was fired at an average depth of 5732 ft in well MWX-2. Since both series were at approximately the same depth as the BSS tool, horizontally polarized primary waves were detected. The wave form was very complex and no horizontal component of the secondary waves could be detected. Vertically polarized secondary wave arrivals were clear, so these were used for determination of the velocity factor. The velocity factor, V_F, was calculated for each shot from the known distance and the primary and secondary wave arrival times, using Equation 7.4.1. Velocity factors for both paths are given in Table 8.4.1 and proved to be close enough together to reasonably consider all 28 values to be one data set. Averaging all values for both paths gives a velocity factor of 23.7 ft/ms, with a standard deviation of 1.2 ft/ms.

8.4.4 ORIENTATION OF THE BSS TOOL

If it is assumed that the direction of polarization of the primary wave is the direction towards the source, as it would be in a homogeneous isotropic medium, then the orientation of the geophone axes can be determined from the same perforation shots used to determine the velocity factor. Since well MWX-3 is very nearly vertical, the elevation calculated from the BSS data can be compared to the elevation to the center of the perforation gun, as a check on the assumption that the direction of polarization is the same as the direction to the source. It is unreasonable to assume that a correct orientation has been obtained if large errors in elevation result. The MWX-1 data set indicates a small scatter about the correct elevation, while the MWX-2 data set has such a small scatter that the even the small average error can be interpreted as a slight upward bias (Table 8.4.2).

The orientation, measured from the y-geophone axis to north, obtained from both sets of perforation shots are also given in Table 8.4.2. Orientation based on perforation shots in well MWX-1 differs from orientation based on perforation shots in well MWX-2 by almost 9.6°, approximately four times the standard deviation of either data set. This indicates that there may be a violation of the assumption that the direction of primary wave polarization is the same as the direction to the source. Since the BSS tool was to be left in the C sandstone, this problem was ignored and all 28 values from the two data sets were combined to give an average orientation of -78.2°, with a standard deviation of 5.2°.

8.4.5 LOCATION OF PERFORATION SHOTS

In order to estimate the accuracy which can be expected from the analyses method, data from the perforation shots were analyzed as if they were microseismic events of unknown location. These locations are shown in

Figure 8.4.1. A few of these locations have horizontal components falling outside of circles of radius 25 ft about the perforation wells, as indicated by the triangle symbols in Figure 8.4.1(a). This is clearly a result of using the average orientation value, and affects perforation shots in well MWX-2 to a greater extent than perforation shots in well MWX-1 because more perforation shots from well MWX-1 were recorded. Figure 8.4.1(b) indicates that all of the projections on the north-south plane lie inside circles of 25 ft radius located at the center of the perforation guns; the center of the BSS tool is indicated by the square symbol on the projection of well MWX-3. Thus, it appears that locations resulting from data from the single BSS tool will be less accurate than locations resulting from the two-tool analysis of the B sandstone data shown in Figure 7.4.3.

8.4.6 LOCATION OF THE FRACTURE

The frac map in Figure 8.4.2 is based on 53 microseismic events located using data digitized during the April 30 and May 12, 1987 stimulation experiments in the fluvial C sandstone. Since there seemed to be no difference between the two data sets, both stimulation experiments were combined into a single frac map. Over a thousand signals were recorded on the analog tape during these two stimulation experiments, but problems with the IDAS software prevented digitization of all but about 300 of these. Flow noise prevented the analysis of most of the signals digitized during the pumping phases. Most locatable events occurred during shut-in, with very little activity during either flow back phase.

Figure 8.4.2(a) indicates a frac azimuth of 63° west of north. However, scatter is large enough that both wing length and azimuth do not seem well defined. The standard deviation resulting from spherical statistics on the set of angles measured from well MWX-1 to microseismic event locations is 23.7°. It would seem reasonable to assume that the 63° azimuth could be off by as much as 20°. Figure 8.4.2(b) shows a west wing

of at least 250 ft and a less well defined east wing of up to 200 ft and Frac height appears to be about 100 ft with a fairly well defined bottom at about 5800 ft and a less well defined top around 5700 ft.

8.4.7 SUMMARY AND CONCLUSIONS

Placing the BSS tool in the target sand does not seem to result in a significantly improved signal as compared with results obtained in previous experiments with BSS tools above the target sand. Analysis of perforation shot data indicates that orientation may be off by at least 9° and that secondary waves are polarized in the vertical direction. Analysis of data recorded during the two stimulation experiments indicates a fracture azimuth of 63° west of north, a fracture height of 100 ft and asymmetric wings of at least 250 ft to the west and at most 200 ft to the east.

Table 8.4.1 Velocity Factors

Perforation Well	Velocity Factor (ft/ms)	Standard Deviation (ft/ms)	Path Length (ft)
MWX-1	24.0	1.3	206
MWX-2	23.1	0.3	190
Average	23.7	1.2	--

Table 8.4.2 Tool Orientation

Perforation Well	Tool Orientation	Standard Deviation	Vertical Error	Standard Deviation
MWX-1	-81.6°	2.5°	2.5°	3.7°
MWX-2	-72.0°	2.1°	3.8°	0.7°
Average	-78.2°	5.2°	--	--

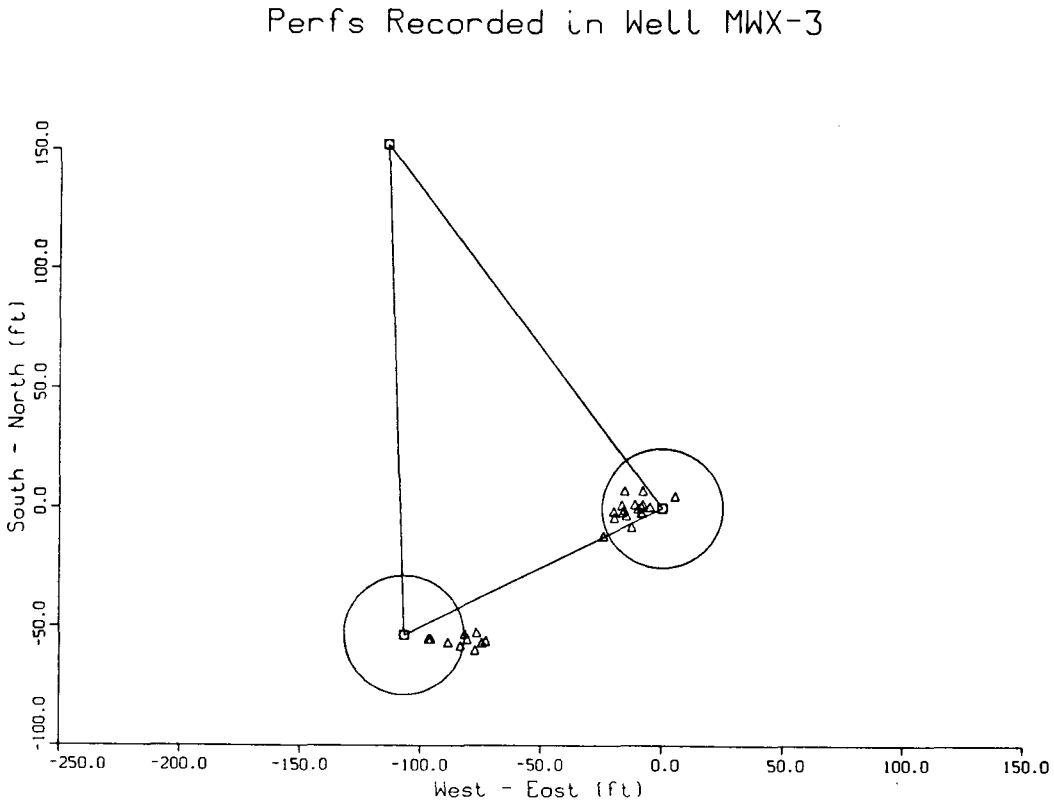

Figure 8.4.1(a). Horizontal projection of perforation shot locations.

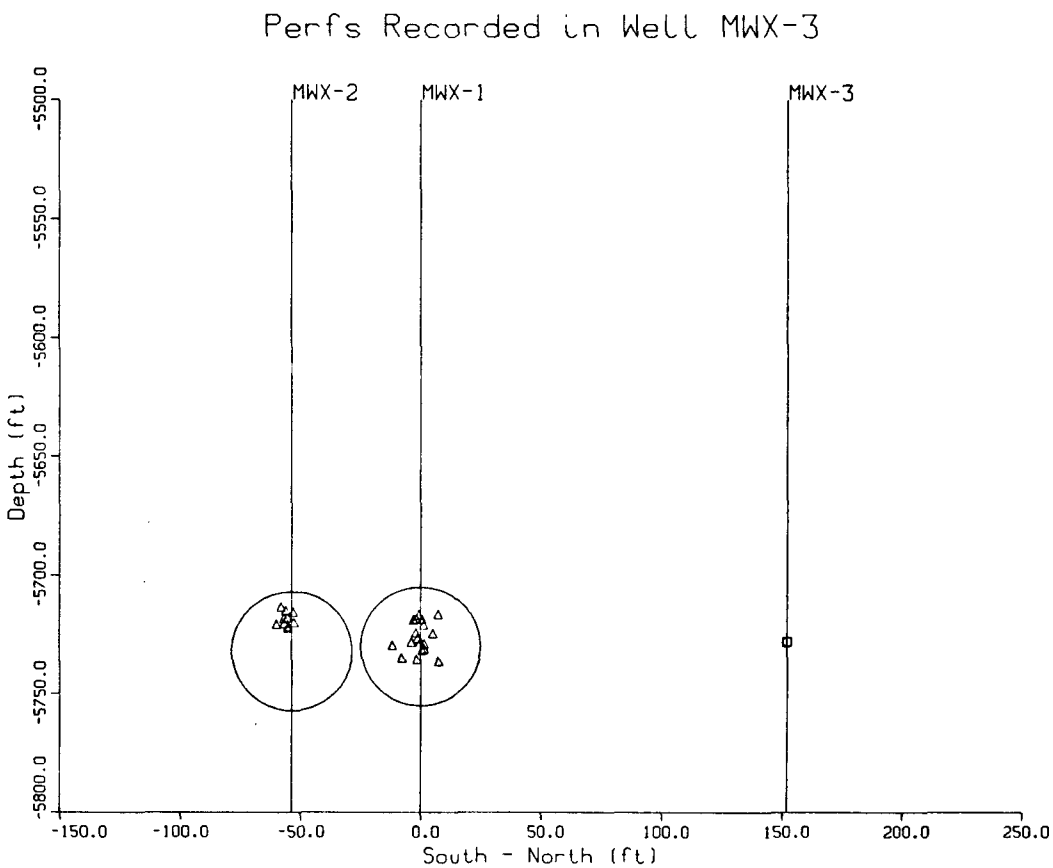

Figure 8.4.1(b). Vertical projection of perforation shot locations.

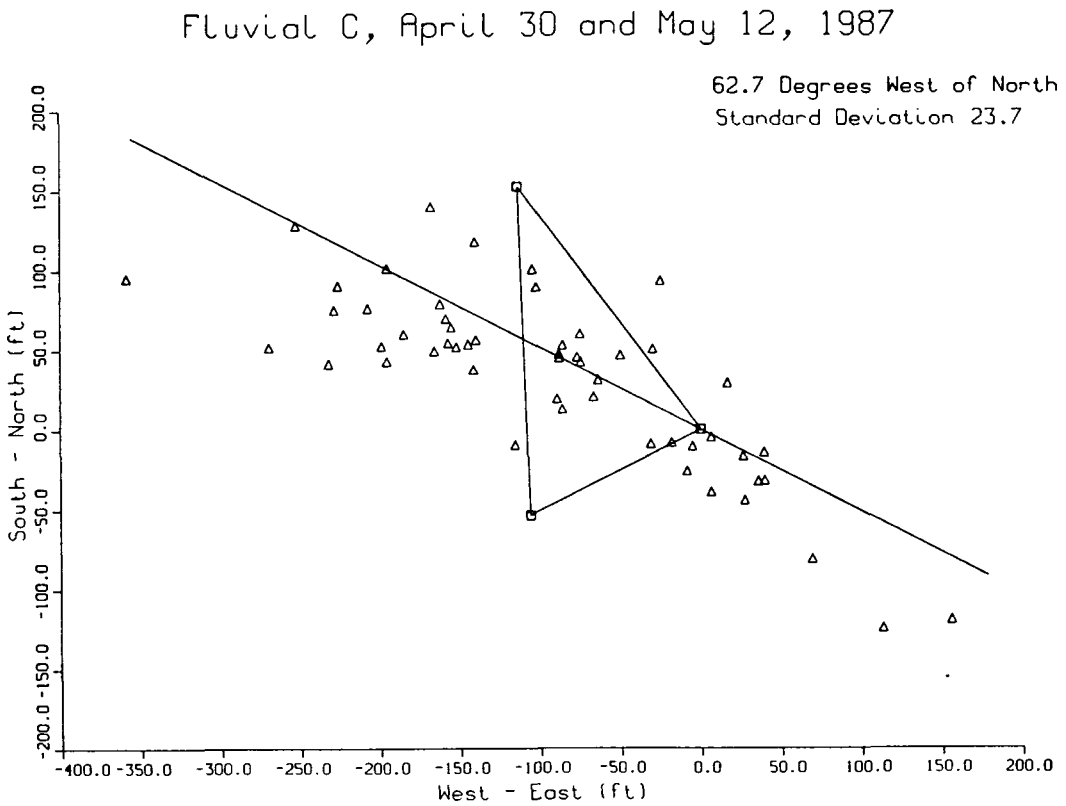

Figure 8.4.2(a). Horizontal projection of microseismic events for two Fluvial C stimulation experiments.

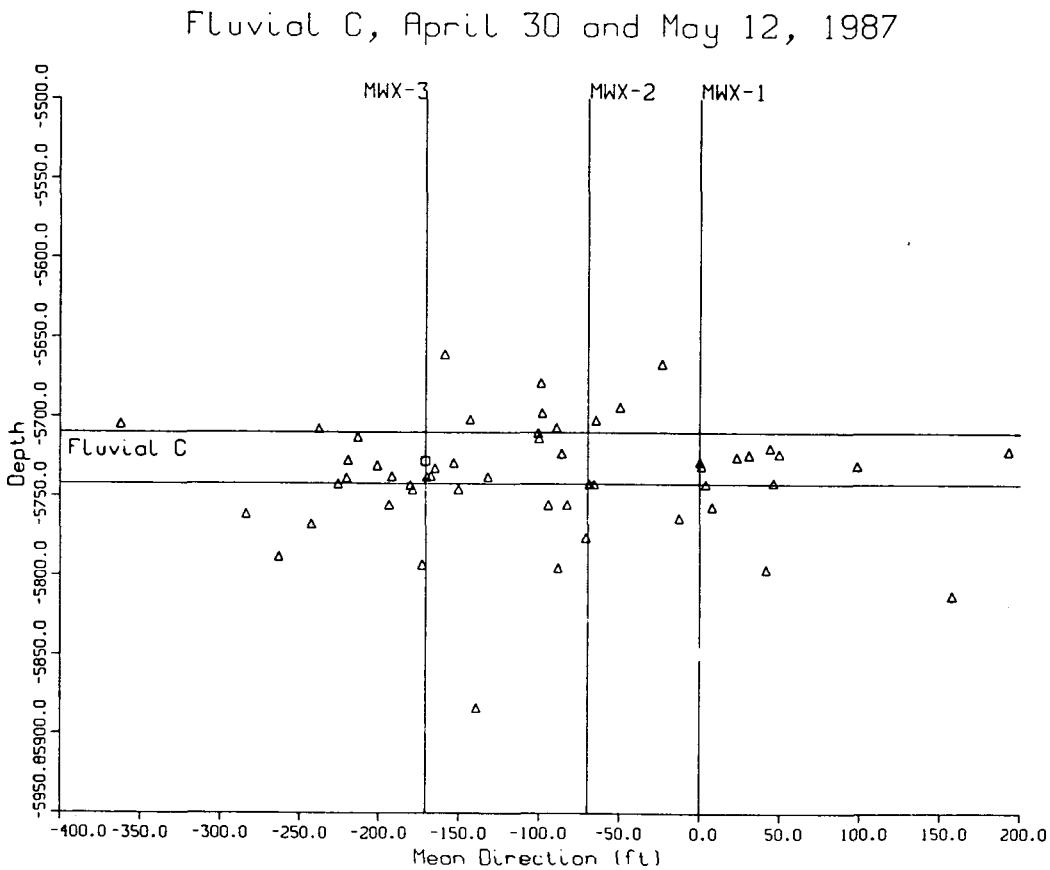

Figure 8.4.2(b). Vertical projection of microseismic events for two Fluvial C stimulation experiments.

9.0 FLUVIAL E SANDSTONE STIMULATION EXPERIMENT

9.1 PRE-STIMULATION RESERVOIR TESTING AND ANALYSIS

P. T. Branagan
CER Corporation

9.1.1 INTRODUCTION

The tight fluvial reservoirs found in the Mesaverde interval at MWX[1] contained interesting candidates for testing and stimulation experiments. Although in situ matrix properties for these reservoirs did not represent a very favorable productive prospect,[2-4] the inclusion of a rather extensive natural fracture system[5] indicated that if these complex reservoirs could be effectively stimulated, it would substantially increase the likelihood that they would become favorable targets for commercial production.

Previous testing and stimulation experiments in underlying paludal[6,7] and coastal[8] reservoirs at MWX made clear the extreme sensitivity of the natural fracture system to invading completion and hydraulic stimulation liquids. Although damage to the reservoir matrix was considered to be detrimental[9] in a relative sense, the more serious problem was clearly maintaining the high productive flow paths of the natural fractures in their original state. Unless certain natural fracture properties could be adequately understood, any hydraulic "stimulation" scheme would not only prove to be ineffective, but could impart sufficient damage to reduce production.[7,10]

The effects of anisotropic natural fractures have been shown to significantly impact post-stimulation gas production.[11] Since average reservoir flow capacity derived from the production wells was not always found to provide sufficient information to describe heterogeneous production behavior,[10] every effort was made to acquire reservoir transients from interference pressure data gathered in the two observation wells during the fluvial tests.

Once adequate well test data were acquired, it was combined with the comprehensive MWX geologic and geophysical data in a series of simulations using a naturally fractured reservoir model. Model parameters were then systematically altered in order to provide the best history match of the well test data. Although a rather simple, single-layered, unbounded model was found to provide a very acceptable history match of the production well, it was the interference well data that required the use of a more complex, multi-layered model to simultaneously match pressure and flow behavior in all three wells.

9.1.2 SITE AND RESERVOIR DESCRIPTION

The fluvial E reservoirs consist of a pair of gas-bearing sandstones located within the Mesaverde Group in the Piceance Basin, Colorado. The sandstone reservoirs in the fluvial interval are characterized as lenticular meander belts[12,13] of limited areal extent with highly heterogeneous characteristics and very low matrix permeability. Figure 9.1.1 is an areal representation of the MWX site, showing the locations of the three MWX test wells and the direction of maximum principal horizontal stress, N78°W. These three experimental test wells were located and spaced in order to provide the most effective information concerning reservoir pressure transient behavior, as well as to serve as observation points for borehole seismic diagnostics during fracturing experiments.[14] The bottomhole location of the three wells in the fluvial E reservoirs, shown by the triangle in Figure 9.1.1, indicates that the distance between wells is approximately 125 to 210 ft.[15-17] Figure 9.1.2 is a cross-sectional plot interpreted from logs and core data[2] and correlated for the three MWX wells. The sandstones of the fluvial E interval are located at a depth of 5525 to 5575 ft.

Extensive geological, sedimentological, log, and core data indicate that the E1 sandstone is characterized as a stream meander belt of fairly large areal extent, having a width in excess of 1500 ft and an unknown length. The E2 sandstone, however, appears to be a splay deposit of very limited size, having a width of possibly 200 to 300 ft. Because of the

limited size and unknown distribution of the E2 sandstone, only the E1 sandstone was perforated and tested.

Table 9.1.1 is a list of some of the salient geologic and geophysical reservoir characteristics for the sandstone in the three wells. The E1 reservoir consists of a low porosity matrix, 6 to 8 percent, with a water saturation between 47 and 52 percent.

Dry core permeability for the E1 sandstone in MWX-1 was found to be about 0.008 md at a confining pressure of 2000 psi.[18] Figure 9.1.3 presents Klinkenberg permeability versus water saturation for an E1 sandstone core sample taken from MWX-2 and corrected for in situ stress conditions.[19] Linear scaling of this measured data, from core at 5942 ft, to the dry permeability resulted in the derived E1 reservoir values. Reviewing Figure 9.1.3 indicates that water saturation of 40 to 60 percent would reduce dry core permeability by a factor of 10 to 100. Therefore, in situ matrix permeability in the E1 sandstone would be on the order of 0.001 md or less.

The integration of core, log, production and well testing data has indicated that the E1 sandstone is naturally fractured. The production characteristics and well test data presented later will show that this sandstone is much more productive than indicated by the matrix permeability. Also, the complexity of this sandstone is significantly increased by the existence of vertical and areal heterogeneities.

9.1.3 PERFORATION AND BREAKDOWN

Completion practices associated with naturally fractured reservoirs should differ markedly from those routinely applied to homogeneous reservoirs, primarily because the intervention processes in the high conductivity fractures differ considerably both in scope and magnitude from the tight matrix alone. Since the salient production stimulation mechanisms in naturally fractured reservoirs depend almost entirely on interaction with the natural fractures to achieve an effective completion,

it is important to take every precaution to minimize damage to the natural fracture system. Matrix damage can also affect optimum production, but when the primary flow paths are natural fractures, then the relative losses are clearly much greater when the fracture system production capacity becomes impaired.

During the course of extensive testing at the Multiwell Experiment (MWX) site, over sixty different perforation and breakdown procedures were performed in a variety of naturally fractured sandstones and other lithologic units. The objectives for MWX testing[1] were most often designed to yield reservoir production characteristics, in situ stresses and/or details of hydraulic fracture interaction and enhancement. Although it was not the expressed intent of the project to determine or evaluate specific perforation and/or breakdown techniques, it was critical that the original reservoir system, which was quickly understood to be highly naturally fractured, not be unalterably affected by these stimulation processes. This was particularly true during well and interference tests that were conducted in ten separate, tight Mesaverde sandstone reservoirs. These reservoirs involved a variety of depositional environments including marine, coastal, paludal and fluvial deposits. Some of these reservoirs were extensive blanket sandstones, while others were lenticular with variable, lateral extent. All contained extremely tight matrix rocks with low porosity[20,21] and were naturally fractured.

The primary goals of the initial MWX completion program, which involved portions of the drilling operations, perforating and breakdown/ microfracturing, were to:

- minimize drilling mud invasion in these overpressured reservoirs;

- establish an undamaged wellbore-to-reservoir connection for all three wells; and

- significantly reduce the volume of liquids injected into the reservoir and natural fracture system during final completion.

Numerous attempts were made at well completions using conventional techniques that included variations of jet charge and bullet perforators, medium (100 BBL) to small (20 BBL) volumes of nondamaging water-based breakdown fluids, and diverting ball sealers. The results were occasionally mixed[22,23] and often provided confusing sets of information. Importantly, it was observed that near-wellbore damage effects were usually diminished in the production well during the course of a 60- to 70-day test, but the observation wells most often did not appear to recover.

Clearly it was important that the phenomena associated with breakdowns and completions be understood in these naturally fractured, low permeability reservoirs. Thus, during the fluvial stimulation experiments, specific efforts were made to acquire additional information concerning non-aqueous breakdown procedures. The primary intent of this research was to:

- attempt several different completion techniques using nitrogen, N_2, gas in the same formation;

- assess results from a tailored pulse propellant fracturing scheme; and

- gain additional knowledge and understanding into natural fracture damage mechanisms and ways to mitigate their effects.

Several different breakdown/microfracturing techniques using non-aqueous forms of fracturing fluids were performed. The background and rationale behind these breakdown schemes are presented in Appendix L. Each of the techniques evaluated are discussed in the following sections.

9.1.3.1 Hydraulic N_2 Fracturing Using Surface Pump Trucks

The initial uses of N_2 at the MWX site involved several breakdown and step/rate injection tests in both coastal[24] and fluvial[25] environments. The primary intent of these tests was to establish closure stress and

fracturing pressure data for impending larger propped foam fracture treatments, and thus, the enhanced production capacity effects of these N_2 fractures were never fully examined. Fracturing was performed using high rate N_2 pump trucks where the maximum rates exceeded 20,000 SCFM and injected volumes totaling almost 1,000,000 SCF. During the course of these treatments, measurements were routinely made of surface injection rates and volume, and surface pressure and bottomhole pressure. Since the volumes were usually rather large, these treatments probably resulted in reasonably long fractures. As a result, these tests would not provide an unambiguous assessment of near wellbore effects nor the effectiveness of small gaseous breakdowns to connect the wellbore with the existing natural fracture set. There would always remain some uncertainty that the lengthy artificial fracture would, by its own presence, substantially enhance production. In addition, variations in perforation conditions and local stress variations would prevent equal treatment of all perforations.

Flowback and short production showed that these treatments successfully enhanced production substantially above that which was possible from the matrix alone. The use of N_2 as a nondamaging stimulation fluid in other fracture-sensitive formations such as the Devonian shale[26-28] had proven to be successful; now these MWX tests (although limited in scope to very short test periods) had shown that these naturally fractured Mesaverde sandstones could also be effectively stimulated with N_2 alone.

9.1.3.2 Perforating in an Underbalanced Column of N_2

To quantify the effectiveness of N_2 as a perforation breakdown fluid a series of differing tests were performed in the E1 sandstone. A slightly different procedure was scheduled for each of the three MWX wells.

The first test involved perforating the observation well, MWX-2, with 20 gm jet charges spaced at 8 per foot in an underbalanced column of N_2. Surface pressure during perforating was about 1000 psi, which for a full N_2 column corresponded to a bottomhole pressure of just about 1200 psi. This procedure differed markedly from the normal perforation process which were

most often performed under a hydrostatic column of 3 percent KCl water. It should be noted that all of the different sandstone reservoirs tested at MWX exhibited reservoir pressure considerably in excess of hydrostatic, ranging from a gradient of 0.82 psi/ft in the Corcoran, to a low of 0.58 psi/ft in the El sandstone, and thus, were all significantly overpressured. Although this underbalanced perforating case was not expected to provide the best connection with the natural fractures, as detailed in Appendix L, nevertheless the well after perforating indicated that it was communicating quite effectively with the natural fractures. This result indicates that the natural fractures were most likely very closely spaced.

9.1.3.3 Perforating in an Overbalanced Column of N_2; N_2 Impulse

The N_2 breakdown scheme for the production well, MWX-1, called for 19 gm jet charge perforators, spaced 2 per foot and phased 120°, to be fired in the casing that contained high pressure N_2. Bottomhole N_2 pressure was set to exceed fracture pressure. This scheme, termed N_2 impulse perforating/breakdown, was designed to simultaneously perforate the well and, at the same time, create fractures that would extend from the wellbore and intersect the natural fracture system.

Figure 9.1.4 is an artist's conception of the test well, MWX-1, showing the prescribed bottomhole pressure prior to perforating and the location of the casing jet perforators. Since the observation well, MWX-2, had previously been perforated, this provided an excellent opportunity to observe the N_2 impulse perforating of MWX-1 at a remote location within the same reservoir (refer to Figures 9.1.1 and 9.1.2). A high accuracy quartz pressure gauge, placed bottomhole in MWX-2, seated in a bottomhole shut-in device, provided an excellent data set.

Figure 9.1.5 is a composite graph showing the measured surface pressure in the frac well, MWX-1, and the reservoir interference pressure being observed in the remote well, MWX-2. The initial pressure increase seen as steps in MWX-1 occurred during the N_2 filling process. The total volume of

N_2 used to fill the 7-in. casing was 350,000 SCF. After surface pressure was brought to about 6000 psi, the jet charges were fired and the well was perforated. Assuming that all the jet charges fired simultaneously or at least within tens of milliseconds of each other, then each perforation was subjected to approximately the same high pressure N_2 impulse. Fracture extension pressure derived from step-rate and in situ stress tests was found to be 4850 psi, thus the initial N_2 pressure at the sand face was at least 2000 psi above fracture pressure.

The dynamics of this N_2 impulse fracturing are more aptly described as impulsive rather than injective. The compressional energy stored in the high pressure N_2 column is almost instantaneously released into the perforations the moment they are created. An expanded view of the pressure data as shown in Figure 9.1.6 discloses the speed with which N_2 pressure dropped following perforating. The average fracturing/injection rate during the first 45 sec after perforating was about 75,000 SCFM. Unfortunately, surface pressure recording from the frac well, MWX-1, failed for about 1.5 minutes during which time the surface pressure fell below 4100 psi (and the corresponding bottomhole extension pressure of 4850 psi). Thus, selecting closure time is not without uncertainty.

Further insight into this fracturing process can be seen from a review of the log-log pressure/derivative pressure group[29] plot shown in Figure 9.1.7. Surface differential pressure, Del p, corresponds to the injection pressure minus the initial fracturing pressure which was taken to be 6011 psi. The early time portion of Del p, and derivative data display a rather constant slope for the first 0.2 minute or about 12 to 14 seconds and then both change significantly. This early time slope is about 0.6 psi/cycle and is reasonably close to the 0.5 psi/cycle slope described by Cinco[30] that represents linear flow within a fracture. Considering the dynamics of this process, turbulence, backstresses, and the continuous storage volume increase as the fracture is created, it is surprising to see such a close correlation between this data and the ideal 0.5 slope. If this 12- to 14-second period does represent the fracture flow regime, then it is probably the period in which the fracture is being created, extended and inflated.

Additional information concerning this fracturing process can be seen in the observation well, MWX-2, data. Referring to Figures 9.1.5 and 9.1.6, there appear to be two superimposed pulses occurring in this interference pressure data. The first pulse occurred almost simultaneously with the perforating in MWX-1 and has a fast rise and fall time, while the second pulse was slower, larger, and continued to rise until data acquisition ceased. The first pulse is most probably the result of a poromechanical response to the creation and extension of the induced fracture in MWX-1. The latter slow rising pulse is the result of the diffusive pressure distribution occurring throughout the natural fracture system. Note that the rise time for the first peak is about 0.3 minute or about 18 to 20 seconds and may well represent the period during which the N_2 induced fracture in MWX-1 is in the process of significant deformation. Once fracture fluid "leak off" becomes the dominate process, extension ceases, the fracture begins to close, and the induced stress diminishes. Modeling this reasonably complex set of processes is in progress and will be presented at a later date.

One final comment is made at this time concerning the derivative group from the MWX-1 data shown in Figure 9.1.7 where a series of damped oscillations appears during the initial seconds of the N_2 impulse. The period for these damped pressure oscillations is a fairly consistent 1.8 seconds. These oscillations may represent a ringing between two differing boundary impedances[31] where the period is the result of the two way transit time for sonic waves in the media. If the transmitting media is the high density N_2, then the distance between the boundaries could be as close as 900 ft. Since this distance is considerably shorter than the surface to bottomhole distance, 5550 ft, then it may represent the fracture tip to wellbore distance. Another possibility is Rayleigh waves induced on the surface of the steel casing or cement.

9.1.3.4 Tailored Pulse Propellant

Surface pressure measurements following the initial perforating of MWX-3 did not indicate that the perforations had connected with the existing

natural fracture system as had been the case with MWX-2 (Section 9.1.3.2). Thus, the tailored pulse breakdown procedure that was conducted in MWX-3 to connect the wellbore to the reservoir. The tailored pulse breakdown procedure entailed the use of a relatively slow burning propellant designed to create a multiple set of fractures radiating like spokes from the perforated wellbore.[32] To create the correct environment for this tailored pulse method to properly initiate multiple fractures, a fluid with a density of about that of water was required as a tamping media in the casing. Since aqueous solutions were not judged appropriate for this application, alternate tamping fluids were considered. Carbon dioxide (CO_2), below 87.8°F and at 1070 psi can exist in liquid form and thus was considered to be an ideal wellbore tamping fluid. At reservoir temperature (150°F) and reduced pressure, the CO_2 would return to the gaseous state, minimizing any residual damage to the natural fracture system. Figure 9.1.8 details the wellbore configuration for this test.

The test procedure called for removal of excess water remaining in the wellbore from previous workover efforts, the tubing removed, and the casing perforated. The well would then be pressured to about 1000 psi with N_2, partly filled with about a 2000-ft head of liquid CO_2; then, a 38-lb propellant package would be placed adjacent to the perforations and ignited. After the propellant was expended and the fractures created, wellbore pressure would be reduced by venting the N_2 gas thus allowing the CO_2 to vaporize. Since the perforated interval was longer than a single propellant package, the procedure was scheduled to be executed in two separate but identical passes. The lower 12 ft (5562 to 5574 ft) of the perforated interval was treated first, while the remaining upper 12 ft (5550 to 5562 ft) was treated two days later.

With some minor delays, the initial procedures appeared to follow the design criteria, and pressure impulse measurements at the surface indicated that the first propellant package had burned properly. However, after a short 12-hr test, the reservoir did not appear to be responding since no significant quantities of reservoir gases were apparent in the wellbore. Several mechanisms were contemplated including the fact that the primary

set of natural fractures might not lie within the portion of the reservoir that had just been fractured. Recall that only the lower most portion of the reservoir had been effectively stimulated by this first test and the upper portion was to be treated in the second pass. Therefore, the well was reconfigured for the second portion of the test, the wellbore was filled with the necessary allocation of liquid CO_2 and N_2 gas, and the propellant package was emplaced at the upper portion of the perforated interval and then ignited. After pressure had been reduced and the CO_2 was permitted to escape, the well produced only very limited quantities of natural gas (<10 MSCFD). After two separate attempts using the propellant fracturing technique, no enhanced production was evident. Subsequent inspection of the casing string showed no apparent damage from either of the propellant shots thus eliminating the possibility of well damage and loss of gas to a thief zone.

A review of the test procedures and subsequent sampling of returned fluids indicated that the original workover water residing in the wellbore prior to perforating had never been adequately purged. Therefore, both of these tests had been seriously compromised by the presence of water adjacent to the perforated interval. Consequently, this test of tailored pulse propellants to create multiple fractures to connect the wellbore with natural fractures could not be considered a valid test of the process. Therefore, the tailored pulse technique still remains a conceptually sound stimulation procedure for naturally fractured reservoirs.

9.1.3.5 N_2 Impulse Using a Bottomhole Pump-Out Plug

Following the attempted tailored pulse fracturing tests in MWX-3 and the failure of the well to flow properly, a remedial treatment was considered. This remedial treatment was conceived to mitigate the possible damage created by the residual wellbore water that had been inadvertently injected into the natural fractures during the previous tests. The treatment essentially involved applying a high pressure N_2 impulse at the perforated interval upon rupture of shear pins in a pump-out plug located

at the bottom of the highly pressurized tubing. This technique was designed to disperse the residual water over a larger portion of the fracture system and thus permit the near wellbore fractures to resume their role as relatively high capacity flow paths for reservoir gases.

Figure 9.1.9 is a schematic of the bottomhole configuration for this remedial treatment. A packer was set at 5527 ft, just above the perforated interval, with shear pins designed to release the pump-out plug at about 6500 psi. The annulus and tubing were connected together at the surface, and both tubulars were pressurized using surface pump trucks. Pressurizing the annulus served two purposes. First, it acted as a large very high flow capacity storage vessel for the impulse. Second, bottomhole annulus pressure was always maintained at a higher pressure than the injection pressure at the perforations. This high bottomhole annulus pressure would tend to minimize any loss of injection gases through micro-annular regions that might exist above the perforated interval. When bottomhole tubing pressure exceeded the prescribed pin shear stress, 6500 psi, the pump-out plug released, creating a very rapid pressure rise at the perforations. This pressure rise to about 6000 psi should be sufficiently fast to permit the extension or at least dilation of the fractures that had been developed by the tailored pulse explosive tests. This process would then disperse the invading water over a much larger area and at least partly restore the near wellbore fractures to their original low liquid saturated value.

Surface pressure measurements indicated that the pump-out plug released at about 6450 psi. Figure 9.1.10 is a linear representation of the surface pressure measured during tubing pressurization and the impulse injection. Maximum surface pressure was 5960 psi which, for a full column of N_2, corresponds to a sand face pressure of about 6450 psi. There is a noticeable pressure rate change during the falloff at about 11.2 minutes which indicates a significant alteration in flow regimes. Figure 9.1.11 shows the log-log/derivative pressure representation of these data for the falloff period. Note that there is considerable difference between this set of curves and those for the simultaneous perforation and N_2 breakdown technique employed in MWX-1, shown in Figure 9.1.7. In this case, fracture

creation was not part of the process as was the situation for the MWX-1. Thus, the fractures in MWX-3 previously created by the tailored pulsed propellant need only be dilated during this process to disperse the trapped liquids.

Following about 48 hrs of production and on-site gas chromatographic monitoring, the well appeared to have responded positively, producing almost 50 MSCFD or about 65 percent of the gas rate produced from the other two wells. Consequently, this technique appears to have sufficient merit to be considered for clean up of near wellbore damage to natural fractures in previously perforated wells.

9.1.3.6 Perforation and Breakdown Summary and Conclusions

The completion of naturally fractured reservoirs differs both in substance and approach from conventional reservoirs. Not only is it improbable that natural fractures will make their presence known during drilling, coring, or perforating, but more important, the damage to sensitive natural fractures can be so severe that fracture flow capacity can be diminished to the point of rendering them useless as flow conduits. Once the hypothesis concerning natural fracture damage is accepted, then completion processes that might tend to impair fracture flow capacity can no longer be considered acceptable practices.

Following a number of intermittent successes and failures at the MWX that employed conventional perforating and aqueous-based breakdown techniques, several different non-aqueous completion schemes were successfully performed. The results of these novel tests are summarized below:

- High rate pumper injection of N_2 alone may not effectively treat the entire perforated interval.

- Perforating in a dry, underbalanced, wellbore column of N_2 successfully connected the wellbore with the highly conductive natural fracture set.

- N_2 impulse perforating/breakdown using high pressure N_2 to simultaneously create fractures during perforating has shown to be field executable and successful in achieving the desired wellbore-reservoir connection.

- Tests of a tailored pulse propellant technique were compromised by the presence of water in the wellbore. Results were confined to describing the field execution and operation of the tailored pulsed fracturing experiment but did not provide an assessment of the technique.

- A remedial treatment of near wellbore natural fracture damage using a N_2 impulse technique that employed a tubing pump-out plug proved to be practical and successful.

- When comparing these techniques to other completion schemes used at the MWX site, indications show that N_2 alone can be effectively employed in breakdown procedures.

Following these experimental efforts, the E1 reservoir was successfully interference tested using all three wells.[33] A great deal of reservoir testing over the past several years at the MWX site underscores the complexities associated with understanding critical mechanisms that complicate the effective completion of naturally fractured reservoirs. Some of these damage processes are now understood and can be circumvented using appropriate well completion techniques.

9.1.4 WELL TESTING, ANALYSIS, AND MODELING

9.1.4.1 Well Testing Operations

One of the primary objectives of the Multiwell Experiment is to develop technology to increase productivity and reserves of tight, lenticular gas reservoirs. To meet this objective, comprehensive multiwell interference tests were used in order to adequately characterize reservoir properties

and production mechanisms. A unique aspect of the MWX is the availability of essential high quality well test data in the production well that is coupled with interference data from two observation wells. The results will show that in the absence of interference data, ambiguous interpretations of the MWX-1 well test data would have occurred primarily due to the complexity of the reservoir. The combination of production well and interference test data allowed a more detailed and reliable reservoir model to be developed, which was considered essential for evaluating the various stimulation options and the subsequent analysis of post-stimulation well and interference tests. A previous experiment in the marine Cozzette[10] sandstone provided the first set of interference test data at MWX and indicated the dominant role that the anisotropic natural fractures played in pre-fracture well test analysis.

The E1 sandstone was tested from June to August of 1987. MWX-1 was designated as the production well and MWX-2 and MWX-3 were used as observation wells. The observation wells were equipped with bottomhole shut-in tools to minimize wellbore volume and storage effects. Bottomhole pressure was recorded in all three test wells using high accuracy quartz pressure gauges with real-time surface display and data storage. This allowed the well testing operations to be monitored and controlled during the test. Daily plots of bottomhole pressure in all three wells and surface flow rate in MWX-1 were used to evaluate the progress of the test. In addition, semi-log, log-log and derivative plots were continuously analyzed to ensure the test was proceeding as planned. This close monitoring allowed test conditions to be changed based on current analytical results.

Figure 9.1.12 illustrates the flow rate and bottomhole pressure in MWX-1, along with corresponding interference pressures from the observation wells, MWX-2 and MWX-3, for the entire test period. (Digitized data for the test period are given in Appendix M.) The E1 sandstone interference tests lasted over 60 days and consisted of the following separate test periods:

- 8-day initial production test.
- 6-day initial pressure buildup test, 1A (bottomhole shut-in).
- 2-day production interference pulse.
- 2-day shut-in interference pulse.
- 2-day production interference pulse.
- 2-day shut-in interference pulse.
- 7.5-day final production test.
- 31-day final pressure buildup test, 1D (bottomhole shut-in).

Bottomhole pressure was closely monitored in MWX-2 during the entire well testing sequence. The initial production testing started before MWX-3 was operational due to remedial work to correct completion difficulties. Interference was detected in both wells during the latter portion of the initial production period, after which time MWX-1 was shut-in. The initial shut-in period, 1A in Figure 9.1.12, was designed to:

- provide initial pressure buildup data to describe the average reservoir characteristics;

- create a pressure transient for interference testing; and

- allow time for MWX-3 to become sufficiently stable to continue interference testing.

Testing of MWX-1 was conducted at a constant bottomhole pressure of 1000 psi. Pressure stabilization was generally acquired after 24 hours. Bottomhole pressure was maintained at 1000 psi to minimize the effects of stress sensitive matrix and natural fracture permeability.[10,19,20] Previous MWX well tests, production data, and laboratory core analysis have indicated that low bottomhole pressure can significantly reduce production.

A series of 2-day pulse tests were conducted after MWX-3 was configured and ready for interference testing and the MWX-1 buildup test had provided sufficient data to allow an initial evaluation of reservoir production. The pulse test included two cycles of 2-day production and 2-day shut-in

periods. Daily evaluation of the MWX-2 and MWX-3 bottomhole pressure clearly indicated pressure interference in both wells directly correlatable to MWX-1 pulsing. Following the last 2-day shut-in, MWX-1 was produced for an additional 7.5 days and then shut-in for an extended 31-day buildup.

9.1.4.2 Well Test Analysis

Horner analysis[22] of the initial buildup (1A), using the late time slope as shown in Figure 9.1.13, yields an average reservoir flow capacity, kh = 0.37 md-ft, a p* = 3200 psi and a skin, s = -2.2. Although the reservoir production mechanisms are considerably more complex than defined by the Horner assumptions, this analysis does provide an average assessment of pre-fracture reservoir flow capacity. For a net height, h, of 28 ft, the average effective permeability, k was 0.013 md.

Figure 9.1.14 is a log-log/derivative plot of the initial buildup, which suggests that reservoir flow regimes are most likely not the result of simple radial flow. A comparison with derivative[29] type curves suggests that the reservoir appears to exhibit characteristics inherent in dual porosity systems. Included in Figure 9.1.14 are matching parameters from the Bourdet family of curves for fractured reservoirs. The match of the late time portion of the derivative curve to the Bourdet dimensionless parameters[29] yields, kh = 0.36 md-ft and a skin, s = -1.7.

9.1.4.3 Reservoir Modeling

Simulation of the E1 reservoir well test data was performed in two parts. The first part involved the use of a relatively simple, single-layered, infinite acting reservoir model, and the second part required the use of a more complex multi-layered, bounded reservoir model. Both models involved the use of a fully transient, naturally fractured, reservoir simulator that permitted the inclusion of anisotropically producing natural fractures[11] and the incorporation of certain reservoir and boundary properties derived from the MWX geologic, and geophysical data. Some parameters of the initial model include:

- log- and core-derived matrix properties, such as porosity and water saturation;

- reservoir areal extent and direction from core, sedimentological and outcrop studies;

- in situ matrix permeability from specialized, restored-state core analysis; and

- fracture orientation from a variety of in situ stress tests and laboratory rock mechanics assessments and outcrop studies.

A very adequate model history match of the production well test data was obtained with the use of a single-layered, unbounded reservoir simulator. Interference pressure histories acquired from the observation wells, along with production well data, required the use of the more complex bounded and multi-layered reservoir model.

9.1.4.3.1 Single-Layered Model

The single-layered simulator used to model the E1 well test data is shown schematically in Figure 9.1.15. Included in Figure 9.1.15 is a list of certain salient reservoir model parameters considered most appropriate to describe in situ properties and that ultimately resulted in a favorable history match of the MWX-1 production well test data. Figure 9.1.16 is a composite Horner plot of the initial MWX-1 pressure buildup and the model history match of that buildup. Field measured flow rates from the beginning of the test until initiating the pressure buildup were used as input to the simulator. Various reservoir model parameters were systematically adjusted and resulted in the simulated pressures, shown in Figure 9.1.16, that were virtual overlays to the field data. A more critical test of the pressure history match can be seen in the composite log-log/derivative plot shown in Figure 9.1.17.

Excellent simulated pressure buildup matches in real time and Horner time were achieved with this model using the reservoir parameters listed in Figure 9.1.15. Note, in the log-log plot of Figure 9.1.17 that wellbore storage had little effect on the buildup data when the bottomhole shut-in tool was employed. Storage effects were virtually eliminated and lasted less than 10 to 15 minutes. Model simulations of the buildup using the full 5500 ft of wellbore volume showed that storage effects would have persisted for almost the entire 120-hour buildup period. This would have so distorted the buildup pressure history that the distinctive slope changes in Figures 9.1.16 and 9.1.17 would have been totally masked, making the data difficult to interpret.

Although this single-layered model provided an excellent history match of the MWX-1 field data, there are nevertheless some shortcomings in this analysis. Note in Figure 9.1.15, that the model's natural fractures were considered to be an isotropic set with a permeability of 10,000 md and widths of 0.0003 in., corresponding to an average fracture flow capacity, $k_f w_f$, of 0.25 md-ft. Two distinct problems occur with this scenario. First, the simulated pressure transients at the observation wells, MWX-2 and MWX-3, were considerably larger than the field data; this suggests anisotropic permeabilities in the reservoir. Secondly, when anisotropic permeabilities of up to 50:1 were introduced into the fracture system, the simulated interference pressures could be matched in only one well. A complicating factor is the fact that the measured pressure in the observation well, MWX-2, was always higher than the observation well, MWX-3, even though it was considerably closer to the production well, MWX-1.

9.1.4.3.2 Multi-Layered, Bounded Model

Since natural fracture anisotropy was not by itself sufficient to permit a single-layer model to simultaneously match all three well pressure histories without altering some other parameter, the geologic and geophysical data were reassessed in order to arrive at a better match of all parameters. A review of the geologic and geophysical data shows that the bulk of the E1 sandstone occurs in MWX-2 and thins toward MWX-3. This

suggests that tighter control of boundary conditions should be imposed in initializing the reservoir model. Furthermore, small lithologic discontinuities, such as very thin shale breaks, were found to act as terminators for vertical natural fractures,[3] and thus the natural fracture system could be considered to be heterogeneously distributed through non-communicating layers.

A new simulator incorporating a multi-layered, heterogenous naturally fractured system was assembled. Since the density of natural fractures was found[3] to be inversely proportional to thickness, then the thinnest layer would be the most conductive, but of course would not necessarily contain the bulk of producible gas. Figure 9.1.18 is a schematic of a three-layer reservoir model devised to simulate the E1 reservoir. The bottom layer (Layer 3) is a thin, 1-ft thick portion of the reservoir that contains a very conductive set of natural fractures. This permits rapid pressure communication between all three wells similar to that seen in the field data shown in Figure 9.1.12. The thick middle layer (Layer 2) consists of an anisotropic fracture set exhibiting a 30:1 permeability ratio. This 24-ft thick layer represents the primary productive portion of the E1 sandstone, producing almost 70 percent of total produced gas. The uppermost layer (Layer 1) is a 7-ft layer that does not significantly contribute to production in MWX-1, since it pinches out between MWX-2 and MWX-1.

Figure 9.1.19 is a composite plot of the field data for all three MWX wells and the model history match of that data. The final matching reservoir model parameters are listed in Figure 9.1.18. Obviously, this model provides a very reasonable match of the entire field test data, not only for the production well, MWX-1, but also for both remote observation wells, MWX-2 and MWX-3.

A Horner plot of field and model data for the final pressure buildup (1D in Figure 9.1.12) is shown in Figure 9.1.20. The log-log/derivative plot for final buildup is also shown in Figure 9.1.21. Note the drop in the pressure derivative occurring in MWX-1 near the end of the test at

400 hrs; this is related to the initiation of production in MWX-3 during recovery of that well's bottomhole pressure gauge. Furthermore, the real drop in MWX-1 pressure at about 600 hrs corresponds to production in MWX-2 during retrieval of that well's bottomhole pressure gauge. This provides additional evidence of the rapid pressure response that occurs between wells, supporting the hypothesis that a very conductive fracture set exists in this El reservoir. The amplitude of these responses, however, underscores the variation or areal heterogeneity of the reservoir.

9.1.5 SUMMARY AND CONCLUSIONS

An extensive set of high quality core, log, geophysical, well test, interference and production data have been acquired from a tight, naturally fractured, lenticular reservoir at the MWX site. Novel completion techniques that used only gas, assured that damaging liquids would not impair reservoir interference test data.

The evaluation of well test and interference data proceeded in three parts:

- analytical well test analysis using Horner, log-log pressure and pressure derivative plotting techniques;
- single-layered reservoir model evaluation and history matching; and
- multi-layered reservoir model evaluation, history matching and interference pressure matching.

The analytical well test analysis from the Horner plot yielded an average reservoir flow capacity, kh = 0.37 md-ft. The log-log pressure and pressure derivative type curve evaluation indicated dual porosity behavior and an average reservoir flow capacity, kh = 0.36 md-ft. However, further details of the reservoir matrix and natural fracture system were not readily available from type curve or other analytical analysis.

A very acceptable match of production and well test data in MWX-1 obtained using a single-layered, naturally fractured reservoir model. Both Horner and log-log pressure and pressure derivative plots were matched using this single-layered model. Basic single-layered reservoir properties included an average matrix permeability, k = 0.002 md, and an isotropic natural fracture set with conductivities, $k_f w_f$ = 0.250 md-ft. It should be noted that a good match of MWX-1 well test data could also be obtained with natural fracture anisotropy of up to 50:1. However, an acceptable history match of the data from the two interference wells could not be obtained using a single-layered model.

Therefore, core, log, and geologic data were reviewed and a three-layer reservoir model was developed which allowed both well test and interference data to be accurately matched. The model consisted of a thin, 1-ft, high permeability layer having an isotropic set of natural fractures with conductivities of 2 md-ft, a 7-ft layer whose anisotropic natural fractures possessed conductivities of 4.1 md-ft and 0.13 md-ft, respectively, and finally a 24-ft thick layer with anisotropic natural fractures with conductivities of 0.83 md-ft and 0.028 md-ft, respectively. The matrix permeability for all three layers was 0.002 md. This final three-layered reservoir model provided a basis for all subsequent hydraulic fracture designs.

The reservoir performance analysis of the E1 reservoir by simulation history matching of well test and interference data from the three MWX wells produced a very detailed picture of the reservoir. The derived model provided significant insight into the complex production characteristics of this tight, lenticular, anisotropic naturally fractured reservoir and yielded the following basic conclusions.

- Reservoir parameters obtained from evaluating single well production data in a naturally fractured reservoir can result in a series of ambiguous interpretations.

- Natural fracture anisotropy, an important property in optimizing hydraulic fracture treatments, may not be evident or obtainable from single well test data.

- Bottomhole shut-in during pressure buildup tests significantly reduces wellbore storage effects to acceptable levels. Without bottomhole shut-in procedures, wellbore storage would have totally masked important reservoir flow regime transition periods, and thus much of this analysis could not have been performed.

- Multi-layered, anisotropic naturally fractured reservoirs may have overall production and pressure buildup characteristics very similar to single-layered, isotropic naturally fractured reservoirs. This could have a major impact on stimulation design and post-stimulation production.

- Anisotropic natural fracture properties are very prevalent in the lenticular Mesaverde reservoirs at the MWX site.

- Standard analytical well test analysis, such as Horner and log-log pressure and pressure derivative type curves, appear to provide representative reservoir characteristics, but do not identify reservoir anisotropy or layering in naturally fractured reservoirs.

9.1.6 REFERENCES

1. Northrop, D. A., et al., "Current Status of the Multiwell Experiment," SPE 12868, presented at the SPE/DOE/GRI Unconventional Gas Recovery Symposium, Pittsburgh, PA, May 13-15, 1984.

2. Kukal, G. C., "Well Log Analysis of the Low Fluvial Interval," CER Report, May 23, 1986.

3. Lorenz, J. C., et al., "Fracture Characteristics and Reservoir Behavior of Stress-Sensitive Fracture Systems in Flat-Lying Lenticular Formations," SPE 15244, presented at the SPE Unconventional Gas Technology Symposium, Louisville, KY, May 18-21, 1986.

4. Sattler, A. R., "The Multiwell Experiment Core Program II," SPE/DOE/GRI 12854, presented at the SPE/DOE/GRI Unconventional Gas Recovery Symposium, Pittsburgh, PA, May 13-15, 1984.

5. Lorenz, J. C., "Characterization and Significance of a Subparallel, Unidirectional, Natural Fracture System in Mesaverde Reservoirs, Northwestern, Colorado," presented at the American Association of Petroleum Geologists, Research Conference on the Analysis of Naturally Fractured Reservoirs, Snowbird, UT, May, 1987.

6. Warpinski, N. R., et al., "Fracturing and Testing Case Study of Paludal, Tight, Lenticular Gas Sands," SPE/DOE 13876, presented at the SPE/DOE Low Permeability Gas Reservoirs Symposium, Denver, CO, May 19-22, 1985.

7. Branagan, P. T., et al., "Case History of Hydraulic Fracture Performance in the Naturally Fractured Paludal Zone: The Transitory Effects of Damage," SPE/DOE 16397, presented at the SPE/DOE Low Permeability Reservoirs Symposium, Denver, CO, May 18-19, 1987.

8. "Multiwell Experiment Final Report III. The Coastal Interval of the Mesaverde Formation," Sandia National Laboratories report, SAND88-3284, May 1989.

9. Raible, C. J. and Gall, B. L., "Fracturing Materials Research," DOE/METC-87/6080, in the Proceedings of the Unconventional Gas Recovery Contractor's Review Meeting, July 1987, 250-259.

10. Branagan, P. T., et al., "Interference Testing of the Naturally Fractured Cozzette Sandstones: A Case Study at the DOE MWX Site," SPE/DOE/GRI 12869, presented at the SPE/DOE/GRI Unconventional Gas Recovery Symposium, Pittsburgh, PA, May 13-15, 1984.

11. Branagan, P. T., et al., "Designing and Evaluating Hydraulic Fracture Treatments in Naturally Fractured Reservoirs," SPE/DOE 16434, presented at the SPE/DOE Low Permeability Reservoir Symposium, Denver, CO, May 18-19, 1987.

12. Lorenz, J. C., "Sedimentology of the Mesaverde Formation at Rifle Gap, Colorado, and Implications for Gas-Bearing Intervals in the Subsurface," Sandia Report, March 1982.

13. Lorenz, J. C., "Predictions of Size and Orientations of Lenticular Reservoir in the Mesaverde Group, Northwestern Colorado," SPE/DOE 13851, presented at the SPE/DOE Symposium on Low Permeability Reservoirs, Denver, CO, May 19-22, 1985.

14. Hommert, P. J., "Multiwell Experiment - Fracture Diagnostics," DOE/METC-87/6080, in the Proceedings of the Unconventional Gas Recovery Contractor's Review Meeting, July 1987, 399-409.

15. "Multi-Well Experiment MWX-1, As-Built Report," CER Report, SAND82-7201, July 1982.

16. Multi-Well Experiment MWX-2, As-Built Report," CER Report, SAND82-7100, August 1982.

17. Multi-Well Experiment MWX-3, As-Built Report," CER Report, SAND84-7132, May 1984.

18. Special Core Analysis Study for Sandia National Laboratories from Core Laboratories, Inc., Document Number 61-4863, 1983.

19. Randolph, P. L., "Porosity and Permeability of Mesaverde Sandstone Core from the DOE Multiwell Experiment," SPE Preprint 11765, 1983 SPE/DOE Symposium on Low Permeability Gas Reservoirs, Denver, CO.

20. Sattler, A. R., "The Multiwell Experiment Core Program II," SPE 12854, presented at the SPE/DOE/GRI Unconventional Gas Recovery Symposium, Pittsburgh, PA, May 13-15, 1984.

21. Randolph, P. L., "Porosity and Permeability of Mesaverde Sandstone Core from the U.S. DOE Multiwell Experiment, Garfield County, Colorado," SPE 11765, presented at the SPE/DOE Low Permeability Gas Reservoir Symposium, Denver, CO, March 4-6, 1983.

22. Branagan, P. T, G. Cotner, and S. J. Lee, "Interference Testing of the Naturally Fractured Cozzette Sandstone: A Case Study at the DOE MWX Site," SPE 12869, presented at the SPE/DOE/GRI Unconventional Gas Recovery Symposium, Pittsburgh, PA, May 13-15, 1984.

23. Branagan, P. T, et al., "Comprehensive Well Testing and Modeling of Pre- and Post-Fracture Well Performance of the MWX Lenticular Tight Gas Sands," SPE 13867, presented at the SPE/DOE Low Permeability Gas Reservoirs Symposium, Denver, CO, May 19-22, 1985.

24. Branagan P. T., "Preliminary Results of the N_2 Fracturing Experiments in the Coastal Yellow Sandstone," CER Corporation, Distribution Memo, June 19, 1985.

25. Warpinski, N. R., "Analysis of the Fluvial B Nitrogen Step-Rate/Flow-Back Tests," Sandia Distribution Memo, October 22, 1986.

26. Komar, C. A. and A. B. Yost, "Practical Aspects of Foam Fracturing in the Devonian Shale," SPE 8345, presented at the 54th SPE Annual Fall Conference, Las Vegas, NV, September 23-26, 1979.

27. Freeman E. R., et al., "A Stimulation Technique Using Only Nitrogen," JPT (December 1983) 2165-2174.

28. Gottschling, J. C., "Nitrogen Gas and Sand: A New Technique for Stimulation of Devonian Shale," JPT (May 1985) 901-907.

29. Bourdet, D., et al., "A New Set of Type Curves Simplifies Well Test Analysis," World Oil (May 1983) 95-106.

30. Cinco-L, H., et al., "Transient Pressure Analysis for Fractured Wells," SPEJ (August 1978) 253-264.

31. Holzhausen, G. R., and R. P. Gooch, "The Effect of Hydraulic Fracture Growth on Free Oscillations of Wellbore Pressure," 26th US Symposium on Rock Mechanics, Rapid City, SD, 621-631.

32. Cuderman J. F., "Design and Modeling of Small Scale Multiple Fracturing Experiments," SAND81-1398, Sandia National Laboratories, 1981.

33. Branagan, P. T., et al., "Pre-Frac Interference Testing of a Naturally Fractured, Tight Fluvial Reservoir," SPE 17724, presented at the Gas Technology Symposium, Dallas, TX, June 13-15, 1988.

TABLE 9.1.1 GROSS FLUVIAL E1 MATRIX PROPERTIES FOR GEOLOGIC AND GEOPHYSICAL DATA

Well	Depth (ft)	Net Pay (ft)	Porosity (ϕ)	Water Saturation (Sw)
MWX-1	5544-5565	21.5	0.060	0.52
MWX-2	5534-5566	33.0	0.077	0.47
MWX-3	5555-5575	20.0	0.059	0.48

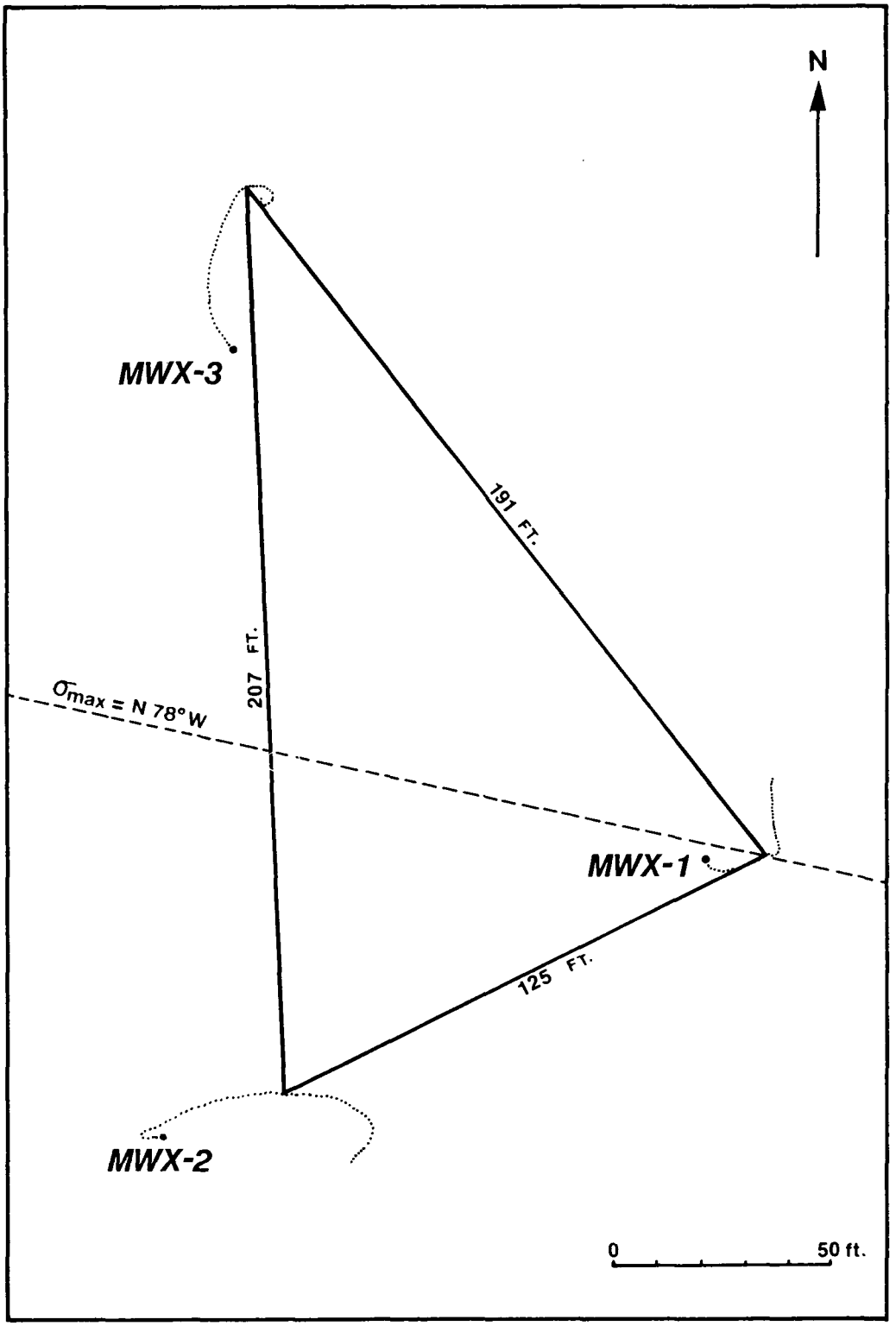

Figure 9.1.1 Areal Representation of MWX Site

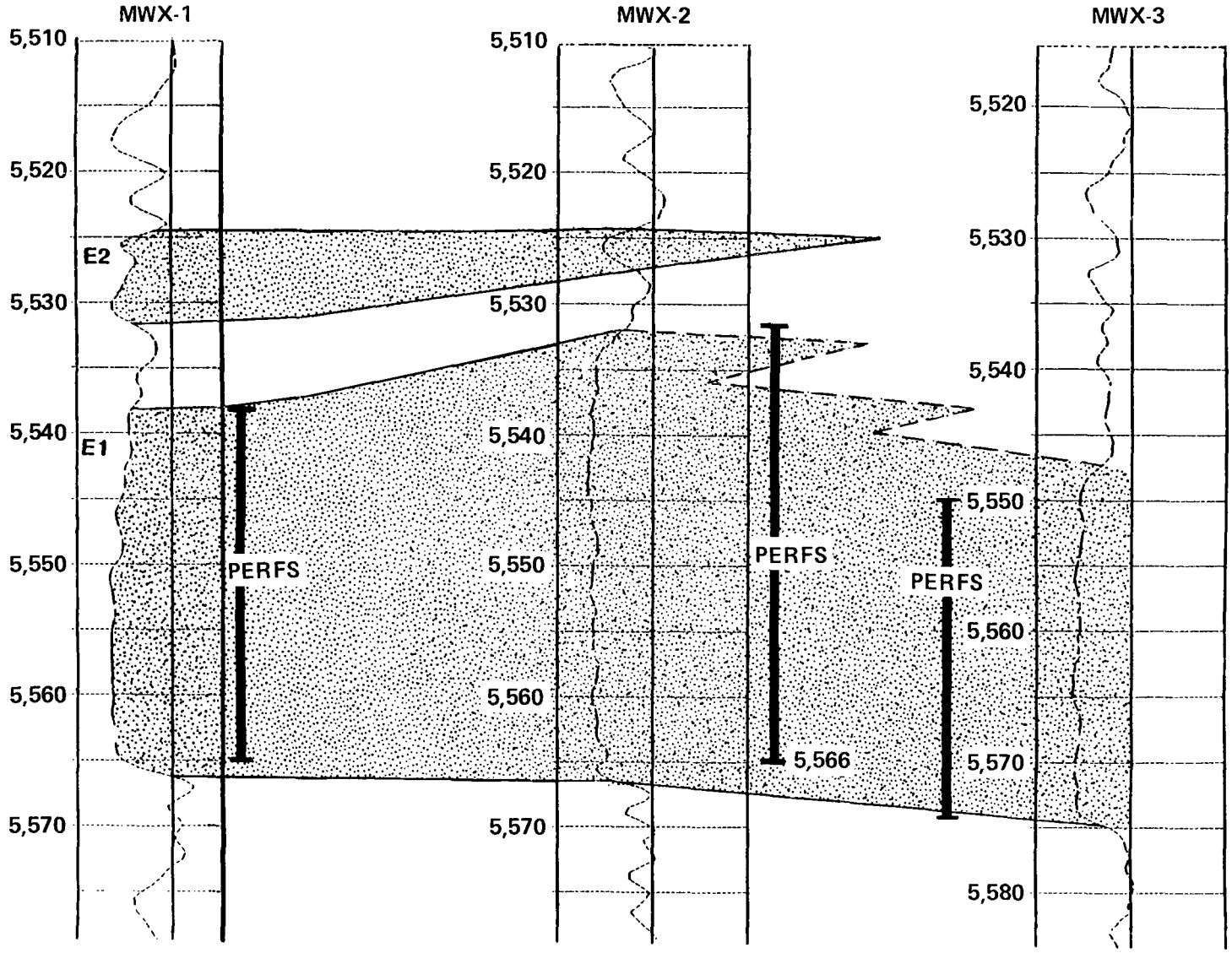

Figure 9.1.2 Cross-Sectional Correlation of Fluvial E Interval

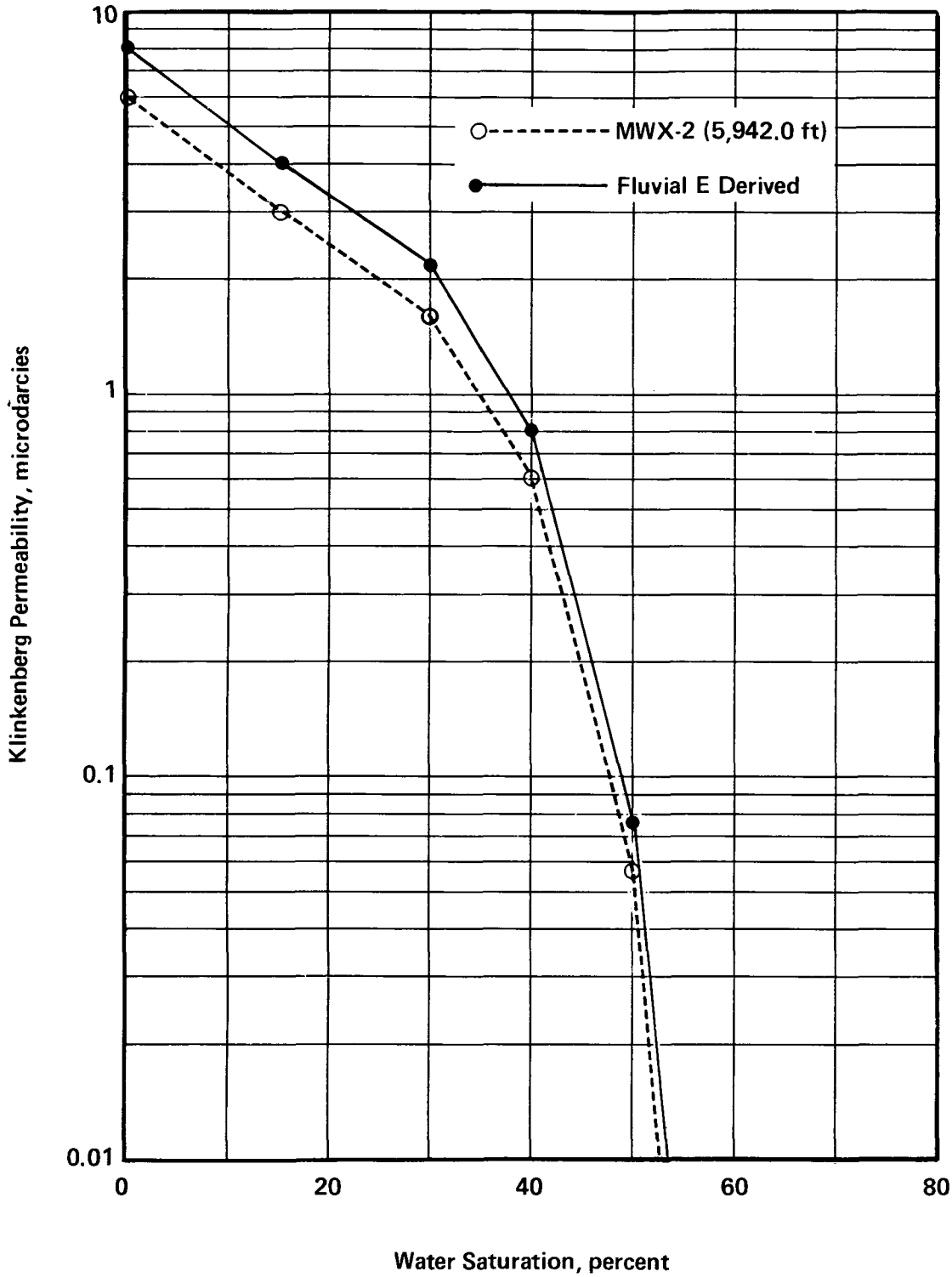

Figure 9.1.3 Effect of Water Saturation on Permeability

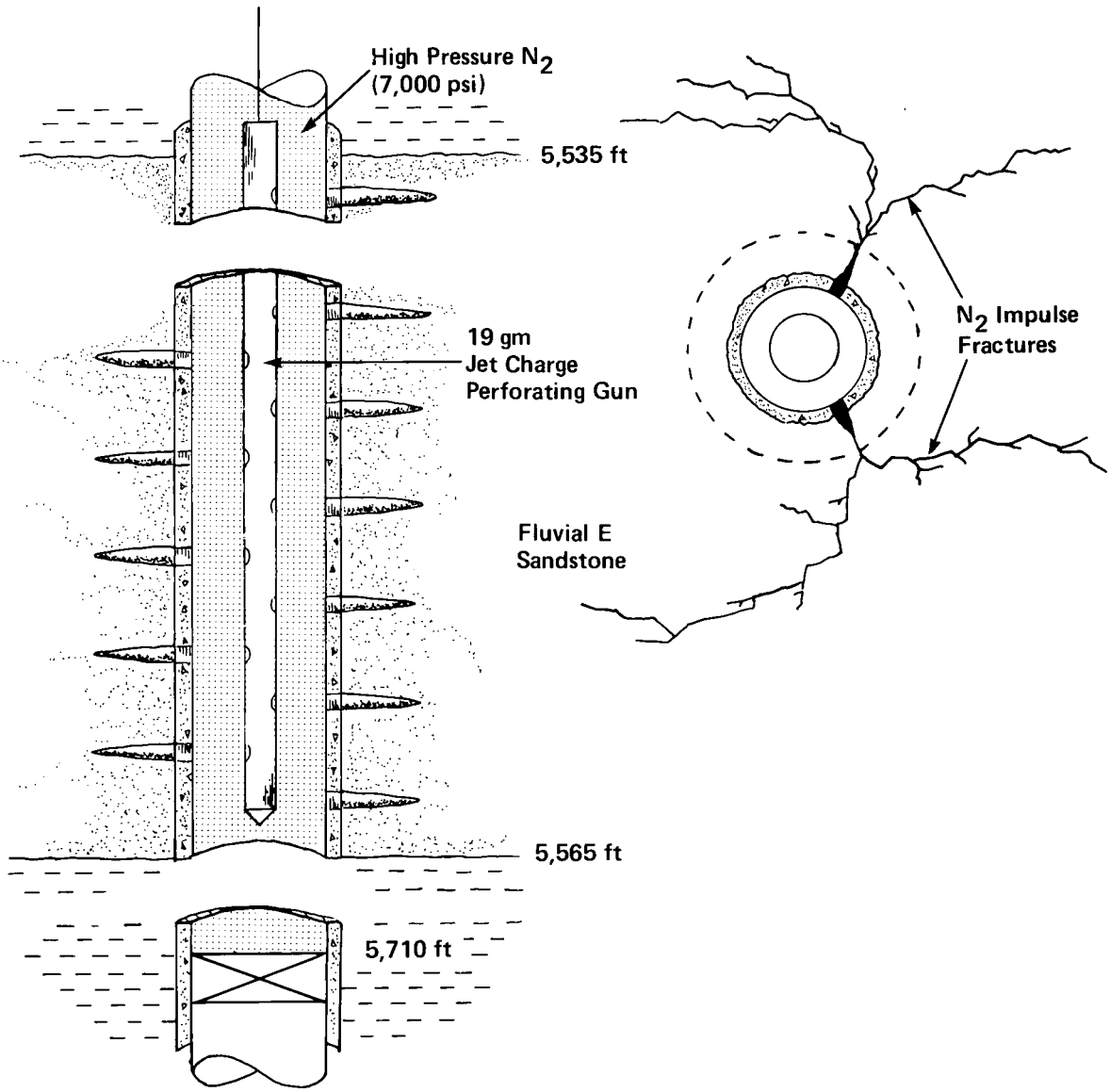

Figure 9.1.4 Nitrogen Impulse Fracturing

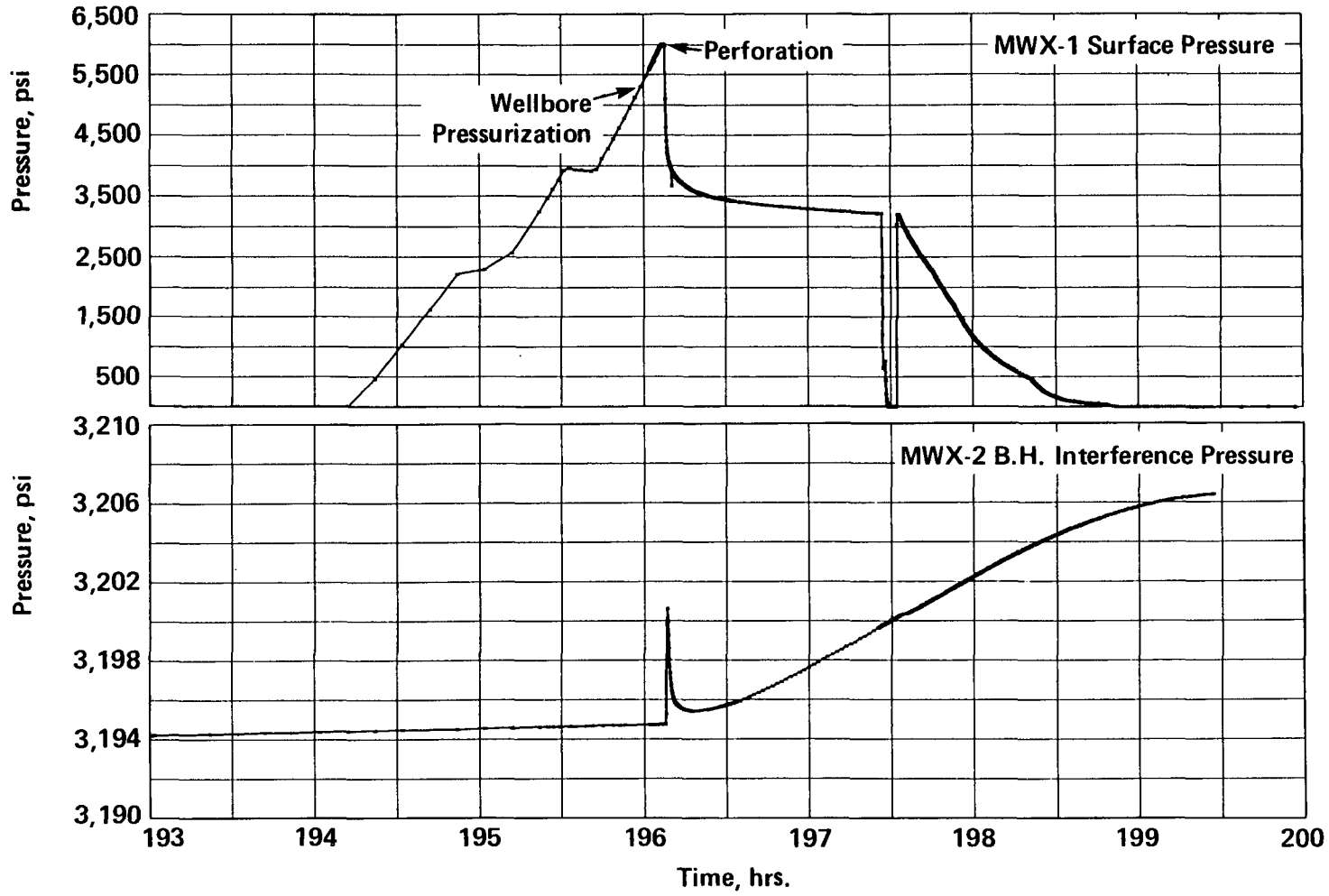

Figure 9.1.5 Frac Well (MWX-1) and Interference Well (MWX-2) Pressures

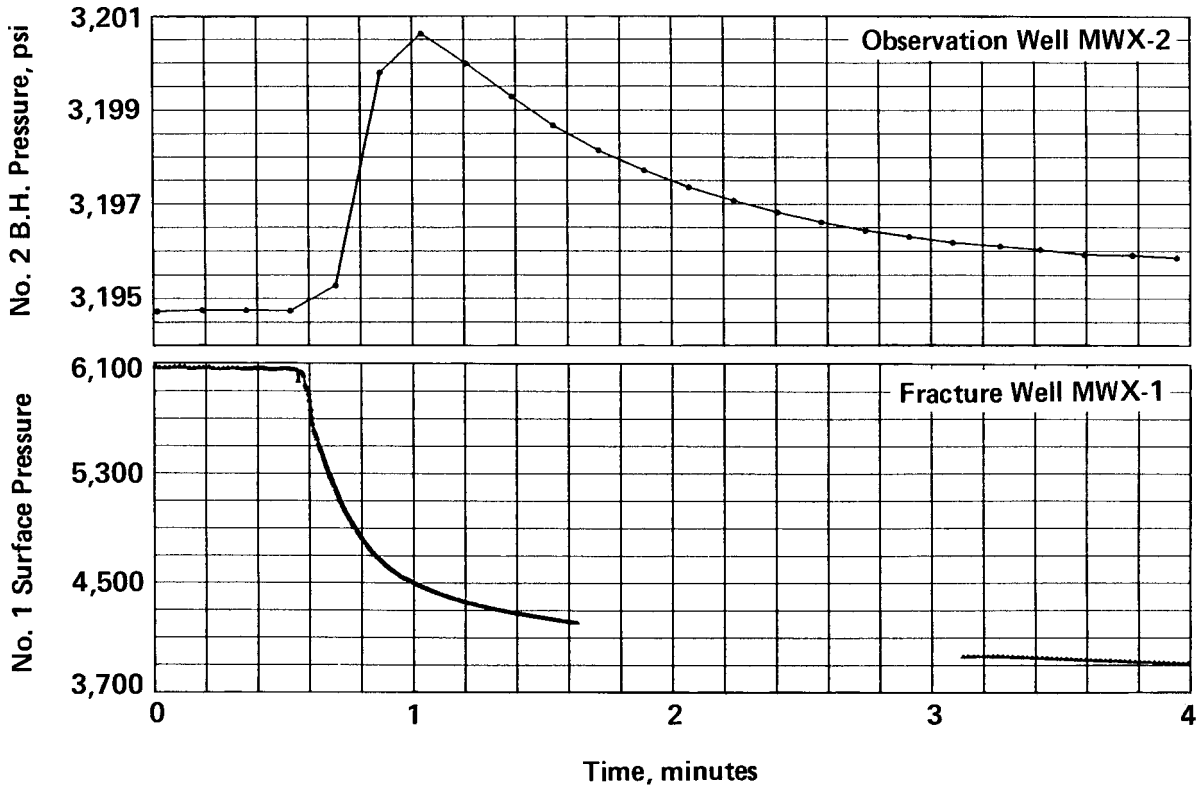

Figure 9.1.6 Expanded Pressure Records, Nitrogen Impulse

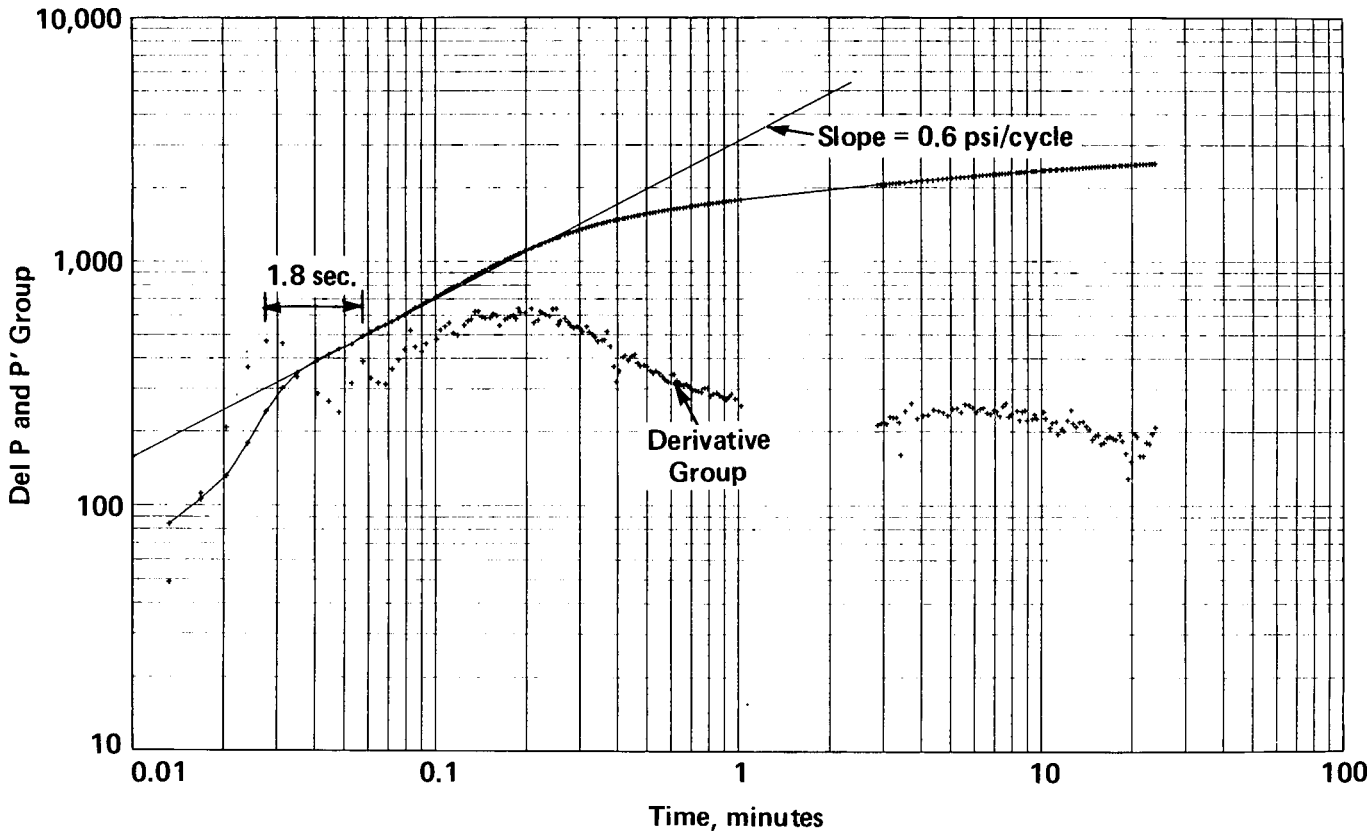

Figure 9.1.7 Expanded Pressure Records, Nitrogen Impulse

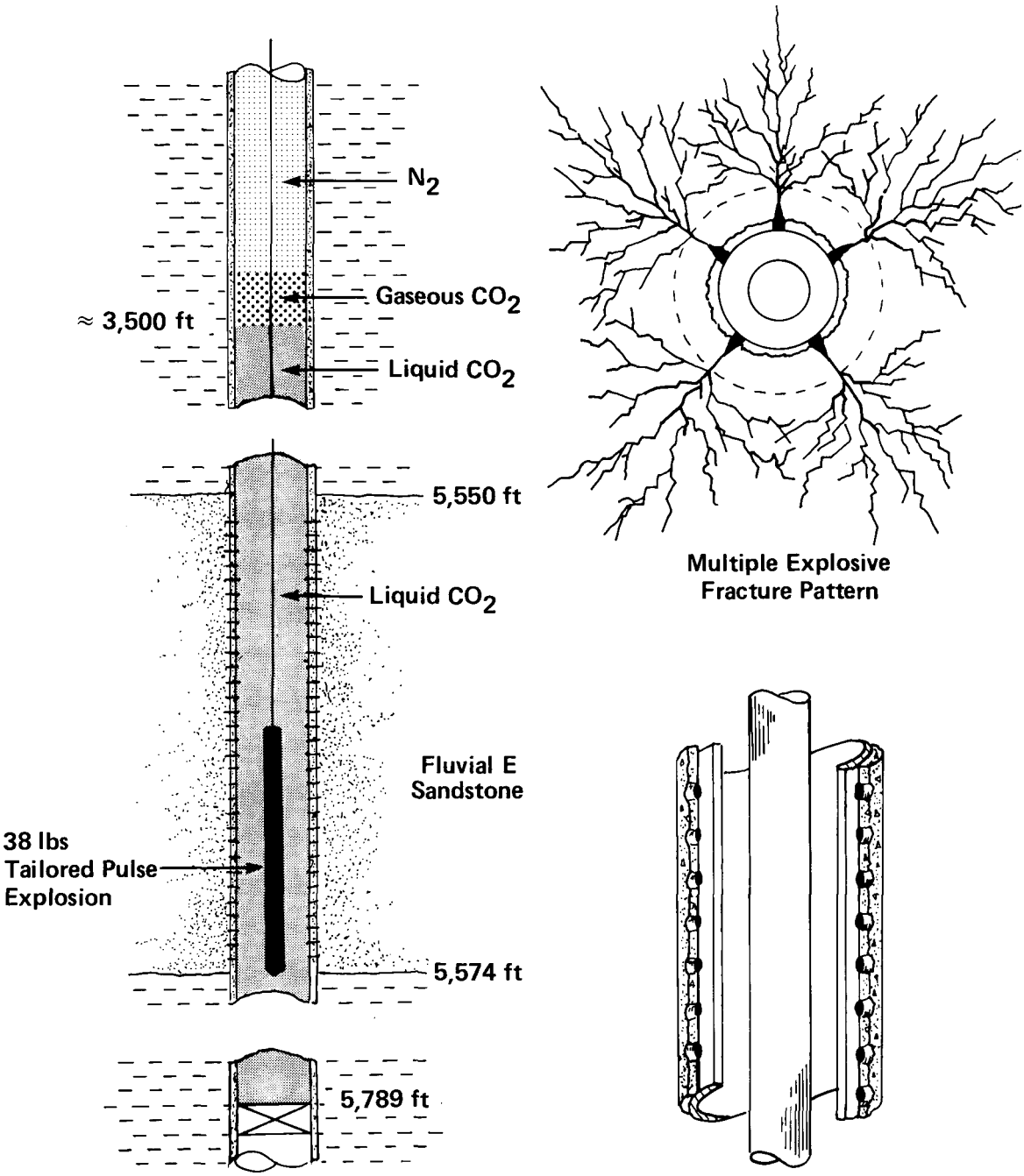

Figure 9.1.8 Tailored Pulse Fracturing

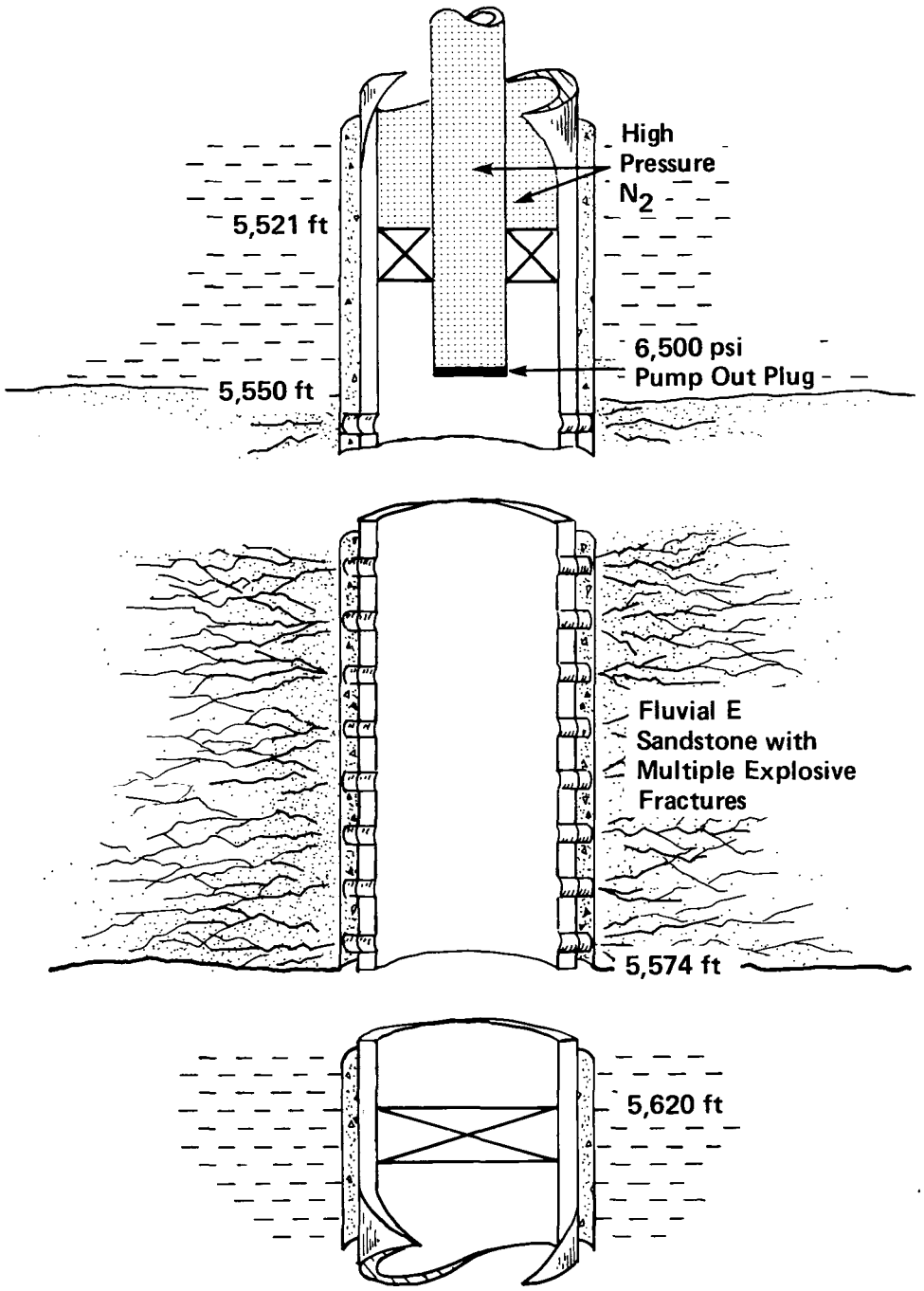

Figure 9.1.9 Nitrogen Tubing Impulse with Pump-Out Plug

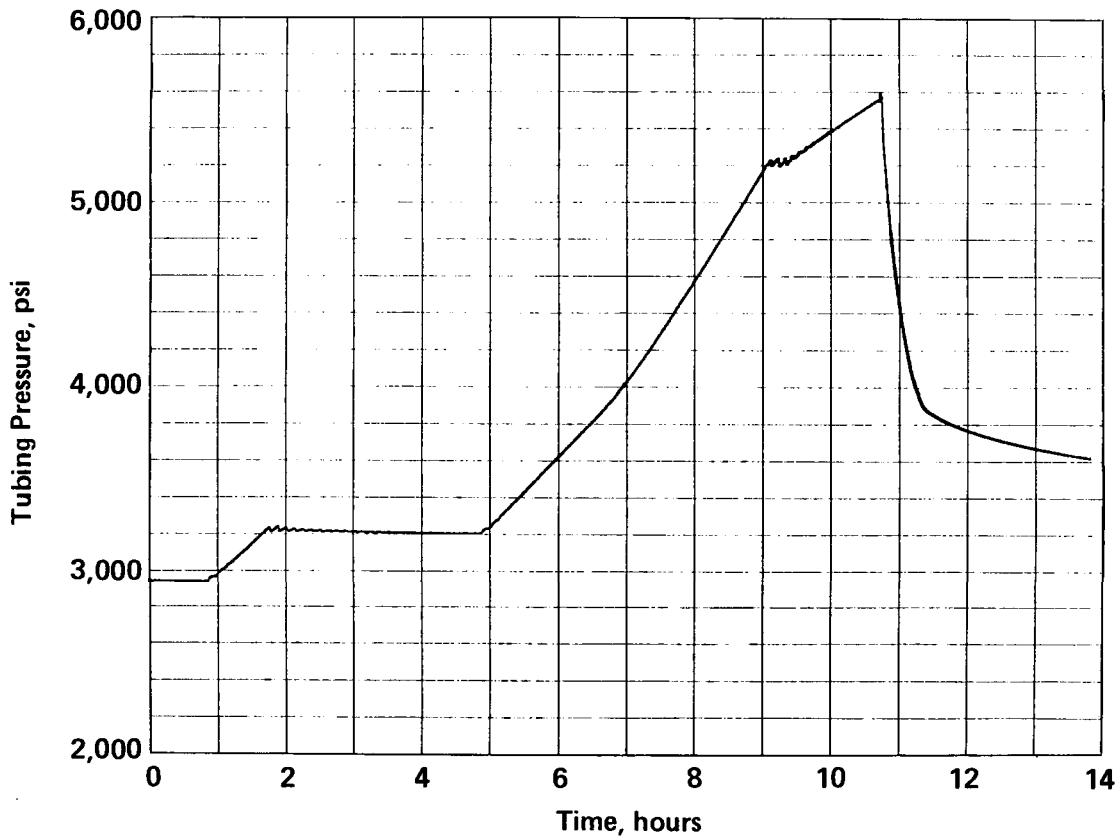

Figure 9.1.10 Nitrogen Tubing Impulse with Pump-Out Plug, Surface Pressure

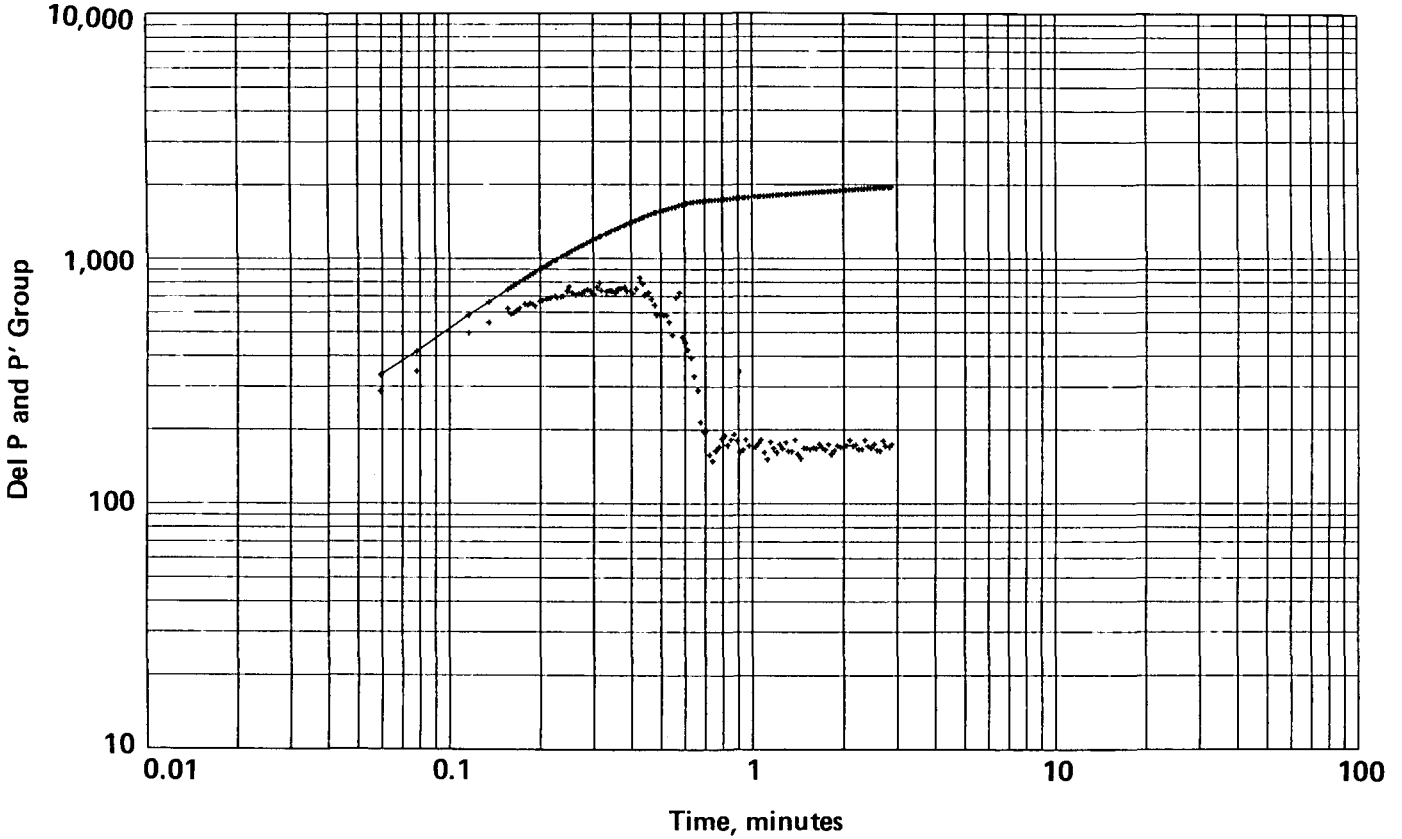

Figure 9.1.11 Nitrogen Tubing Impulse with Pump-Out Plug, Pressure Fall-Off

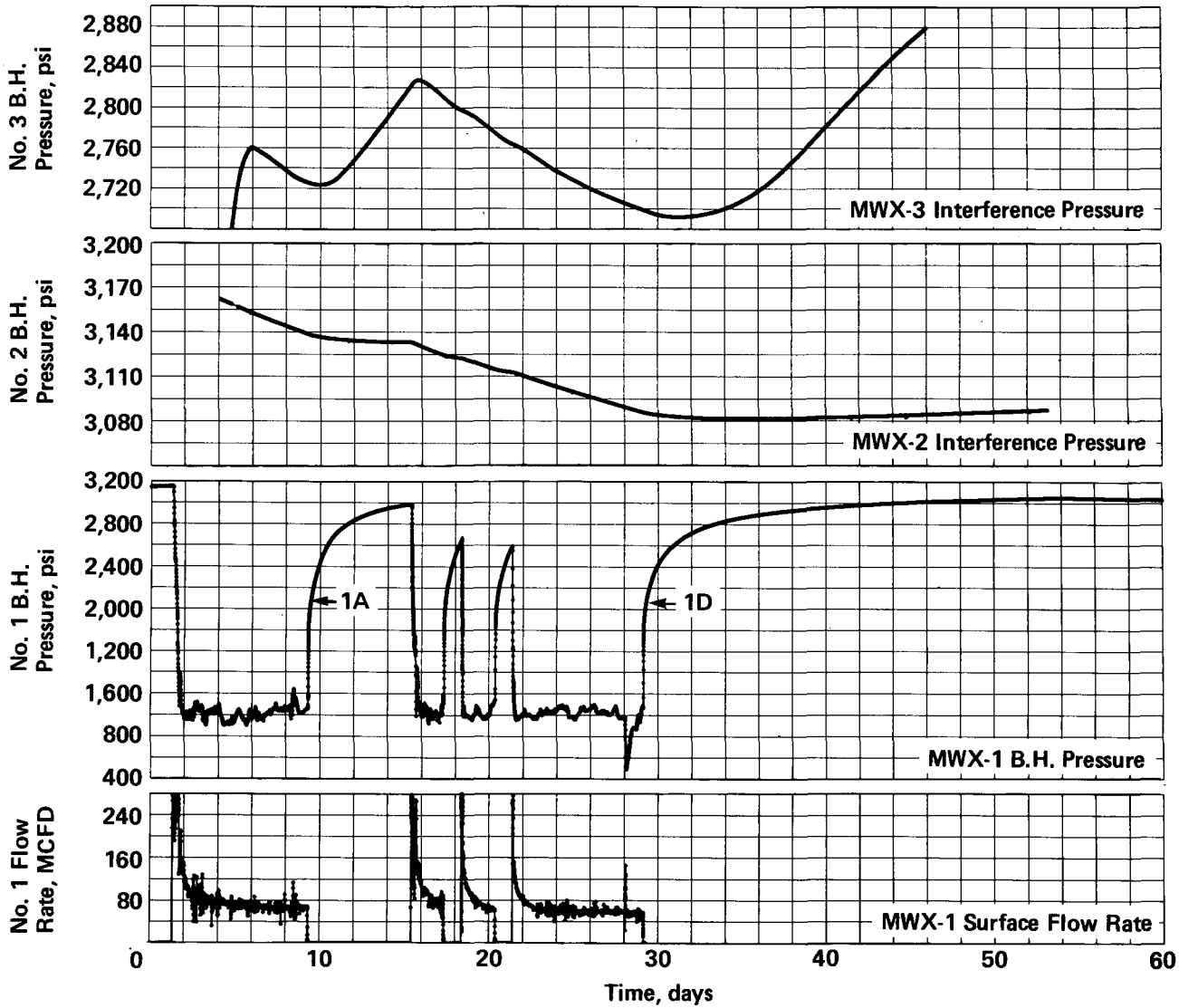

Figure 9.1.12 Flow Rate and Bottomhole Pressures; Pre-Frac Test Period

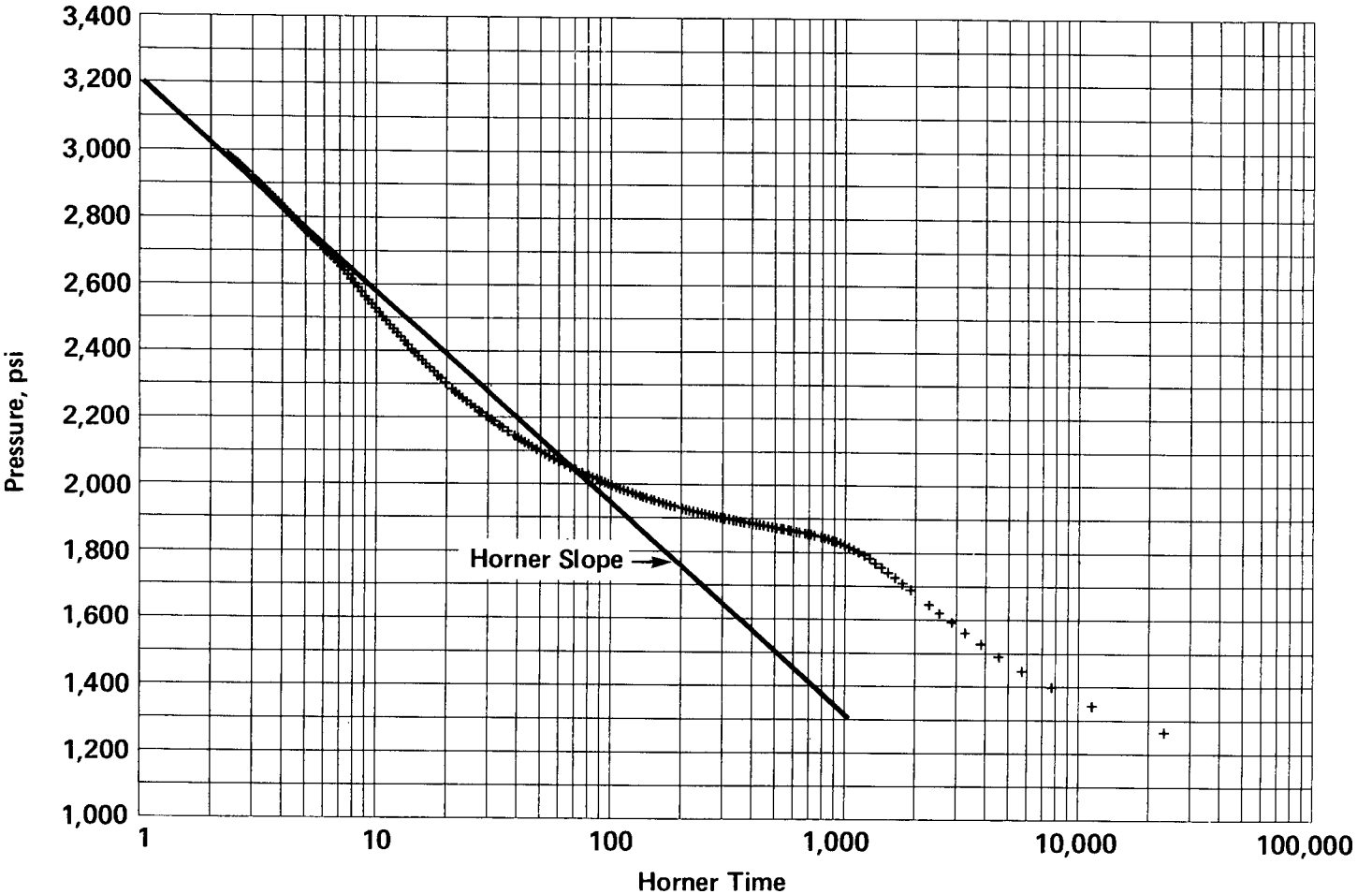

Figure 9.1.13 Initial Buildup Test, Horner Plot

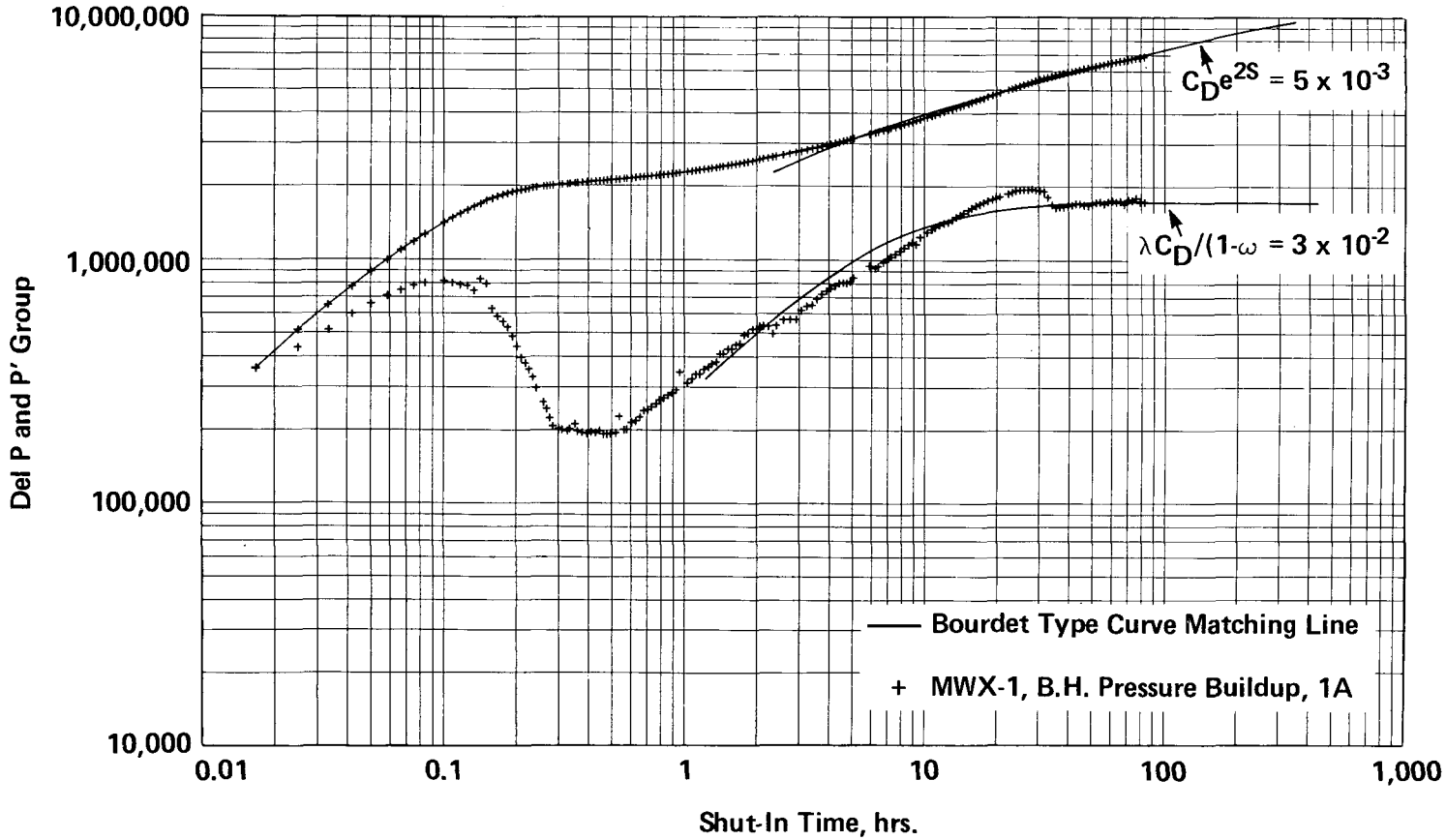

Figure 9.1.14 Initial Buildup Test, Log-Log and Derivative Plots

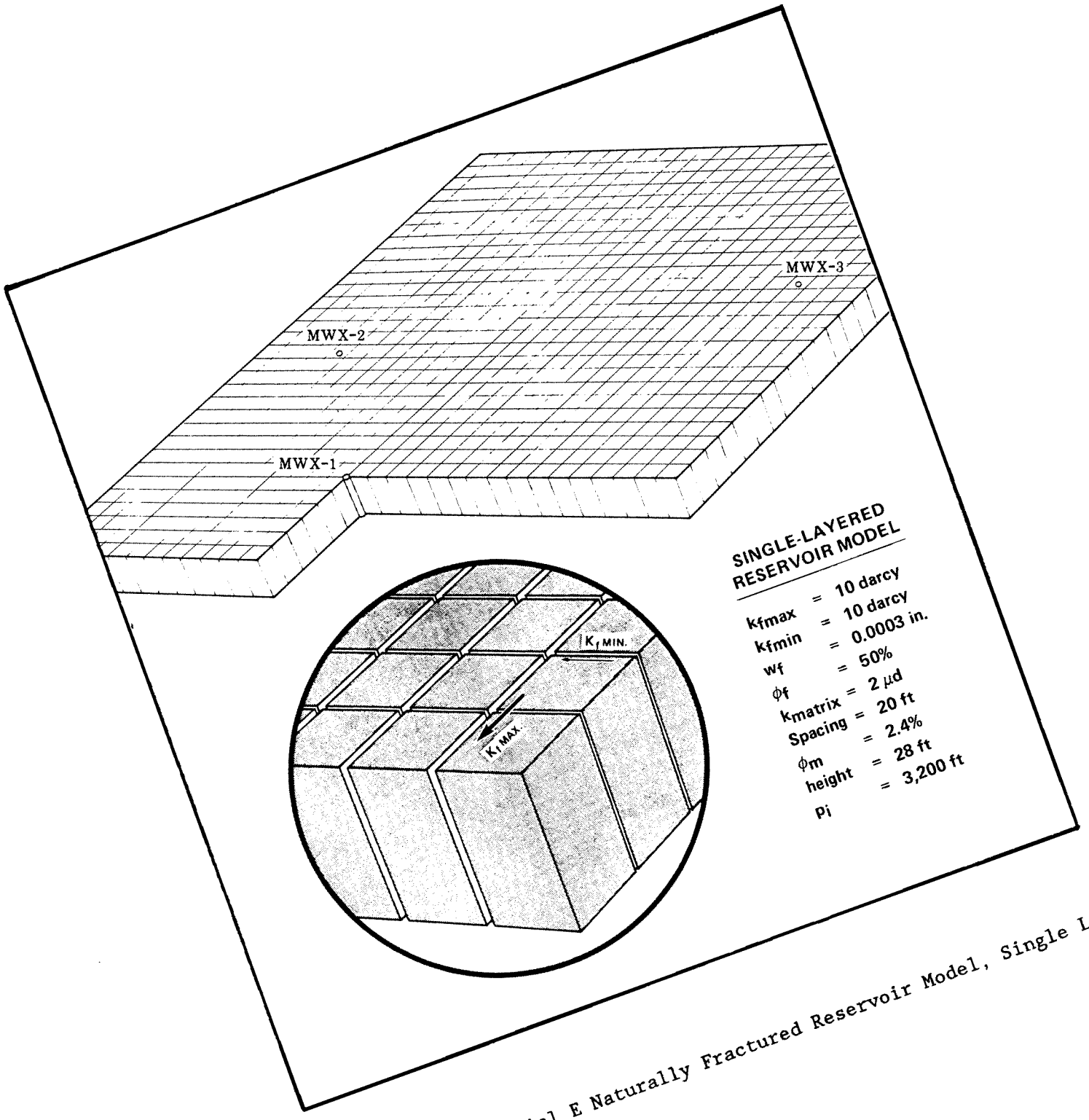

Figure 9.1.15 Fluvial E Naturally Fractured Reservoir Model, Single Layer

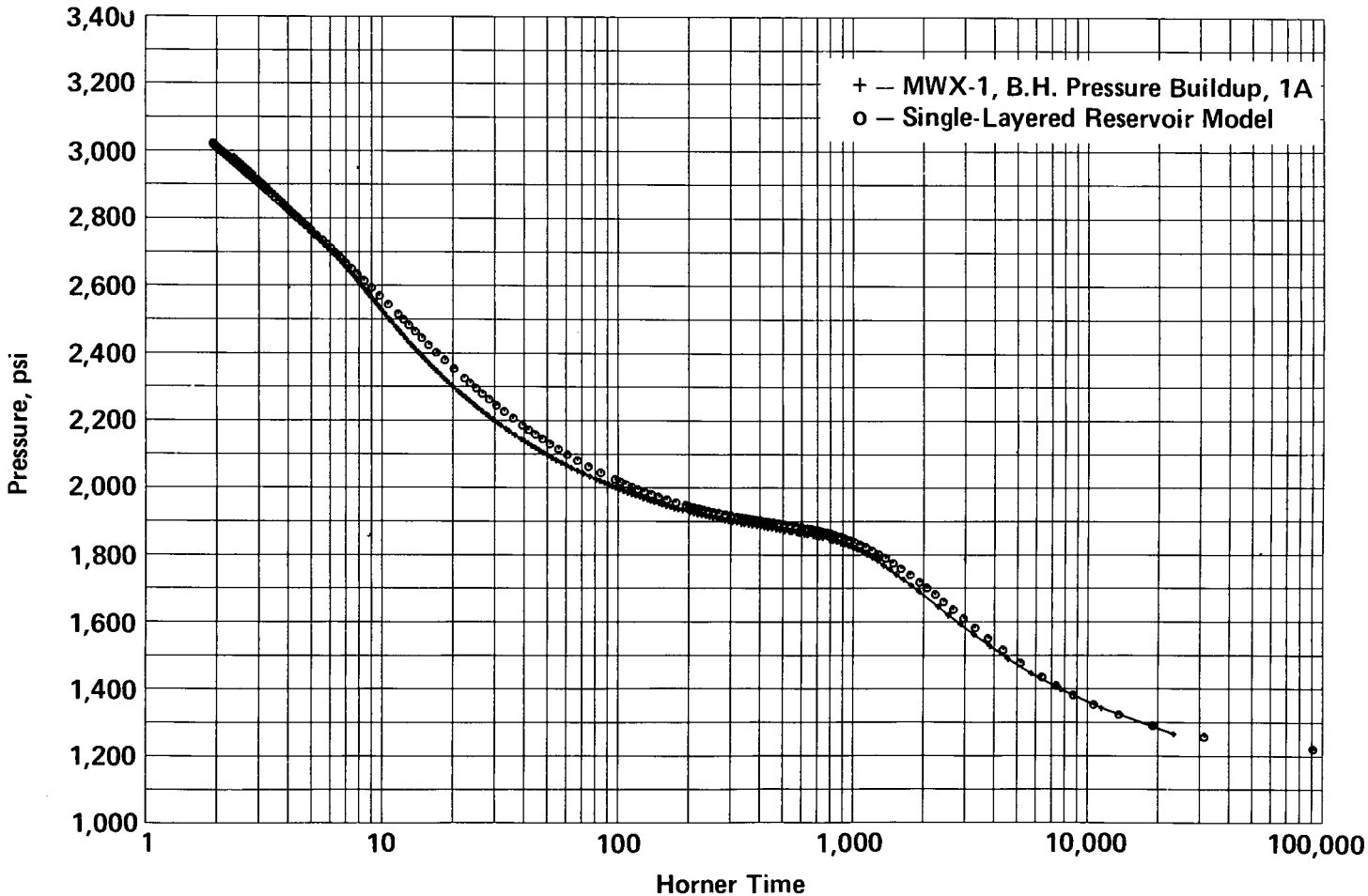

Figure 9.1.16 Comparison of Simulated and Field Pressure Data

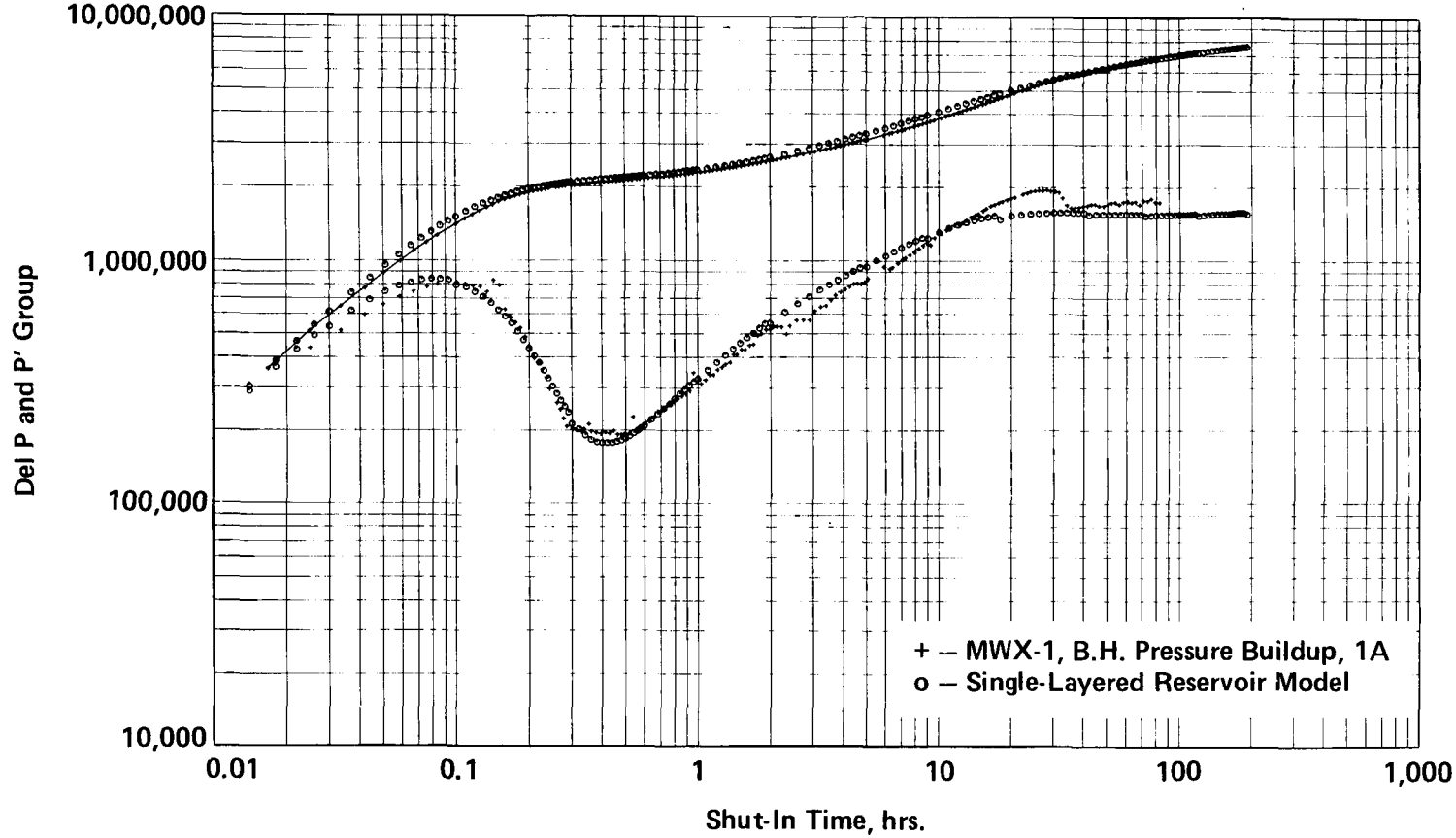

Figure 9.1.17 Comparison of Simulated and Field Pressure Data

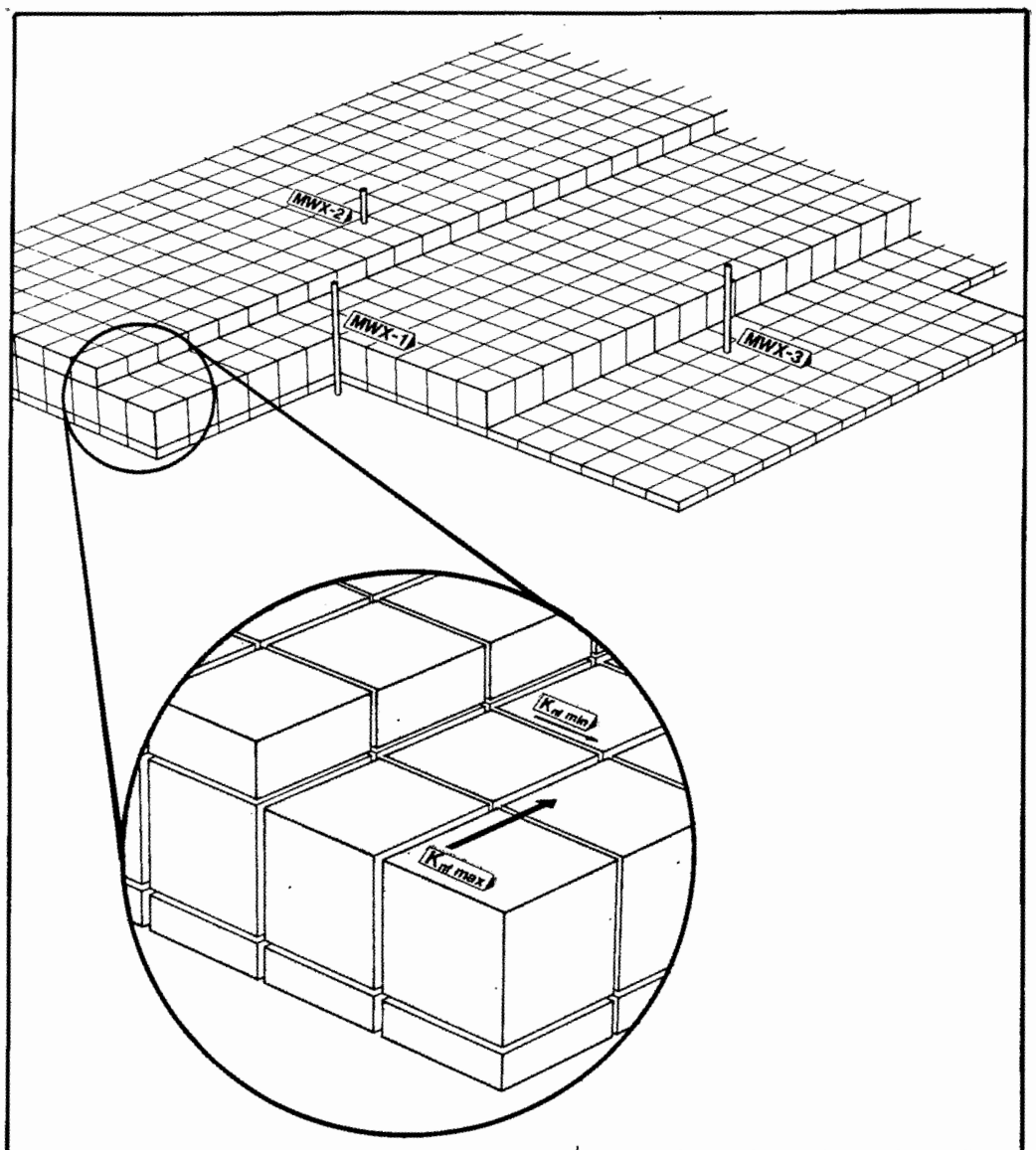

	Layer 1	Layer 2	Layer 3
k_{fmax}	165 darcy	33 darcy	80 darcy
k_{fmin}	5.5 darcy	1.1 darcy	80 darcy
w_f	0.0003 in.	0.0003 in.	0.0003 in.
ϕ_f	50%	50%	50%
k_{matrix}	2 μd	2 μd	2 μd
Spacing	20 ft	20 ft	20 ft
ϕ_m	2.4%	2.4%	2.4%
height	7 ft	24 ft	1 ft
p_i	3,200 psi	3,200 psi	3,200 psi

Figure 9.1.18 Fluvial E Naturally Fractured Reservoir Model, Multi-Layer

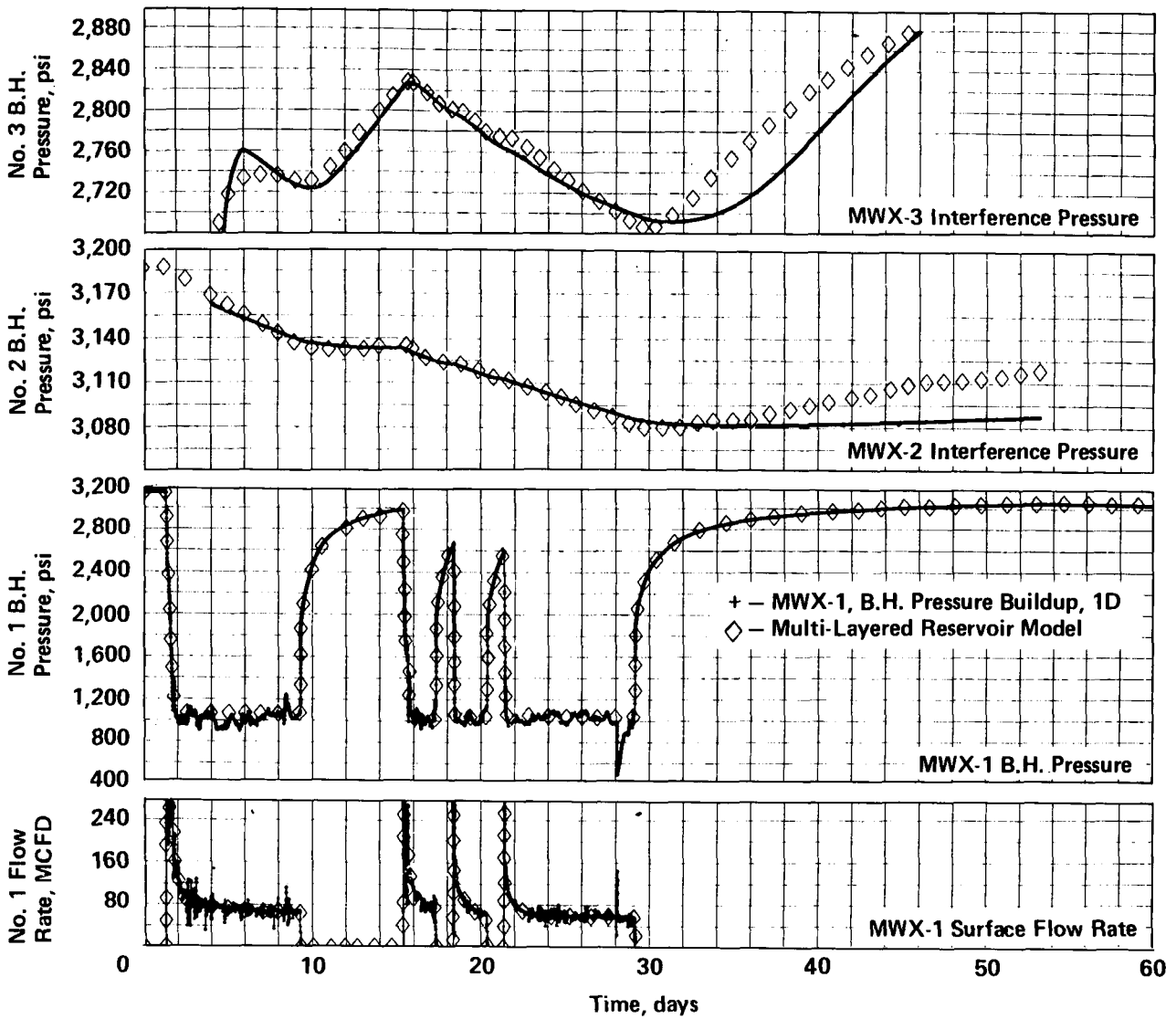

Figure 9.1.19 Comparison of Simulated and Field Flow and Pressure Data

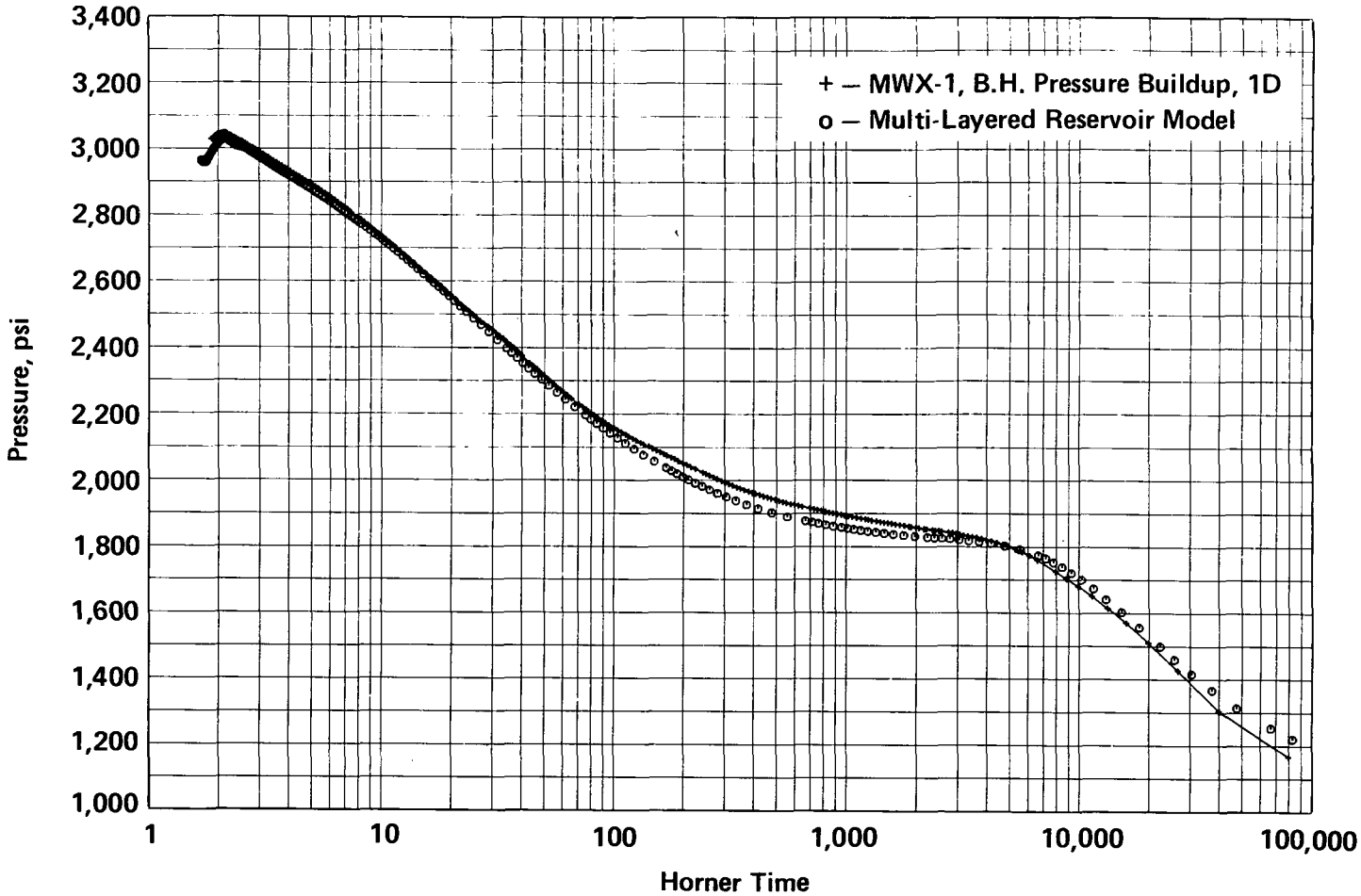

Figure 9.1.20 Comparison of Simulated and Field Pressure Data

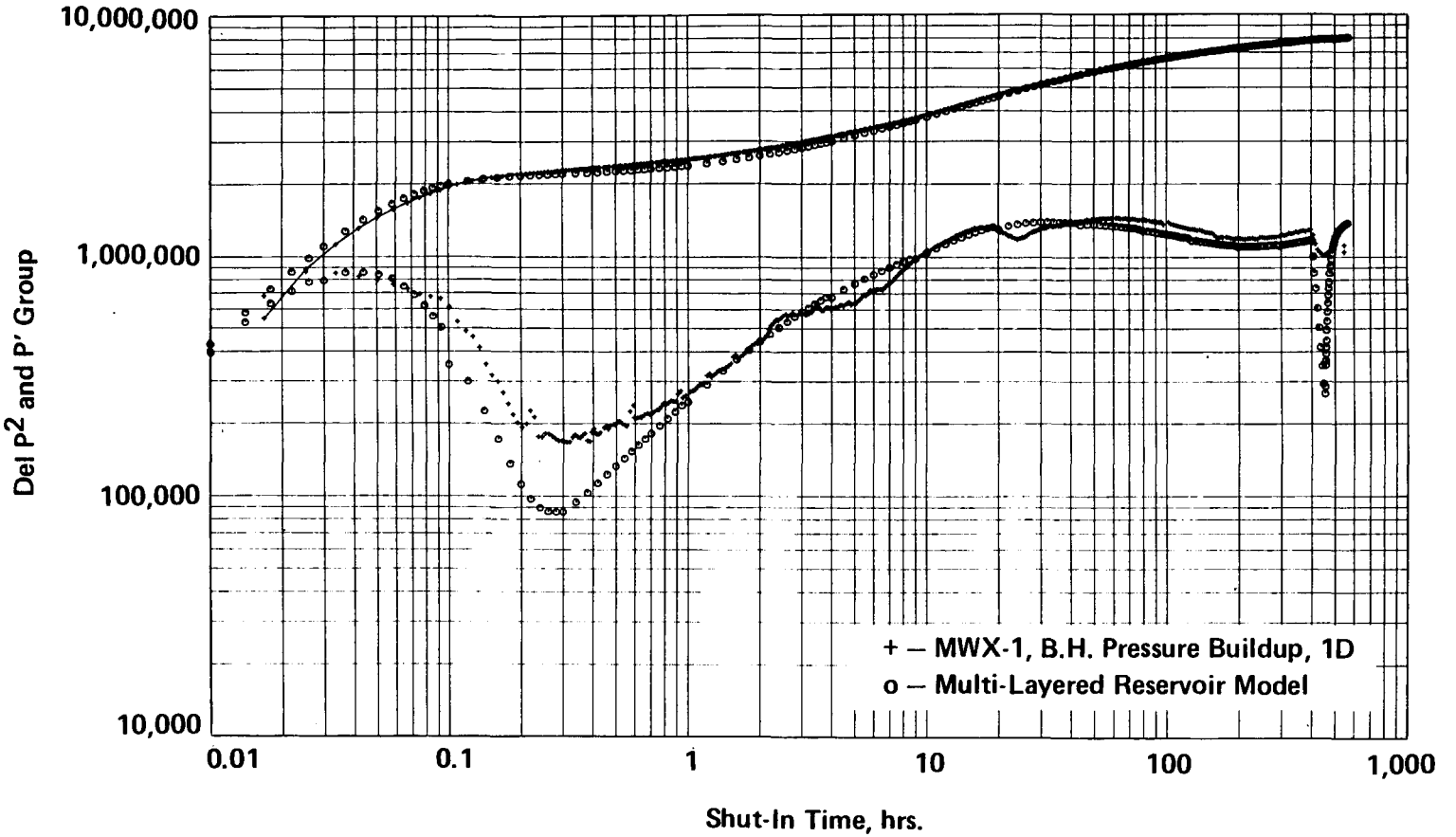

Figure 9.1.21 Comparison of Simulated and Field Pressure Data

FLUVIAL E SANDSTONE STIMULATION EXPERIMENT

9.2 STIMULATION AND ANALYSIS

N. R. Warpinski
Sandia National Laboratories

9.2.1 OBJECTIVE

During September, 1987, a stimulation experiment was conducted in the fluvial E sandstone. This experiment consisted of pump-in and flow-back tests conducted on September 10 and 11, a nitrogen foam minifrac on September 12, and the stimulation treatment on September 23. The objective of this experiment was to successfully stimulate a fluvial lens without screening out and with minimum damage to the natural fracture system. Fine, 100-mesh sand was used to control the accelerated leakoff that was observed in the two previous fluvial zones, and a new breaker system was employed to minimize damage.

9.2.2 BACKGROUND

The fluvial zone of the Mesaverde in the Piceance basin is the nonmarine interval with the largest lenticular reservoirs[1] and, thus, the greatest potential for gas production. In addition, at MWX the greatest number of natural fractures are observed in the lower part of the fluvial. Testing of the fluvial zone began with a stimulation experiment in the fluvial B sandstone at about 5830 ft. The results of this experiment were disappointing, in large part because of a screenout that occurred only a few minutes after sand entered the perfs. Subsequent analysis (see Section 7.2) of this experiment suggested that the reason for the screenout was an intensified leakoff condition that occurred above a threshold pressure, with leakoff increasing by a factor of 50. The intensified leakoff is probably a result of the large number of natural fractures in this zone.

A limited experiment (see Section 8.1) was then conducted in the C sandstone at about 5720 ft to investigate the intensified leakoff and determine if it could be stopped with 100-mesh sand. 100-mesh sand was

chosen as the optimum leakoff additive because the natural fractures were also the primary gas production mechanism and additives that would totally plug the natural fractures were unacceptable. Two minifracs were conducted in the C sandstone, the first one using nitrogen foam. This first minifrac showed that the intensified leakoff condition was present in the C sandstone, at a threshold pressure about 875 psi above closure; it also showed that fracture containment was not as good as previous tests and fracture height growth occurred. The second minifrac, a nitrogen foam treatment with four stages of 100-mesh sand, resulted in more normal fracture behavior, with the 100-mesh sand reducing leakoff by a factor of 3-4. The 100-mesh sand also appeared to limit height growth. However, when the 100-mesh sand was stopped and a nitrogen foam overflush was injected, the positive effects of the 100-mesh sand appeared to fade away. Analyses of the pressure declines from both minifracs also suggested that the leakoff after shut-in was about a factor of two greater in the second treatment, possibly because the 100-mesh sand provided added conductivity in the natural fractures. The end result was the 100-mesh sand appeared to provide several favorable properties: reduced leakoff, limited height growth, and increased natural fracture conductivity near the hydraulic fracture.

These results were then used in a full-scale stimulation experiment in the E sandstone at about 5550 ft. The E sandstone is the thickest sandstone in the naturally fractured, lower fluvial interval.

9.2.3 RESERVOIR DATA

As shown in Figure 9.2.1, the E sandstone is a 24- to 35-ft-thick sand that is seen in all three wells. In MWX-1, the production well, the gross sand thickness is about 28 ft with 5-7% porosity and 50% water saturation. It is a meanderbelt sandstone (see Section 3.0) with a clear fining-upward trend. Complete core was only obtained in MWX-1, so only a gross estimate of meanderbelt width of 1800 ft is possible. A best estimate of lens dimensions and orientations is shown in Figure 9.2.2. The hydraulic

fracture azimuth[2] in this zone is about N80°W based on anelastic strain recovery data, and about N67°W based on differential strain curve analysis.

The best estimate of rock and reservoir properties is given in Table 9.2.1 and additional information is compiled in Section 5.0.

The 13-μd effective permeability is an average system permeability determined during prefrac interference testing. The reservoir is actually an anisotropic, naturally fractured flow system with the primary permeability direction nearly the same as the hydraulic fracture orientation.

Nineteen mineralized fractures (see Section 3.4) were observed in E sandstone core, with the majority of them vertical with strikes from N65°W to N75°W. However, one fracture had a strike of N35°W, four fractures were nearly horizontal, and two fractures were shear fractures. These data suggest that the natural fracture system in this interval may be more interconnected than previous zones.

The well testing also indicated a more interconnected fracture system. Interference pulses were observed in both observation wells (a first for the nonmarine section at MWX) and rates of about 65 MCFD were sustained, compared to less than 20 MCFD in the B sandstone.

Young's modulus of the E sandstonestone is 4.7×10^6 psi and Poisson's ratio is 0.16. The mudstone below the E sandstone has a Young's modulus of 3.58×10^6 and a Poisson's ratio of 0.13. No other rock property data are available.

The in situ stresses in the fluvial, as determined with small volume hydraulic fractures in MWX-2 are shown in Figure 9.2.3. Stress contrasts around the E sandstone are generally about 600-700 psi, and are much less than around the B sandstone or in the coastal and paludal zones. Notice that slightly higher in the section the stress contrasts decrease to only a

couple of hundred psi. The stress in the E sandstone is deduced from the pump-in and flow-back tests given in this analysis. No stress tests were possible in the E sandstone. The stress in the F sandstone was measured to be 4520 psi, while the stress in the C sandstone was 4575 psi. Closure stress in the E sandstone is 4550 psi, as will be shown later.

Figure 9.2.4 shows a containment calculation, assuming the stresses in MWX-1 are similar to those in MWX-2. Good fracture containment will occur for treating pressures below 600 psi above closure (5150 psi). Above this pressure level, fracturing into the F sandstone and above is likely.

9.2.4 WELLBORE CONFIGURATION

The wellbore configuration for these tests is shown in Figure 9.2.5. A bridge plug was set at 5610 ft with sand on top to 5600 ft. The zone was perforated from 5535-5565 ft with two shots/ft, using 19-gm, 0.43-in.-diameter, 120° phasing perforations. The perforations were broken down by pressurizing the annulus with nitrogen to 7000 psi bottom-hole and perforating under this pressure (Section 9.1.3.3). This appeared to give an excellent perforation breakdown with no liquids. Tubing was landed open ended at 5452 ft with a bottom-hole pressure/temperature gage at about 5400 ft in the tubing. Treatment fluids were injected down the annulus.

9.2.5 FRACTURE DESIGN

The purpose of this stimulation was to create a propped hydraulic fracture of about 750-ft length with minimum damage to the natural fracture system, using 100-mesh sand to control the intensified leakoff. To minimize liquids and possible liquid damage, a 75-quality nitrogen foam with 20 lb/1000 gal Xanthan gum gel in the water phase was chosen. A new breaker system was also developed by Dowell-Schlumberger and a 75-quality foamed water/breaker prepad was added to enhance gel break. The design for the minifrac is given in Table 9.2.2.

The total flow rate is about 23 bpm at bottom-hole pressure and temperature conditions. The purpose of the nitrogen pump-up stage is to displace any residual water out through the perfs and to get the wellbore up to a high enough initial pressure that the foam in the tubulars will be stable.

The design for the main frac is given in Table 9.2.3. The first pad is straight 75-quality foam while the second pad contains 0.5-ppg 100-mesh sand to start plugging natural fractures (and possibly controlling height growth). When the intermediate strength proppant stages are started, 100-mesh sand is reduced to 0.25 ppg. The use of 100-mesh through the entire job is based on the C sandstone results which showed that the effect of 100-mesh sand fades rapidly after active injection stops (Section 8.1). McDaniel and Willingham[3] show that these proportions of 100-mesh and 20/40-mesh proppant will reduce fracture conductivity by no more than a factor of two; this is insignificant in this 13-μd reservoir.

9.2.6 INSTRUMENTATION AND DIAGNOSTICS

Bottom-hole pressure and temperatures, as well as all surface flow rates, pressures, temperatures, and sand concentrations, were measured during the treatments. Figure 9.2.6 shows a schematic of the instrumentation system as given by Cipolla et al.[4] (this report is included as Appendix N). Also included in this report are the QC operations, all of the measured data, and the complete treatment operations. Not shown in Figure 9.2.6 are the bottom-hole gages. After the minifrac and the main frac, temperature logs were run to estimate fracture height, and a gamma ray log was run to locate tagged proppant. During all injections, borehole seismic units were positioned at depth in the offset wells to try to locate microseismic events from the hydraulic fracturing process.

9.2.7 PRE-MINIFRAC INJECTION AND FLOW-BACK TESTS

Prior to the minifrac, a pump-in/shut-in, a step-rate/flow-back and three pump-in/flow-back tests were conducted in MWX-1. The injection fluid was 2.5%-KCl water. The purpose of these tests was to determine closure stress, fracturing pressures, and initial leakoff data.

9.2.7.1 Pump-in/Shut-in Test.

The pump-in/shut-in test has been found to be a good closure stress measurement technique as well as an initial leakoff indicator. KCl water was pumped into the E sandstone at 9.8 bpm for about 10 minutes, with a shut-in time of nearly 70 minutes. The bottom-hole pressure and temperature for the entire test are show in Figure 9.2.7 while the pressure and flow data during the injection and the Nolte-Smith plot[5] are given in Figure 9.2.8. Fracturing proceeds normally with the pressure increasing slightly during the injection to a maximum value of 5060 psi.

The pressure decline and a limited Nolte pressure decline type curve[6] are shown in Figure 9.2.9. Closure is so rapid that only the early time data are usable. The resultant leakoff coefficient is about 0.00077 $ft/\sqrt{min}$. This is considerably higher than the leakoff in the C sandstone with KCl water, which was about 0.0003 $ft/\sqrt{min}$, and probably is due to the better natural fracture system in the E sandstone.

Figure 9.2.10 shows a square root of time plot and the derivative of pressure with respect to the square root of time. Closure appears to occur at about four minutes after shut-in, at a pressure between 4500 and 4600 psi (the endpoints of the transition zone between the two linear segments). The G function curve, as used by Castillo[7] is shown in Figure 9.2.11. There is no clear linear portion of the G function to help choose the closure stress. The segment between two and four minutes has an average dP/dG, or P^*, of about 550 psi, which yields a leakoff coefficient of 0.00085 $ft/\sqrt{min}$.

The linearized G function curves[7] are shown in Figures 9.2.12 and 9.2.13. The 1.0 power seems to provide the best linearization of G, which would indicate that leakoff is reservoir compressibility and permeability dominated, an interesting possibility. The slope is about 0.25 which yields an M value of 4.92×10^{-7} for a leakoff coefficient of 0.00077 ft/$\sqrt{}$min at 4800 psi and 0.00084 at 5060 psi, the maximum pressure achieved. At these pressures there is no significant pressure sensitive leakoff that is evident in the pressure decline.

9.2.7.2 Step-Rate/Flow-Back Test

The step-rate test is used to determine the minimum fracturing pressure, which is an upper limit on the closure stress. The flowback immediately afterwards is used to determine the value of the closure stress, if the flowback rate is correct. Figure 9.2.14 shows the bottomohole pressure and temperature during the test. The injection data are shown in Figure 9.2.15; rate steps are from one to 9.8 bpm as the pressure increased from 4300 to 5100 psi. Linear and semilog step-rate plots are shown in Figure 9.2.16 but no clear fracture initiation rate is seen. A reasonable estimate of the minimum fracturing pressure would be 4850 psi; this is an upper limit on the closure pressure.

The flow-back data are given in Figure 9.2.17. The initial flowback rate is one bpm, but it slowly drops to nearly 0.9 bpm at 35 minutes when the pressure is well below closure. While there is an inflection in the pressure data, the exact point is difficult to discern. A five-point regression of the derivative of the bottom-hole pressure is shown in Figure 9.2.18a, but no clear closure is seen here either. A sixth order polynomial fit was also tried, and the resultant fit is the solid line through the pressure data points in Figure 9.2.17. The first and second derivatives are shown in Figures 9.2.18b and 9.2.18c, respectively. The inflection point is located at 31.7 minutes at 4445 psi, but confidence in the accuracy of this point is low because of the long linear portions of the curve between the positive and negative curvature segments.

9.2.7.3 Pump-In/Flow-Back Tests

The pump-in/flow tests are short injection pumps followed by flowbacks at various rates to determine the closure stress. The bottom-hole pressure and temperature for the first pump is shown in Figure 9.2.19 and the injection data are shown in Figure 9.2.20. The relative flattening of the Nolte-Smith plot at the end of the pump may indicate the start of some height growth.

The pressure and rate data for the flowback after the first pump are shown in Figure 9.2.21. The flowback rate drops from an initial value of 0.55 bpm to about 0.45 bpm at 40 minutes, when the pressure is clearly below closure. The five-point regression derivatives, shown in Figure 9.2.22a, and the least-square polynomial-fit derivatives shown in Figures 9.2.22b and 9.2.22c, do not indicate closure. The rate is clearly too low.

The bottom-hole pressure and temperature for the second pump-in/flow-back test are shown in Figure 9.2.23 and the injection data for this test are shown in Figure 9.2.24. The slope of the pressure during this injection appears more normal than the first pump-in/flow-back test. The flowback data after the second pump-in are given in Figure 9.2.25. The flowback rate, which starts a little over 1.5 bpm, slowly drops to almost 1.2 bpm at 30 minutes. There is clearly a slope reversal in this test, but the inflection point is again not very clear. Derivatives from five point regressions and least-square polynomial fits are shown in Figure 9.2.26. Two possible curvature reversals exist, one at about 17 minutes where the pressure is 4615 psi and another at about 24 minutes where the pressure is 4300 psi. More likely the true closure stress is somewhere in between.

The bottom-hole pressure and temperature for the third pump-in/flow-back test are shown in Figure 9.2.27 and the injection data are given in Figure 9.2.28. The flow-back data are shown in Figure 9.2.29; the flow-back rate was the maximum possible rate with the on-site flow-back valve, at an initial rate of about 1.75 bpm but dropping to 1.4 bpm at 25 minutes. No obvious inflection point can be seen in the pressure data of Figure 9.2.29

and neither can it be seen in the derivative data in Figure 9.2.30. Again, two slight curvature reversals appear to occur.

It is not clear whether the problem is the slight rate decrease during the test or something about the formation, but flow-back tests do not seem to give an accurate or reproducible measurement for the closure stresses in these tight, lenticular sands. This was also true in C sandstone experiments. The best closure stress measurement is obtained from a KCl water pump-in/shut-in test. Based on the pump-in/shut-in test and the surrounding stress tests, the closure stress was taken to be 4550 psi.

9.2.8 MINIFRAC

The purpose of the minifrac is to provide leakoff information, characterize height growth potential and determine other useful fracture parameters. The minifrac is conducted by injecting a volume that is generally about the size of the pad and then by shutting in the well and monitoring the pressure decline. The pressure decline yields useful leakoff data while the injection phase, when analyzed using a pressure-history match technique, provides height growth potential and other parameters. The operational details for the minifrac are given in Appendix N, while digitized stimulation data are presented in Appendix O.

The bottom-hole pressure and temperature for the minifrac are shown in Figure 9.2.31 and the injection data are given in Figure 9.2.32. The initial pressure behavior is due to fracturing with nitrogen gas. When the foam hits the perfs (at about 11 minutes), the pressure rises again to a new level indicative of the higher foam viscosity. The rate changes from about 18 to 26 minutes were due to problems with a nitrogen pump truck. These rate changes caused the density and pressure changes at the same time. The Nolte-Smith plot is shown in Figure 9.2.33, but it is hard to evaluate the frac behavior from this curve because of the rate changes.

The pressure decline and the Nolte type curve derived from this falloff are shown in Figure 9.2.34. The early part of the pressure decline fits the theoretical type curves well, but after a dimensionless time of about 1.2 at 4800 psi, the pressure deviates rapidly. Later data do not fit the theoretical type curves at any P* value. Assuming the early time data are correct, the P* value is about 250 psi for a leakoff coefficient of 0.00063 ft/$\sqrt{\text{min}}$. This is an order of magnitude greater than leakoff in the C sandstone.

The pressure versus G function curve is shown in Figure 9.2.35. As seen in the derivative plot, there is a short, early-time, linear portion and a late-time linear segment. The early time segment, which is probably most representative of fracture conditions, has a P* value of 340 psi, which yields a leakoff coefficient of 0.00085 ft/$\sqrt{\text{min}}$. A linearized pressure vs G function curve, shown in Figure 9.2.36, does not help much. The slope is about 3.3 in the early time segment, for an M value of 0.000024 and a leakoff coefficient of 0.00095 ft/$\sqrt{\text{min}}$ at 5000 psi (shut-in) and 0.001 ft/$\sqrt{\text{min}}$ at 5400 psi (injection).

The nonlinear pressure decline behavior may be due to many possible problems. It looks like closure behavior, but there is no way closure could occur at 4900 psi based on stress tests, pump-in/shut-in, and step rate tests. More likely, it is some dual leakoff behavior of the natural fractures or some interaction between height growth and leakoff.

9.2.9 MINIFRAC PRESSURE HISTORY MATCH

A pressure history match of the minifrac, combined with the pressure decline analysis, can provide the best possible estimate of parameters, both during pumping and shut-in. Because these fractures are generally of considerably greater length than height, a pseudo-3-D, Perkins and Kern geometry, multistage simulator is used. Input data include measured rock properties and stresses, service company rheological data, measured flow

rates (altered for bottom-hole conditions), and the base leakoff coefficient determined from the pressure decline analysis.

Figure 9.2.37 shows the final history math of the minifrac, including the nitrogen fracturing phase and the foamed water prepad. Parameters for this match are shown in Table 9.2.4.

In order to get the model calculations to turn the sharp corner at 850 psi (14 minutes), accelerated or intensified leakoff was again applied. The threshold pressure is 850 psi and the factor of increase in leakoff is 50. (See similar results in B and C sandstones, Sections 7.2 and 8.1). The pressure decrease that starts at about 17 minutes is assumed to be due to height growth into some lower stress region, possibly downward into the D sandstone. Approximately 15-30 ft of height growth, depending on how the shape factor is chosen, is needed to model the pressure decline between 17 and 26 minutes. Rate changes account for some of the pressure changes. The final fracture length is 620 ft with a height of 115-130 ft.

The relatively sharp break in the pressure at 14 minutes could also be obtained with significant height growth, but then there would be so much fluid volume in storage that the pressure decline would be very slow. As is, the initial pressure decline could not be matched with a constant fluid leakoff, which is reasonable if dilated natural fractures are closing. However, the B sandstone could be modeled with an instantaneous drop in leakoff coefficient to the base level when the pressure dropped below the threshold value, so some characteristics of the fracturing and intensified leakoff may be different for different fluvial sands. Fracturing behavior in the C and E sandstones appears to be fairly similar.

As usual, this match is by no means unique; it is only the best representation that can be made with the particular simulator using the estimated fracture parameters. The final height was chosen to agree with the geophone data for the main frac (shown later), but no total length measurement could be made. This again shows the need for diagnostic tools that can give the total fracture geometry.

Based on these results and calculations, a decision was made to use 100-mesh sand throughout the entire propped treatment to control the intensified leakoff and possibly height growth. The expected benefits of 100-mesh sand, including enhanced natural fracture permeability near the hydraulic fracture, far outweighed the factor-of-two loss in conductivity (at least for this 13-μd reservoir).

9.2.10 MINIFRAC CLEANUP AND LOGGING

Prior to the minifrac, 517 bbl of KCl water were injected into the formation and 223 bbl were recovered. During the minifrac, about 130 bbl of liquid were injected, of which 74 were flowed back within 24 hours. However, the well died and, during the following week recoveries of 15 and 12 bbl were obtained with two reverse circulations with nitrogen. This cleanup was sufficient to get the well flowing at about 30 MCFD. Total injected liquids prior to the main frac were 647 bbl; total recovered liquids were 324 bbl. This shows how easy it is to damage the natural fracture system with liquids.

Two post-minifrac temperature logs were run, but they exhibited no features that could be interpreted as fracture height. The only feature seen was the perforated interval.

9.2.11 STIMULATION

The purpose of the E sandstone stimulation was to create a propped fracture of 750-ft length without seriously damaging the natural fracture system. 100-mesh sand was used throughout the treatment to control the intensified leakoff and 75-quality nitrogen foam was used to minimize liquids. The operational details and digitized data for the stimulation are given in Appendices N and O, respectively.

The bottom-hole pressure and temperature throughout the experiment are shown in Figure 9.2.38. Initial fracturing with nitrogen and some water

occurs at about 5250 psi, while foam hits the perfs at about 12 minutes. Shut-in occurs at 49 minutes and a long pressure decline follows so treatment parameters can be estimated. More details of the injection data can be seen in Figure 9.2.39. The 100-mesh sand seems to control both the leakoff and the height growth, as can be seen by the pressure behavior after 100-mesh sand hits the perfs at about 18 minutes. The larger pressure rise occurring after 30 minutes corresponds to increased sand concentrations in the fracture. The pressure drop at about 44 minutes corresponds to a short loss of sand injection that occurred at about 36 minutes, as seen in the density plot. The rate was fairly constant throughout the test. The Nolte-Smith plot is shown in Figure 9.2.40. The results look fairly normal for these lenticular sands.

The pressure decline and the resultant Nolte type curve are given in Figure 9.2.41. The value of P^* is about 255 psi with a resultant leakoff coefficient of 0.00085 $ft/\sqrt{min}$, which is similar to the minifrac result. Plots of pressure versus the G function and dP/dG, shown in Figure 9.2.42, result in a P^* value of about 205, yielding a leakoff coefficient of about 0.0007 $ft/\sqrt{min}$. It should be noted that this is a late time P^* value for a fracture with proppant in it. If the fracture walls are closing on the proppant relatively early, then the late time data are meaningless. An early time P^* value of about 280, from about 18-32 minutes, yields a leakoff coefficient of 0.00093 $ft/\sqrt{min}$. Any of these are possible. The linearized G function curve is shown in Figure 9.2.43, but it adds no improvement over the P vs G plot of Figure 9.2.42. No estimate is made of fracture length because the intensified leakoff makes such a calculation meaningless.

Based on these results, the fracture appears to have been executed close to design. Slightly less proppant was injected than design because of a limit on total amount of intermediate-strength proppant (Proflow) available. Gel viscosities were also somewhat lower than specified.

9.2.12 STIMULATION PRESSURE HISTORY MATCH

A pressure-history-match analysis was also performed on the stimulation data, using the same model and basic parameters as were obtained from the minifrac analysis. The resultant match is shown in Figure 9.2.44. The initial 11 minutes are fracturing by nitrogen, with some slugs of water and foamed water interspersed because of foam quality control problems at the start of the job. No attempt was made to match all the features of this phase.

Fracturing with 75-quality foam starts at about 11 minutes, with an initial pad for 7-8 minutes and a pad containing 100-mesh sand for another 8 minutes. As in the minifrac, intensified leakoff occurs at about 850 psi above closure, at about 13 minutes. The one-ppg proppant stage starts at 28 minutes, the three-ppg stage at 33 minutes and the four-ppg stage at 42 minutes. However, at 43-45 minutes, the blender temporarily sanded out and a slug of foam without proppant was injected. Proppant pumping resumed for three minutes and shut-in occurred at 48 minutes.

Based on the earlier minifrac results, additional height growth was started at 18 minutes and reduction of the intensified leakoff was started at 20 minutes, just after the 100-mesh sand was injected. By the end of the job, the intensified leakoff was reduced by a factor of five, suggesting that the 100-mesh sand, along with the 20-40 mesh, was fairly effective in controlling leakoff. Most of the pressure increase after 32 minutes is due to increasing proppant concentration as the slurry dehydrates. In fact, even though the 100-mesh sand fairly effectively controlled leakoff, the concentration of the three-ppg stage reached 16-17 ppg near the three-ppg front at the end of the job. It is a good possibility that we had a screenout at the very end of the job with such high proppant concentrations.

The total length derived from this model was 885 ft, but only 490 ft was propped and only 390 ft had high sand concentrations. The height was 115-130 ft, depending on how the area shape factor is interpreted; this value was a constrained parameter based on geophone results. As with the minifrac, some artificial height features were needed to arrive at this

value. The stress test data suggest that considerable height growth will occur at relatively low pressures. Nolte has suggested[8] that the restricted height growth may be due to the yield stress characteristics of foams in the narrow fracture in the higher stress shales. This would certainly retard vertical growth if the yield stress is large enough. This match also needed a slight increase in the closure stress so these results would match the minifrac results. This may be caused by the additional two weeks of buildup and the nitrogen and fluid injected during the minifrac tests.

The only negative result that was obtained from this analysis is an apparent low conductivity spacer about 50 ft wide and 100 ft into the fracture. This spacer was the result of the sand out at the surface for two minutes during the four-ppg stage. The spacer may cut productivity from the hydraulic fracture proppant-tip region. Realistically, however, it is likely that mixing within the fracture improved the conductivity in this region.

As always, this pressure-history-match is not unique, but it does help to provide a basic understanding of the particular fracture treatment. Many of these parameters can be adjusted, within bounds, to get a slightly different result, but fracture length is not likely to vary by more than 100 ft (assuming the maximum height value is correct) and the intensified leakoff factor appears to lie between 40 and 80. Other parameters have similar bounds.

9.2.13 POST-FRAC TEMPERATURE AND GAMMA RAY LOGS

Figure 9.2.45 shows two post-frac temperature logs that were run about one-half hour apart, just after the pressure decline period. These indicate that fracture top is around 5520 ft, about 15 ft above the perforations. The fracture bottom cannot be seen. These results are somewhat questionable since these logs were run upward. Two logs run downward showed no change in temperature until well into the perforated interval. It wasn't clear whether there was a problem with the temperature tool or its ability to log

downward, or whether there was no temperature gradient until a downward run disturbed the fluid. We have always had difficulty getting good temperature logs after foam fracs.

Figure 9.2.46 shows a gamma ray log that was run after the stimulation. Some evidence of tagged proppant is clearly seen below 5520 ft and it possibly extends higher. The largest spike is seen at the bottom of the perforated interval, suggesting that significant growth may have occurred downward. Propped height near the well above appears to be at least 50 ft.

9.2.14 FLOW-BACK, CLEANUP AND PRODUCTION

Immediately after the temperature logs, the well was opened up for flowback, at a fairly constant two-bpm foam rate. Initially the flow-back was performed up the annulus until pressures dropped low enough to pull the pressure/temperature tool into the lubricator. The flowback was then switched to the tubing. Very little sand was brought back with the fluid and 127 bbl of the 286 bbl of injected liquids were recovered within 12 hours. Within two days, the well was producing 300 MCFD, dropping to 200-220 MCFD after a 16-day flow period. Of the 956 bbl of liquids injected during all fracture tests, 636 bbl were recovered.

9.2.15 SUMMARY AND CONCLUSIONS

The fluvial E sandstone stimulation experiment has probably been the most successful stimulation experiment at MWX. The fracture was conducted with only minor problems, all instrumentation functioned properly, diagnostics provided some information on fracture geometry, and production was increased from 65 MCFD to 220 MCFD. It appears that the intensified leakoff phenomenon was present again, but the 100-mesh sand controlled it very well. Propped frac length was probably 400 ft, with the possibility of a low conductivity region about 100 ft into the frac.

Fracture height growth was relatively limited, considering the low stress contrasts (~600 psi). This may be due to the complex bedding, the restricted width, the yield stress of the foam, or some combination of the above. Diagnostics indicate that total fracture height was about 120 ft.

Pressure-history-match analysis suggests that the propped length is 400 ft, based on the 120-ft height observed by the geophones. As discussed in Section 9.4, the length estimate from the geophones could be either the total length of the fracture or only as far as the geophones can detect usable signals.

The fast cleanup and resultant flow indicates that the fluid system did little damage to the natural fractures. The breaker prepad may have helped, along with avoiding the high pressures of a screenout and controlling the accelerated leakoff rate with 100-mesh sand.

This experiment shows how important a careful prefrac characterization is to the final results. The B sandstone, with no cross fracture set, produced about 15-18 MCFD prefrac and 25-30 MCFD postfrac (admittedly with some operational problems during stimulation) compared to 65 MCFD and 220 MCFD in this zone. Two reservoirs which are relatively close (325 ft) performed completely differently. The key, of course, is the natural fracture system. These submicrodarcy rocks would never produce without the aid of the natural fractures, but the natural fractures are still very marginal if they only bring the effective permeability to 13 μd. Recognizing the characteristics of the fracture system and avoiding any damage to these fractures is very important for successful stimulation and production.

9.2.16 REFERENCES

1. Lorenz, J. C. and Finley, S. J., "Differences in Fracture Characteristics and Related Production of Natural Gas in Different Zones of the Mesaverde Formation, Northwestern Colorado," SPE 16809, proceedings of 62nd Annual SPE Technical Conference, Dallas, TX, September 27-30, 1987.

2. Warpinski, N. R. and Teufel, L. W., "In Situ Stresses in Low Permeability, Nonmarine Rocks," SPE 16402, proceedings SPE Symposium on Low Permeability Reservoirs, Denver, CO, pp 125-138, May 18-19, 9187.

3. McDaniel, R. R. and Willingham, J. R., "The Effect of Various Proppants and Proppant Mixtures on Fracture Permeability," SPE 7573, proceedings 53rd SPE Annual Fall Technical Conference, Houston, TX, October 1-4, 1987.

4. Cipolla, C., R. Wilmer, D. Cowley, and D. Ferguson, "Multiwell Experiment Fluvial E Fracturing Operations Quality Control and Monitoring Results," CER Corporation Report, October 16, 1987.

5. Nolte, K. G. and M. B. Smith, "Interpretation of Fracturing Pressures," JPT, Vol. 33, No. 9, pp 1767-1775, September, 1981.

6. Nolte, K. G., "A General Analysis of Fracturing Pressure Decline with Application to Three Models," SPE Formation Evaluation, Vol. 1, No. 6, pp 571-583, December 1986.

7. Castillo, J. L., "Modified Fracture Pressure Decline Analysis Including Pressure-Dependent Leakoff," SPE 16417, presented at SPE/DOE Low Permeability Reservoirs Symposium, Denver, CO, pp 273-281, May 18-19, 1987.

8. Nolte, K., personal communication.

Table 9.2.1

E Sandstone Reservoir Data

Bottom-Hole Pressure	3200 psi
Bottom-Hole Temperature	160°F
Matrix Permeability	0.1-1.0 μd at 2000 psi and 50% S_w
Effective Permeability	13 μd from well tests
Porosity	5%-7%
Water Saturation	50%
Young's Modulus	4.7×10^6 psi
Poisson's Ratio	0.16

Table 9.2.2

Minifrac Design

Stage	Fluid	Volume (gal)	N_2 Rate (SCFM)	Liquid Rate (bpm)
Pump-up	N_2	-	25000	0
Prepad	Foamed H_2O	2000	25000	5.7
Minifrac	Foam	10000	25000	5.7
Flush	Foam	7800	25000	5.7

Table 9.2.3

Stimulation Design

Stage	Fluid	Volume (gal)	Proppant (ppg)	Rate (BPM)	100-Mesh-Sand (ppg)
Pump-up	N_2	-	-	17	-
Prepad	Foam H_2O Breaker	4000	-	23	-
Pad 1	Foam	6000	-	23	-
Pad 2	Foam	8000	-	23	0.50
1	Foam	5000	1	23	0.25
2	Foam	9000	3	23	0.25
3	Foam	10000	4	23	0.25
Flush	Foam	7800	-	23	-

Total Volume Injected	42000 gal
Total Volume Pumped	49800 gal
Total 20/40 Proppant (Proflow)	72000 lb
Total 100-Mesh Sand	10000 lb

Table 9.2.4

Parameters for History Match

Stage	n'	k' (lb-sec$^{n'}$/ft^2)	C ft/$\sqrt{\text{min}}$
Water	1	0.00001	0.005
Nitrogen	1	0.00000052	0.011
Foamed Water	0.6	0.0015	0.002
Foam	0.5	0.01	0.0008

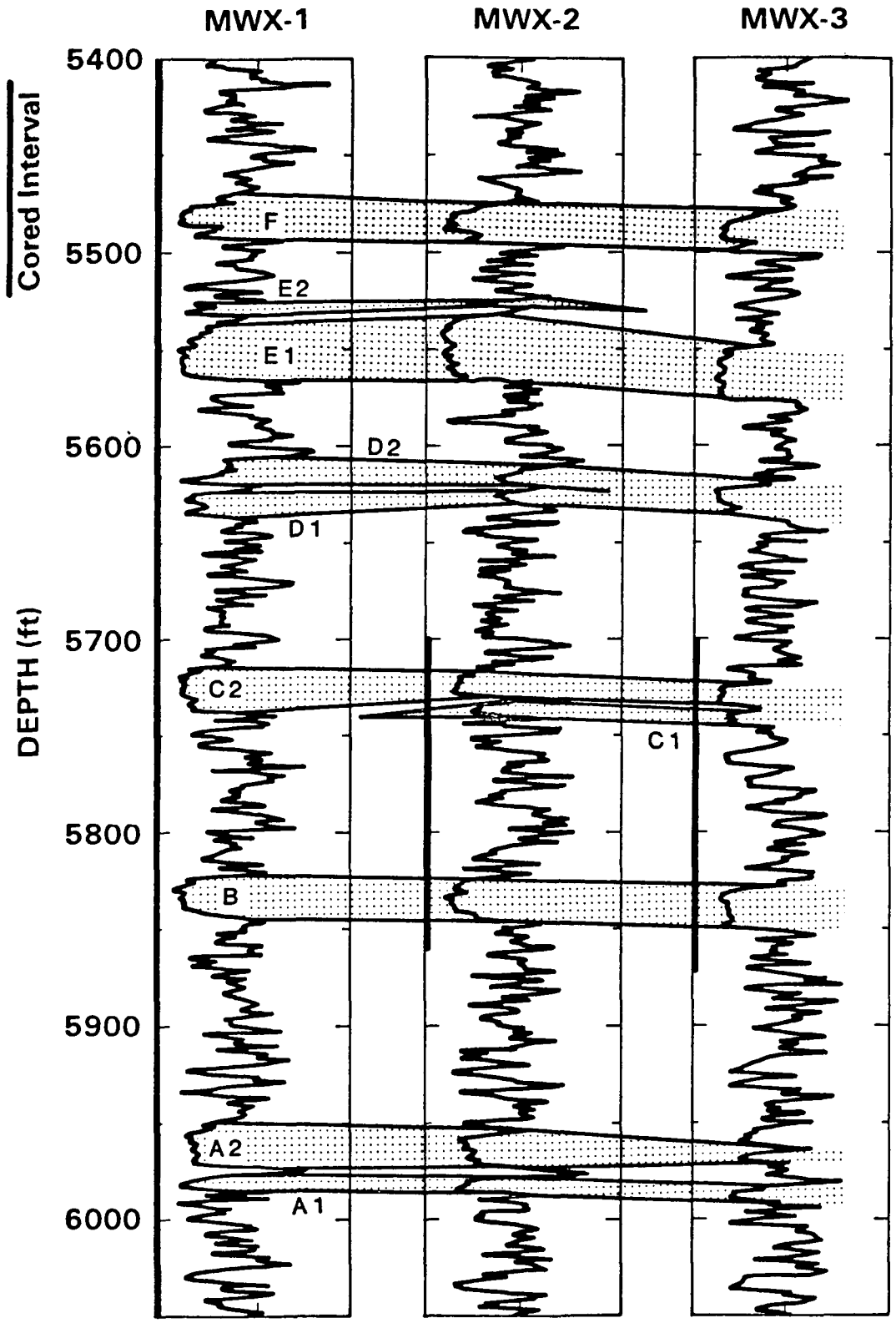

Figure 9.2.1. Fluvial Lithology

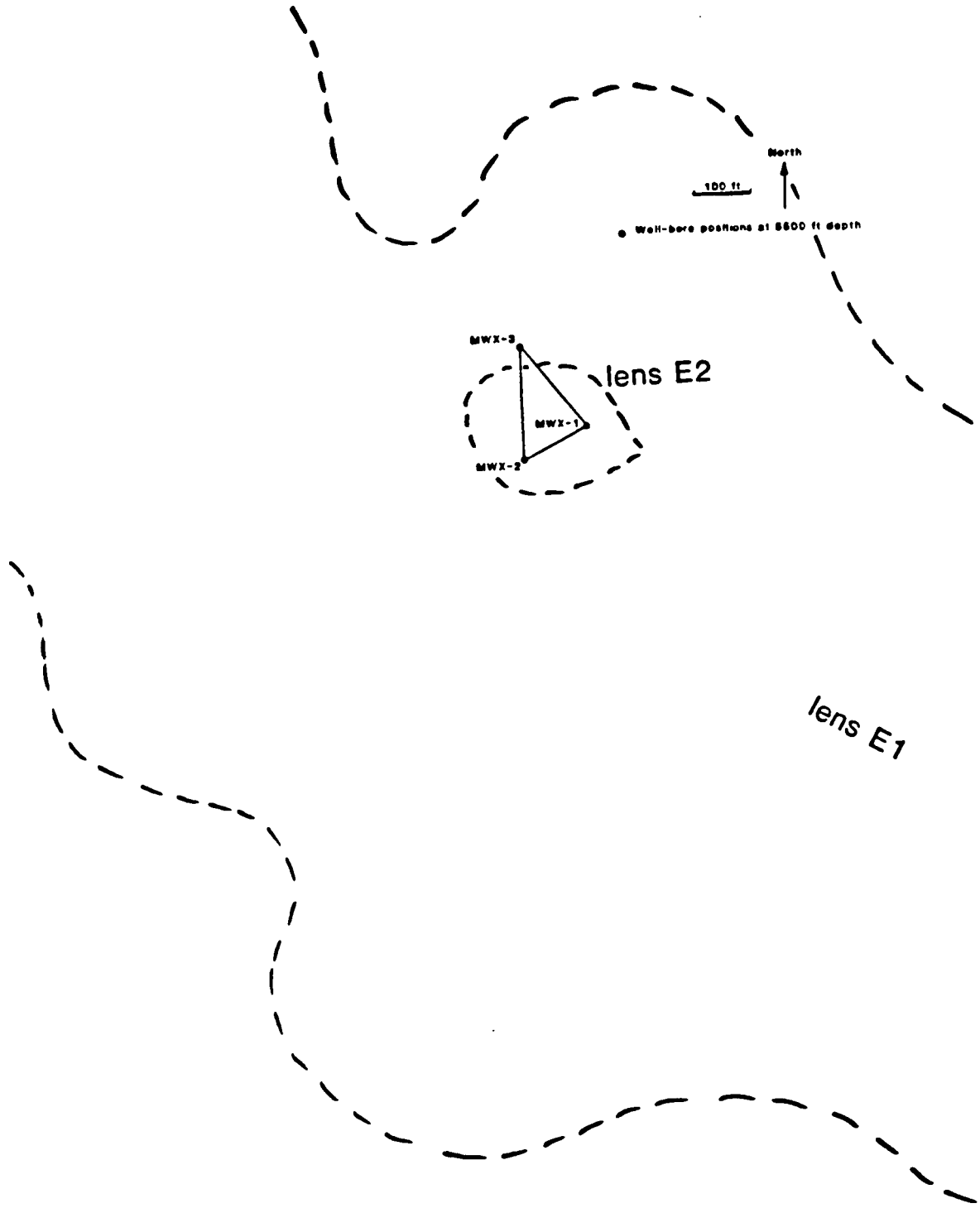

Figure 9.2.2. Estimated Lens Size and Orientation of E Sandstone

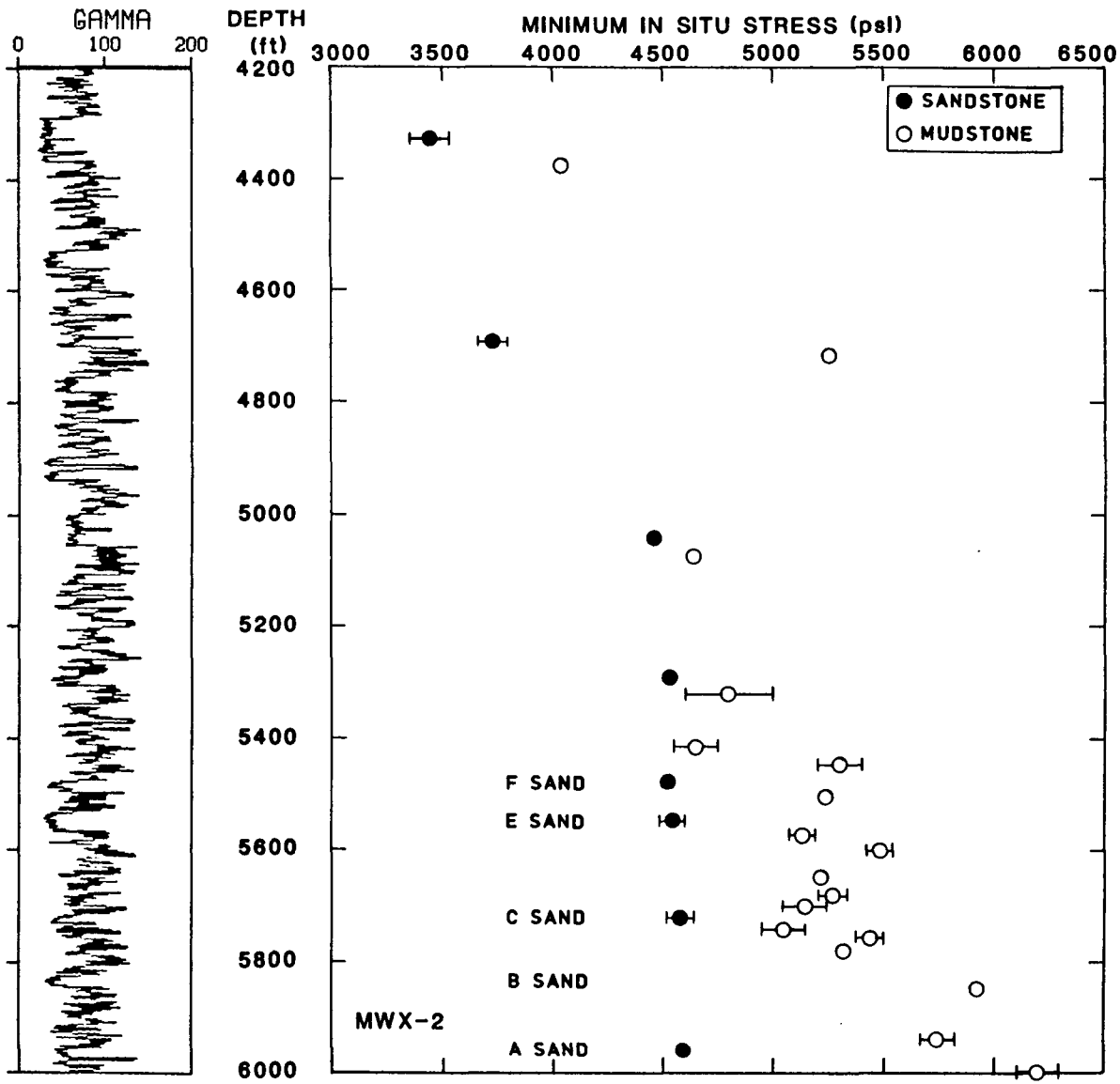

Figure 9.2.3. Measured Stress Distribution

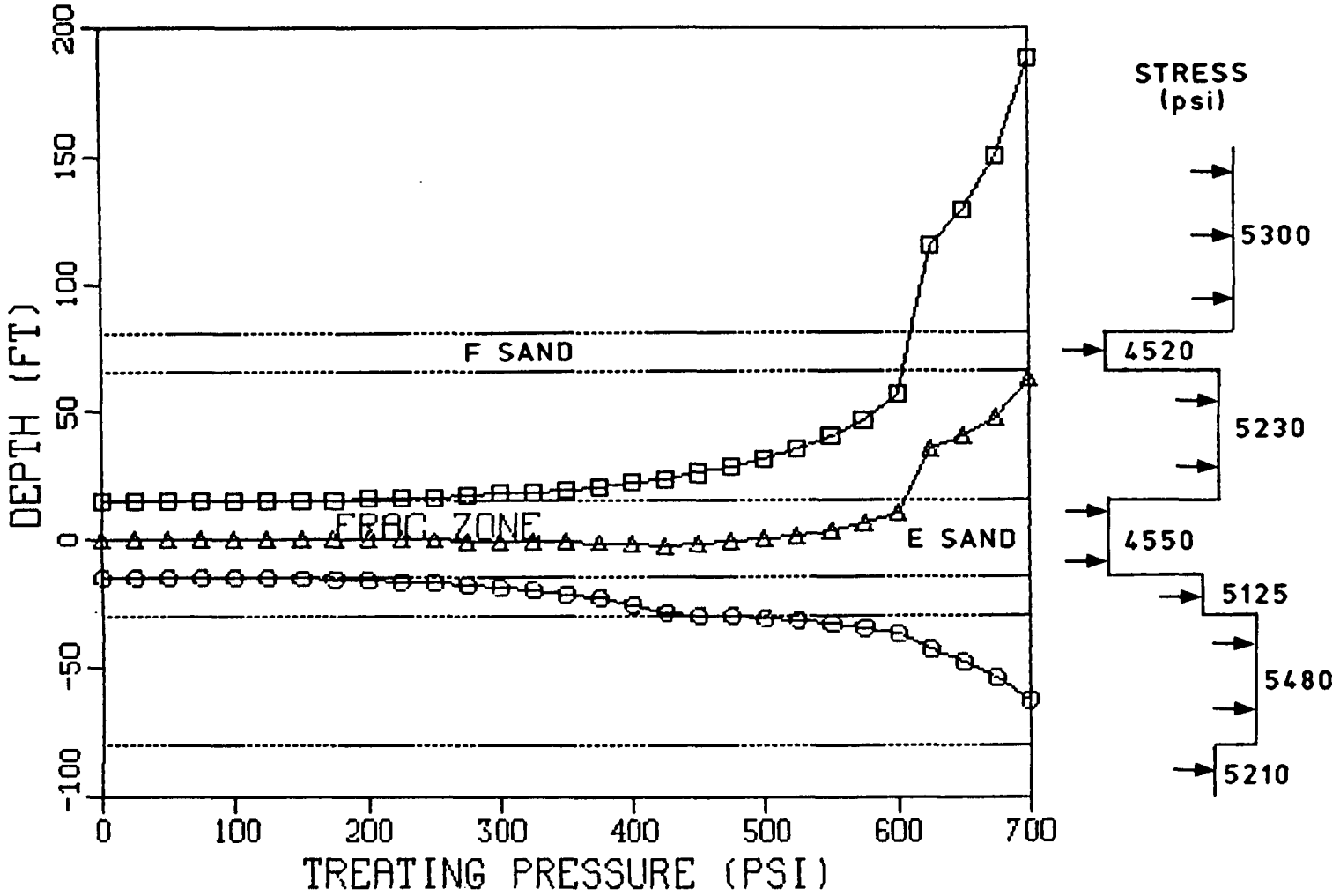

Figure 9.2.4. Calculated Stress Containment

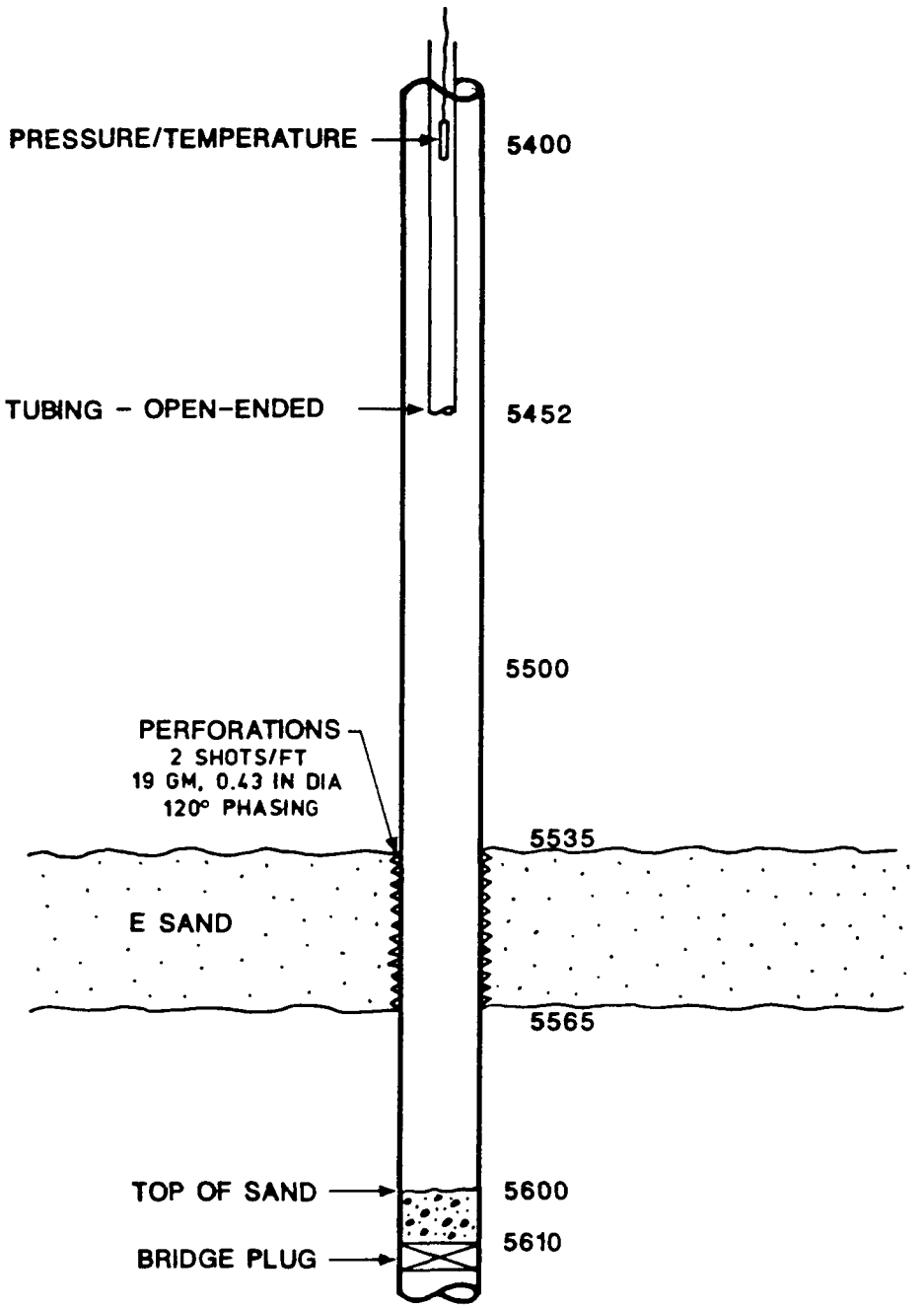

Figure 9.2.5. Wellbore Configuration

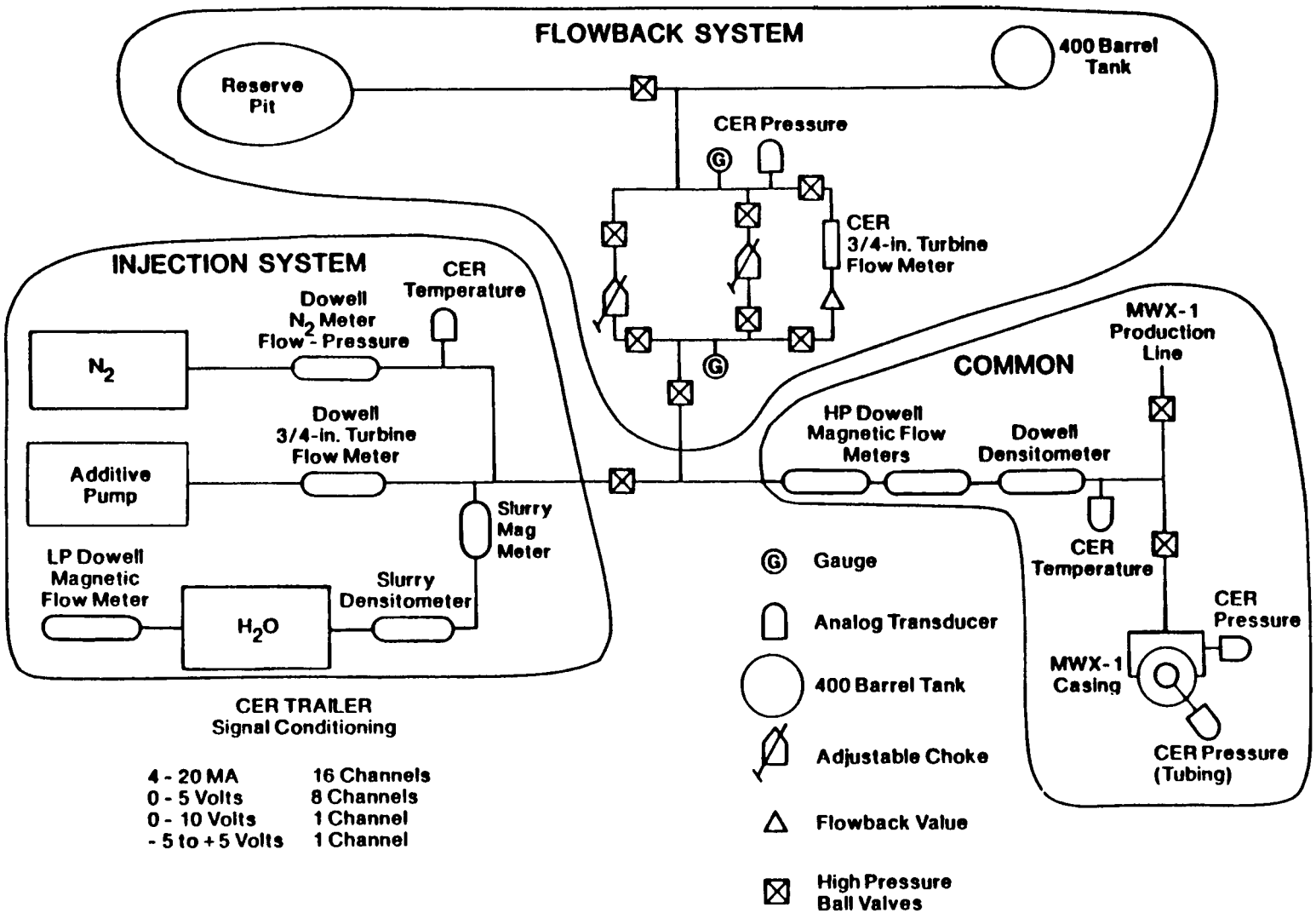

Figure 9.2.6. Instrumentation Schematic

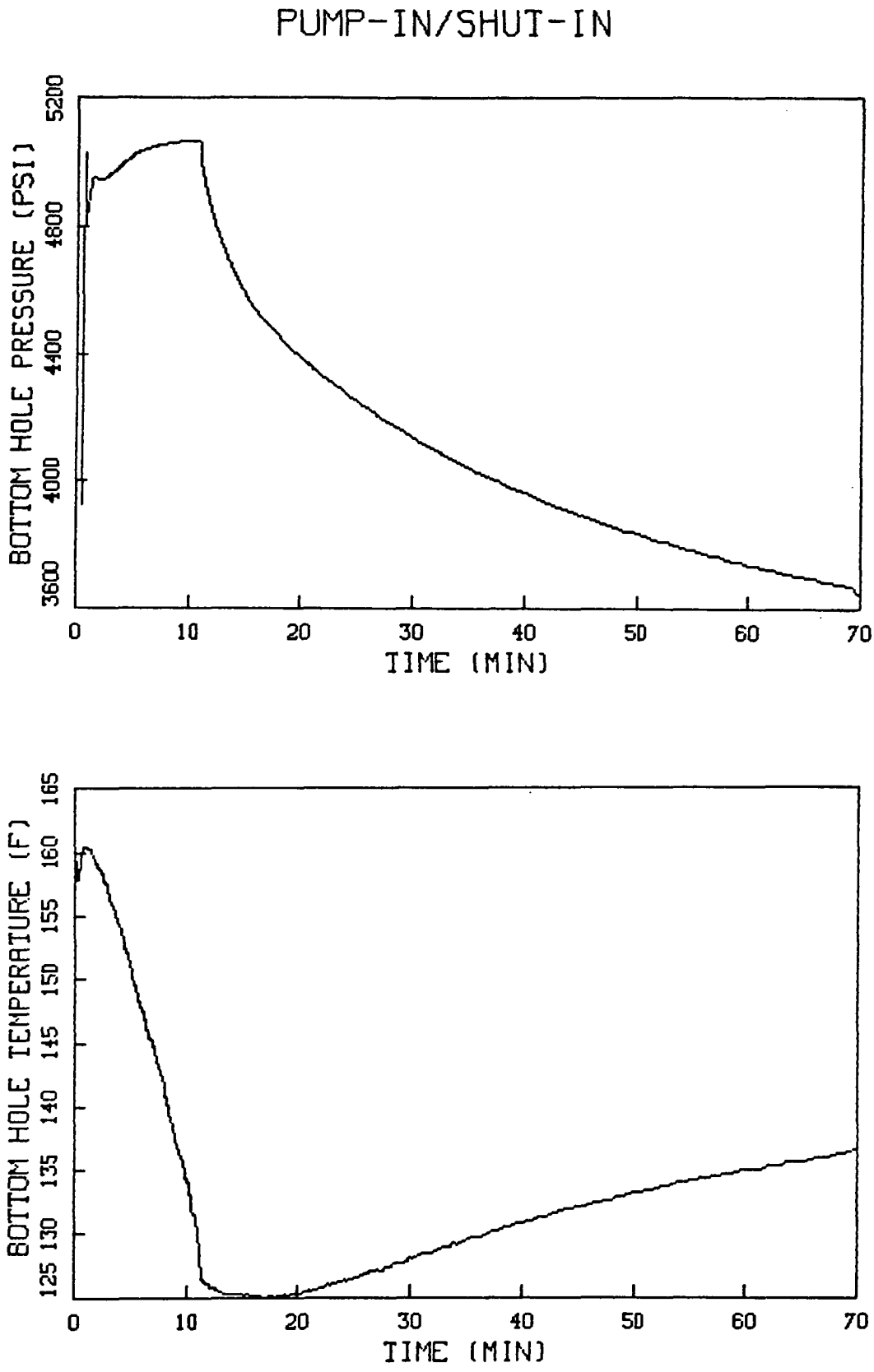

Figure 9.2.7. Pump-In/Shut-In Pressure and Temperature Data

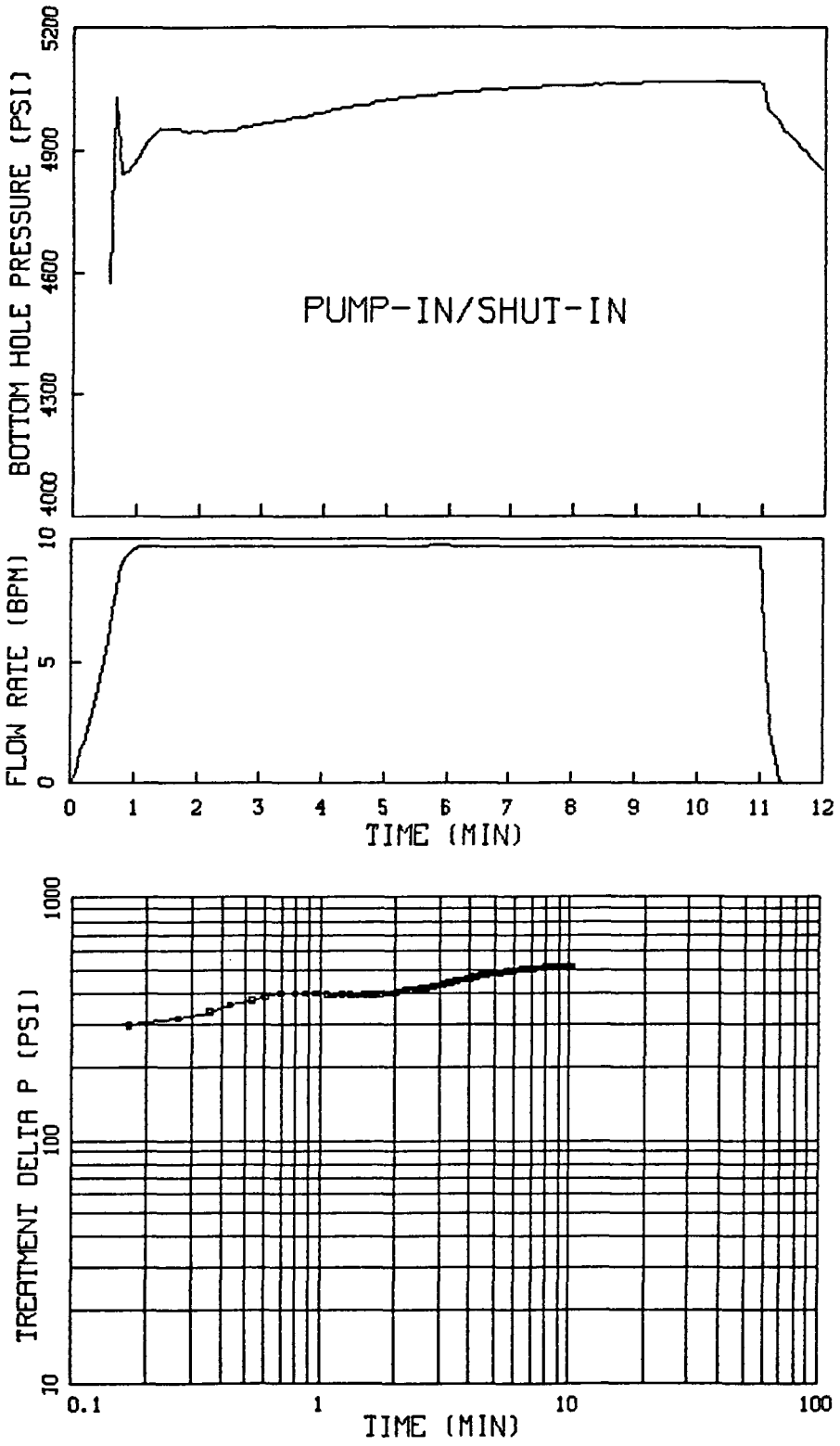

Figure 9.2.8. Pump-In/Shut-In Injection Data

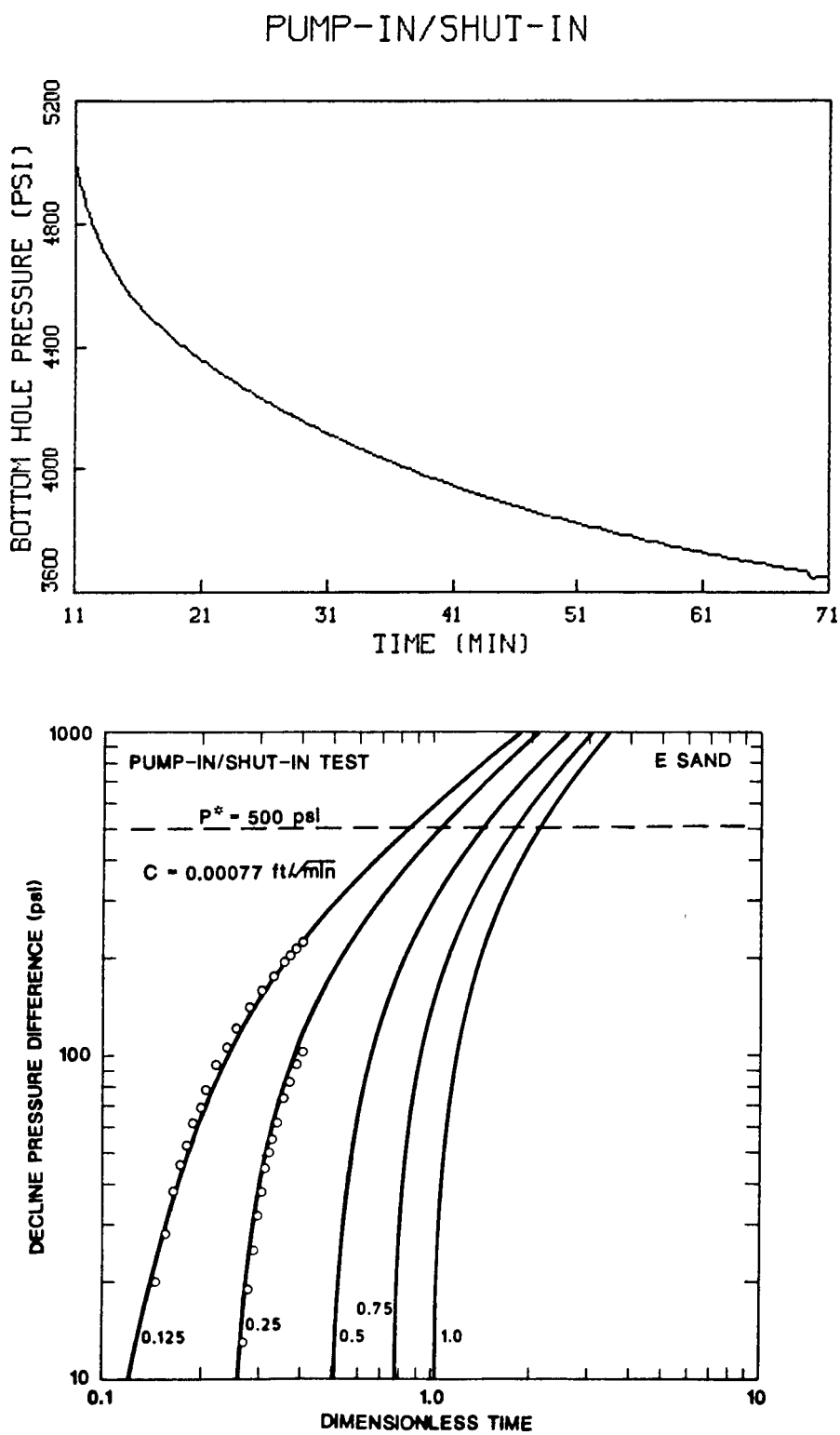

Figure 9.2.9. Pump-In/Shut-In Pressure Decline Data

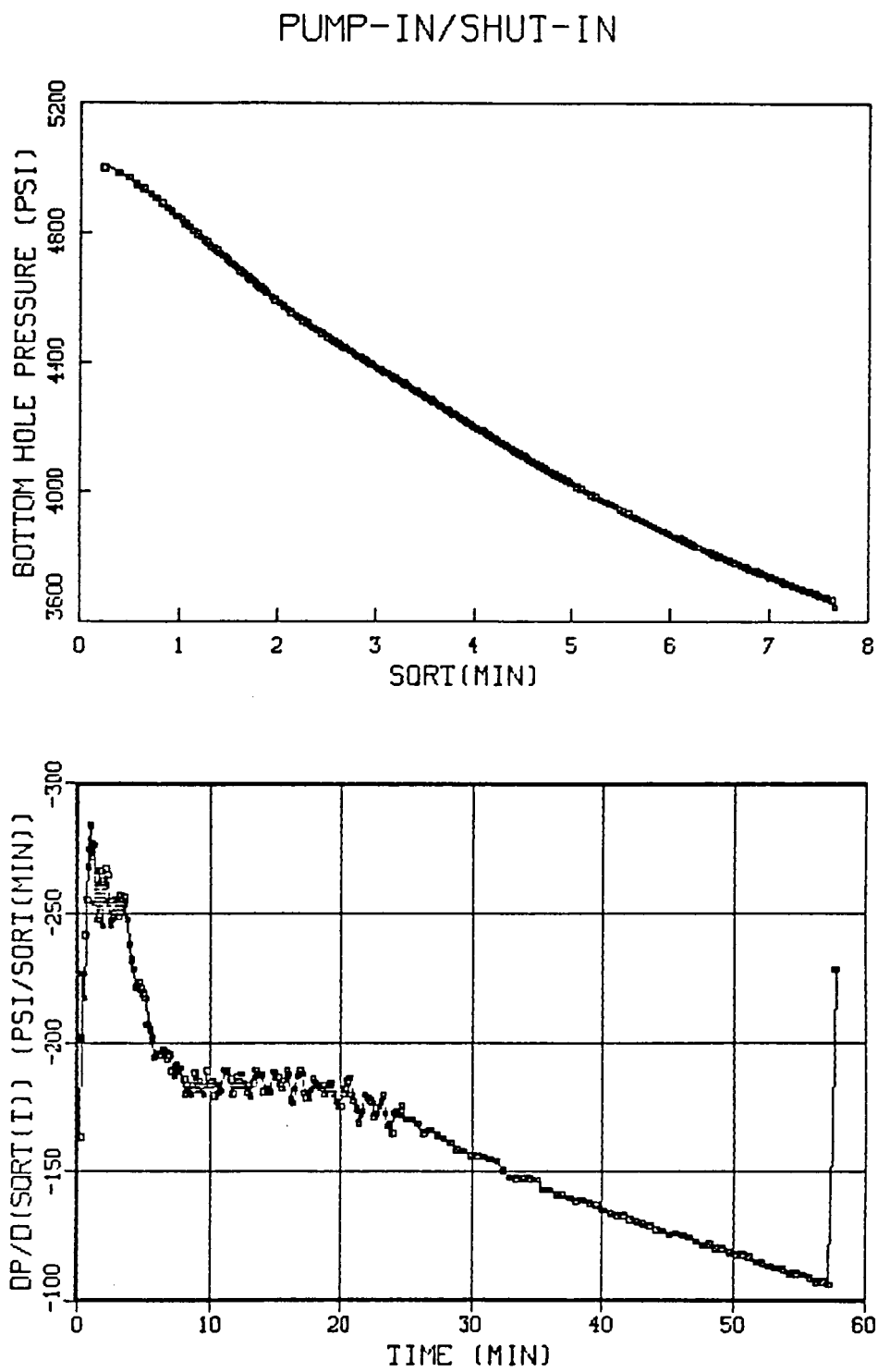

Figure 9.2.10. Pump-In/Shut-In Square-Root-of-Time Plots

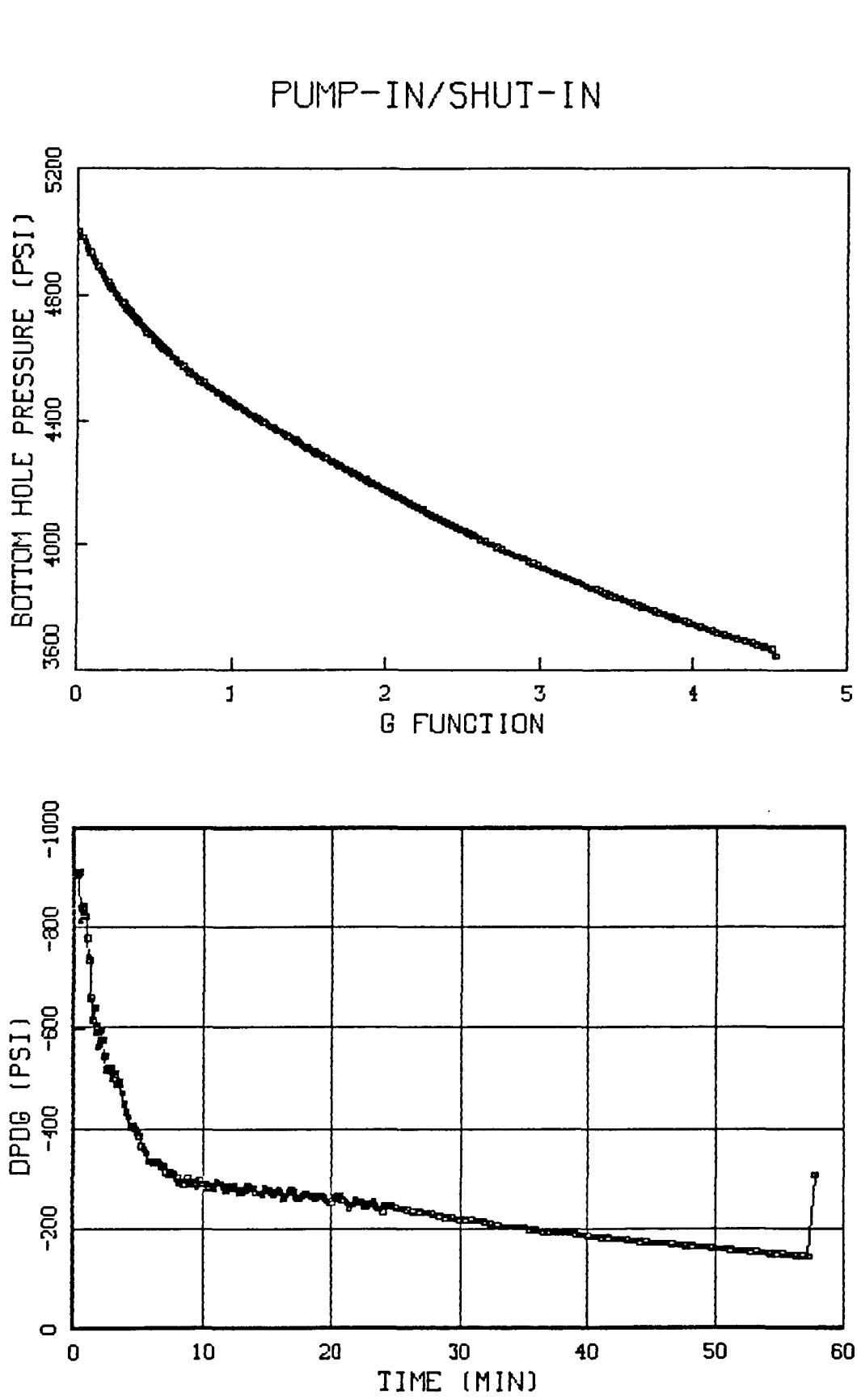

Figure 9.2.11. Pump-In/Shut-In Pressure vs G Function Curves

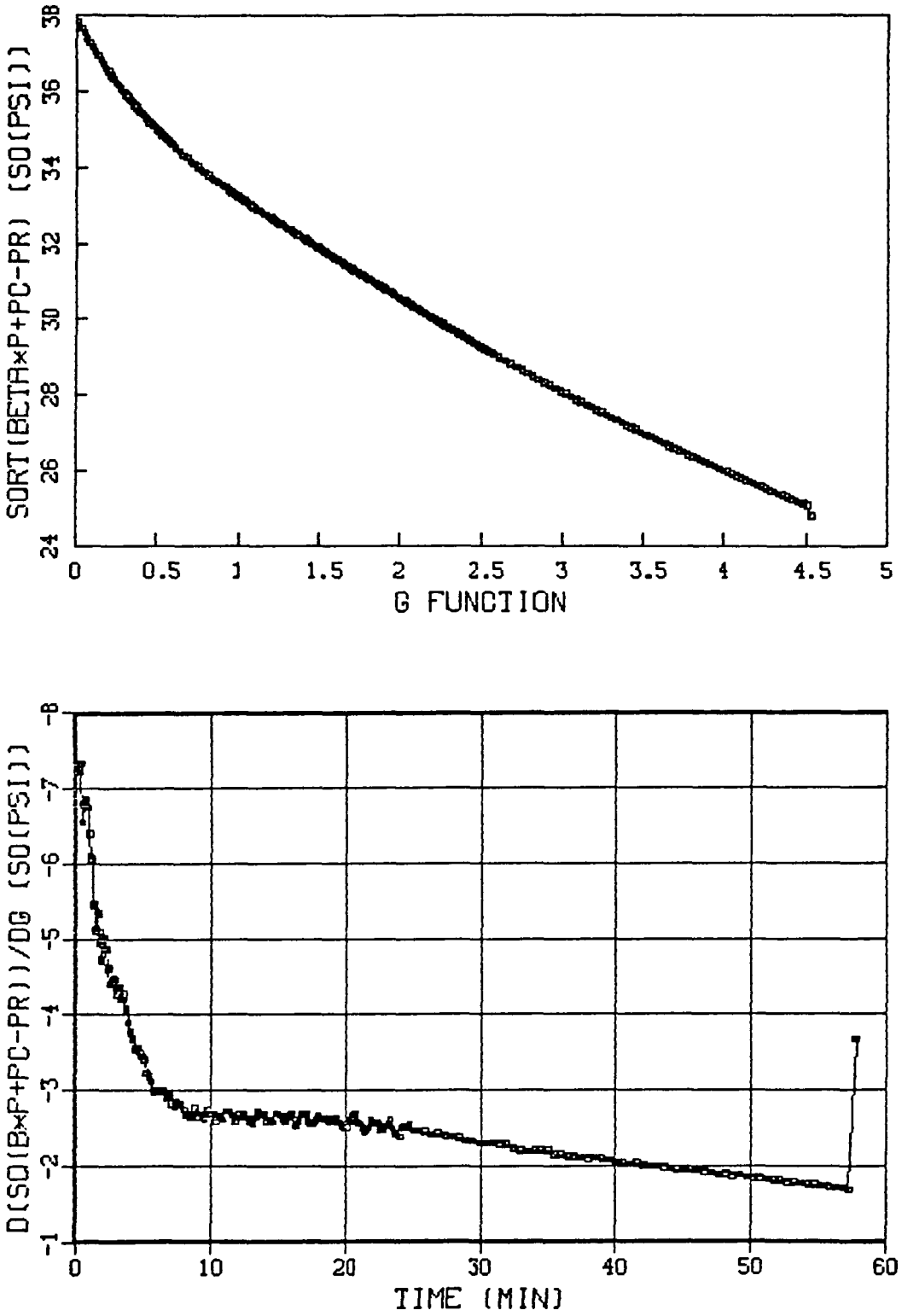

Figure 9.2.12. Pump-In/Shut-In Linearized G Function Curves, Exponent = 1/2

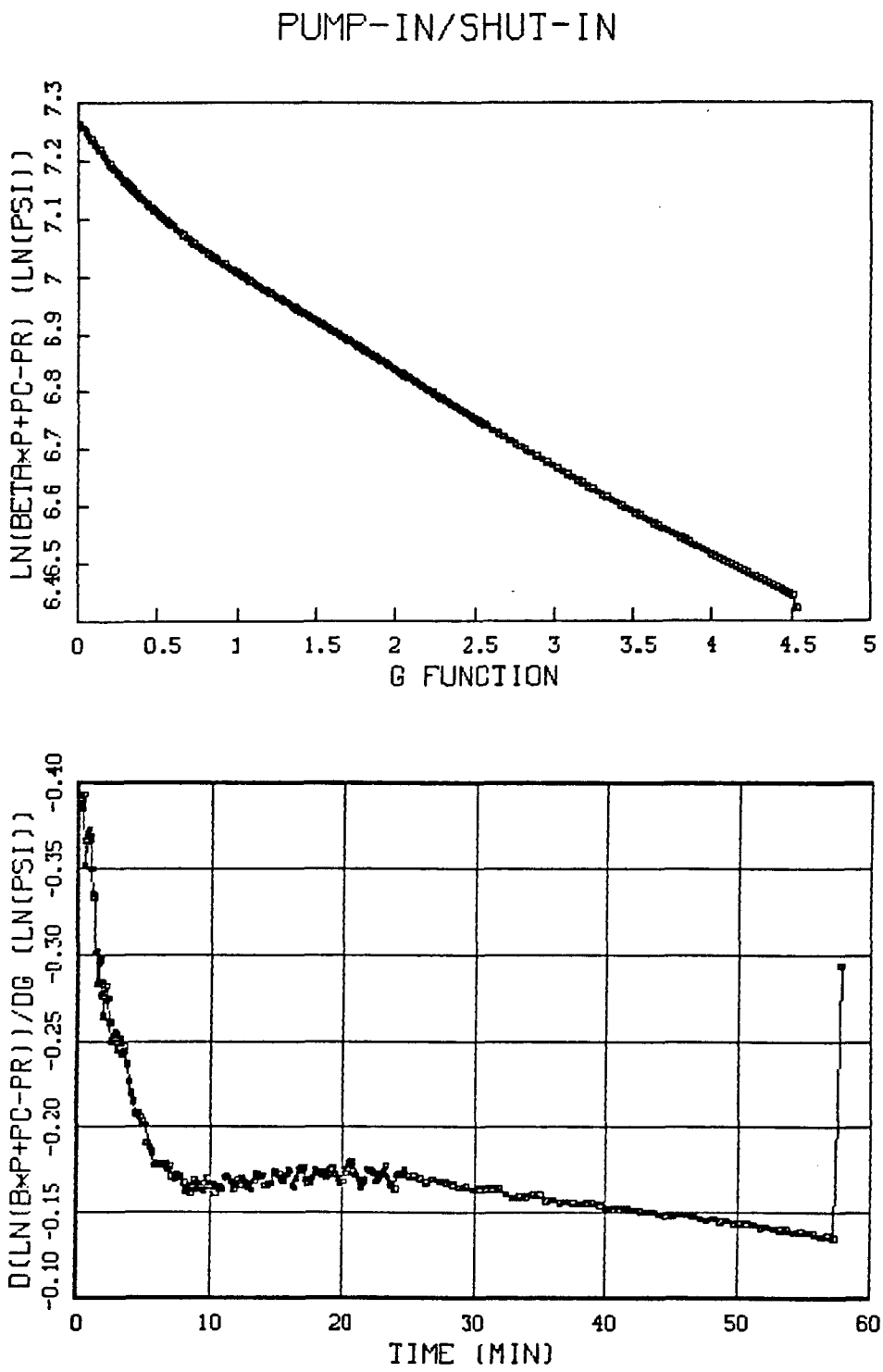

Figure 9.2.13. Pump-In/Shut-In Linearized G Function Curves, Exponent = 1

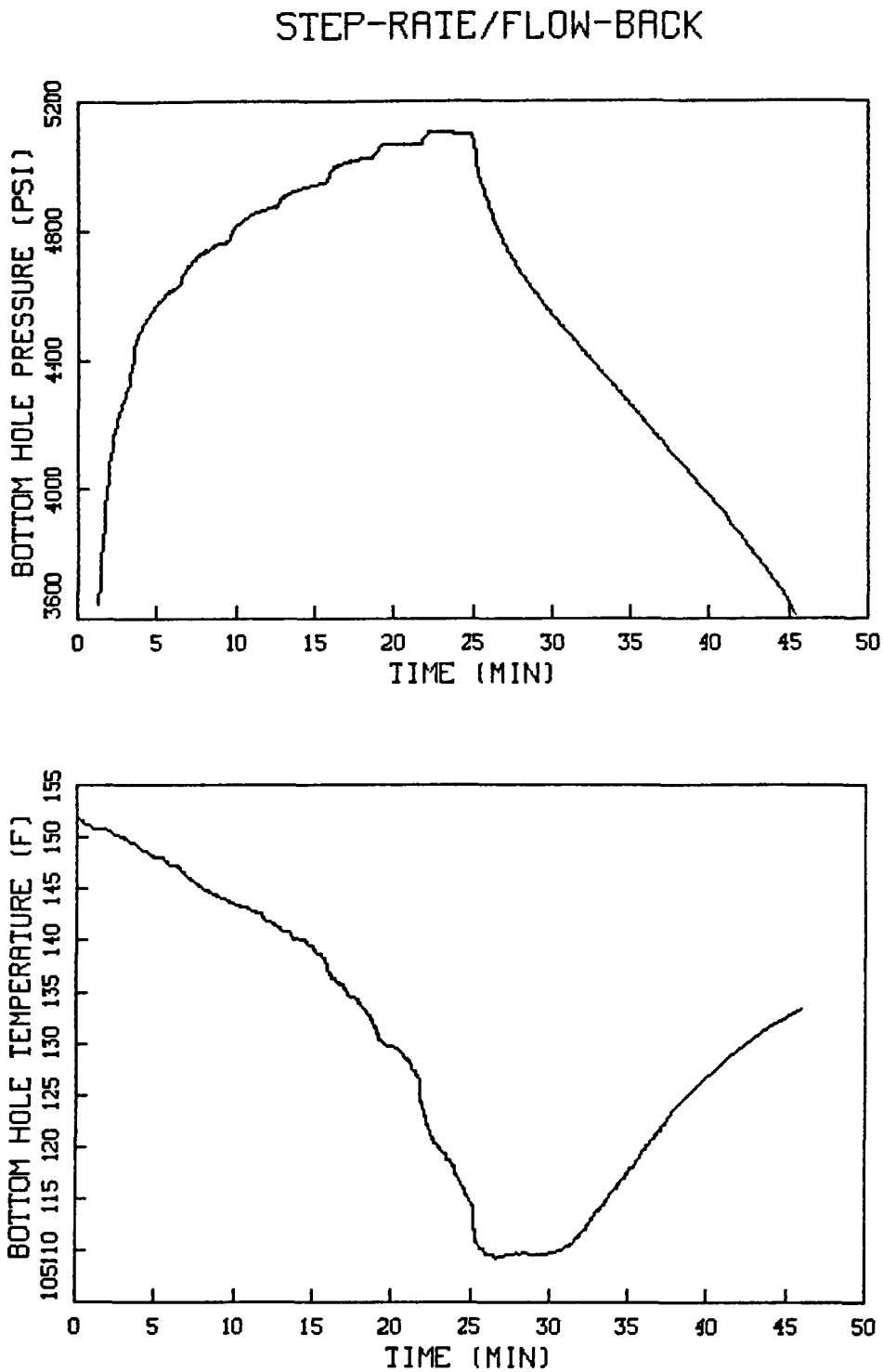

Figure 9.2.14. Step-Rate/Flow-Back Pressure and Temperature Data

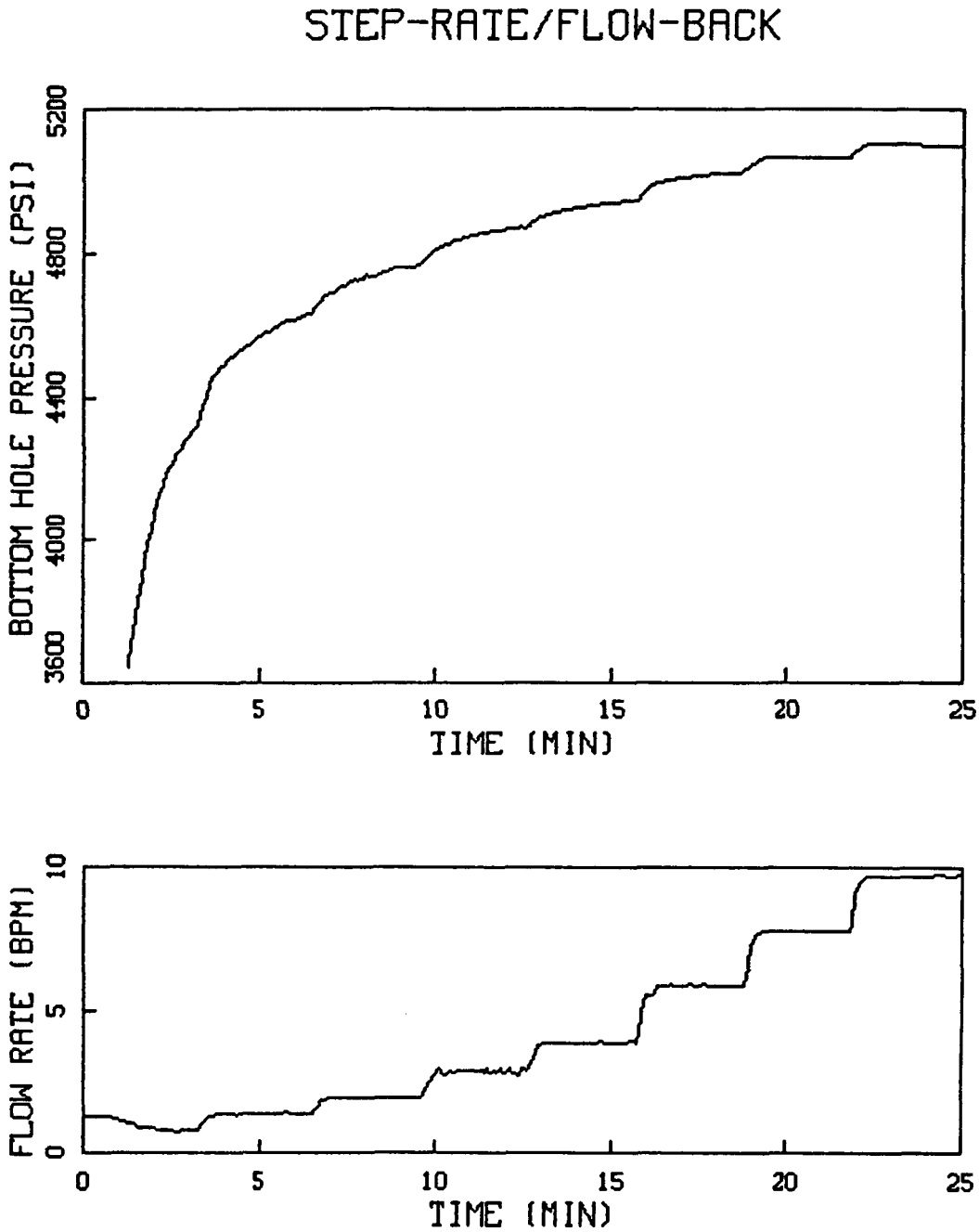

Figure 9.2.15. Step-Rate/Flow-Back Injection Data

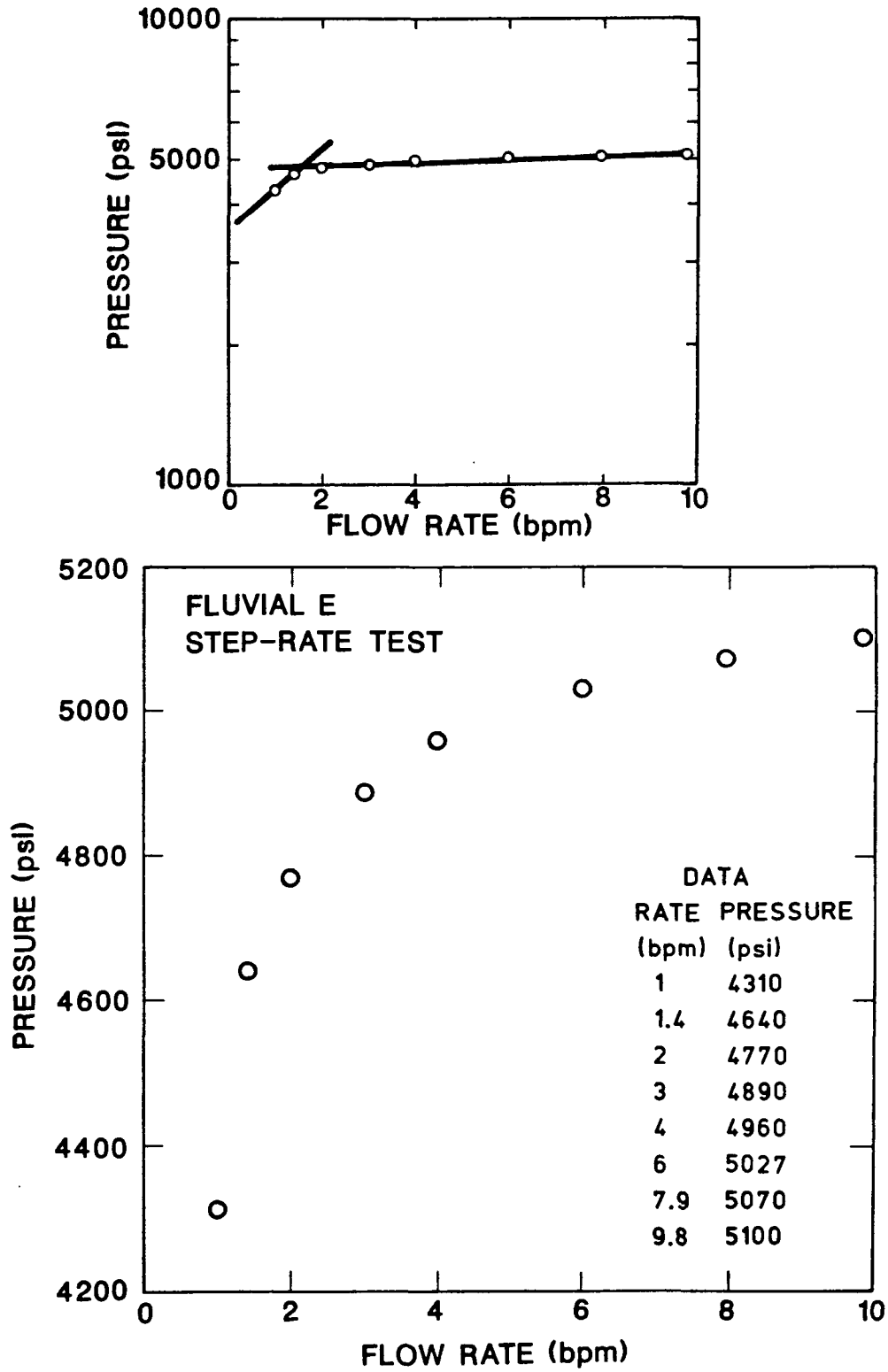

Figure 9.2.16. Step-Rate Pressure vs Flow-Rate Curves

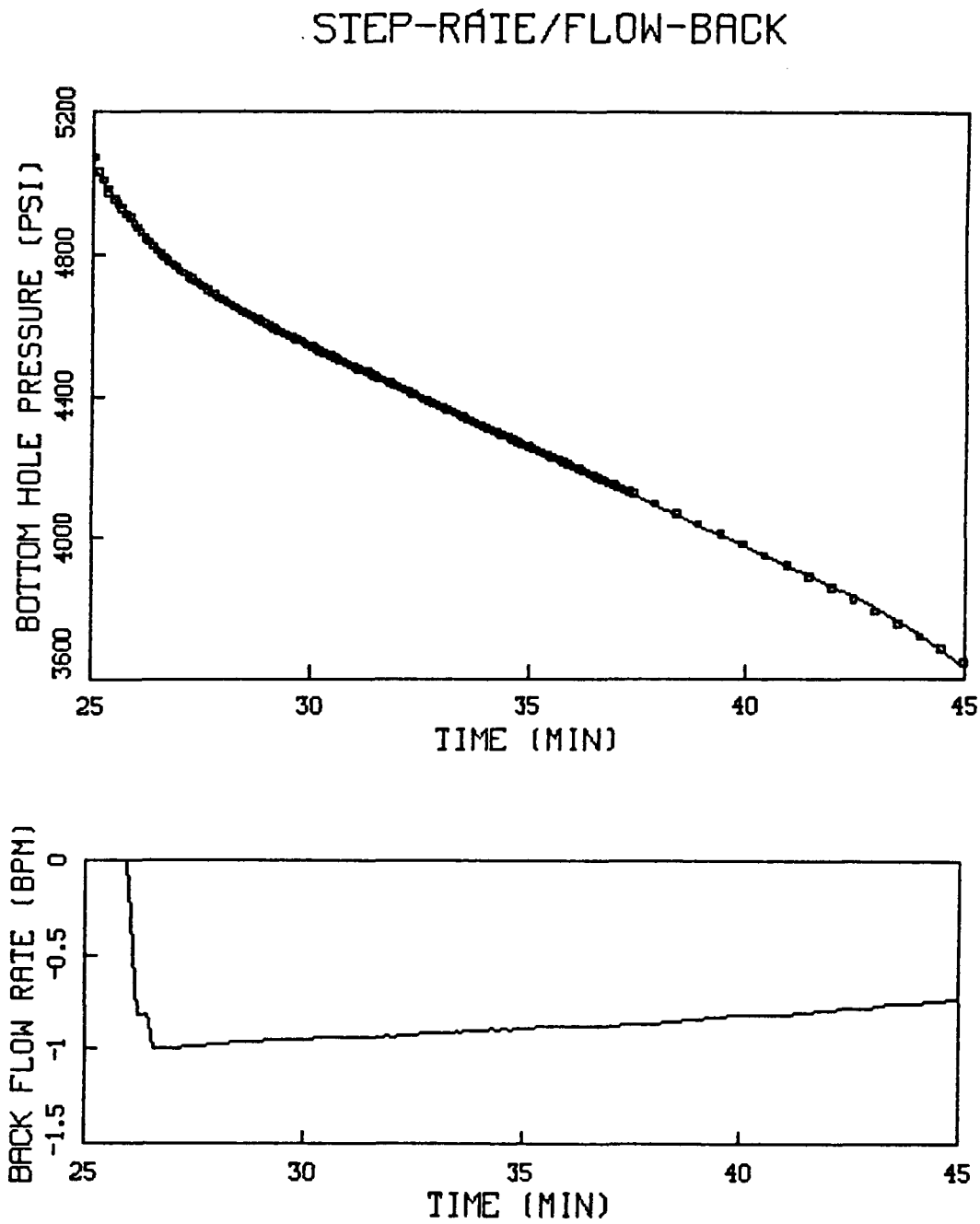

Figure 9.2.17. Flow-Back Data After Step-Rate Test

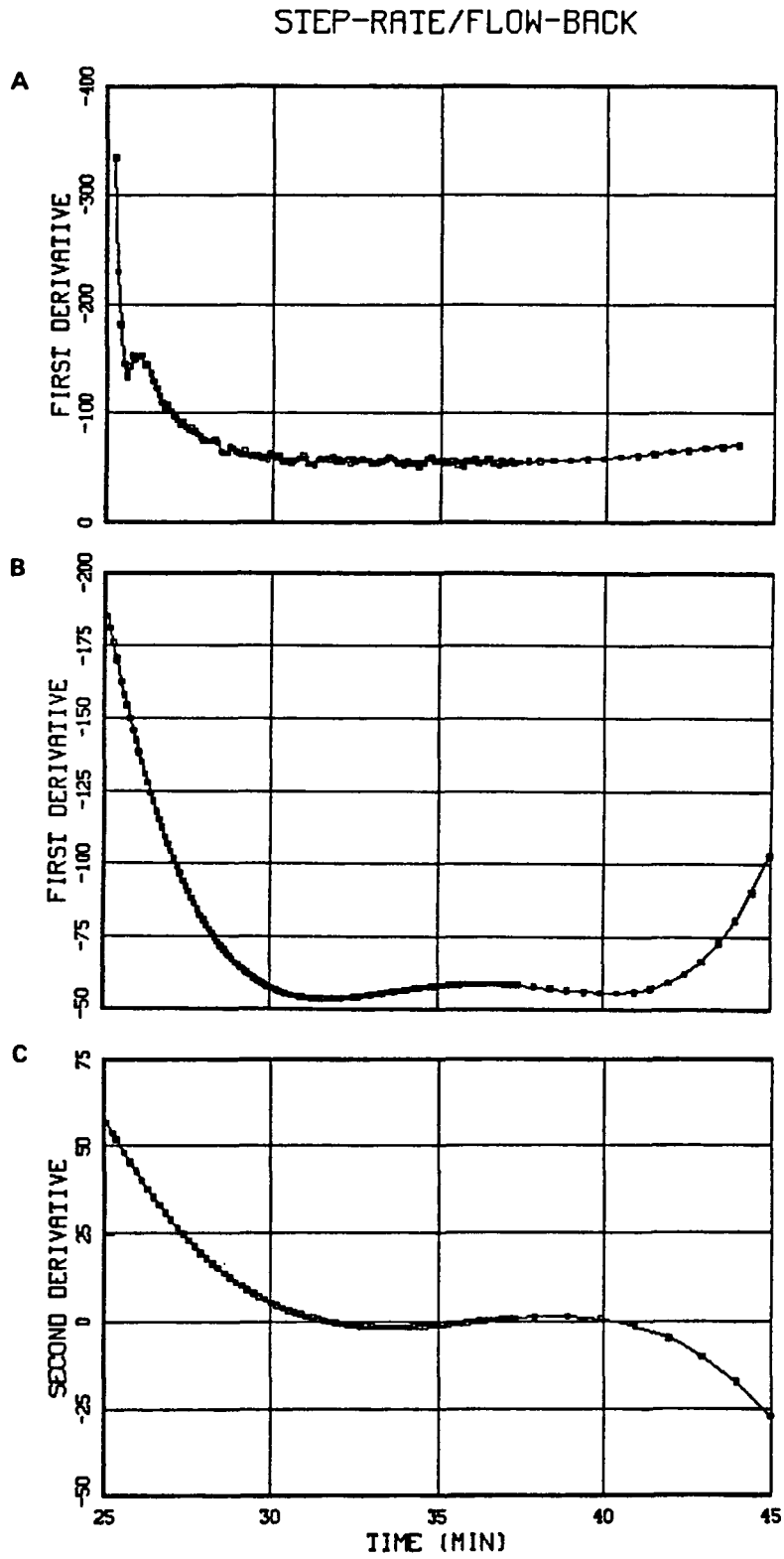

Figure 9.2.18. Flow-Back Derivative Results After Step-Rate Test

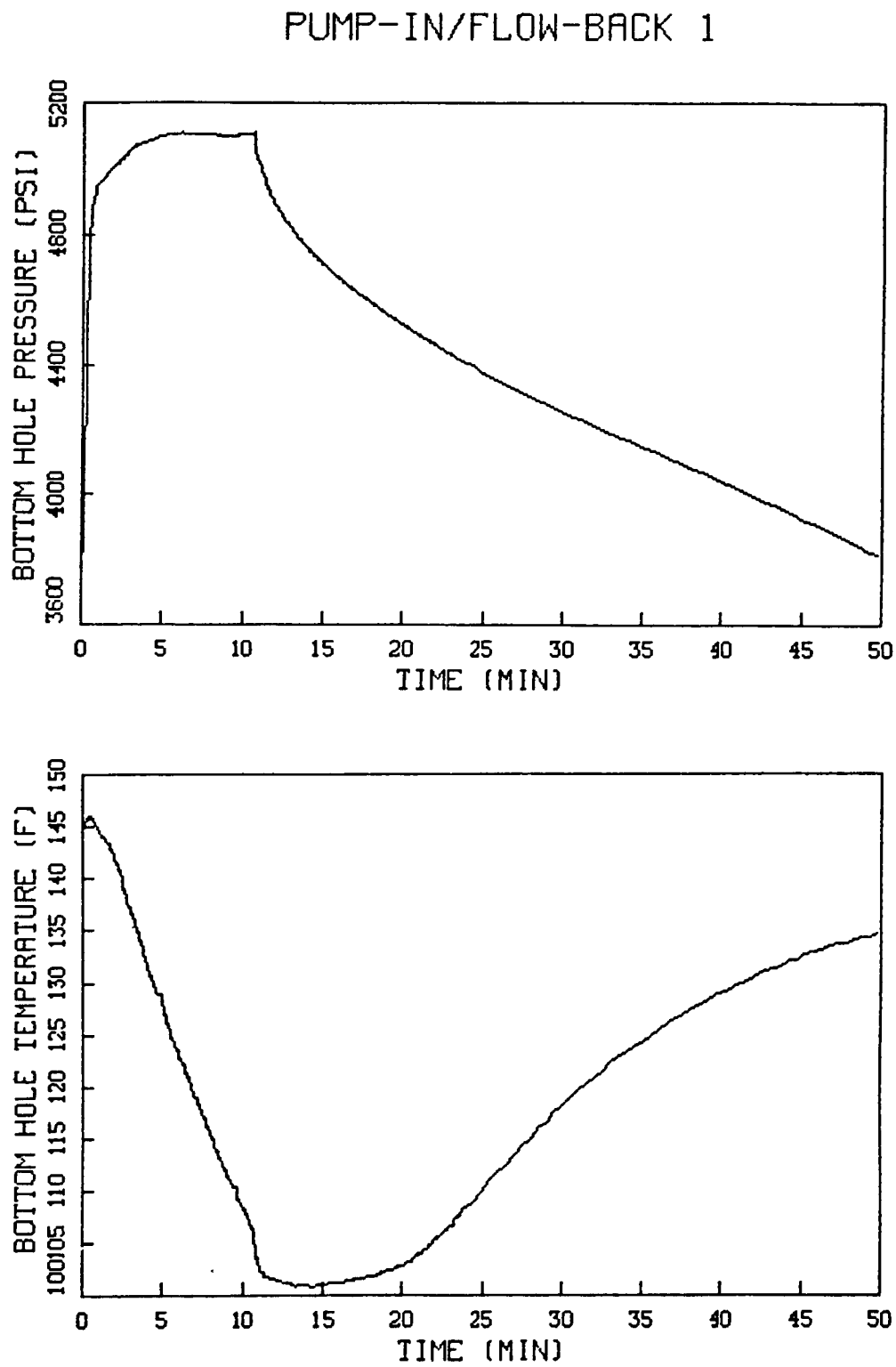

Figure 9.2.19. Pump-In/Flow-Back #1 Pressure and Temperature Data

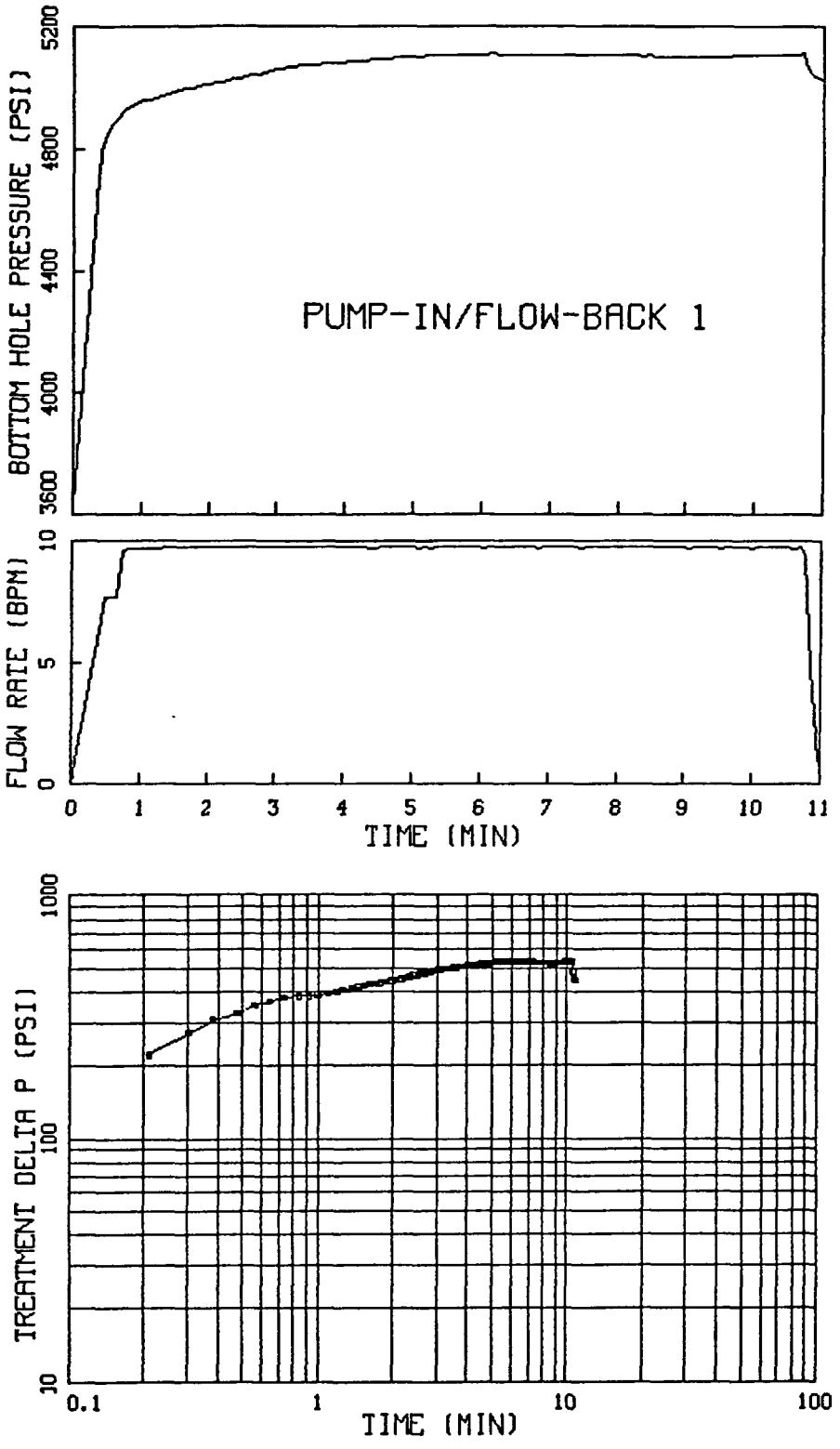

Figure 9.2.20. Pump-In/Flow-Back #1 Injection Data

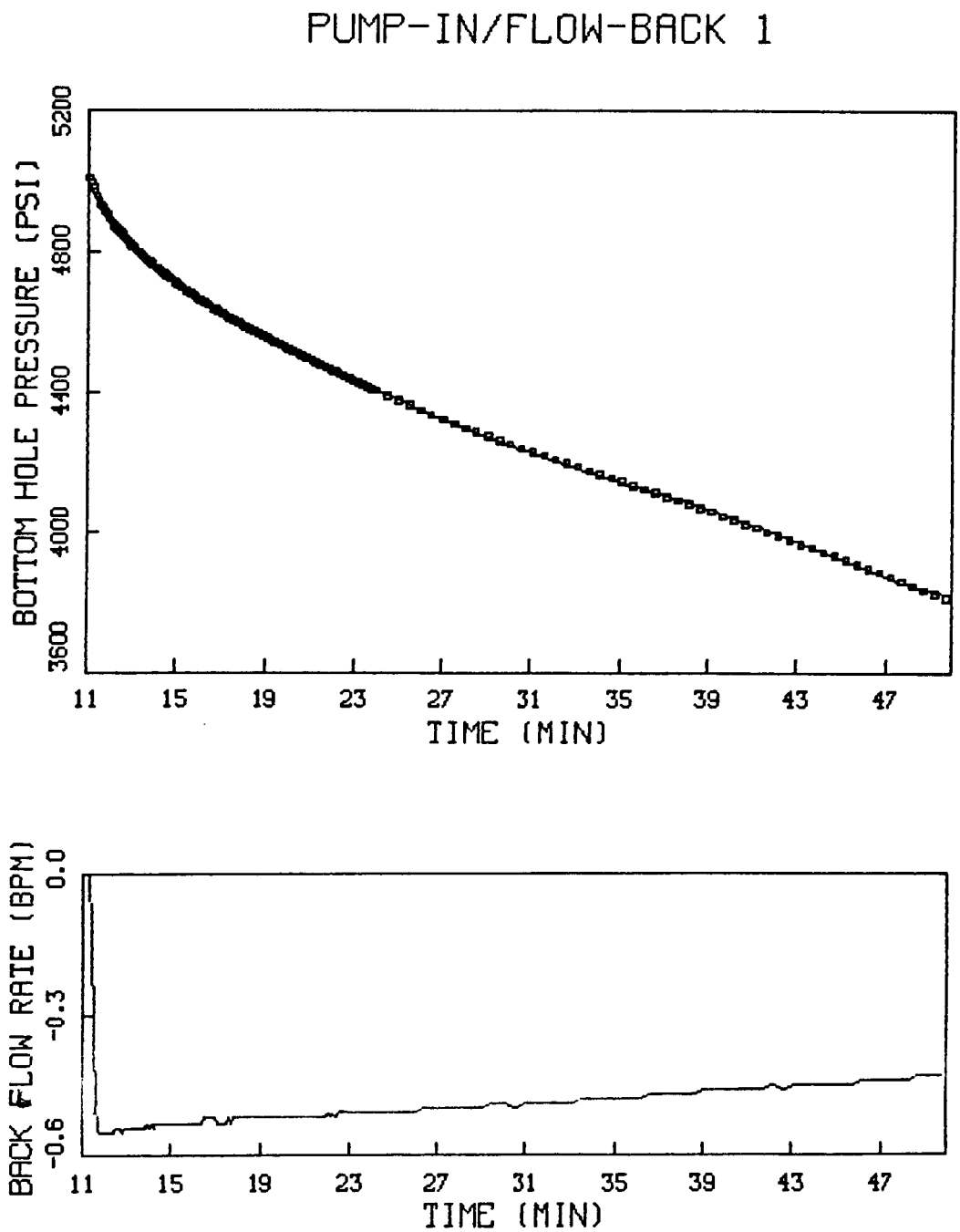

Figure 9.2.21. Flow-Back Data for Pump-In/Flow-Back #1

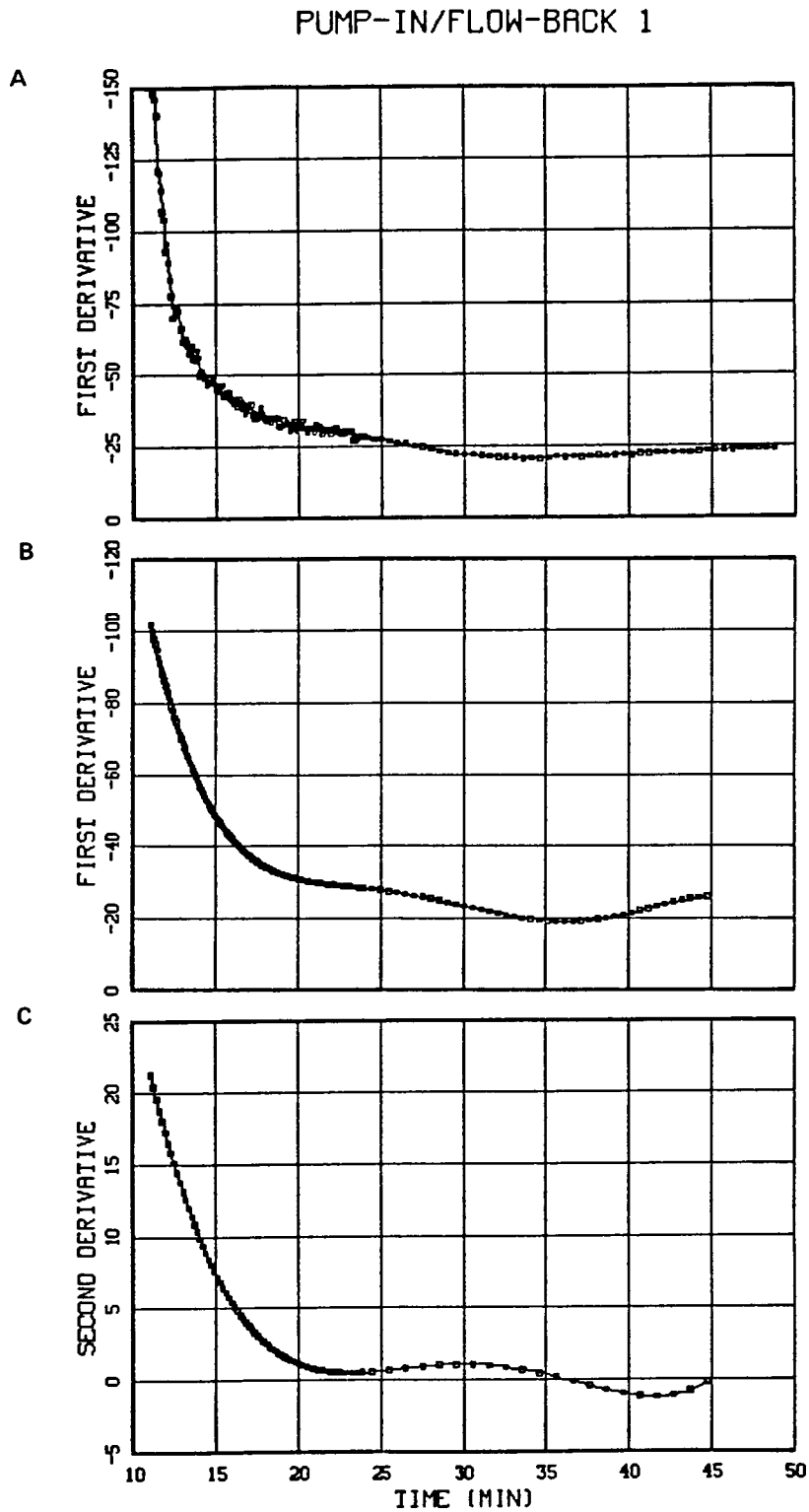

Figure 9.2.22. Flow-Back Derivative Results for Pump-In/Flow-Back #1

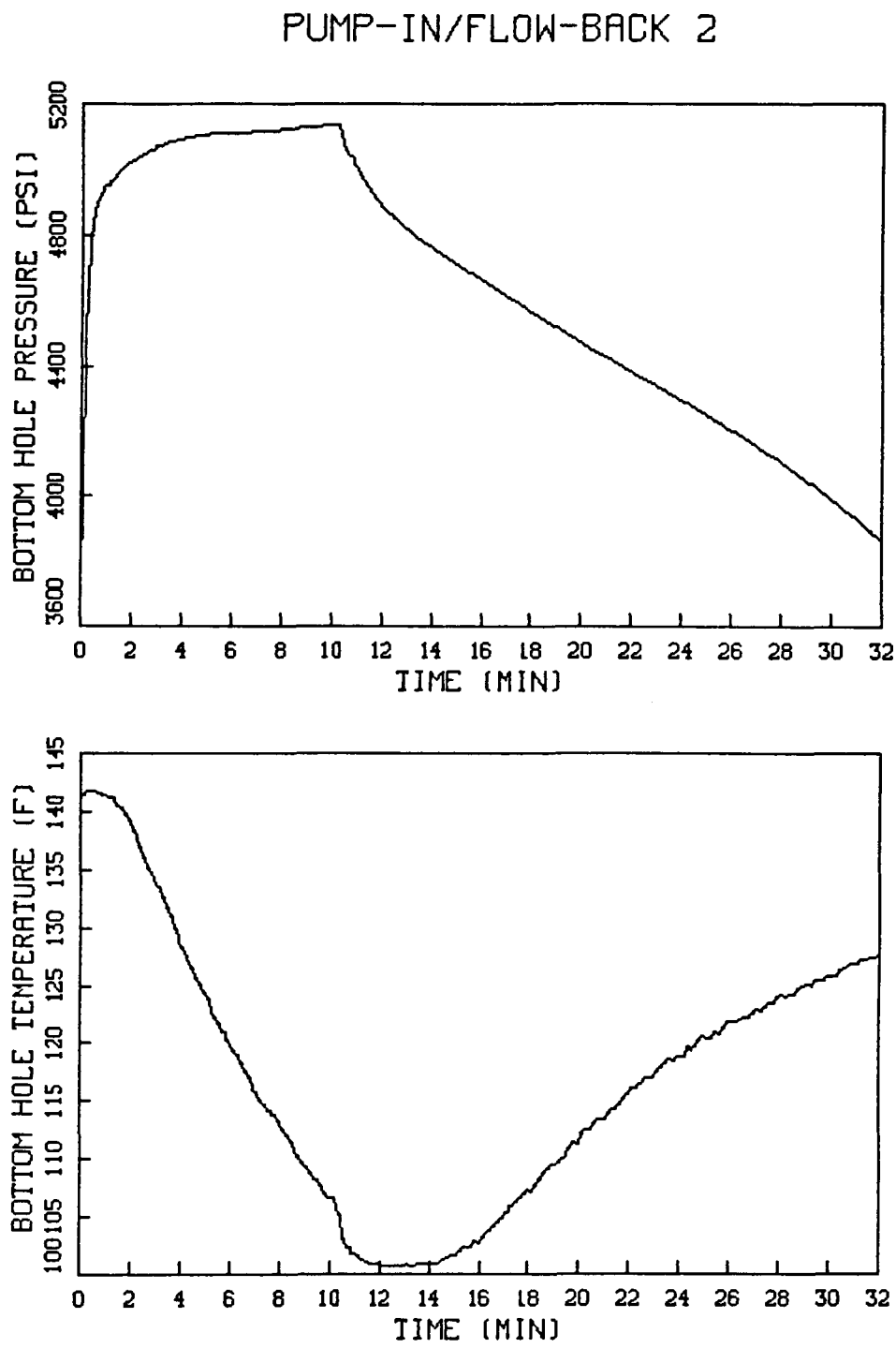

Figure 9.2.23. Pump-In/Flow-Back #2 Pressure and Temperature Data

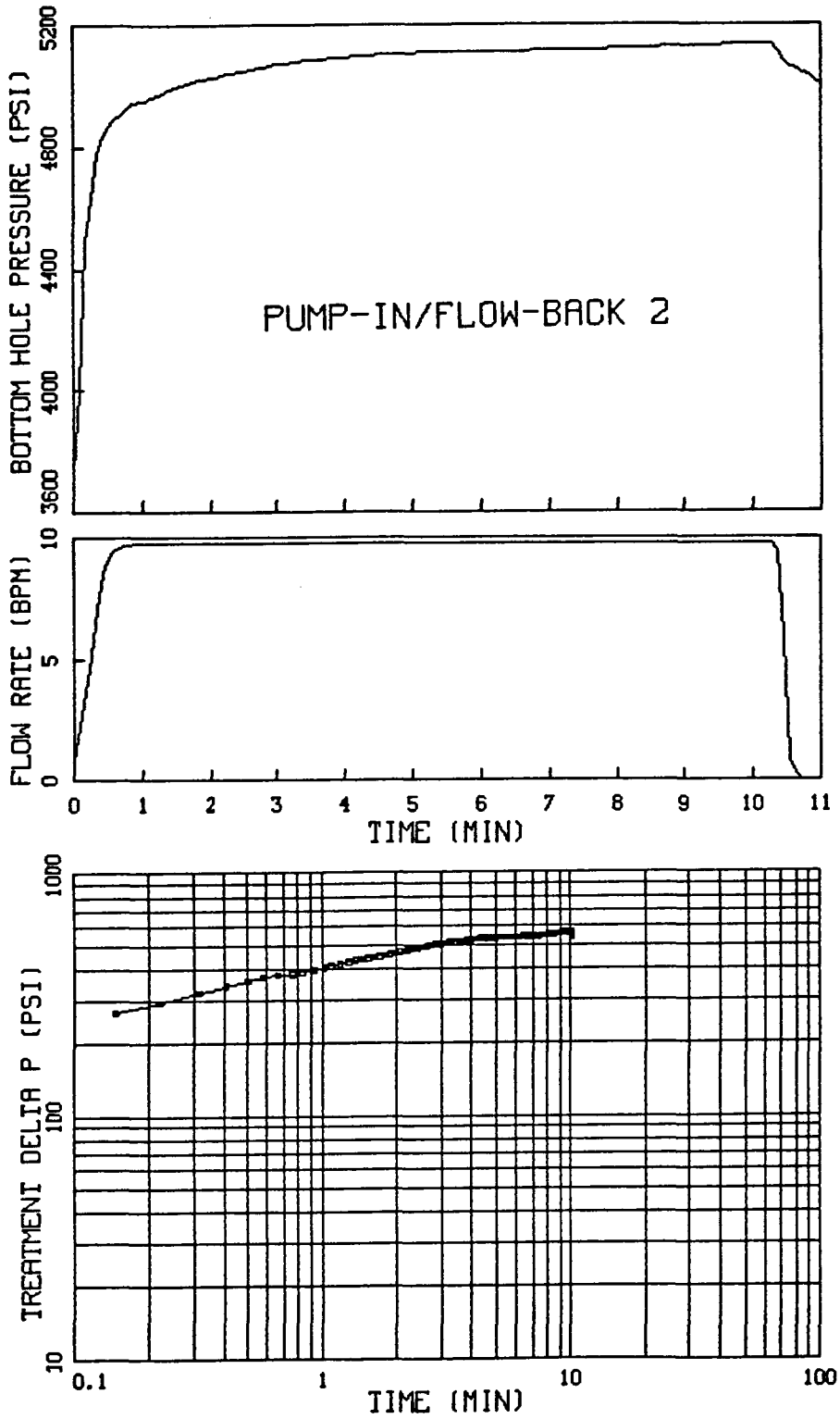

Figure 9.2.24. Pump-In/Flow-Back #2 Injection Data

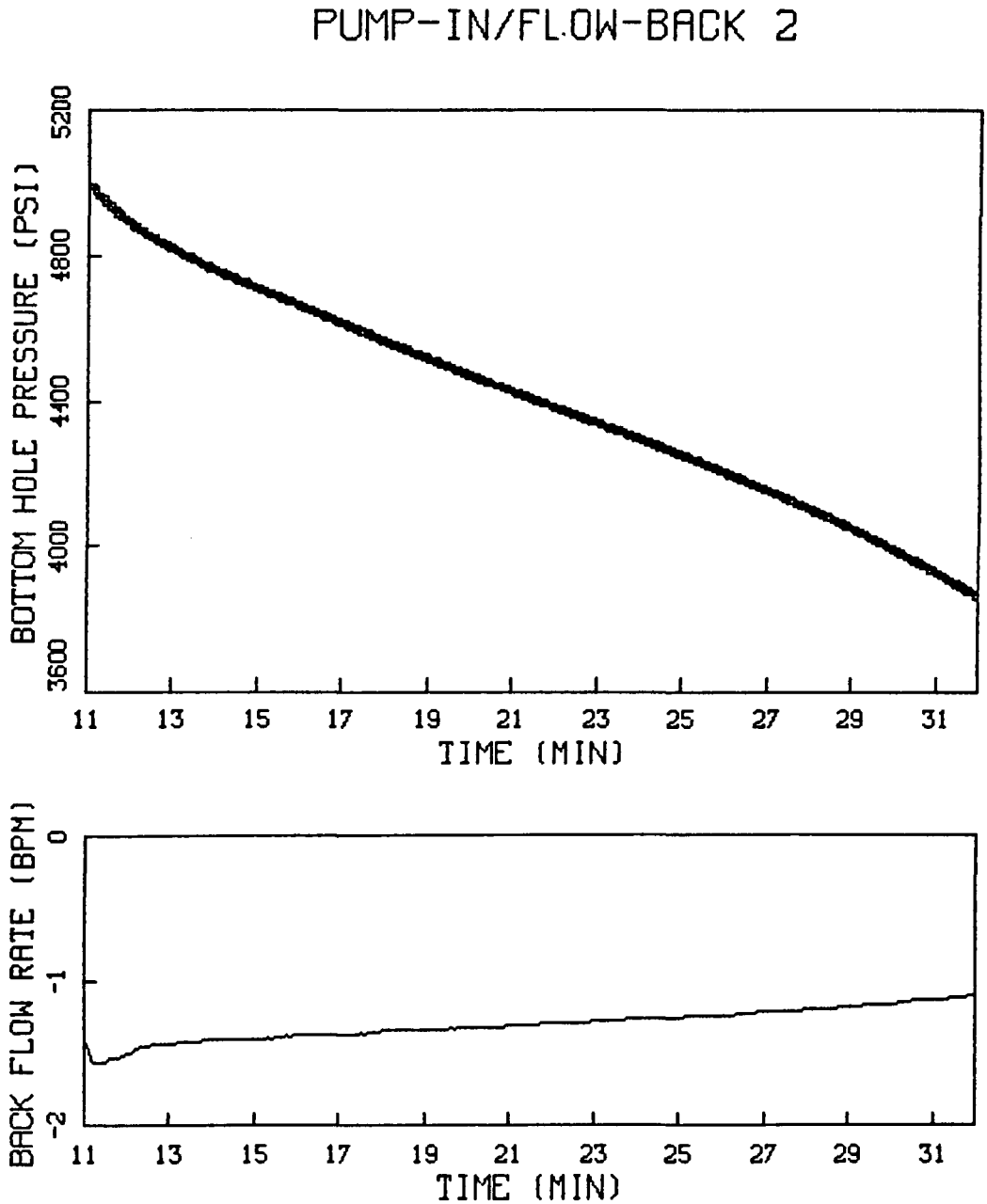

Figure 9.2.25. Flow-Back Data for Pump-In/Flow-Back #2

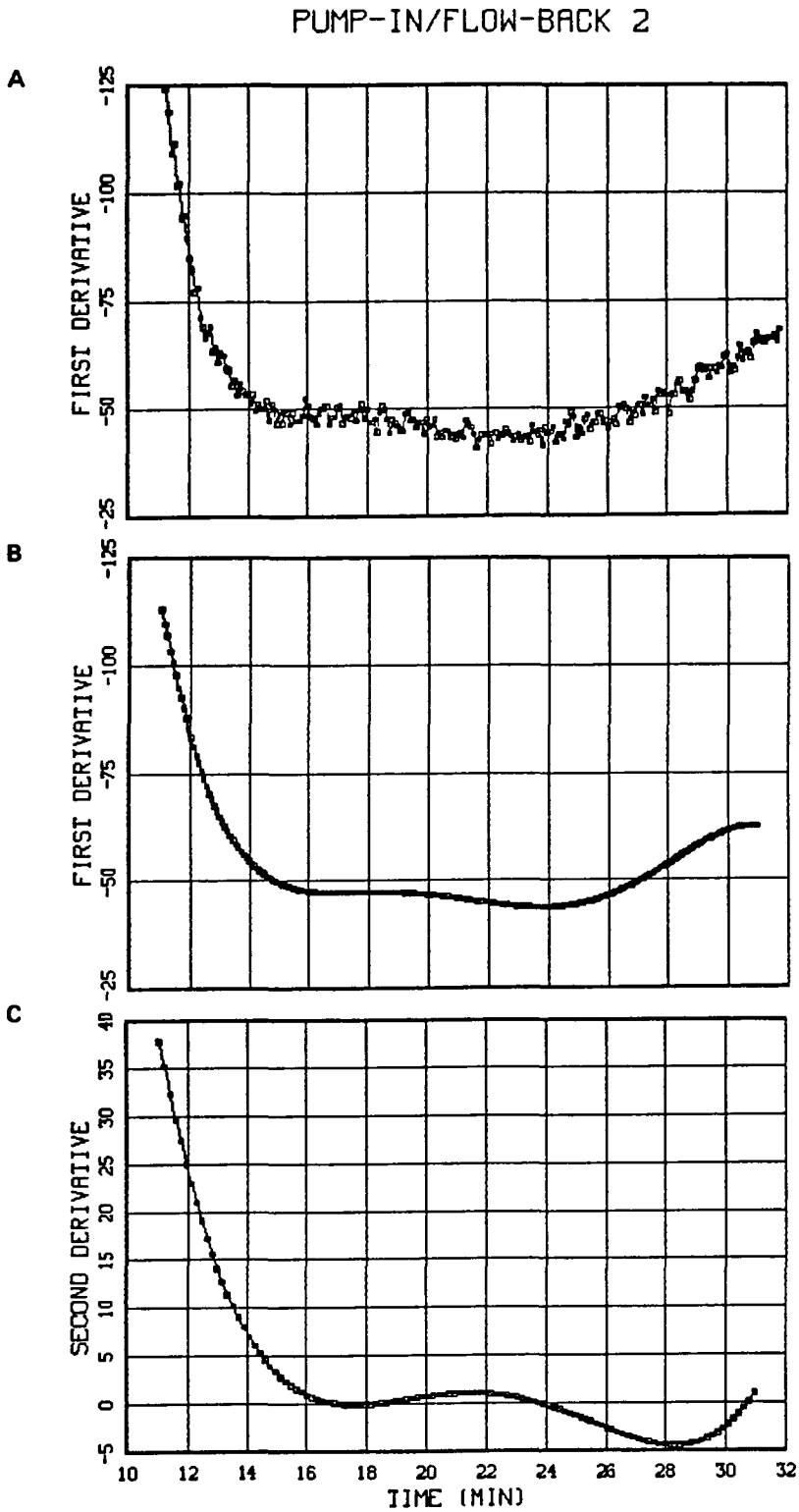

Figure 9.2.26. Flow-Back Derivative for Pump-In/Flow-Back #2

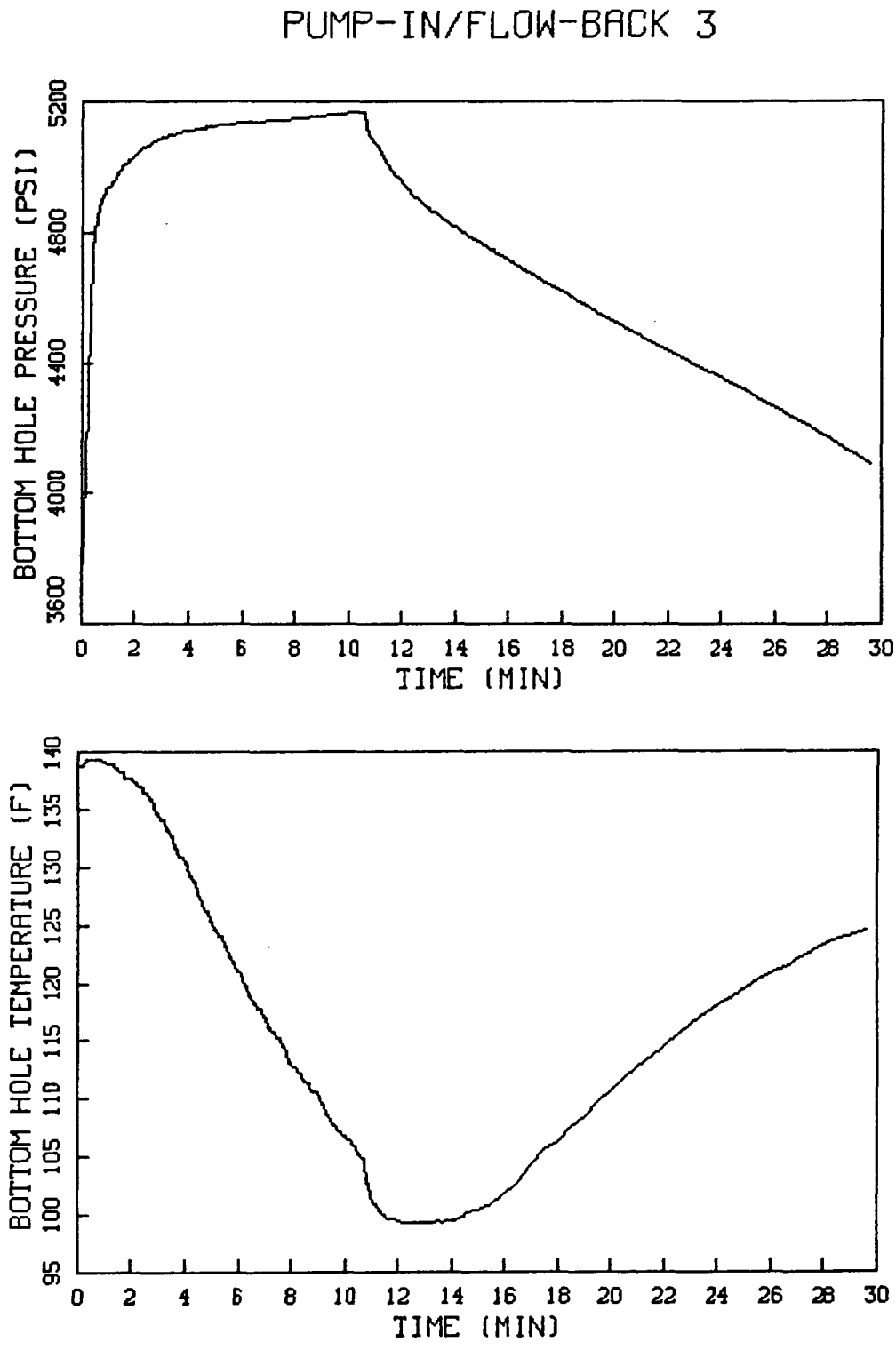

Figure 9.2.27. Pump-In/Flow-Back #3 Pressure and Temperature Data

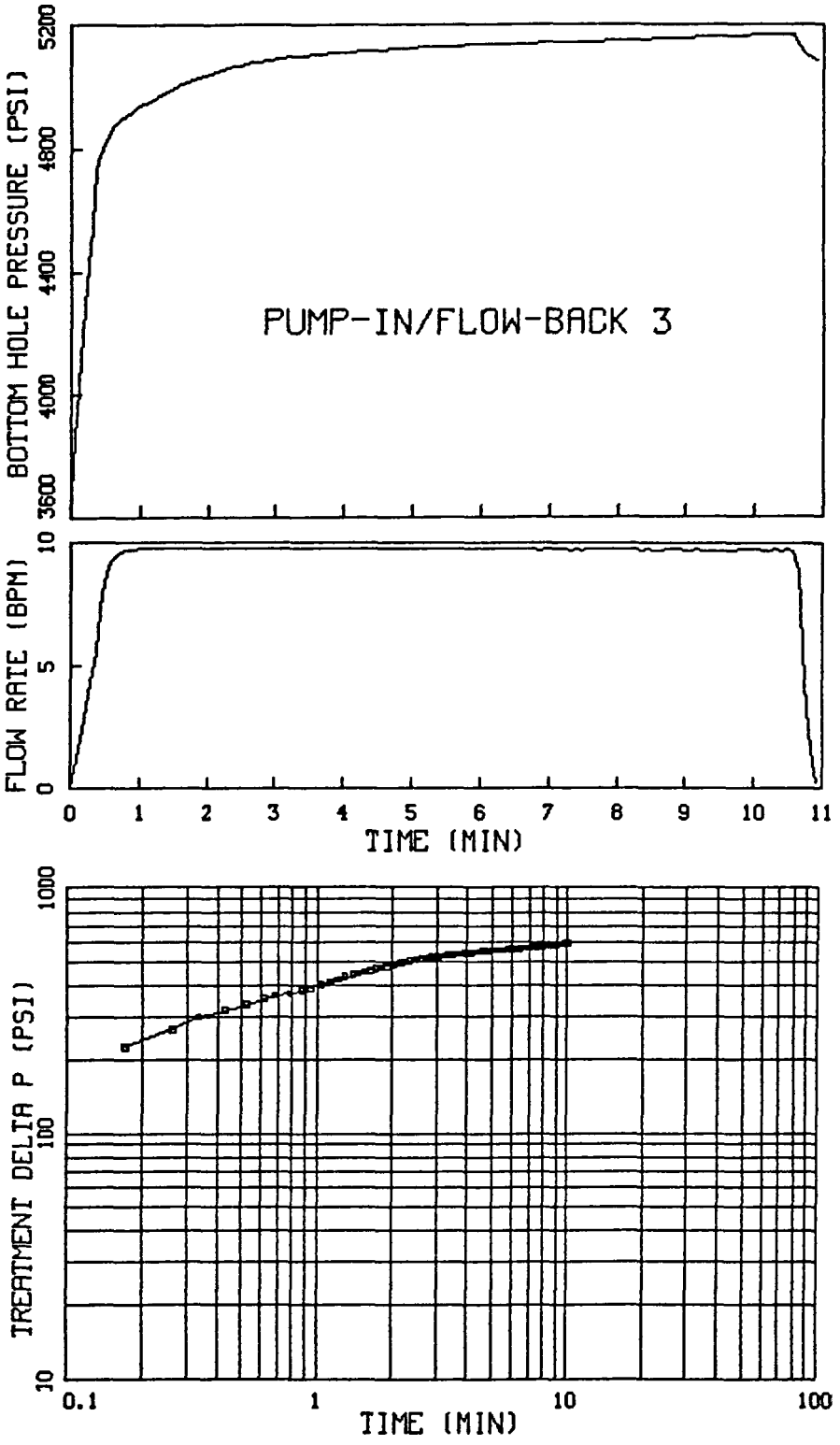

Figure 9.2.28. Pump-In/Flow-Back #3 Injection Data

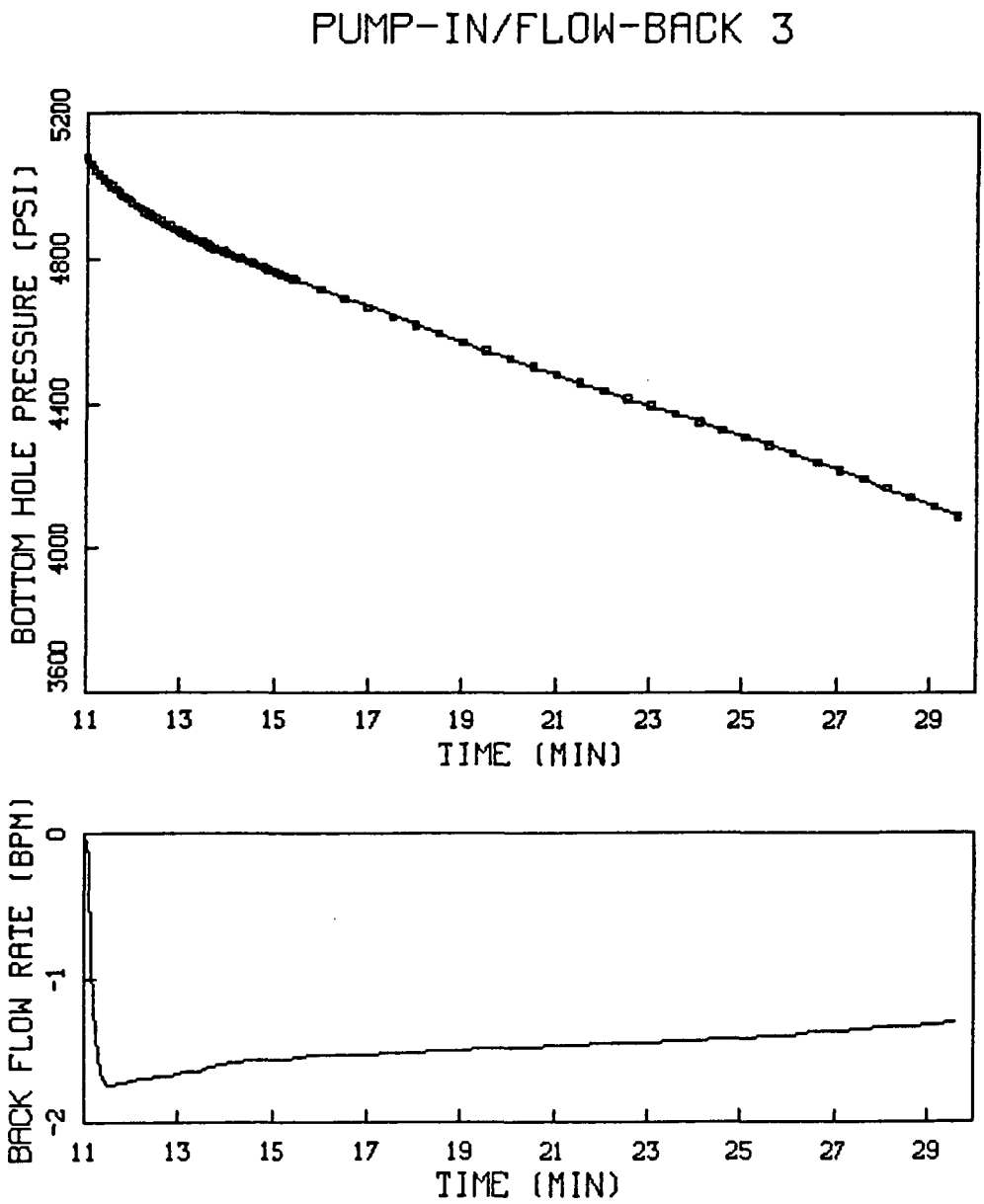

Figure 9.2.29. Flow-Back Data for Pump-In/Flow-Back #3

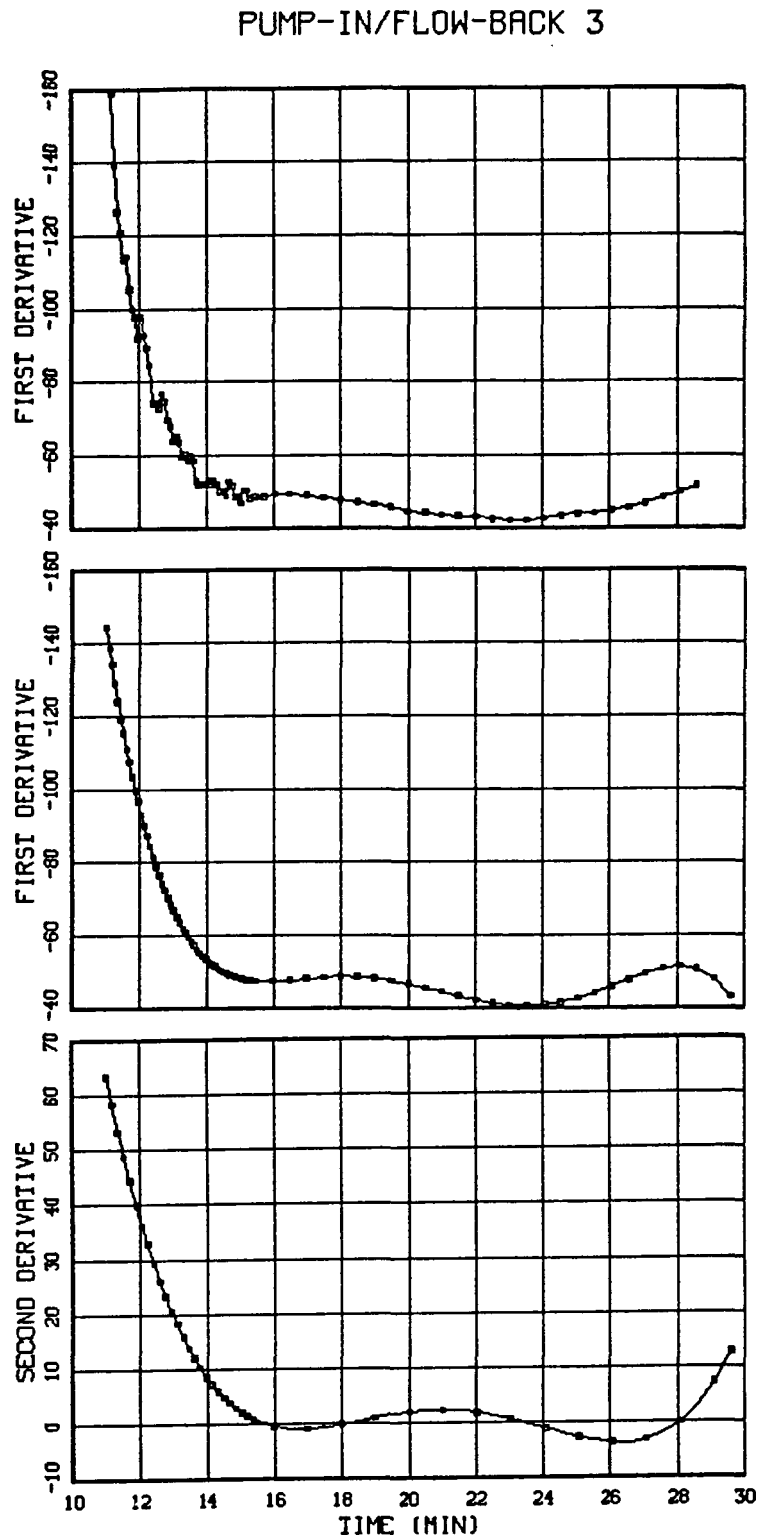

Figure 9.2.30. Flow-Back Derivatives for Pump-In/Flow-Back #3

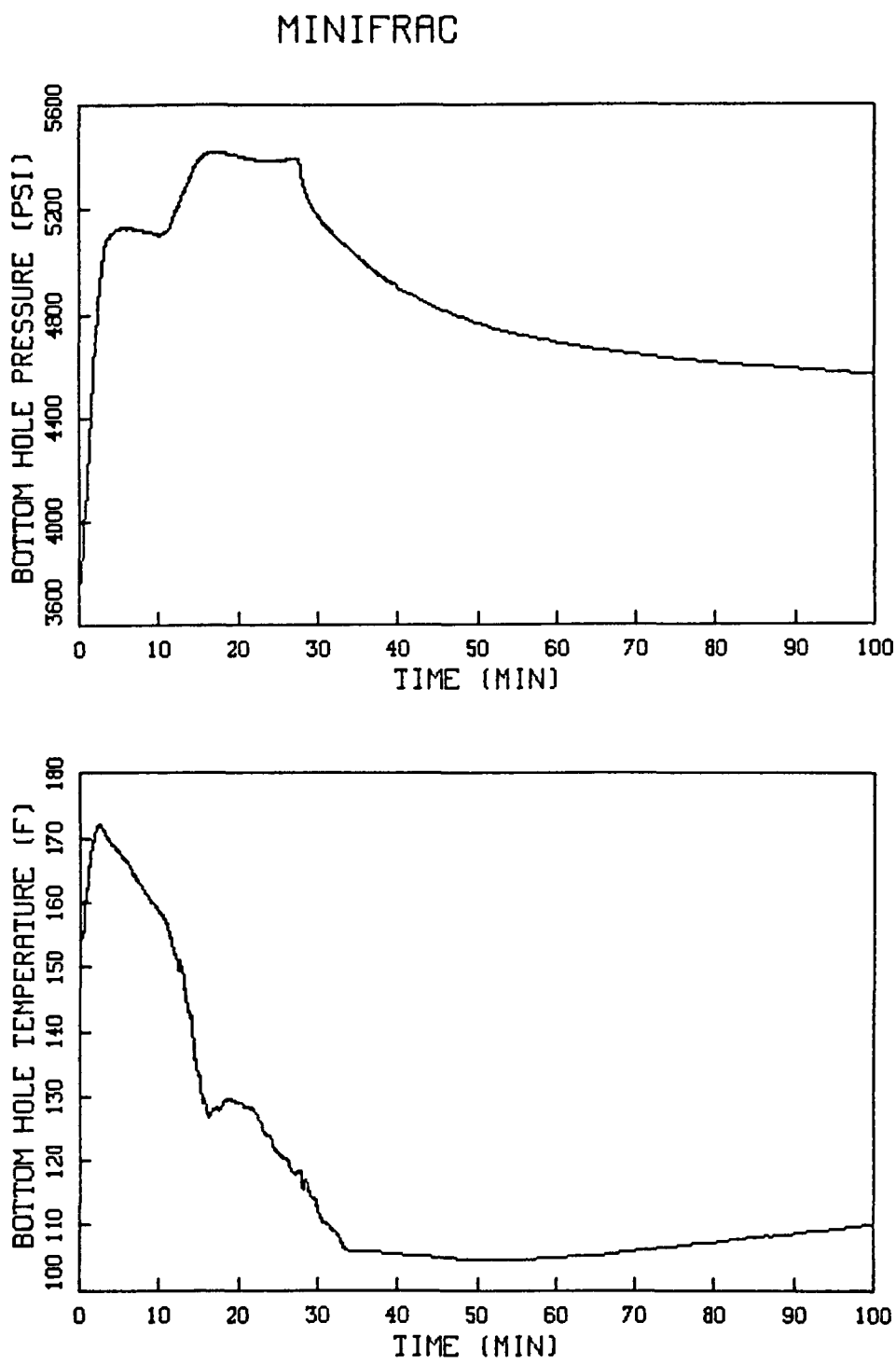

Figure 9.2.31. Minifrac Pressure and Temperature Data

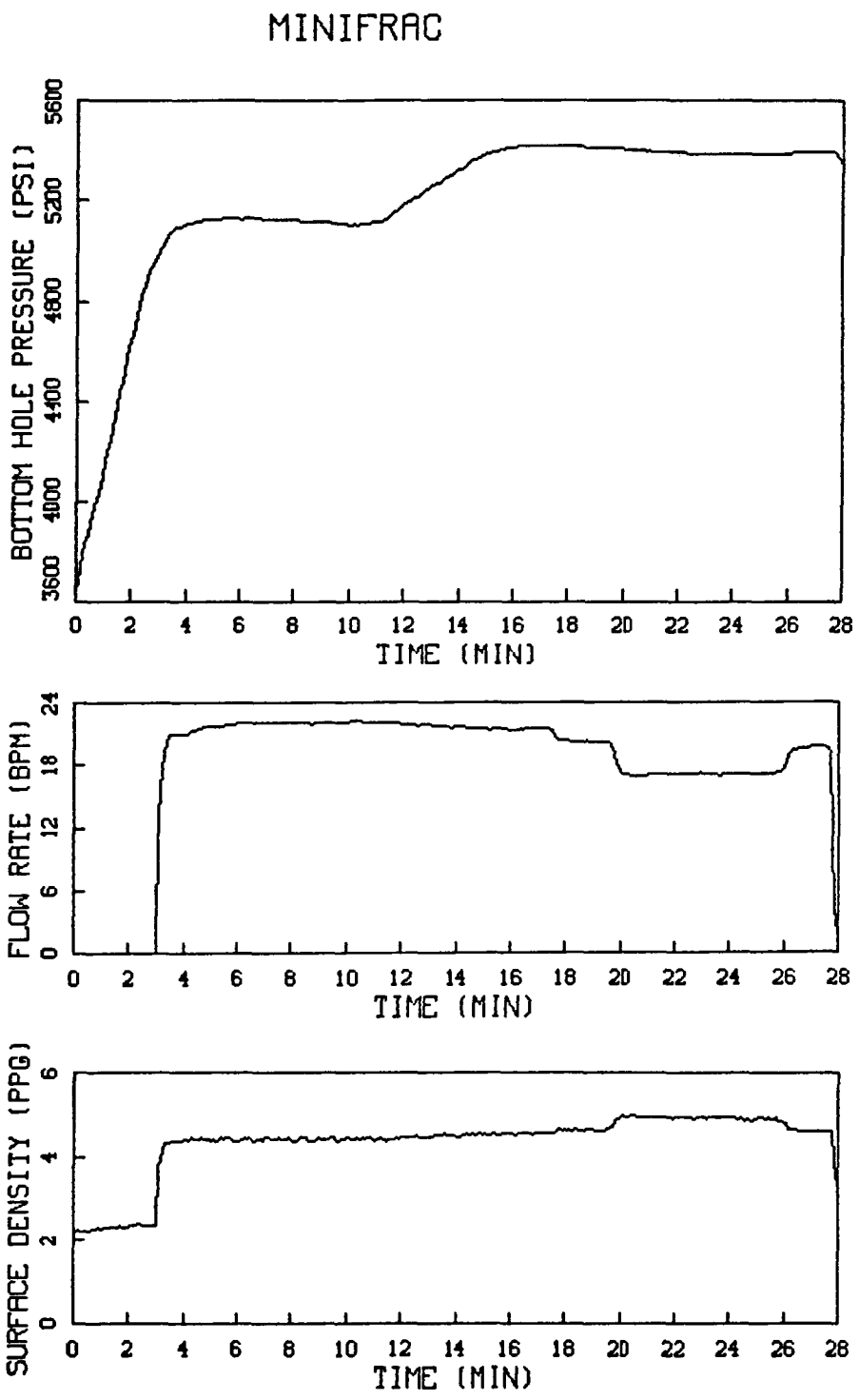

Figure 9.2.32. Minifrac Injection Data

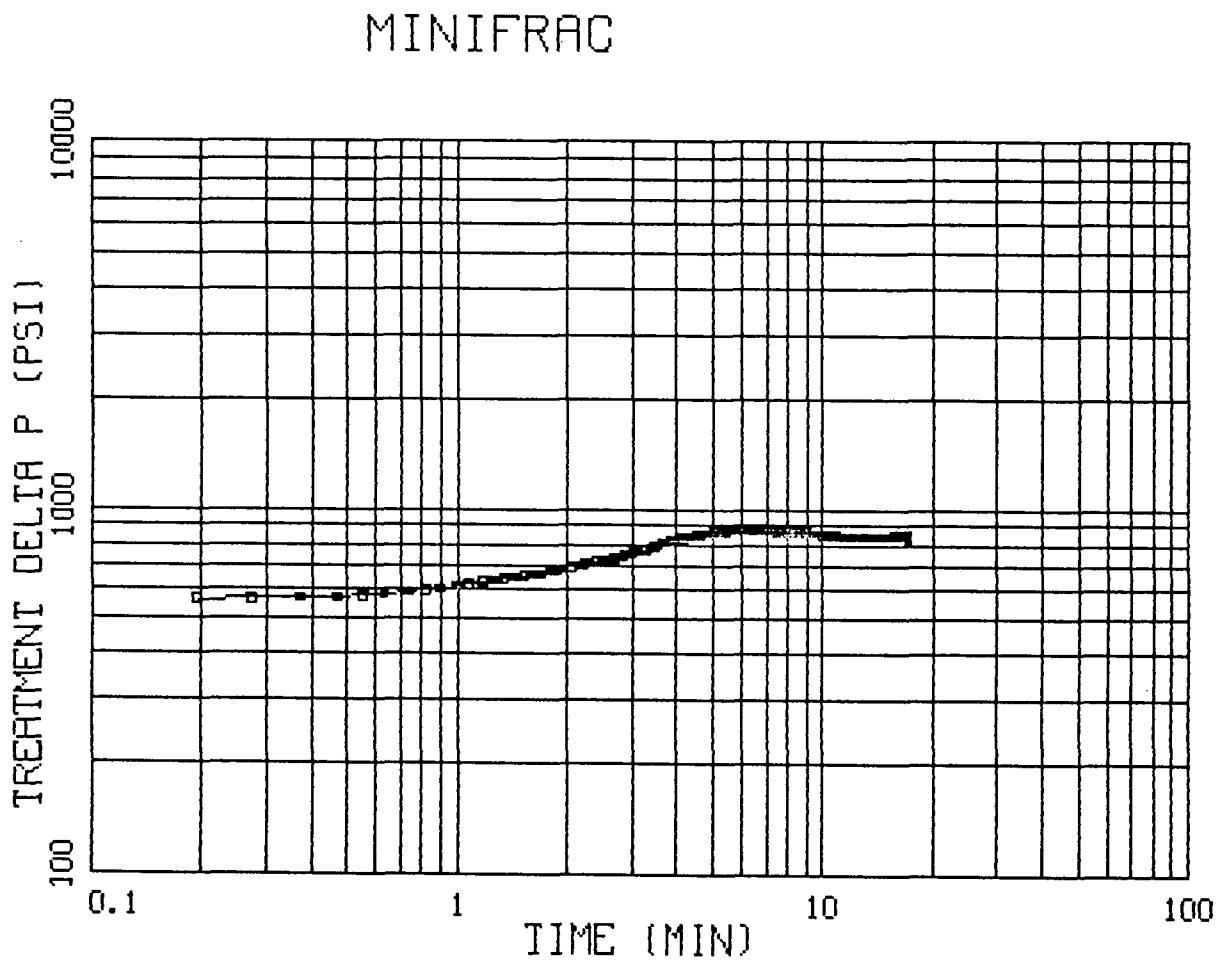

Figure 9.2.33. Minifrac Nolte-Smith Plot

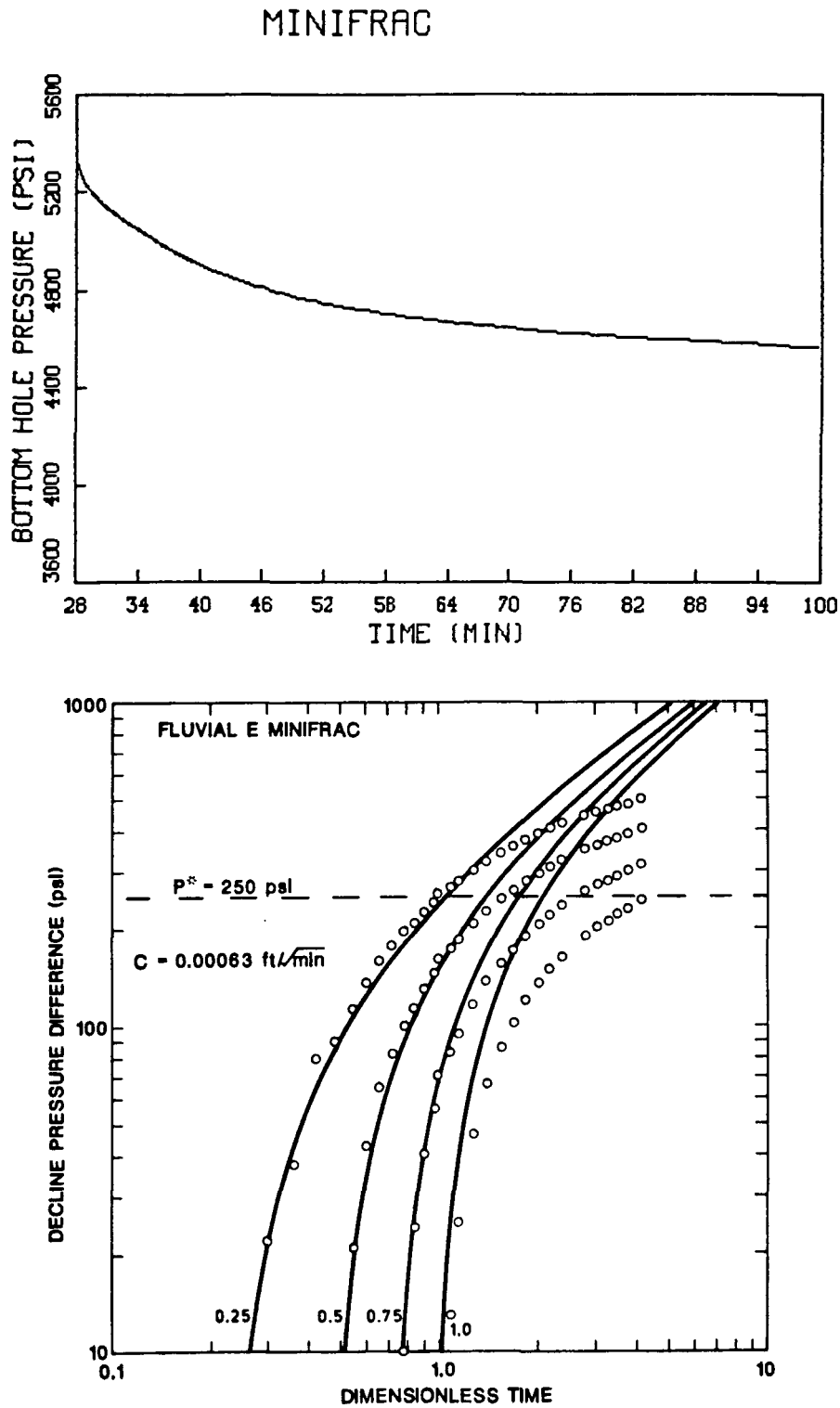

Figure 9.2.34. Minifrac Pressure Decline Results

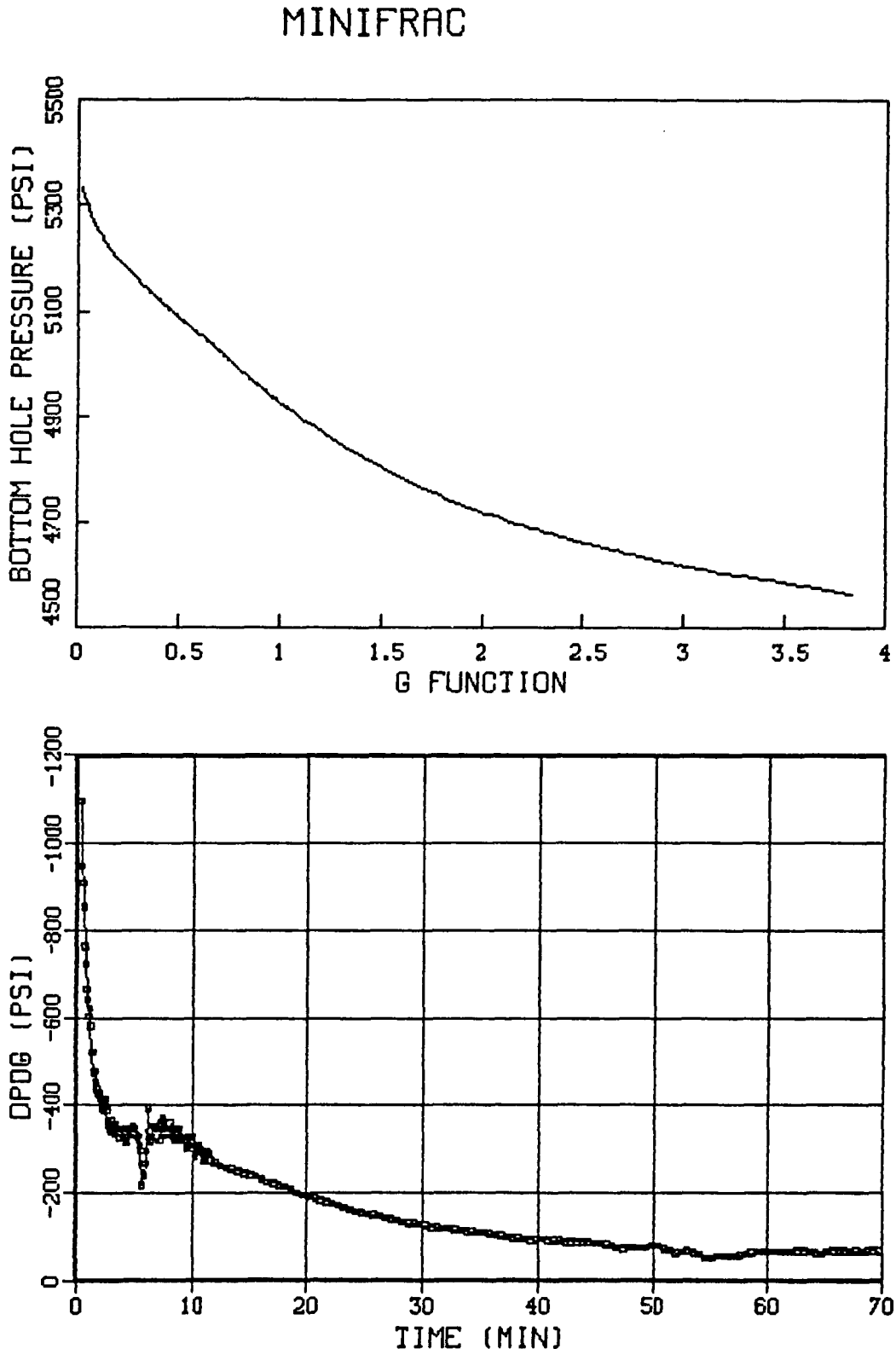

Figure 9.2.35. Minifrac Pressure vs G Function Results

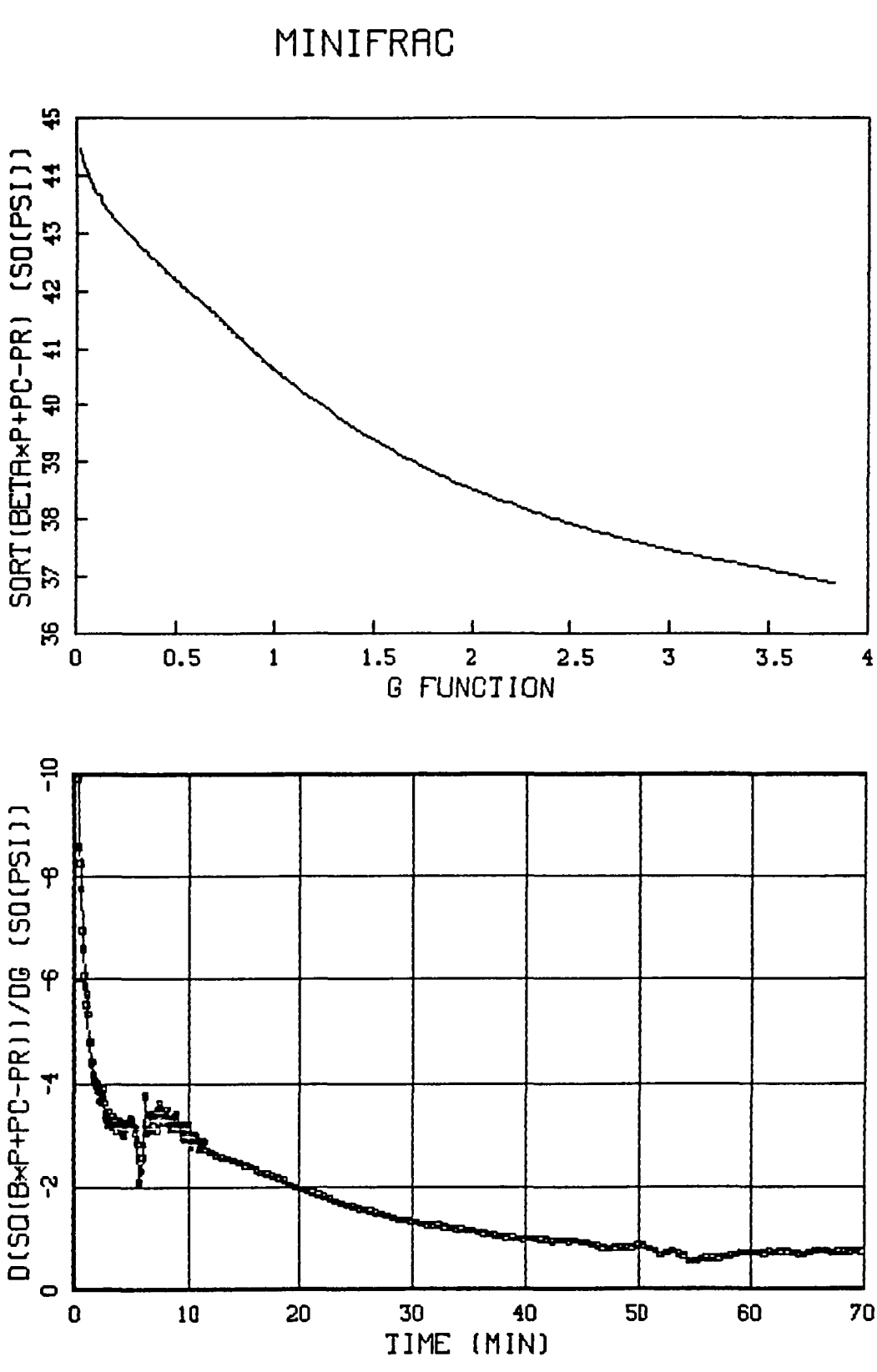

Figure 9.2.36. Minifrac Linearized G Function Results, Exponent = 1/2

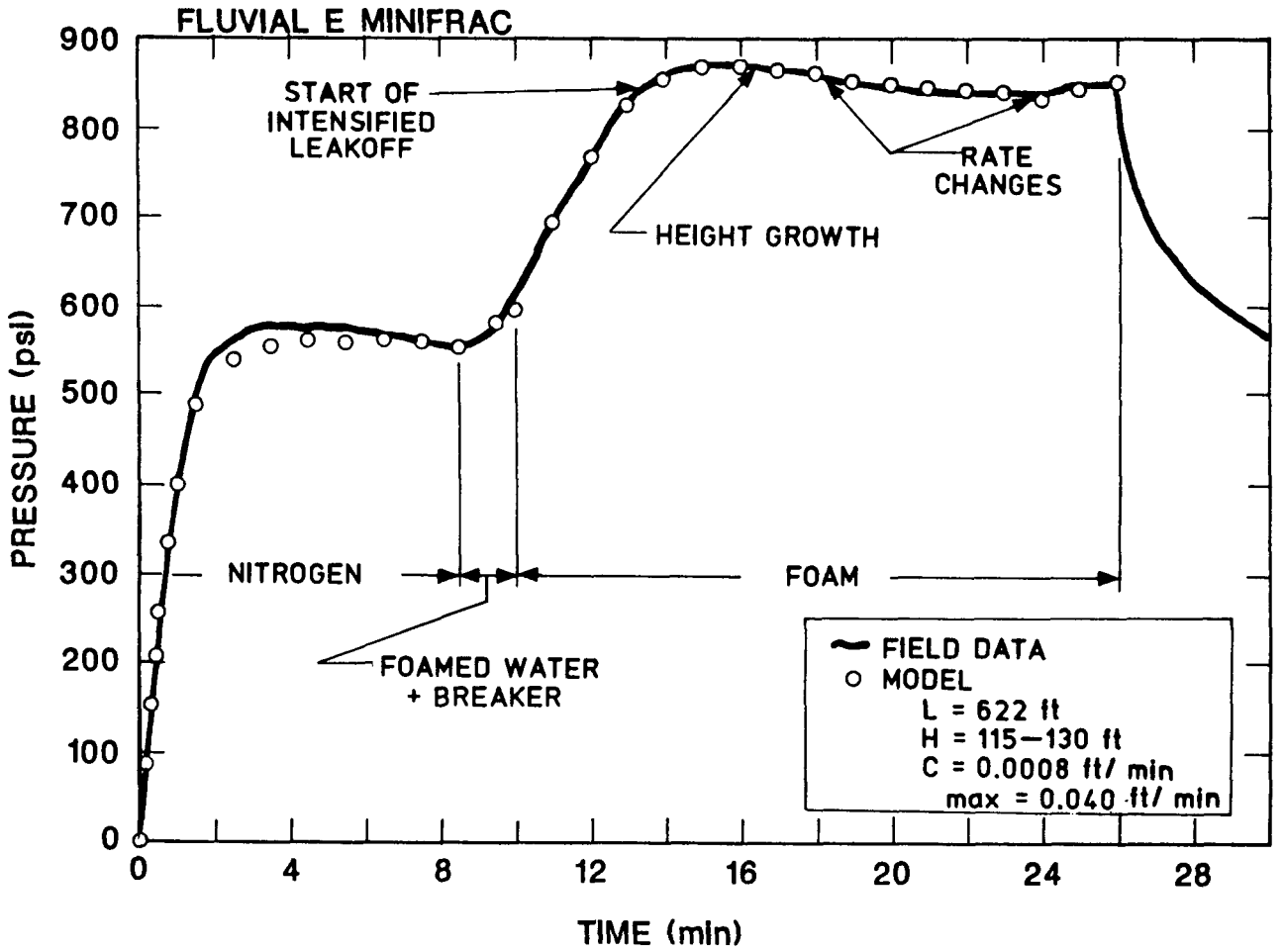

Figure 9.2.37. Minifrac Pressure-History-Match Results

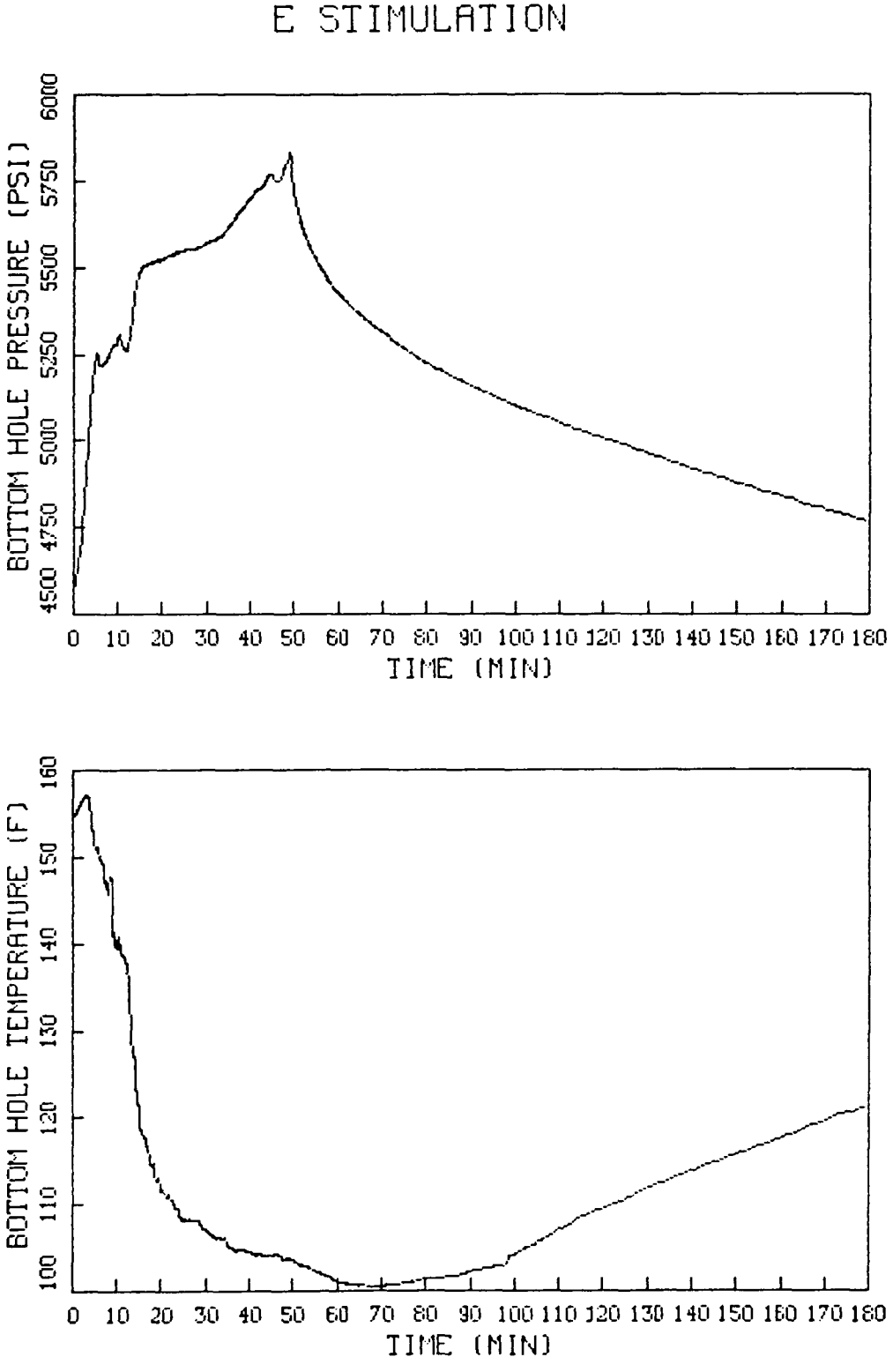

Figure 9.2.38. Stimulation Pressure and Temperature Data

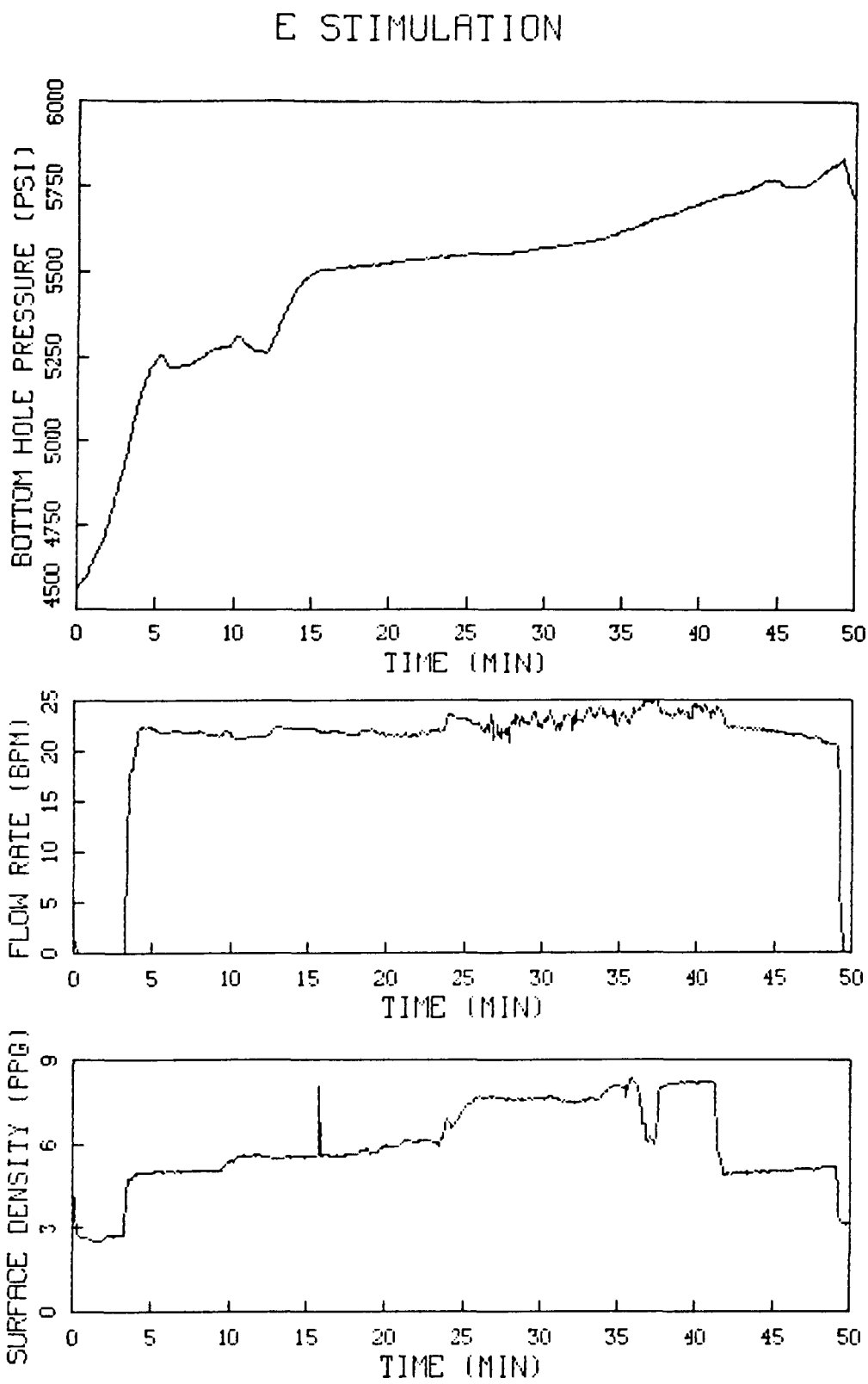

Figure 9.2.39. Stimulation Injection Data

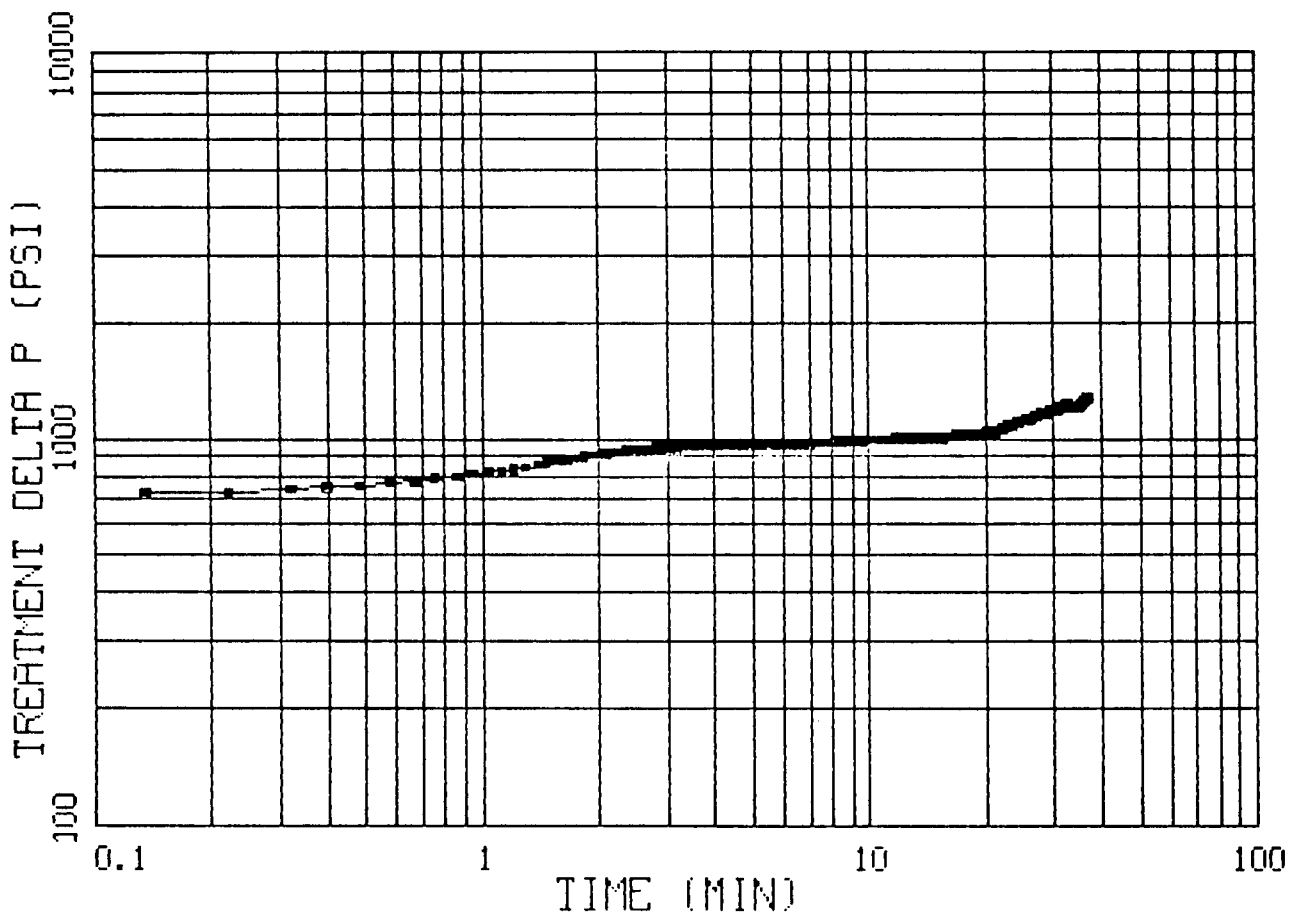

Figure 9.2.40. Stimulation Nolte-Smith Plot

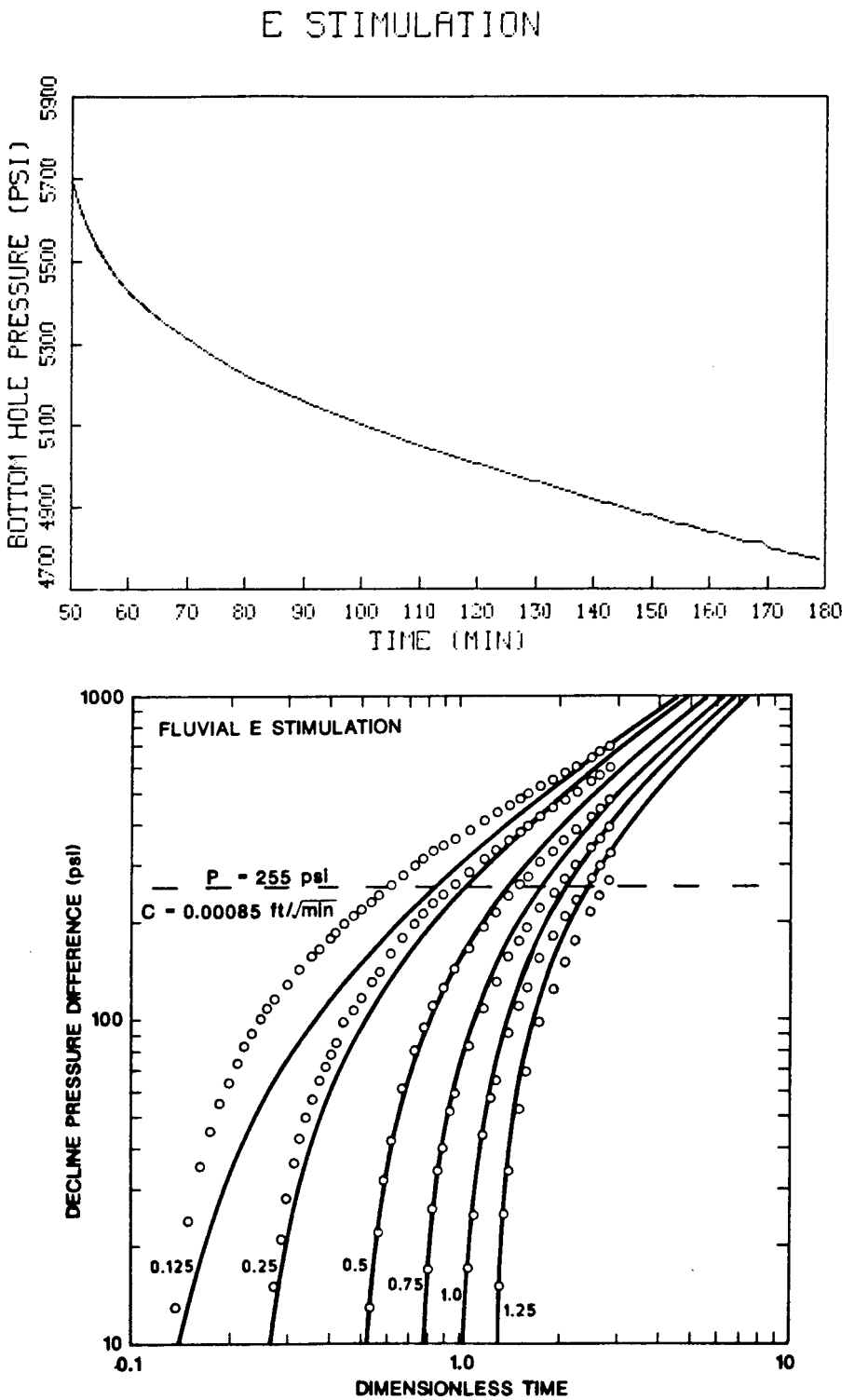

Figure 9.2.41. Stimulation Pressure Decline Results

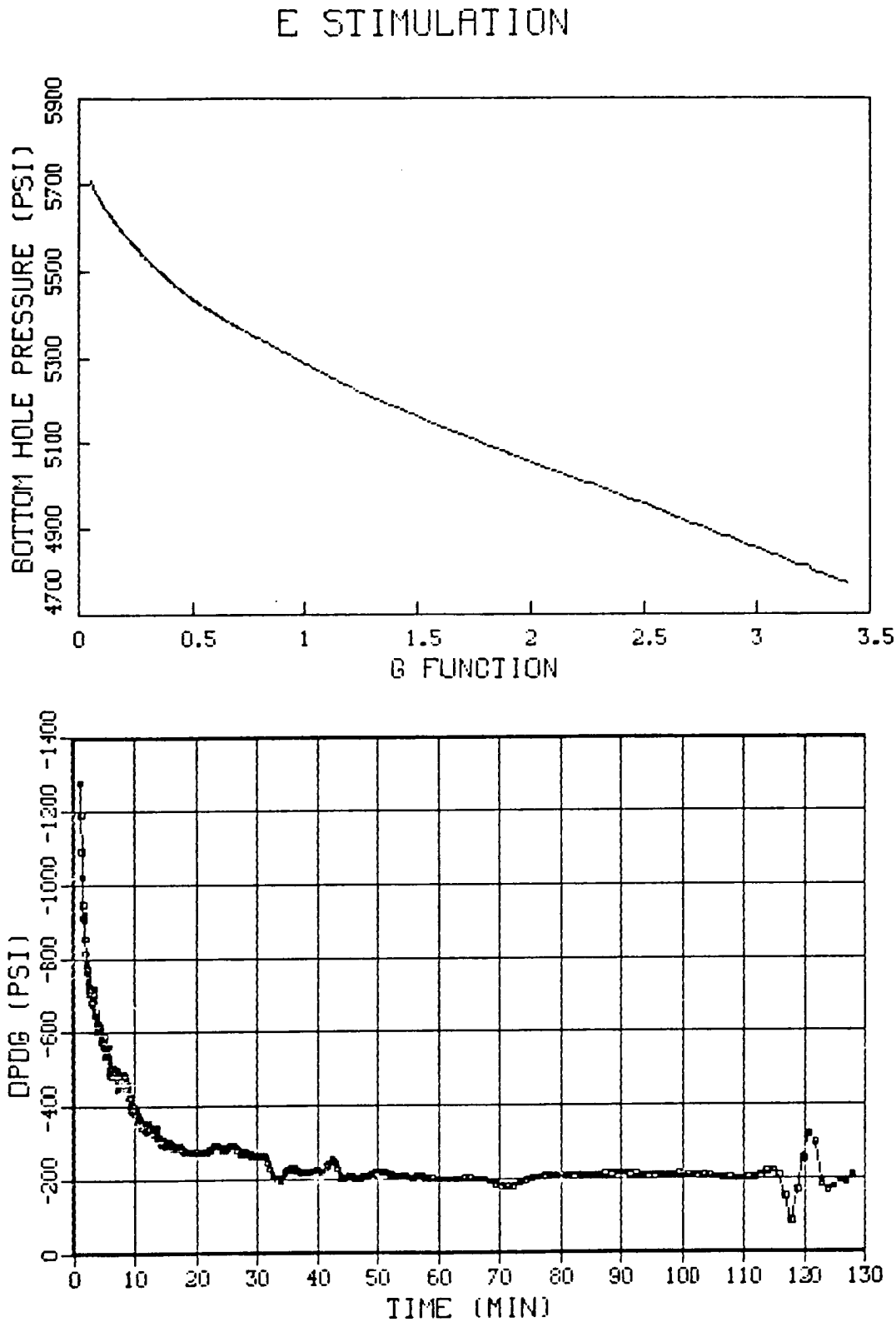

Figure 9.2.42. Stimulation Pressure vs G Function Results

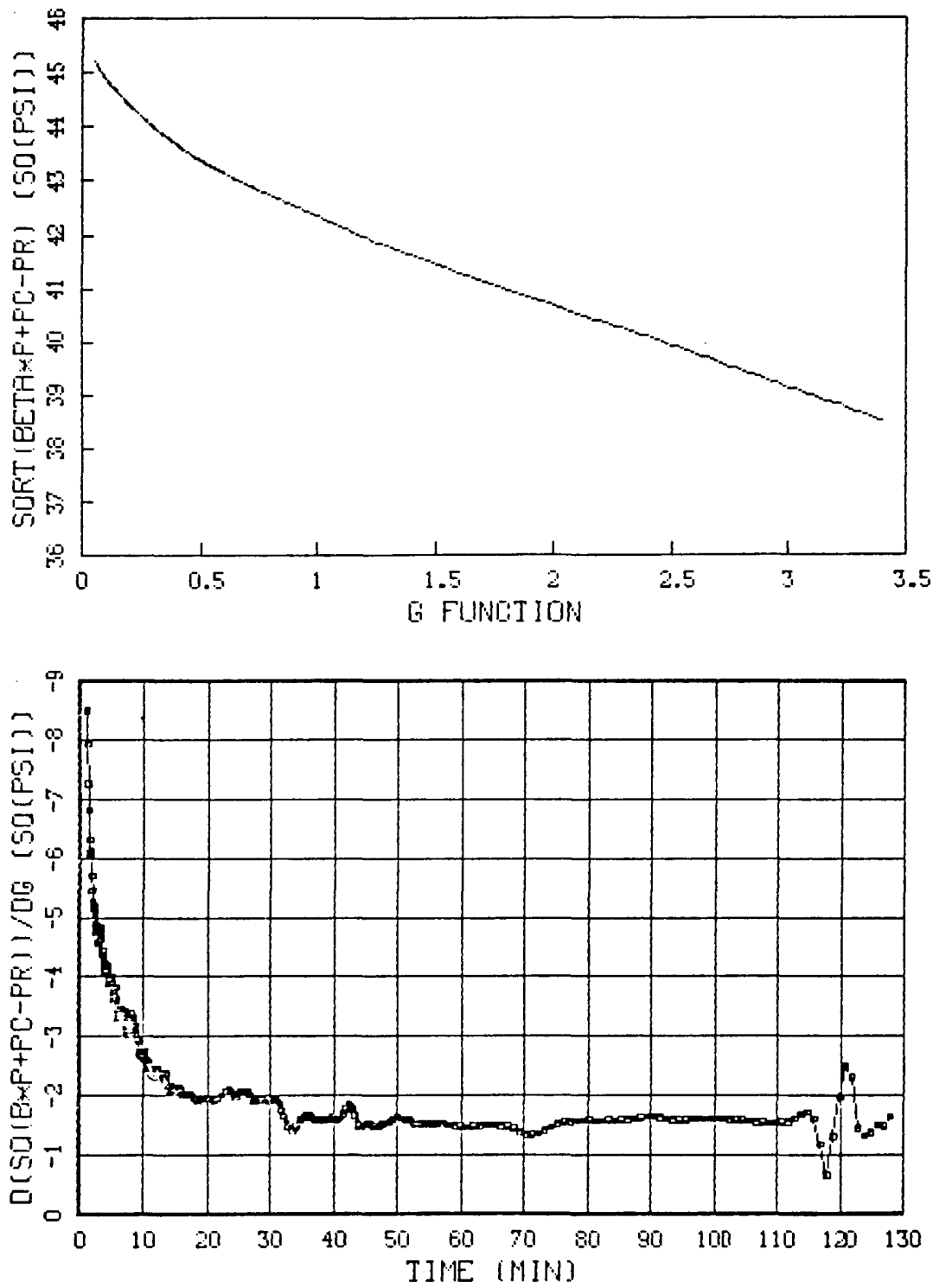

Figure 9.2.43. Stimulation Linearized G Function Results, Exponent = 1/2

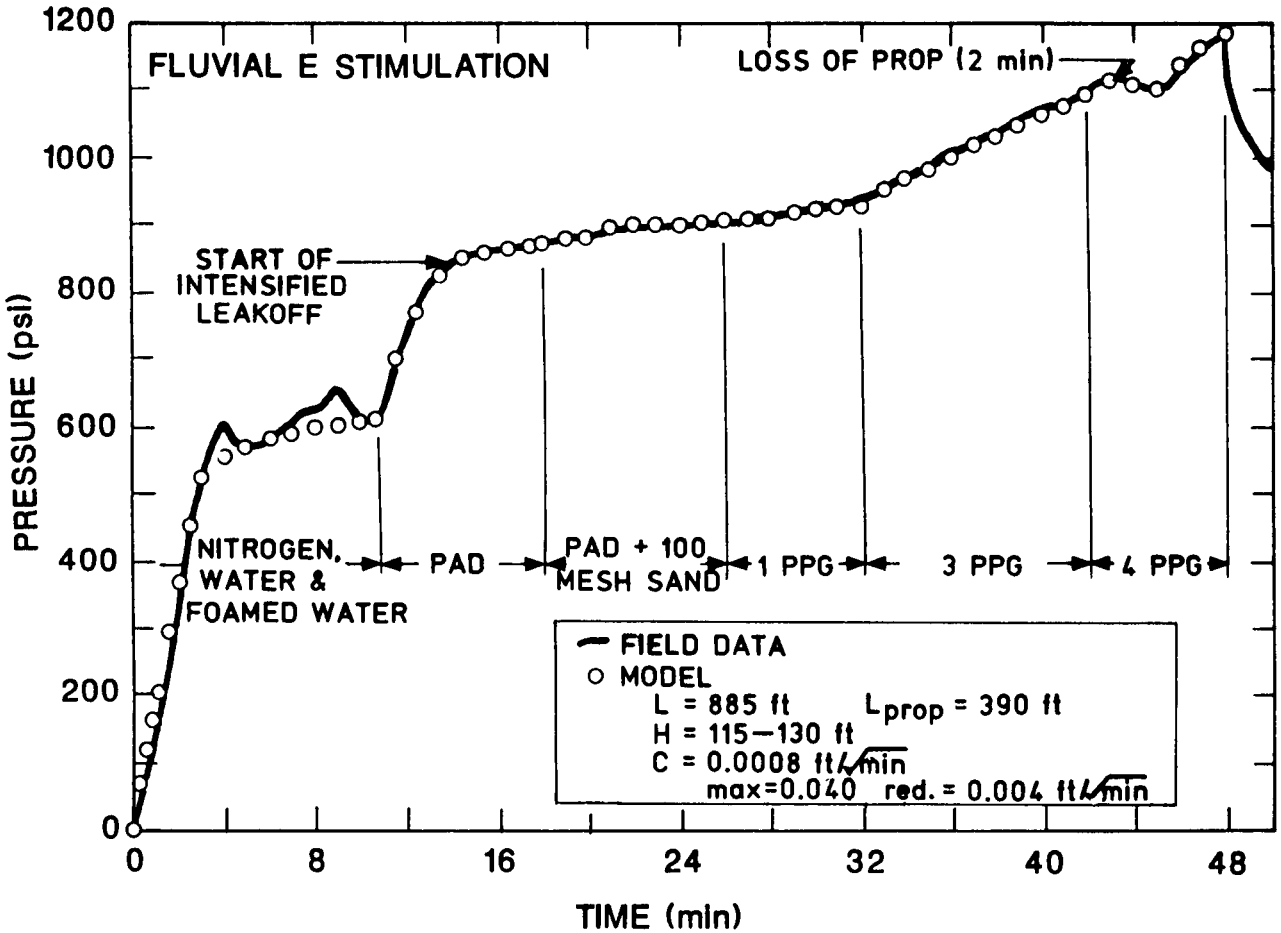

Figure 9.2.44. Stimulation Pressure-History-Match Results

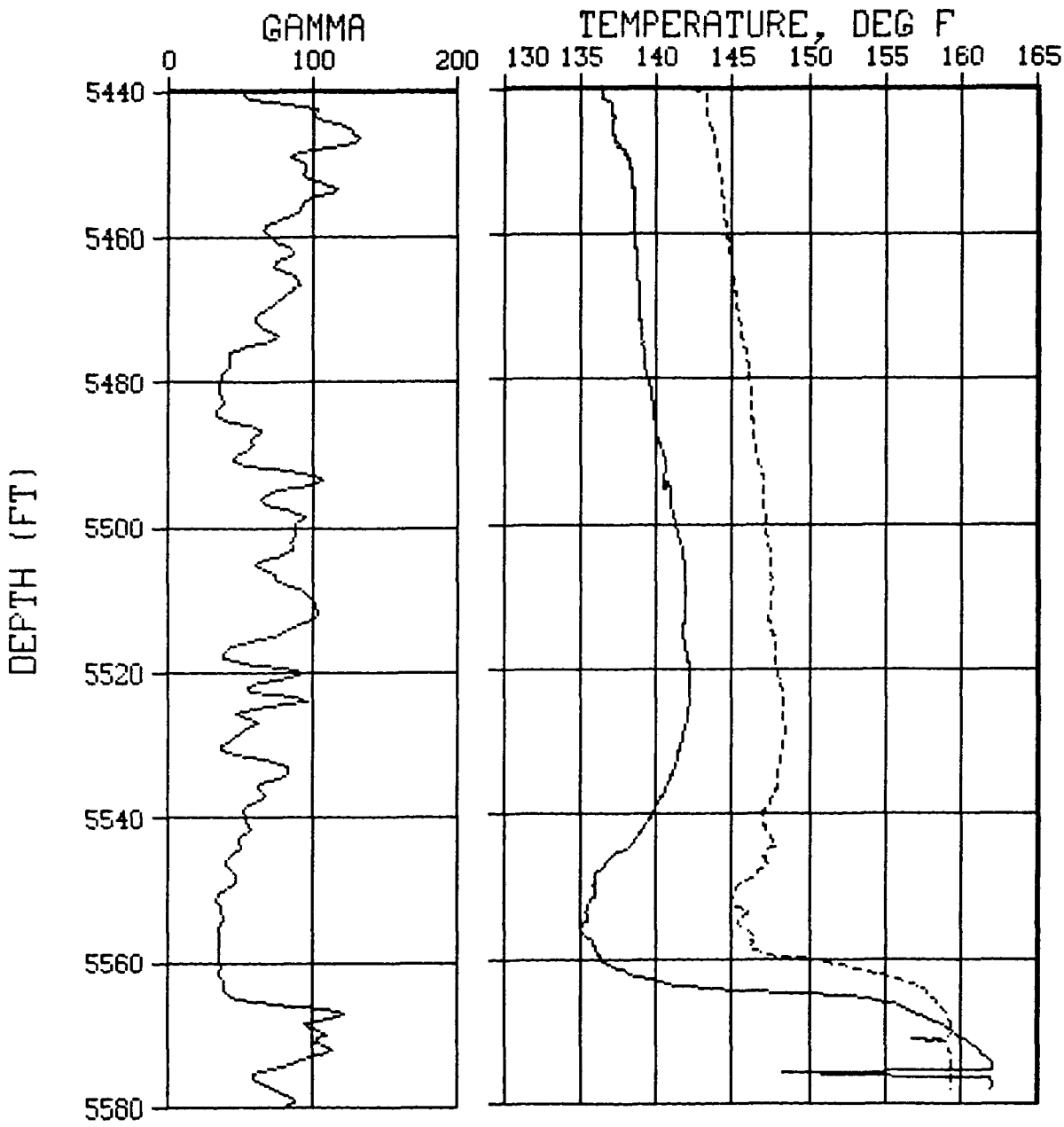

Figure 9.2.45. Post-Frac Temperature Logs

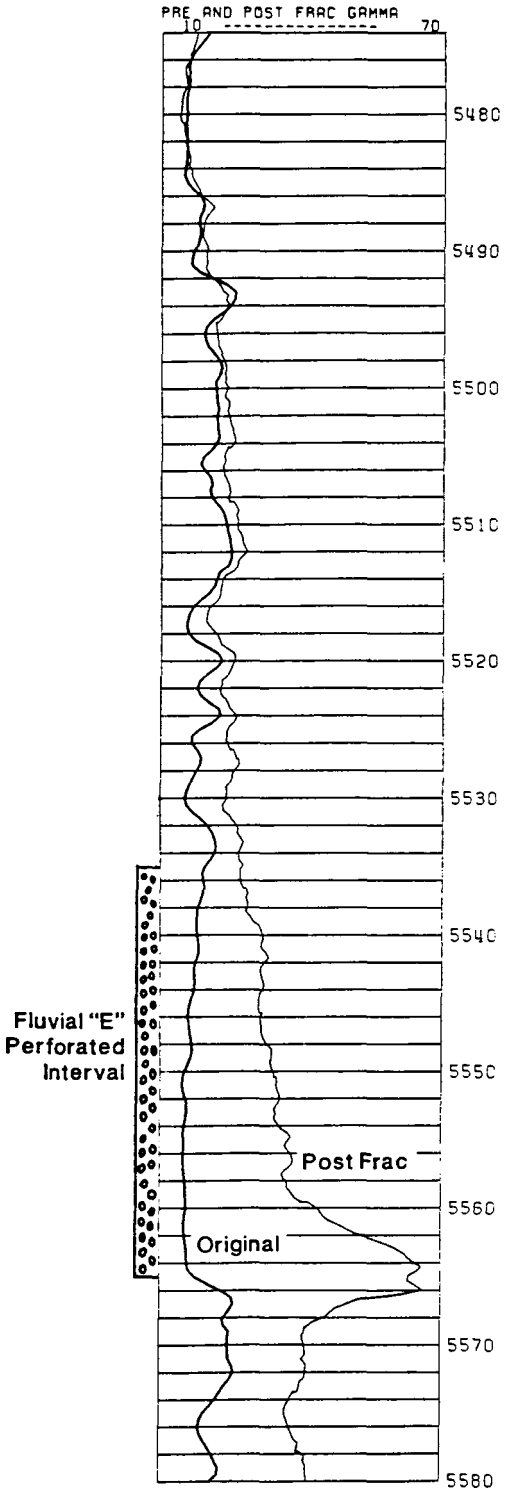

Figure 9.2.46. Gamma Ray Log

FLUVIAL E SANDSTONE STIMULATION EXPERIMENT

9.3 POST-STIMULATION RESERVOIR TESTING AND ANALYSIS

P. T. Branagan
CER Corporation

9.3.1 CLEANUP AND WELL TESTING

Immediately after the post-stimulation pressure decline and temperature logs, MWX-1 was flowed back at a fairly constant rate of 2 BPM. Very little sand was returned, and 127 BBL of the 286 BBL of fluid were recovered within 12 hours. Within two days, the well was on a flare and producing 300 MCFD. The well was produced at 250 MCFD for 5 days and was then shut-in for two days to prepare for the post-frac production test.

On October 2, 1987, the post-frac testing began. The downhole configurations on all three wells were the same as in the pre-frac testing. The test sequence consisted of:

- 16-day production test,
- 2-day interference shut-in pulse,
- 7-day production test, and
- 42-day pressure buildup test.

Data from the production well, MWX-1, during these test periods are shown in Figure 9.3.1, and includes the bottomhole pressure and the surface gas and liquid flow rates. (Digitized data for the period are given in Appendix P.) Note that liquid production, presumably returns from the fracture treatment, diminishes to less than 10 BPD after the first several days of flowback. Gas flow rate at the end of the 16-day production test was 200-220 MCFD at a bottomhole flowing pressure of 1000 psi, showing a productivity enhancement ratio of 3.4. Thus, the propped fracture resulted in substantial production enhancement in this naturally fractured, low matrix permeability reservoir.

Figure 9.3.2 is a composite plot showing the production and bottomhole pressure for MWX-1 and the corresponding bottomhole pressure in the two observation wells, MWX-2 and MWX-3. Note that the interference pressure perturbance at the closest well, MWX-2, is larger than in the more distant well, MWX-3, and is contrary to the pre-frac observation data.

9.3.2 ANALYTIC RESERVOIR ASSESSMENT

Using a linear flow analysis technique, an estimate of propped fracture length can be obtained from the MWX-1 pressure record. This linear flow analysis technique calculates propped fracture wing length, L_f, using the following,

$$L_f = 4.065\ qB/mh\ (\mu/k\phi c_t)^{0.5} \qquad (1)$$

where

q = flow rate, MSCFD
B = reservoir volume factor, CF/SCF
m = slope of the square root plot, psi/(hr)**0.5
h = net height, ft
μ = gas viscosity, cp
k = average reservoir permeability, md
ϕ = porosity,
c_t = total system compressibility, 1/psi.

Substituting the values obtained from the post-frac testing for flow rate, q, and slope, m, from the square root of time plot of Figure 9.3.3, along with the pre-frac average reservoir parameters for net height, h, porosity, ϕ, and average reservoir permeability, k, and the correct fluid properties for the test, results in a propped fracture length, L_f = 54 ft.

Although this propped fracture length of 54 ft appears small, it represents the fracture length that needs to be extended in the average pre-frac reservoir to provide a production increase of 3.4. This small calculated value of L_f is often obtained when this type of linear analysis

is applied to the more complex flow regimes inherent in an anisotropically producing, naturally fractured reservoir.

A review of the square root of time plot (Figure 9.3.3) reveals that the straight line portion of the data represents a 24-hour linear flow period. Figure 9.3.4 is the log-log/derivative plot of the buildup data. As can be seen from the early time 1/2 slope, it confirms the short 20- to 30-hour linear flow period. Thus, the flow regimes in the final post-frac testing buildup period were marked by early time, 20- to 30-hour linear flow that subsequently transitioned into a regime indicative of a dual porosity reservoir. Figure 9.3.5 is a composite log-log/derivative plot for the pre- and post-frac bottomhole pressure buildup data. In both cases, the use of a bottomhole shut-in device minimized the detrimental wellbore storage interval. From this composite plot, the linear flow period amounting to about 20 to 30 hours is readily discernable during the post-frac test and clearly differentiates it from the pre-frac test data. Furthermore, note the late time dip in the post-frac derivative data that does not appear in the pre-frac data. This change in the derivative plot suggests that a different interporosity flow regime was present during the latter portion of the post-frac test.

Recall that the propped fracture length, L_f = 54 ft, was derived from the use of average pre-frac reservoir properties. The average pre-frac reservoir conductivity, kh = 0.36 md-ft, divided by the net height for the thickest productive layer, 28 ft, results in an average reservoir permeability, k = 0.013 md (Section 9.1). To provide a range for propped fracture length, consider that the average reservoir conductivity may be reduced because of some form of damage to the natural fracture system that connects this reservoir to the propped fracture and wellbore. This damage mechanism has been shown to have significantly affected the paludal stimulations and has been the subject of considerable investigation at MWX. Assume then that the natural fractures adjacent to the propped fracture are completely plugged and do not contribute to production. Therefore, the only productive portion of the reservoir that remains in contact with the propped fracture is the tight matrix rock. Substituting the matrix value, k_m = 0.002 md into Equation 1, yields a propped fracture length, L_f =

150 ft. This suggests that some form of natural fracture production impedance may have existed during the post-frac testing period if the induced propped fracture actually extended beyond 54 ft into the reservoir.

One other possibility for the apparent short, calculated fracture length may result from the fact that the average permeability, k, used in Equation 1, did not include the effects of the considerable anisotropy, which from the pre-frac modeling was found to be about 30 to 1. When that permeability ratio is included in the calculation, fracture length increases to about 150 ft. Although this result is in better agreement with other diagnostic data that indicated a propped fracture length around 400 ft, it still represents a short fracture and thus some combination of natural fracture damage and the recurring anisotropy most probably existed during the post-frac testing and slightly limited production.

Figure 9.3.6 is a Horner plot of the post-frac bottomhole pressure data and further illustrates the complexity that exists in the flow regimes during the pressure buildup. Estimates of reservoir behavior based on Horner analysis are not appropriate since the flow regimes appear to represent some form of linear flow and the complex interaction between the natural fractures and the tight matrix. Except for the very late portions of the test, it could even be considered that the reservoir was exhibiting radial or pseudo-radial flow. Thus, Horner analysis would not be appropriate with this buildup data set.

Interference is clearly seen in both observation wells as seen in Figure 9.3.2, and, as in the pre-frac tests, the response was much faster in MWX-2 than in MWX-3. However, the interference pressure in MWX-2 during the post-frac testing appears to be not only faster but also larger in magnitude than during the pre-frac tests. This suggests that the propped fracture is in closer proximity to MWX-2 than to MWX-3 and is as expected from the current in situ stresses and well location.

9.3.3 RESERVOIR MODELING

A large number of reservoir simulations were conducted in an attempt to model the reservoir behavior during this post-frac testing period. Variations in simulation or modeling parameters included:

- propped fracture properties,
- natural fracture damage, and
- matrix variations near the propped fracture.

The initial attempts to include a simple, simulated propped fracture into the multilayered pre-frac model described in Section 9.1.4.3.2, provided less than an acceptable match to the measured data. Figure 9.3.7 is an overlay of data obtained from one of these model runs along with the field test data. In this case, the simulated propped fracture was considered to extend through both reservoir layers, have a propped fracture length of 400 ft, and have a dimensionless fracture conductivity in excess of 100. This large dimensionless fracture conductivity is consistent with the bottomhole pressure data shows an early period of linear flow with no apparent period of bilinear flow. The absence of a bilinear flow period implies that the propped fracture must possess a relatively high conductivity. Note that during the flow periods, the model provides reasonably good adherence with the field data, but fails to provide an appropriate match with the pressure buildup data. A supplementary presentation of the data is seen in the composite log-log/derivative plot shown in Figure 9.3.8, and contains the bottomhole pressure buildup data acquired from the field and the matching pressure data from the simulator. This plot amplifies the poor match.

A systematic series of model parameter variations in simulated propped fracture conductivity, length and porosity, separately or in concert, did not significantly improve the match. Although corresponding values of model and field production rates and pressure could be achieved during flow periods, the final bottomhole pressure simulation, particularly when displayed in the log-log/derivative format, was never consistent to warrant serious consideration as a suitable match.

Since some damage from the foam stimulation treatment to the natural fracture system was considered probable, particularly in view of previous post-frac reservoir behavior in the paludal, coastal and fluvial intervals, the reservoir simulator was modified to include damage to the natural fractures. This damage was introduced in the model reducing the conductivity of those natural fractures that were immediately adjacent to the propped fracture. The magnitude of the damage and its spacial extent were varied over a wide range. The process involved the actual changing of natural fracture properties, such as reducing the original high permeability to a considerably lower value, while jointly reducing fracture porosity. This process is a considerably more accurate representation of real in situ damage mechanism than the more common practice that involves the inclusion of arbitrary skins.

Figure 9.3.9 is a composite log-log/derivative plot that includes the field data and the model output for a case which contained some damage to the natural fractures that were directly connected with the simulated propped fracture. Note that although there is a considerable change in the shape of these curves for the modified fracture system as compared to the unaltered system shown in Figure 9.3.8, there are still considerable differences when compared to the field data. Altering the degree of natural fracture damage along the length of the propped fracture as well as developing damage that had deeper and deeper penetration into the natural fractures provided an interesting simulation, but still did not produce an acceptable match for the pressure buildup data.

The final changes in the stimulated reservoir model involved reducing the matrix permeability of the thinnest, least productive of the model layers. This reduction in the matrix permeability of the thin, 1 ft, highly fractured layer was aimed at replicating some form of matrix degradation presumably caused by the treatment process. Further, this reduced matrix permeability, k_m = 0.0001 md, may also indicate that original value of matrix permeability, k_m = 0.002 md, used in the pre-frac modeling was initially set at too large a value. Figure 9.3.10 is a composite plot for this final model run and the field data. This model includes a propped fracture with wing length, L_f = 500 ft, the reduced

matrix permeability, k_m = 0.0001 md, in the thin, 1-ft layer, and some damage to the anisotropic natural fractures that abut the propped fracture. Included in this composite data plot is the pressure match for the observation well, MWX-2.

9.3.4 POST-STIMULATION TESTING SUMMARY

The post-frac field testing of the fluvial E sandstone was successfully performed during the fall of 1987. The test period covered over two months of extensive data acquisition. Although the test was reasonably complicated, few operational problems were encountered and none compromised the testing sequence. The measured data included an excellent set of bottomhole interference pressures from both observation wells, MWX-2 and MWX-3, and is considered to be the most comprehensive post-frac data set acquired at MWX. The productivity increase from 65 MCFD to 220 MCFD, a factor of 3.4, attests to the fact that the foam stimulation treatment of this complex naturally fractured reservoir was effective from a reservoir stimulation standpoint. In addition, the stimulation was an operational success.

A review of the bottomhole pressure buildup data from the fracture well, MWX-1, particularly in the form of the log-log/derivative plot, underscores the complexity of the flow regimes that existed in the reservoir and propped fracture. The very early portion of the data provides a clear indication that the primary flow regime was linear and implies that the propped fracture was a highly conductive flow channel. This reservoir linear flow period was followed in about 24 hrs by a flow regime indicative of the transition period normally associated with dual or interporosity flow behavior. Since the linear flow period, that began within minutes of shut-in, was considered to be the result of linear flow within the reservoir as opposed to fracture linear flow, the propped fracture conductivity would by necessity be large.

The final history match of the entire post-frac well test of the fluvial E provides a good correspondence between field observation and model parameters. The simulation, however, involved considerable model

parameter variation and underscores the complexity of the in situ processes and our limited understanding of them.

One of the more salient conclusions drawn from this extensive set of modeling runs is that the original pre-frac model of the fluvial E reservoir required modification beyond just the addition of a simple propped fracture for the model to match the behavior observed in the post-frac testing. These alterations involved the inclusion of some damage to the natural fractures that intersect the high conductivity propped fracture, as well as a significant change in the late time interporosity flow mechanisms that was modeled by reducing the matrix permeability in one of the model layers.

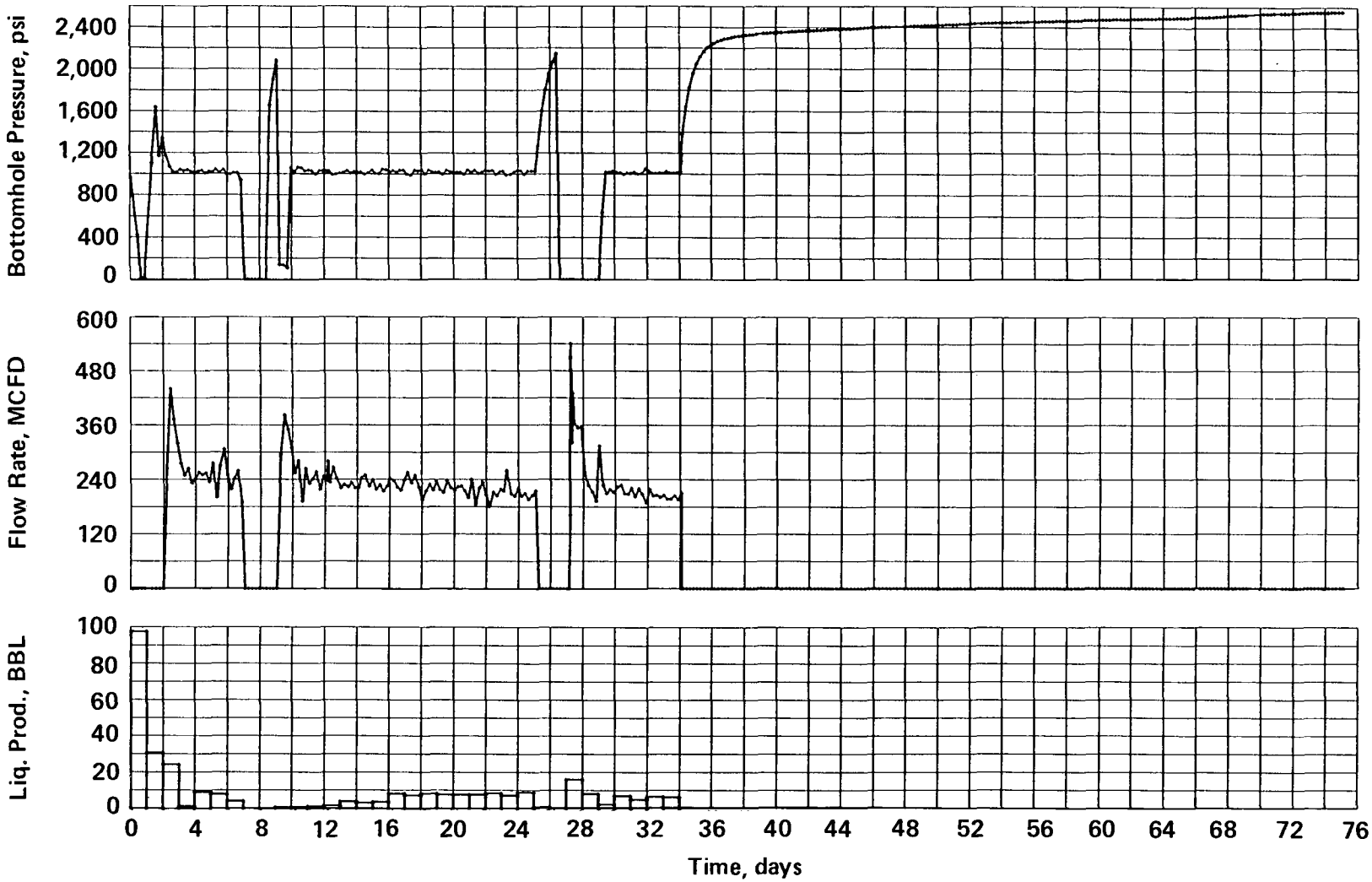

Figure 9.3.1 Post-Frac Flow and Pressure Data

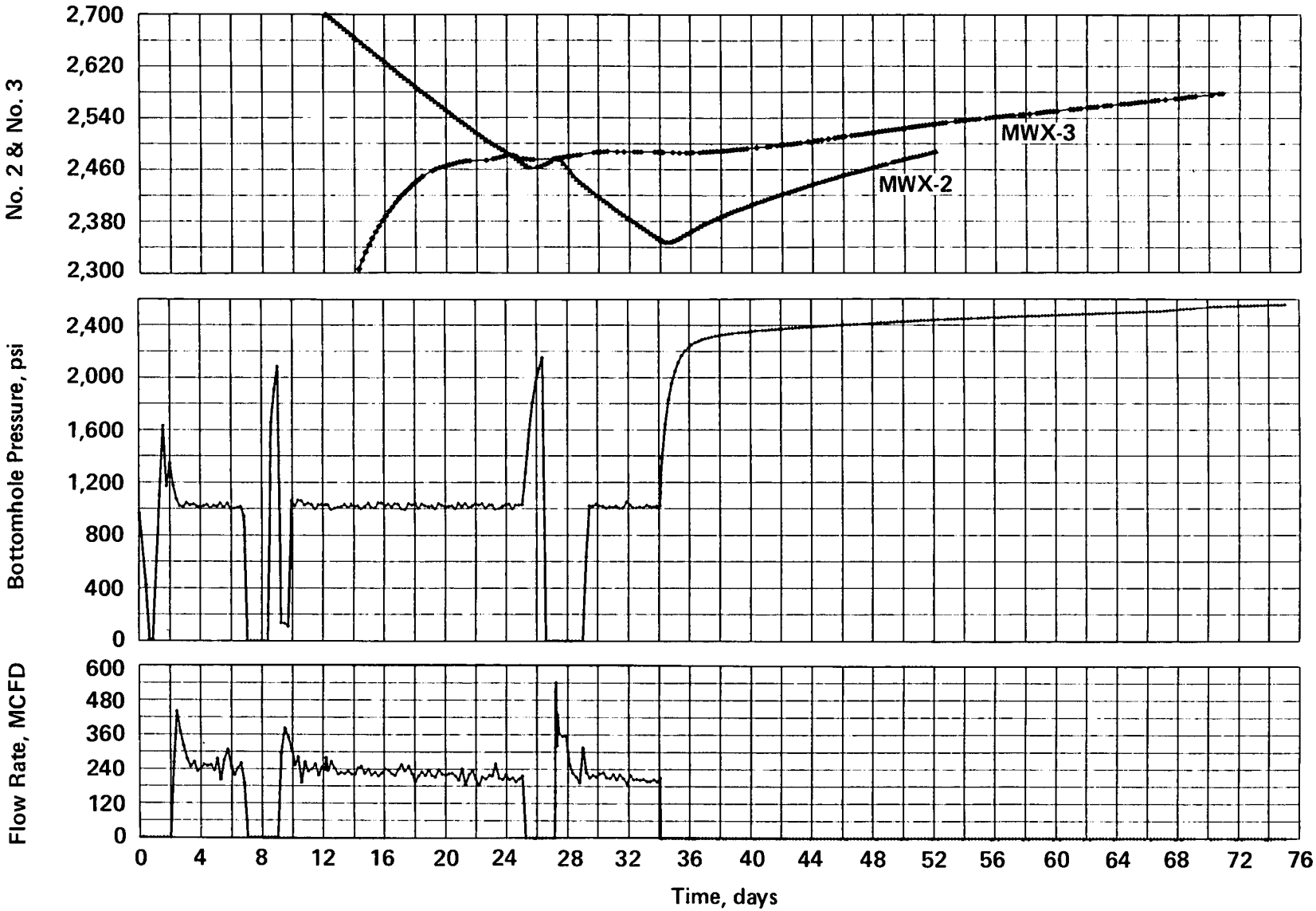

Figure 9.3.2 Post-Frac Flow and Bottomhole Pressure Data

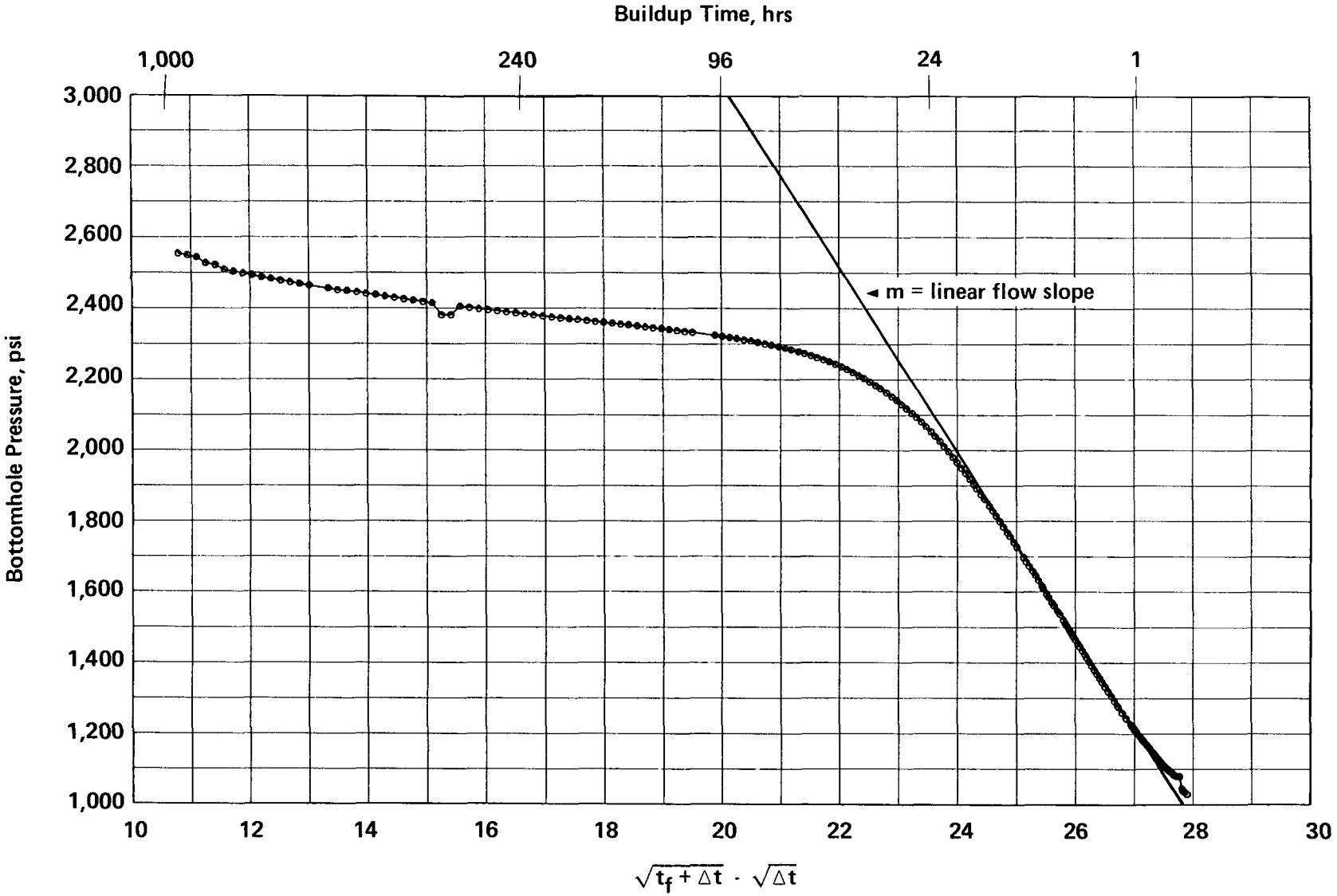

Figure 9.3.3 Post-Frac Buildup Test, Square Root Plot

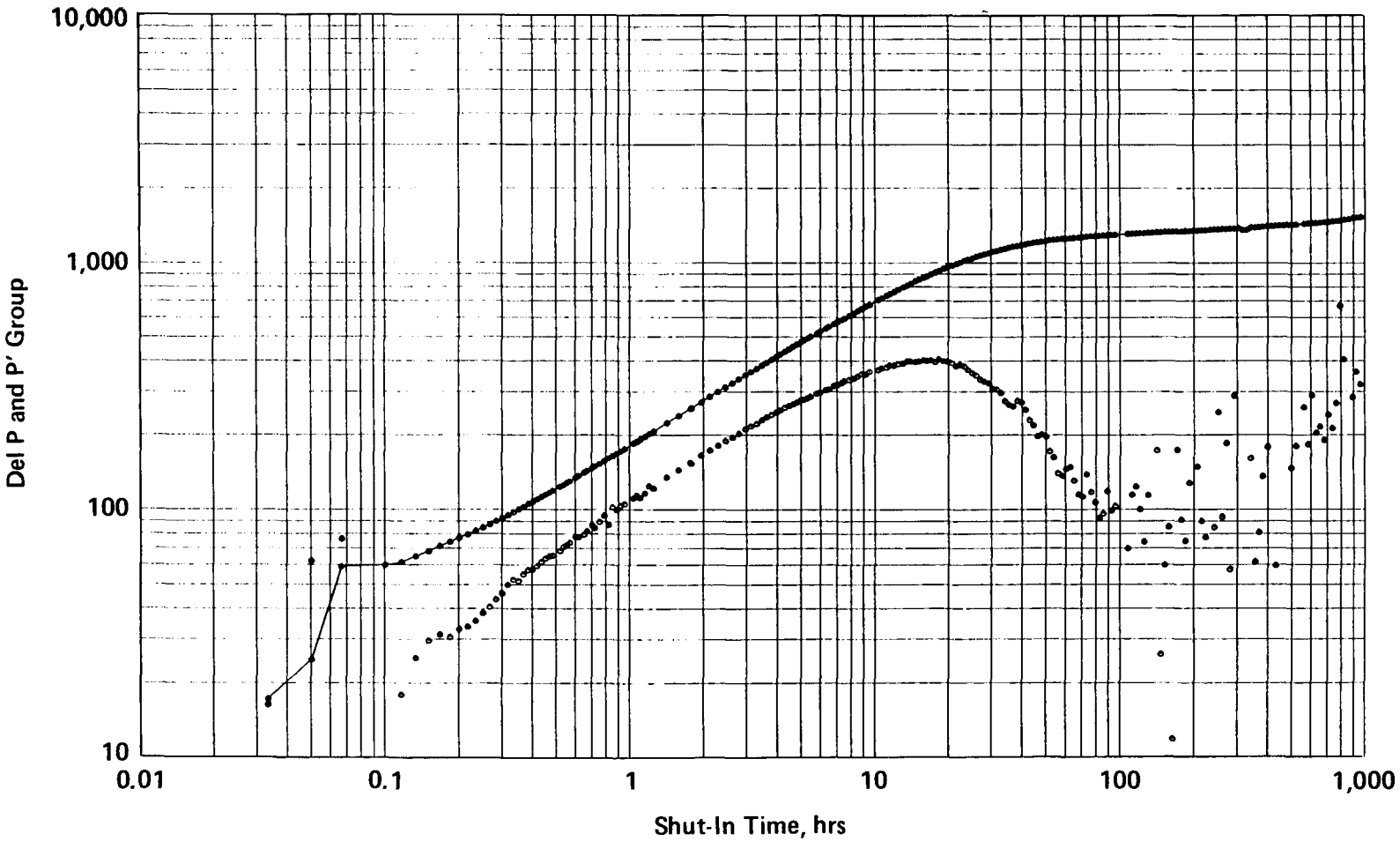

Figure 9.3.4 Post-Frac Buildup Test, Log-Log and Derivative Plots

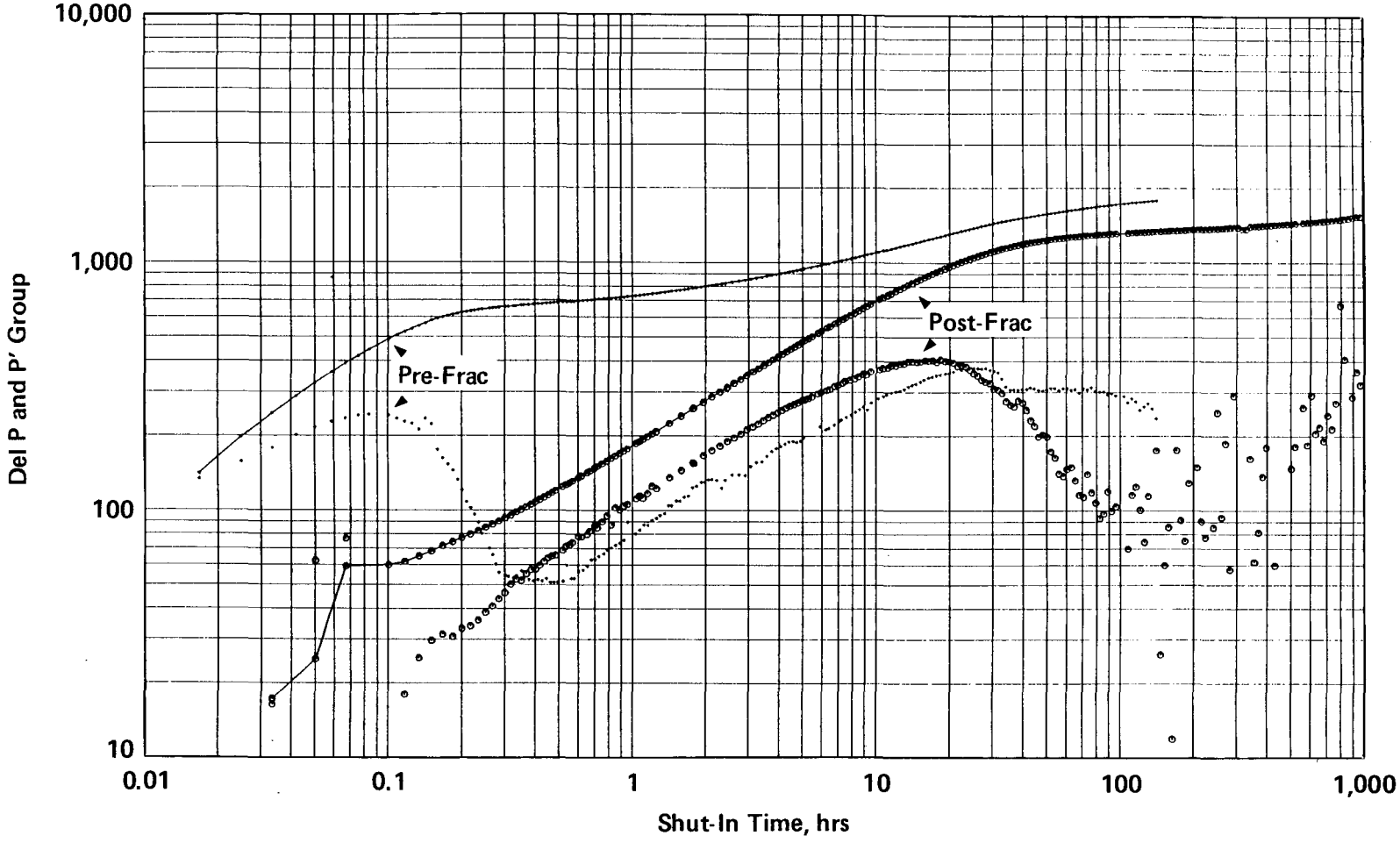

Figure 9.3.5 Comparison of Pre-and Post-Frac Buildup Pressure Data

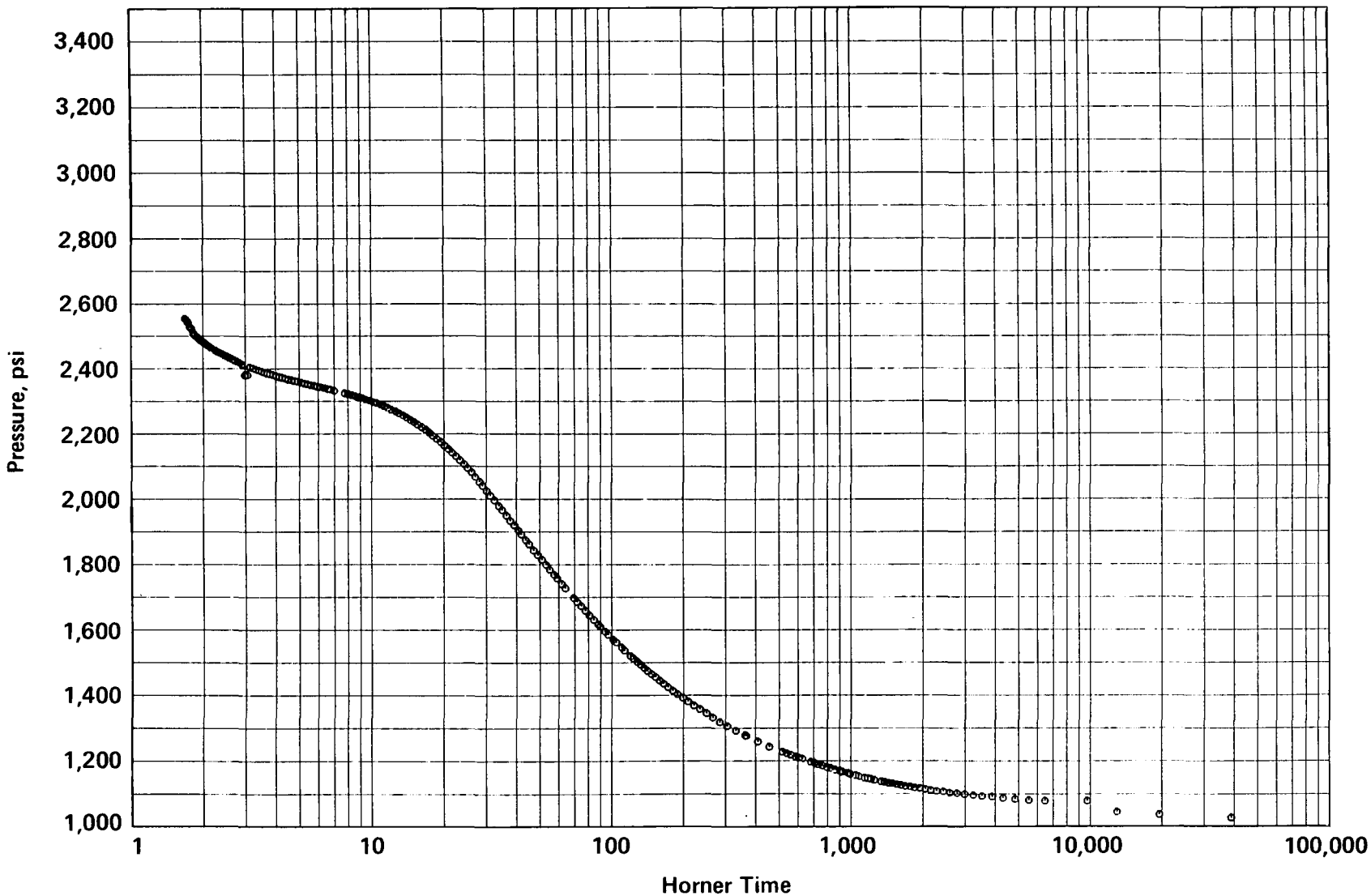

Figure 9.3.6 Post-Frac Buildup Test, Horner Plot

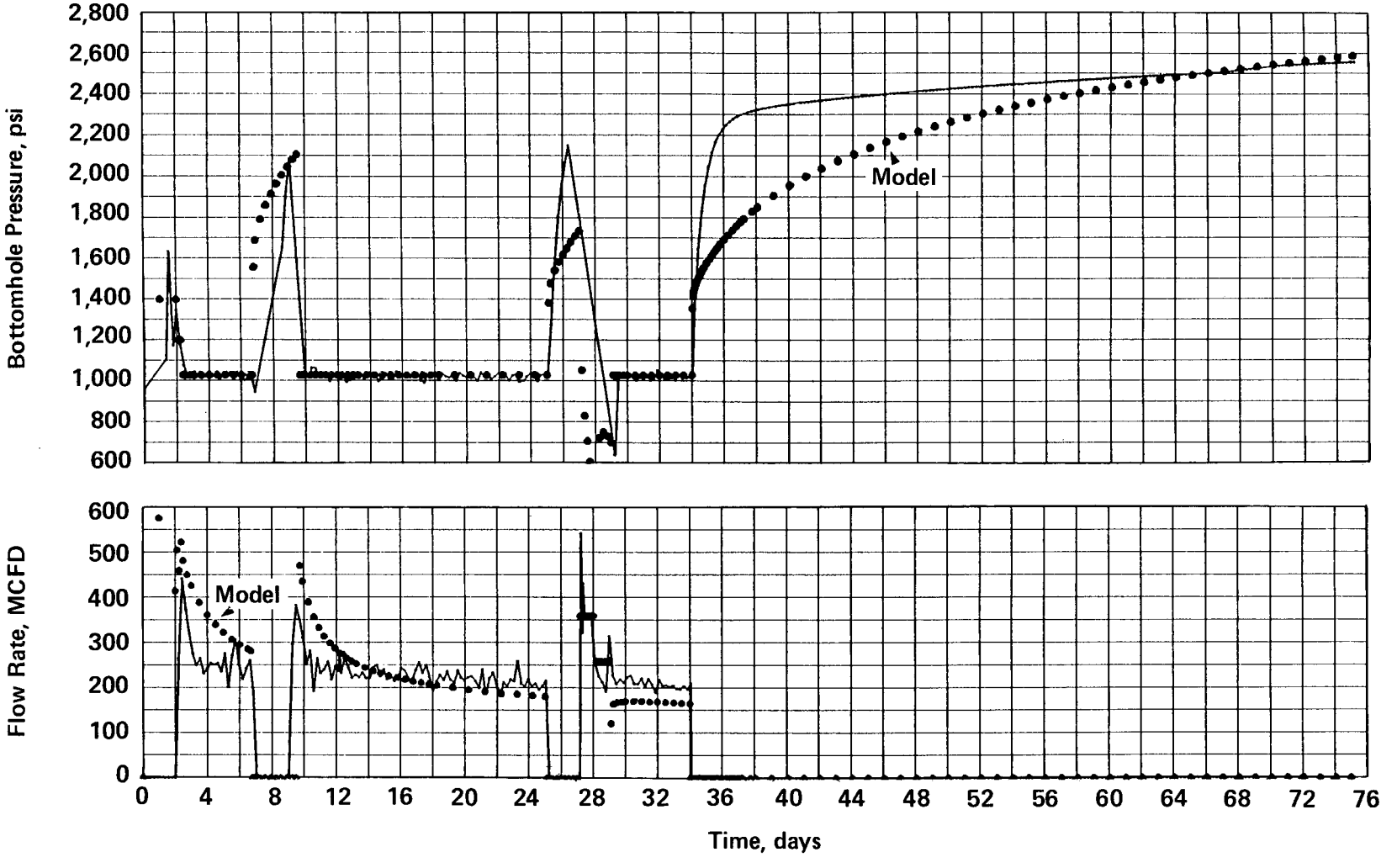

Figure 9.3.7 Comparison of Simulated and Field Data, Initial Match

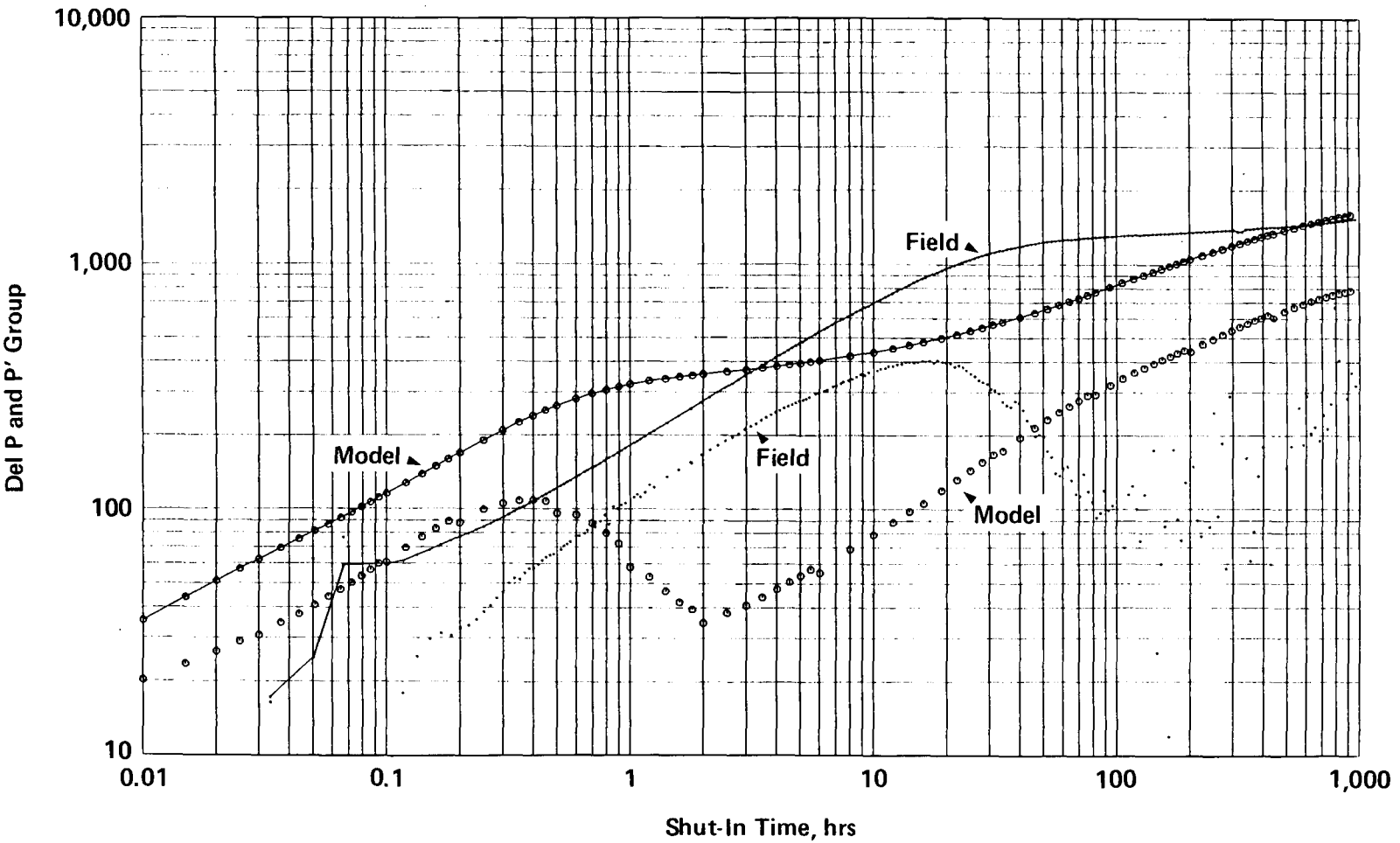

Figure 9.3.8 Comparison of Simulated and Field Data, Initial Match

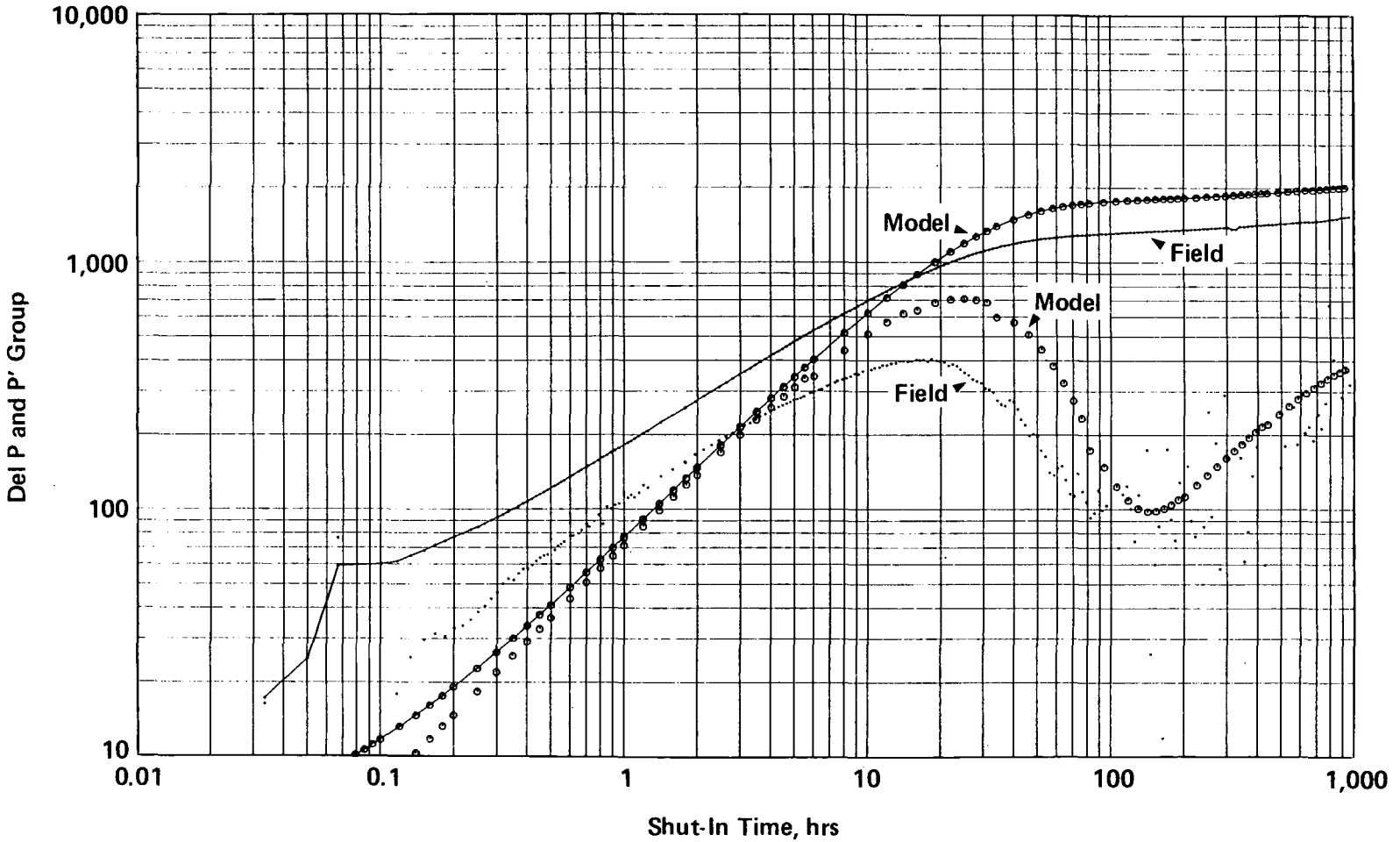

Figure 9.3.9 Comparison of Simulated and Field Data, Subsequent Match

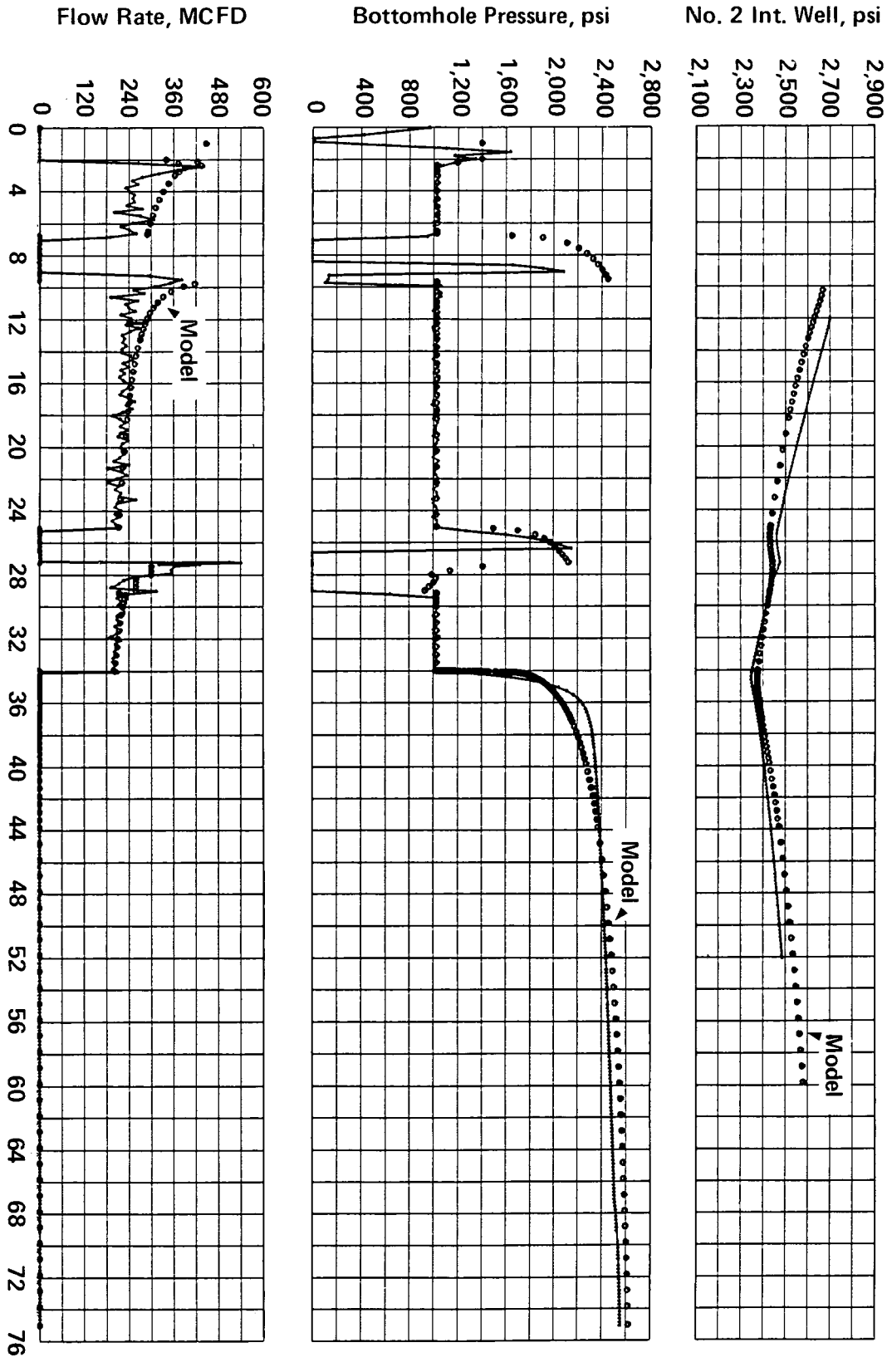

Figure 9.3.10 Comparison of Simulated and Field Data, Final Match

FLUVIAL E SANDSTONE STIMULATION EXPERIMENT

9.4 BOREHOLE SEISMIC FRACTURE DIAGNOSTICS

B. J. Thorne
Sandia National Laboratories

9.4.1 INTRODUCTION

Redesign of the geophone array, new analog to digital (A/D) hardware and small refinements in data-reduction techniques have resulted in good estimates of hydraulic fracture height and wing length. The BSS was upgraded to include a four axis geophone array using geophones with higher frequency response. Improved digitization hardware made possible the acquisition and processing of data that would not have been possible with the previous system. The accuracy of the perforation data set was less than observed in the fluvial B experiment (Section 7.4.7). Nevertheless, a reasonable determination of the azimuth, wing length, and height of the September 23, 1987, hydraulic fracture in the fluvial E sandstone was possible.

9.4.2 INSTRUMENTATION UPGRADE

Careful analysis of the data set produced during the August 1, 1985, coastal stimulation experiment led to the conclusion that frequency content up to 1 kHz must be included for successful analysis. Subsequent data sets, particularly the fluvial B experiment data set, have confirmed this conclusion. Since the Mark Products L-25 geophones used in all previous BSS tools have nonlinear response above 400 Hz, obtaining accurate data to 1 kHz required the redesign of the geophone array using geophones with higher frequency capability. In addition, differences in the frequency content of vertical and horizontal components observed in all data sets have made determination of inclination much more difficult than determination of azimuth. While this difficulty is probably due to

properties of the clamp arm and/or well casing, differences between the horizontal and vertical geophones could be eliminated as a possible source of this problem by using identical geophones on all axes. Both of these objectives were accomplished by using Geo Space GS-14-L9 geophones which have a flat frequency response beyond 1 kHz and can be placed at any angle between 0° to 90° from the vertical.

In order to produce the most uniform response from all axes, it was decided to use a geophone array with the four axes arranged so that all axes make the same angle with the vertical and with the plane of the clamp arm. This arrangement has the additional advantage of providing redundancy. If any single channel should fail, the remaining three axes can be used to construct a complete triaxial data set. This geometry results in an array that is compact and easy to build. With this geometry it would be possible to use 10 geophones per axis in less space than was required for the old three geophone per axis array. For this experiment, four geophones per axis were used which produced about the same output voltage as the old three-geophone-per-axis array. The new geophone array contains a vertical exciter and two horizontal exciters oriented parallel and perpendicular to the plane of the clamp arm. These exciters can be individually activated from the surface to confirm operation of the entire system and to analyze the resonance properties of the BSS tool while clamped in the well casing or hanging from the wireline.

During the fluvial B experiment, problems with the software for the Phoenix Data IDAS A/D converter limited data acquisition to six channels and required over 30 seconds to write each event to disc. This resulted in missing many events and rendered the system incapable of digitizing all eight channels from two of the new four axes BSS tools. Phoenix Data was not able to correct these problems and would not release the source code so that we could correct them ourselves. The Phoenix IDAS A/D converter was replaced with a Metrabyte DASH 16F data acquisition plug-in board for the

IBM-XT which is capable of digitizing up to 16 channels at a total rate of 100 kHz. The Metrabyte board was coupled to the analog channels through an event detector which triggers the IBM-XT to store data when any one of a preselected set of four of the 16 channels exceeds a preset voltage. The new system is capable of simultaneously digitizing eight channels at a rate of 12.5 kHz per channel and can write an event to disk in less than two seconds. For this data set a digitization rate of 10 kHz per channel was used. Linear interpolation was applied to center all four channels from each tool to a common time. Figure 9.4.1(a) shows time histories of the four data traces for the first 25 ms of a typical microseismic event recorded in well MWX-2. Figure 9.4.1(b) shows the resulting horizontal and vertical signals, together with horizontal and vertical hodograms of the first 2.4 ms of the primary wave. Note the good signal to noise ratio of the time histories and the clear direction of breakout of the hodograms.

9.4.3 DETERMINATION OF THE VELOCITY FACTOR

Before the distance to the source can be determined, the velocity factor, V_P, must be established (Section 7.4.3). This is accomplished by analysis of data from seismic sources at known locations. In this case, 17 ten-gram perforation shots were fired at an average depth of 5555 ft in well MWX-3 with a BSS tool in place at a depth of 5480 ft in well MWX-2. The velocity factor, V_F, was calculated for each shot from the known distance and the primary and secondary wave arrival times, using Equation 7.4.1. Without moving the BSS tool in well MWX-2, a second BSS tool was placed in well MWX-3 at a depth of 5450 ft. Then 14 ten-gram perforation shots were fired at an average depth of 5555 ft in well MWX-1, which were detected in MWX-2 and MWX-3. Velocity factors shown in Table 9.4.1 proved to be the same for all three paths, so all three data sets were combined to give an average value of 19.8 ft/ms.

9.4.4 ORIENTATION OF BSS TOOLS

If it is assumed that the direction of polarization of the primary wave is the direction towards the source, as it would be in a homogeneous isotropic medium, then the orientation of the geophone axes can be determined from the same perforation shots used to determine the velocity factor. Since the wells at the MWX site are very nearly vertical, the elevation calculated from the BSS data can be compared to the elevation to the center of the perforation gun, as a check on the assumption that the direction of polarization is the same as the direction to the source. It is unreasonable to assume that a correct orientation has been obtained if large errors in the elevation result. Table 9.4.2 gives the vertical errors for the three paths. The average vertical error detected in MWX-2 due to perforation shots in well MWX-3 was 2.9° with a standard deviation of 13.3°, indicating a rather large scatter about the correct value. Perforation shots detected in MWX-2 from well MWX-1 result in an average error of 0.0° with a standard deviation of only 2.7°. These same perforation shots result in an average vertical error of 16.7° when detected in well MWX-3 with a standard deviation of 11.0°, indicating both a large scatter and a strong upward bias. Previous perforation shot series in wells MWX-1 and MWX-2 with a BSS tool at a depth of 5480 ft (1670 m) in well MWX-3 yielded much better results. However, excessive background noise required that the BSS tool in well MWX-3 be placed further from the bridge plug.

The orientations, measured from the y-geophone axis to north, obtained from both sets of perforation shots are also given in Table 9.4.2. The perforation shots in well MWX-1 confirm the orientation of the BSS tool in well MWX-2 obtained from the perforation shots in well MWX-3 to within a fraction of the 3.4° and 4.6° standard deviations of the two data sets. Thus, the assumption that the direction of primary wave polarization is the same as the direction towards the seismic source is reasonable for the BSS

tool in well MWX-2. The previous perforation shot series in wells MWX-1 and MWX-2 confirmed the orientation of a BSS tool in well MWX-3 at a depth of 5480 ft. However, it was impossible to check the orientation of the BSS tool at the final depth of 5450 ft in well MWX-3 since perforations could not be fired in MWX-2 due to the presence of the BSS tool in that well. In view of the absence of confirmation of orientation at the final depth and the large vertical errors obtained from the perforation shots, the orientation of the BSS tool in well MWX-3 is questionable.

9.4.5 LOCATION OF PERFORATION SHOTS

In order to estimate the accuracy which can be expected, data from the perforation shots in well MWX-1 were analyzed as if they were microseismic events of unknown location. The locations resulting from analysis of the MWX-3 data were inaccurate, as might be expected from the large vertical errors and questionable orientation. The locations determined from well MWX-2 were more accurate. These locations, together with locations determined for the perforation shots in well MWX-3 are given by the triangle symbols in Figure 9.4.2. Some of these locations have horizontal components which fall outside of circles of radius 25 ft about the perforation wells, as indicated in Figure 9.4.2(a). Figure 9.4.2(b) indicates that many of these locations lie outside of ellipsoids with horizontal axes of 25 ft and vertical axis of 30 ft located at the center of the perforation guns. The location of the bottom of the BSS tool in MWX-2 is shown by the square symbols. Thus, it appears that locations resulting from data in well MWX-3 are very questionable and that locations determined using data from well MWX-2 alone will be less accurate than locations resulting from the two-well analysis that was possible for the fluvial B experiment data (Figure 7.4.3).

9.4.6 LOCATION OF THE FRACTURE

The frac map in Figure 9.4.3 is based on 160 microseismic events

located using data from well MWX-2. It is the result of analysis of over 600 signals digitized during the September 23, 1987 main frac in the fluvial E sandstone. Of these 160 microseismic events, four occurred during the pumping phase, 72 occurred during the shut in phase and 84 occurred during the flow back phase.

Activity was very intense during the one hour and 15 min of the pumping phase. Yet only four microseismic events could be located from the 140 signals detected at a trigger level of 4.5 volts because of the high level of background noise. This high background noise is probably the result of fluid moving through the formation as well as from the pumping equipment itself.

During the shut in phase, background noise was not a problem, and 72 microseismic events were located from 340 signals which were digitized at a trigger level of 3 volts. Many of the unanalyzable signals seemed to be associated with vertical oscillations, possibly resulting from tube waves in the fluid-filled portion of the casing below the bridge plug.

Background noise increased only slightly during the flow back phase, but activity was so intense that it was necessary to increase the trigger level to 5 volts for the first hour in order to avoid rapid saturation of available disk space. Over 800 signals which exceeded the 3 volt level were recorded on analog tape during the first hour of the flow back phase, including 180 which exceeded the 5 volt level and were digitized. After the first hour of the flow back phase, the trigger level was reduced to 3 volts and only 40 signals were digitized during the next hour. From these 220 signals, 84 microseismic events were located. Again, vertical oscillations seem to dominate the unanalyzable signals.

All of these signals were also recorded in well MWX-3. However, almost all azimuths derived from well MWX-3 data were within eight degrees of the

average perforation shot azimuth. Since the scatter in the perforation shot azimuths was almost eight degrees, and confirmation of orientation had not been possible for the final tool position, it was concluded that orientation of the tool in well MWX-3 is unknown. However, it was possible to confirm that the positions of the 160 microseismic events derived from MWX-2 data are consistent with primary wave arrival times in well MWX-3. This was done by using differences between primary wave arrival times in wells MWX-2 and MWX-3, together with differences in distances and the velocity factor, to compute reasonable primary and secondary wave velocities for the two paths.

Figure 9.4.3 shows symmetric wings of 250 ft length. Vertical positions indicate a fairly well defined top and bottom, giving a frac height of about 120 ft. The 60° west of north frac azimuth is around 10° from what was expected from previous tests. The standard deviation resulting from spherical statistics on the set of angles measured from well MWX-1 to microseismic event locations is 14.9°. The locations resulting from analysis of just well MWX-2 data in the fluvial B yielded an azimuth that was 12° different from the azimuth determined from locations based on analysis of data in both wells, Figure 7.4.5(a). For these reasons it would seem logical to assume that the azimuth shown in Figure 9.4.2 could be off by as much as 15°.

9.4.7 SUMMARY AND CONCLUSIONS

The most recent upgrade of the BSS for the fluvial E stimulation has allowed the collection of data from microseismic activity with a significant increase in frequency content and without missing a significant amount of activity while writing digitized data to disk. It was possible to orient the BSS tool in well MWX-2 from perforation shots in well MWX-1 with very small errors in elevation and small scatter in azimuth. This orientation was confirmed by perforation shots in well MWX-3 even though

the scatter in vertical error for this data set was large. However, the perforation shots in well MWX-1 yielded large errors in elevation when analyzed from data collected in well MWX-3, casting serious doubt on the orientation of the BSS tool in well MWX-3. Using only data from well MWX-2 resulted in the ability to locate perforation shots somewhat less accurately than was possible in the fluvial B by using data from both observation wells.

Data from the fluvial E stimulation on September 23, 1987, confirm that well MWX-3 data contain no usable directional information. Analysis of data from well MWX-2 indicates a fracture azimuth of 60° west of north, a fracture height of about 120 ft and symmetric wings of 250 ft.

Table 9.4.1 Velocity Factors

Observation Well	Perforation Well	Velocity Factor (ft/ms)	Standard Deviation (ft/ms)	Path Length (ft)
MWX-2	MWX-3	19.8	1.3	219
MWX-2	MWX-1	20.4	2.7	146
MWX-3	MWX-1	19.2	3.3	218

Table 9.4.2 Tool Orientation

Observation Well	Perforation Well	Tool Orientation	Standard Deviation	Vertical Error	Standard Deviation
MWX-2	MWX-3	48.0°	3.4°	2.9°	13.3°
MWX-2	MWX-1	49.0°	4.6°	0.0°	2.7°
MWX-3	MWX-1	-1.6°	3.9°	16.7°	11.0°

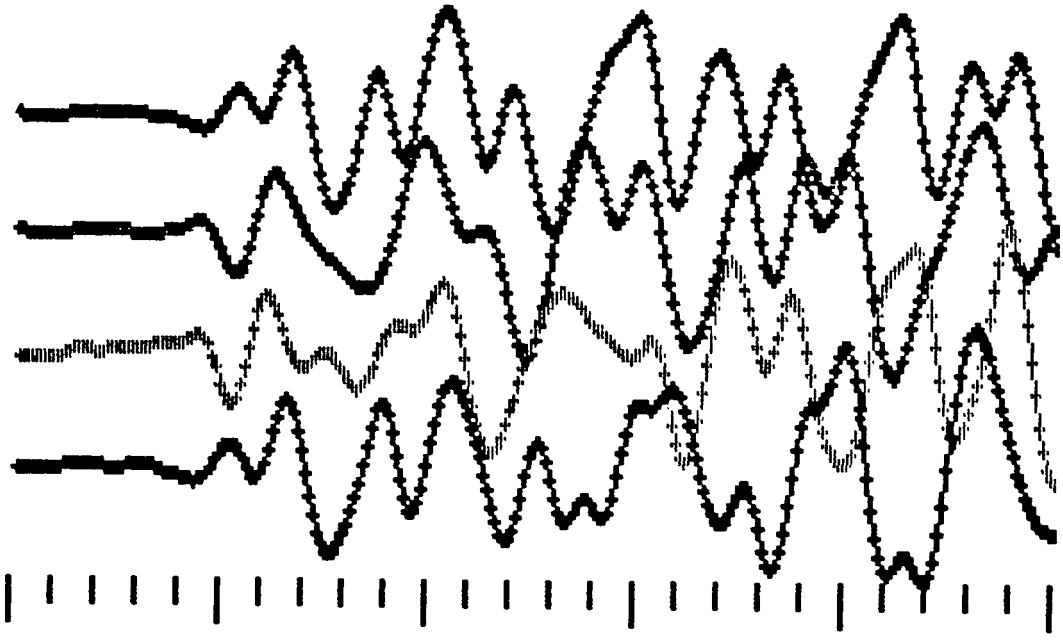

Figure 9.4.1(a). Four axes geophone data for a typical microseism.

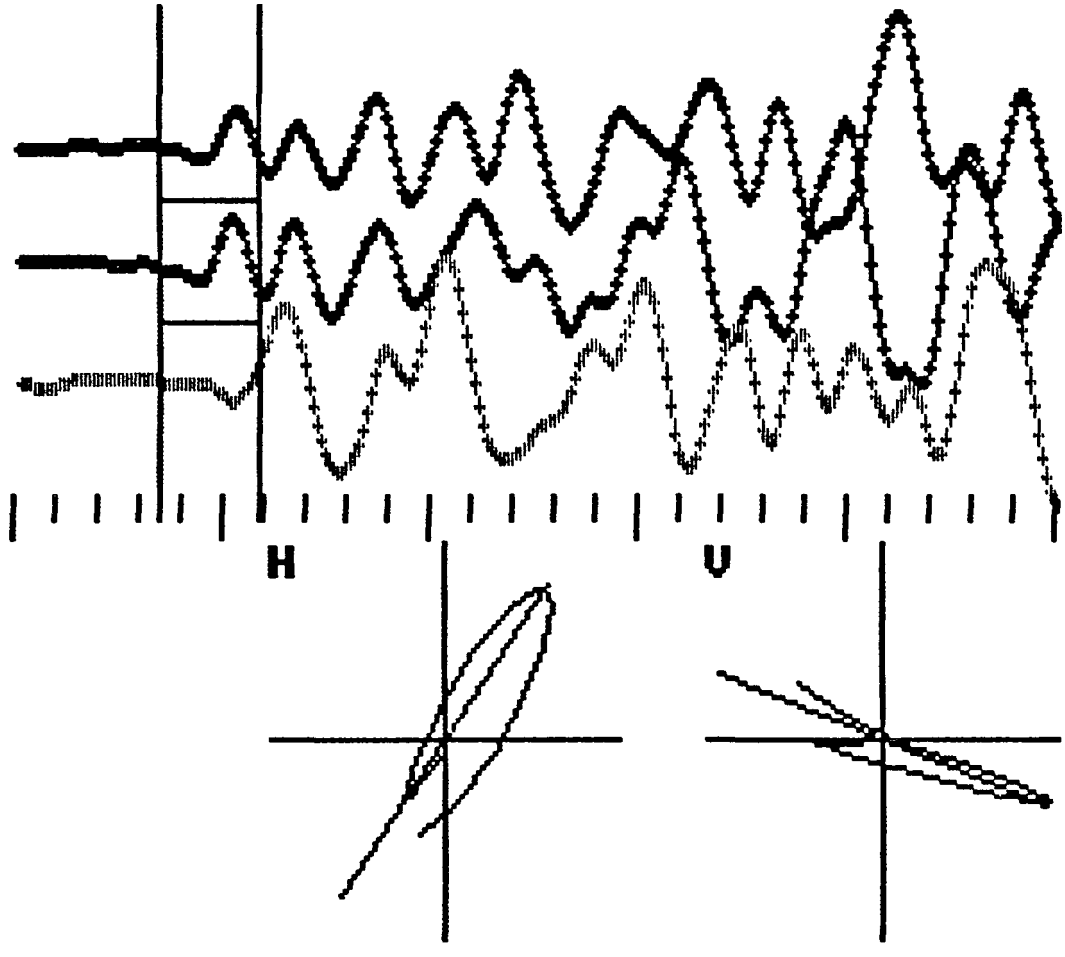

Figure 9.4.1(b). Tri-axial data and hodograms for above microseism.

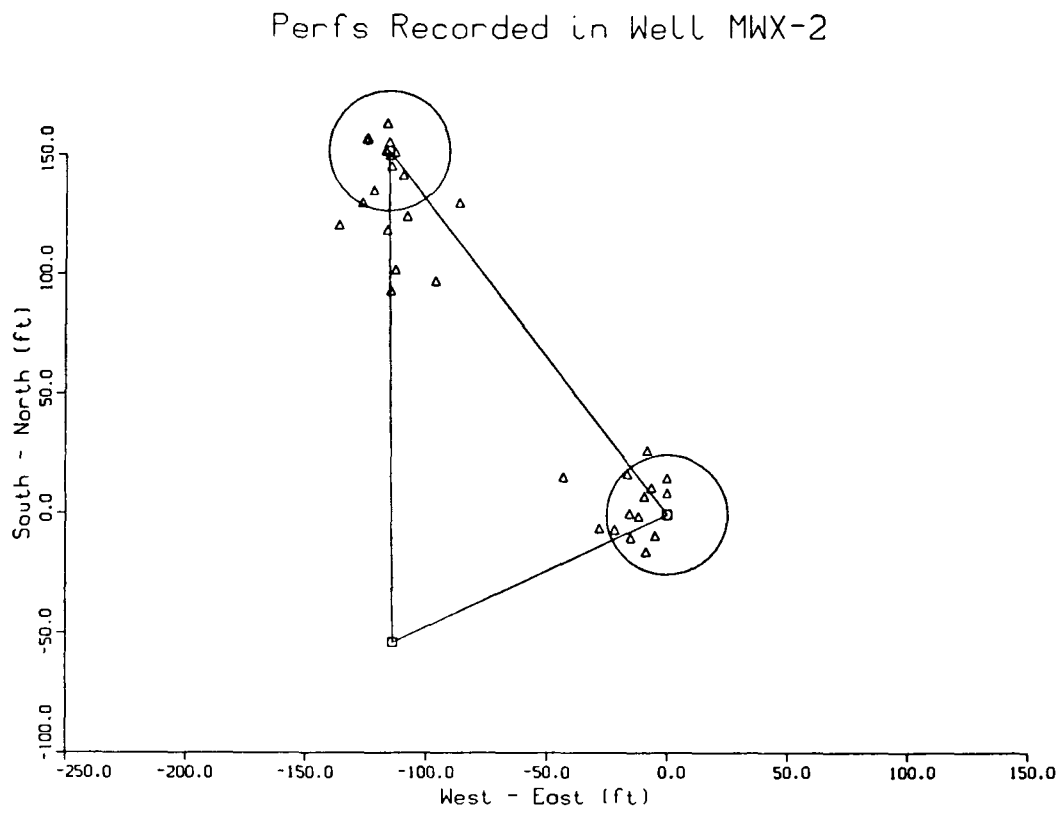

Figure 9.4.2(a). Horizontal projection of perforation shot locations.

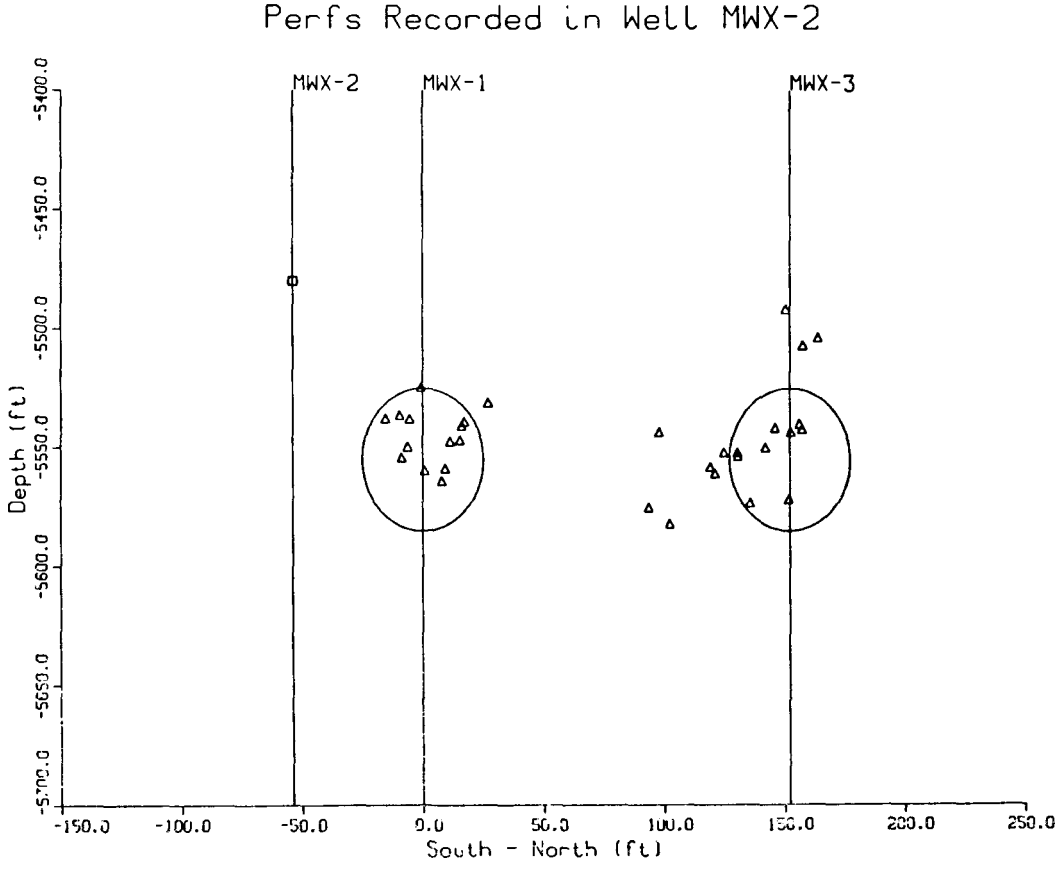

Figure 9.4.2(b). Vertical projection of perforation shot locations.

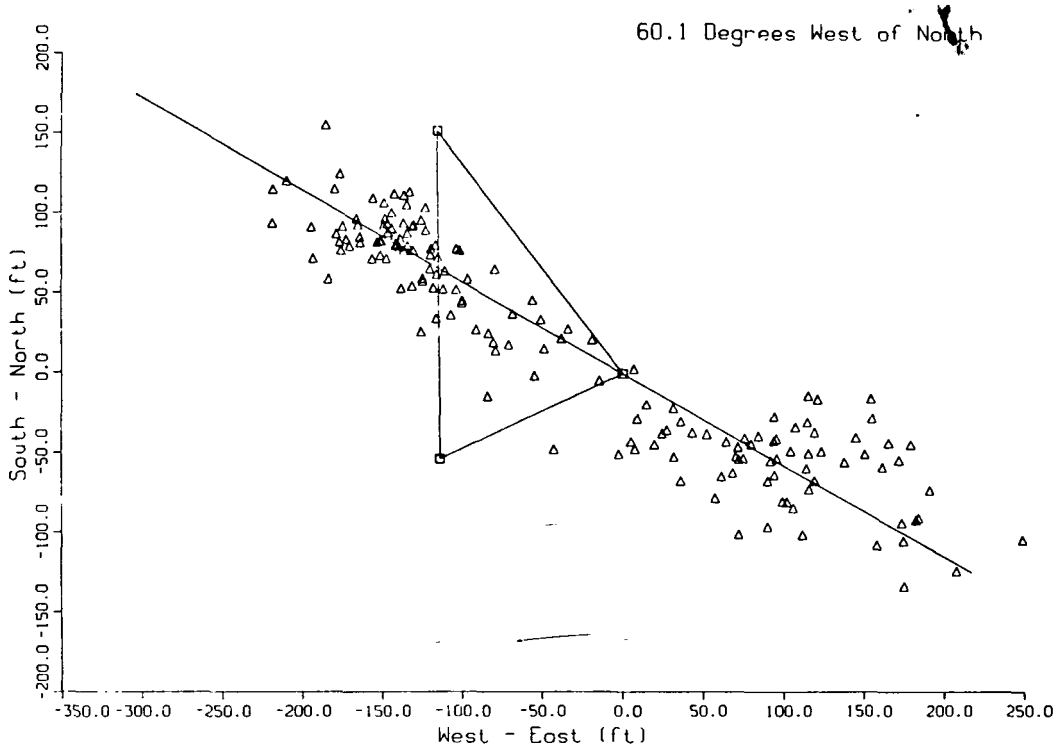

Figure 9.4.3(a). Horizontal projection of microseismic events for the Fluvial E stimulation experiment.

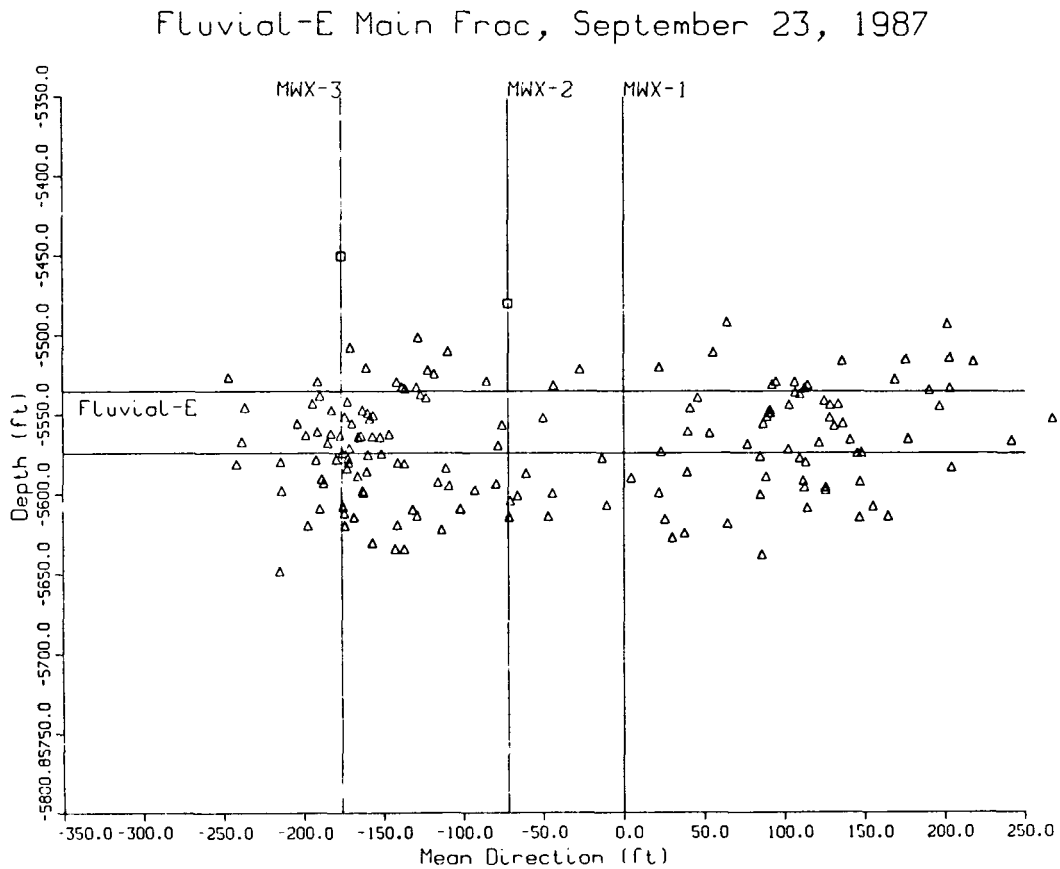

Figure 9.4.3(b). Vertical projection of microseismic events for the Fluvial E stimulation experiment.

10.0 LABORATORY WORK SUPPORTING THE FLUVIAL ZONE STIMULATIONS

A. R. Sattler
Sandia National Laboratories

10.1 INTRODUCTION

Pre- and post-frac laboratory studies supported the fluvial zone stimulation design, execution, and analyses conducted in the B, C, and E sandstones of the lower fluvial zone at 5822-5845 ft, 5720-5738 ft, and 5535-5565 ft, respectively (Figure 10.1). The fluid system common to all stimulations was a 75 quality nitrogen foam which contained 20 lb/1000 gal of a temperature-stable gelled biopolymer in the water phase. A thorough description of these supporting laboratory studies with attendant discussions are described in References 1-3. Laboratory studies were conducted mainly in support of the propped stimulations of the fluvial B and E sandstones. These studies were largely concerned with estimating and controlling the damage to the natural fracture system.

The matrix rock in the fluvial zone is extremely tight. Permeabilities are in the few tenths of a microdarcy range, and are among the less permeable of the tight Mesaverde sandstones studied (Section 5).[4-6] Capillary pressures are several hundred psi, and this rock is prone to imbibition and increased saturation from water-based fluids.

Extensive pre-stimulation testing in the marine, paludal, coastal, and fluvial zones showed that production was dominated by natural fractures.[4-6] Core and outcrop analyses indicated that the natural fracture system in the Mesaverde at the MWX site consists of narrow, subparallel, mineralized fractures. These fractures are relatively numerous in the fluvial zone and are mostly extension fractures (Section 3). The width distribution of these fractures in the fluvial zone again shows that most of the fractures are narrow (Figure 10.2). Dry Klinkenberg permeability and relative permeability measurements were made on many core plug samples (Section 5.4) and on some whole core samples containing these mineralized natural fractures at confining stresses estimated to exist in the reservoir.

These data generally show that even highly mineralized natural fractures significantly improved the permeability over that of the matrix rock (Figure 10.3).

Experience from the earlier paludal and coastal zone stimulations indicated that not only do natural fractures dominate the pre-stimulation production, but damage to these narrow natural fracture systems can be a very important factor in determining post-stimulation production. Apparently there is an interaction between the stimulation fluids employed and the natural fractures. Field evidence for this stimulation fluid/natural fracture interaction is:

- Observations of high treating pressures during stimulations. These high pressures are primarily due to high in situ stresses in the sandstones and the abutting materials.

- Evidence of increased leakoff at high pressures during treatments, most likely into natural fractures. This appears to occur above a threshold pressure and may result in factor-of-fifty leakoff increase. This may be the mechanism responsible for early screenouts observed in two stimulations.

- Post-stimulation well test data clearly show that a conductive fracture was created, but it is necessary to include damage to the natural fractures which intersect the created hydraulic fracture in order to match the low production rates.

Over the course of the MWX stimulation experiments, the laboratory program was expanded to study the production problems which very likely resulted from stimulation damage to the narrow natural fracture system. By the time the preparations for the fluvial series of stimulations has begun, laboratory studies had all but eliminated matrix and proppant-related effects as major factors in most stimulation production for these tight Mesaverde sandstones at MWX (References 7-11). While studies of matrix and

proppant related effects were conducted on some fluvial zone core, by far the largest amount of laboratory work was concerned with:

- Characterizing the nature of the damage to the natural fracture system from tests of permeability degradation of both natural and artificially created fractures exposed to stimulation fluids. This included study of the effects of fine mesh sand and nonaqueous stimulation fluids.

- Designing a breaker system for use with the biopolymer to minimize the damage by gel residue to the natural fracture system.

- Analyzing the original and returned stimulation fluids for polymers and gel decomposition products to determine the state of the residual polymer in the formation.

This section is therefore devoted mainly to the discussion of the above three topics because of an apparently strong relationship between post-stimulation production and the degree of stimulation fluid damage to the natural fracture system. However, all work supporting the stimulations is mentioned and referenced.

10.2 PERMEABILITY DAMAGE AND LEAKOFF

Polymer damage to matrix and to fractured core was studied by measuring permeability degradation under simulated reservoir conditions.

10.2.1 Matrix

Earlier laboratory studies helped eliminate matrix related effects as a significant factor in post-stimulation production. Permeability degradations of matrix rock exposed to stimulation fluid are small, and leakoff into the matrix is small.[7-11] There appeared to be little to no polymer penetration into the matrix rock. However, cleanup times could be

long with several thousand pore volumes of gas passing through the core before its maximum post-exposure value could be attained. Permeabilities were usually within 80% - 90% of the pre-exposure value.

10.2.2 Natural Fractures in Core

Some limited permeability damage measurements were made with naturally fractured core samples. Figure 10.4 shows the effective gas permeability of the naturally fractured core from the Canyon Sands Formation in Texas[12] as a function of net confining stress after exposures to HPG gel and to HPG gel plus fine-mesh sand. This core was a tight sandstone with narrow fractures and was expected to provide an indication of the effects that would be experienced by MWX core. Several observations can be drawn from Figure 10.4.

- Successive exposures to brine and to the gel each reduce the fracture permeability threefold.

- The permeability of the fractured core decreases with increasing confining pressure.

- Fine-mesh sand (200-300 mesh) decreases the permeability of the core even more.

10.2.3 Artificially Fractured Core

The lack of sufficient natural fractured samples with similar flow properties prevented conducting systematic studies on the effects of stimulation fluids on Mesaverde core. Artificially created fractures in core (cracked core) yielded reasonably reproducible "fractured" core samples for systematic study of permeability degradation and leakoff of the fracture fluids used in MWX stimulations. The exposure of either natural or artificially fractured core to stimulation fluids and the resulting permeability measurements could be expected to provide comparative data on

damage to gas flow properties. A major difference is that the natural fractures at the MWX site are usually mineralized while the artificially created fractures are not.

The preparation and conditioning of the artificially fractured core samples, along with the apparatus used, are described elsewhere.[2,3] The more narrow (<30 μm), lower-permeability artificial fractures (<100 to 200 μd) are the main concern since they are believed to be more representative of fractures occurring at the MWX site.

Reductions in permeabilities of cracked core were observed after injection and cleanup of brines, surfactants, and breaker formulations without any gel. Brine/surfactant solutions generally reduced permeabilities about 25% while brine/surfactant/breaker solutions reduced permeabilities by around 50% (Table 10.1).[1-3]

Permeability damage was measured on cracked core exposed to the polymers used in MWX, HPG and biopolymer, as well as on the hydroxyethyl-cellulose (HEC) polymer.[1-3] HEC was a candidate polymer for the foam system. Some of the biopolymer solutions used with the artificial fractures contained breaker and fine-mesh sand. The work was conducted at estimated reservoir net stress and temperature. Table 10.1 shows the various combinations of these fluid systems used and the results are summarized as follows:

- The permeability reductions were very high for artificially fractured core exposed to all the polymers.

- Breaker added to biopolymer may have mitigated permeability damage, although the resulting damage was still very high.

- Fine-mesh sand (100 mesh) did not increase permeability damage in the presence of a breaker although it did appear to increase permeability damage without a breaker.

Scanning electron microscope (SEM) photos of cracked core exposed to biopolymer show considerable dried polymer both around the crack entrance and lining the sides of the crack.[3,6] Similar results were found in SEM photos of cracked core exposed to HPG.

Some limited investigations were made to determine if permeability damage would be smaller if the cracked core was exposed to nonaqueous gelled stimulation fluids.[1,3] Cracked core was exposed to a low-pH methanol system that has an HEC type polymer to provide proppant transport and foam stability. The core sample employed had a matrix permeability of 3 μd and was at irreducible water saturation. Table 10.1 shows successive permeability degradation to the sample after exposure to brine-methanol and to gelled methanol fluids. Table 10.2 shows that the permeability damage of cracked core was about the same after exposure to either gelled methanol or biopolymer, HEC, and HPG gels.

Leakoff was often measured when stimulation fluids were passed through the artificial fractures.[1,3] The leakoff is plotted as a function of the square root of time for systems of biopolymer with breaker and surfactant with and without the 100-mesh sand (Figure 10.5). This fine sand was usually filtered at the crack entrance of the core sample, where it increased the filter-cake buildup. The 100-mesh sand reduced the laboratory leakoff values by a factor of 2.5, and (from pressure history matching, Section 8.1) the 100-mesh sand appeared to reduce leakoff about a factor of 3.5 in the fluvial C sandstone minifracs. The laboratory-derived leakoff values are somewhat smaller than the accelerated and fine-mesh-sand-affected field leakoff estimates.

10.3 BREAKER SYSTEM DEVELOPMENT

Because of the extreme stability of the biopolymer, various options for fracture fluid systems were considered after the coastal stimulation and prior to the fluvial stimulations. A decision was made to use a gelled fluid in the foam system and to develop a breaker for use with the biopolymer.[13-19]

A breaker system should allow the viscosity of a stimulation fluid to remain reasonably high and stable over the short term to carry the proppant and any fine-mesh sand out into the hydraulically created fracture. In the longer term, the viscosity of the stimulation-fluid system should degrade to facilitate cleanup and recovery of the polymer.

A satisfactory breaker system that can be used with the biopolymer in tight sandstone stimulations was developed as a result of the laboratory work supporting the coastal, fluvial B, and fluvial E stimulations where the biopolymer foam was employed.

The cyanuric acid was used as a breaker stabilizer to help control the reaction rate of the breaker (NaOCl) in the stimulation of the B sandstone. Laboratory tests conducted suggested that 3-5 lb/1000 gal would be an adequate amount of breaker stabilizer as cyanuric acid does not dissolve readily. A hot oiler was employed to heat the frac water to about 80°F to facilitate dissolution of the cyanuric acid. After heating the water and adding the cyanuric acid the fluid was circulated in the tanks by the frac pumps to further assist in the dissolution. These extra procedures were avoided in the subsequent stimulation of the E sandstone because a more common and soluble chemical, NH_4Cl was used as the stabilizer.

The design of the liquid phase of the stimulation fluid for both stimulations included 20 lb/1000 gal of biopolymer and 15 gal/1000 gal of 5% NaOCl breaker. For the B sandstone stimulation 3 lb/1000 gal cyanuric acid was used as the stabilizer. For the E sandstone stimulation 3 lb/1000 gal NH_4Cl was used for the stabilizer. In both stimulations, a 2.75% KCl solution was used. Figures 10.6-10.8 show the behavior, all measured at a representative formation temperature of 150°F, of laboratory and field designed fluids for the B and E stimulations.

The concentration of the KCl is also an important factor in controlling the reaction rate of the breaker. The 2.75% KCl concentration appeared optimum for this purpose. (The use of KCl concentration to control the reaction rate is protected in a Dowell Schlumberger Canadian patent 1185778, April 23, 1985. A similar US patent is pending.)

Field quality control tests and analyses suggested that the breaker actually used in the B sandstone stimulation was not at designed strength.[20] This may have contributed to a post-stimulation production that was only about 1.5 that of pre-stimulation production (although many different factors were involved).

A breaker prepad was used in the propped E sandstone stimulation. The breaker concentration chosen was 30 gal/1000 gal of 5% NaOCl solution. Laboratory tests on core samples indicated that little, if any, formation damage would occur from the prepad.[21] No stabilizer was needed in the prepad. Laboratory data indicated that the breaker used in the E sandstone stimulation was 16% stronger than designed. Post-stimulation production was over threefold greater than pre-stimulation production.

10.4 BIOPOLYMER DEGRADATION

The biopolymer used at MWX is extremely temperature-stable.[1] Samples of the biopolymer were heated at 195°F (90°C) for about 60 days with little degradation in molecular weight (Figure 10.9).[21] Viscosities degraded very little in a shorter 72-hour test (Figures 10.6 through 10.8) at 150°F (65°C). Thus chemical breakers are required for stimulation clean-up.

The effectiveness of the breaker systems in the B and E sandstone stimulations was studied by analyzing both stimulation and returned fluids. Both carbohydrate content and viscosities were analyzed (Table 10.3).[21-31] The carbohydrate content indicates how much biopolymer is in the solution. Measurement of the viscosities of the returned fluids indicates whether a viscosity decrease has occurred. A viscosity decrease may occur due to the effect of both the breaker and formation temperature on the biopolymer or due to dilution of the frac fluid. In the case of the B sandstone stimulation, the viscosity was reduced in some of the samples collected, but the amount of biopolymer relative to that in the stimulation fluid was somewhat low. This suggests that the returned fluid had been diluted rather than broken. Overall, no more than about 30% of the biopolymer was recovered from the B sandstone stimulation.

A viscosity break was not seen in the first returned fluid samples after the E sandstone stimulation, but apparently the first sample came from the flush after stimulation and the sample was not exposed to formation temperatures. Later returned fluid samples showed considerable viscosity reduction; moreover, the carbohydrate content of those samples approximated that of the stimulation fluid (Table 10.3). About 70% of the biopolymer was recovered from the E sandstone.

Three observations can be drawn from the three propped stimulations with biopolymer foam:

- Unbroken biopolymer remained in the formation for some time after the coastal zone stimulation; there was no breaker in the stimulation fluid.

- The state of the biopolymer after the B sandstone stimulation could not be determined. The reduction in viscosity could have been from either the breaker or a dilution of the biopolymer in the returned fluid. Only a small fraction of the biopolymer was recovered for this treatment.

- The biopolymer had undergone substantial viscosity degradation after the E sandstone stimulation. A large fraction of the biopolymer was recovered.

10.5 DISCUSSION

Alternatives other than the biopolymer were considered for the fluvial B sandstone stimulation. The use of HEC polymer with an enzyme breaker was carefully considered. However, the enzyme breaker was ineffective at formation temperatures.[7] The viscosity of this HEC system at formation temperatures was low[31] and the laboratory stability of the HEC foam was considerably less than that of the biopolymer foam.[32] A decision was made to use the biopolymer because of its foam stability and low residue, and also to develop an effective breaker system to use with this polymer. A

laboratory program was initiated to develop this breaker system which was used in the stimulation of the B sandstone. However, it was difficult to dissolve the cyanuric acid stabilizer under field conditions, and quality control measurements suggested that the breaker was substantially weaker than its design. Returned fluid analyses could not indicate the status of the biopolymer.

Different stimulation fluid systems were again considered after the B sandstone stimulation. There appeared to be few nondamaging fluid options available for stimulation of the E sandstone that did not entail a large risk of uphole or downhole screenouts. Laboratory work showed that the commonly used polysaccharide gels were damaging to narrow fracture systems. Long-term stimulation experience, verified by a literature survey,[33-35] indicated that failure to use a properly viscosified base fluid, with proper leakoff and foam stability characteristics, would risk a screenout, especially in these fractured formations.

It was decided to again use the biopolymer-stabilized foam for stimulating the E sandstone because of foam stability, proppant transport, and leakoff considerations. However, there was a significant difference in this fluid system from that of the earlier biopolymer fluid systems. A prepad consisting of a breaker solution was employed. Also, NH_4Cl stabilizer was substituted for cyanuric acid. Polymer damage might be mitigated by the use of such a prepad consisting of a breaker solution. This approach would put additional breaker in the formation and would entail little risk of premature viscosity degradation because the gel had no contact with the additional breaker until the gel was in the formation itself. This fluid scheme might actually place some breaker in natural fractures as they open up a higher treating pressures. The breaker strength was 16% higher than the design value; this was probably helpful.

There was a substantial production increase as a result of the fluvial E stimulation. The effects of damage were not obvious and the fraction of biopolymer recovered was high. This interval contains a secondary natural fracture set and such a formation may be less susceptible to severe damage from stimulation fluids; but this can't be determined from existing data.

Accelerated leakoff was mitigated by fine-mesh sand both in the second C sandstone minifrac and in the propped E sandstone stimulation. This is consistent with the laboratory work.

10.6 CONCLUSIONS

Natural fractures dominate pre-stimulation production in these Mesaverde sandstones. How well these fractures remain open after a stimulation is a very important factor in post-stimulation production efficiency. Ample field and laboratory data from MWX experience support the following conclusions:

- Interactions between natural fractures and stimulation fluids have been seen in the stimulations through high treating pressures, accelerated leakoff, and highly increased values of reservoir kh values upon reversal of gas flow.

- Laboratory work on stimulation fluid degradation corroborates the premise that fluid damage was involved in some of the MWX post-stimulation production problems. Based on tests during cleanup, unbroken polymer remained in the formation after some stimulations.

- Interactions of naturally fractured and artificially fractured core samples and stimulation fluids were apparent. Successive permeability degradations were seen after exposure of these core samples to brine and gel. The resulting final permeability degradations can be very large.

- An effective breaker package has been designed for use with the biopolymer. The fluid system includes a breaker prepad and the resulting fluid system is apparently satisfactory for stimulations of naturally fractured, tight sandstone reservoirs.

10.7 REFERENCES

1. Sattler, A. R., et al., "Stimulation-Fluid Systems for Naturally Fractured Tight Gas Sandstones: A General Case Study from Multiwell Experiment Stimulations," SPE 17717, Proceedings of the SPE Gas Technology Symposium, Dallas, TX, June 1988.

2. Gall, B. L., "Permeability Damage to Natural Fractures Caused by Fracturing Fluid Polymers," SPE 17542, Proceedings of the 1988 SPE Rocky Mountain Regional Meeting and Exhibition, Casper, WY, May 1988.

3. Gall, B. L., et al., "Permeability Damage to Artificially Fractured Cores from the Department of Energy Multiwell Experiment," National Institute for Petroleum and Energy Research (NIPER), Final Report for Sandia National Laboratories, Contract 95-4340, May 1988.

4-6. Northrop, D. A., MWX Project Group at Sandia National Laboratories and CER Corporation "Multiwell Experiment Final Report: I. The Marine Interval of the Mesaverde Formation," SAND87-0327, April 1987; "II. The Paludal Interval of the Mesaverde Formation," SAND88-1008, May 1988; III. The Coastal Interval of the Mesaverde Formation," March, 1989.

7. Raible C. J., NIPER Quarterly Report for Sandia National Laboratories, Contract NIPER85-68B, January through March 1986.

8. Raible, C. J., and B. L. Gall, "Laboratory Formation Damage in Western Tight Sands," SPE/DOE 13903, Proceedings of the 1985 SPE/DOE Joint Symposium on Low Permeability Reservoirs, Denver, CO, May 1985.

9. Volk, L. J., et al., "A Method for Evaluation of Formation Damage Due to Fracturing Fluids," Proceedings of the 1983 SPE/DOE Symposium on Low Permeability Reservoirs, Denver, CO, March 1983.

10. Sattler, A. R., et al., "Laboratory Studies for the Design and Analysis of Hydraulic Fracture Stimulations in Lenticular, Tight, Gas Reservoirs," SPE/DOE/GRI 15425, Proceedings of the Unconventional Gas Technology Symposium, Louisville, KY, May 1986.

11. Sattler, A. R., et al., "Integration of Laboratory and Field Data for Insight on the Multiwell Experiment Paludal Stimulation," SPE/DOE 13891, Proceedings of the 1985 SPE/DOE Joint Symposium on Low Permeability Reservoirs, Denver, CO, May 1985.

12. Raible C. J., NIPER Quarterly Report for Sandia National Laboratories, Contract NIPER85-68B, July through September 1986.

13-19. Gill, P. J., Dowell Schlumberger, Denver, Series of Reports to Sandia on the Breaker for the Biopolymer, August 8, 29, September 22, 23, 1986, June, August, September 1988.

20. Nimerick, K. H., Dowell Schlumberger (Tulsa) Report on Breaker Tests on E Sandstone Core, August 1987.

21. CER Corporation Multiwell Experiment Report, "MWX Fluvial B Fracturing QC and Operational Data," February 1987.

22. Raible, C. J., NIPER Quarterly Report for Sandia National Laboratories, Contract NIPER 85-68B, April through June 1986.

23-24. Ainley, B. R., Dowell Schlumberger (Tulsa), Returned Fluid Analyses Reports to Sandia, December 1986, April 1987.

25-29. Nimerick, K. H., Dowell Schlumberger (Tulsa), Returned Fluid Analyses Reports to Sandia, August 1987, September 1987, November 1987, December 1987, January 1988.

30. Gill, P. J., Dowell Schlumberger (Denver), Returned Fluid Analyses Reports to Sandia, November, December 1986, October 20, 28, 1988.

31. Dowell Schlumberger Engineering Data Handbook, Fracturing Fluids, 1984.

32. Wendorf, C. L. and B. R. Ainley, "Massive Hydraulic Fracturing of High Temperature Wells with Stable Frac Foams," SPE 1057, Presented at the 56th Annual SPE Technical Conference, Dallas, TX, 1981.

33. Parks, C., "Characterizing Polymer Solutions by Viscosity and Functional Testing," Presented at National Meeting of American Chemical Society, Anaheim, CA, September 1986.

34. Harris, P. C., "Effects of Texture on Rheology of Foam Fracturing Fluids," SPE 15427, Presented at the 60th Annual SPE Technical Conference, Las Vegas, NV, September 1985.

35. Watkins, C. L., et al., "A New Crosslinked Foam Fracturing Fluid," SPE 12027, Presented at the 58th Annual SPE Technical Conference, San Francisco, CA, October 1983.

Table 10.1
Gas Permeability Damage of Cracked Cores Resulting from Fracturing Fluid Surfactant and Breaker Solutions, Methanol, and Gelled Methanol

Sample	Solution Additive	Exposure Time (hr)	k_g (md)	Reduction (%)
MWX-2 5837.0	2% KCl	18	0.117	
	2% KCl + Surfactants	18	0.086	27
MWX-2 5836.8B	2% KCl	3	0.110	
	2% KCl + Surfactants + Breaker	18	0.060	45
MWX-2 5836.8C	2% KCl	18	0.140	
	2% KCl + Surfactants + Breaker	18	0.070	50
MWX-1 5841.0	Brine	3	0.047	
	Methanol	1	0.038	20
	Gelled Methanol	2	0.020	58

Table 10.2
Permeability to Gas of Cracked MWX Cores Before and After Gel Damage

Sample	Gel Type	kg Before Gel (md)	kg After Gel (md)	Reduction (%)
	20 lb Biopolymer			
MWX-3 5727.1A		0.190	0.020	90
MWX-1 5842.0A	(Breaker)	0.045	0.019	58
MWX-3 5727.1B-1	(100 Mesh)	0.052	0.024	54
MWX-3 5727.1B-2	(100 Mesh)	0.107	0.023	79
MWX-1 5548.7B	(100 Mesh)	0.136	0.017	88
MWX-1 5548.7C-2	(100 Mesh)	0.239	0.024	90
MWX-1 5548.7C-3	(100 Mesh)	0.372	0.020	94
MWX-2 5736.1B*	(Breaker)	0.072	0.024	66
MWX-2 5736.1A*	(Breaker+100 Mesh)	0.076	0.030	61
MWX-1 5727.4B*	(Breaker)	0.041	0.013	68
	HEC/Water			
MWX-2 5736.1	(Breaker)	0.073	0.034	53
MWX-1 5836.8B	(Breaker)**	0.153	0.030	80
MWX-1 5836.8A	(Breaker)***	0.063	0.013	78
	Other			
MWX-1 5842.0	20-lb Biopolymer	0.045	0.019	58
MWX-1 5842.0	40-lb HPG	0.042	0.022	48
MWX-1 5841.9	20-lb Gelled Methanol	0.047	0.020	42
MWX-1 5841.9	HEC/Methanol	0.047	0.020	57

*Surfactant Added
**(3-Day Test)
***(8-Day Test)

Table 10.3
Correlations of Carbohydrate and Viscosity Measurements from Returned Fluid Analyses

Stimulation	Time from Frac (hr)	Carbohydrates (%)	Viscosity (cp @170 sec^{-1}) (150°F)
Fluvial B	Frac Fluid	0.25	11.4
	24	0.10	1.2
	36	0.10-0.13	1.2
Fluvial E	Frac Fluid	0.22	12.0
	2	0.20	12.0
	5.5	0.18	3.6
	8	0.15	3.6
	100	0.05	2.4

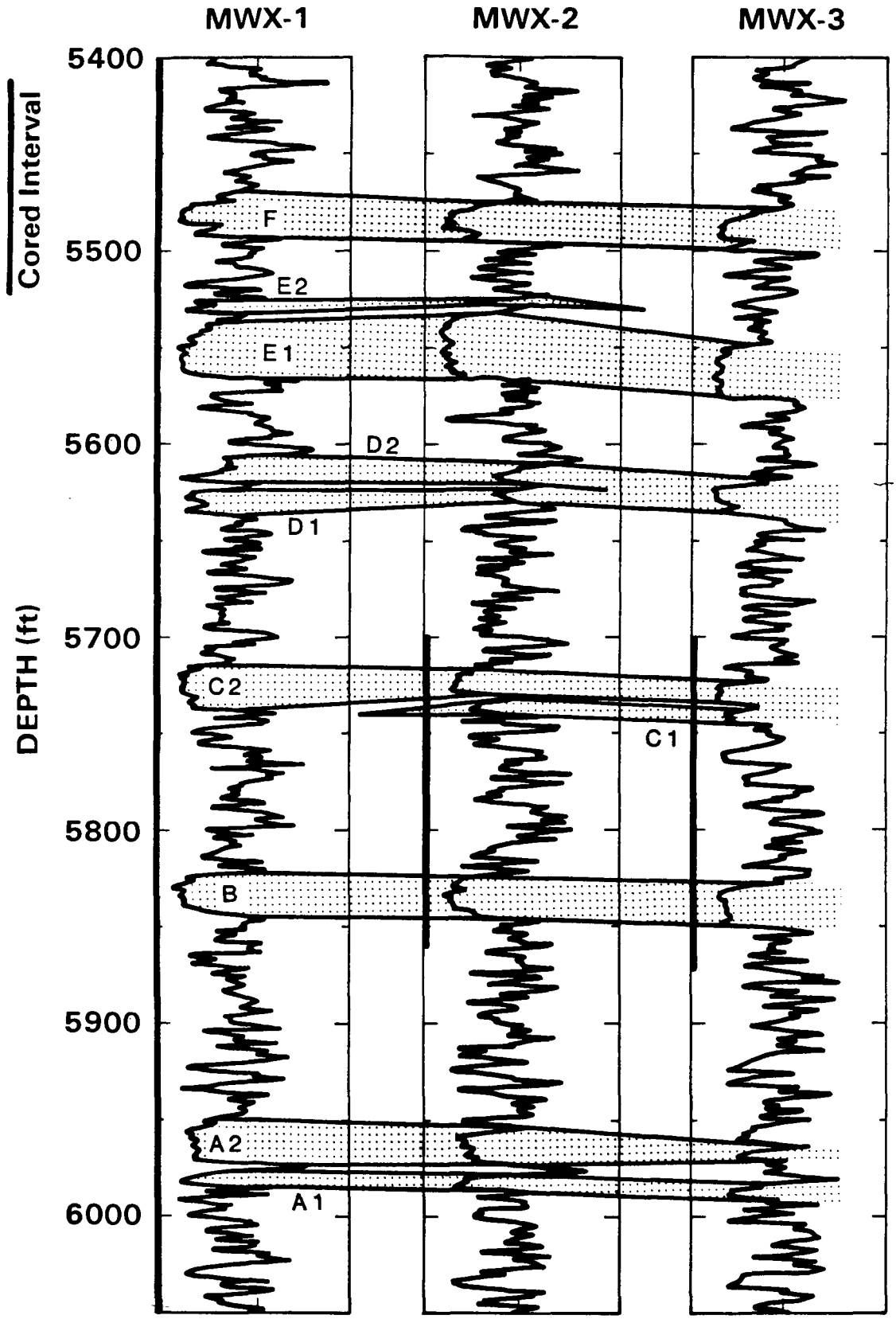

Figure 10.1. The Lower Fluvial Zone at the MWX Site

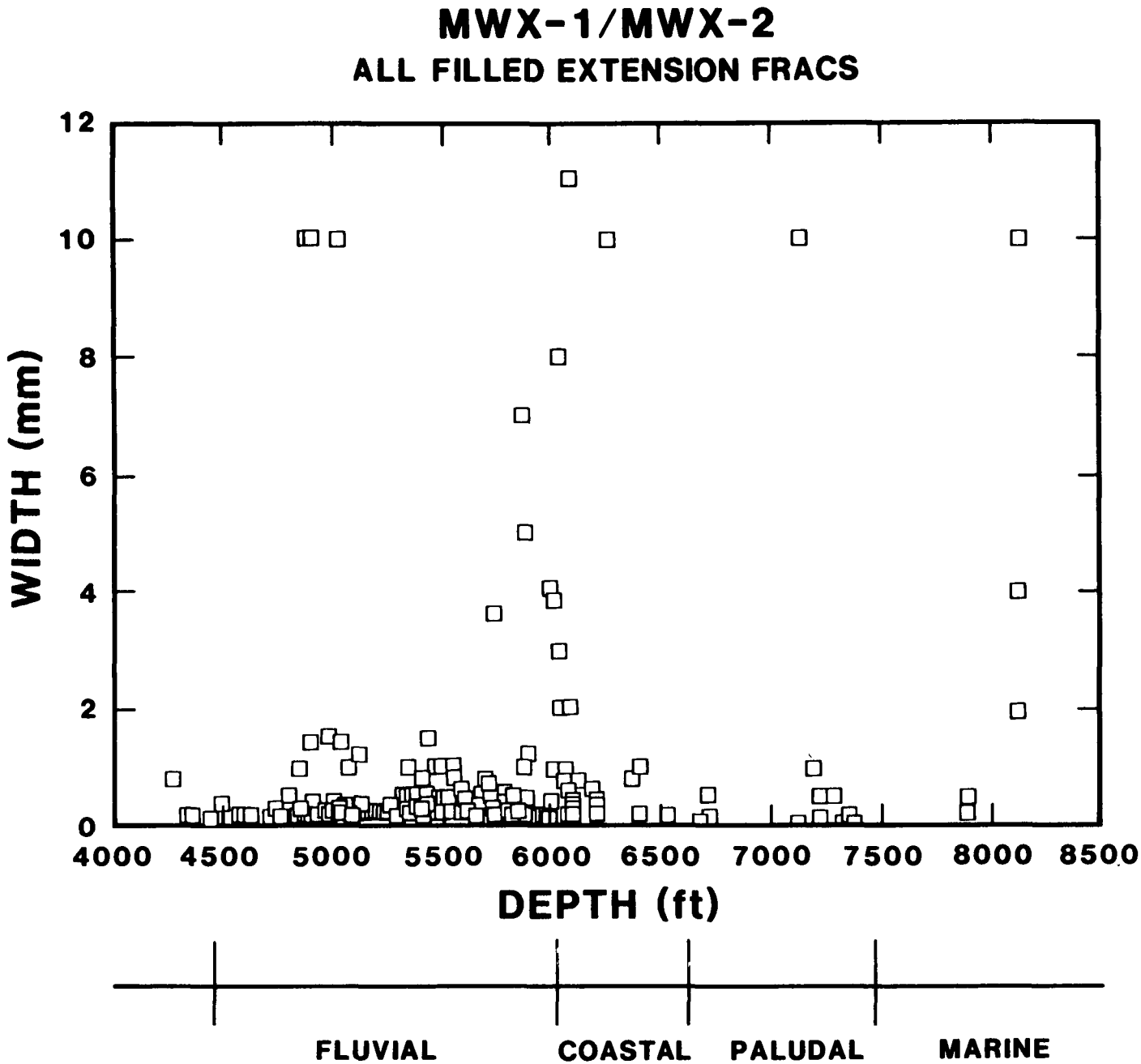

Figure 10.2. Fracture Width Distribution vs. Depth from MWX Core

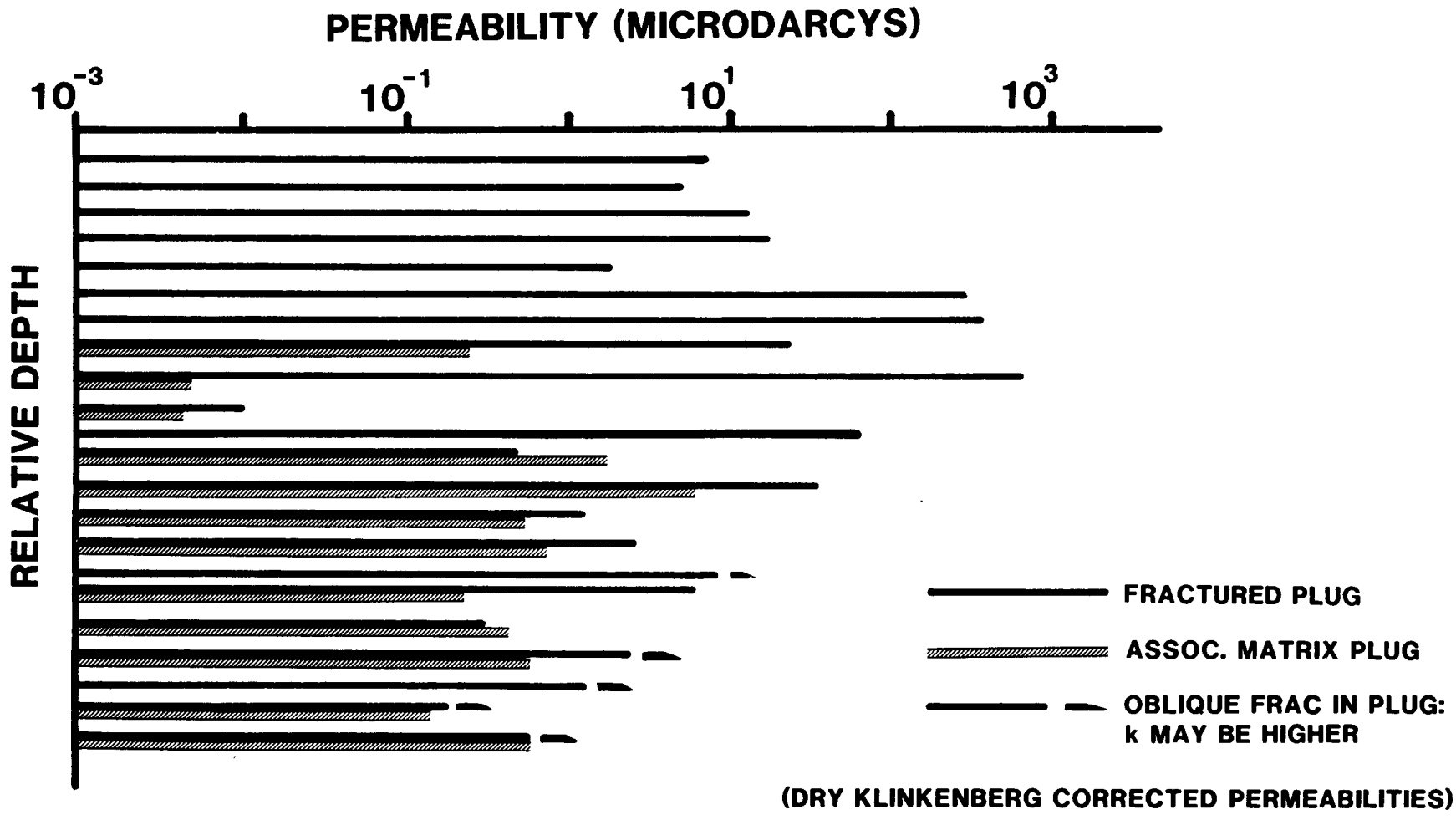

Figure 10.3. Permeability of Fractured Core vs. Permeability of Matrix Rock

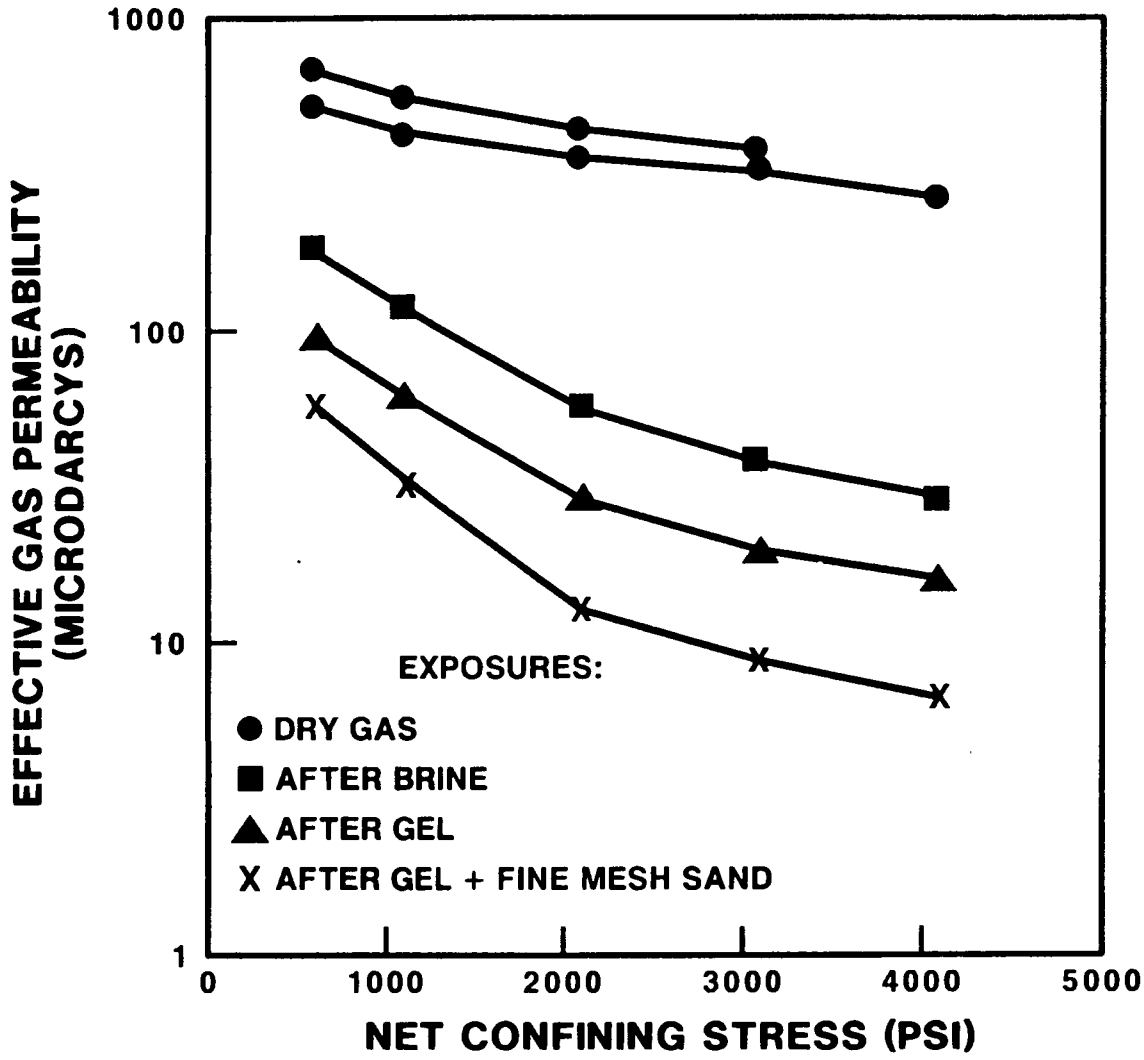

Figure 10.4. Permeability Degradation of Naturally Fractured Core

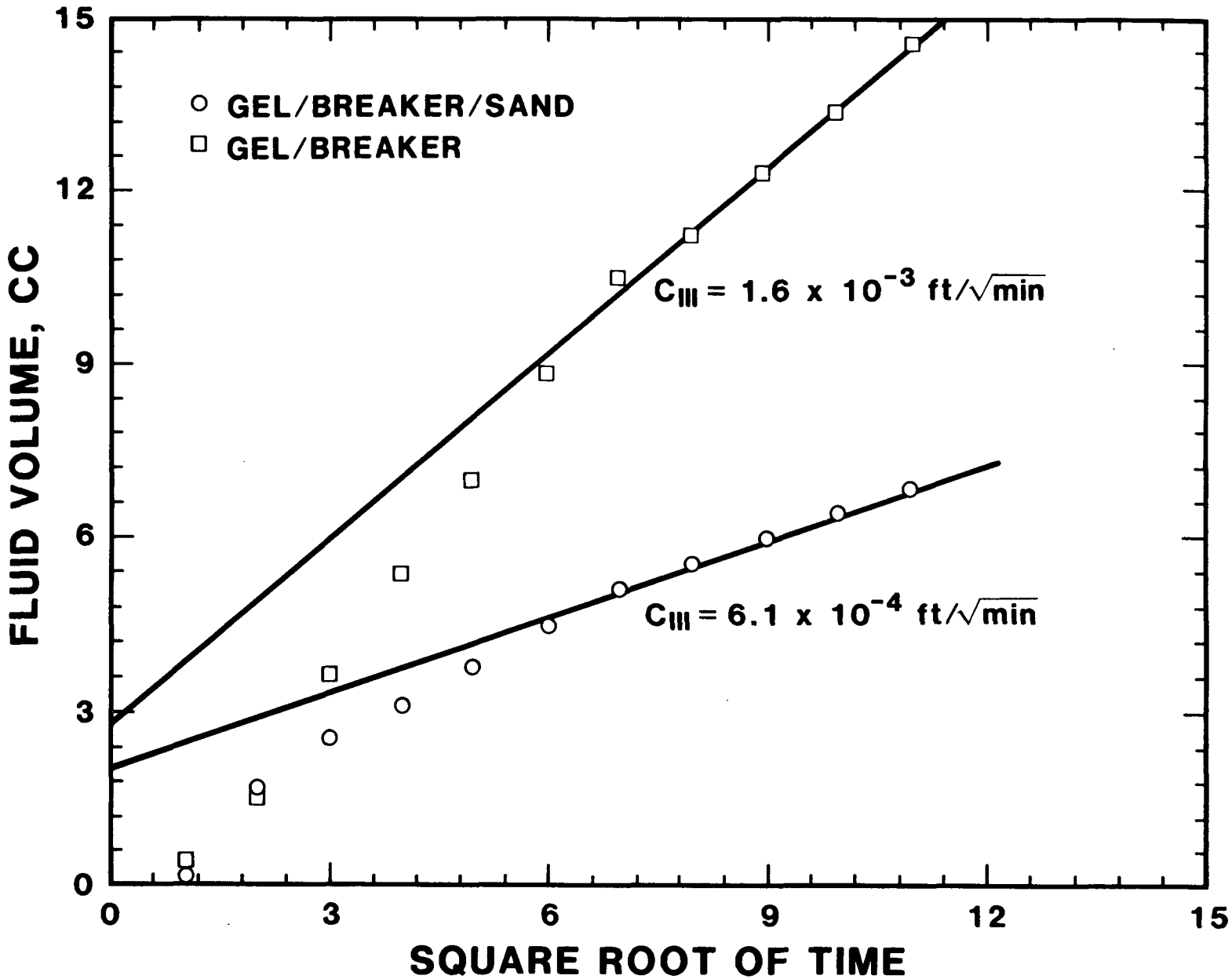

Figure 10.5. Leakoff in Core With and Without Fine Mesh Sand

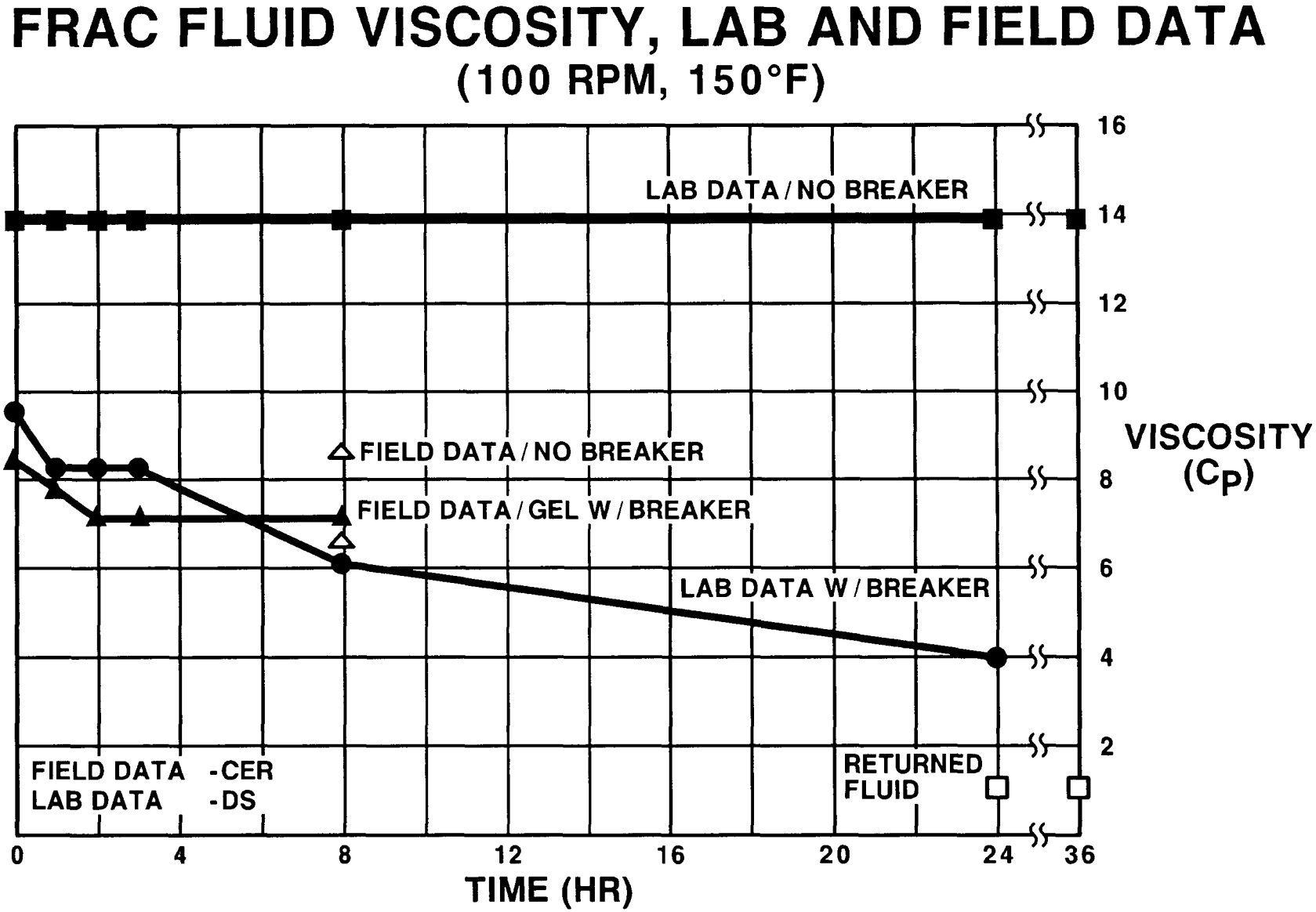

Figure 10.6. Viscosity vs. Time for Gel Used in the Stimulation of the Fluvial B Sandstone

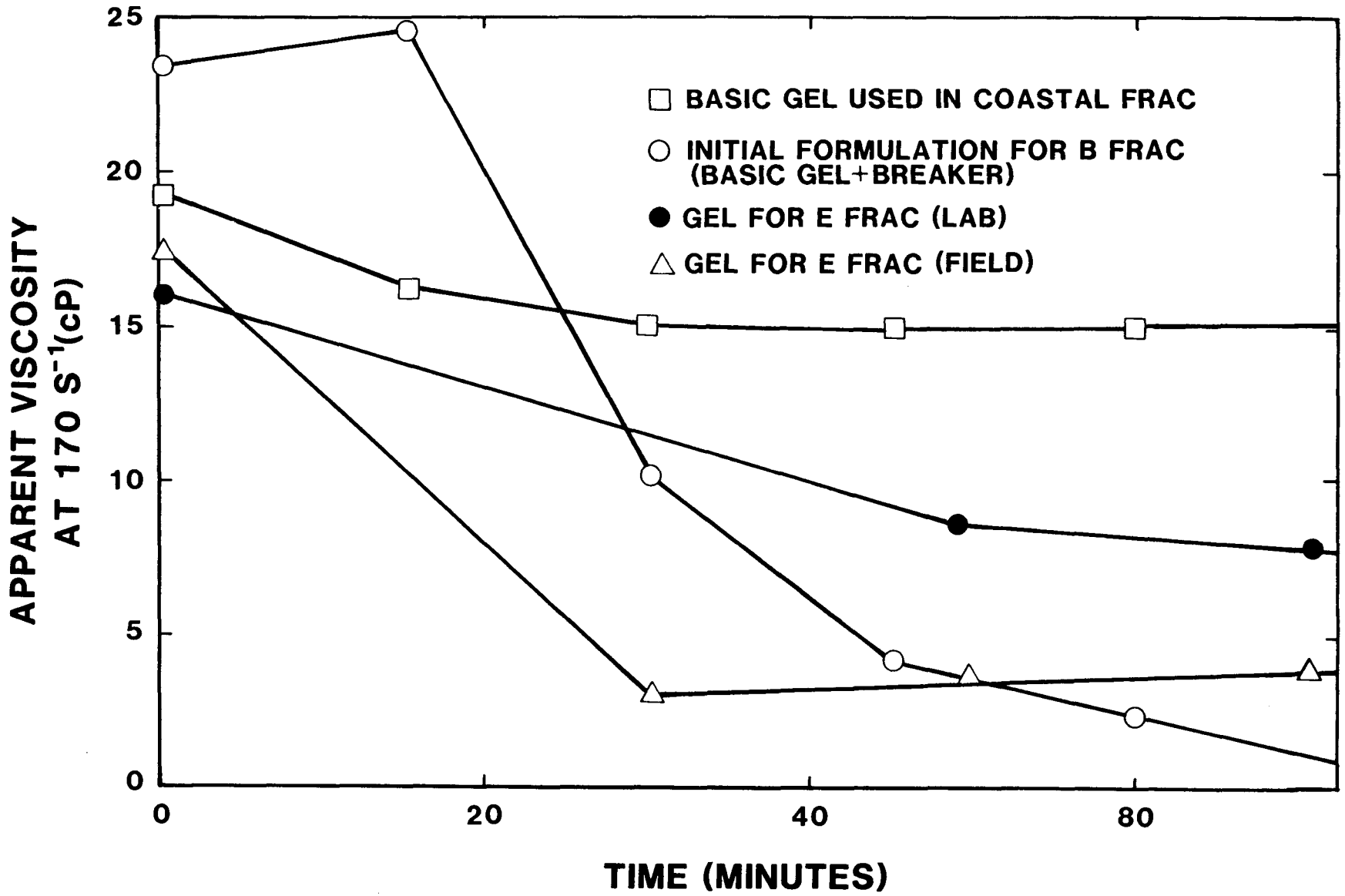

Figure 10.7. Viscosity vs. Time for Gel Used in the Stimulation of the Fluvial E Sandstone (Short Term)

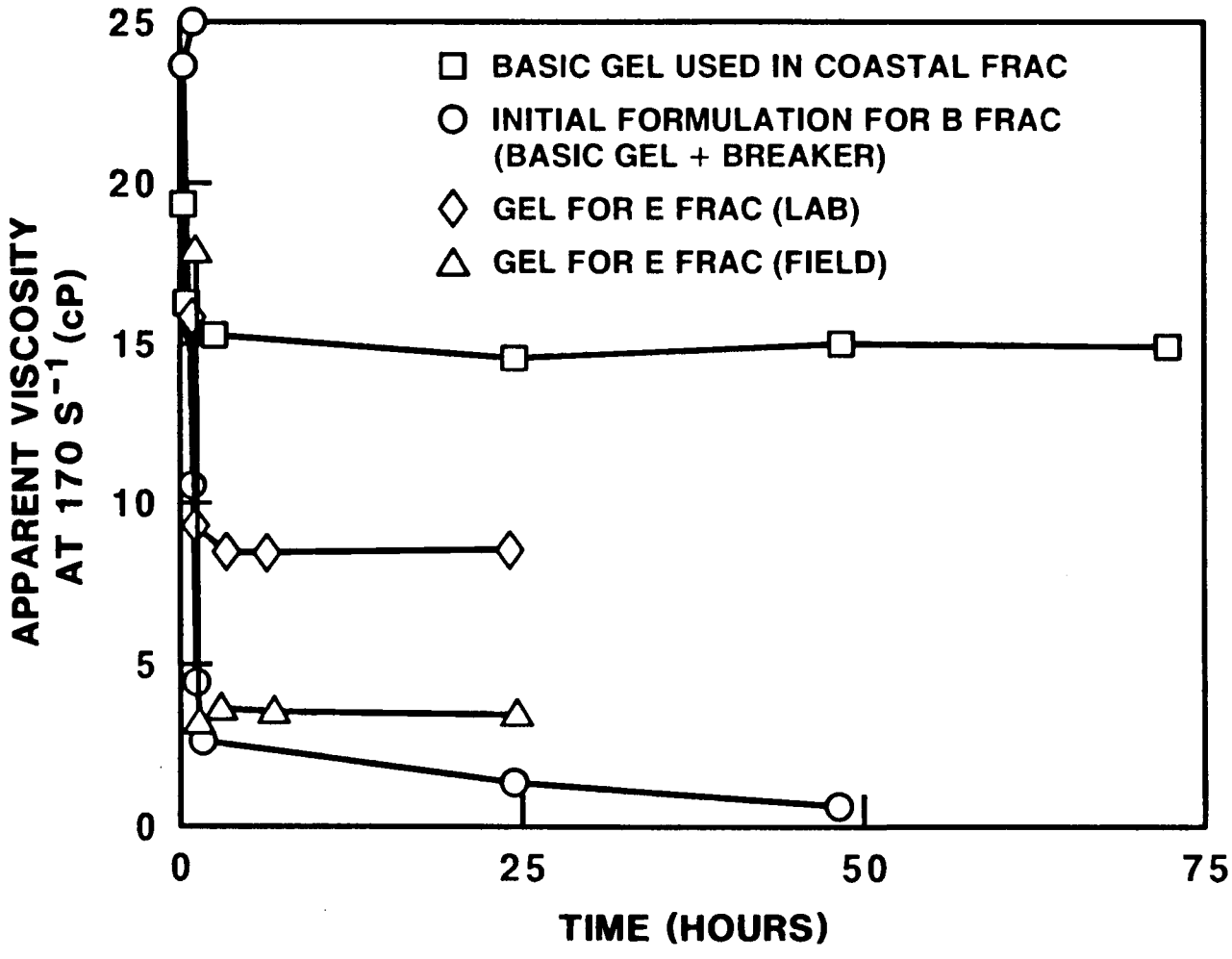

Figure 10.8. Viscosity vs. Time for Gel Used in the Stimulation of the Fluvial E Sandstone (Long Term)

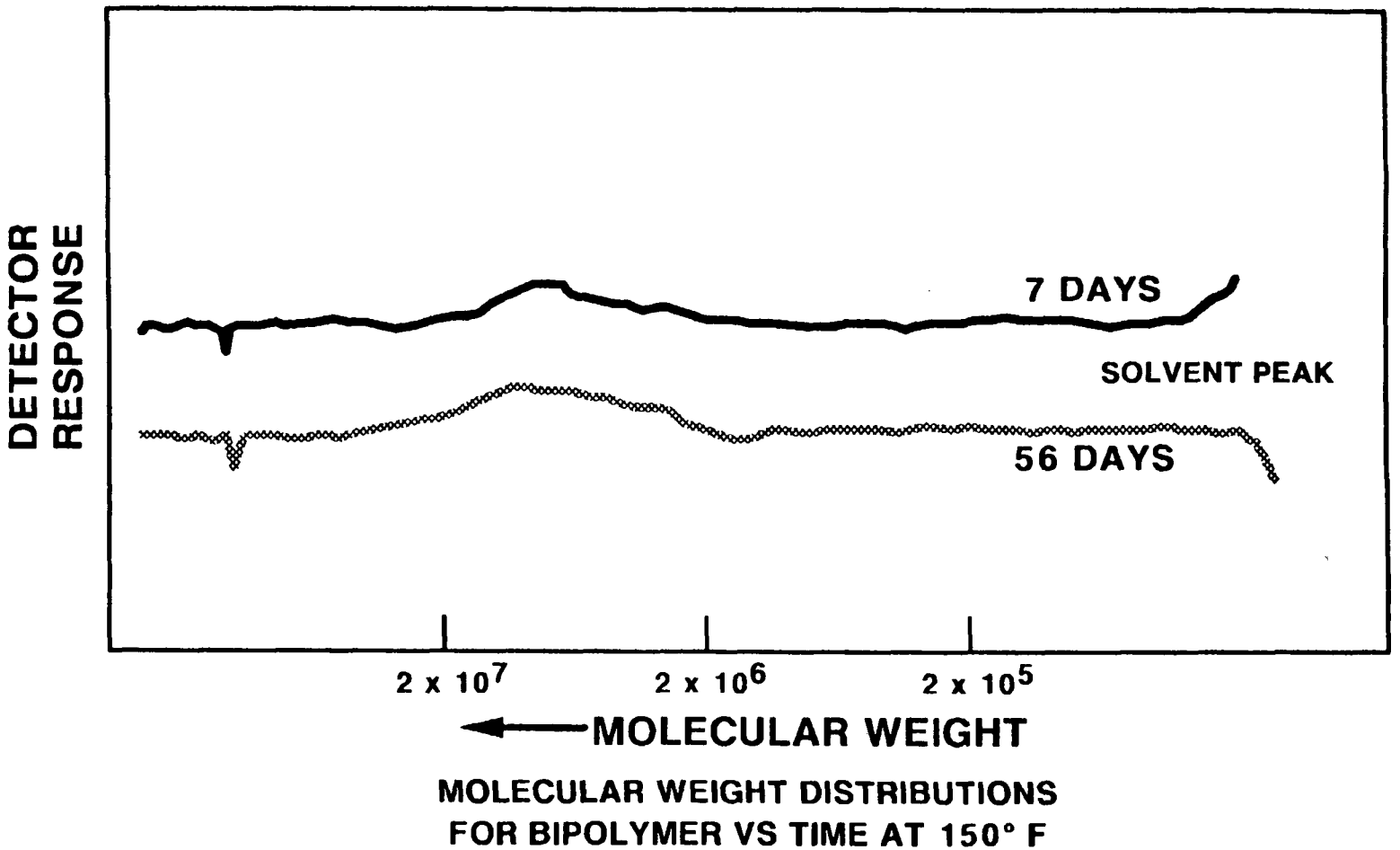

Figure 10.9. Molecular Weight of Biopolymer vs. Time

11.0 BIBLIOGRAPHY

S. J. Finley
Sandia National Laboratories

The technical output from the Multiwell Experiment resides in an MWX Data File which is maintained in the project office at Sandia National Laboratories in Albuquerque, NM.

The MWX Data File is intended to be "results-oriented." Thus, it includes such entries as (1) data reports from contractors and others, (2) memoranda, informal reports and compilations of results and analyses, (3) formal publications and reports, and (4) in limited cases, planning documents, review meeting summaries, etc. It is not intended to include every sheet of paper ever written on MWX or every bit of data taken. In general these are entries which are referenceable and which convey data.

The MWX Data File has the following overall organization:

1.0 Well data by well
1.1 Well logs by well and logging program; analyses
1.2 Core and fluid analyses by type and performer
1.3 Core-log correlation
1.4 Geology by topic
1.5 Environmental
1.6 Geophysics by type
1.7 Stress testing by interval
1.8 Well testing by interval
1.9 Stimulation and fracture diagnostics by interval
3.1 General reviews and status reports
3.3 Quarterly reports
3.5 Topical meetings, displays and workshops
3.7 Technical Review Panel
3.8 Plans

A computer-based index to the MWX Data File is also maintained in which each entry is indexed by accession number, data file number, author(s), title, company, date, alternate report number, key word(s), and comments/notes. Thus, searches, retrieval, and summaries of various types can be made readily. Two listings from this index are presented:

(A) A listing is given in this section of publications and formal reports which include information on the fluvial interval. (These are selected from the index through the key words "formal" and "fluvial.")

(B) A listing of the complete MWX Data File index data is given in Appendix Q for those entries which contain results for the fluvial interval.

```
**************************************************************************
ACCES NUM  N00644
REPORT NUM 1.2.55.007
AUTHOR     BROWER,KR
AUTHOR     MORROW,NR
TITLE      FLUID FLOW IN CRACKS AS RELATED TO LOW PERMEABILITY GAS SANDS
CORP AUTH  NMPRRC
DATE       830314
ALT NUMBER SPEDOE11623
NOTES      PRESENTED AT THE 1983 SPEDOE SYMPOSIUM ON LOW PERMEABILITY
           RESERVOIRS HELD IN DENVER CO, MARCH 14-16, 1983.
**************************************************************************
ACCES NUM  N00301
REPORT NUM 1.4.2.012
AUTHOR     EATOUGH,MO
TITLE      MINERALOGIC AND PETROLOGIC OVERVIEW OF CORE SAMPLES FROM THE
           DEPT. OF ENERGY'S WESTERN GAS SANDS PROJECT MULTIWELL EXPERIMENT,
           PICEANCE BASIN, COLORADO
CORP AUTH  BENDIX
DATE       830300
ALT NUMBER SPEDOE11764
NOTES      THIS PAPER WAS PRESENTED AT THE 1983 SPE/DOE SYMPOSIUM ON LOW
           PERMEABILITY HELD IN DENVER, COLORADO, MARCH 14-16, 1983
**************************************************************************
ACCES NUM  N00847
REPORT NUM 1.4.4.047
AUTHOR     FINLEY,SJ
AUTHOR     LORENZ,JC
TITLE      CHARACTERIZATION OF NATURAL FRACTURES IN MESAVERDE CORE FROM THE
           MULTIWELL EXPERIMENT
CORP AUTH  SAND
DATE       880900
ALT NUMBER SAND88-1800
**************************************************************************
ACCES NUM  00862
REPORT NUM 1.4.4.051
AUTHOR     FINLEY,SJ
AUTHOR     LORENZ,JC
TITLE      CHARACTERIZATION AND SIGNIFICANCE OF NATURAL FRACTURES IN
           MESAVERDE RESERVOIRS AT THE MULTIWELL EXPERIMENT SITE
CORP AUTH  SAND
DATE       890306
ALT NUMBER SPE19007
NOTES      PRESENTED AT 1989 SPE JOINT ROCKY MOUNTAIN REGIONAL MEETING
           AND LOW PERMEABILITY RESERVOIR SYMPOSIUM, MARCH 6-8,1989,
           DENVER,CO
**************************************************************************
ACCES NUM  N00308
REPORT NUM 1.4.2.013
AUTHOR     HEINZE,DM
TITLE      MINERALOGY AND PETROLOGY ASPECTS OF THE MESAVERDE FORMATION AT
           RIFLE GAP, COLORADO, SPECIFIC TO THE SEDIMENTOLOGY AND
           GAS-BEARING INTERVALS IN THE SUBSURFACE
DATE       830300
ALT NUMBER SAND830287
**************************************************************************
ACCES NUM  N00577
REPORT NUM 1.1.4.014
AUTHOR     KUKAL,GC
AUTHOR     HILL,RE
TITLE      IMPROVED SHALY SAND ANALYSIS IN HEAVY DRILLING MUDS: A SIMPLE
           TECHNIQUE  FOR USING THE PHOTOELECTRIC MEASUREMENT
CORP AUTH  CER
DATE       850600
NOTES      PRESENTED AT SPWLA 26TH ANNUAL LOGGING SYMPOSIUM, DALLAS, TEXAS
           JUNE 17-20  1985
```

```
**********************************************************************
ACCES NUM  N00636
REPORT NUM 1.3.010
AUTHOR     KUKAL,GC
AUTHOR     HILL,RE
TITLE      LOG ANALYSIS OF CLAY VOLUME: AN EVALUATION OF TECHNIQUES AND
           ASSUMPTIONS USED IN AN UPPER CRETACEOUS SAND-SHALE SEQUENCE
CORP AUTH  CER
DATE       860000
NOTES      TO BE PRESENTED AT THE 1986 SOCIETY OF PROF. WELL LOG  ANALYSTS
           MEETING, HOUSTON, TEXAS
**********************************************************************
ACCES NUM  N00574
REPORT NUM 1.1.4.011
AUTHOR     KUKAL,GC
AUTHOR     SIMONS,KE
TITLE      LOG ANALYSIS TECHNIQUES FOR QUANTIFYING THE PERMEABILITY OF SUB-
           MILLIDARCY SANDSTONE RESERVOIRS
CORP AUTH  CER
DATE       850500
ALT NUMBER SPEDOE13880
NOTES      PRESENTED AT THE SPE/DOE 1985 LOW PERMEABILITY GAS RESERVOIR
           SYMPOSIUM  DENVER, COLORADO, MAY 19-22 1985.
**********************************************************************
ACCES NUM  N00160
REPORT NUM 1.6.2.002
AUTHOR     LEE,MW
TITLE      VERTICAL SEISMIC PROFILES AT MULTI-WELL EXPERIMENT SITE, GARFIELD
           COUNTY, COLORADO
CORP AUTH  USGS
DATE       831100
ALT NUMBER USGS OPEN FILE REPORT 84-168
**********************************************************************
ACCES NUM  N00500
REPORT NUM 1.6.2.004
AUTHOR     LEE,MW
AUTHOR     MILLER,JJ
TITLE      ACQUISITION AND PROCESSING OF AZIMUTHAL VERTICAL SEISMIC PROFILES
           AT MULTIWELL EXPERIMENT SITE, GARFIELD COUNTY, COLORADO
CORP AUTH  USGS
DATE       850400
ALT NUMBER USGS OPEN FILE REPORT 85-427
**********************************************************************
ACCES NUM  N00294
REPORT NUM 1.4.3.033
AUTHOR     LORENZ,JC
TITLE      SEDIMENTOLOGY OF THE MESAVERDE FORMATION AT RIFLE GAP, COLORADO
           AND IMPLICATIONS FOR GAS-BEARING INTERVALS IN THE SUBSURFACE
DATE       820300
ALT NUMBER SAND820604
**********************************************************************
ACCES NUM  N00309
REPORT NUM 1.4.3.037
AUTHOR     LORENZ,JC
TITLE      RESERVOIR SEDIMENTOLOGY IN MESAVERDE ROCKS AT THE MULTI-WELL
           EXPERIMENT SITE
DATE       830600
ALT NUMBER SAND83-1078
**********************************************************************
ACCES NUM  N00793
REPORT NUM 1.4.4.041
AUTHOR     LORENZ,JC
AUTHOR     FINLEY,SJ
TITLE      DIFFERENCES IN FRACTURE CHARACTERISTICS AND RELATED PRODUCTION
           OF NATURAL GAS IN DIFFERENT ZONES OF THE MESAVERDE FORMATION,
           NORTHWESTERN, COLORADO
```

CORP AUTH SAND
DATE 870927
ALT NUMBER SPE16809
NOTES PRESENTED AT THE ANNUAL SPE CONFERENCE IN DALLAS,TX SEPT. 27-30,1987
****
ACCES NUM N00845
REPORT NUM 1.4.5.016
AUTHOR LORENZ,JC
AUTHOR FINLEY,SJ
TITLE SIGNIFICANCE OF DRILLING- AND CORING-INDUCED FRACTURES IN MESAVERDE CORE, NORTHWESTERN COLORADO
CORP AUTH SAND
DATE 880900
ALT NUMBER SAND88-1800
****
ACCES NUM N00504
REPORT NUM 1.4.3.023
AUTHOR LORENZ,JC
AUTHOR HEINZE,DM
AUTHOR CLARK,JA
AUTHOR SEARLS,CA
TITLE DETERMINATION OF WIDTHS OF MEANDER-BELT SANDSTONE RESERVOIRS FROM VERTICAL DOWNHOLE DATA, MESAVERDE GROUP, PICEANCE CREEK BASIN, COLORADO
CORP AUTH SAND
DATE 850500
NOTES PUBLISHED IN AAPG BULLETIN, V.70, P710-721
****
ACCES NUM N00780
REPORT NUM 1.4.3.040
AUTHOR LORENZ,JC
AUTHOR RUTLEDGE,AK
TITLE LATE CRETACEOUS MESAVERDE GROUP OUTCROPS AT RIFLE GAP, PICEANCE CREEK BASIN, NORTHWESTERN COLORADO
CORP AUTH SAND
DATE 870000
ALT NUMBER 68
NOTES GEOLOGICAL SOCIETY OF AMERICA CENTENNIAL FIELD GUIDE - ROCKY MOUNTAIN SECTION, 1987
****
ACCESS NUM N00847
REPORT NUM 3.1.021
AUTHOR LORENZ,JC
AUTHOR WARPINSKI,NR
AUTHOR TEUFEL,LW
AUTHOR BRANAGAN,P
AUTHOR SATTLER,AR
AUTHOR NORTHROP,DA
TITLE RESULTS OF THE MULTIWELL EXPERIMENT, IN SITU STRESSES, NATURAL FRACTURES, AND OTHER GEOLOGICAL CONTROLS ON RESERVOIRS
CORP AUTH SAND
CORP AUTH CER
DATE 880830
NOTES EOS VOL 69, NO 35, P 817,825-826
****
ACCES NUM N00104
REPORT NUM 1.2.55.001
AUTHOR MORROW,NR
TITLE RELATIONSHIP OF PORE STRUCTURE TO FLUID BEHAVIOR IN LOW PERMEABILITY GAS SANDS, FIRST ANNUAL REPORT
CORP AUTH NMPRRC
DATE 831000
ALT NUMBER DOEBC10216-13
****
ACCES NUM N00328

```
REPORT NUM 1.2.55.005
AUTHOR     MORROW,NR
TITLE      RELATIONSHIP OF PORE STRUCTURE TO FLUID BEHAVIOR IN LOW
           PERMEABILITY GAS SANDS
CORP AUTH  NMPRRC
DATE       840500
ALT NUMBER NMERDI2703303
**********************************************************************
ACCES NUM  N00705
REPORT NUM 1.2.55.012
AUTHOR     MORROW,NR
TITLE      RELATIONSHIP OF PORE STRUCTURE TO FLUID BEHAVIOR IN  LOW
           PERMEABILITY GAS SANDS: YEAR THREE
CORP AUTH  NMPRRC
DATE       850200
ALT NUMBER NMERDI 2-72-4309
**********************************************************************
ACCES NUM  N00447
REPORT NUM 1.2.55.004
AUTHOR     MORROW,NR
AUTHOR     BROWER,KR
AUTHOR     KILMER,NH
TITLE      RELATIONSHIP OF PORE STRUCTURE TO FLUID BEHAVIOR IN LOW
           PERMEABILITY GAS SANDS
CORP AUTH  NMPRRC
DATE       820000
ALT NUMBER DOE BC 10216-14
**********************************************************************
ACCES NUM  N00704
REPORT NUM 1.2.55.011
AUTHOR     MORROW,NR
AUTHOR     BROWER,KR
AUTHOR     KILMER,NH
TITLE      RELATIONSHIP OF PORE STRUCTURE TO FLUID BEHAVIOR IN LOW
           PERMEABILITY GAS SANDS, 1984 FINAL REPORT
CORP AUTH  NMPRRC
DATE       840900
ALT NUMBER DOEBC10216-13
**********************************************************************
ACCES NUM  N00669
REPORT NUM 1.2.55.009
AUTHOR     MORROW,NR
AUTHOR     WARD,J
AUTHOR     BROWER,KR
TITLE      ROCK MATRIX AND FRACTURE ANALYSIS OF FLOW IN WESTERN TIGHT GAS
           SANDS, 1985 ANNUAL REPORT
CORP AUTH  NMPRRC
DATE       860200
ALT NUMBER DOEMC21179-2032
**********************************************************************
ACCES NUM  N00470
REPORT NUM 1.4.3.026
AUTHOR     PETERSON,RE
TITLE      GEOLOGICAL AND PRODUCTION CHARACTERISTICS OF THE NON-MARINE PART
           OF THE  MESAVERDE GROUP, RULISON FIELD AREA,PICEANCE BASIN,
           COLORADO
CORP AUTH  CER
DATE       840514
ALT NUMBER SPE 12835
NOTES      PRESENTED AT THE SPE/DOE/GRI UNCONVENTIONAL GAS RECOVERY
           SYMPOSIUM IN  PITTSBURGH PA, MAY 13-15,1984.
**********************************************************************
ACCES NUM  N00295
REPORT NUM 1.4.3.034
AUTHOR     PETERSON,RE
TITLE      WESTERN GAS SANDS PROJECT: AN APPROXIMATION OF CONTINUITY OF
```

```
            LENTICULAR MESAVERDE SANDSTONE LENSES, UTILIZING CLOSE WELL
            CORRELATIONS, PICEANCE BASIN, NORTHWEST COLORADO
CORP AUTH   CER
DATE        821100
ALT NUMBER DOENV102493
**********************************************************************
ACCES NUM   N00312
REPORT NUM 1.4.3.028
AUTHOR      PETERSON,RE
AUTHOR      KOHOUT,J
TITLE       APPROXIMATING THE DIMENSIONS OF LENTICULAR MESAVERDE GROUP
            SANDSTONE LENSES UTILIZING CLOSE WELL CORRELATIONS (2.2)
CORP AUTH   CER
DATE        831018
ALT NUMBER DOEMETC843
NOTES       PRESENTED AT WGSS PROGRAM REVIEW, OCTOBER 18-19, 1983,
            MORGANTOWN, WV
**********************************************************************
ACCES NUM   N00305
REPORT NUM 1.4.3.035
AUTHOR      PETERSON,RE
AUTHOR      KOHOUT,J
TITLE       AN APPROXIMATION OF CONTINIUITY OF LENTICULAR MESAVERDE SANDSTONE
            LENSES UTILIZING CLOSE-WELL CORRELATIONS, PICEANCE BASIN,
            NORTHWESTERN COLORADO
CORP AUTH   CER
DATE        830300
ALT NUMBER SPEDOE11610
NOTES       THIS PAPER WAS PRESENTED AT THE 1983 SPE/DOE SYMPOSIUM ON LOW
            PERMEABILITY HELD IN DENVER, COLORADO, MARCH 14-16, 1983
**********************************************************************
ACCES NUM   N00300
REPORT NUM 1.2.12.020
AUTHOR      RANDOLPH,PL
TITLE       POROSITY AND PERMEABILITY OF MESAVERDE SANDSTONE CORE FROM THE
            U.S. DOE MULTIWELL EXPERIMENT, GARFIELD COUNTRY, COLORADO
CORP AUTH   IGT
DATE        830300
ALT NUMBER SPEDOE11765
NOTES       THIS PAPER WAS PRESENTED AT THE 1983 SPE/DOE SYMPOSIUM ON LOW
            PERMEABILITY HELD IN DENVER, COLORADO, MARCH 14-16, 1983
**********************************************************************
ACCES NUM   N00326
REPORT NUM 1.2.12.021
AUTHOR      RANDOLPH,PL
AUTHOR      SOEDER,DJ
AUTHOR      CHOWDIAH,P
TITLE       POROSITY AND PERMEABILITY OF TIGHT SANDS
CORP AUTH   IGT
DATE        840513
ALT NUMBER SPEDOEGRI12836
NOTES       PRESENTED AT THE 1984 SPE/DOE/GRI UNCONVENTIONAL GAS RECOVERY
            SYMPOSIUM, PITTSBURGH, PENNSYLVANIA, MAY 13-15, 1984
**********************************************************************
ACCES NUM   N00323
REPORT NUM 1.2.26.005
AUTHOR      SATTLER,AR
AUTHOR      HECKES,AA
AUTHOR      CLARK,JA
TITLE       PRESSURE CORE MEASUREMENTS IN TIGHT SANDSTONE LENSES DURING THE
            MULTIWELL EXPERIMENT
CORP AUTH   SAND
DATE        840513
ALT NUMBER SPE12853
NOTES       PAPER WAS PRESENTED AT THE 1984 SPE/DOE/GRI UNCONVENTIONAL GAS
            RECOVERY SYMPOSIUM HELD IN PITTSBURGH, PA, MAY 13-15, 1984
```

```
**************************************************************************
ACCES NUM  N00572
REPORT NUM 1.6.4.002
AUTHOR     SEARLS,CA
TITLE      THE MULTIWELL EXPERIMENT GEOPHYSICS PROGRAM FINAL REPORT
CORP AUTH  SAND
DATE       850900
ALT NUMBER SAND 85-1013
**************************************************************************
ACCES NUM  N00297
REPORT NUM 1.6.4.003
AUTHOR     SEARLS,CA
AUTHOR     LEE,MW
AUTHOR     MILLER,JJ
AUTHOR     ALBRIGHT,JN
AUTHOR     FRIED,J
AUTHOR     APPLEGATE,JK
TITLE      A COORDINATED SEISMIC STUDY OF THE MULTI-WELL EXPERIMENT SITE
CORP AUTH  SAND
CORP AUTH  USGS
CORP AUTH  LANL
CORP AUTH  CSM
DATE       830300
ALT NUMBER SPEDOE11613
NOTES      THIS PAPER WAS PRESENTED AT THE 1983 SPE/DOE SYMPOSIUM ON LOW
           PERMEABILITY HELD IN DENVER, COLORADO, MARCH 14-16, 1983
**************************************************************************
ACCES NUM  N00302
REPORT NUM 1.2.25.018
AUTHOR     SENSENY,PE
TITLE      LABORATORY MEASUREMENTS OF MECHANICAL PROPERTIES OF SANDSTONES
           AND SHALES
CORP AUTH  RSI
ALT NUMBER SPEDOE11762
NOTES      THIS PAPER WAS PRESENTED AT THE 1983 SPE/DOE SYMPOSIUM ON LOW
           PERMEABILITY HELD IN DENVER, COLORADO, MARCH 14-16, 1983
**************************************************************************
ACCES NUM  N00329
REPORT NUM 1.2.12.022
AUTHOR     SOEDER,DJ
AUTHOR     RANDOLPH,PL
TITLE      POROSITY, PERMEABILITY AND PORE STRUCTURE OF THE TIGHT MESA
           VERDE SANDSTONE, PICEANCE BASIN, COLORADO
CORP AUTH  IGT
DATE       840916
ALT NUMBER SPE13134
NOTES      PRESENTED AT THE 59TH ANNUAL TECHNICAL CONFERENCE AND  EXHIBITION
           HELD IN HOUSTON, TEXAS, SEPTEMBER 16-19, 1984
**************************************************************************
ACCES NUM  N00474
REPORT NUM 1.4.5.003
AUTHOR     SPENCER,CW
AUTHOR     KEIGHIN,CW
TITLE      GEOLOGIC STUDIES IN SUPPORT OF THE U.S. DOE'S MULTI-WELL
           EXPERIMENT,GARFIELD  COUNTY, COLORADO.
CORP AUTH  USGS
DATE       841100
ALT NUMBER OFR 84757
NOTES      SUMMARY OF USGS WORK ON MWX
**************************************************************************
ACCES NUM  N00515
REPORT NUM 1.2.26.006
AUTHOR     TEUFEL,LW
TITLE      PREDICTION OF HYDRAULIC FRACTURE AZIMUTH FROM ANELASTIC STRAIN
           RECOVERY  MEASUREMENTS OF ORIENTED CORE
CORP AUTH  SAND
```

DATE 820825
NOTES PRESENTED AT THE 23RD U.S. SYMPOSIUM ON ROCK MECHANICS, BERKELEY,CA AUGUST 25-27, 1982
****
ACCES NUM N00513
REPORT NUM 1.9.5.004
AUTHOR TEUFEL,LW
AUTHOR HART,CM
AUTHOR SATTLER,AR
AUTHOR CLARK,JA
TITLE DETERMINATION OF HYDRAULIC FRACTURE AZIMUTH BY GEOPHYSICAL, GEOLOGICAL, AND ORIENTED CORE METHODS AT THE MULTI-WELL EXPERIMENT SITE, RIFLE, CO.
CORP AUTH SAND
DATE 840916
ALT NUMBER SPE 13226
NOTES PRESENTED AT THE 59TH ANNUAL SPE MEETING HOUSTON TX, SEPTEMBER,1984
****
ACCES NUM N00760
REPORT NUM 1.9.3.010
AUTHOR THORNE,BJ
AUTHOR MORRIS,HE
TITLE ADVANCES IN BOREHOLE SEISMIC FRACTURE DIAGNOSTICS
CORP AUTH SAND
DATE 870518
ALT NUMBER SPEDOE 16405
NOTES PRESENTED AT THE 1987 SPEDOE JOINT SYMPOSIUM ON LOW PERMEABILITY RESERVOIRS, MAY 18-19, 1987, DENVER, CO.
****
ACCES NUM N00849
REPORT NUM 1.9.3.018
AUTHOR THORNE,BJ
AUTHOR MORRIS,HE
TITLE PASSIVE SEISMIC MONITORING OF HYDRAULIC FRACTURE EXPERIMENTS AT THE MULTIWELL EXPERIMENT SITE
CORP AUTH SAND
DATE 880800
ALT NUMBER SAND88-1284
****
ACCES NUM N00853
REPORT NUM 1.9.3.020
AUTHOR WARPINSKI,NR
TITLE DUAL LEAKOFF BEHAVIOR IN HYDRAULIC FRACTURING OF TIGHT LENTICULAR GAS SANDS
CORP AUTH SAND
DATE 881002
ALT NUMBER SPE 18259
NOTES PRESENTED AT THE 63RD ANNUAL TECHNICAL CONFERENCE AND EXHIBITION OF THE SOCIETY OF PETROLEUM ENGINEERS HELD IN HOUSTON TEXAS,OCT.2-5,1988. B, C, AND E SANDS
****
ACCES NUM N00852
REPORT NUM 1.9.3.019
AUTHOR WARPINSKI,NR
AUTHOR BRANAGAN,P
AUTHOR SATTLER,AR
AUTHOR CIPOLLA,C
AUTHOR LORENZ,JC
AUTHOR THORNE,BJ
TITLE A CASE STUDY OF A STIMULATION EXPERIMENT IN A FLUVIAL, TIGHT, SANDSTONE GAS RESERVOIR
CORP AUTH SAND
CORP AUTH CER
DATE 881002
ALT NUMBER SPE 18258

NOTES PRESENTED AT THE 63RD ANNUAL TECHNICAL CONFERENCE AND EXHIBITION OF THE SOCIETY OF PETROLEUM ENGINEERS HELD IN HOUSTON TEXAS, OCT. 2-5,1988, E SAND

****

ACCES NUM N00759
REPORT NUM 1.7.5.002
AUTHOR WARPINSKI,NR
AUTHOR TEUFEL,LW
TITLE IN SITU STRESSES IN LOW PERMEABILITY, NONMARINE ROCKS
CORP AUTH SAND
DATE 870518
ALT NUMBER SPEDOE 16402
NOTES PRESENTED AT THE 1987 SPEDOE JOINT SYMPOSIUM ON LOW PERMEABILITY RESERVOIRS, MAY18-19,1987, DENVER,CO.

****

ACCES NUM N00703
REPORT NUM 1.2.55.010
AUTHOR WEI,KK
AUTHOR MORROW,NR
AUTHOR BROWER,KR
TITLE THE EFFECT OF FLUID, CONFINING PRESSURE, AND TEMPERATURE ON ABSOLUTE PERMEABILITIES OF LOW PERMEABILITY SANDSTONES
CORP AUTH NMPRRC
DATE 840916
ALT NUMBER SPE 13093
NOTES PRESENTED AT THE 59TH ANNUAL TECHNICAL CONFERENCE AND EXHIBITION HELD IN HOUSTON, TEXAS SEPT 16-19,1984

12.0 APPENDICES

The following appendices appear as microfiche in pocket on back cover:

A. Site Description and Operations (F. R. Myal, CER)
B. Petrographic Data Sheets (Bendix)
C. Core Laboratories Core Data
D. Institute of Gas Technology (IGT) Core Data
E. RESPEC Core Data
F. Fluvial B Pre-Frac Well Test Data (CER)
G. Fluvial B Stimulation Operations and QC (CER)
H. Fluvial B Stimulation Data (Sandia)
I. Fluvial B Post-Frac Well Test Data (CER)
J. Fluvial C Stimulation Operations and QC (CER)
K. Fluvial C Stimulation Data (Sandia)
L. Completions Background and Analyses (P. T. Branagan, CER)
M. Fluvial E Pre-Frac Well Test Data (CER)
N. Fluvial E Stimulation Operations and QC (CER)
O. Fluvial E Stimulation Data (Sandia)
P. Fluvial E Post-Frac Well Test Data (CER)
Q. Fluvial MWX Data File Entries (S. J. Finley, Sandia)